

Fire and Polymers IV

Downloaded by 212.166.64.10 on October 22, 2009 | <http://pubs.acs.org>
Publication Date: November 24, 2005 | doi: 10.1021/bk-2006-0922.fw001

ACS SYMPOSIUM SERIES **922**

Fire and Polymers IV

Materials and Concepts for Hazard Prevention

Charles A Wilkie, Editor
Marquette University

Gordon L. Nelson, Editor
Florida Institute of Technology

**Sponsored by the
ACS Division of Polymeric Materials: Science and
Engineering, Inc.**



American Chemical Society, Washington, DC

In Fire and Polymers IV; Wilkie, C., et al.;
ACS Symposium Series; American Chemical Society: Washington, DC, 2005.



Library of Congress Cataloging-in-Publication Data

Fire and polymers IV : materials and concepts for hazard prevention / Charles A. Wilkie, editor ; Gordon L. Nelson, editor.

p. cm. — (ACS symposium series ; 922)

“Developed from a symposium sponsored by the Division of Polymeric Materials: Science and Engineering, Inc. at the 228th National Meeting of the American Chemical Society, Philadelphia, PA, August 23–26, 2004”—

Includes bibliographical references and index.

ISBN-13: 978-0-8412-3948-7 (alk. paper)

1. Polymers—Fire testing—Congresses. 2. Fire resistant polymers—Congresses.

I. Wilkie, C. A. (Charles A.), 1941- II. Nelson, Gordon L., 1943- III. American Chemical Society. Division of Polymeric Materials: Science and Engineering, Inc. IV. American Chemical Society. Meeting (228th : 2004 : Philadelphia, Pa.). V. Series.

TH9446.5.P65F553 2005
628.9'223—dc22

2005048309

The paper used in this publication meets the minimum requirements of American National Standard for Information Sciences—Permanence of Paper for Printed Library Materials, ANSI Z39.48–1984.

Copyright © 2006 American Chemical Society

Distributed by Oxford University Press

ISBN 10: 0-8412-3948-7

All Rights Reserved. Reprographic copying beyond that permitted by Sections 107 or 108 of the U.S. Copyright Act is allowed for internal use only, provided that a per-chapter fee of \$30.00 plus \$0.75 per page is paid to the Copyright Clearance Center, Inc., 222 Rosewood Drive, Danvers, MA 01923, USA. Republication or reproduction for sale of pages in this book is permitted only under license from ACS. Direct these and other permission requests to ACS Copyright Office, Publications Division, 1155 16th Street, N.W., Washington, DC 20036.

The citation of trade names and/or names of manufacturers in this publication is not to be construed as an endorsement or as approval by ACS of the commercial products or services referenced herein; nor should the mere reference herein to any drawing, specification, chemical process, or other data be regarded as a license or as a conveyance of any right or permission to the holder, reader, or any other person or corporation, to manufacture, reproduce, use, or sell any patented invention or copyrighted work that may in any way be related thereto. Registered names, trademarks, etc., used in this publication, even without specific indication thereof, are not to be considered unprotected by law.

PRINTED IN THE UNITED STATES OF AMERICA

Foreword

The ACS Symposium Series was first published in 1974 to provide a mechanism for publishing symposia quickly in book form. The purpose of the series is to publish timely, comprehensive books developed from ACS sponsored symposia based on current scientific research. Occasionally, books are developed from symposia sponsored by other organizations when the topic is of keen interest to the chemistry audience.

Before agreeing to publish a book, the proposed table of contents is reviewed for appropriate and comprehensive coverage and for interest to the audience. Some papers may be excluded to better focus the book; others may be added to provide comprehensiveness. When appropriate, overview or introductory chapters are added. Drafts of chapters are peer-reviewed prior to final acceptance or rejection, and manuscripts are prepared in camera-ready format.

As a rule, only original research papers and original review papers are included in the volumes. Verbatim reproductions of previously published papers are not accepted.

ACS Books Department

Preface

In the United States we each have about a 40% lifetime probability of being involved in a fire big enough to cause the local fire department to arrive at our door. 1.6 million fires occur in the United States annually, resulting in \$12.3 billion in damage. Although the United States has one of the highest rates of fire in the world, fire is a worldwide problem. Most fires involve the combustion of polymeric materials. Flame retardants continue to be the largest single class of additives sold for use in plastics and flame retardants alone constitute a \$1 billion (plus) worldwide business. Thus, a clear need exists for a peer-reviewed book on the latest topics in fire science from a polymer perspective.

Because fire and polymers are an important social issue and because of the interest in and the complexity of fire science, a symposium was organized at the 228th American Chemical Society (ACS) National Meeting in Philadelphia, Pennsylvania. The symposium builds upon previous symposia in 1989, 1994, and 2000. Thirty-eight papers from the leading world experts were presented. From those presentations, 28 chapters were carefully selected for incorporation into this volume.

Acknowledgements

We gratefully acknowledge the ACS Division of Polymeric Materials: Science and Engineering, Inc. (PMSE) for providing the venue for the symposium. We acknowledge Cyndi Johnsrud for her extensive assistance with the myriad of details in preparation for the symposium and associated reception and in the preparation and organization of PMSE preprints from the symposium. We gratefully acknowledge Elementis Specialties, Astaris LLC, Great Lakes Chemical Corp., Isolatek International, Martin Marietta (Magnesia Specialties),

Nanocor, Southern Clay Products, Inc., ATOFINA Chemicals, Inc., and Luzenac/Borax for their interest in the symposium, and in support of the associated reception and of international speaker travel.

Gordon L. Nelson
College of Science
Florida Institute of Technology
150 West University Boulevard
Melbourne, FL 32901-6975

Charles A. Wilkie
Department of Chemistry
Marquette University
P.O. Box 1881
Milwaukee, WI 53201-1881

Fire and Polymers IV

Chapter 1

Fire Retardancy in 2005

Gordon L. Nelson¹ and Charles A. Wilkie²

¹Florida Institute of Technology, 150 West University Boulevard,
Melbourne, FL 32901–6975

²Department of Chemistry, Marquette University, P.O. Box 1881,
Milwaukee, WI 53201–1881

Fire is a worldwide problem. It claims thousands of lives and causes significant loss of property every year. In the volume problems are discussed and solutions delineated. This peer-reviewed volume is designed to be representative of the state-of-the-art. This chapter places current work in perspective.

Introduction

In the United States every 20 seconds a fire department responds to a fire somewhere in the country. A fire occurs in a structure at the rate of one every 61 seconds. A residential fire occurs every 79 seconds. A fire occurs in a vehicle every 101 seconds. There is a fire in an outside property every 42 seconds. The result is 1.6 million fires per year (2003) attended by public fire departments. In 2003 those fires accounted for \$12.3 billion in property damage and 3925 civilian fire deaths (one every 134 minutes) and 18,125 injuries (one every 29 minutes). Some 105 fire fighters died in the line of duty in 2003. Fires have declined over the period 1977 to 2003, most notably structural fires, from 1,098,000 to 519,500. Civilian fire deaths in the home (80% of all fire deaths) declined from 6,015 in 1978 to 3,145 in 2003. While those declines are

progress, recent years have been static, and the United States still maintains one of the highest rates of fire in the world. Just as the U.S. has a high fire rate, the fire death rate in the US varies by state, from 37.9/million population in Arkansas to 3.1/million in Utah. Importantly, 70% of fire deaths in the U.S. occurs in homes without working smoke alarms, this despite years of effort to achieve a high penetration (1-3)

The higher rate of fire in the United States versus most industrialized countries is probably a product of five factors: (1) the U.S. commits fewer resources to fire prevention activities; (2) there is a greater tolerance in the U.S. for "accidental" fires (no one is at fault); (3) Americans practice riskier and more careless behavior than people in other countries (example, the use of space heaters); (4) homes in the U.S. are not built with the same degree of fire resistance and compartmentation as in some countries; and (5) most importantly, people in the U.S. have more contents or "stuff" than those in other countries (i.e., higher fire load) as well as a higher number of ignition sources (higher use of energy).

Polymers form a major part of the built environment. Fire safety depends upon those materials. Polymers are "enabling technology." Advances in numerous technologies depend on appropriate advances in polymers for success. While polymers are both natural and synthetic, this book focuses entirely on the fire safety aspects of synthetic polymers. Production of synthetic plastics resins totaled over 169 million metric tons worldwide in 2003 (4). The U.S. constitutes about one quarter of worldwide plastics consumption, the European Union only slightly less, and Japan about 9 %. In Table I one finds plastics production figures by resin for North America (5). In Table II one finds plastics use data by resin for North America (6).

All organic polymers are combustible. They decompose when exposed to heat, their decomposition products burn, smoke is generated, and the products of combustion are highly toxic. The prime toxic product is CO in concert with CO₂. Toxicity is made more complex by the pervasive presence of alcohol on the part of fire victims. Fire is not a single material property. Fire performance combines ease of thermal decomposition, ignition, flame spread, heat release, ease of extinction, smoke generation, toxic potency and other properties. Regulations use specific tests covering these properties with engineering assessments for materials and systems as deemed appropriate for a particular application. Thus, for example, it is appropriate in small appliances to only worry about ignitability by a Bunsen burner flame or a needle flame, since in the application, from an internal point of view, that is the size of a fire source possible in real appliance failures.

**Table I North American Plastics Production^a – 1999 and 2003
(millions of pounds, dry weight basis)**

<i>Resin</i>	<i>1999 production</i>	<i>2003 production</i>
Epoxy	657	578
Urea and melamine ^c	2985	3174
Phenolics (gross wt) ^c	4388	4442
Total thermosets	8030	8194
LDPE ^c	7700	7804
LLDPE ^c	8107	11137
HDPE ^c	13864	15709
PP ^c	15493	17665
ABS ^{c,m}	1455	1262
SAN ^{c,m}	123	121
Other styrenics ^{c,m}	1644	1596
Nylon ^{c,m}	1349	1279
PVC ^c	14912	14702
Thermoplastic polyester	4846	7587
Total thermoplastics	75964	85255
Engineering resins ^c	2765	2619
All other resins	10702	10913
Grand total	97461	106974

Notes: ^a US, Canada and Mexico as noted, ^c Canada included, ^m Mexico included

Table II. Resins sales by major markets (millions of pounds)

<i>Major market</i>	<i>2003</i>	<i>%</i>
Transportation	4732	5.9
Packaging	27464	34.3
Building and construction	14495	18.2
Electrical/electronic	2862	3.6
Furniture and furnishings	3361	4.2
Consumer and institutional	14194	17.8
Industrial/machinery	962	0.8
Adhesives/inks/coatings	1170	1.5
All others	2021	2.5
Exports	9009	11.2
Total selected plastics^a	80270	100.0

a versus Table I, including engineering resins but excluding thermoplastic polyester

This volume is about the latest research at the intersection of the fields of fire and polymers. Much work continues focused on improving the fire performance of polymers through a detailed understanding of polymer degradation chemistry. New and refined analytical techniques facilitate that analysis. Creative chemists continue to develop new approaches and new, more thermally stable structures. Mathematical fire models continue to become more sophisticated. Tests are becoming better understood.

There are many diverse approaches to enhancing the fire stability of polymers. In the past the most common approach involved the addition of additives. Fifteen years and more ago halogenated fire retardants (with antimony oxide) were the additives of choice to enhance the fire retardancy of many polymers. At this time there is a strong emphasis on non-halogenated fire retardants, and nano-scale additives in particular.

As one looks at previous Fire and Polymers volumes, topics have clearly changed over the years. In 1990 fire toxicity was the first section with six papers. In 1995 there again was a section on fire toxicity with seven chapters. In 2001 there was but one paper and in this volume, 3. In 1990 there was a section on cellulose, in 2001 only 1 chapter, and in this volume none. In the 1995 volume there were twelve chapters on tests and regulations, in 2001, 2, and in this volume, none. In the current volume, half of the papers are on nanocomposites. Only two papers have a focus on halogen materials specifically. This is not to say that very traditional materials are not being used. Indeed, the use of halogen flame retardants continues to grow. However, this peer-reviewed volume is designed to represent the state of the art (7-9).

References

1. Karter, Jr., M. J. Fire Loss in the United States During 2003; National Fire Protection Association: Quincy, MA, October 2004.
2. Fire Loss; National Fire Protection Association; <http://www.nfpa.org>.
3. USFA State Fire Statistics; <http://www.usfa.fema.gov/statistics/state/>
4. Plastics in Europe, An analysis of plastics consumption and recovery in Europe; Association of Plastics Manufacturers; Summer 2004.
5. APC Year End Statistics for 2003; <http://www.americanplasticscouncil.org>
6. APS Plastics Industry Producer's Statistics Group; <http://www.americanplasticscouncil.org>.

7. Fire and Polymers, Hazards Identification and Prevention; Nelson, G. L.; Ed.; American Chemical Society: Washington, DC, 1990.
8. Fire and Polymers II, Materials and Tests for Hazard Prevention; Nelson, G. L.; Ed.; American Chemical Society: Washington, DC, 1995.
9. Fire and Polymers, Materials and Solutions for Hazard Prevention; Nelson, G. L. and Wilkie, C. A.; Eds.; Washington, DC, 2001.

Chapter 2

A Review of Recent Work in the Fire Retardancy of Nanocomposites

**Charles A. Wilkie, Xiaoxia Zheng, Grace Chigwada,
Marius Costache, Bok Nam Jang, and Jinguo Zhang**

**Department of Chemistry, Marquette University, P.O. Box 1881,
Milwaukee, WI 53201-1881**

Recent work from this laboratory on various aspects of the fire retardancy of polymer-clay nanocomposites is reviewed. The principal areas of interest are: the amount of clay that is required, the mechanisms by which nanocomposite formation enhances fire retardancy, the role of the surfactant and synergy between conventional fire retardants and nanocomposite formation. This is used to set a pathway for the future of nanocomposites in fire retardancy.

The age of polymer/clay nanocomposites began in the 1990s with the work done at Toyota of blends of polyamide-6 (PA-6) with clay and the observations that the heat distortion temperature increased by 90 °C with no loss of mechanical properties (1). Work that has turned out to be very germane was carried out much earlier by Blumstein, who found that the presence of clay during a polymerization reaction had an influence on the product that was formed (2). It is typically felt that there are four areas in which nanocomposites can be important: to enhance the barrier properties, to enhance fire retardancy, to improve the mechanical properties and to increase the heat distortion temperature. In this paper, we will focus almost exclusively on the fire performance from nanocomposites. The initial work on fire retardancy of polymer/clay nanocomposites probably originated at the National Institute of Standards and Technology (NIST) and this group has led the effort within the United States to capitalize on this technology.

Nanocomposite formation involves taking some layered material, most commonly an alumino-silicate or a silicate in the early days but now just as likely a double layered hydroxide (or salt), carbon nanotubes, polyhedral oligosilsesquioxanes, POSS, or a host of other materials. As long as the gallery space is sufficiently organophilic, polymer (or monomer) is able to enter this space and expand the clay layers. Three different types of materials may be described: an immiscible nanocomposite, also known as a microcomposite, occurs when the clay is not well-dispersed but rather acts as a filler; an intercalated nanocomposite occurs when the clay layers do expand, pushed apart by the polymer and the registry between the initial clay layers is maintained; a delaminated nanocomposite (also known as exfoliated) arises when the clay layers are pushed apart so far that the registry between the clay layers is lost.

Over the past five years, the work of this laboratory has been primarily directed towards understanding and enhancing the role of nanocomposites in fire retardancy. At this stage it seems appropriate to review some of this work and to make some predictions for the future.

The work that has been carried out in the laboratories at Marquette University has involved several significant areas: the amount of clay that is effective, the role of the surfactant, the use of cone calorimetry to evaluate the nanodispersion, the mechanism by which nanocomposites function and synergy between nanocomposite formation and conventional fire retardants.

Mechanisms of Fire Retardancy by Nanocomposites

The usual clay loading that has been used is in the range of 3 to 5% organically-modified clay (3). The amount of clay has been reduced to 0.1% and one still sees a reduction in the peak heat release rate (PHRR) but it is somewhat reduced at this level (4). Typically, the reduction in PHRR is about the same when the clay concentration is between 0.1 and 1% and that reduction is between one-third to one-half of the reduction seen at 3 or 5% organically-modified clay. There does not appear to be any advantage in using more than 3 to 5% clay for fire retardant applications. It is of interest to note that the type of nanocomposite, whether intercalated or delaminated, does not seem to influence the fire properties as measured by cone calorimetry (5).

Realizing that antioxidants function at the 0.1% level, we questioned if there may be some antioxidant effect occurring due to the presence of the clay; perhaps some radical trapping process was occurring. In examining the composition of clay, one may be struck by the amount of iron that is present in the clay. Fortunately there are clays available that are rich in iron and there are also clays that have very little iron. A comparison of these by cone calorimetry

showed that at low amounts of clay (less than 3%), there was a significantly smaller reduction in PHRR for clays that did not contain iron than for those which did contain iron (6). When the clay content reached about 3%, both offered about the same level of reduction. The only mechanism that had been proposed at that time was the barrier effect mechanism (7). Simply stated, this asserts that the clay forms a barrier at the surface of the polymer which prevents, at least for a time, mass transport of polymer to the vapor phase and also insulates the surface of the degrading polymer from the heat source. It is apparent that there must be a certain amount of clay present to form this surface. At less than this value, which may be about 3%, some radical trapping by the paramagnetic iron in the clay occurs, which has some effect in reducing the PHRR. When sufficient material is present, a significant barrier is produced and the barrier mechanism is the dominant process.

In collaboration with Jianqi Wang, we have probed the surface of the degrading polymer using X-ray photoelectron spectroscopy and we have been able to show that at about 400 °C for both polystyrene and poly(methyl methacrylate) nanocomposites, one observes the loss of carbon and an accumulation of oxygen, silicon and aluminum on the surface of the degrading material (8,9,10). Since all of these changes occur at the same temperature, they must be linked. One would expect that the polymer would volatilize in this temperature region, leading to the loss of carbon at the surface. It is of interest to compare this with the behavior of poly(vinyl chloride), in which carbon accumulation is observed both for the virgin polymer and for its nanocomposites (11). Since PVC is a char-forming polymer, one expects this effect.

The barrier mechanism is a physical process which can prevent the loss of material but one wonders if there is not also chemistry involved in the process. Initially we used TGA/FTIR to study the degradation of polystyrene nanocomposites and made the interesting observation that there are differences in the infrared spectra of the evolved products in the region around 1600 cm^{-1} (12). In this region there are two equally strong peaks when virgin polystyrene is degraded at about 1600 and 1630 cm^{-1} . The first of these may be assigned to the aromatic stretching frequency while the later is due to double bonds. When the degradation of polystyrene nanocomposites was studied, it was noted that this later peak became less intense. Additional work has now been carried out on this system which enables further elucidation of the process which is occurring. (13) The degradation of polystyrene proceeds by random scission, producing radicals; in the absence of clay, these radicals undergo further reaction, leading to the formation of monomeric styrene and styrene oligomers. In the presence of the clay, these radicals are at least momentarily contained by the clay and this enables radical recombination reactions, which leads to the formation of products that are different from those observed in the degradation of polystyrene

alone. In the degradation of virgin polystyrene, only three major volatile products are observed, monomeric styrene, styrene dimer and styrene trimer. When the nanocomposite undergoes thermal degradation, a very large number of products with retention times, and hence molecular weights, that are close to that of the dimer.

Work has also been performed on ethylene vinyl acetate copolymers, EVA, and its nanocomposites with similar results (14). EVA undergoes thermal degradation in two steps, the first is chain stripping in which acetic acid is lost with the formation of double bonds where the acetate had been connected to the chain. In the second step, this partially unsaturated material undergoes random scission, leading to the formation of alkanes, 1-alkenes and α,ω -dienes ranging from a nine carbon chain up to a 31 carbon chain. In the presence of an organically-modified clay, the α,ω -dienes are no longer produced or are in much lower amount and the amount of alkanes relative to alkenes is increased. A radical recombination pathway, quite similar to that suggested for polystyrene nanocomposites, has been suggested to explain this result.

Role of the Surfactant

A common problem in nanocomposites formulations is the thermal instability of the surfactant that is required to permit compatibility between the clay and the polymer. Typically the organically-modified clay begins to thermally degrade at about 200 °C, which can create a problem for those materials that must be processed at higher temperatures. We have explored several different pathways to enhance the thermal stability of the organically-modified clay. The most typical material that is used is some 'onium' salt and this is most often ammonium. The degradation of the surfactant in the clay is believed to proceed by a Hofmann elimination which involves the loss of an olefin from the long chain and then, at higher temperatures, the loss of the amine, leaving a proton as the counterion for the clay. Previous work has shown that phosphonium-modified clays show enhanced thermal stability compared to that of the ammonium clays (5). This suggested that it might be advantageous to study a heavier element from the same family to try to understand what controls the thermal stability of the organically-modified clay. Accordingly, a stibonium-modified clay was prepared and studied (15). The degradation of this stibonium-modified clay begins at about the same temperature as other onium-substituted clays but only the first step of the degradation occurs, at 500 °C, only 15% of the mass has been lost. Unfortunately, the clay is not well-nanodispersed throughout the polymer and the cone calorimetric results reflect this.

Another approach is to use a carbocation rather than an onium ion as the counterion of the clay. It is most likely that one would think of the trityl

(triphenylmethyl) ion as the typical carbocation, however we chose to use the tropylium ion, because it should have better thermal stability than does trityl. A tropylium-modified clay does show enhanced thermal stability and nanocomposites have been formed with styrene (16). With the usual onium salts, one must have at least one long chain on the nitrogen to permit good compatibility between the clay and the polymer. In this study, a styryltropylium cation, the structure of which is shown in Figure 1, was used to obtain this compatibility. The tropylium-modified clay does not show as good a nanodispersion nor as large a reduction in the peak heat release rate as is usually observed for styrene nanocomposites with the usual onium surfactants. The thermal stability, as measured by TGA, is quite good, there is less than 3% mass loss at 600 °C. These are very encouraging results and they suggest that carbocation-modified clays should continue to be pursued for higher temperature applications. The best guess is that longer chains must be added to enhance compatibility between the polymer and the clay.

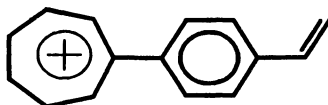


Figure 1. The styryltropylium cation that has been used to organically-modify clays.

Another approach has been to prepare oligomerically-modified clays. This has been accomplished using oligomers of molecular weight in the range of 5000 from styrene (17,18,19), methyl methacrylate (17,18,20), butadiene (21,22) and caprolactone (23). The oligomerically-modified clays of styrene, methyl methacrylate and butadiene have been prepared using copolymers which contain one or, at most, two units of vinylbenzyl chloride, which has been used to quaternize an amine to give the ammonium salt that was ion-exchanged onto the clay. The thermal stability of these oligomerically-modified clays is significantly better than the commonly used clays; the styrene-containing clay has only lost 7% of its mass at 350 °C.

Nanocomposites have been prepared using polystyrene, poly(methyl methacrylate), high impact polystyrene, HIPS, acrylonitrile-butadiene-styrene terpolymer, ABS, polypropylene and polyethylene. One might anticipate that a clay which contains a cation containing a styrene oligomer will be nicely compatible with polystyrene while a methacrylate-containing clay will show good compatibility with methyl methacrylate. Surprisingly, this is not the case and we find that the styrene-containing clay shows good compatibility with many polymers. The commonly used surfactants have a molecular weight in the range of 200 while these oligomeric surfactants are close to 5000; thus the inorganic

content of the clay is greatly reduced. While a commonly used clay has 75% inorganic content, these oligomerically-modified clays have an inorganic content in the range of 25 to 30% and so much more clay is required to give the inorganic clay content that is required for fire retardancy. For the styrene-containing oligomerically-modified clay, which contains 27% inorganic content, the oligomerically-modified clay content must be about 15% or greater (inorganic content is 4%) to achieve the same level of reduction in PHRR that is usually seen for polystyrene nanocomposites.

The caprolactone-containing clay has given larger reductions in PHRR for polystyrene, HIPS, polypropylene and polyethylene than has been seen with any other surfactant. While there are some compatibility issues between some polymers and the polycaprolactone, this oligomerically-modified clay has great potential for fire retardancy.

Cone Calorimetry as a Means to Evaluate Nanodispersion

Nanodispersion is typically evaluated by the combination of X-ray diffraction, which gives the d-spacing or the distance between the clay layers, and transmission electron microscopy, which provides an actual image of the clay in the polymer. This can be a tedious process and it is also time consuming so there have been efforts to develop new techniques for this purpose. At NIST an NMR technique has been developed that uses relaxation times to determine the type of nanodispersion. Since clays contain paramagnetic iron, this will effect the proton relaxation time. In an immiscible nanocomposite, the average distance between an iron atom and a proton on the polymer is large and there will be a minimal change. In an intercalated system, this distance is decreased, leading to a lower relaxation time. Finally, the delaminated system will have the closest approach between the iron in the clay and the protons of the polymer and this will lead to the lowest relaxation time (24).

The NIST scientists have also shown that a microcomposite shows very little reduction in PHRR while nanocomposites do show an appreciable reduction. The reduction in PHRR is not constant for all polymers but shows a good deal of variation between polymers. Table I presents the maximum reduction that has been observed both for clay (17,18,23,25) and graphite (26) nanocomposites. We assert that when one reaches a comparable reduction in PHRR for one of these polymers, one has achieved good nanodispersion. The low value for PMMA in comparison to all of the other polymeric systems suggests that there may be something special about this polymer. Based upon the work that has been done on the mechanisms of action of nanocomposites in fire retardancy has led to the suggestion that the presence of the clay can change the pathway of thermal degradation. In the case of PMMA, only one product,

monomer, is observed during thermal degradation so there is no possibility of changing the pathway to favor one over another. For PMMA, we surmise that the only mechanism that is operative is the barrier mechanism and this gives the low value. In the other polymers, there are several products that are formed during thermal degradation and the presence of the clay has a significant influence on the course of thermal degradation. The agreement between the two different nano-dimensional materials suggests that this is valid. There are also numerous examples where the TEM images have shown that the nano-dispersion was less than perfect and the reduction in PHRR did not reach the expected level. A notable example has been work with the tropylium-modified clay (16) where the TEM image shows obvious examples of the presence of tactoids and the reduction in PHRR for a polystyrene nanocomposite is only 32% rather than the 65% expected for this polymer. Further development of cone calorimetry as a tool to evaluate the nano-dispersion will require a more complete understanding than is now available on the mechanism of fire retardation due to nanocomposites and the factors that control the reduction in PHRR.

Table I. Reduction in PHRR for various polymers with both clay and expandable graphite as the nano-dimensional material

<i>Polymer</i>	<i>Clay</i>	<i>Expandable graphite</i>
Polystyrene	66	48
HIPS	58	36
ABS	45	48
Polypropylene	59	
PP-g-MA	54	
Polyethylene	51	
Polyamide-6	63	62
PMMA	25	35

Synergy between Nanocomposite Formation and Conventional Fire Retardants

The age of the nanocomposite has created a lot of excitement in the world of fire retardancy, since the results from cone calorimetry show significant reductions in the peak heat release rate. However, all of these nanocomposites still burn; in most cases, ignition of a nanocomposite occurs more easily in a cone calorimeter experiment than does the virgin polymer and they all are not classified by the UL-94 protocol. The earlier time to ignition has been noted with a number of additives in polymers and it has been suggested that the additive may absorb the heat better than does the polymer, thus creating local hot

spots at which ignition may initiate (27). Regardless of the explanation, the fact is that nanocomposites alone do not solve any fire problem, but they can be a component of the solution. With this in mind, we have examined a series of combinations of nanocomposites with conventional fire retardants, including phosphorus, halogen and metal hydroxide systems.

Phosphorus fire retardants may either be added as additives or else they may be chemically combined with the clay. There may be an advantage to incorporating the phosphorus into the clay cation because that way, if the clay is well-dispersed, the phosphorus fire retardant will also be well-dispersed. This has been accomplished by preparing a surfactant which contains some phosphate moiety on the cation; a typical structure is shown in Figure 2.

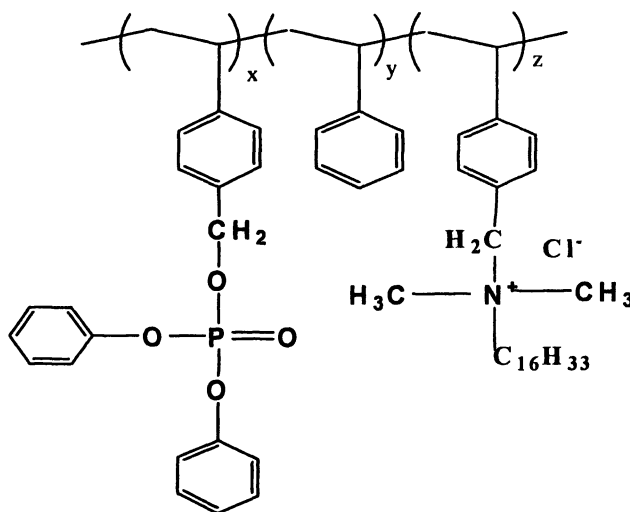


Figure 2. Structure of the cation in a phosphate-containing clay.

Good nano-dispersion has been achieved for this system and the reduction in the peak heat release rate is better than what has been achieved using clay alone, suggesting that the presence of phosphorus is playing a role in the fire retardancy of polystyrene. (28) Up to about 20% phosphate, there may be a linear relationship between the phosphate content and the reduction in PHRR. At higher levels of phosphate, it appears that the reduction levels off and the relationship is no longer linear. A plot of heat release rates for a series of clays containing different amounts of phosphate, shown in Figure 3, illustrates this observation.

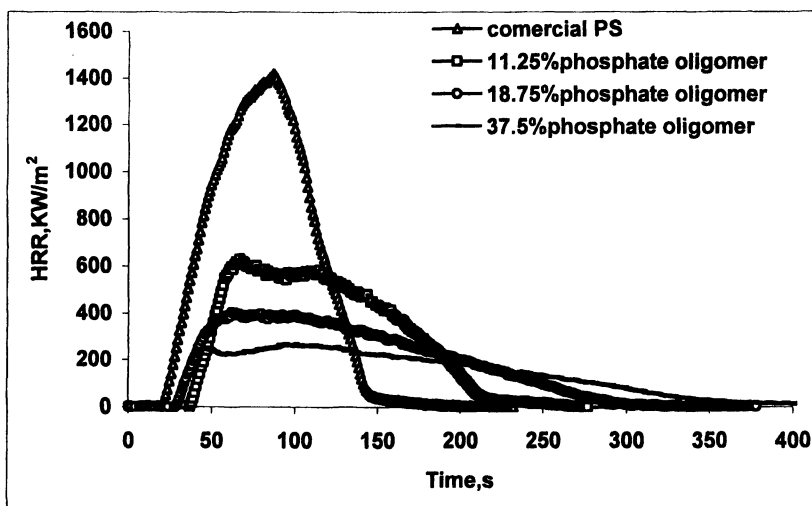


Figure 3. Heat release rate curves for styrene nanocomposites formed using phosphate-containing clays. Reprinted from reference 23, Copyright 2003, with permission from Elsevier.

In other cases, phosphates have been incorporated as additives to either polystyrene (29) or vinyl ester resins (30). In both cases, a large number of conventional phosphorus-containing fire retardants were evaluated using a high throughput method. A brief mention of the high throughput evaluation method is warranted. The procedure that has been developed in these laboratories is to prepare nanocomposites as cylinders and to place the end of the cylinder in contact with a flame for one minute, then to measure the time for which the sample continues to burn. Since this does not correspond to any conventional test, it was necessary to show that rapid extinguishment in this test did correlate with some conventional test, such as the cone calorimeter. Accordingly, those samples which extinguished quickly, as well as some samples which showed a much longer burning time, were prepared on a larger scale and evaluated by cone calorimetry. It was very satisfying to find that samples that showed rapid extinguishment also showed large reductions in PHRR while those that burned for some time did not show large reductions.

The two materials which showed the most promise in the high throughput evaluation were tricresylphosphate and resorcinol diphosphate and these have been further evaluated. Samples were evaluated with varying amounts of

phosphate and varying amounts of clay; the amount of clay did not seem to be important, in agreement with previous work on nanocomposites, but there was an increasing reduction in PHRR as the fraction of phosphate increased. A comparison of the heat release rate curves for polystyrene and its nanocomposite with and without a phosphate is shown in Figure 4. From this figure, one can see that the combination of the components gives the most efficacy.

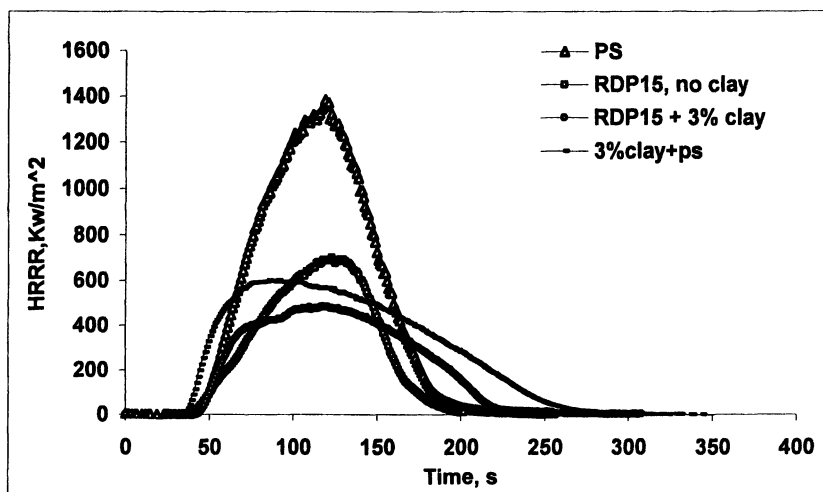


Figure 4. Heat release rates curves for polystyrene and its nanocomposite and both with 15% RDP. Reprinted from reference 29, Copyright 2003, with permission from Elsevier.

When one obtains cone calorimetric data on a polymer-clay nanocomposite, the usual result is that the peak heat release rate is significantly reduced, and the mass loss rate is also reduced so it is believed that the reduction in MLR leads to the reduction in PHRR. The other parameters, such as total heat released or quantity of smoke produced are usually not changed by nanocomposite formation and, as noted above, the time to ignition is usually decreased. For a polystyrene nanocomposite which also contains 10% tricresylphosphate, the reduction in PHRR is 80%, which is much larger than what is usually seen for polymer-clay nanocomposites (55%), and the total heat released is reduced by 57%, while it is unchanged with the clay alone, and the smoke is approximately doubled. These changes are slightly more than additive, suggesting that there is some synergy between nanocomposite formation and the presence of a phosphate. Similar effects have been seen with the vinyl ester resins.

Halogen-containing additives have been studied both with polypropylene (31) and polystyrene (32,33). The PHRR of PP-g-MA is little changed by the presence of decabromodiphenyl oxide, DBDO, but is significantly reduced upon nanocomposite formation, with a decreased time to ignition, and it is still further reduced when the bromine-containing fire retardant, antimony oxide and the nanocomposite are combined. It is very significant to note that the time to ignition of the nanocomposite is increased in the presence of bromine.

Dibromostyrene has been examined as a fire retardant both by incorporating it onto the clay cation (32), by the preparation of oligomers that contain styrene and dibromostyrene, and using the same copolymers as additives (33). Both the reductions in PHRR and in total heat released are much better when the additive is used rather than the bromine-containing clay. It is very significant to note that this has been accomplished when the amount of bromine is less than 6%, rather than the 20% that is normally used for polystyrene.

Expectations for the Future of Nanocomposites in Fire retardancy

Some of the problems that must be solved for the most efficacious usage of nanocomposites in fire retardancy are:

- Develop new high temperature surfactants that will enable melt blending of polymers, such as polycarbonate, that must be processed at higher temperature.
- Develop an understanding of the role that intercalation and/or delamination plays in fire retardancy.
- Fully understand the mechanisms by which nanocomposites enhance the reduction in peak heat release rate.
- Develop an understanding of the reasons why a nanocomposite has a shorter time to ignition than the virgin polymer.
- Develop appropriate combinations of nanocomposites and other additives to achieve fire retardancy.
- Understand the influence that the different processing methods may have on intercalation or delamination of the system and how this effects fire retardancy.
- Develop an understanding of the effect of the clay modifier on fire retardancy.

References

1. Kojima, Y.; Usuki, A.; Kawasumi, M.; Okada, A.; Fukushima, Y.; Kurauchi, T.; Kamigaito, O. *J. Mater. Res.*, **1993**, *7*, 1185-1189.
2. Blumstein, A. *J. Poly. Sci.: Part A*. **1965**, *3*, 2653-2664. *J. Polym. Sci.: Part A*. **1965**, *3*, 2665-2672. Blumstein, A.; Billmeyer, F.W.; *J. Polym. Sci.*

- Part A-2*, 1966, 4, 465-474. Blumstein, A.; Blumstein, R.; Vanderspurt, T.H. *J. Colloid Interface Sci.*, 1969, 32, 236-247. Blumstein, A.; Malhotra, S.L.; Watterson, A.C. *J. Polym. Sci.: Part A-2*, 1970, 8, 1599-1615. Blumstein, A.; Parikh, K.K.; Malhotra, S.L.; Blumstein, R. *J. Polym. Sci.: Part A-2*, 1971, 9, 1681-1691.
3. Alexandre, M.; Dubois, P. *Mater. Sci. Eng.* 2000, R28, 1-63.
 4. Zhu, J.; Wilkie, C.A. *Polym. Int.*, 2000, 49: 1158-1163.
 5. Zhu, J.; Morgan, A.B.; Lamelas, F.J.; Wilkie, C.A. *Chem. Mater.*, 2001, 13, 3774-3780.
 6. Zhu, J.; Uhl, F.M; Morgan, A.B.; Wilkie, C.A. *Chem. Mater.*, 2001, 13: 4649-4654.
 7. Gilman, J.W.; Jackson, C.L.; Morgan, A.B.; Harris, Jr., R.; Manias, E.; Gainnelis, E.P.; Wuthenow, M.; Hilton, D.; Phillips, S.H. *Chem. Mater.* 2000, 12, 1866-1873.
 8. Wang, J.; Du, J.; Zhu, J.; Wilkie, C.A. *Polym. Degrad. Stab.*, 2002, 77, 249-252.
 9. Du, J.; Zhu, J.; Wilkie, C.A.; Wang, J. *Polym. Degrad. Stab.*, 2002, 77, 377-381.
 10. Du, J. Wang, J.; Su, S.; Wilkie, C.A. *Polym. Degrad. Stab.*, 2004, 83, 29-34.
 11. Du, J.; Wang, D.; Wilkei, C.A.; Wang, J. *Polym. Degrad. Stab.*, 2003, 79, 319-324.
 12. Su, S.; Wilkie, C.A. *Polym. Degrad. Stab.*, 2004, 83, 347-362.
 13. Jang, B.N.; Wilkie, C.A. *Polymer*, in press.
 14. Costache, M.; Wilkie, C.A. manuscript in preparation
 15. Wang, D.; Wilkie, C.A. *Polym. Degrad. Stab.*, 2003, 82, 309-315.
 16. Zhang, J.; Wilkie, C.A. *Polym. Degrad. Stab.* 2004, 83, 301-307.
 17. Su, S.; Jiang, D.D.; Wilkie, C.A. *Polym. Degrad. Stab.*, 2004, 83, 321-331.
 18. Su, S.; Jiang, D.D.; Wilkie, C.A. *Polym. Degrad. Stab.*, 2004, 83, 333-346.
 19. Su, S.; Jiang, D.D.; Wilkie, C.A. *Polym. Degrad. Stab.*, 2004, 84, 269-277..
 20. Su, S.; Jiang, D.D.; Wilkie, C.A. *Polym. Advanc. Tech.*, 2004, 15, 225-231.
 21. Su, S.; Jiang, D.D.; Wilkie, C.A. *Polym. Degrad. Stab.*, 2004, 84, 279-288..
 22. Su, S.; Jiang, D.D.; Wilkie, C.A. *J. Vinyl Add. Tech.*, 2004, 10, 44-51.
 23. Zheng, X.; Wilkie, C.A. *Polym. Degrad. Stab.* 2003, 82, 441-450.
 24. VanderHart, D.L.; Asano, A.; Gilman, J.W. *Macromol.*, 2001, 34, 3819-3822. VanderHart, D.L.; Asano, A.; Gilman, J.W. *Chem. Mater.*, 13, 3781-3795, 3796-3809. Bourbigot, S.; Gilman, J.W.; VanderHart, D.L.; Awad, W.H.; David, R.D.; Morgan, A.B.; Wilkie, C.A. *J. Polym. Sci. Part B: Polym. Phys.* 2003, 41, 3188-3213.
 25. Gilman, J.W.; Kashiwagi, T.; Giannelis, E.P.; Manias, E.; Lomakin, S.; Lichtenham, J.D.; Jones, P. in *Fire retardancy of Polymers The Use of Intumescence*, Eds., M. Le Bras, G. Camino, S. Bourbigot, R. Delobel, Royal Society of Chemistry, Cambridge, 1998, pp. 203-221.

-
26. Uhl, F.M.; Wilkie, C.A. *Polym. Degrad. Stab.*, **2002**, *76*, 111-122. Uhl, F.M.; Wilkie, C.A. *Polym. Degrad. Stab.* **2004**, *84*, 215-226. Uhl, F.M.; Yao, Q.; Nakajima, H.; Manias, E.; Wilkie, C.A. *Polym. Degrad. Stab.*, in press. Uhl, F.M.; Yao, Q.; Wilkie, C.A. *Polym. Adv. Tech.*, in press.
 27. Bundy, M.; Gilman Sr., J.W. private communication.
 28. Zheng, X.; Wilkie, C.A. *Polym. Degrad. Stab.*, **2003**, *81*, 539-550.
 29. Chigwada, G.; Wilkie, C.A. *Polym. Degrad. Stab.*, **2003**, *81*, 551-557.
 30. Chigwada, G.; Jash, P.; Jiang, D.D.; Wilkie, C.A. *Polym. Degrad. Stab.* In press.
 31. Zanetti, M.; Camino, G.; Canavese, D.; Morgan, A.B.; Lamelas, F.J.; Wilkie, C.A. *Chem. Mater.*, **2002**, *14*, 189-193.
 32. Chigwada, G.; Jash, P.; Jiang, D.D.; Wilkie, C.A. *Polym. Degrad. Stab.*, in press.
 33. Wang, D.; Echols, K.; Wilkie, C.A. *Fire Mater.*, in press.

Chapter 3

Combined Fire Retardant Action of Phosphonated Structures and Clay Dispersion in Epoxy Resin

G. Camino¹, G. Tartaglione¹, A. Frache¹, C. Manfredi²,
P. Finocchiaro³, and L. Falqui⁴

¹Politecnico di Torino, Sede di Alessandria, Centro di Cultura per l'Ingegneria delle Materie Plastiche, INSTM Research Unit, Viale T. Michel 5, 15100 Alessandria, Italy

²Università degli Studi di Torino, Dip. Chimica I.F.M., INSTM Research Unit, Via P. Giuria 7, 10125 Torino, Italy

³Università degli Studi di Catania, Dip. di Metodologie Fisiche e Chimiche per l'Ingegneria, INSTM Research Unit, V.le A. Doria 6, 95125 Catania, Italy

⁴Istituto per lo Studio delle Macromolecole, CNR, Sezione di Genova, Via De Marini, 6-16149 Genova, Italy

In this work epoxy-clay nanocomposites were synthesized by *in situ* polymerization of a prepolymer (diglycidyl ether of bisphenol-A) [DGEBA] crosslinked with methyl tetrahydrophthalic anhydride [MTHA] filled with organically-modified and natural montmorillonites. The morphology of epoxy-montmorillonite composites was assessed by X-ray diffraction and transmission electron microscopy. A phosphorus containing fire retardant monomer, 2,2-Bis (3-diethoxyphosphonyl-4-hydroxyphenyl) propane [BisP] or 5,5'-Bis (diethoxyphosphonyl)-6,6'-dihydroxy-3,3',3'-tetramethyl-1,1'-spirobiindane [SpiroP], was copolymerized with DGEBA to prepare a halogen free fire retardant polymer/layered silicate nanocomposite suitable for electrical and electronic applications. Thermogravimetry shows that in nanocomposites the epoxy matrix chars in nitrogen as in air, independent of the presence of the phosphorus-containing comonomer, whereas the pure epoxy matrix chars only in air. The rate of heat release in the nanocomposite combustion is

strongly reduced as compared to the pure epoxy resin. An additive or synergistic fire retardant effect is found in nanocomposites prepared by copolymerization of the phosphorus containing fire retardant materials.

Introduction

Epoxy resins are widely used in applications where insulation must be ensured at high working temperatures. In order to obtain the best possible heat resistance, it is necessary to develop crosslinked systems based on thermally stable co-reactants. This means that aliphatic chain segments should be minimized to the greatest extent possible in both the resin and the curing agents, functionality should be high, and the distance between crosslinking points should be as short as possible. In practice, alicyclic or aromatic mono- or di-anhydride curing agents are preferable to the amine curing agents. Among the amines, aromatics based di- or polyamines are the most preferable.

To increase their flame resistance epoxy resins are generally fire retarded with halogenated additives, such as tetrabromobisphenol A. However, the use of such low molecular weight additives tends to negatively effect the mechanical properties of the resulting material (1,2). Therefore, recent studies have successfully explored the use of flame retardants co-reacted with the resin, such as phosphine oxide, to give an inherently flame retardant polymer(1, 3, 4).

In recent years polymer/layered silicate (PLS) nanocomposites containing a small amount (≤ 10 wt%) of layered silicate have attracted great interest because they frequently exhibit remarkably improved mechanical and physical properties when compared to either the matrix polymers alone or conventional micro- and macro-composite materials. The use of nanocomposites shows several advantages, compared to microscopic fillers, because of the large filler-matrix contact surface which improves physical and mechanical properties at low loading (5-9).

Furthermore, in the last ten years it has been found that exfoliated nanocomposites prepared by forcing polymer molecules to penetrate into the galleries of the silicate, can noticeably improve flame resistance and thermal stability (10-16). This phenomenon is generally due to the creation of a ceramic protective layer on the surface of the burning material resulting from a reassembling of the dispersed layers of clay. The protective superficial layer formed provides a barrier to both heat and mass transfer thereby leading to cooling of the polymer and reducing the rate of evolution of combustible volatiles feeding the flame (14,17-19). The overall observed result is improved flame retardancy.

This effect can be induced with as low a concentration of silicate as 2-5 wt% (12,16,20,21). A silicate content above 10 wt% increases the viscosity of the epoxy resin formulation, making it difficult to process, and does not give better fire retardant properties. In fact in order to create a ceramic insulative skin on the surface of the polymer a very low concentration of exfoliated layered filler is actually required, therefore silicate concentrations >10 wt% often do not promote any additional barrier effect as was shown in the case of EVA nanocomposites (19).

In order to meet the most demanding fire retardancy requirements, the strategy pursued involves a combination of nanocomposites with conventional fire retardants. Preliminary results show that the use of classical fire retardants in nanocomposites could reduce the amount of additive required (22).

The present research concerns the thermal properties and combustion behaviour of epoxy-clay nanocomposites synthesised by *in situ* polymerisation of a prepolymer (diglycidyl ether of bisphenol-A) crosslinked with methyl tetrahydrophthalic anhydride. The inorganic phase was montmorillonite and the flame retardants were dihydroxyarylphosphonates.

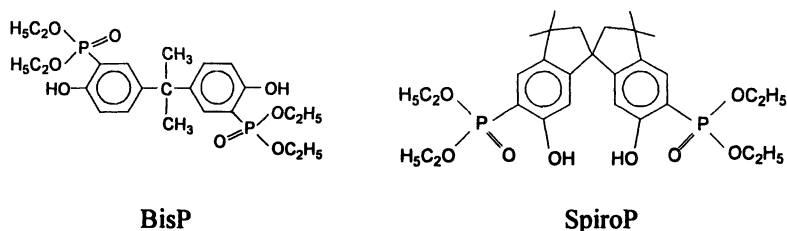
Experimental

Materials

The polymeric matrix used for the epoxy-montmorillonite hybrid composites synthesis was the diglycidyl ether of bisphenol-A [DGEBA] (Vantico, LY 575) cured by methyl tetrahydrophthalic anhydride [MTHA] (Vantico, HY 917). To prepare the pure epoxy resin [ER], 1% of imidazole (Sigma Aldrich) was added to DGEBA.

Our studies (23) on epoxy-composites containing 10% wt. of a number of layered silicates showed substantial delamination/exfoliation for NANOFIL 848 when compared to the microcomposite obtained with NANOFIL 757. Therefore commercial sodium montmorillonite and octadecyl ammonium exchanged montmorillonite (respectively NANOFIL 757 and NANOFIL 848, Süd Chemie) were used to prepare the materials [ER/757 and ER/848 respectively]. The fire retardant comonomers used (Scheme 1) were 2,2-Bis (3-diethoxyphosphonyl-4-hydroxyphenyl) propane [BisP] and 5,5'-Bis (diethoxyphosphonyl)-6,6'-dihydroxy-3,3,3',3'-tetramethyl-1,1'-spirobiindane [SpiroP], synthesized according to the literature (24). Dihydroxy arylphosphonates amount was 5 wt% in both cases.

In order to evaluate the contribution of phosphonate to fire retardancy of the polymer matrix, reference materials were also prepared using the same amount (5 wt%) of the corresponding phosphorous free comonomer.



Scheme 1: Fire retardant comonomers structures

Methods

EpoxyResin/Clay samples

Mixtures of DGEBA and silicates were prepared by dispersing montmorillonite powder (1.055 g) in DGEBA (5.00 g) by sonication for 1 h at 80°C using an ultrasonic bath (EMME GI, model AC14). The anhydride curing agent (90 phr) was added to the DGEBA/montmorillonite mixture at 80°C with manual stirring. Before curing, the mixtures (ca 10.55 g) were centrifuged, outgassed and poured into an aluminium mold. Curing was performed for 15 hrs at 120°C in a vented oven to produce the epoxy resin or the nanocomposite containing 10 wt.% organo-clay.

The reference resin was prepared using the same procedure without addition of clay. The crosslinking reaction of the pure epoxy resin was catalyzed by adding 1% imidazole with respect the total weight of the mixture to DGEBA, since in previous research we confirmed the need for a catalyst to promote polymerization (19). Imidazole was not necessary to synthesize the composites due to the catalytic effect of the phyllosilicate on the epoxy ring opening (19, 25). Samples cured without imidazole also showed better thermal stability, so imidazole was not used to prepare the filled materials.

EpoxyResin/Nanofil 848/Phosphonate samples

The fire retardant comonomer (5 wt.%) was stirred with tetrahydrophthalic anhydride until an homogenous solution was obtained then it was added to the DGEBA/Nanofil 848 mixture and processed as above. The reference resins or composites containing the comonomer either with or without phosphorus were prepared by the same procedure used to prepare the parent phosphorus containing epoxy resins or composites from DGEBA or DGEBA/comonomer mixtures.

Characterization

Nanocomposite morphology was investigated by means of X-ray diffractometry (XRD) and transmission electron microscopy (TEM). The X-ray diffractometer was a Philips instrument with CoK α radiation ($\lambda = 0.179$ nm). TEM was performed with a Zeiss EM 900 apparatus at 80 KeV. Thermal analysis (TGA) was performed using a TA Instrument thermobalance, TGA 2050, under nitrogen or air flow (100ml/min), at a heating rate of 10°C/min. Combustion studies were made using an oxygen consumption calorimeter (Fire Testing Technology Limited FFT Cone Calorimeter model). Heat flux: 50 kW/m², Sample: 75 mm diameter, 5 mm thick \pm 5 % . Heat Release Rate (HRR) measurements were carried out in duplicate or triplicate with an estimated experimental error of \pm 10%.

Results and Discussion

Morphological Characterization

X-Ray Diffraction (XRD). Nanocomposite preparation by “in situ” polymerization was carried out in two stages: the first involved the intercalation of the DGEBA epoxy prepolymer into the organically-modified silicate by sonication, while the second involved the curing of the intercalated prepolymer. Thermoset nanocomposites prepared by “in situ” polymerization of epoxy intercalated layered silicates may lead to intercalated or delaminated/exfoliated nanocomposites (6,26-30).

The morphology of the composites was determined by X-ray diffraction following each of the two steps of their preparation: after sonication to estimate the DGEBA preswelling in the montmorillonite galleries and after curing. Table I shows that the unmodified sodium clay NANOFIL 757 undergoes a negligible increase of interlayer spacing upon sonication with DGEBA.

However, the diffraction pattern of the organoclay DGEBA/NANOFIL 848 mixture after sonication shows a shift of the basal diffraction peak to a lower angle (figure 1A and 1B), which indicates an increase of the montmorillonite d-spacing due to swelling by DGEBA from 1.78 to 2.90 nm (Table 1).

Curing of the NANOFIL 848 based composites leads to disappearance of the diffraction peak (figure 1C), indicating that either the clay layers are randomly distributed in the polymer matrix or are separated by a distance larger than 4.5 nm, a distance two or threefold greater than that of the original

Table I. Variation of *d*-spacing of pristine MMT and after 1h sonication evaluated by X Ray Diffraction

	<i>d</i> -spacing (nm)		Δ <i>d</i> -spacing (nm)
	<i>Clay</i>	<i>Mixture DGEBA/Clay</i>	<i>Mixture-Clay</i>
NANOFIL 757	1.13	1.30	0.17
NANOFIL 848	1.78	2.90	+1.12

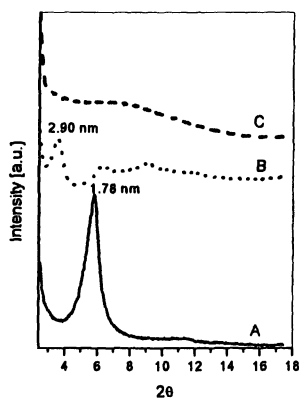


Figure 1. X-ray diffraction patterns of NANOFIL 848 in different physical states: (A) clay powder, (B) clay in DGEBA suspension after 1h sonication, (C) intercalated clay (10 %wt.) in anhydride-cured epoxy nanocomposite

organoclay. This morphology is referred as a delaminated or exfoliated structure (8). As shown in figure 1C, the clay layers behave independently of each other when they are randomly distributed in the polymer matrix. Similarly, when a phosphorylated comonomer was copolymerized within the structure of the epoxy resin, a delaminated/exfoliated nanocomposite was obtained with NANOFIL 848. On the other hand, in the composite containing 10 wt% Na⁺-montmorillonite (NANOFIL 757) the d-spacing of the DGEBA/clay mixture remains unchanged on curing, indicating that a microcomposite should be formed. This morphology is due to the hydrophilic nature of the completely inorganic filler NANOFIL 757 and to the bulky epoxy resin used.

Transmission Electron Microscopy (TEM). The morphologies of the composites initially suggested by XRD were confirmed by transmission electron microscopy. Figure 2 presents TEM micrographs of the samples containing NANOFIL 757 [ER/757], NANOFIL 848 [ER/848] and both NANOFIL 848 and comonomer BisP [ER/848/BisP]. Figure 2A shows a TEM micrograph of sample [ER/757]; large aggregates around 5 micron in diameter are present, in agreement with the microcomposite morphology found with XRD measurements. For ER/848 and ER/848/BisP samples, a disordered intercalated/exfoliated morphology, with a mostly delaminated structure, has been observed in both cases.

In Figure 2B (x 30000) the morphology of ER/848 is shown; an extensive examination of the distance between the clay layers inside stacks has been carried out. The interlamellar distance varies from 4 to 18 nm for ER/848 and from 8 to 18 nm for ER/848/BisP nanocomposites. Thus a hybrid intercalated/exfoliated morphology is evident according to XRD results and by the definition due to Vaia (8), which assumes that a two-threefold increase of the organoclay interlamellar distance corresponds to an exfoliated structure. In Figure 2c and 2d TEM micrographs at higher magnification (x50000) of the epoxy resin filled with NANOFIL 848 [ER/848] and of the epoxy resin containing in addition the phosphorylated comonomer BisP [ER/848/BisP] are shown, respectively.

Thermal Characterization

Thermogravimetry (TGA, DTG). Thermal properties have been investigated by thermogravimetric analysis and figure 3 shows thermogravimetric curves for the unfilled epoxy resin and epoxy composites under both N₂ and air flow. In nitrogen, the pure epoxy resin thermally degrades through a two step process with maximum rate at 301 and 414°C, leaving a 4% residue.

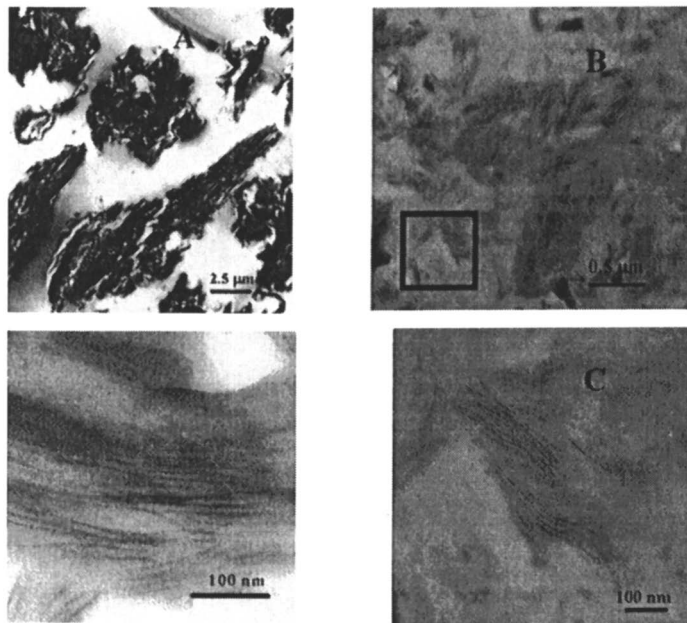


Figure 2. TEM images of ER/MMT samples: *A) ER/Nanofil 757(x3000); B) ER/848(x30000); C) ER/848(x50000), square domain of figure2B; D) ER/848/bisP(x50000).*

The filled epoxy resins undergo a degradation mechanism very similar to the one we proposed for typical epoxy resins (31-35). The first step of degradation at 300°C involves water elimination that results in formation of C-C unsaturations (31-36). Carbon-oxygen bonds in the beta position to these unsaturations (allylic bonds) become the thermally weakest bonds in the epoxy network and they break, giving fragments of the crosslinked structure that eventually are small enough to volatilize at these temperatures. The volatilization of the fragments is however limited up to 350°C, due to competitive rearrangements, such as cyclization, that produce relatively stable structures. These cyclic structures break down in the second step of figure 3A, under a nitrogen atmosphere between 350-450°C. In this elevated temperature region, an extensive breaking of chemical bonds of the epoxy network takes place, including C-phenyl bonds of bisphenol A, leading to almost complete volatilization. A minor amount of charred residue is formed (ca. 4%) due to limited recombination of reactive species to a thermally stable charred material of reactive degrading species during decomposition.

The epoxy network shows good resistance to thermal oxidation, as shown by the coincidence of the weight loss curves in nitrogen and air up to 400°C. However charring of the epoxy network in the second degradation step takes place in air with a higher yield (ca. 20% at 400°C) than in nitrogen, due to catalysis by oxygen. Complete oxidation-combustion of the char takes place in air with maximum rate at 535°C (figure 3A).

In the nanocomposite ER/848 the contribution to the weight loss in the first step is strongly reduced (figure 3 B). Moreover, the nitrogen and air thermogravimetric curves are coincident throughout the degradation process of the epoxy network, *i.e.* to 500°C, because the clay layers catalyze a charring process in nitrogen which does not occur in the neat resin. Therefore the presence of air does not show any additional charring effect to that brought about by the clay. However, the thermogravimetric curve of the nanocomposite shows a maximum rate of weight loss at a lower temperature (388-395°C) than the neat resin (410-414°C).

The presence of the phosphorylated comonomer does not modify the main features of the thermogravimetric behavior of the nanocomposite in nitrogen or air, as it can be seen for example by comparing figure 3B with figure 3C, apart from a further decrease of the temperature of maximum rate of weight loss to 370-377°C.

In the nanocomposite the typical surface shielding action displayed by the clay layers in thermally oxidizing or burning layered silicate nanocomposites (17, 18) is evident in figures 3B and 3C. The oxidation of the charred residue is

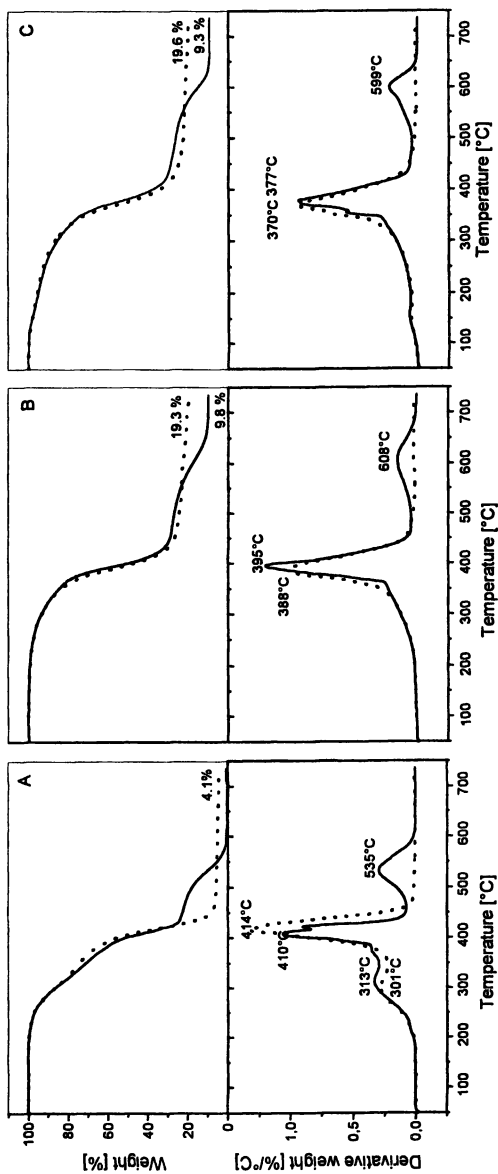


Figure 3: Thermogravimetric curves under N₂(...) and air flow(—) of: (A) neat ER, (B) ER/848 (C) ER/848/BisP

delayed with a shift of the maximum rate from 535°C in figure 3A to 600°C as compared to the neat epoxy resin in figure 3B and 3C.

Cone calorimetry. The flame retardant properties of the neat resin and of the composites have been investigated by cone calorimetry. In a typical experiment the heat release rate (HRR) is recorded as a function of time. In figure 4, it is seen that the peak of heat release rate (PHRR), which is a major parameter in controlling flame propagation of fires (37), is decreased by 38% in the nanocomposite (curve b) as compared to the neat resin (curve a) and shifted from 90s to 115s.

Introduction of phosphorus in the epoxy network of the nanocomposite leads to a substantial increase in the time to ignition from 34.5 s for the neat resin (curve 4.a) and ER/848 (curve 4.b) to ca. 50 s for the phosphonated nanocomposite (curve 4.c and 4.d). In addition a further decrease in the PHRR which is larger in the case of the BisP comonomer (48% or 68% as compared to the nanocomposite or to the neat resin respectively) than in that of SpyroP comonomer (20% or 51% as reported in table II.

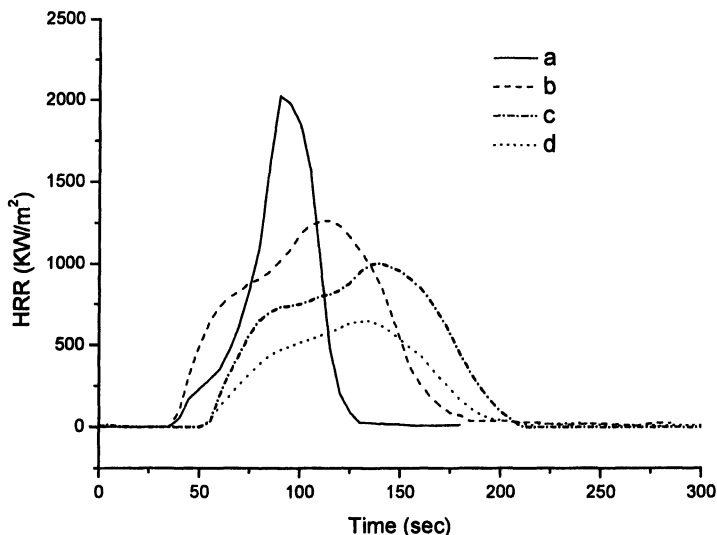


Figure 4. Cone calorimeter analysis of: a) neat ER, b) ER/848, c) ER/848/SpyroP d) ER/848/BisP.

Thus the phosphorylated comonomer further improves the fire retardant effect arising from the nanodispersed clay layers in the epoxy network.

Table II. Comparison of T_{ignition} and HRR of ER-samples

MATERIAL	$T_{\text{ignition}}/[\text{s}]$	HRRmax/[KW/m ²]	Improvement %
ER/pure	34.5	2030	
ER/Nanofil 848	34.5	1250	38%
ER/bisP	40	1440	30%
ER/848/bisP	48	645	68%
ER/spiroP	34.5	1900	6%
ER/848/spiroP	49	1000	51%

Indeed figure 5 shows that copolymerization of the bisphenol structure (curve 5.c) leads to a decrease of about 10% in the PHRR of the neat resin (curve 5.a) that increases to 30% when the bisphenol structure also contains phosphorus atoms (curve 5.b). Combination of the clay with the fire retardant comonomer BisP leads to a reduction of PHRR of the neat resin by 68% which can be accounted for by combination of PHRR reductions respectively resulting from surface protection by reassembling clay layers and action of phosphorus.

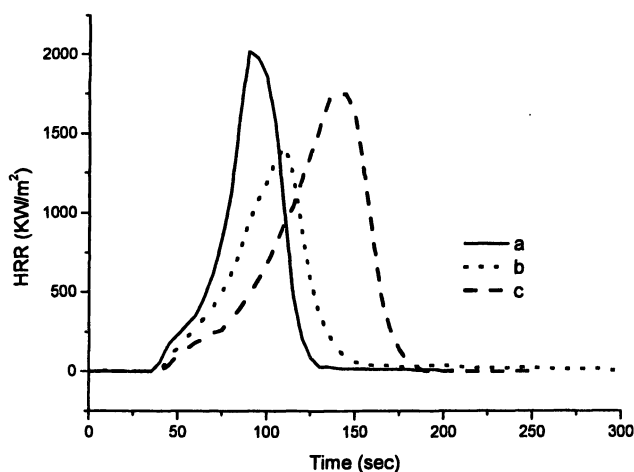


Figure 5. Cone calorimeter analysis of: a) neat ER, b) ER/BisP 5%wt., c) ER/Bisphenol 5%wt.

However, in the case of the Spyro comonomer, the mechanism of combined fire retardancy seems more complex. Indeed, figure 6 shows that the spymethyl structure tends to lower the time to ignition (curve c), possibly by reducing the thermal stability of the network, while the PHRR is not changed.

The introduction of phosphorus has a slight effect in increasing the time to ignition back to that of the neat resin but has a negligible effect on PHRR (curve b). However the nanocomposite ER/848/SpyroP, based on the same polymer matrix (ER/SpyroP), shows a consistent increase in the time to ignition and

reduction of PHRR (figure 4, curve c) as compared to the nanocomposite ER/848 prepared with the only DGEBA based polymer network (figure 4, curve a). This might be due to a catalytic effect of the clay layers on the chemical reactions induced by phosphorus moieties (31-34), which are responsible for the fire retardant action. Such chemical reactions may not take place in the degrading polymer matrix in the absence of clay.

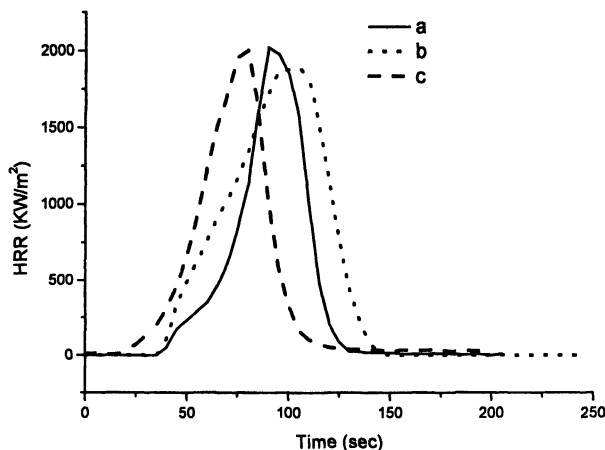


Figure 6. Cone calorimeter analysis of: a) neat ER, b) ER/SpyroP 5%wt., c) ER/Spyromethyl 5%wt.

Conclusions

The nanocomposite epoxy resin prepared by *in situ* polymerization of DGEBA intercalated in an octadecylammonium exchanged montmorillonite and cured with methyl tetrahydrophthalic anhydride, shows an intercalated-exfoliated morphology with evidence of ordered exfoliated structures.

Introduction of a phosphorylated comonomer (BisP) in the epoxy network, gives a nanocomposite with a much larger average clay platelet interlayer distance and evidence of ordered delaminated structures as in the DGEBA resin.

The epoxy resin undergoes thermal volatilization in a two step process with partial charring in air. Nanocomposites catalyze charring in nitrogen independent of the presence of the phosphorylated comonomer.

The maximum rate of heat release is decreased by 38% in the nanocomposite with 10% montmorillonite, compared to the neat resin. The presence of 5% of copolymerized phosphorylated comonomer in the epoxy network of the nanocomposite leads to an increase in the time to ignition and further decrease of maximum rate of heat release, depending on type of

comonomer. In the case of BisP a reduction of 68% is found, attributable to the effects of clay on the DGEBA resin and of copolymerization of DGEBA with the phosphorylated comonomer. Whereas in the case of SpyroP the reduction of the maximum rate is 51% which results from a synergistic effect of the combination clay - phosphorylated comonomer, which used alone has a negligible effect on the maximum.

Thus, it can be concluded that combination of typical fire retardants with slow burning nanocomposites is a viable approach to comply with the general demand to reach requested fire retardant performances with lower additives loadings. Furthermore, a bonus is gained in this combined approach due to the general improvement of physical and mechanical properties of relatively small amounts of nanofillers.

Acknowledgments

The authors like to thank Mr. G. Dondero for technical support in performing TEM analysis.

References

1. Levchik, S.V.; Camino, G.; Luda, M.P.; Costa, L.; Muller, G.; Costes, B.; Henry, Y.; *Polym. Adv. Tech.*, **1996**, *7*, 823.
2. Ho, S.M.; Lee, Y.J.; *MRL Bull. Res. Dev.*, **1998**, *2*, 27.
3. Varma, I.K.; Gupta, U.; *J. Macromol. Sci. Chem.*, **1986**, *23*, 19.
4. Levchik, S.V.; Camino, G.; Luda, M.P.; Costa, L.; Muller, G.; Costes, B.; *Polym. Degrad. Stab.*, **1998**, *60*, 169
5. Giannelis, E. P.; *Adv. Mater.*, **1996**, *8*, 29.
6. Zanetti, M.; Lomakin, L.S.; Camino, G.; *Macromol. Mater. Eng.*, **2000**, *279*, 1.
7. Alexandre, M.; Dubois, P.; *Mater. Sci. Eng. R*, **2000**, *28*, 1.
8. Vaia, R.A.; "Polymer-clay nanocomposites", Eds. T.J. Pinnavaia and G.W. Beall, John Wiley & Sons Ltd, New York, **2000**, 244.
9. Ray S.S., Okamoto, M.; *Prog. Polym. Sci.*, **2003**, *28*, 1539
10. Wang Z., Pinnavaia T., *J. Chem. Mater.*, **1998**, *10*, 1820.
11. Gilman, J.W.; *Appl. Clay Sci.*, **1999**, *15*, 31.
12. Gilman, J.W.; Kashiwagi, T.; Nyden, M.; Brown, J.E.T.; Jackson, C.L.; Lomakin, S.; Giannelis, E.P.; Manias, E.; *Chemistry and Technology of Polymer Additives*, Blackwell Science Ltd, Oxford, **1999**, 249.
13. Kojima, Y.; Usuki, A.; Kawasumi, M.; Okada, A.; Fukushima, Y.; Kamigaito, O.; *J. Mater. Res.*, **1993**, *8*, 1185.

14. Zanetti, M.; Camino, G.; Mulhaupt, R.; *Polym. Degrad. Stab.*, **2002**, *74*, 413.
15. Gilman, J.W.; Jackson, C.L.; Morgan, A.B.; Harris R., Manias, E.; Giannelis, E. P.; *Chem. Mater.*, **2000**, *12*, 1866.
16. Gilman, J.W.; Kashiwagi, T.; Giannelis, E. P.; Manias, E.; Lomakin, S.; Lichtenhan, J.D.; Jones, P.; *Fire Retard. Polym.*, **1998**.
17. Zanetti, M.; Kashiwagi, T.; Falqui, L.; Camino, G.; *Chem. Mater.*, **2002**, *14*, 885.
18. Zanetti, M.; Camino, G.; Reichert, P.; Mülhaupt, R.; *Macromol. Rapid. Comm.*, **2001**, *22*, 176.
19. Torre, L.; Frulloni, E.; Kenny, J.M.; Manfredi, C.; Camino, G.; *J. Appl. Polym. Sci.*, **2003**, *90*, 2532.
20. Gilman, J.W.; Kashiwagi, T.; Lichtenhan, J.D.; *Sampe J.*, **1997**, *33(4)*, 40.
21. Lee, J.; Giannelis E. P.; *Polym. Preprints*, **1997**, *38*, 688.
22. Zanetti, M.; Camino, G.; Canavese, D.; Morgan, A.B.; Lamelas, F.J.; Wilkie, C.A.; *Chem. Mater.*, **2002**, *14*, 189.
23. Camino, G.; Tartaglione, G.; Frache, A.; Falqui L. *in preparation*
24. Consiglio, G.A.; Failla, S.; Finocchiaro, P.; Siracusa, V.; *Phosphorus, Sulfur and Silicon*, **1998**, *134/135*, 413.
25. Kaviratna, L.; Pinnavaia, P. D.; *J. Phys. Chem. Solids*, **1996**, *57*.
26. Zilg, C.; Thomann, R.; Finter, J.; Mulhaupt, R.; *Macromol. Mater. Eng.*, **2000**, *280/281*, 41.
27. Zilg, C.; Reichert, P.; Dietsche, F.; Engelhard, T.; Mulhaupt, R.; *Kunstst-Plast. Eur.* **1998**, *88*, 1812.
28. Le Baron, P.C.; Wang, Z.; Pinnavaia, T.J.; *Appl. Clay Sci.*; **1999**, *15*, 11.
29. Lagaly, T.; *Appl. Clay Sci.*, **1999**, *15*, 30.
30. Brown, J.M.; Curliss, D.; Vaia, R.A.; *Chem. Mater.*, **2000**, *12*, 3376-3384.
31. Camino, G.; *Chemistry and Technology of Polymer Additives*, Eds. S. Al-Malaica, A. Golovoy, C.A. Wilkie, Blackwell Science Ltd, Oxford, **1999**, 108.
32. Levchik, S.V.; Camino, G.; Luda, M.P.; Costa, L.; Muller, G.; Costes B.; *Polym. Degrad. Stab.*, **1998**, *60*, 169.
33. Levchik, S.V.; Camino, G.; Luda, M.P.; Costa, L.; Muller, G.; Costes, B.; Henry, Y.; *Polym. Adv. Tech.*, **1996**, *7*, 823.
34. Levchik, S.V.; Camino, G.; Costa, L.; Luda, M.P.; *Polym. Degrad. Stab.*, **1996**, *54*, 317.
35. Levchik, S.V.; Camino, G.; Luda, M.P.; Costa, L.; Costes, B.; Henry, Y.; Morel, E.; Muller, G.; *Polym. Adv. Tech.*, **1995**, *6*, 53.
36. Kandola, B.K.; Horrocks, A.R.; Myler, P.; Blair, D.; *Fire and Polymers*, Ed. G.L. Nelson, C.A. Wilkie, *ACS Symposium Series*, American Chemical Society, Washington, DC, 797.
37. Babrauskas, V.; "Ignition Handbook", Published by Fire Science Publishers, A division of Fire science and Technology Inc., Issaquah, WA 98027, **2003**.

Chapter 4

Thermal Degradation and Flammability of Poly(methyl methacrylate) Containing TiO₂ Nanoparticles and Modified Montmorillonite

A. Laachachi^{1,2}, M. Cochez¹, M. Ferriol¹, E. Leroy²,
and J. M. Lopez Cuesta^{2,*}

¹Laboratoire de Chimie et Applications, E.A. n° 3471 Université de Metz,
Rue Victor Demange 57500 Saint-Avold, France

²Centre des Matériaux de Grande Diffusion, Ecole des Mines d'Alès 6,
Avenue de Clavières, 30319 Alès Cedex, France

*Corresponding author: Jose-Marie.Lopez-Cuesta@ema.fr

The thermal stability and flame resistance of various formulations of PMMA containing micrometric or nanometric TiO₂ and/or organically-modified montmorillonites (OMMT), were studied by thermogravimetric and cone calorimeter experiments. Synergistic effects of fire retardancy between OMMT and TiO₂ were observed, leading to an improvement of PMMA thermal stability together with higher ignition times, reduced heat released, and a significant increase of total burning time. These improvements do not seem to be dependent on the preparation mode of PMMA/oxide nanocomposites since solvent casting and blend mixing lead to quite similar results.

Introduction

Several types of mineral fillers permit an improvement in polymer flame retardancy (1). Recently, the use of modified phyllosilicates, generally referred to as organoclays (2,3), has brought great expectations to this field. Depending upon the processing conditions and characteristics of both the polymer matrix and organoclay, the *in situ* dispersion of organoclay inside the host polymer by melt blending can be more or less achieved, leading to intercalated or exfoliated nanocomposites. The effect of the resulting microstructure on thermal stability and improvement of fire retardancy is not clearly established. Nevertheless, organoclays seems to be very attractive as a new class of components in flame-retardant systems (4-7). The flame retardant mechanism involved seems to be based on the formation of a carbonaceous-silicate char, which builds up on the surface during burning due to a change of polymer degradation pathway in presence of clay particles (4). This char layer can appear even in polymers which do not usually char upon burning (eg. polyolefins). However, most authors conclude that these lamellar nanoparticles have to be used in combination with other additives in order to meet required fire resistance performance (7). Other nanoparticles, such as silica or carbon nanotubes, can be used, leading to synergistic multicomponent systems (8-10).

Metal oxides are considered as emerging nanoparticles with promising effects on polymer thermal degradation (11-14). It can be expected that their nanometric size makes them suitable for synergistic effects with organoclays, allowing the combination of both fire retardancy and enhanced mechanical properties.

In this paper, results obtained with poly(methyl methacrylate) (PMMA) and particles of titanium oxide (TiO_2), alone and in combination with organo-modified montmorillonites (OMMT), are presented.

Experimental

Materials and processing

Two poly(methyl methacrylate) polymers were used in this study. They were supplied by Aldrich ($M_w=350000$ g/mol, denoted HMW) and Atofina (Orogas, $M_w=93000$ g/mol, denoted LMW) respectively. The organically-modified montmorillonite (OMMT) used was a natural montmorillonite modified with dimethyldihydrogenated tallow ammonium salt (Cloisite 15A -

Southern Clay). Both nanometric ($n\text{TiO}_2$, Degussa P25, median particle size 21 nm, S_{BET} 48 $\text{m}^2\cdot\text{g}^{-1}$) and micrometric titanium dioxide ($m\text{TiO}_2$, Panreac, median particle size 0.2 μm , S_{BET} 5.8 $\text{m}^2\cdot\text{g}^{-1}$) were used. HMW/ $n\text{TiO}_2$ filled polymer samples were prepared by dissolving PMMA in chloroform (1g per 50 cm^3). The solution was stirred at 50°C for 30 min before the addition of $n\text{TiO}_2$, which was ultrasonically treated for a few hours at room temperature in order to obtain good dispersion. Afterwards, the samples were dried for 4 hrs at 170 °C to complete the evaporation of chloroform. Other compositions were prepared by melt blending. LMW pellets and fillers ($n\text{TiO}_2$,OMMT) in appropriate ratio, were mixed in an internal mixer (Haake PolyLab 60 cm^3) for 7 min at 225 °C and 50 rpm. The resulting nanocomposites were then pelletized using a rotary cutter mill, and finally compression molded at 250°C and 100 bars for 5 min in order to obtain 100×100×4 mm^3 specimens. Compositions of 5, 10, 15 and 20 wt% total loading were prepared for LMW/ TiO_2 compositions, 10% for LMW/OMMT composition and 5% $n\text{TiO}_2$ + 5% OMMT loading for LMW/ $n\text{TiO}_2$ -OMMT compositions.

Instrumentation

Glass transition temperatures (T_g) were measured on solvent cast samples (20-25 mg) on a Setaram DSC-92 apparatus at a heating rate of 10 $^{\circ}\text{C}\cdot\text{min}^{-1}$; these are believed accurate to ± 0.5 °C. The limiting oxygen index (LOI) of 200 mg samples was determined with an apparatus described in NFT 51-07 using a modified procedure (15). Thermal gravimetric analyses (TGA) in air of 20-25 mg samples were performed at 10 $^{\circ}\text{C}\cdot\text{min}^{-1}$ with a Mettler-Toledo TGA/SDTA 851e thermobalance. Flammability properties of PMMA and its nanocomposites prepared by melt blending were studied using a cone calorimeter (Fire Testing Technology). 100×100×4 mm^3 specimens were exposed to an irradiance of 35 $\text{kW}\cdot\text{m}^{-2}$ and the heat release rates was measured with a precision of $\pm 5\%$. X-ray diffraction patterns were recorded on a Philips PW 1700 X-ray diffractometer using $\text{Cu K}\alpha$ radiation. TEM observations of composites were performed using a Hitachi H800 MT at 200kV.

Results and discussion

Morphology of nanocomposites

TEM micrographs of HMW/ $n\text{TiO}_2$, LMW/ $n\text{TiO}_2$, LMW/OMMT, LMW/OMMT- $n\text{TiO}_2$ composites at 10% global filler loading were obtained in order to observe the distribution of $n\text{TiO}_2$ particles and the intercalated or

exfoliated state of organoclay. Figure 1 shows that the shape of $n\text{TiO}_2$ is nodular and that it is rather well distributed, either in HMW or LMW PMMA, but that a few aggregates in the micrometric range are also present. Aggregation processes can be explained by the absence of any surface treatment on the $n\text{TiO}_2$ particules.

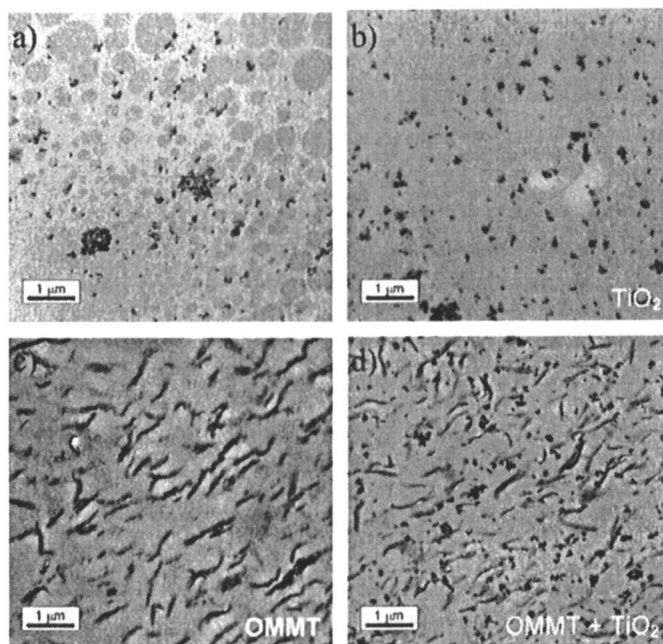


Figure 1: TEM micrographs of HMW/ $n\text{TiO}_2$ (a) LMW/ $n\text{TiO}_2$ (b), LMW/OMMT (c), LMW/OMMT- $n\text{TiO}_2$ (d) compositions

Figure 1 reveals a mixed intercalated-exfoliated morphology for OMMT. The presence of intercalated structures was confirmed by X-ray diffraction analysis which shown larger d-spacings for PMMA-OMMT and PMMA-Oxide-OMMT composites ($d=3.6$ nm) than for pure OMMT ($d=2.9$ nm).

Glass transition temperature and LOI measurements of TiO_2 nanocomposites

LOI values of the HMW/ $n\text{TiO}_2$ composite increases as a function of $n\text{TiO}_2$ loading (from 18% for unfilled PMMA to 23.4% for 20 w. % of $n\text{TiO}_2$). Increasing LOI values suggest an improvement of the fire retardancy of the filled polymer. Glass temperature transition T_g also increases with $n\text{TiO}_2$

percentage, from 122°C for unfilled PMMA to 132°C for 20 w. % of nTiO₂. Moreover, one observes a roughly linear relationship between LOI and Tg. A similar correlation was found earlier for PMMA filled with Sb₂O₃ (16). The increase in the thermal stability of the polymer in the presence of such mineral fillers has been discussed in the literature on the basis of the restriction of mobility of the polymer chains resulting from their adsorption on the oxide surface via the methoxycarbonyl group, and of steric hindrance due to the presence of solid particles (17). In the present case of TiO₂, it can be assumed that the adsorption of polymer on the oxide particle surface is also responsible for the increase in thermal stability, probably by inhibiting a key step of the degradation mechanism. However, it is difficult to identify this step, since the oxidative degradation mechanism of PMMA is complex and depends on the type of PMMA and its mode of polymerization, according to several authors (18-21).

Thermal stability of TiO₂ and OMMT nanocomposites

TGA curves obtained in air for HMW and HMW/nTiO₂ compositions are presented in Figure 2.

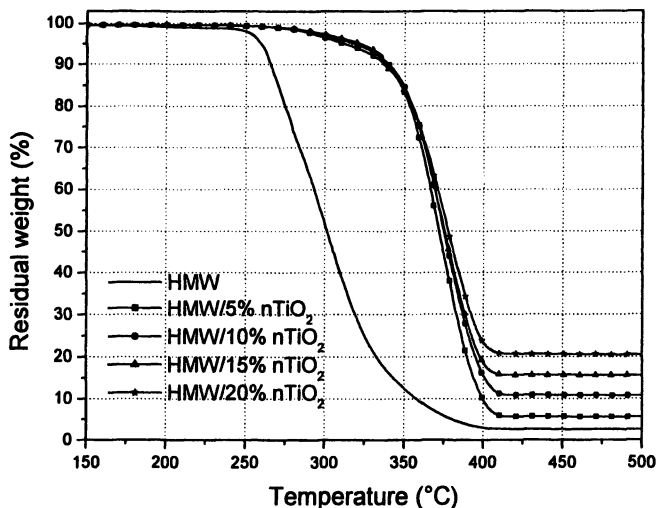


Figure 2: TGA curves obtained for HMW/nTiO₂ compositions

The thermal stability of the polymer is significantly improved by about 70 °C for all compositions even at the lowest oxide content. This improvement of thermal stability due to oxide nanoparticles is also seen in filled LMW with a

thermal stability shift around 50°C. Figure 3 shows the TGA curves of OMMT and LMW/OMMT. For this nanocomposite, the onset temperature of degradation is lower (248°C) than in pure LMW (270°C). This can be ascribed to the low onset degradation temperature of OMMT itself (224°C), due to the thermal decomposition of interlayer interfacial agents. Nevertheless, a comparison between a linear combination of the TGA curves of pure LMW, OMMT and the experimental curve of LMW/OMMT can not account for the difference in thermal stability observed between pure LMW and nanocomposite. Consequently, it seems that the presence of OMMT leads to a similar effect of mobility restriction of the polymer chains for both oxides. Nevertheless, this effect seems weaker according to the respective position of the TGA curves. However, the LMW-5% n TiO₂-5%OMMT nanocomposite degradation presents an onset temperature (278°C) shifted significantly towards higher temperatures in comparison to the LMW-10%OMMT nanocomposite. Moreover, the combination 5% n TiO₂/5%OMMT leads to a degradation temperature shift close to that observed for 10% n TiO₂ and higher than that obtained for 10%OMMT.

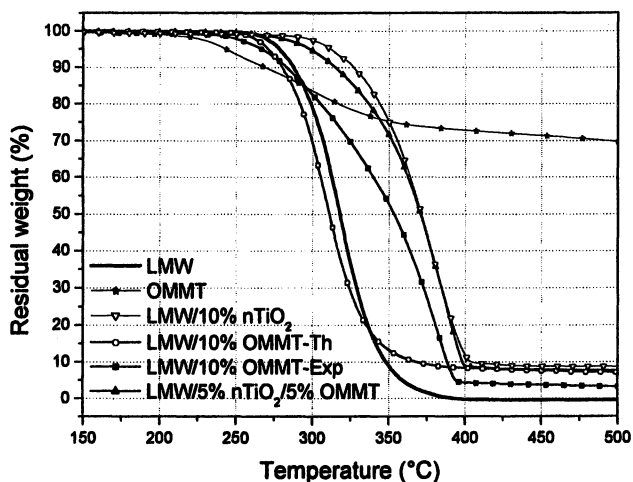


Figure 3: TG curves obtained for LMW, OMMT and OMMT and/or nanometric TiO₂ composites. For LMW-10%OMMT, a theoretical curve (Th) corresponding to a linear combination between experimental curves of LMW and OMMT is plotted. Finally, one can also notice that despite the different nature of the PMMA used, the influence of the elaboration mode of composites seems relatively weak, regarding the improvement of thermal stability.

Fire testing of PMMA nanocomposites samples prepared by melt blending

PMMA-TiO₂ nanocomposites

The heat release rate curves of LMW/nTiO₂ nanocomposites (Figure 4) show that increasing the percentage of filler reduces the peak value of heat release rate (PHRR), in comparison to pure PMMA. In parallel, the time to ignition increases significantly (more than 20s) for LMW/nTiO₂ nanocomposites, in comparison to LMW (69s). A very strong increase for the time of flameout (TOF) and total burning time is observed for 15 and 20 wt% of nTiO₂. A comparison between nTiO₂ and mTiO₂ was also carried out to investigate the effect of particle size and specific surface area on the heat release rate of PMMA. The reference used was the PHRR value of unfilled LMW PMMA and a reduction of 39 % for LMW/mTiO₂ microcomposite was observed compared to 45 % for LMW/nTiO₂ nanocomposite. In both cases the ignition time increased by about 20 s in comparison with unfilled PMMA. The stability of TiO₂ was checked using X-ray diffraction performed on specimens containing TiO₂ nanoparticles before and after cone calorimeter tests.

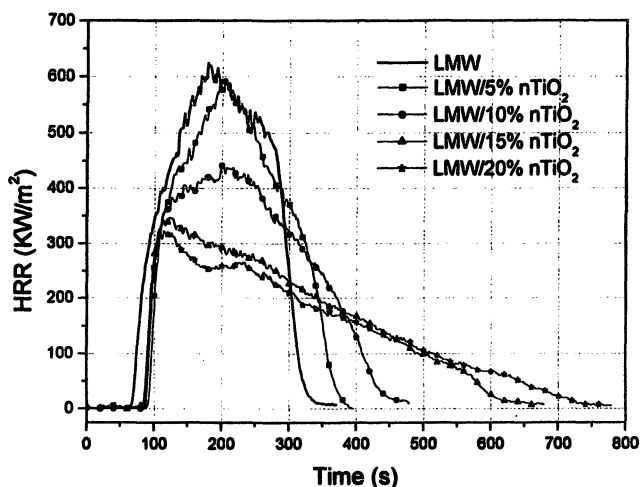


Figure 4. Heat Release Rate curves obtained for pure LMW and 5 to 20 wt.% nTiO₂ compositions.

The residual weight for LMW/nTiO₂ samples corresponds roughly to the percentage of oxide initially introduced. Nevertheless, for the highest loadings studied (15 % and 20%), the nanocomposite residues exhibit a certain cohesion,

showing that a mainly inorganic layer has built up progressively during burning as polymer ablation was occurring. Figure 5 shows that a slightly charred structure appears during the degradation of the composite in the case of nTiO₂, while practically no char appears on the LMW/mTiO₂ residue.

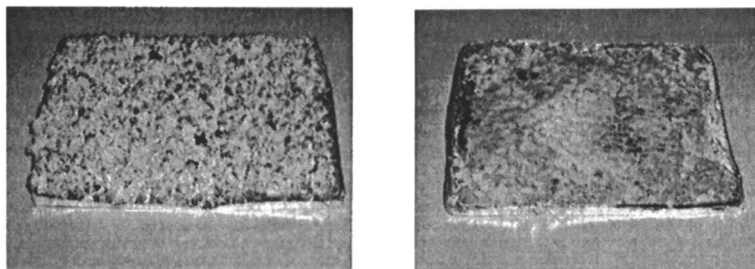


Figure 5. Photos of the cone Calorimeter residues of LMW/15% nTiO₂ (left) LMW/15% mTiO₂ (right).

The TGA of residues obtained for 15% filler loading lead to mass losses of 0.2% for mTiO₂ and 2.7% for nTiO₂; both mass losses occurred mainly around 400°C. These results account for a modification of the degradation pathway of PMMA due to the presence of the filler and this can be ascribed to catalytic activity leading to charred structures. Moreover, in the case of nTiO₂, the cohesive mainly inorganic layer formed on the burning surface during cone calorimeter experiments may behave as an insulating and protective barrier for the polymer beneath.

This different flame retardant behavior between nTiO₂ and mTiO₂ could be explained by an enhancement of the heat transfer between TiO₂ and PMMA, due to the increase in the interfacial area upon decreasing the particle size. TiO₂ particles have a relatively high thermal diffusivity ($1.96 \cdot 10^{-6} \text{ m}^2 \cdot \text{s}^{-1}$, calculated from literature data (22-24)), which may result in a reduction of both temperature and surface tension gradients inside the polymer melt. Such gradients are actually the driving forces propelling degradation gas bubbles through the melt (25) and therefore, their decrease will slow the flow of combustible gaseous degradation products from the melt to the surface, resulting in a decrease of heat released during the combustion.

PMMA-OMMT and PMMA- TiO₂-OMMT nanocomposites

Figure 6 shows the heat release rate curves corresponding to LMW/OMMT compositions and 10 wt % LMW/OMMT-nTiO₂ at a 10 wt % global loading. The LMW/OMMT nanocomposite exhibits much lower HRR values than that of

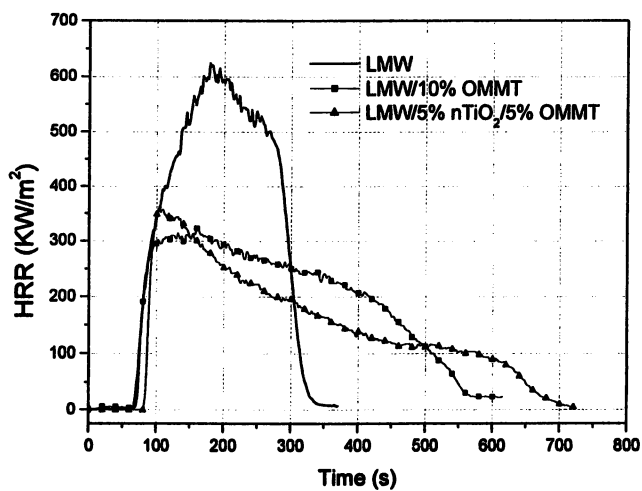


Figure 6. Heat Release Rate curves of LMW and LMW/10 wt.% fillers (OMMT and OMMT-nTiO₂).

LMW, as observed by Wilkie et al. (26). Even though the total heat release (THR) remains constant at about $110 \text{ MJ}\cdot\text{m}^{-2}$, the time of flame out is significantly enhanced from 318 to 555 s.

The PHRR value for LMW/OMMT ($315 \text{ kW}/\text{m}^2$) is lower than that for LMW/nTiO₂ ($440 \text{ kW}/\text{m}^2$). Nevertheless, this better burning behavior, resulting in a longer burning time, is counterbalanced by a shorter time to ignition (74s, compared to 87s for LMW/nTiO₂), in agreement with TGA measurements. It is important to note that since TGA experiments are made on microscopic samples, they cannot reflect the degradation mechanisms occurring in cone calorimeter experiments, which may involve heat and mass diffusion phenomena through sample thickness.

The residues after the cone calorimeter tests reveal significant charring for the LMW/OMMT composite (Figure 6). The final mass loss observed for these samples (taking into account the weight loss of OMMT itself, see Figure 2), indicates that the residual weight corresponds only to the remaining mineral portion of the nanofiller (6%wt of the initial sample).

In order to obtain a more complete view of the burning behavior, a LMW/OMMT specimen was placed in the cone calorimeter with the same radiant heat flux, but the test was stopped after 200s, between ignition and complete degradation of the sample. A strong charring had occurred on the upper side of the sample, while the rest of the sample appeared not significantly degraded. Both parts of the sample were expanded and the remaining polymer was foamed. The global thickness of the partially degraded sample was more than two times higher than the initial value. Such a behavior has been observed in EVA filled with flame retardant systems containing OMMT (9), in which it could be ascribed to three phenomena caused by the composition and morphology of OMMT: charring, viscosity increase and heterogeneous bubble nucleation.

The combination of OMMT and nTiO₂ in LMW leads to enhanced flame retardancy: TTI increases from 74 for OMMT alone to 86 s for LMW/nTiO₂-OMMT. At the same time, TOF increases from 555 s to 791 s. Even though the PHRR is lower for OMMT alone ($315 \text{ kW}/\text{m}^2$ compared to $365 \text{ kW}/\text{m}^2$ when nTiO₂ is added), the total heat release (THR) is lower when the two types of nanofillers are combined (100 instead of $110 \text{ MJ}/\text{m}^2$).

The residual weight at 320 s (TOF for pure PMMA) increases from 38 % for LMW/OMMT to 48 % for LMW/nTiO₂-OMMT, in comparison with LMW. Taking into account the mass loss of OMMT itself, this means that it was counterbalanced by an increased charring fraction issuing from the polymer in the presence of n-TiO₂, which suggests catalytic activity for nTiO₂.

This is supported by TGA performed on the residues. The weight loss for LMW/OMMT is 13%wt, while it is 26%wt in the case of LMW/nTiO₂-OMMT. Observation of the photographs of the residues for both samples containing OMMT after combustion (Figure 7) shows that the cohesive character of the residue is enhanced in the presence of nTiO₂. This may be due to the additional char fraction.

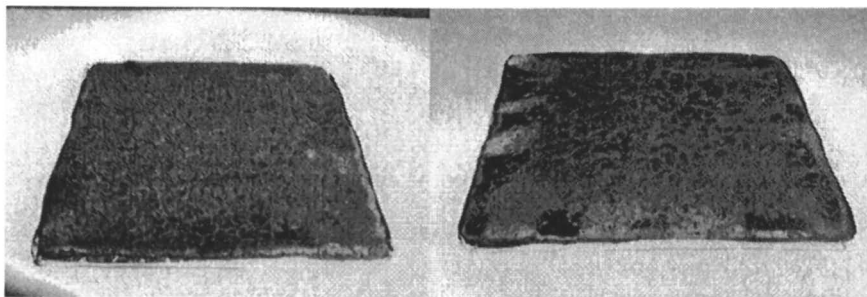


Figure 7. Photos of the cone calorimeter residues of 10 wt.% LMW/OMMT (left), LMW/TiO₂-OMMT (right).

Conclusion

The thermal and flammability properties of PMMA nanocomposites containing OMMT and/or TiO₂ nanoparticles were investigated by TGA and cone calorimeter experiments and compared to those of PMMA alone and PMMA/TiO₂ microcomposites. From the results obtained, an improvement of thermal stability and flammability properties was observed, which increases with the amount of oxide nanoparticles. The improvement of thermal stability does not seem to be dependent on the mode of preparation of the composites, since solvent casting and melt blending lead to quite similar results for two PMMA differing in their average molecular weight. A synergistic effect on thermal stability and fire performance has been achieved by the combination of oxide nanoparticles and organoclays, resulting in longer ignition times, reduced total heat and a significant increase in time of flameout. These results are ascribed to the formation of an expanded char due to morphology and composition of OMMT, and to the high diffusivity, high specific surface area and possible catalytic effect of nTiO₂,

References

1. Rothon, R (Ed.), *Particulate-Filled Polymer Composites*, Chap.6, Longman Scientific and Technical, 1995
2. Giannelis, E. P., *Adv. Mater.* **1996**, *8*, 29.
3. Pinnavaia, T.J.; Beall, C.W. (Eds), *Polymer-Clay nanocomposites*, Wiley, 2001
4. Gilman, J.W. ; Jackson, C.L. ; Morgan, A.B. ; Harris, R.; Manias, E. ; Giannelis, E.P.; Wuthenow, M.; Hilton, D.; Phillips, S.H., *Chem. Mater.* **2000**, *12*, 1866.

5. Porter, D.; Metcalfe, E.; Thomas, M.J.K., *Fire Mater.* **2000**, *24*, 45.
6. Zanetti, M.; Camino, G; Mühlaupt, R., *Polym. Degrad. Stab.* **2001**, *74*, 413.
7. Le Bras, M.; Wilkie, C. ; Bourbigot, S. ; Duquesne, S. ; Jama, C. (Eds). *Fire Retardancy of Polymers: The Use of Mineral Fillers*, The Royal Society of Chemistry, Oxford, 2005.
8. Beyer, G., *Fire Mater.* **2001**, *25*, 193.
9. Ferry, L.; Gaudon, P.; Leroy, E.; Lopez-Cuesta, J.M., in Le Bras, M.; Wilkie, C.; Bourbigot, S.; Duquesne, S.; Jama, C. (Eds). *Fire Retardancy of Polymers: The Use of Mineral Fillers*, p. 345, The Royal Society of Chemistry, Oxford, 2005.
10. Dubois, P., Oral communication, MoDeSt Conference, 30th Sept-2nd Oct. 2004, Lyon, France
11. Kuljanin, J.; Marinovic-Cincovic, M.; Zec S.; Comor, M.I.; Nedeljkovic, J.M., *J.Mat. Sci. Lett.* **2003**, *22*, 235.
12. Yeh, J.T.; Hsieh, S.H.; Cheng, Y.C.; Yang, M.J.; Chen, K.N., *Polym. Degrad. Stab.*, **1998**, *61*, 399.
13. Weil, E., Oral communication, MoDeSt Conference, 1st-4th Jul. 2002, Budapest, Hungary
14. Laoutid, F.; Ferry, L.; Lopez-Cuesta, J.M.; Crespy, A., *Polym. Degrad. Stab.*, **2003**, *82*, 357
15. Cochez, M.; Ferriol, M.; Weber, J.V.; Chaudron, P.; Oget, N.; Mieloszynski, J.L, *Polym. Degrad. Stab.* **2000**, *70*, 455
16. Laachachi, A.; Cochez, M.; Ferriol, M.; Leroy, E.; Lopez-Cuesta, J.M.; Oget, P., *Polym. Degrad. Stab.*, **2004**, *85*, 641
17. Zulfigar, S.; Masud, K., *Polym. Degrad. Stab.* **2002**, *78*, 305
18. Hirata, T.; Kashiwagi, T.; Brown, J.E., *Macromolecules* **1985**, *18*, 1410
19. Kashiwagi, T.; Inaba, A.; Brown, J.E., *Macromolecules*, **1986**, *19*, 2160
20. Peterson, J.D.; Vyazovkin, S.; Wight, C.A., *Macromol. Rapid Comm.*, **1999**, *20*, 480
21. Peterson, J.D.; Vyazovkin, S.; Wight, C.A., *J. Phys. Chem.* ,**1999**, *B* *103*, 8087
22. Chase, M.W., NIST-JANAF Thermochemical Tables, 4th edition, J. Phys. Chem. Ref. Data, Monograph 9, 1998.
23. Shackelford, J.F.; Alexander, W. *Materials Science and Engineering Handbook*, CRC Press, Boca Raton, U.S.A, 2000
24. Jahromi, S.A.J.; Ali Pour, M.M.; Beirami, A. *Eng. Failure Anal.* **2003**, *10*, 405
25. Butler, K., Extended Abstracts and Presentations from the Workshop on Fire Growth and Spread on Objects, March 4-6, 2002, NIST.
<http://fire.nist.gov/bfrlpubs/flamespread/Abstract/Butler%20Abstract.pdf>
26. Zhu, J.; Start, P.; Mauritz, K. A.; Wilkie, C. A., *Polym. Degrad. Stab.* **2002**, *77*, 253
27. Lewin, M., *Fire Mater.* **2003**, *27*, 1.

Chapter 5

The Effects of Inorganic–Organic Cations on EVA–Magadiite Nanocomposite Flammability

Alexander B. Morgan¹, Paul D. Whaley², Thomas S. Lin²,
and Jeffrey M. Cogen²

¹Core R&D, The Dow Chemical Company, Midland, MI 48674

²Wire and Cable R&D, The Dow Chemical Company, Somerset, NJ 08873

There are several organoclays which have been used in polyethylene-co-vinyl acetate (EVA) nanocomposite synthesis, most commonly montmorillonite and fluorinated synthetic mica. One type of clay, magadiite, and the effects of its cations on nanocomposite flammability has not been thoroughly studied in EVA. In our study we investigated the effects of an organically treated magadiite and four inorganic magadiites on EVA flammability. Thermogravimetric analysis, transmission electron microscopy, and X-ray diffraction analyses found that the organically treated magadiite led to nanocomposite formation whereas the inorganic magadiites gave microcomposite structures. Flammability performance by cone calorimeter testing showed that the organically treated magadiite nanocomposite gave the best flammability performance.

Introduction

Polymer-clay nanocomposites are now a widely studied class of materials due to their great improvements in flammability and mechanical properties when compared to traditional composites (1). Numerous studies show that polymer-clay nanocomposites have significantly reduced heat release rates (HRR), which indicate a higher level of fire safety under real world fire conditions (2,3). However, polymer-clay nanocomposites by themselves do not seem to pass existing regulatory tests, even with the lowered HRR (4,5,6). To address this issue, polymer-clay nanocomposites have been combined with conventional flame retardant additives to generate systems with superior flame retardancy and balance of mechanical properties (7,8,9,10).

Most of the work on polymer-clay nanocomposite materials for flammability applications has been done with montmorillonite clay. Very little work has been done with other layered silicates, such as magadiite, although there have been a few papers on the use of magadiite as a clay for nanocomposite use (11,12,13). Synthetic magadiite clay has some advantages over natural clay, namely in the areas of color and transition metal impurities. Due to the presence of iron in the clay (14) structure, natural clays are colored and often produce a brown to tan base color in the final polymer nanocomposite. Also, the iron impurities could promote degradation of the polymer matrix over long periods of time, which could cause long-term heat aging problems for a wire and cable jacketing compound. Magadiite, composed only of silicon and oxygen (and whatever cation is incorporated during synthesis), is white and has no transition metal impurities in its structure. Products where coloration is important (such as different colored wires and cables) should begin with a base white, or color-free, polymeric material. Also, the lack of iron in magadiite should be beneficial in the long term stability of the polymeric material.

In this paper, we use magadiite as the layered silicate, and focus on the effects of the clay cation (organic or inorganic) on the flammability of the resulting polymer-magadiite nanocomposite. Magnesium hydroxide was combined with the magadiite-polymer nanocomposite to lower flammability further and meet regulatory tests. To address the effects of the clay cation, which serves as the interface between clay and polymer, we investigated one organic cation and four inorganic cations. For the organic cation, we chose a dimethyl, di(hydrogenated tallow) ammonium salt to give an organically treated clay, or organoclay. Organoclays are better suited for polymer nanocomposite synthesis in hydrophobic (polyolefin) polymers (1,15). The base sodium magadiite can also be ion exchanged with inorganic cations to generate new inorganic clays. Inorganic clays typically give microcomposites in polyolefins (1,16) but there may be some benefit to inorganic substitution in reacting with the $\text{Mg}(\text{OH})_2$ under fire conditions. Also, the polar co-monomer in EVA could

interface with the inorganic clay, allowing better dispersion than would normally be expected. The inorganic cations chosen were calcium, magnesium, and hydrogen. The hydrogen exchange is one that requires some additional explanation, as its final structure is different from all of the other clays in this study. The hydrogen exchanged clay is sodium magadiite treated with a protic acid, such that the proton (H^+ cation) exchanges with the sodium; however, in so doing, the ionic nature of magadiite is lost. The anionic site on magadiite can best be thought of as a SiO^{-1} anion, and when reacted with H^+ it forms a silanol ($Si-OH$) site. In effect this makes H^+ Magadiite a layered *silica* rather than an ionically exchanged *silicate*. This silica structure may have some additional benefit in flame retardancy over ionically exchanged silicate in that it may form silicate glasses under fire conditions, as well as help lessen polymer flow due to thermal degradation (17,18).

To measure how each magadiite affected the flammability performance of the resulting composite, UL-94 vertical burning test and cone calorimeter testing were utilized. To understand the composite structure generated by each of the magadiites, each formulation was analyzed by thermogravimetric analysis (TGA), X-ray diffraction (XRD), and transmission electron microscopy (TEM).

Experimental Section

Polyethylene-co-vinyl acetate (EVA, 3.0 melt index, 28% vinyl acetate), linear low density polyethylene-graft-maleic anhydride (LLDPE-g-MA, 2.0 melt index, 0.3wt% MA), magnesium hydroxide, dimethyl di(hydrogenated tallow) ammonium chloride (Akzo Nobel Arquad2HT, 25% by weight in isopropanol). Sodium magadiite was prepared as previously described (19). Cation exchanges on magadiite (with either organic or inorganic cations) were conducted via conventional ion exchange processes.

EVA-magadiite nanocomposites (Table I) were prepared by melt compounding in a ThermoHaake mixer with 250 cc mixing head. The initial RPM was set to 10, polymer was added first and mixed at 170 °C until molten, followed by other additives which were fed into the mixing bowl and the RPM increased to 50 for 10 minutes. Material was then removed from the mixing bowl and allowed to cool. From the cooled sample, UL-94 burn bars and cone calorimeter plaques (100mm × 100mm × 3.2mm) were made via compression molding at 155 °C.

Table I. EVA + Mg(OH)₂ + Magadiite (MGD) Formulations.

Formulation ID	EVA + NaMGD	EVA + Arq2HT MGD	EVA + CaMGD	EVA + MgMGD	EVA + H+MGD	EVA + 63% Mg(OH) ₂	EVA + 58wt% Mg(OH) ₂
EVA	31	31	31	31	31	31	36
Sodium Magadiite	5	0	0	0	0	0	0
0.5 H+ Arq2HT Magadiite	0	0	0	0	0	0	0
1.0 Na+ Arq2HT Magadiite	0	5	0	0	0	0	0
Calcium Magadiite	0	0	5	0	0	0	0
Magnesium Magdiite	0	0	0	5	0	0	0
H+ Magadiite	0	0	0	0	5	0	0
Mg(OH) ₂	58	58	58	58	58	63	58
LLDPE-g-MA	6	6	6	6	6	6	6

TGA data were collected with a TA Instruments TGA 2950, under nitrogen, at 20 °C/min, from 25 °C to 700 °C. All samples were run in triplicate for repeatability analysis, and the data presented in Table II is an average of those three samples. XRD data were collected on a Bruker AXS diffractometer using Cu K α radiation ($\lambda=0.1505945$ nm) with a 0.02 2 θ step size and a 2 s count time. Samples used for XRD were compression molded at 155 °C to give 25mm diameter (2 mm thick) disks in synchronous rotation mode. Nanocomposites were viewed by TEM by having the nanocomposite thin-sectioned at 90nm using a Reichert-Jung Ultracut E (Serial # 393365) with a FC-4E cryo-chamber attachment (Serial # 402389) at -95°C and collected on a copper grid. Sections were examined with a JEOL JEM-1230 TEM (Serial # EM18440018) running at an accelerating voltage of 120 kV. Images were recorded digitally with a Gatan Multiscan CCD camera, Model 749 (Serial # C2060401).

UL-94 Testing was performed with a minor modification to the standard procedure (20). Rather than test two sets of samples each conditioned at different humidity, only one set of 5 bars was tested with no conditioning. Cone Calorimeter experiments were conducted in triplicate on a FTT Cone Calorimeter at a heat flux of 35 kW/m² and exhaust flow of 24 L/s using the standardized cone calorimeter procedure (ASTM E-1354-99). Data collected has an error of $\pm 10\%$ and was calculated using a specimen surface area of 100 cm².

Results and Discussion

The summary of the data collected (TGA, XRD, TEM, UL-94 V, cone calorimeter) is listed below in Table II. TGA data does not show any significant

differences between the formulations tested, but when compared to the EVA control, there are some slight differences at the 1, 5, and 10wt% loss temperatures. The TGA data here served as a test to confirm loading of the inorganic additives (magadiite and Mg(OH)₂). In regards to this point, the TGA data was within the expected ranges.

Table II. Analytical Data for EVA formulations

Formulation ID	EVA + NaMGD	EVA + Arq2HT MGD	EVA + CaMGD	EVA + MgMGD	EVA + H+MGD	EVA + 63% Mg(OH) ₂	EVA + 58wt% Mg(OH) ₂	EVA Control
XRD (X-Ray Diffraction)								
d-spacing (100) measured (nm)	1.52	4.4	1.35	1.37	no peak	n/a	n/a	n/a
d-spacing (100) difference (nm)	-0.02	-0.6	?	0.03	n/a	n/a	n/a	n/a
TGA (Thermogravimetric Analysis)								
1wt% loss (deg C)	333	298	339	342	343	345	341	324
5wt% loss (deg C)	366	369	371	373	371	373	369	352
10wt% loss (deg C)	383	393	389	390	388	390	386	369
loss @ 700 C (wt%)	53.73	57	54.8	53.26	53.74	55.24	58.39	99.97
UL 94 Vertical Burn								
Average Thickness (mm)	3.45	3.58	3.33	3.56	3.38	3.35	3.4	known
1st Flame Applications (s)	0,0,0,0,0	0,0,0,0,0	0,0,0,0,0	0,0,0,0,0	0,0,0,0,0	0,0,0,0,0	0,0,0,1,0	to fail
2nd Flame Applications (s)	0,0,0,0,0	4,0,0,0,0	0,0,0,0,4	0,0,0,0,0	0,0,0,0,0	0,0,1,0,0	3,7,43,261,7	UL-94 V
Classification	V-0	V-0	V-0	V-0	V-0	V-0	NR	NR
Cone Calorimeter (avg. data)								
Tig (s)	140	111	132	134	128	143	142	84
Peak HRR (kW/m ²)	255	123	165	133	131	188	293	1632
Avg HRR (kW/m ²)	129	80	94	81	92	101	149	603
Total Heat Evolved (MJ/m ²)	66	72	64	61	63	67	72	113
Time to Peak HRR (s)	488	173	270	220	258	530	437	213

TEM and XRD Data

Since it is well known that the degree of clay dispersion is related to flammability performance in polymer nanocomposites,³ XRD and TEM were used to understand the degree of clay dispersion in the magadiite-containing formulations. XRD and TEM are used together in polymer nanocomposite analysis since, by themselves, they do not describe all aspects of polymer nanocomposite structure and dispersion (21). XRD measures the degree of spacing change between clay plates, which can suggest polymer intercalation (a positive d-spacing change), organic treatment rearrangement / degradation (a negative d-spacing change) or no polymer/clay nanoscale interaction (no or insignificant d-spacing change). XRD does not indicate overall clay dispersion, merely the degree of spacing change for the clay particles that diffracted X-rays. Disordered clay particles will not be detected by the XRD technique (21). TEM

becomes complimentary to XRD by showing the overall quality of the clay dispersion, and showing the size of the clay particles in relation to each other and the rest of the polymer matrix. TEM does not measure d-spacing however, so it needs to be combined with XRD data to determine what changes occurred at the nanoscale.

In Table II, XRD data is described in two categories; data for organomagadiites and data for inorganic magadiites. For the EVA + Arquad 2HT treated magadiite (Arq2HTMGD) sample, a small amount of d-spacing decrease was observed. We believe this decrease to be due to an alkyl chain rearrangement rather than degradation, as the melt processing of the nanocomposite formulations was kept below 200 °C and the amount of d-spacing decrease is not as large as known decompositions reported in the open literature (22,23). For the inorganic magadiite samples, the spacings were unchanged, although in the case of calcium magadiite and H⁺ magadiite, almost no peak for the clay was observed, making it difficult to assign a d-spacing change. As the TEM data show, there was no d-spacing change with these two inorganic magadiites, but instead, the magadiite became disordered during melt compounding, resulting in structures that did not diffract X-rays.

TEM for the EVA + Arq2HTMGD sample shows good overall microscale dispersion, but higher magnification images show that the dispersion could be further improved. The organomagadiite appears to be in the form of smaller multi-plate, well ordered agglomerates which are dispersed into the EVA phase between the Mg(OH)₂ particles. The primary clay tactoids have been broken up, and smaller clay stacks can be seen, thus suggesting nanocomposite formation. To be more specific, the nanoscale particle is several layers thick, rather than an intercalated stack or a single clay plate.

TEM for the inorganic magadiites is significantly different than that of the organomagadiite sample. XRD data for all of the inorganic magadiite samples suggests that these clays only produced microcomposites. TEM confirms that all of the formulations made with inorganic magadiites (Figures 1, 2) are microcomposites. In Figure 1, a large fibrous-looking mass can be seen in the low magnification image; this is the sodium magadiite (NaMGD). Similar large masses can be seen in Figures 1 and 2 for the other magadiites. These large masses were not seen with the H⁺ Magadiite (H+MGD, Figure 2, Right) sample, suggesting that the primary clay particles were smaller than in the other samples. However, TEM images (Figures 1-3) are not those which typically suggest polymer intercalation. It appears that the primary clay particles sheared apart, but did not intercalate, giving well-ordered magadiite clay stacks (24). The TEM images are very different than those observed in previous EVA + montmorillonite work, where XRD did detect d-spacing increase, and clay particles were observed that suggested polymer intercalation (21,28,29,30).

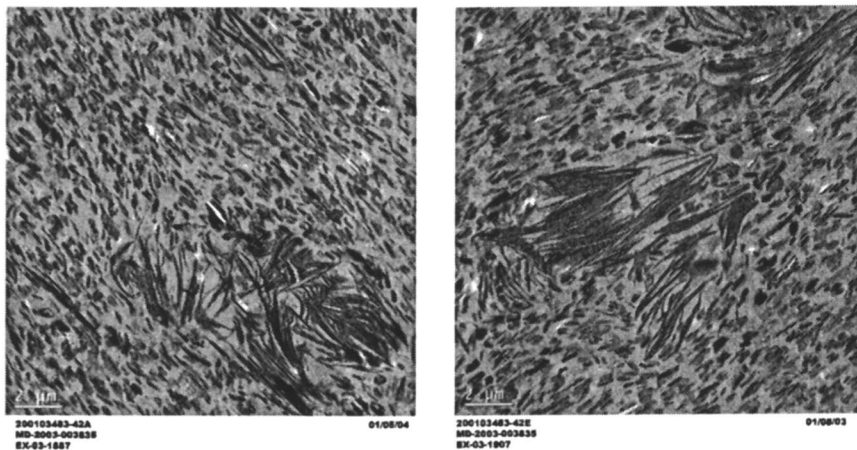


Figure 1. TEM Images of NaMGD (Left) and calcium magadiite (CaMGD) (Right) in EVA/Mg(OH)₂.

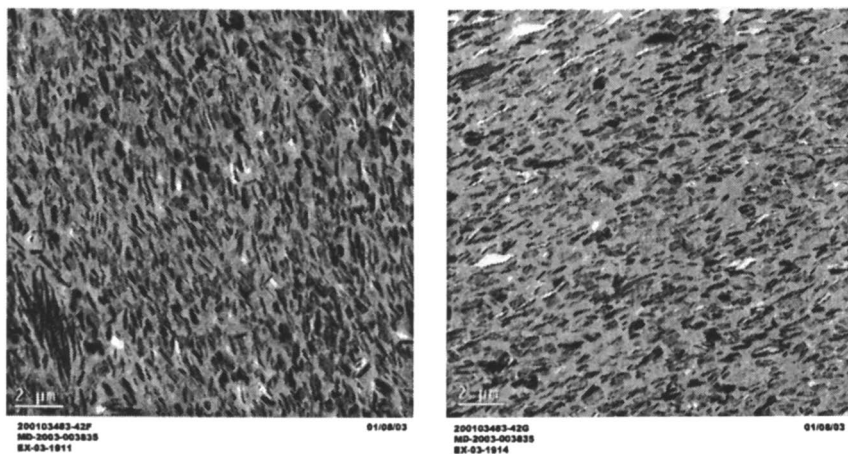


Figure 2. TEM Images of Magnesium magadiite (MgMGD) (Left) and H⁺MGD (Right) in EVA/Mg(OH)₂.

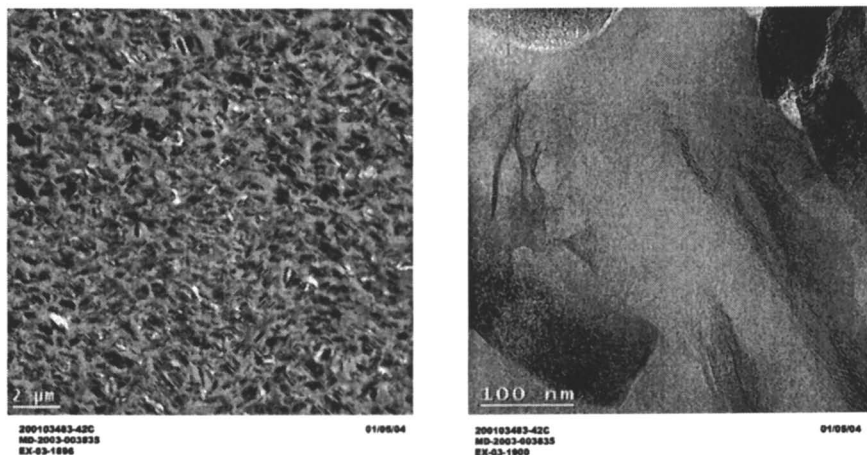


Figure 3. TEM Images of Arq2HT MGD in EVA/Mg(OH)₂.

Cone Calorimeter and Flammability Data

Each of the formulations was tested by UL-94 V and cone calorimetry to measure flammability performance. As the data in Table II show, all of the magadiite containing samples performed the same under UL-94 as the 63wt% Mg(OH)₂ control sample. Since UL-94 was unable to differentiate between these materials, cone calorimeter testing was undertaken. Cone calorimeter testing can generate a variety of flammability parameters which can be of use to understanding the fire safety performance of a material (25,26). In Table II, some of this flammability data is summarized, including time to ignition (Tig), Peak HRR, average HRR, total heat evolved and time to peak HRR. It is also informative to view the actual data, so the full HRR curves were plotted to help determine which magadiite provided superior flame retardancy. The EVA+MGD+Mg(OH)₂ formulations show reductions in peak HRR of 84% to 92% compared to the EVA control. The Mg(OH)₂ only samples have reductions in peak HRR of 88% and 82% compared to the EVA base polymer. EVA nanocomposites by themselves (without magnesium hydroxide) have shown reductions of peak HRR in the area of 40 to 60% (9,27,28,29,30).

In Figure 4, the HRR curves for the two Mg(OH)₂ only samples and the organomagadiite nanocomposites are compared. The magadiite nanocomposite shows lower peak HRR, but earlier time to peak HRR than the Mg(OH)₂ only samples. Interestingly, the difference in HRR curve shape and peak HRR in Figure 4 is most pronounced when comparing the 63wt% Mg(OH)₂ and the 58wt% Mg(OH)₂ EVA samples. Even though there is just a 5wt% difference in total FR loading, the sample with higher loading has a much lower peak HRR and average HRR than the sample with slightly lower loading.

In Figure 5, the HRR curves for the inorganic magadiite formulations and the two control samples are compared. The sodium magadiite sample had a higher peak HRR than the high loading control sample and the other inorganic magadiite samples. The calcium magadiite sample was only slightly better in peak HRR than the high loading control sample, but not better than the other two inorganic magadiite samples. The magnesium and H^+ magadiite samples showed superior flammability performance when compared to the other inorganic magadiites and the two control samples. The MgMGD and H^+ MGD nanocomposites had similar Tig and HRR curves, and were significantly better in peak HRR performance than the other samples.

In Figure 6, the HRR curves for the organomagadiite and the two inorganic magadiites with the best performance in regards to peak HRR are shown. Amongst these three formulations, there are some flammability differences. The organomagadiite has a slightly earlier time to peak HRR than the inorganic magadiite samples, but the peak HRR is lower, and HRR drops off quickly after ignition before rising again later to another peak. The inorganic magadiites have similar behavior, but they take longer to reach peak HRR. However, the inorganic magadiites show slightly higher average HRR when compared to the organomagadiite. There is still a some difficulty in the interpretation of cone calorimeter data when the sample has been tested at a single heat flux,³¹ and these changes in HRR may not be significant given that all of these formulations passed the UL-94 V test at the same rating and thickness. But since peak HRR is considered to be one of the key elements leading to flame spread (26) materials that keep peak HRR low are desirable in regards to fire safety.

Conclusions

In this study, EVA was combined with various inorganic cation exchanged magadiites and one alkyl ammonium exchanged magadiite which gave a nanocomposite that was not easily defined by traditional nanocomposite analysis. TEM and XRD data suggest that no polymer intercalation occurred in these samples, but the primary clay agglomerates were broken up in the case of the organomagadiite, giving a nanocomposite where the reinforcing particle was several clay layers thick. The inorganic magadiite samples were all microcomposites by XRD, TEM, and fit the classic definition of a traditional composite with micron-size clay particles. The one possible exception was the H^+ magadiite sample, where the primary particles seem to have broken apart during compounding. We speculate that the $Mg(OH)_2$ may have had a favorable interaction with the silanols on the H^+ magadiite structure, thus breaking apart the primary tactoids, but at this time we cannot envision an experiment to test this hypothesis.

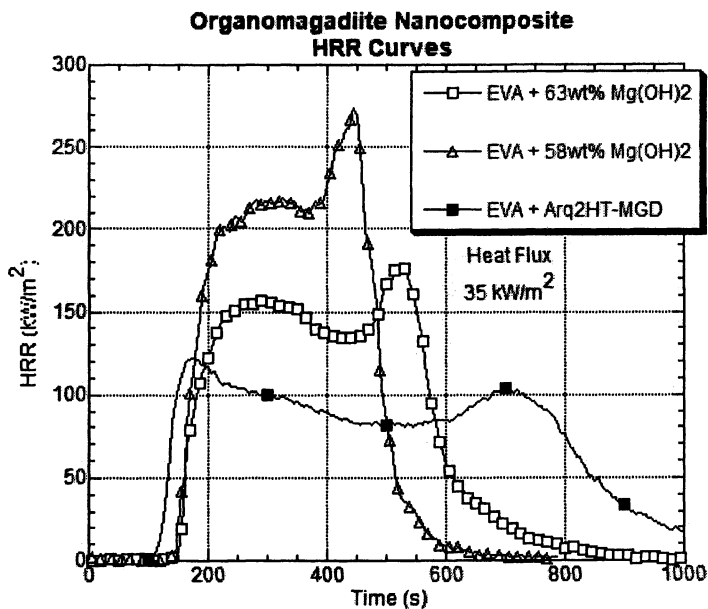


Figure 4. HRR of EVA+Mg(OH)₂ and Arq2HT-MGD formulations.

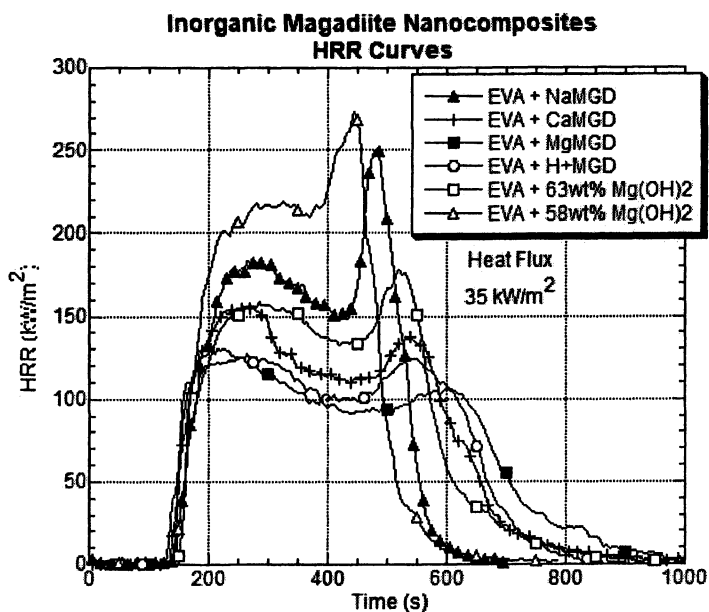


Figure 5. HRR of EVA+Mg(OH)₂ and inorganic MGD formulations.

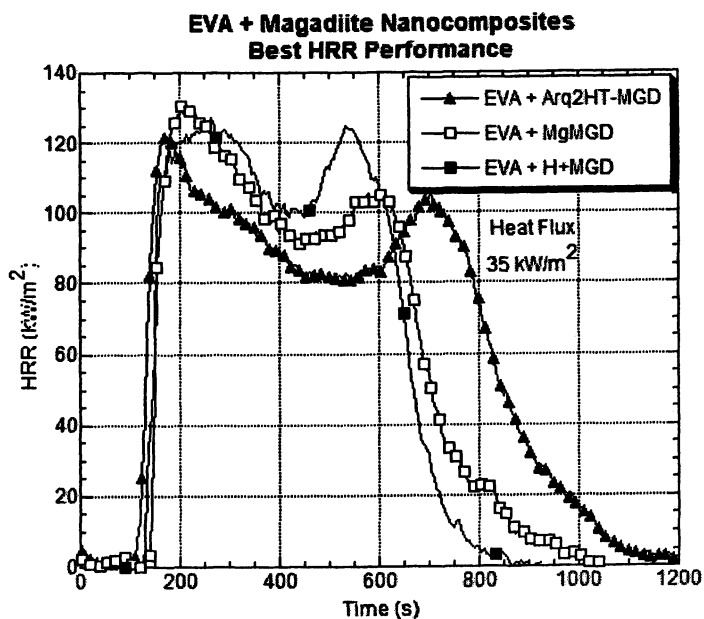


Figure 6. HRR Curves of EVA+Mg(OH)₂+ MGD formulations.

In regards to flammability, all of the magadiite samples gave UL-94 V-0 performance at 3.2mm thickness, but different performance under cone calorimeter testing. By cone calorimeter, only three of the magadiite containing samples had improved flammability when compared to the $Mg(OH)_2$ only control samples, namely the Arq2HT, Mg, and H^+ magadiites. The result for the Arq2HT magadiite was not too surprising, as organoclay nanocomposites always show greatly reduced peak HRR. However, numerous literature examples have shown that microcomposites do not have a significant effect on reducing peak HRR, which makes the HRR results of the Mg and H^+ magadiite microcomposites surprising. Therefore, the improved flame retardancy could be due to some inorganic chemical reaction at high fire temperatures (17,18), not to nanocomposite structure. This is an important observation, as it indicates that a nanocomposite may not always be needed to obtain good flammability behavior when using a layered silicate. However, an important consideration when choosing between inorganic magadiites (microcomposites) and organic magadiites (nanocomposites) is the final balance of properties. Since the inorganic magadiites are microcomposites, their balance of mechanical properties may not be as good as the balance of properties provided by the organomagadiite nanocomposites.

Acknowledgements

We would like to thank Ron Patrick for cone calorimeter measurements, Dan Crane for magadiite synthesis, and Joseph Harris for TEM measurements.

References

1. Ray, S. S.; Okamoto, M. *Prog. Polym. Sci.* **2003**, *28*, 1539-1641
2. Gilman, J. W.; Jackson, C. L.; Morgan, A. B.; Harris, R.; Manias, E.; Giannelis, E. P.; Wuthenow, M.; Hilton, D.; Phillips, S. H. *Chem. Mater.* **2000**, *12*, 1866-1873.
3. Gilman, J. W. *App. Clay Science* **1999**, *15*, 31-49.
4. Chigwada, G.; Wilkie, C. A. *Polym. Degrad. Stab.* **2003**, *80*, 551-557.
5. Bartholmai, M.; Schartel, B. *Polymers Adv. Technol.* **2004**, *15*, 355-364.
6. Morgan, A. B.; Chu, L. L.; Harris, J. D. *Proceedings of Flame Retardants 2004* January 27-28, 2004. Interscience Communications, London, UK. Pp 85-96,
7. Zanetti, M.; Camino, G.; Canavese, D.; Morgan, A. B.; Lamelas, F. J.; Wilkie, C. A. *Chem. Mater.* **2002**, *14*, 189-193.
8. Dabrowski, F.; Le Bras, M.; Cartier, L.; Bourbigot, S. *J. Fire Sciences* **2001**, *19*, 219-241.
9. Beyer, G. *Fire Mater.* **2001**, *25*, 193-197.

10. "Polymer-Layered Silicate Nanocomposites with Conventional Flame Retardants" Gilman, J. W.; Kashiwagi, T. in "Polymer-Clay Nanocomposites" ed. Pinnavaia, T. J.; Beall, G. W. John Wiley & Sons. 2000. PP. 193-206.
11. Wang, D.; Jiang, D. D.; Pabst, J.; Han, Z.; Wang, J.; Wilkie, C. A. *Polym. Eng. Sci.* **2004**, *44*, 1122-1131.
12. Isoda, K.; Kuroda, K.; Ogawa, M. *Chem. Mater.* **2000**, *12*, 1702.
13. Wang, Z.; Pinnavaia, T. J. *Chem. Mater.* **1998**, *10*, 1820.
14. Zhu, J.; Uhl, F. M.; Morgan, A. B.; Wilkie, C. A. *Chem. Mater.* **2001**, *13*, 4649-4654.
15. Reichert, P.; Nitz, H.; Klinke, S.; Brandsch, R.; Thomann, R.; Mulhaupt, R. *Macromol. Mater. Eng.* **2000**, *275*, 8-17.
16. "Flammability of Polymer Clay Nanocomposites Consortium: Year One Annual Report" Gilman, J. W.; Kashiwagi, T.; Morgan, A. B.; Harris, R. H.; Brassell, L.; VanLandingham, M.; Jackson, C. L. *National Institute of Standards and Technology Internal Report (NISTIR) 6531*, **2000**.
17. "NEW FLAME RETARDANTS CONSORTIUM: FINAL REPORT. Flame Retardant Mechanism of Silica" Gilman, J. W.; Kashiwagi, T.; Nyden, M.; Harris, R. H. *National Institute of Standards and Technology Internal Report (NISTIR 6357)*, **1999**.
18. Kashiwagi, T.; Gilman, J. W.; Butler, K. M.; Harris, R. H.; Shields, J. R. Asano, A. *Fire Mater.* **2000**, *24*, 277-289.
19. Garces, J.M.; Lakso, S.R.; Schoeman, B.J.; Ulmer, D.C., Patent Application WO 01/83370 A2.
20. UL-94: Test for Flammability of Plastic Materials for Parts in Devices and Applications [ASTM D3801-96]
21. Morgan, A. B.; Gilman, J. W. *J. App. Polym. Sci.* **2003**, *87*, 1329-1338.
22. Xie, W.; Gao, Z.; Pan, W-P.; Hunter, D.; Singh, A.; Vaia, R. *Chem. Mater.* **2001**, *13*, 2979-2990.
23. Xie, W.; Xie, R.; Pan, W-P.; Hunter, D.; Koene, B.; Tan, L-S.; Vaia, R. *Chem. Mater.* **2002**, *14*, 4837-4845.
24. Dennis, H. R.; Hunter, D. L.; Chang, D.; Kim, S.; White, J. L.; Cho, J. W.; Paul, D. R. *Polymer* **2001**, *42*, 9513-9522.
25. Babrauskas, V. *Fire Mater.* **1995**, *19*, 243-252.
26. Babrauskas, V.; Peacock, R. D. *Fire Safety Journal* **1992**, *18*, 255-272.
27. Riva, A.; Zanetti, M.; Braglia, M.; Camino, G.; Falqui, L. *Polym. Degrad. Stab.* **2002**, *77*, 299-304.
28. Zanetti, M.; Camino, G.; Thomann, R.; Mulhaupt, R. *Polymer* **2001**, *42*, 4501-4507.
29. Zanetti, M.; Camino, G.; Mulhaupt, R. *Polym. Degrad. Stab.* **2001**, *74*, 413-417.
30. Zanetti, M.; Kashiwagi, T.; Falqui, L.; Camino, G. *Chem. Mater.* **2002**, *14*, 881-887.
31. Schartel, B.; Braun, U. *e-Polymers* **2003**, Article #13, <http://www.e->

Chapter 6

Fire Retardancy of Polypropylene- Metal Hydroxide Nanocomposites

Jinguo Zhang and Charles A. Wilkie

Department of Chemistry, Marquette University, PO Box 1881,
Milwaukee, WI 53201

The combination of metal hydroxides (aluminum or magnesium) with an organically-modified clay has been studied as a potential fire retardant system for polypropylene. The combination of polypropylene with 5% inorganic clay and 20% of the metal hydroxide gives an 80% reduction in the peak heat release rate, which is the same as what is obtained when 40% of the hydroxide is used alone. This means that more polymer can be used, which could be an advantage in some situations.

Introduction

Aluminium trihydrate (ATH) and magnesium hydroxide (MDH) are well-known fire retardants for polypropylene (1); they are attractive because of their low price and good performance. The limitation of ATH and MDH is that high loadings are required to achieve good fire retardant performance; the normal loading is at least 40%, and the typical loading is 60% (2). Such a high loading will cause significant degradation in mechanical properties. On the other hand, much has been heard recently about polymer-clay nanocomposites, which show greatly enhanced mechanical as well as fire and barrier properties (3). Beyer (4)

showed that with ethylene vinyl acetate copolymers, EVA, one could replace 18-20% ATH with 5% organically-modified clay and maintain the same peak heat release rate, PHRR. In other words, the amount of polymer that is present can be increased by 13 to 15%.

Normally one must use maleic anhydride as a compatibilizer for polypropylene, which could again degrade the mechanical properties. Recent work from this laboratory has shown that a new oligomerically-modified clay can be melt blended with polypropylene to give intercalated and delaminated nanocomposites (5,6). This work is based on this discovery and herein we examine the combination of polypropylene with ATH and MDH and an oligomerically-modified clay.

Experimental

Materials. Aluminum trihydrate, $\text{Al}_2\text{O}_3 \cdot 3\text{H}_2\text{O}$, OL-107/LE, and magnesium hydroxide, $\text{Mg}(\text{OH})_2$, H7, which are uncoated materials, were obtained from Martinswerke GmbH, a company of Albemarle Corporation. The majority of the other chemicals used in this study, including isotactic polypropylene (melt index $230^\circ\text{C}/2.16 \text{ Kg } 4\text{g}/10\text{min}$) and solvents, were obtained from the Aldrich Chemical Company. The oligomerically-modified clay, COPS, was synthesized according to the published procedure (5). The inorganic clay content in COPS clay is 30%; it contains about 70% of the surfactant. Throughout the paper, the loading of inorganic clay is referenced; the loadings of oligomerically-modified clay that have been used are 3%, 10% and 17%, which corresponds to 1%, 3% and 5% inorganic clay loading. Polypropylene, COPS clay and ATH or MDH were pre-mixed in a beaker, then blended in Brabender Plasticorder at 180°C for 10 min at 60 rpm. The mixture then was removed from the mixer and cut into pieces. A Leistritz 18 mm co-rotating twin screw extruder, L:D ratio = 40:1, was used at a feed rate of 2 Kg/hr and a screw speed of 400 rpm. The utilization of ATH with polypropylene is limited industrially because the usual mixing temperature is above the temperature at which ATH will undergo thermal degradation.

Instrumentation. X-ray diffraction was performed on a Rigaku Geiger Flex two-circle powder diffractometer; generator tension was 50 kV at a current of 20 mA. Scans were taken at $2\theta = 1.0 - 10$ at a 0.1 step. Cone calorimetry was performed on an Atlas CONE-2 according to ASTM E 1354-92 at an incident flux of $50 \text{ kW}/\text{m}^2$ using a cone shaped heater; exhaust flow was set at 24 L/s. Cone samples were prepared by compression molding the sample into $100 \times 100 \times 3\text{mm}$ square plaques. Typical results from cone calorimetry are considered to be reproducible to $\pm 10\%$ (7). Thermogravimetric analysis (TGA) was performed on a SDT 2000 machine at 15mg scale under a flowing nitrogen

atmosphere at a scan rate of 20 °C/min. Temperature are reproducible to $\pm 3^\circ\text{C}$, while the error on the fraction of non- volatile materials is $\pm 2\%$. Tensile properties are obtained on Reliance RT/5 (MTS) at 5mm/min crosshead speed; the reported values are based on the average of 5 determinations.

Results and Discussion

Characterization of nanocomposite formation by X-ray diffraction

The formation of a nanocomposite is accompanied by an increase in the gallery spacing, which can be evaluated using X-ray diffraction, XRD. The compositions that have been studied as well as the 2θ values and the corresponding d-spacing are recorded in Table I while the actual XRD traces are shown in Figure 1. It is obvious that COPS clay itself has a large d-spacing and this is maintained in the polypropylene nanocomposites, but there is no increase in the d-spacing. The same results have been previously reported for COPS-polypropylene nanocomposites and the TEM data suggests that the clay is well-dispersed and that the system is partially delaminated (5).

Table I. XRD data for COPS clay and its PP nanocomposites

<i>PP</i>	<i>ATH</i>	<i>MDH</i>	<i>COPS</i>	2θ	<i>d-spacing,</i> <i>nm</i>
0	0	---	100	2.1	4.2
63	20	---	17	2.2	4.0
70	20	---	10	2.0	4.4
77	20	---	3	---	---
63	---	20	17	2.1	4.2

Thermogravimetric analysis

Both a surface treated and an untreated form of ATH and MDH have been studied; the TGA curves, which show no difference between the treated and untreated samples, are shown in Figure 2 while the data is reported in Table II. The data consists of the temperatures at which 10%, $T_{0.1}$, which is considered to be the onset of the degradation, and 20%, $T_{0.2}$, which is another measure of

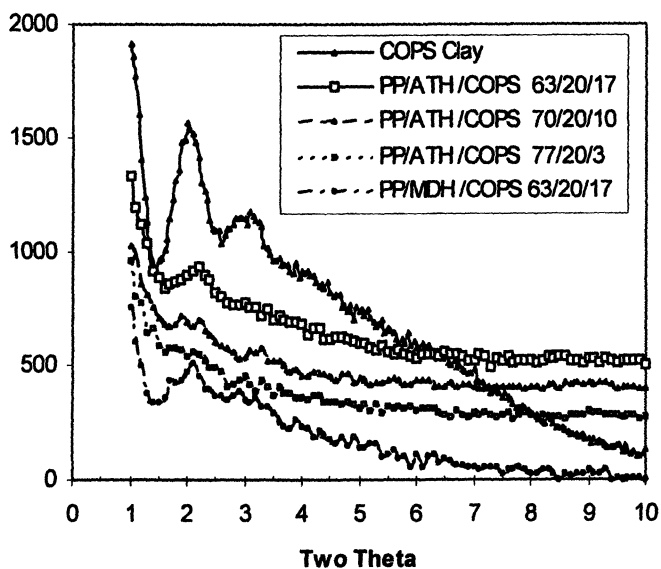


Figure 1. X-ray diffraction pattern of COPS clay and its PP nanocomposites

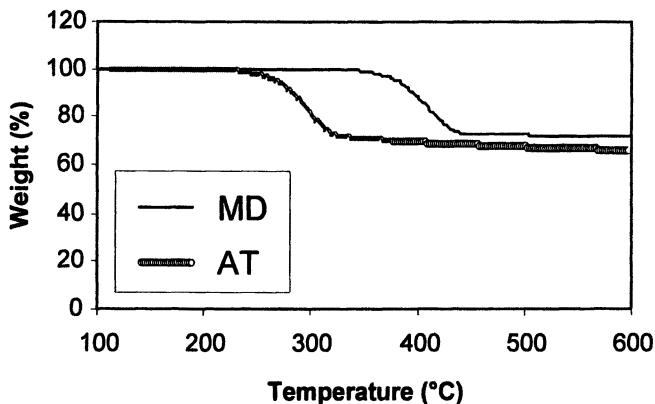


Figure 2. TGA curves of different metal hydroxides

Table II. TGA results for metal hydroxides

	$T_{0.1}(\text{ }^{\circ}\text{C})$	$T_{0.2}(\text{ }^{\circ}\text{C})$	Char at 600°C (%)
ATH	282	301	67
MDH	404	425	70

thermal stability, of the mass has been lost as well as the fraction of non-volatile which remains at 600 °C. (8) It is clear that MDH has a much higher thermal stability than does ATH.

Thermogravimetric analysis of the combinations of polypropylene with the metal hydroxides, without the addition of clay, have been studied and the TGA curves are shown in Figures 3 and 4 while these results are tabulated in Table III. It is clear that ATH is less stable than the polymer so the degradation of these blends commences at lower temperature, while the higher stability of MDH means that these degrade at higher temperature. The fraction of non-volatiles that remains at 600 °C is what is expected based upon the amount of metal hydroxide that is present.

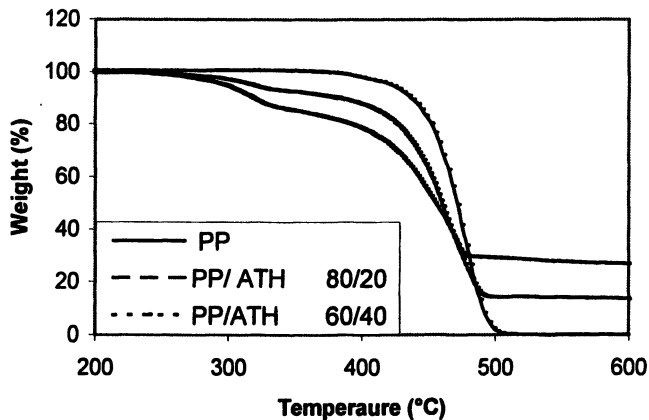


Figure 3. TGA curves of PP and its ATH composites

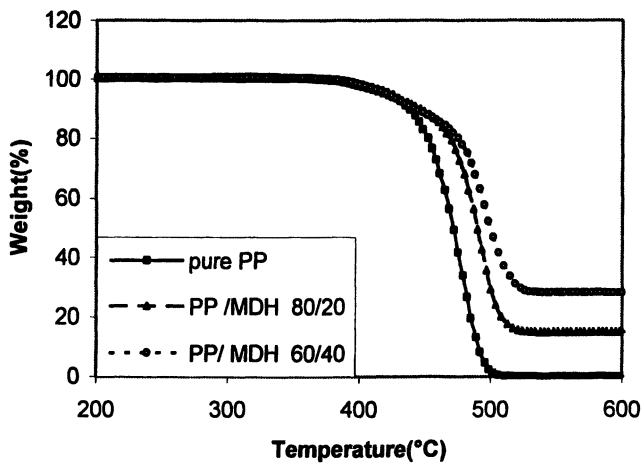
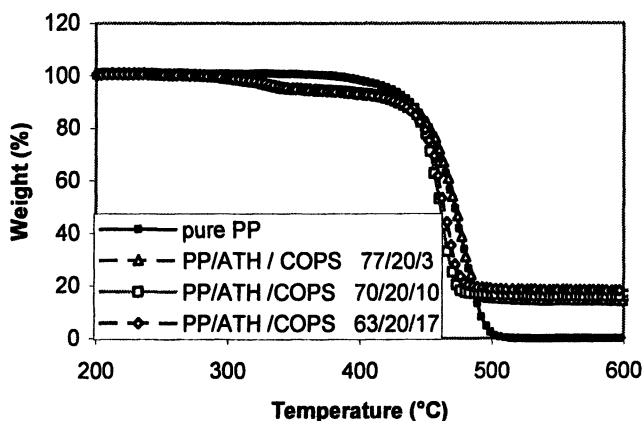


Figure 4. TGA curves of PP and its MDH composites

Table III. TGA data of PP and its metal hydroxides composites

PP	ATH	MDH	$T_{0.1}$ (°C)	$T_{0.5}$ (°C)	Char at 600 °C (%)
100	---	---	436	472	0
80	20	---	384	460	13
60	40	---	320	455	27
80	---	20	446	490	15
60	---	40	442	499	28

Upon the addition of clay to the polypropylene-ATH system, the onset temperature of the degradation increases by 40 °C while the temperature at which 50% degradation occurs is either slightly increased or unaffected and the fraction of non-volatile residue is unchanged. Apparently the addition of clay has a very positive effect on the degradation process; the TGA curves are shown in Figures 5 and 6 and the results are tabulated in Table IV.

*Figure 5. TGA curves of PP - ATH nanocomposites*

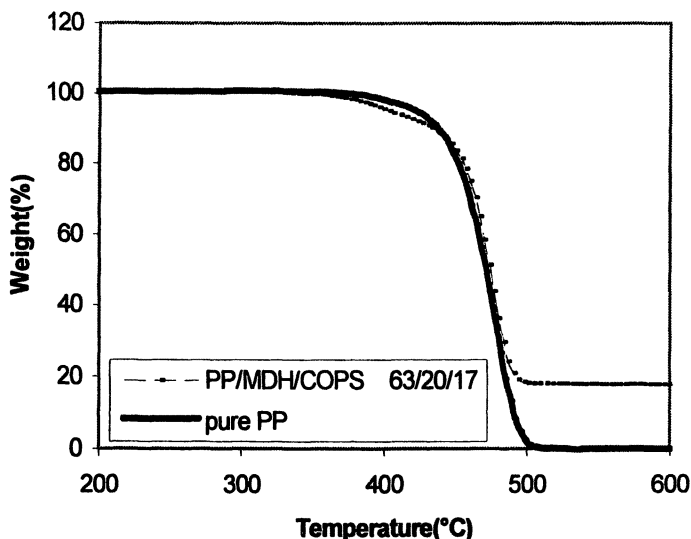


Figure 6. TGA curve of PP - MDH nanocomposites

Table IV. TGA data of PP - metal hydroxides nanocomposites

PP	ATH	MDH	COPS	$T_{0.1}$ (°C)	$T_{0.5}$ (°C)	Char at 600 °C (%)
100	---	---	---	436	472	0
77	20	---	3	428	472	14
70	20	---	10	432	462	16
63	20	---	17	425	464	18
63	20	17	---	435	476	18

Cone calorimetry

The fire properties of these nanocomposites were evaluated using the cone calorimeter, which enables the measurement of the time to ignition (t_{ign}), the heat release rate curve and especially its peak value (PHRR), the amount of smoke evolved, known as the specific extinction area (SEA), the mass loss rate (MLR) and the total heat released (THR). The usual observations for nanocomposites are that there is a significant reduction in PHRR and in time to ignition while the total heat released is unchanged. This means that the nanocomposites are actually easier to burn than the virgin polymer and the shape of the heat release curve is changed but all of the polymer is eventually burned. The purpose of this work was to see if a combination of a metal hydroxide with a clay would have

the same effect in polypropylene that Beyer found in EVA, significant reduction in PHRR at lower loading of the metal hydroxide when clay is present (4). The results for the polypropylene-ATH system are presented in Table V and the heat release rate curves are shown in Figure 6. The combination of 63% polypropylene, 20% ATH and 17% COPS clay (5% inorganic clay) gives about the same value for PHRR and THR that is obtained when 60% polypropylene and 40% ATH are combined. The advantage of the clay-containing composition is that there is approximately 15% more polymer present in the composition, which would be expected to improve the mechanical properties.

Table V. Cone calorimeter data for polypropylene and ATH and their nanocomposites.

PP	ATH	COPS	t_{ign}^a, s	PHRR ^a Kw/m ² (% reduction)	SEA ^a (m ² /kg)	MLR ^a (g/sm ²)	THR ^a (MJ/m ²)
100	---	---	26±4	1967 ±50	584±20	29.7±0.3	112±9
80	20	---	27±3	817±40 (59)	681±32	15.4±1.6	90±2
60	40	---	28±2	467±5(76)	677±147	8.6±0.1	70±6
77	20	3	21±1	677±38 (66)	839±17	16.4±0.7	84±6
70	20	10	20±2	592±18 (70)	1037±39	14.2±0.1	77±4
63	20	17	18±1	536±16 (73)	1143±18	12.6±0.6	74±1

^a t_{ign} , time to ignition; PHRR, peak heat release rate; SEA, specific extinction area, a measure of smoke; MLR, mass loss rate; THR, total heat released.

For the MDH system, only 5% inorganic clay loading was used in combination with MDH as a fire retardant in polypropylene and the results are quite similar to those seen with ATH. The combination of 20% MDH, 17% oligomerically-modified clay (5% inorganic content) and 63% polypropylene gives a very similar value for PHRR and THR but there is a substantial increase in smoke, no doubt due to the presence of styrene in the clay. This system, like that with ATH, has the advantage of an increased organic content which may lead to enhanced mechanical.

It is not possible to melt blend samples that contain more than 40% MDH in the Brabender mixer so these samples were mixed in a twin screw extruder and the results are shown in Table 7 while the heat release rate curves are shown in Figure 9. The best reduction in PHRR, 86%, is obtained for a system that contains 40% PP and 60% MDH and this also shows the best reduction in the total heat released and in mass loss rate. If one replaces 10% of the MDH with COPS clay, the results are almost as good. This corresponds to about 3% inorganic clay, which is a reasonable amount, so it is surprising that the results are not more encouraging.

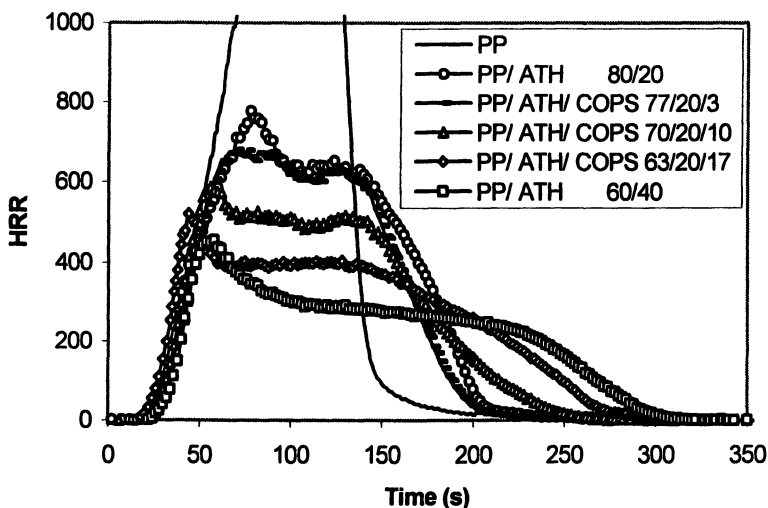


Figure 7. Comparison of the heat release rate (HRR) plots for virgin polypropylene and polypropylene with ATH and their nanocomposites at 50KW/m^2 heat flux.

Table VI. Cone calorimeter data for PP and its MDH composites

PP	MDH	COPS	t_{ign}^a , s	PHRR, ^a Kw/m ² (% reduction)	SEA ^a (m ² /kg)	MLR ^a (g/sm ²)	THR ^a (MJ/m ²)
100	---	---	26±4	1967 ±50	584±20	29.7±0.3	112±9
80	20	---	31±1	1000±50 (49)	664±39	19.4±1.1	98±1
60	40	---	34±1	433±21 (78)	668±33	8.9±1.8	75±5
63	20	17	24±1	476±20 (76)	1123±30	13.5±0.4	70±3

^a t_{ign} , time to ignition; PHRR, peak heat release rate; SEA, specific extinction area, a measure of smoke; MLR, mass loss rate; THR, total heat released.

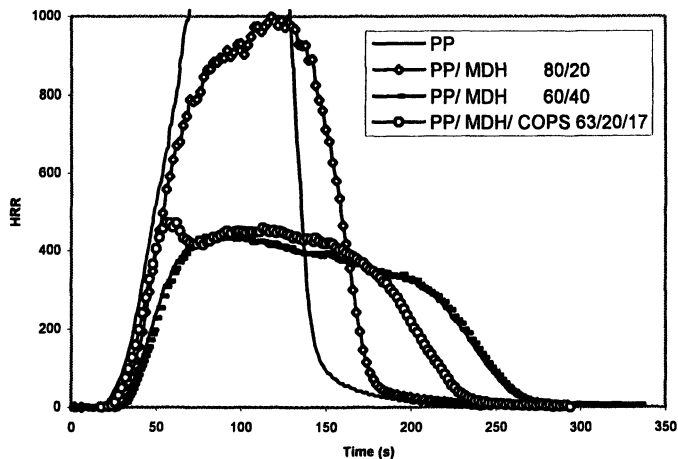


Figure 8. Comparison of the heat release rate (HRR) plots for virgin polypropylene and combinations with MDH and oligomerically-modified clay at 50KW/m² heat flux.

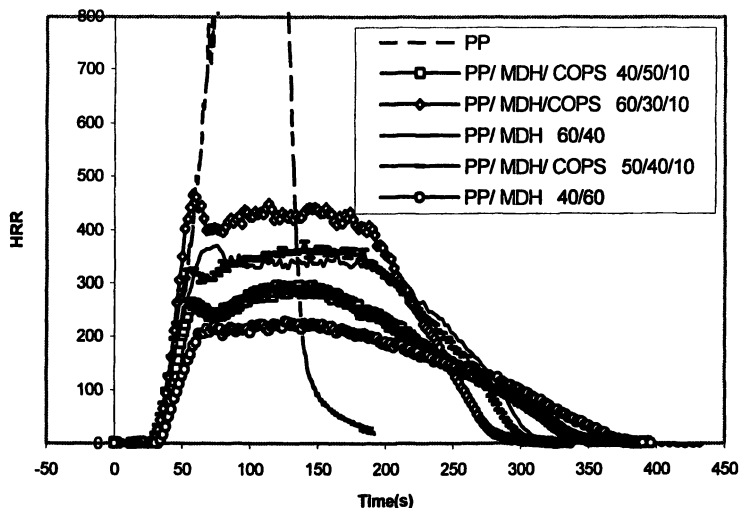


Figure 9. Heat release rate curves for PP-MDH-COPS clay combinations.

Table VII. Cone calorimeter data for PP and its MDH composites

PP	MDH	COPS	t_{ign}^a , s	PHRR, ^a Kw/m ² (% reduction)	SEA ^a (m ² /kg)	MLR ^a (g/sm ²)	THR ^a (MJ/m ²)
100	0	0	30±5	1684 ±155	427±36	34.5±3.5	89±6
60	40	0	3±1	377±16 (78)	529±91	11.5±0.2	71±1
40	60	0	29±3	228±12 (86)	529±91	8.4±0.7	51±1
60	30	10	24±3	471±15 (72)	764±27	13.6±0.3	80±1
50	40	10	23±2	385±9 (77)	757±14	11.7±0.3	69±2
40	50	10	22±4	304±16	765±58	10.0±0.4	59±3

^a t_{ign} , time to ignition; PHRR, peak heat release rate; SEA, specific extinction area, a measure of smoke; MLR, mass loss rate; THR, total heat released.

Tensile properties

In addition to fire properties, tensile properties were also evaluated. The peak stress, modulus and strain at break are listed in Tables IX and X for various systems. The substitution of 20% of the metal hydroxides with 17% COPS causes little change in modulus and there is a slight increase in the strain at break for the ATH system which is not present for MDH.

Table VIII. Comparison of the tensile properties of PP -ATH composites

<i>PP</i>	<i>ATH</i>	<i>COPS</i>	<i>Peak stress (Mpa)</i>	<i>Modulus (Gpa)</i>	<i>Strain at break (%)</i>
80	20	---	30.3	4.2	18.5
60	40	---	25.9	6.0	0.8
63	20	17	25.9	4.8	1.3

Table IX. Comparison of the tensile properties of PP -MDH composites

<i>PP</i>	<i>MDH</i>	<i>COPS</i>	<i>Peak stress (Mpa)</i>	<i>Modulus (Gpa)</i>	<i>Strain at break (%)</i>
80	20	0	26.4	4.8	5.9
60	40	0	22.6	5.8	1.8
63	20	17	26.9	5.7	0.8

Conclusion

Polypropylene nanocomposites can be formed by melt blending the polymer with metal hydroxides and COPS clay. The combination of 20% Al(OH)₃ or Mg(OH)₂ with 5% inorganic clay in polypropylene gives an 80% reduction in PHRR, which is the same reduction that is obtained when 40% Al(OH)₃ or Mg(OH)₂ is used. In the absence of clay, the ATH-containing polymer undergoes degradation at a lower temperature than in the presence of the clay. There is some interaction between the components. Further work is required to optimize the system, but it appears likely that one can devise a fire retardant polypropylene system by the use of metal hydroxides and nanocomposite formation.

References

1. Walter, M. D. *Recent Advances in Flame Retardancy of Polymeric Materials* 1998, 9, 274-285
2. Snyder, C. A. *Plastics Compounding* 1985, 8, 41-3, 45, 4
3. Zhu, J; Morgan, A. B.; Lamelas, F. J.; Wilkie, C. A. *Chem Mater* 2001, 13, 3774-3780.
4. Beyer, G. *Fire Mater.*, 2002, 25, 193-197.
5. Su, S.; Jiang, D. D.; Wilkie, C. A. *Polym. Deg. Stab* 2004, 83, 321-331.
6. Su, S.; Jiang, D. D.; Wilkie, C. A. *Polym. Deg. Stab* 2004, 83, 333-346
7. Gilman, J. W.; Kashiwagi, T.; Nyden, M.; Brown, J. E. T.; Jackson, C.L.; Lomakin, S.; Gianellis, E.P.; Manias, E. in *Chemistry and Technology of Polymer Additives*; Al-Maliaka, S.; Golovoy, A.; Wilkie, C.A., Eds.; Blackwell Scientific: London, 1999; pp. 249-265.
8. J. Zhu, J.; Start, P.; Mauritz, K.A.; Wilkie, C.A.; *J. Polym. Sci., Part A: Polym. Chem.*, 2002, 40, 1498-1503.

Chapter 7

PVC and PVC–VAc Nanocomposites: Negative Effects on Thermal Stability

**Marco Zanetti^{*}, Simona Valesella, Maria Paola Luda,
and Luigi Costa**

**Università degli Studi di Torino, Dipartimento di Chimica IFM,
Via P. Giuria 7, 10125 Torino, Italy**

^{*}Corresponding author: marco.zanetti@unito.it

Polymer layered silicate nanocomposites constitute a new class of materials with unique properties offering new technological and economic opportunities. The organic modification of clay, forming the so-called organoclay, opened the possibility to make nanocomposites with a wide range of polymers. However, in spite of the organic treatment of the clay, preparation of PVC nanocomposite via direct melt compounding still poses many problems due the rather low stability of PVC to the influence of heat. Intercalated PVC/organoclay and PVC-VAc/organoclay nanocomposites were prepared via direct melt compounding. The thermal degradation of PVC nanocomposites was studied in thermogravimetry where it was observed a destabilizing effect.

Polymer layered silicate nanocomposites (PLSN) constitute a new class of materials with unique properties offering new technological and economic opportunities (1,2). In particular, the PLSNs demonstrated to be a promising material as far as the flame retardant. In literature many examples of flame retardant improvements due to the nanoscopic dispersion of clays in thermoplastic polymer are reported. It has been in fact assessed that polymers that normally burn fast without char formation (i.e. PP (3,4), PE (5,6) and EVA(7)) can burn slowly with char formation once they have been transformed in nanocomposites.

It has been evidenced that the mechanism of flame retardant of PLSN acts essentially in condensed phase^{3,7} These papers show that the primary parameter responsible for the lower heat released rate (HRR) of the nanocomposites is the mass loss rate (MLR) during combustion, which is significantly reduced from those values observed for the pure polymer. This is due to the formation on the surface of a char-clay refractory material, which creates a protective shield for the polymer that slows down the flame feeding from the thermal decomposition in the nanocomposite.

In the other hand a similar behavior is well known in the so-called char former polymer such as PVC. Exposed to heat, PVC eliminates the chlorine atoms as HCl forming carbon carbon double bond ordered in polyenic sequences that evolve on heating to aromatized thermally stable charred structures through inter- and intra-molecular Diels-Alder reactions (8). Char forming reactions reduce the fuel feeding the flame and the residue formation creates a shield able to hinder the combustion cycle. In spite of this benefit, the diminishing of PVC flammability through the nanocomposite formation represents an interesting challenge.

The surface modification of clay with onium salt, forming the so-called organoclay, opened the possibility to make nanocomposites with a wide range of polymers. However, the limited thermal stability of alkyl ammonium cations and the processing instability of some polymers such as PVC pose many problems in the nanocomposite preparation via direct melt compounding as recently observed by Wan et al. (9).

In this paper we report our studies on the thermal stability of PVC and PVC-VAc nanocomposites prepared via melt blending with different organoclay. PVC is also one of the most widely used materials in electrical cable construction, especially in its flexible plasticized form, obtained by means of plasticizer. For this reason we studied also the thermal behavior of a flexible PVC formulation, containing epoxidized soybean oil as plasticizer.

The nanocomposite formation has been verified by means of X-ray diffractometry (XRD). The thermal degradation behavior has been studied in thermogravimetry.

Experimental

Materials

The polymers used were ETINOX 630 produced by Aiscondel S.A. (Spain), which is a polyvinylchloride obtained by suspension polymerization, with K-value 65 and SC5710 produced by EVC (Italy), which is a poly(vinylchloride-co-vinylacetate) obtained by suspension polymerization, with K-value 57 and a VAc content of 10.5% wt. The processing additives used for PVC were Naftomix TGRX530, Onepack of lead stabilizer and lubricant produced by Chemson Polymer Additive (Germany), tribasic lead sulphate (TLS) and lubricant Realube RL/105, both produced by Reagens Spa. (Italy). In order to prepare plasticized PVC epoxidized soybean oil (ESO) produced by Reagens S.p.A. Italia and containing 6.2-6.4% of oxiranic oxygen, trade name: Reagens EP/6, has been used.

As nanofiller were used: Somasif ME100, Co-Op Ltd Japan (FH) which is sodium-exchanged fluorohectorite-like synthetic silicate; Somasif MAE, Co-Op Ltd Japan (FH/DT) which is FH exchanged with a dimethyl ditallow ammonium cation (tallow: containing 70, 25, 4, and 1 mol % of C18, C16, C14, and C12 carbon chains, respectively); Cloisite 20A, Southern Clay products Texas (MMT/DT), which is a montmorillonite exchanged with a dimethyl ditallow ammonium cation.

Compounding

PVC/clay composite and PVC/organoclay nanocomposites were prepared via direct melt compounding using a twin-screw extruder MD-30 (Bausano & sons), tailoring the extrusion profile to avoid any thermal degradation of the nanocomposites. The components were first heated to 110 °C in a pre-mixer and then cooled to room temperature. The twin-screw extruder operated with 7 heating zone: 175°C, 170°C, 170°C, 165°C, 175°C, 160°C, 100°C. The mixing time calculated by speed screw (20 R.p.m.) corresponds to 8 min. The characteristics and the names of the materials are illustrated in Table I.

Characterization

The interlayer spacing of the clay was studied by means of wide angle X-ray scattering (WAXS) using a Philips diffractometer with Co K α radiation ($\lambda=0.179$ nm). The WAXS patterns of the thin films of the hybrids were obtained.

The interlayer distance was determined by the diffraction peak, using the Bragg equation.

Thermodegradation was determined on approx. 10 mg samples in a TGA 2950 balance (TA Inc.) with alumina sample pan in a 60 cm³/min nitrogen flow (gas chromatography purity 99.999%) and with a 10°C/min heating ramp. Thermo-oxidation was determined in the same way in 60 cm³/min airflow.

Table I. Characteristics and the names of the materials

<i>Abbreviation</i>	<i>Composition (% wt.)</i>	<i>Type</i>
PVC	ETINOX630 (94.3) + TGRX530 (2.8) + TLS (2.8) + RL/105 (0.1)	Stabilized polymer
PVC/FH	ETINOX630 (90) + FH (4.5) + TGRX530 (2.7) + TLS (2.7) + RL/105 (0.1)	Microcomposite
PVC/FH-DT	ETINOX630 (90) + FH/DT (4.5) + TGRX530 (2.7) + TLS (2.7) + RL/105 (0.1)	Nanocomposite
PVC/MMT-DT	ETINOX630 (90) + MMT/DT (4.5) + TGRX530 (2.7) + TLS (2.7) + RL/105 (0.1)	Nanocomposite
PVC-VAc	SC5710 (94.3) + TGRX530 (2.8) + TLS (2.8) + RL/105 (0.1)	Stabilized polymer
PVC-VAc/FH	SC5710 (90) + FH (4.5) + TGRX530 (2.7) + TLS (2.7) + RL/105 (0.1)	Microcomposite
PVC-VAc/FH-DT	SC5710 (90) + FH/DT (4.5) + TGRX530 (2.7) + TLS (2.7) + RL/105 (0.1)	Nanocomposite
PVC-VAc/MMT-DT	SC5710 (90)+MMT/DT(4.5)+TGRX530 (2.7)+TLS (2.7)+RL/105 (0.1)	Nanocomposite
PVC-ESO	ETINOX630 (73)+ESO(21)+TGRX530(3)+TLS(3) +RL/105 (0.1)	Stabilized and plasticized polymer
PVC-ESO/MMT-DT	ETINOX630 (70) + ESO(20) + MMT-DT (4.5) + TGRX530 (2.7) + TLS (2.7) + RL/105 (0.1)	Nanocomposite

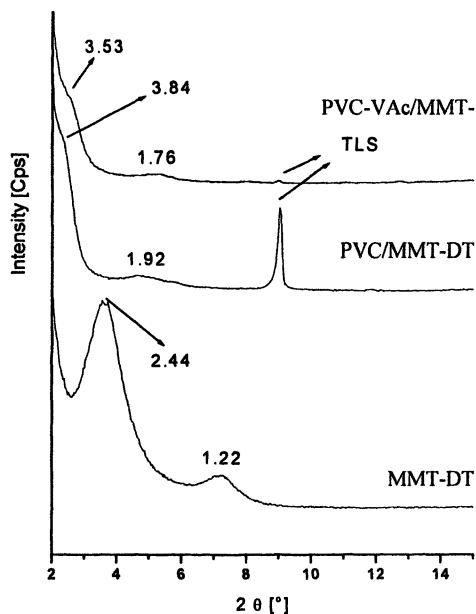


Figure 1. Comparison between the WAXS of MMT-DT with the relative composites, based on PVC (PVC/MMT-DT) and PVC-VAc (PVC-VAc/MMT-DT).

Results and Discussion

Nanocomposite morphology

In figure 1 is reported the comparison between the XRD patterns of MMT-DT, PVC/MMT-DT and PVC-VAc/MMT-DT. Mixing the organoclay with the PVC the d_{001} interlayer spacing is increased from 2.44 nm to 3.84 nm indicating the formation of an intercalated nanocomposite. The peak around $2\theta=9$, corresponding to a d spacing of 0.98 nm, is due to the presence of tribasic lead sulphate (TLS). A smaller interlayer spacing (3.53 nm) was obtained using the PVC-VAc as polymer matrix. The amount of intercalated polymer is reasonably the same and the lower distance between the clay lamina is due to the higher chain flexibility caused by the presence of vinyl acetate pendant group.

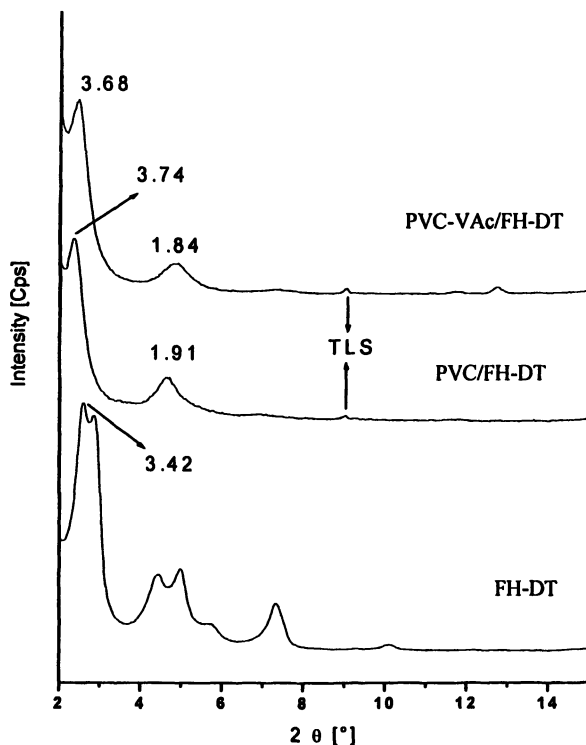


Figure 2. Comparison between the WAXS of FH-DT with the relative composites, based on PVC (PVC/FH-DT) and PVC-VAc (PVC-VAc/FH-DT).

Intercalated nanocomposites were obtained even using FH-DT, as shown in figure 2 where the intercalation was reached with an increasing of the d spacing of the organoclay from 3.42 nm to 3.74 nm and 3.68 nm for PVC and PVC-VAc respectively. In absence of organic treatment the same fluorohectorite was not able to reach the intercalation of the polymers as shown in figure 3. The WAXS pattern of PVC/FH and PVC-VAc/FH show the same peaks of the FH indicating that the silicate dispersed in the polymer matrix retained the stacked structure of the pristine clay. The WAXS of figure 4 indicates the formation of an intercalated nanocomposite even in the case of plasticized PVC. The presence of the plasticizer increased the intercalation grade of the polymer shifting the d_{001} interlayer spacing of the nanocomposite to 4.01 nm.

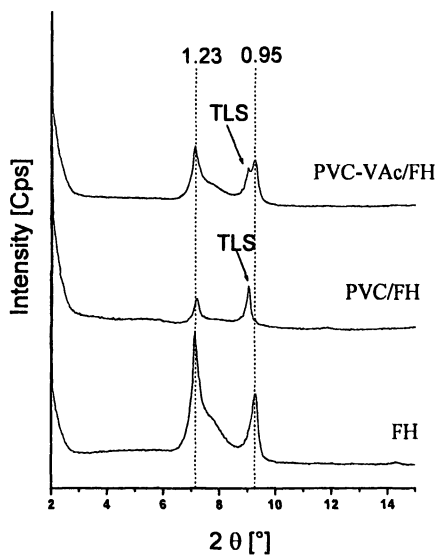


Figure 3. Comparison between the WAXS of FH with the relative composites based on PVC (PVC/FH) and PVC-Vac (PVC-VAc/FH).

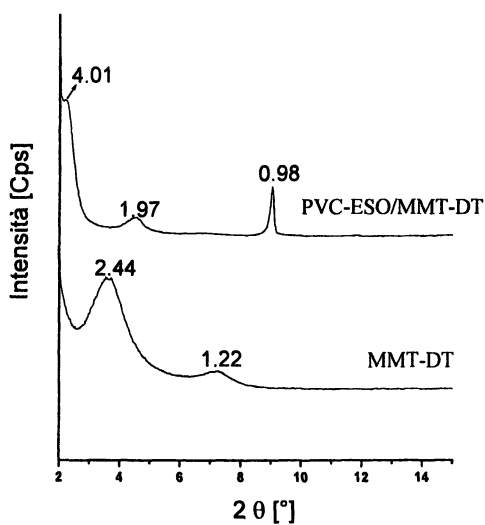


Figure 4. Comparison between the WAXS of MMT-DT and the relative composite with plasticized PVC (PVC-ESO/MMT-DT).

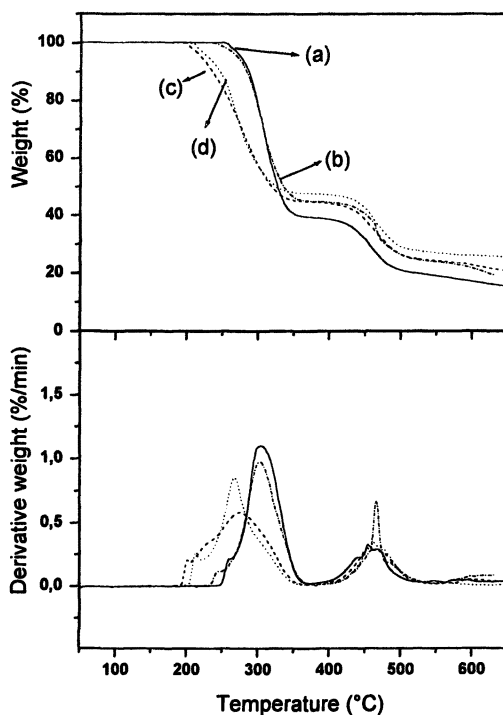


Figure 5. TGA in nitrogen flow of PVC (a), PVC/FH (b), PVC/FH-DT (c) and PVC/MMT-DT (d).

Thermal degradation

In Figure 5 the thermogravimetry curves (TGA) under nitrogen flow of PVC, of the microcomposite (PVC/FH) and of the two nanocomposites (PVC/FH-DT and PVC/MMT-DT) are reported. As can be seen the thermal degradation process takes place with two main weight loss steps. In its earliest stages, the thermal degradation of PVC involves the sequential loss of hydrogen chloride molecules accompanied by the generation of conjugated polyene sequences. The PVC/FH behaves as the pure polymer: the presence of the microdispersed FH did not change the thermal degradation pathway of PVC, with the exception of the amount of residue corresponding to the clay added. In the same figure is possible to see that both nanocomposites shows a strong effect of destabilization reducing of 50°C the onset temperature of HCl elimination. After the complete elimination of HCl (above 305°C) the nanocomposites behaves as the microcomposite. The organic treatment of organoclay exhibits a limited thermal stability, as we observed in a precedent work (10). The thermal decomposition of alkyl ammonium salts is known to take place

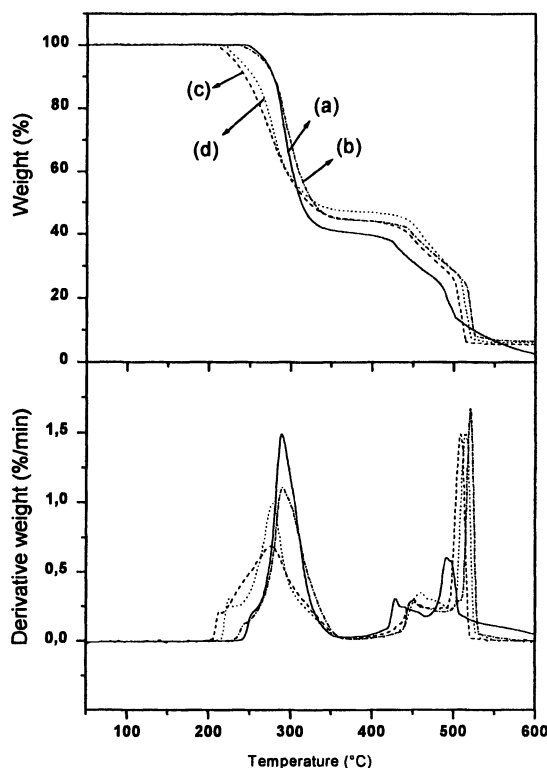


Figure 6. TGA in airflow of PVC (a), PVC/FH (b), PVC/FH-DT (c) and PVC/MMT-DT (d).

with the Hofmann mechanism (11) leading to volatilization of amine and the corresponding olefin. As result strong protonic catalytic sites are created on the layer of the clay. Both radical and molecular mechanisms have been proposed to explain the HCl elimination reaction of PVC as recently reviewed by Starnes (12). It is well known that the thermal degradation is accelerated by the catalytic effect of evolving HCl and by this point of view the protonated sites of the clay layers may act as acidic catalyst able to accelerate the HCl loss.

With the exception of the weight loss at 500°C due to the combustion of the carbonaceous residue, the TGA in air (figure 6) do not show differences with those performed under nitrogen flow. In literature the major effect of thermal stabilization of nanocomposites has been observed in air flow where the organoclay layers demonstrate to be very effective in decreasing the oxidative reaction trough a shielding effect as well enhancing the char form reaction. As observed previously, the negative effects of the organoclay on thermal stability of PVC occur at temperature lower than the thermal oxidation temperature

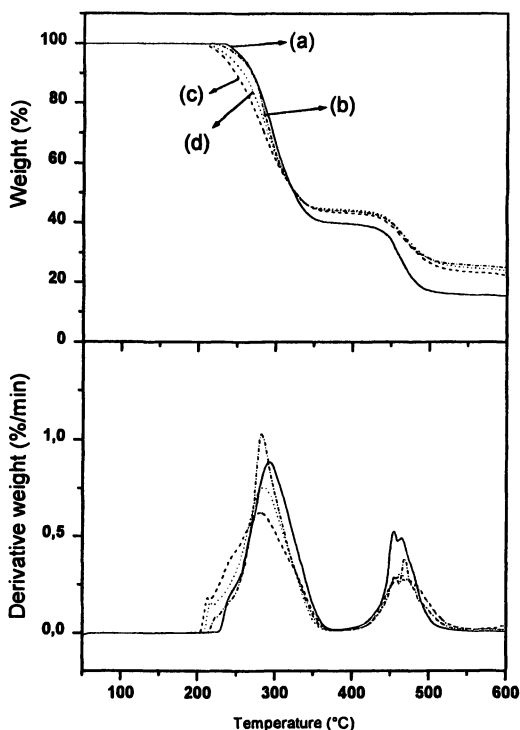


Figure 7. TGA in nitrogen flow of PVC-VA (a), PVC-VA/FH (b), PVC-VA/FH-DT (c) and PVC-VA/MMT-DT (d).

frustrating the possible beneficial effect of the organoclay. There is, indeed, just a minimal effect of stabilization in the nanocomposites above 450°C. This effect is reached even by the microcomposite (PVC/FH).

In Figure 7 the TGA under nitrogen flow of PVC-VAc, of the microcomposite (PVC-VAc/FH) and of the two nanocomposites (PVC-VAc/FH-DT and PVC-VAc/MMT-DT) are reported. The PVC-VAc is characterized by a lower thermal stability if compared with PVC. The electron effect of the chlorine activates the vinyl acetate group enhancing the elimination of acetic acid. As observed in the case of PVC, the microcomposite (curve b) behaves similar to the polymer matrix (curve a) leaving an increased amount of residue corresponding to the silicate added. The nanocomposites show an enhanced thermal instability starting the weight loss at lower temperature than the PVC-VAc. The onset temperatures are located around 200°C and are close to those observed for the PVC nanocomposites (figure 5). Above 305° C the nanocomposites behaves as the microcomposite.

Performing the thermogravimetry under air flow (figure 8) the behavior of copolymer samples is very similar to that observed for the homopolymer

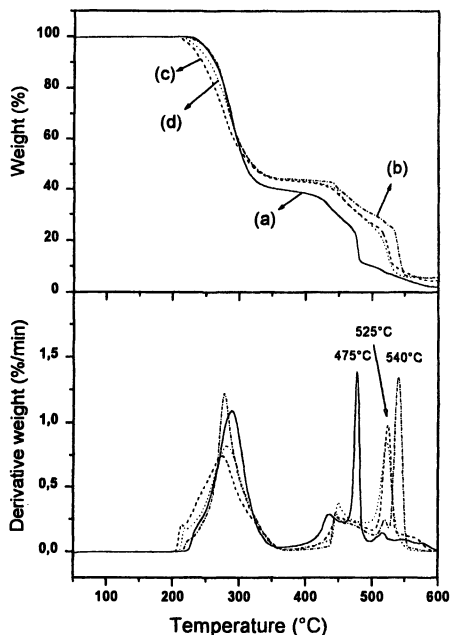


Figure 8. TGA in air flow of PVC-VA (a), PVC-VA/FH (b), PVC-VA/FH-DT (c) and PVC-VA/MMT-DT (d).

samples in the same conditions. Below 400°C the weight loss of all the samples is the same observed under nitrogen flow. Above 450°C all the sample are subjected to the chain breaking as well to combustion phenomena. The combustion is associated to a rapid weight loss evidenced by a sharp peak in the derivative TG curve. PVC-VAc shows the combustion peak at 475°C while the nanocomposites (PVC-VAc/FH-DT and PVC-VA/MMT-DT) show this peak at 525°C, indicating a stabilization effect against the combustion. The microcomposite (PVC-VAc/FH) seems to be even more stable showing a combustion peak at 540°C.

Concerning the plasticized PVC, as can be seen in figure 9, the presence of ESO increased the thermal stability of PVC as indicated by the increasing of the onset temperature from 246°C to 261°C. The formation of an intercalated nanocomposite affected the thermal stability of the polymer diminishing the onset temperature to 240°C that is, however, higher than the onset temperature observed for the PVC and PVC-VAc nanocomposites (220°C). Heating the samples in air flow (figure 10), the behavior of the plasticized PVC nanocomposite as well the plasticized PVC is the same observed in nitrogen flow up to 450°C. Above this temperature the nanocomposite shows a small stabilization effect probably due to the hindered escape of the volatile products caused by the clay layers.

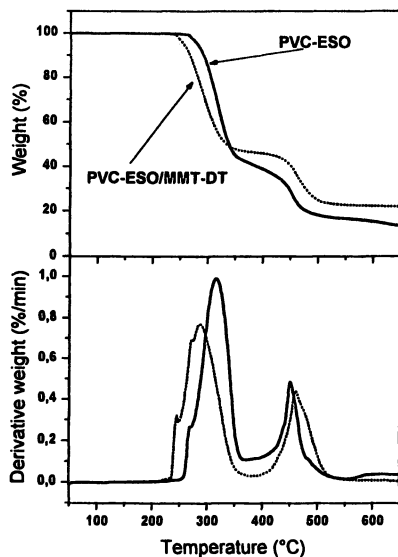


Figure 9. TGA in nitrogen flow of PVC plasticized with soy oil (PVC-ESO) and the plasticized PVC nanocomposite (PVC-ESO/MM-DT)

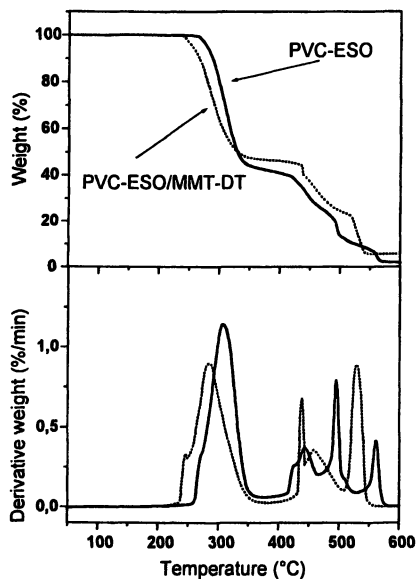


Figure 10. TGA in air flow of PVC plasticized with soy oil (PVC-ESO) and the plasticized PVC nanocomposite (PVC-ESO/MM-DT).

Concerning the plasticized PVC, as can be seen in figure 9, the presence of ESO increased the thermal stability of PVC as indicated by the increasing of the onset temperature from 246°C to 261°C. The formation of an intercalated nanocomposite affected the thermal stability of the polymer diminishing the onset temperature to 240°C that is, however, higher than the onset temperature observed for the PVC and PVC-VAc nanocomposites (220°C). Heating the samples in air flow (figure 10), the behavior of the plasticized PVC nanocomposite as well the plasticized PVC is the same observed in nitrogen flow up to 450°C. Above this temperature the nanocomposite shows a small stabilization effect probably due to the hindered escape of the volatile products caused by the clay layers.

Conclusion

Nanocomposites of PVC, PVC-VAc and plasticized PVC were prepared by melt compounding using a twin-screw extruder. As observed in WAXS analysis all the nanocomposites showed an intercalated morphology while the absence of an organic treatment of the clay did not lead to a nanocomposite formation. A destabilizing effect due to presence of the intercalated organoclay was observed in all cases in thermogravimetry. Polymer layered silicate nanocomposites have been demonstrated to possess enhanced properties compared to the virgin polymers. In the field of flame retardant the benefits of nanocomposites are usually associated to an enhanced stability to thermal oxidation in the temperatures range between 150 and 350°C. This statement seems to be inapplicable to PVC where the formation of a nanocomposite led to a lower thermal stability of the polymer. PVC is a char former polymer and the absence of advantages deriving from nanocomposite formation demonstrate that the improved thermal oxidative stability, observed for other non char former thermoplastic polymer, originates from a chemical effect on the thermo-oxidation pathway of the polymer matrix.

Acknowledgement

Authors wish to thank Mr Eraldo Bausano and Dr. Riccardo Sangiorgio at Bausano & sons for their kind help and use their facilities.

References

- 1 Giannelis, E. P. *Adv. Mater.* **1996**, *8*, 29-35.
- 2 Zanetti, M.; Lomakin, S.; Camino, G. *Macromol. Mater. Eng* **2000**, *279*, 1-9.
- 3 Gilman, J. W.; Jackson, C. L.; Morgan, A. B.; Harris, R.; Manias, E.; Giannelis, E. P.; Wuthenow, M.; Hilton, D.; Phillips, S. H. *Chem. Mater.* **2000**, *12*, 1866-1873.
- 4 Zanetti, M.; Camino, G.; Canavese, D.; Morgan, A. B.; Lamelas, F. J.; Wilkie, C. *Chem. Mater* **2002**, *14*, 189-193.
- 5 Zhang Jinguo; Wilkie, C. A. *Pol Deg Stab* **2003**, *80*, 163-169.
- 6 Zanetti, M.; Costa, L. *Polymer* **2004**, *45*, 4367-4373.
- 7 Zanetti, M.; Kashiwagi, T.; Falqui, L.; Camino, G. *Chem. Mater.* **2002**, *14*, 881-887.
- 8 Starnes, W. H. In *Developments in Polymer Degradation-3*; Barking, Ed.; Applied Science Publisher.: 1981, p 152.
- 9 Wan, C.; Zhang, Y.; Zhang, Y. *Polymer Testing* **2004**, *23*, 299-306.
- 10 Zanetti, M.; Camino, G.; Reichert, P.; Mulhaupt, R. *Macromol Rapid Comm* **2001**, 176-180.
- 11 Jhon March *Advanced Organic Chemistry*; McGraw-Hill Kogakusa Ltd: Tokyo, 1977.
- 12 Starnes Jr. W.H. *Progress in polymer science* **2002**, *27*, 2133-2170.

Chapter 8

Thermal Stability and Fire Behavior of Intumescent Systems in Presence of Layered Inorganic Fillers and Silica

S. Duquesne¹, J. Lefebvre¹, S. Bourbigot¹, R. Delobel²,
and P. Recourt³

¹ Laboratoire Procédés d'Elaboration de Revêtements Fonctionnels (PERF), École Nationale Supérieure de Chimie de Lille (ENSCl)/USTL, B.P 108, F-59652 Villeneuve d'Ascq Cedex, France

² Centre de Recherche et d'Étude sur les Procédés d'Ignifugation des Matériaux (CREPIM), Parc de la Porte Nord, Rue Christophe Colomb, 62700 Bruay-la-Buissière, France

³ Laboratoire Processus et Bilans des Domaines Sédimentaires-UMR 8110-USTL F-59655 Villeneuve d'Ascq Cedex, France

This study focus on the potential synergistic effects that can be achieved by combining inorganic fillers with conventional fire retardants, such as intumescent systems. Modification of the thermal stability of an intumescent formulation by the addition of the fillers is first investigated. Thermal stabilization is observed in the high temperature range and the formation of "ceramic like" structure may be proposed. In the second part, the influence of the nature of the particles on the fire retardant performance is investigated. The best performance is achieved when layered particles (montmorillonite or layered double hydroxide) are used compared to spherical particles (silica), whatever the fire tests. It is assumed that when layered particles are added the char integrity is maintained, leading to better fire performance.

The need for continual improvement in the performance of polymeric materials (thermoplastic, thermoset...) leads to the emergence of new technologies. In the field of flame retardancy, it is necessary to develop fire retardant systems with high efficiency at low content, which are also environmentally friendly. Intumescent systems appear to be good candidates (1). However, to be efficient such systems have to be used at relatively high levels (around 20-30%). As a consequence, synergism in intumescent systems is only now developing. Previous studies demonstrated that the use of zeolite leads to a synergistic effect in intumescent formulations (2). The zeolites are framework silicates consisting of interlocking tetrahedra of SiO_4 and AlO_4 . In the field of silicates, clays, and in particular montmorillonite (MMT), appear as interesting minerals to improve the fire retardant properties of polymers.

Due to the nanoscale of the silicate layers composing the MMT, its incorporation into a polymer matrix could lead to the formation of a nanocomposite, a new generation of materials combining a basic matrix (polymer, ceramic, metal...) and nanofillers (clays, lamellar double hydroxides (LDH), silica, calcium carbonate...). Nanocomposites appear to be an interesting solution, making it possible to combine properties and could thus satisfy the needs for industry as regards new materials (3-5). The use of nanoparticles as the reinforcement phase of a polymeric matrix significantly improves various properties of the materials, particularly their fire retardant properties (6-8). However, in spite of very favorable effects on certain characteristic parameters (decrease in heat release rate, in the velocity of burning, in dripping...), the nanocomposites cannot pass successfully the "trades" tests, such as UL94. Combining the nanofiller with traditional fire retardants, it is possible to improve the properties while decreasing the proportion of the fire retardant (9-11).

The association of intumescent systems with mineral fillers, in particular those dispersable at a nanoscale such as MMT, appears very promising (11-12). In an intumescent system, the reactions that occur between an acid source, a carbonization agent and a blowing agent lead to the formation of an expanded charred layer that insulates the substrate from the heat source (1). In an MMT-polymer nanocomposite, it is usually accepted that the MMT accumulates at the surface with a small amount of carbonaceous char creating a protective surface barrier/insulation layer (13-15).

The investigation of the effects of the nature of the mineral filler on the fire retardant properties of intumescent systems appear particularly interesting. The charred layer developed in an intumescent system mainly comes from the phosphorylation reaction between the hydroxyl group of the carbonaceous agent and the phosphoric acid released from the acid source (16). The hydroxyl groups contained in the clay (in MMT in particular) or in the LDH may contribute to such a reaction and the hydroxyl content of the nanofiller could be a deciding factor. The aspect ratio and the shape of the filler is also an important parameter, since the creation of a tortuous pathway generally leads to good fire retardant

performance (17). Finally, since the dehydration of either MMT or LDH is an endothermic phenomenon, it may also contribute to the fire retardant action.

This study examines the combination of an intumescent system with inorganic fillers in an ethylene vinyl acetate copolymer (EVA) matrix. In a first part, the thermal stability of the minerals, as well as of the intumescent formulations, is investigated. Secondly, the influence of the nature of the filler on the improvement of the fire retardant properties is discussed.

Experimental

Materials

The copolymer used is EVA (ethylene/vinyl acetate copolymer) containing 19wt.-% vinyl acetate (Exxon's Escorene UL0019) hereafter called EVA. Southern Clay Products Inc supplied the montmorillonite, Cloisite 30B (abbreviated notation 30B) for which the negative charges of its layers are compensated with methyl tallow bis(2-hydroxyethyl) ammonium ions. The silica has been provided by Degussa (Aerosil 200, average primary particule size = 12nm, SiO₂ content > 99.8%). The lamellar double hydroxide (abbreviated notation LDH) is prepared by reacting Al(NO₃)₃ with Mg(NO₃)₂, then adding an aqueous NaOH solution followed by aging at 80°C for two days. Exchange of NO₃⁻ with dodecyl sulfate (DS) is carried out at 60°C for 2 days to obtain organically-modified LDH (abbreviated notation LDH-DS). Al(NO₃)₃·9H₂O and Mg(NO₃)₂·6H₂O, sodium dodecyl sulfate (SDS) and NaOH were purchased from the Aldrich Chemical Company and used as received. LDH-DS was characterized by X-ray powder diffraction (Figure 1) and IR spectroscopy (Figure 2).

The X-ray diffraction pattern of LDH-DS shows three diffraction peaks at $2\theta=2.75^\circ$ and $2\theta=5.30^\circ$ (d-spacing = 32.3Å) and $2\theta=12.10^\circ$ (d-spacing = 7.4Å). Two structures are observed: one corresponding to pristine LDH where the galleries are occupied by NO₃⁻ (d-spacing=7.4 Å) (18) and one corresponding to LDH intercalated with DS (d-spacing = 32.3Å) (19). The FTIR spectra of LDH and LDH-DS confirm those results. They show a broad absorption band around 3500cm⁻¹ attributed to O-H stretching of the hydroxyl groups of LDH. A strong absorption in the spectrum of LDH-DS at 1384cm⁻¹ demonstrates that DS has not exchanged all the nitrate ions. However, bands in the range 1250-1100cm⁻¹, attributed to sulfate, and 3000-2850cm⁻¹, attributed to C-H stretching, demonstrate that DS partially substitutes NO₃⁻ ions. The band centred at 1000cm⁻¹ may also be attributed to DS (Figure 3). The shift between the bands of SDS and LDH-DS may be attributed to modification of the coordination of intercalated sulfate (20).

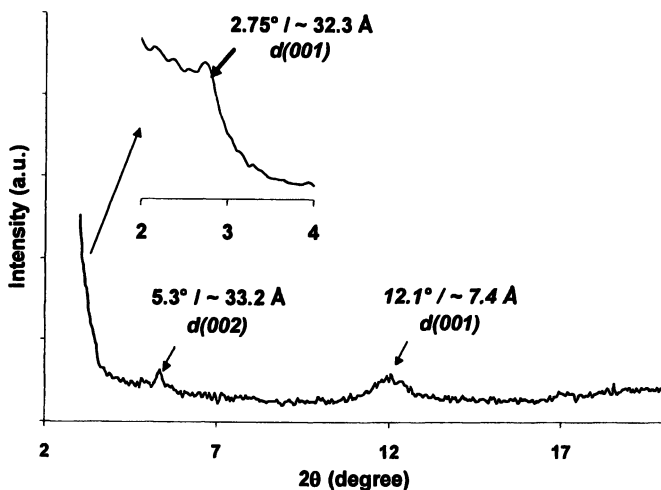


Figure 1: XRD pattern of LDH-DS.

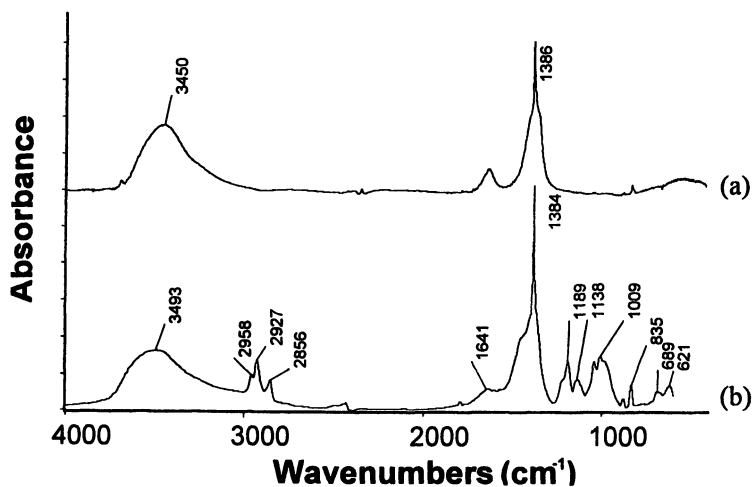


Figure 2: FTIR spectra of LDH (a) and LDH-DS (b).

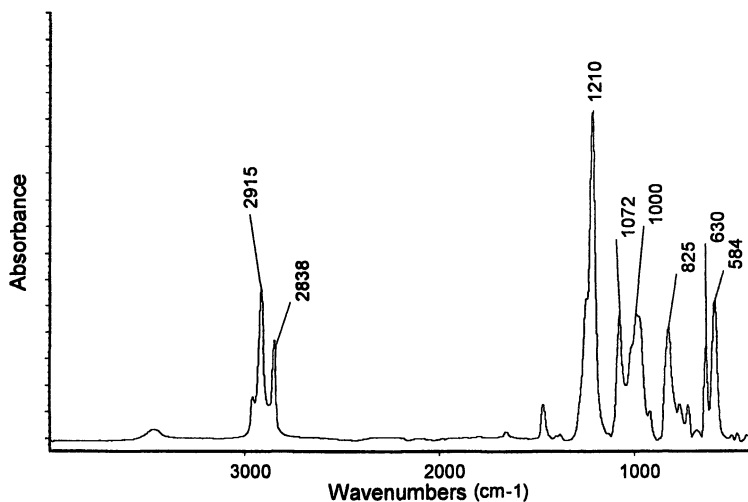


Figure 3: FTIR spectra of SDS.

The intumescent system is a mixture of ammonium polyphosphate (APP supplied by Clariant – Exolit AP422) and polyamide 6 supplied by Nyltech (PA-6).

Methods:

Formulations (Table I) were mixed at 230°C using Brabender mixer. Sheets were then obtained using a Daragon pressing machine.

Table I: Composition of the formulations.

Name	Nanofiller	%EVA	%APP	%PA6	%Nanofiller
REF	-	60	33.3	6.7	0
F-30B	30B	57.1	33.3	6.4	3.2
F-A200	A200	57.1	33.3	6.4	3.2
F-LDH-DS	LDH-SD	57.1	33.3	6.4	3.2

Thermal analyses were performed on powdery material using a Setaram MTB 10-8 thermobalance under gas flow at heating rate 10°C/min (from 20 to 800°C). LOI was measured using a Stanton Redcroft instrument on specimens (100x10x3 mm³) according to the standard ‘oxygen index’ test (ASTM D2863/77). The UL-94 tests were carried out on 100x13x1.6 mm³ specimens according to the American National Standard UL-94 (Test for flammability of plastics materials for part in devices and appliance, Underwriter laboratories,

Northbook, ANSI/ASTM D-635/77). The heat rate release (HRR) is measured using oxygen consumption calorimetry (samples were exposed to a Stanton Redcroft Cone Calorimeter according to ASTM 1356-90 and ISO 5660 under a heat flux of 50 kW/m² which corresponds to the evolved heat before the flashover). The cone calorimeter is also used to determine the following principal fire properties: total heat release (THR), time to ignition, total CO and CO₂ emission and total smoke release. All experiments were repeated 3 times and the values are considered to be reproducible to within $\pm 10\%$.

Results and Discussion

Thermal stability of the nanofillers

The thermal stability of the fillers is compared in Figure 4. The thermal degradation of the organically-modified montmorillonite (Cloisite 30B) takes place in two major steps in the temperature range 200-800°C. Several phenomena overlap in the temperature range 200-400°C. The thermal degradation of 30B is attributed to the thermal desorption and thermal decomposition of the organic ion, combined with a rearrangement of the intercalated chains of the organoclay (21). The thermal decomposition is assumed to take place by the Hofmann mechanism (22) for the interlayer cations as well as for the physisorbed cations. However, it is generally assumed that degradation of the free surfactant occurs at slightly lower temperature than the surfactant located between the silicate layers. Moreover, the interlayer water in the smectite structure is removed below 350°C.

These phenomena lead to the collapse of the interlayer structure, accompanied by a significant decrease in the interlayer spacing, a migration of interlayer cations and new charge balance schemes in interlayer structure. In the higher temperature range ($T > 500^\circ\text{C}$), the degradation is attributed to dehydroxylation and phase transformations which occur in most smectites (23).

The thermal degradation of LDH-DS occurs in three main steps. In the first step of degradation, 50-110°C, physically absorbed and interlayer water is lost (24). The dehydroxylation of LDH sheets occur in the temperature range 230-470°C (25). The decomposition of the dodecyl sulfate takes place in the temperature range 290-460°C.

The thermogravimetric curve of silica shows only one degradation step between 30-140°C, attributed to loss of absorbed water (26).

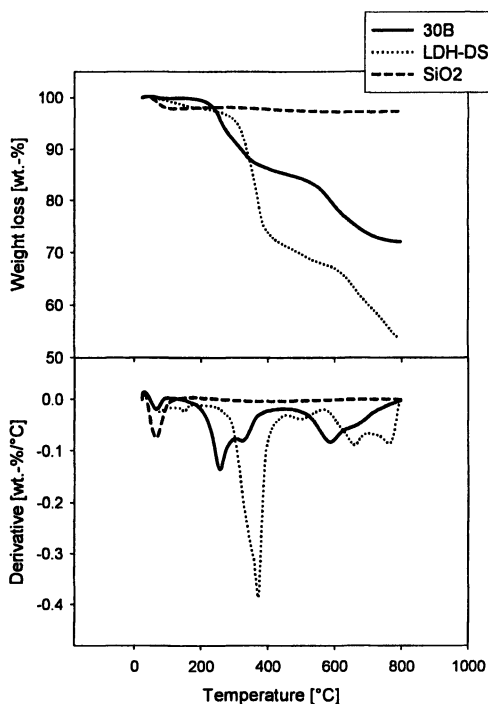


Figure 4: TG curves of the nanofillers.

Thermal stability of the intumescent formulations.

The thermogravimetric curves of the intumescent formulations are compared in Figure 5. Whatever the formulation, the mechanism of degradation can be described as a four steps mechanism.

TGA curves of the intumescent formulations containing the fillers are similar to those of the reference from ambient temperature up to 480°C. In this temperature range, three steps of degradation are observed. The first, between 250 and 400°C, may be attributed to the deacetylation of the EVA matrix leading to the formation of unsaturated carbon-carbon bonds along the polymer chain (27). At the same time, the thermal degradation of the ammonium polyphosphate begins. In the temperature range 420–480°C, two degradation steps overlap. These two steps lead to the formation of carbonaceous residues of around 35wt.% for the reference and F-LDH-DS and around 40wt.% for F-30B and F-A200. They result from phosphorylation reactions (12) between the polymer or its degradation products (either EVA or nylon) and the additives, leading to the formation of a phosphocarbonaceous material. The amount of

residue for F-30B and F-A200 is higher than the mineral content added in the formulation (around 2.2% for 30B and 3.2% for A200). As a consequence, it may be assumed that the particles interact in the formulation and lead to the thermal stabilization of the systems. In a previous study (12) dealing with the use of polyamide 6 nanocomposite (commercial grade supplied by UBE, Japan) as the char forming agent in a similar intumescent formulations, it has been shown that the montmorillonite allowed the thermal stabilization of the phosphocarbonaceous structure.

In the high temperature range, 480-800°C for F-30B and F-A200 and 600-800°C for F-LDH-DS, an important stabilization of the system is observed (between 15 and 20wt.% compared with the reference). This cannot be attributed to the mineral content. A reaction occurs between the mineral particles and the intumescent system. In this range of temperature, it may be assumed that a ceramic like structure is formed from a reaction between the mineral (SiO_2 ,

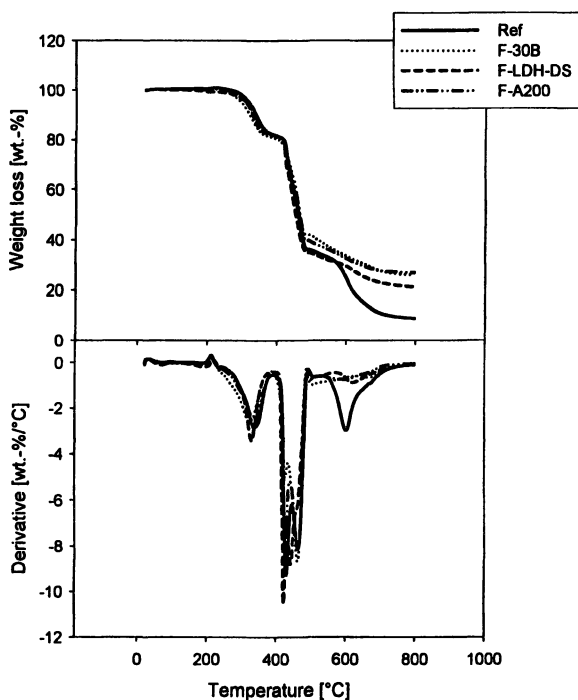


Figure 5: Thermogravimetric curves of the intumescent formulations

Al₂O₃, MgO ...) and the phosphate (1,12). However, analytical data is needed to identify further these structures.

Fire performance of the intumescent formulations.

The fire retardant performance of the intumescent formulations is reported in Table II. An intumescent phenomenon is observed whatever the materials. The fire retardant performance of the intumescent systems containing a layered inorganic filler (MMT or LDH) is higher than that of the reference. In particular, the use of 30B leads to a UL94 V-0 rating and to an increase in the oxygen index at 4 vol.%. The fire retardant performance is lower when LDH is used in comparison with 30B but further investigations are needed to compare these systems. The addition of silica to the intumescent system leads to a dramatic decrease in the fire retardant performance, which is opposite to what was found by Wei et al. (28), where a synergistic effect was observed for low silica loading (1-4wt.%) while an antagonist effect is observed for high loadings (>6wt.%). However, in this study the carbon source is pentaerythritol and the total additive amount is lower (30wt.%). Under the UL94 protocol, the sample burns totally after the first flame application, while, for the reference, the sample never burns totally but a high combustion time leads to non-classification (NC).

Table II: Fire retardant performance of the intumescent formulations.

	REF	F-30B	F-LDH-DS	F-A200
Maximum after flame time (sec)	60	4	28	>60
Total after flame time for 5 specimens (sec)	126	15	60	-
Flaming drops	Yes	No	Yes	Yes
Time before first drop (sec)	1	-	5	20
UL-94 rating	NC	V0	V2	NC
LOI (vol.-%)	28±1	32 ±1	29 ±1	26 ±1

The change in the flammability properties of the intumescent system by addition of silica or of layered nanoparticles can be partially explained. The addition of mineral particles, of whatever kind, in EVA leads to a sharp increase in the viscosity of the material as demonstrated by the increase in the time before the first drip and by the observation of the sample after the UL-94 tests (Figure 6).

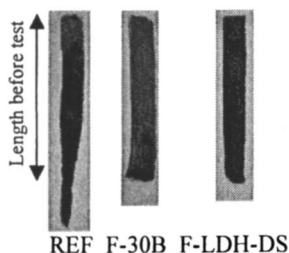


Figure 6: Samples after UL94 tests

The increase in viscosity is particularly high for the silica containing material. In that case, the heat cannot be removed by dripping, which maintains the combustion triangle (heat, fuel, air) and as a consequence the test samples totally burn. In the case of layered inorganic fillers, competitive phenomenon occur leading to an increase in the flame retardancy of the intumescent system. The viscosity of the burning F-30B and F-LDH-DS increase as in the case of A-200, however in these cases, it is reasonable to assume that the mechanical stability of the char is improved since the aspect ratio of 30B or LDH-DS is very high compared to A200, which increases the rigidity of the intumescent shield. Higher mechanical stability of the intumescent shield avoids the formation of cracks (29) and so the heat and mass transfer are limited, leading to interruption of the combustion triangle. This assumption will be confirmed by the cone calorimeter measurements and the data is presented in *Table III* and in Figure 7.

Table III: Cone calorimeter data of the intumescent formulations

	REF	F-30B	F-LDH-DS	F-A200
Peak HRR t1 (kW/m ²)	267	270	233	336
Peak HRR t2 (kW/m ²)	299	202	284	261
Total heat release (MJ/m ²)	68	69	74	68
Time to ignition (sec)	36	76	44	61
Total CO emission (kg/kg)	0.04	0.03	0.03	0.03
Total CO ₂ emission (kg/kg)	2.0	2.2	2.1	1.8
Total smoke release (-)	1422	1392	1367	1407

Whatever the formulations, the HRR versus time curve shows two peaks, the first before 200 sec (t1) and a second between 300 sec (REF) and 500sec (F-30B), which is the typical behavior of intumescent systems.

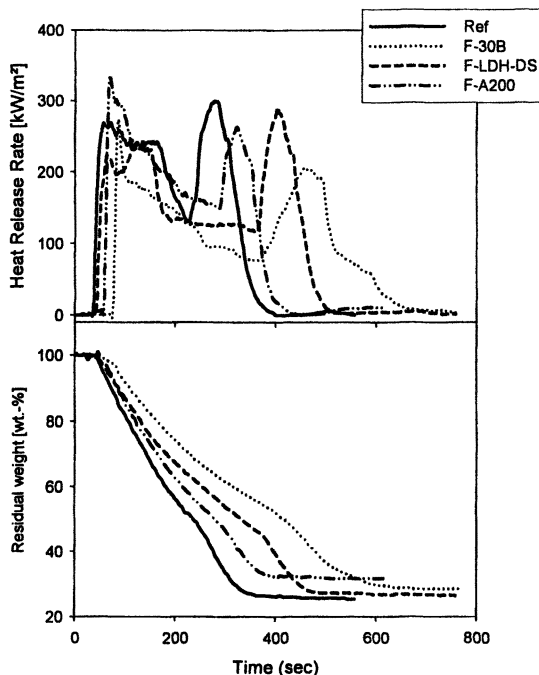


Figure 7: Heat Release Rate and Weight Loss Curves of the intumescent formulations.

The first peak is attributed to the formation of the intumescent protective shield that leads to a decrease of heat and mass transfer between the flame and the material. When this shield is formed, the HRR decreases and a plateau is in some cases observed. The second peak corresponds to the destruction of the intumescent layer leading to a sharp emission of flammable gases, the higher the time for the second peak, the higher the thermal and mechanical stability of the intumescent shield. Then, a thermally stable residue is formed (around 30% of the initial mass of the sample).

When Cloisite 30B is added to the intumescent system, the first peak HRR is narrower. However, its value is similar to that of the reference and an increase in the time to ignition is observed. The second peak heat release is sharply reduced (decrease of 30% when compare to the reference) and occurs around 200 sec later. The weight loss occurs in two steps for REF and F-30B but the curve for F-30B is shifted towards higher time. The CO, CO₂ and smoke emission are not affected by the presence of MMT within the intumescent system. Those results demonstrate that the formation of the intumescent shield is modified when 30B is

added to EVA/APP/PA6 and that the intumescent shield which is formed is thermally and/or mechanically more stable.

The F-LDH-DS material shows a decrease in the first peak HRR (decrease in 12% compared to the reference) and a delay in the second peak (around 150 sec). The other parameters are not affected by the presence of the mineral filler. Finally, the addition of silica to the intumescent system leads to a sharp increase in the first peak HRR (26% compared to the reference) demonstrating a decrease in the fire performance when using this mineral.

The delay of the second peak HRR when inorganic particules are used in the intumescent system confirms that the thermal (as demonstrated in the high temperature range of the TGA experiments) and the mechanical stability of the intumescent shield is increased.

Conclusion

This study demonstrates the potential synergistic effects that can be achieved when layered inorganic fillers are combined with an intumescent system. It may reasonably be accepted that the increase in the fire performance is due to an increase in the thermal and mechanical stability of the intumescent shield. The fire performance decreases when using silica particles, whereas the thermal stability of the formulation increases in the high temperature range, similar to the formulation containing the layered particle. Further analyses are needed to determine if the assumed increase in the mechanical stability is only attributed to a physical reinforcement and/or if the chemistry of those systems play a crucial role as well.

References

1. Bourbigot, S.; Le Bras, M.; Duquesne, S.; Rochery, *Macromol. Mater. Eng.* **2004**, *289*, 499-511.
2. Bourbigot, S.; Le Bras, M.; Delobel, R.; Tremillon, J.M. *J. Chem. Soc., Faraday Trans.* **1996**, *92*, 3435-3444.
3. Alexandre, M.; Dubois, P. *Mater. Sci. Eng. R*: **2000**, *R28*, 1-63.
4. Ray, S.S.; Okamoto, M. *Prog. Polym. Sci.* **2003**, *28*, 1539-1641.
5. Utracki, L.A. *Clay-containing polymeric nanocomposites*; Rapra Technology Limited: Shropshire, UK, 2004.
6. Giannelis, E.P. *Annual Technical Conference - Society of Plastics Engineers*. **1996**, *54th(Vol. 3)*, 2998-3003.
7. Gilman, J.W.; Kashiwagi, T.; Lichtenhan, J.D. *International SAMPE Symposium and Exhibition*. **1997**, *42(Evolving Technologies for the Competitive Edge, Book 2)*, 1078-1089.
8. Gilman, J.W. *App. Clay Sci.* **1999**, *15*, 31-49.

9. Chigwada, G.; Jiang, D.D.; Wilkie, C.A. *Polym. Mater. Sci. Eng.* **2004**, *91*, 156-157.
10. Beyer, G. In *Proc. Conf. Recent Adv. Flame Retardancy Polym. Mater. Stamford, CT*, **2001**.
11. Duquesne, S.; Jama, C.; Delobel, R.; Le Bras, M. In *Proc Conf. Additives 2003*. San Francisco, CA, **2003**.
12. Bourbigot, S.; LeBras, M.; Dabrowski, F.; Gilman, J.W.; Kashiwagi, T. *Fire Mater.* **2000**, *24*, 201-208.
13. Gilman, J.W.; Kashiwagi, T.; Giannelis, E.P.; Manias, E.; Lomakin, S.; Lichtenhan, J.D.; Jones, P. In: *Fire Retardancy of Polymers: The use of intumescence*; Le Bras, M.; Camino, G.; Bourbigot, S.; Delobel, R., Eds.; The Royal Society of Chemistry: Cambridge, UK, **1998**; pp 203-221.
14. Kashiwagi, T.; Harris, R.H.; Zhang, X.; Briber, R.M.; Cipriano, B.H.; Raghavan, S.R.; Awad, W.H.; Shields, J.R. *Polymer* **2004**, *45*, 881-891.
15. Lewin, M. *Fire Mater.* **2003**, *27*, 1-7.
16. Delobel, R.; Ouassou, N.; Le Bras, M.; Leroy, J.M. *Polym. Degrad. Stab.* **1989**, *23*, 349-357.
17. Zanetti, M.; Kashiwagi, T.; Falqui, L.; Camino, G. *Chem. Mater.* **2002**, *14*, 881-887.
18. Villegas, J.C.; Giraldo, O.H.; Laubernds, K.; Suib, S.L. *Inorg. Chem.*, **2003**, *42*, 5621-5631.
19. Zhao, H.; Nagy, K.L. *J. Coll. Interface Sci.* **2004**, *274*, 613-624.
20. Bubniak, G.A.; Schreiner, W.H.; Mattoso, N.; Wypych, F. *Langmuir*, **2002**, *18*, 5967-5970.
21. Lee, J.W.; Lim, Y.T.; Park, O.O. *Polym. Bull.* **2000**, *45*, 191-198.
22. Zanetti, M.; Camino, G.; Reichert, P.; Mülhaupt, R. *Macromol. Rapid Commun.* **2001**, *22*, 176-180.
23. Gu, B.X.; Wang, L.M.; Minc, L.D.; Ewing, R.C. *J. Nuc. Mater.* **2001**, *297*, 345-354.
24. Wang, J.; Wei, M.; Rao, G.; Evans, D.G.; Duan, X. *J. Solid State Chem.* **2004**, *177*, 366-371.
25. Yang, W.; Kim, Y.; Liu, P.K.T.; Sahimi, M.; Tsotsis T.T. *Chem. Eng. Sci.* **2002**, *57*, 2945-2953.
26. Wang, L.; Wang, Z.; Yang, H.; Yang, G. *Mater. Chem. Phy.* **1999**, *57*, 260-263.
27. Le Bras, M.; Bourbigot, S.; Siat, C.; Delobel, R. In: *Fire Retardancy of Polymers: The use of intumescence*; Le Bras, M.; Camino, G.; Bourbigot,

- S.; Delobel, R., Eds.; The Royal Society of Chemistry: Cambridge, UK, 1998; pp 266-279.
28. Wei, P.; Hao, J.; Du, J.; Han, Z.; Wang, J. *J. Fire Sci.* **2003**, *21*, 17-28
29. Duquesne, S.; Delobel, R.; Le Bras, M.; Camino, G. *Polym. Degrad. Stab.* **2002**, *77*, 333-344.

Chapter 9

Fire Retardancy of Polystyrene Nanocomposites Using Naphthenate-Containing Clays

Grace Chigwada, David D. Jiang, and Charles A. Wilkie

Department of Chemistry, Marquette University, P.O. Box 1881,
Milwaukee, WI 53201-1881

Polystyrene (PS) clay nanocomposites have been prepared both by bulk polymerization and melt blending (MB) processes using naphthenate-containing (Np) organically-modified clays. The number of alkyl chains was varied from 1-3 and the dispersion of the clay in the polymer was determined both by X-ray diffraction (XRD) and transmission electron microscopy (TEM). Thermal stability was probed by thermogravimetric analysis (TGA) and the fire properties were evaluated using the cone calorimeter. As the number of long alkyl chains on the ammonium cation increases, it becomes more difficult for polymer to enter the gallery space and one cannot obtain good nano-dispersion and the fire retardancy is not enhanced.

Polymer clay nanocomposites have attracted substantial attention over the past few decades because they possess superior physical and mechanical properties compared to the virgin polymer or microcomposites (1). Since the discovery by Toyota scientists in the 1980s that a clay loading as low as 5% can result in enhanced chemical and physical properties in polyamide-6-nanocomposites (2), considerable work has been done with other polymer systems and these have shown increased modulus (3,4), reduced gas permeability (5,6,7), improved heat distortion temperature (1), and reduced flammability (7,8,9,10,11).

For nanocomposite formation to be effective in reducing the flammability of the polymer, there is need for the clay to be well dispersed in the polymer matrix. This is made possible by modification of the clay to impart organophilicity. This modification is achieved via cationic exchange reactions between the naturally occurring alkali metal cations residing between the aluminosilicate layers and alkyl ammonium surfactants. While ammonium is the most common cation that is used, other onium salts, such as stibonium (12), tropylium (13) and phosphonium (1,14), have also been used.

From much of the work that has been done to date, it is at times difficult to obtain good nano-dispersion of the clay in the polymer. In order to improve the dispersion, the inorganic clay has also been organically-modified using of an oligomeric-containing cation. This was achieved by using oligomers of styrene (15), methyl methacrylate (15,16) and other polymers (17,18,19). These oligomerically-modified clays offered a significant improvement in thermal stability and fire retardancy.

In this work we investigate how increasing the number of long alkyl chains and the presence of a naphthenate (Np) group affects the nano-dispersion, and hence the fire retardancy, of polystyrene (PS) for samples prepared both by bulk polymerization and melt blending.

Experimental

Materials. The majority of chemicals used in the study, including 1-chloromethyl naphthenate, benzyl bromide, styrene, polystyrene, methanol, ethanol, tetrahydrofuran (THF), N, N dimethyl hexadecylamine, didecyl methyl amine, trilaurylamine, and benzyl peroxide (BPO), were obtained from the Aldrich Chemical Company. Montmorillonite was kindly provided by Southern Clay Products, Inc.

Instrumentation. X-ray diffraction (XRD) measurements were performed using a Rigaku powder diffractometer with a Cu tube source ($\lambda=1.54\text{\AA}$); generator tension was 50 kV at a current of 20 mA. Scans were taken from $2\theta = 1.0 - 10$, step size = 0.1 and scan time per step of 10s using the high-resolution mode. Bright field transmission electron microscopy (TEM) images were

obtained at 60 kV with a Zeiss 10c electron microscope. The samples were ultramicrotomed with a diamond knife on a Rigchert-Jung Ultra-Cut E microtome at room temperature to give ~70nm thick section. The sections were transferred from the knife-edge to 600 hexagonal mesh Cu grids. Thermogravimetric analysis, TGA, was performed on a Cahn unit under a flowing nitrogen atmosphere at a scan rate of 20 °C per minute from 20 °C to 600 °C. All TGA experiments have been done in triplicate; the reproducibility of temperature is ± 3 °C while amount of nonvolatile residue is reproducible to $\pm 2\%$. Cone calorimeter measurements at 35kWm^{-2} were performed using an Atlas Cone 2; the spark was continuous until the sample ignited. All samples were run in triplicate and the average value is reported; results from cone calorimeter are generally considered to be reproducible to $\pm 10\%$ (20).

Preparation on Naphthenate Np salt. In a 250 mL round-bottomed flask was placed 5.0 g (28 mmol) of 1-(chloromethyl)naphthenate in 100 mL methanol, then 9.1 g (34 mmol) of dimethylhexadecylamine was gradually added with magnetic stirring. The solution was stirred at 50-60 °C for several hours. The solvent was then evaporated at 70 °C, giving an off-white solid. ^1H NMR CDCl_3 : δ 8.728-8.700 (d, $J=8.4$ 1H), δ 7.980-7.842 (m, 3H), δ 7.704-7.653 (t, $J=7.8$ 1H), δ 7.538-7.439 (m, 2H), δ 5.745 (s, 2H), δ 3.345 (s, 6H), δ 1.791-1.723 (p, 2H), δ 1.432-1.301 (b, 28H), δ 0.903-0.853 (t, $J=6.6$ 2H).

Preparation of methyl-Naphthenatedidecylmethylammonium salt NpDD. In a 250 mL round-bottomed flask was placed 5.0 g (28 mmol) of 1-(chloromethyl)naphthenate in 100 mL ethanol, then 8.83 g (28.3 mmol) didecylmethylamine was added to the solution with stirring. The solution was then refluxed for 48 hrs, followed by cooling to room temperature. The solvent was then removed under vacuum, leaving the product as a white solid. ^1H NMR, CDCl_3 : δ 8.628-8.657 (d, $J=8.7$ 1H), δ 7.975-7.87 (m, 3H), δ 7.737-7.686 (t, $J=7.5$ 1H), δ 7.574-7.487 (m, 2H), δ 5.582 (s, 2H), δ 3.760-3.689 (q, $J_1=7.2$, $J_2=14.1$ 4H), δ 3.223 (s, 3H) δ 1.138- δ 1.374 (m, 32H), δ 0.862 - 0.906 (t $J=6.3$ 6H).

Preparation of NpTL and BTL Salts. In a 100 mL round-bottomed flask was placed 2.5 g (29 mmol) of benzyl bromide in 40mL anhydrous ethanol. To this solution was added 7.68 g (29.4 mmol) of trilaurylamine. The solution was refluxed for 96 hrs, followed by cooling to room temperature. The solvent was evaporated under vacuum, leaving a yellowish white solid. The solid was recrystallized from ether. ^1H NMR, CDCl_3 : δ 7.60-7.4 (m, 5H), δ 4.92 (s, 2H), δ 3.92-3.21 (t $J=213$ 6H), δ 1.20-1.39 (m, 60H), δ 0.8-0.93 (t $J=39$ 9H). The same procedure was used with 1-(chloromethyl) naphthenate in place of bromobenzene.

Modification of the clay. The ammonium salts prepared above were dissolved in 100ml of THF while the clay was dispersed in 200ml of 2:1 water:THF solution. These were combined and stirred at RT for 24 hours,

followed by filtration and continuous washing with water until no chloride ion was evident, testing with a silver nitrate solution.

Preparation of Nanocomposites. Both bulk polymerization and melt blending processes were utilized for the preparation of nanocomposites, following the procedures outlined in the literature (8,21,14).

Results and Discussion

Four different ammonium salts, which contain one naphthenate or benzene group, and with either one, two or three other long chains have been prepared and used to make new organically-modified clays. The structures of these ammonium salts are shown in Figure 1.

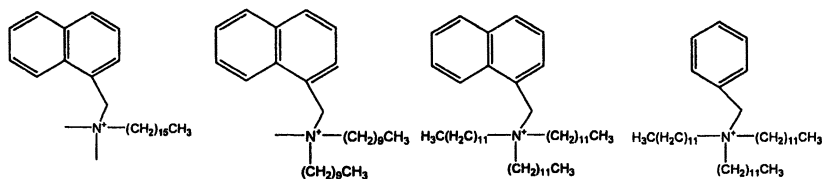


Figure 1. Structures of the naphthenate-containing ammonium salts; these are referred to herein as Np, NpDD, NpTL and BTL (from left to right)

X-Ray diffraction (XRD)

XRD enables one to determine the distance between the clay layers, using the Bragg equation. As the distance increases, the value of 2θ will decrease. The results for all of the clays and their polystyrene nanocomposites are shown in Table I; Figure 2 shows a representative set of XRD traces for the collection of the nanocomposites prepared using the organically-modified clays.

For nanocomposites prepared using Np modified clay, it is interesting to note that both bulk and blending processes result in the formation of samples with lower 2θ values than the original clay. The fact that a peak is observed for samples prepared by melt blending shows that the presence of a Np group has a significant effect, since it has been shown that nanocomposites prepared by melt blending using an organically modified clays containing a single long alkyl chain do not show formation of an intercalated system (20). On the other hand increasing the number of the alkyl long chains does not seem to enhance the d-spacing between the clay layers. This may be attributable to crowding in the gallery space as the number of long chains increases, which can be verified by TEM.

Table I. XRD data for the clays and their polystyrene nanocomposites.

<i>Sample</i>	2θ	<i>d-spacing, nm</i>
10A clay	4.3	2.1
Np clay	3.7	2.4
BTL clay	3.1	2.9
NpTL clay	3.3	2.7
NpDD clay	3.7	2.4
PS+1%Np clay, Bulk	2.7	3.3
PS+3%Np clay, Bulk	2.7	3.3
PS+5%Np clay, Bulk	2.4	3.7
PS+7%Np clay, Bulk	2.6	3.4
PS+1%Np clay, MB	2.7	3.3
PS+3%Np clay, MB	2.6	3.4
PS+5%Np clay, MB	2.6	3.4
PS+10%Np clay, MB	2.7	3.3
PS+1%NpDD clay Bulk	3.1	2.9
PS+3% NpDD clay, Bulk	3.2	2.8
PS+5% NpDD clay, Bulk	3.1	2.9
PS+3%NpDD clay, MB	4.4	2.0
PS+5% NpDD clay, MB	4.4	2.0
PS+10% NpDD clay, MB	4.3	2.1
PS+3%BTL clay, MB	3.2	2.8
PS+3%BTL clay, Bulk	3.0	3.0
PS+5%BTL clay, MB	3.3	2.7
PS+3%NpTL clay, MB	3.6	2.5

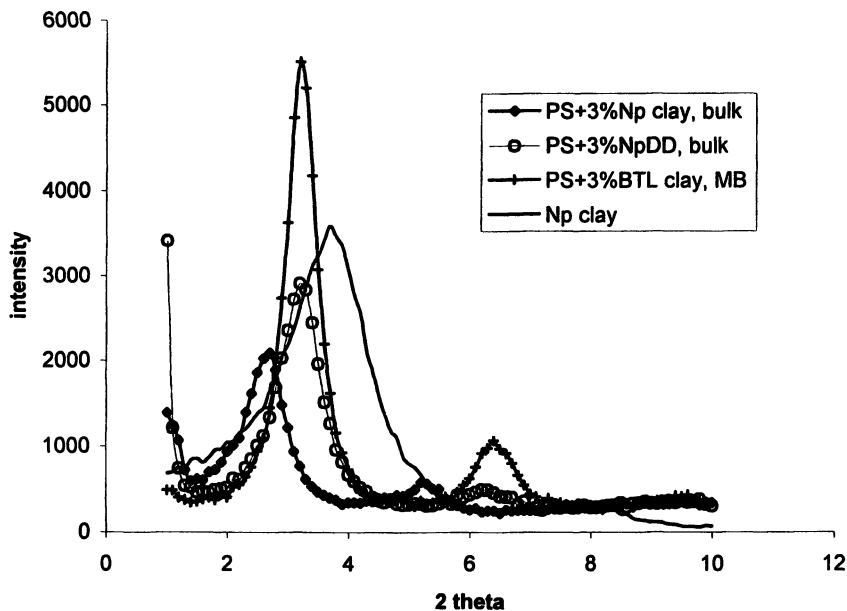


Figure 2. XRD traces for PS-Np clay nanocomposites by bulk polymerization

Transmission electron microscopy (TEM)

The dispersion of the polymer within the clay is evaluated by TEM. Two images are usually required, the low magnification image provides information on the quality of the nano-dispersion, *i.e.*, is it a microcomposite or a nanocomposite, while the high magnification image enables one to determine if intercalation or delamination has occurred. In general, one can say that the nano-dispersion is much better for systems that have been bulk polymerized rather than melt blended. The only melt blended system that exhibits good nano-dispersion is the naphthenate salt with a single long chain, which agrees with the XRD data. The nano-dispersion is quite good and intercalated systems are obvious for both the clays that contain either one or two long chains, but this is not the case where three long chains are present. Representative TEM images of the Np and the NpDD clay are shown in Figures 3 and 4, respectively, while Figure 5 shows the TEM image of the Np clay prepared by melt blending and showing good nano-dispersion.

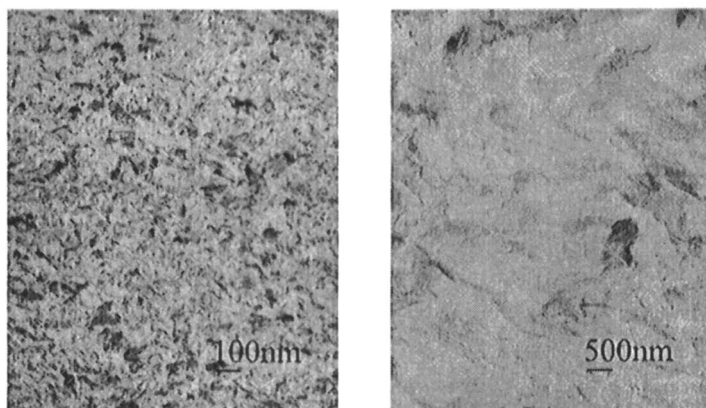


Figure 3. TEM images at high (right) and low (left) magnification for PS/Np clay nanocomposites prepared by bulk polymerization.

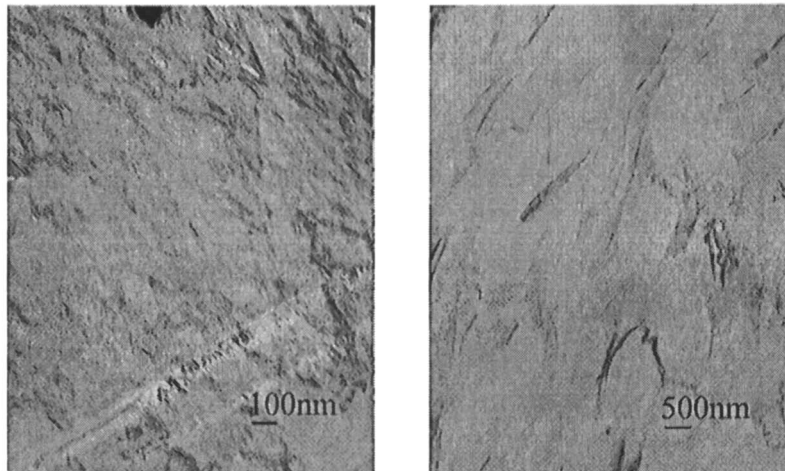


Figure 4. TEM images at high (right) and low (left) magnification for PS + 3% NpDD clay nanocomposites prepared by bulk polymerization

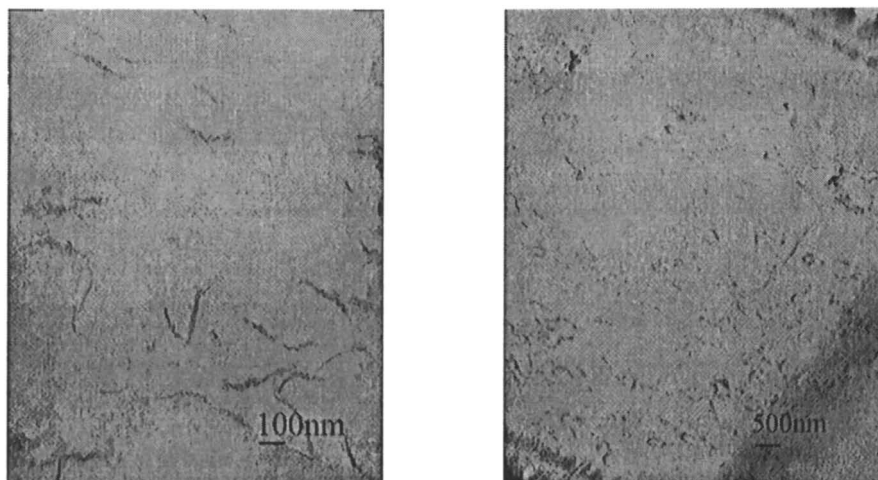


Figure 5. TEM images at high (right) and low (left) magnification for PS/Np clay nanocomposites prepared by melt blending.

Thermogravimetric analysis

The thermogravimetric analysis data for the naphthenate-containing organically-modified clays and the nanocomposites prepared by bulk polymerization and melt blending is shown in Table II for all of the clays. The data reported include the onset temperature of degradation, as measured by temperature at which 10% of the sample is lost, T_{10} , the mid-point of degradation, T_{50} , another measure of thermal stability, and the fraction of the non-volatile residue remaining at 600 °C, denoted as char. For polystyrene nanocomposites, both the onset temperature and the mid-point temperature usually increase by about 50 °C. The organically-modified clays undergo thermal degradation by a Hofmann elimination reaction that commences at about 200 °C for the typical commercially available clays. These clays show the same onset temperature; these are not any more thermally stable than commercial clays. The residue from the clay alone is in the range of 62 – 72%, the more long chains the greater is the organic content of the clay and thus the lower is the inorganic content.

For the nanocomposites it is clear that in the presence of Np modified clay, a clay with a single long chain, the onset and 50% degradation temperatures are higher than those of the virgin polymer for samples prepared both by bulk polymerization and melt blending. For the NpDD, NpTLC and BTLC both the

initial and 50% degradation temperatures are decreased. This is surprising in the case of the cation that contains two long chains, because evidence from XRD and TEM support good nano-dispersion in this case, and may be due to the presence of excess organic material. We generalize to say that an increase in the number of long chains on the cation is not promising for enhanced thermal stability.

Table II. TGA data for polystyrene nanocomposites.

<i>Sample</i>	<i>T10</i>	<i>T50</i>	<i>%Char</i>
Commercial PS	412	445	0
10A clay	282	-	62
Np clay	289	-	63
NpDD clay	240	-	72
PS+1%Np-clay bulk	417	453	1
PS+3%Np-clay bulk	426	464	2
PS+5%Np-clay bulk	419	462	4
PS+1%Np-clay M.B	421	457	3
PS+3%Np-clay M.B	422	458	4
PS+5%Np-clay M.B	421	459	6
PS+10%Np-clay M.B	421	462	9
PS+1%NpDD-clay bulk	315	415	1
PS+3%NpDD-clay bulk	338	431	6
PS+5%NpDD-clay bulk	341	438	6
PS+3%NpDD-clay M.B	395	438	3
PS+5%NpDD-clay M.B	393	439	5
PS+10%NpDD-clay M.B	400	444	9
BTL clay	317	-	57
PS+3%BTL clay, MB	395	436	5
PS+5%BTL clay, MB	386	432	4
PS+3%BTL clay, Bulk	230	433	7
NpTL clay	335	-	56
PS+3% NpTL clay, MB	392	433	5

Cone calorimetry

The parameters that may be evaluated from cone calorimetry include the heat release rate, the time to ignition and the time to peak heat release rate, specific extinction area (SEA), a measure of smoke and the mass loss rate. One

of the parameters that has been given special attention in flame retardancy is the peak heat release rate, PHRR as this gives the information about the size of the fire. In literature it has been shown that nanocomposite formation gives rise to the maximum reduction in PHRR while a microcomposite gives little or no reduction. The magnitude of the reduction is very polymer dependent; the usual reduction for polystyrene systems is in the range of 50 – 60%. The time to ignition is a measure of how easy it is to ignite the material, and nanocomposites typically give a shorter time to ignition than does the virgin polymer. The decrease in peak heat release rate is usually associated with a decrease in the mass loss rate while the total heat released is usually unchanged, indicating that ultimately everything will burn. The cone calorimetric data for all of the styrene systems is collected in Table III while representative heat release curves for a few systems are shown in Figures 6 to 8. It is obvious that bulk polymerization gives a much better reduction in PHRR than does melt blending. It is also clear that one long chain is better than either two or three, which are about the same, for a reduction in the peak heat release rate. The most reasonable suggestion is that the presence of multiple long chains occupies too much of the gallery space and does not leave room for the polymer to enter this space.

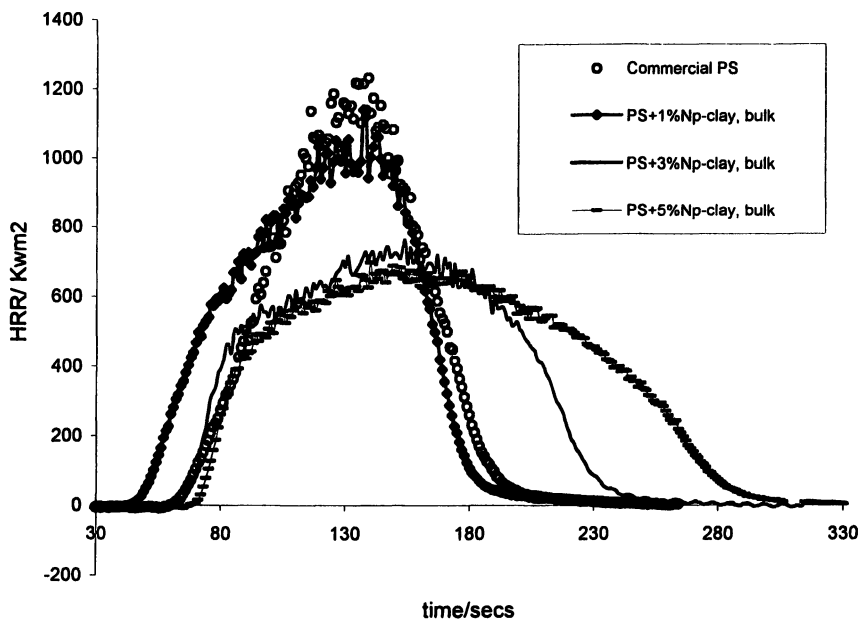


Figure 6. Heat release rate curves for bulk polymerized styrene nanocomposites of the Np clay

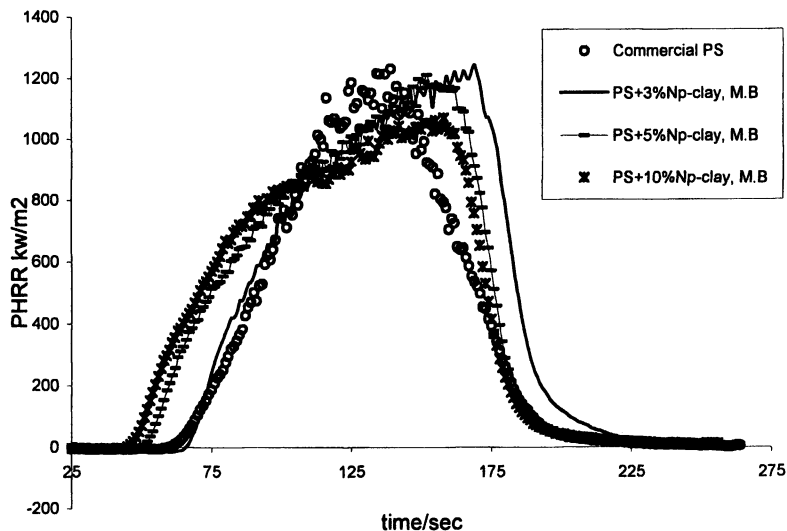


Figure 7. Heat release rate curves for melt blended polystyrene in the presence of the Np clay.

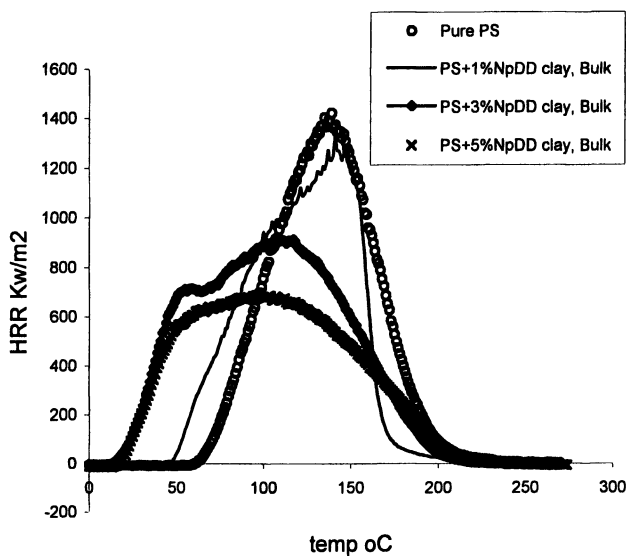


Figure 8. Heat release rate curves for bulk polymerized styrene with the NpDD clay.

Table III. Cone calorimetric data for polystyrene nanocomposites

<i>Sample</i>	<i>t_{ign}^a s</i>	<i>PHRR^a Kw/m² (% reduction)</i>	<i>THR^a MJ/m²</i>	<i>MLR^a g/sm²</i>	<i>SEA^a m²/kg</i>
Commercial PS	61±3	1338±142	95±2	24±3	1203±54
PS+1%Np-clay, bulk	41±3	1110±90 (17)	89±3	24±1	1198±1
PS+3%Np-clay, bulk	62±2	807±118 (40)	92±7	19±1	1356±73
PS+5%Np-clay, bulk	60±7	675±38 (50)	97±4	16±1	1411±89
PS+7%Np-clay, bulk	62±4	754±34 (44)	92±3	16±1	1443±84
PS+3%Np-clay, M.B	56±7	1255±23	99±5	23±1	1284±271
PS+5%Np-clay, M.B	50±3	1299±124	101±4	24±1	1166±47
PS+10%Np-clay, M.B	47±4	1082±31 (19)	99±1	23±1	1251±5
PS + 1% NpDD, bulk	16±5	1571±98	109±9	21±3	1386±50
PS+3% NpDD, bulk	15±3	887±141 (40)	90±23	16±1	1543±26
PS+5% NpDD, bulk	21±6	725±49 (51)	89±4	15±1	1543±26
PS+3% NpDD, MB	43±3	1299±147	112±3	21±2	1420±172
PS+5% NpDD, MB	44±1	1315±181 (12)	97±3	20±1	1283±72
PS+10%NpDD, MB	37±7	1064±44 (28)	97±3	20±1	1420±144
PS+3%BTL, bulk	15±2	852±85	92±4	17±1	1569±75
PS+3%BTL, MB	56±4	982±90	90±2	21±1	1413±87
PS+3% NpTL, MB	49±3	1076±88	94±3	21±1	1229±77

^a *t_{ign}*, time to ignition; PHRR, peak heat release rate; THR, total heat released; MLR, mass loss rate; SEA, specific extinction area, a measure of smoke.

Conclusion

From this study it has been shown that the presence of a naphthenate group on the cation of the clay can help to achieve good nano-dispersion by a melt blending process, even when only one long chain is present on the cation, which is unlike the situation with other organically-modified clays. Since fire retardancy follows along with good nano-dispersion, this permits enhanced fire retardancy for polystyrene nanocomposites. In general, nano-dispersion is achieved more easily by bulk polymerization than by melt blending. As one increases the number of long chains attached to the cation, the possibility of the polymer entering the gallery space is decreased.

Acknowledgement

A portion of this work has been performed under the sponsorship of the Office of Naval Research under grant number N00014-03-1-0172 and their support is gratefully acknowledged.

References

1. Xie, W.; Xie, R.; Pan W-P.; Hunter, D.; Koene, B.; Tan, L-S.; Vaia, R. *Chem. Mater.*, **2002**, 14, 4837-4845.
2. Kojima, Y.; Usuki, A.; Kawasumi, M.; Okada, A.; Fukushima, Y.; Kurauchi, T.; Kamigaito, O. *J. Mater Res*, **1993**, 8, 1185-1189.
3. Messersmith, P.B.; Giannelis, E.P. *Chem Mater*. **1994**, 6, 1719-1725.
4. Lan, T.; Pinnavaia, T.J. *Chem Mater*. **1994**, 6, 216-219.
5. Yano, K.; Usuki, A.; Kamigaito, O. *J. Polym. Sci.; Part A: Polym. Chem.* **1993**, 31, 2493-2498.
6. Yano, K.; Usuki, A.; Okada, A. *J. Polym. Sci.; Part A: Polym. Chem.* **1997**, 35, 2289-2294.
7. Messersmith, P.B.; Giannelis, E.P. *J. Polym. Sci.; Part A: Polym. Chem.* **1995**, 33, 1047-1057.
8. Zhu, J.; Morgan, A.B.; Lamelas, F.J.; Wilkie, C.A. *Chem. Mater.* **2001**, 13, 3774-3780.
9. Gilman, J.W.; Jackson, C.L.; Morgan, A.B.; Harris, R., Jr.; Manias, E.; Giannelis, E.P.; Wuternow, M.; Hilton, D.; Phillips, S.H. *Chem. Mater.* **2000**, 12, 1866-1873.

10. Pinnavia, T, J . *Chem. Mater.* **2002**, 14, 4088-4095.
11. Zhu, J.; Wilkie, C. A. *Polym. Int.* **2000**, 49, 1158-1163.
12. Wang, D.; Wilkie, C. A. *Polym. Degrad. Stab.* **2002**, 82, 309-315.
13. Zhang, J.; Wilkie, C. A. *Polym. Degrad. Stab.* **2004**, 83, 301-307
14. Zheng, X and Wilkie, C.A, *Polym.Degrad.Stab.***2003**, 81, 539-550.
15. Su, S.; Jiang, D.D.; Wilkie, C.A. *Polym. Degrad. Stab.*, **2004**, 83, 321-331
16. Su, S.; Jiang, D.D.; Wilkie, C.A. *Polym. Degrad. Stab.*, **2004**, 83, 333-346
17. Su, S.; Jiang, D.D.; Wilkie, C.A. *Polym. Degrad. Stab.*, **2004**, 84, 279-288
18. Su, S.; Jiang, D.D.; Wilkie, C.A. *J. Vinyl Add. Tech.*, **2004**, 10, 44-51
19. Zheng, X and Wilkie, C.A, *Polym.Degrad.Stab.***2003**, 82, 441-450
20. Gilman J.W.; Kashiwagi, T.; Nyden, M.; Brown, J.E.T.; Jackson, C.L.; Lomakin, S. in *Chemistry and Technology of Polymer Additives*, Eds. Al-Maliaka, S.; Golovoy, A.; Wilkie, C.A. London Blackwell Scientific; **1999**, pp. 249-265
21. Wang, D.; Zhu, J.; Yao, Q.; Wilkie, C.A. *Chem. Mater.*, **2002**, 14, 3837-3843.

Chapter 10

Effect of Interfaces in Metal Hydroxide-Type and Intumescent Flame Retarded Nanocomposites

Gy. Marosi, S. Keszei, Sz. Matkó, and Gy. Bertalan

Department of Organic Chemical Technology, Budapest University
of Technology and Economics, Budapest, Hungary

Multipurpose interfacial structure of (reactive) surfactant and thermally adaptive elastomer layers have been formed. Interlayer of reactive surfactants may serve for good dispersion and chemical coupling in EVA systems, containing $\text{Mg}(\text{OH})_2$ and clay. The distribution of nanoparticles could be determined by micro Raman technique even in presence of ~50% $\text{Mg}(\text{OH})_2$. Use of activating/deactivating interphase is a versatile way to match the action of flame retardant to the degradation profile of the polymer. Increase of the viscosity in the temperature range of 390-470°C by modification of the interphase has a strong influence on the fire retardancy. In intumescent PP system, a boroxosiloxane based adaptive interphase protects the additive during processing, while at higher temperature delivers it to the surface and then holds the reinforcing nanoparticles in the char together. Combination of a polysiloxane interphase with an “expandable nanocomposite” structure resulted in the lowest RHR value.

Polymer composites require **chemical and mechanical compatibilization**. Both can be performed by appropriate **multilayer interphase (IP)** according to a concept proposed earlier (1). Chemical compatibilization is achieved by thin layers of surfactant or coupling agent (2,3), while a thicker macromolecular (elastomer) interlayer may release the local stresses in the interfacial zone (mechanical compatibilization) (4). Further progress was achieved by introducing **grafted elastomers** and **reactive surfactants** (5-7). Reactive surfactants have two functional groups (for reacting with both phases) and exhibit amphiphilic character (for absorbing at interfaces preferably).

In the field of flame retardancy only a few papers paid attention to the interfaces until the appearance of nanocomposites (8,9). **Nanocomposite** technologies adapted the use of surfactants, multilayer IP (introducing maleic anhydride grafted macromolecular interlayer) (10,11) and reactive surfactants (such as vinylbenzyl dodecyl dimethylammonium chloride) (12).

Simplification is, however, characteristic of most of the works dealing with nanostructured FR polymers: importance of compatibility is pronounced without considering the special IP requirements of fire retardancy. Thus most of the IP modifiers proposed for nanoparticles strive only for the better dispersion. In montmorillonite (MMT) containing FR systems, for example, cationic surfactants, increasing the extent of exfoliation, are applied universally. It is not clarified; however, exactly which (exfoliated, intercalated or tactoid) structure is the most advantageous for certain FR systems. More conscious IP design is needed for optimization of FR performance. This paper tries to contribute to the clarification of this picture, considering all the surface related aspects of flame retardancy.

Experimental

Ethylene-vinyl acetate copolymer (EVA) IBUCCELL K 100 with VA content of 28% (H.B. Fuller); polypropylene (PP) Tipplen H535 type, density: 0.9 g/cm³, melt index: 4 g/10 min at 21.6 N, 230°C (product of TVK Co. Hungary); non-modified Na-montmorillonite (MMT), Microtec (Eurotrade Ltd. Hungary); organophilic montmorillonite, Bentone SD-1 (OMM), coated with long chain alkyl amine (Rheox. Inc.); polybutene/polysiloxane intercalated OMM (IMM), laboratory product, prepared by solvent method; magnesium hydroxide (Mg(OH)₂) (Dead Sea Bromine Group) were investigated. Two types of intumescent system were applied one consisting of ammonium polyphosphate (APP, Exolit AP 422, Clariant, Germany) and polyol (POL, pentaerythritol, Aldrich) in a ratio of 3:1, the other contained a APP and a phosphorylated polyol char forming component. *Polyboroxosiloxane* (BSil) elastomer was prepared in our laboratory according to a process described earlier (7,13). The total amount of the additives in intumescent PP was 30%, including 2% MMT and/or BSil.

The compounds were prepared in a Plasti Corder PL2000 internal-mixer (Brabender) at a rotor speed of 180 rpm, at 180°C, in 10 min. Sheets (120x120x2mm) were obtained by compression moulding using Collin P 200 E type laboratory press at 180°C and a pressure of 5 MPa. Rheological data were collected by AR 2000 Thermal Scanning Rheometer (TA Instruments) in a parallel plate configuration. The samples of 25x25x2 mm size were heated from 130 to 550°C at a heating rate of 15°C/min at 8Hz frequency. Raman imaging was performed by a LabRam type confocal Raman microscope (Jobin Yvon, France). The excitation source was a frequency doubled Nd-YAG laser emitting at 532nm. Chemical imaging by scanning electron microscope was performed in a JEOL JSM-5500 LV system equipped with IXRF type energy-dispersive X-ray analyzer (EDX). X-ray diffraction (XRD) analysis was carried out using Philips PW 1050 model diffractometer with CuK α radiation. Fire resistance was characterized by Cone calorimeter (Stanton Redcroft, ASTM E1354-04, heat flux of 50 kW/m², sample surface area: 100 cm², Al tray of 10 X 10 X 0.3 cm size, replicate samples:3, CV:3%, exhaust gas flow: 0.024m³/s), UL 94 (ASTM D-635/77) and Limiting Oxygen Index measurements (LOI, ASTM D 2863).

Results and Discussions

Examples of the IP types being advantageous in FR systems are taken from our recent work, referring also to the available relevant papers in the literature.

Dispersing, Coupling Interphases

Inclusions of high surface energy tend to interact with each other, forming aggregates in polymer composites. In FR polymer systems aluminium/magnesium hydroxides and nanoparticles represent high surface area for such interactions either because of the high concentration of the additives or because of their high specific surface area. The submicron particles can be hardly dispersed without interfacial modification excepting some nanoparticles of low surface energy such as nanotubes, which exhibit good dispersion without using any organic treatment (14) Reactive coupling, used to enhance the adhesion between the phases, can be achieved with coupling agents (such as alkoxy silanes), which, however, generally do not exhibit surface active character. Therefore we prefer to use reactive surfactants in order to combine the coupling and surfactant functions (15). Various types have been synthesised by means of Diels-Alder reaction or by esterification (7). Dienophile compounds, e.g. maleic anhydride, was used as reaction partners to the Diels-Alder reaction. One example is shown in Figure 1, which shows also the Raman spectroscopic monitoring of the reaction.

The most characteristic change in course of the reaction is the decrease of the band at 1658 cm^{-1} belonging to the $\nu(\text{C}=\text{C})$ vibration of the unsaturated fatty acid. (The $\nu(\text{C}=\text{C})$ vibration of maleic anhydride was detected at 1637 cm^{-1}) At the beginning of the reaction the small peak at 1854 cm^{-1} indicates the dissolution of MAA, which disappears as the reaction proceeds.

Such reactive surfactant has been used in various FR composites. For example it proved to be suitable to improve the processability of ATH filled PP at lower temperature and reduce the dripping at higher temperature (16). Reactive surfactant was used for achieving coupling at the interfaces also in intumescent FR polypropylene system reinforced with natural fibres (17).

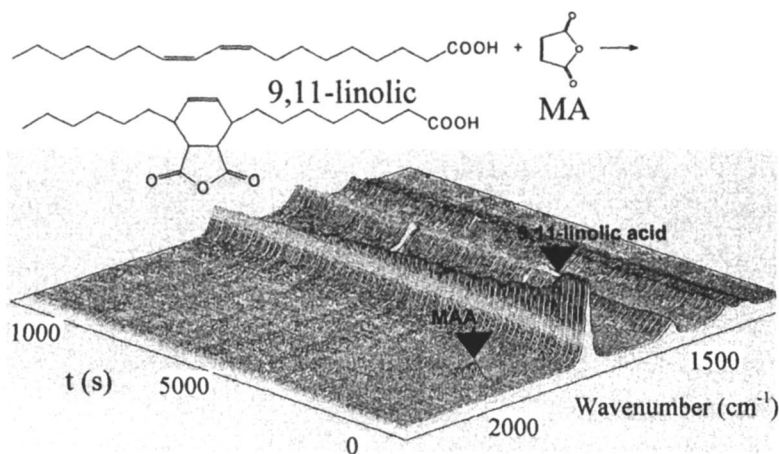


Figure 1. Synthesis of reactive surfactant and its Raman spectroscopic monitoring

Elastomer Interphases

Elastomer IP, proposed first in CaCO_3 filled PP, was an apolar compatibilizing layer (18). Later CaCO_3 with a silicon elastomer was found to act as FR additive in ethylene-acrylate copolymer (19). Factors affecting the elastomer IP formation during the compounding process are: ratios of melting temperatures, viscosities and polarities of the polymer components (20).

Comparing to other elastomers we found better flame retardancy in PP when polysiloxane elastomer IP was applied (8). Based on this knowledge we introduced polysiloxane elastomer between the galleries of MMT resulting in elastomer intercalated MMT (IMM). This was combined with $\text{Mg}(\text{OH})_2$ in a system having the following composition: EVA: $\text{Mg}(\text{OH})_2$:IMMT (of 8:8:1

weight ratio). A great challenge was to examine the distribution of nanoparticles in such a highly filled system because in presence of ~50% magnesium hydroxide the position of the minor amount of the layered silicate might be masked. Raman imaging was tried for this purpose since the individual components can be distinguished from each other based on their characteristic chemical structure. The distribution of silicate layers in highly filled polymer compound can be well demonstrated by the Raman mapping (Figure 2). In Figure 2 the bright areas represent the distribution and size of the non-modified and various modified MMT particles in the polymer matrix (no shading effect of the $\text{Mg}(\text{OH})_2$ occurs). In the EVA- $\text{Mg}(\text{OH})_2$ -MMT compound (Figure 2/a), large size (~20 μm) of the non-modified MMT agglomerates could be well observed. Fine dispersion of OMM of EVA- $\text{Mg}(\text{OH})_2$ -OMM compound can be observed in Figure 2/b. The image of the EVA- $\text{Mg}(\text{OH})_2$ -IMM compound is shown in Figure 2/c. The dispersion is also fine but less uniform than in the compound containing the OMM. According to XRD results similar arrangement of the compared MMT types occurs in EVA without $\text{Mg}(\text{OH})_2$ (21).

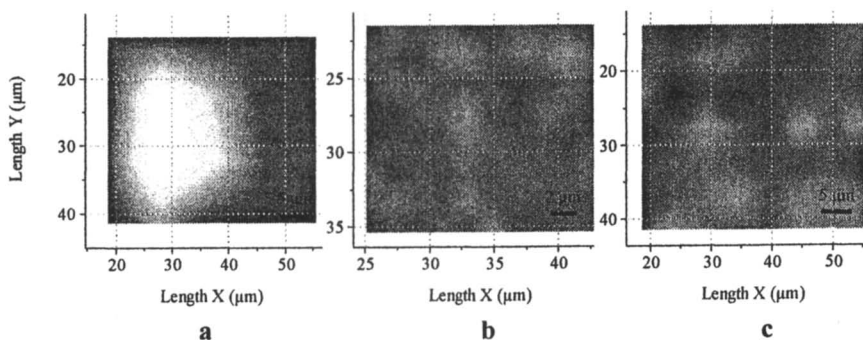


Figure 2. Raman imaging of a) EVA- $\text{Mg}(\text{OH})_2$ -MMT, b) EVA- $\text{Mg}(\text{OH})_2$ -OMM, c) EVA- $\text{Mg}(\text{OH})_2$ -IMM

Deactivating / Activating Interphases

Although the flame retardant action should be matched with the degradation profile of polymers, high costs do not allow designing different flame retardants for each polymer of different degradation profile. Coating layers applied for chemical or mechanical compatibilization may affect the FR performance especially when the unmodified or modified surface has a catalytic activity.

Deactivation of FR particles may be caused by coating layers. A good example is the above mentioned EVA-Mg(OH)₂-IMMT system where the polymer IP around MMT controls the temperature dependence of the compatibility but simultaneously diminishes the activity of the surface atoms of MMT. A considerable increase of LOI and UL 94 data could be realized in this system by adding some uncovered MMT (see in Table I). This result suggests catalytic activity of the clay on the formation of carbonaceous char (as found earlier in PS-clay system (22)) probably through its Fe-ions at the surface (23), which should not be covered entirely. In this case partial coating is the optimal IP structure performing both compatibility-control and catalytic action.

Similar behavior was found in PA: combination of nanoclay with phosphinate flame retardant additive was most advantageous if the MMT was not coated. Interfacial layer around the MMT particles hindered the catalytic activation of phosphinate (24).

Table I. FR Characteristics of EVA Systems Containing MMT-s and Mg(OH)₂

<i>Components</i>	<i>LOI</i>	<i>UL94</i>
EVA	19	No rating
EVA:Mg(OH) ₂ (8:1)	33	V-1
EVA:Mg(OH) ₂ :MMT (8:8:1)	34	V-2
EVA:Mg(OH) ₂ :OMM (8:8:1)	33	V-2
EVA:Mg(OH) ₂ :IMM (8:8:1)	36	V-2
EVA:Mg(OH) ₂ :MMT:IMM (16:16:1:2)	43	V-0

Activating nanolayer was formed by zinc hydroxystannate (ZnHSt) around Mg(OH)₂. The 4.7 nm thickness of the layer was determined by surface analysis (25). Improvement of thermal stability and FR performance was lower if the ZnHSt was applied as separate particles than as coating layer (16). Activating interaction was observed also between APP and MMT (26), which could be controlled by polyorganosiloxane coating layer (27). Activating layers can be formed by special surface active molecules. The synthesis of reactive surfactants of FR function, called synergistic reactive surfactant (SRS), has been reported recently (7). Such additives, applied in intumescent nanocomposites, perform quite complex tasks, combining the above mentioned double action (dispersion and coupling) with FR activity (28). Melamine polyphosphate-polyol system, which is too stable at the degradation temperature of PP, has been activated for application in polyolefins (29). Activating effect is ascribed also to the char forming polymers in intumescent nanocomposites according to the blending approach (30).

These results suggest an economic strategy of selecting a few general flame retardants and shifting their action temperature close to the degradation range of the polymer matrix, by means of deactivating or activating interphases.

Rheology Modifying Interphases

Rheological behavior plays a key role in the FR performance of the materials. IPs may promote the formation of microgel type network (Figure 3) and thus reduce the dripping (31,32) and influence the degradation process of the matrix polymer.

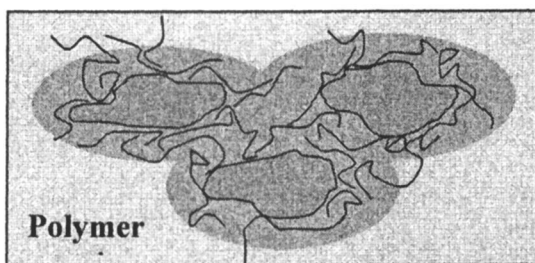


Figure 3. Microgel structure of interacting interphases around FR (nano)particles

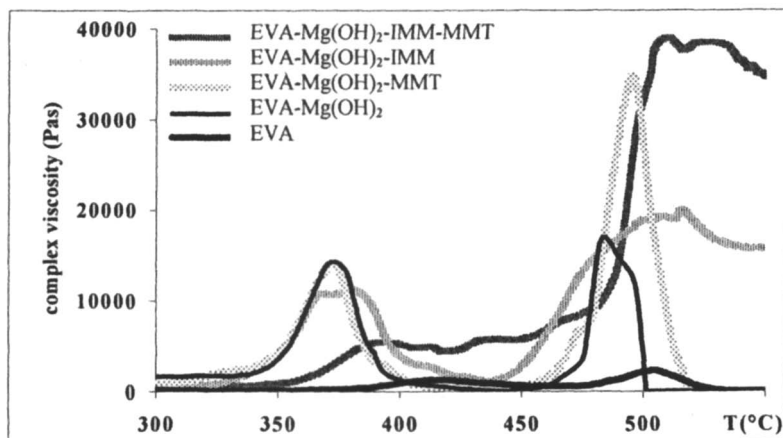


Figure 4. Viscosity-temperature plots of EVA and FR-EVA containing MMT

According to separately published (33) rheological measurements of materials in Table I the level of exfoliation was the highest in case OMM containing system, but, it does not correlate with the highest FR performance because the relationship between rheology and flame retardancy is complex. Figure 4 shows the thermal dependence of viscosity, which is affected most significantly by IMM+MMT. This additive system not only keeps the viscosity at a relatively high value, but even increases it gradually in the temperature range of 390-470°C, where other compositions lose their melt strength. This feature leads to good flame resistance.

Protecting Interphases

The chemical and thermal sensitivity of fire retardants can be overcome by protective coating layers (13). APP has to be protected against hydrolytic degradation at higher temperature and against early reaction with polyols in intumescent systems. Various layers have been proposed for protecting the APP particles (40,41), but the stable, multifunctional, IPs formed during processing are most advantageous. Shear stress resistant silicone elastomer IP was found suitable for preserving the stability under processing conditions (13). The chemical composition of the in-line formed interlayer around APP particles could be analyzed by SEM-EDX method (Figure 5).

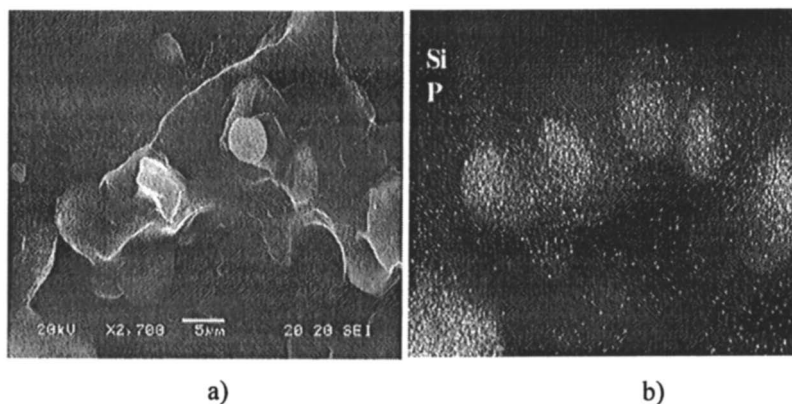


Figure 5. SEM (a) and SEM-EDX (b) images of BSIL-coated APP particles in PP

The protecting effect was confirmed by the decrease of the conductivity of water used for extracting the FR product (from 200 μS of the reference sample to 50 μS of protected APP).

Transporting (Adaptive) Interphases

The homogeneously dispersed FR additives should be transferred to the surface at high temperature in order to maximize their insulating effect against fire. In case of MMT the nanoparticles may be driven by lower surface free energy especially in systems involving a silicon-containing component into the FR mechanism (36). In such case, however, the low value of the work of adhesion (W_a) leads to poor dispersion after compounding. On the other hand, the nanoparticles treated with thermally stable surfactants have no driving force to move to the surface. This paradoxical situation could be solved by forming an *adaptive IP*, which contains thermally sensitive compatibilizing branches formed by a reactive surfactant (see in chapter *Dispersing, coupling interphases*) and incompatible (BSIL) elastomer IP. The compatibilizing units will decompose at the temperature of fire leaving an incompatible coating layer behind. (The elimination of the compatibilizing unit could be determined by the disappearance of their characteristic Raman band.) The migration of the silicone layer coated MMT nanoparticles to the surface could be proven using micro-Raman and XPS analyses (26). The improvement of the fire retardancy of intumescent FR-PP owing to the described mechanism is shown in Figure 6. The decrease of LOI after the maximum suggests that above the concentration needed for interface-modification the applied elastomer is less advantageous, probably due to its softening effect.

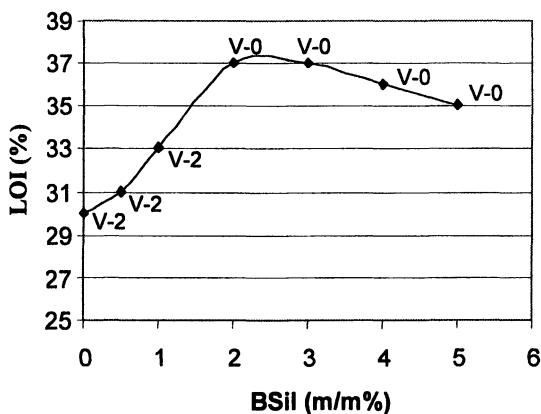


Figure 6. LOI and UL 94 values of FR-PP depending on the concentration of BSIL

Separating Interphases

A competition exists at the surface of the solid phase between the rate of action of fire spreading and FR additives. Migration is not always rapid enough in delivering nanolayers to the surface; therefore a new adaptive concept has been developed based on separating IP. A material utilizing this mechanism contains interlayer of relatively low decomposition temperature intercalated between nanolayers. At the early stage of fire action the gaseous degradation products of the IP separate the nanolayers and drive them to the surface. To the best of our knowledge, this is the most rapid method for forming nanolayer-reinforced surface char barrier. Such material, called “*expandable nanocomposite*”, has been published recently (28,37). The intercalation of phosphorylated polyol (PPOL) flame retardant caused characteristic change in the XRD spectra of OMM as shown in Figure 7. The intercalation of relatively thick layers of PPOL is indicated by the lack of Bragg reflection, while the first and second Bragg reflections of OMM correspond to $\sim 31 \text{ \AA}$, and 19.5 \AA periodic distance. In addition to the advantageous decrease and delay of the RHR peak, another special feature of the expandable PP-nanocomposite is the delay of its ignition time (after a reproducible spike at ignition) as shown in Figure 8.

Most recently we tried to utilize the separating IP concept in epoxy resins but no positive result was detected (38). The crosslinked structure probably hinders the rapid movement of nanoparticles to the surface.

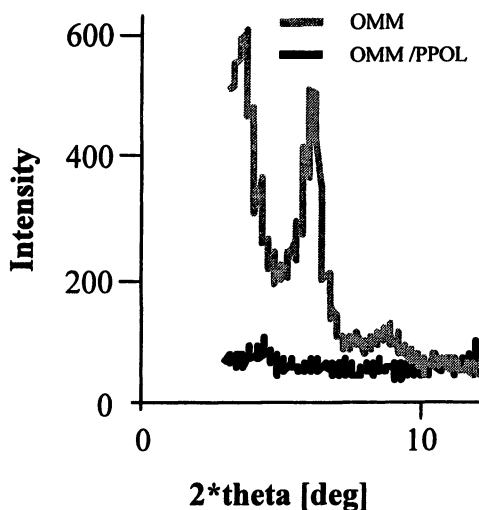


Figure 7. XRD plots of OMM and with phosphorylated polyol intercalated OMM

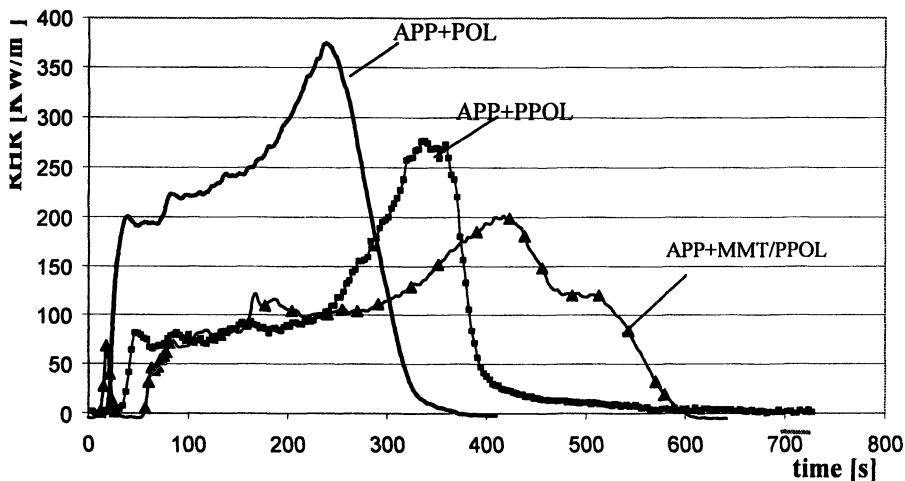


Figure 8. Cone Calorimeter curves of 70%PP+(APP: POL=3:1); PP+(APP: PPOL=3:1); PP+APP+MMT/PPOL: 65%PP+24%APP+11%MMT/PPOL (MMT/PPOL is OMM (1 part) intercalated with phosphorylated polyol (10 part))

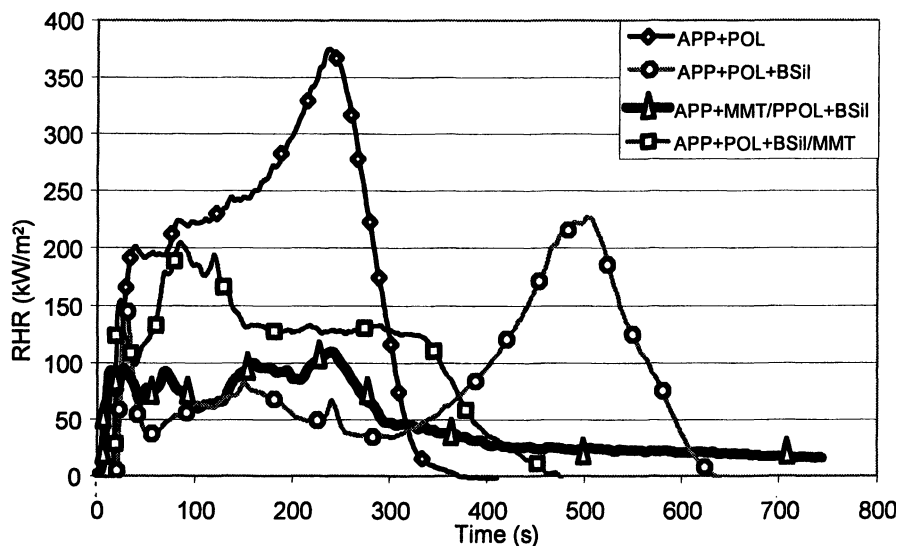


Figure 9. Cone Calorimeter curves of 70%PP+ (APP: POL=3:1); 68%PP+(APP: POL=3:1)+2%BSiI; PP+APP+MMT/POL+BSiI: 63%PP+24%APP+11%MMT/POL+2%BSiI

Ceramizing Interphases

The mechanism in which the accumulation of clay particles on the surface of burning material is accelerated by bubbles of degradation products was found ineffective in PA recently (39). In that case the bubbles at the sample surface pushed the accumulated clay particles outward from the bursting area therefore island-like floccules formed instead of a continuous net-like structure of a clay filled protective layer. This result suggests that the nanoparticles on the surface of a material are more effective if they are bonded to each other. The polysiloxane IP, discussed in the previous chapters, at high temperature may promote the merging of FR components on the surface. The mechanical resistance of the solid residue was evaluated by Thermal Scanning Rheometer in case of metal hydroxide and intumescent type FR systems (40). The plots in Figure 4 reflect, above 450°C, the resistance of the residue against destructive mechanical effects. Decline of the curve around 480-500°C corresponds to less flame retardancy, while sustained high viscosity to better FR performance, in accordance with the LOI and UL 94 data cited in Table I.

Boron atoms built in the polysiloxane elastomers promote the ceramization of the surface layer in case of fire (32). According to XPS measurements partially organic character of the ceramic layer is preserved even after longer flame treatment resulting in mechanically resistant char (13,41).

Combining the most advantageous IP structures the RHR curve could be kept under 100 kW/m² and burning terminated within 300 s (see in Figure 9).

Conclusion

Interfacial structure affects not only the interaction of the phases but also the mechanism of flame retardancy. Interfacial additives are effective at a very low concentration (~1%). Instead of solving all the interfacial issues with a special additive we proposed a multilayer structure, which may act as thermally adaptive interphase. At lower temperature its dispersing, stabilizing, compatibilizing and rheology optimizing effect is active, while at high temperature, caused by the fire, its transporting and ceramizing function becomes active. The catalytic activity of MMT on the charring process can be influenced by interface modification. Expandable MMT (with intercalated gas forming additive) represent the most rapid way to deliver the nanolayers to the surface but this mechanism requires a ceramizing interphase for keeping the nanoparticles together when the gas bubbles try to escape.

References

1. Bertalan, Gy.; Rusznák, I.; Huszár, A.; Székely, G.; Trézl, L.; Horváth, V.; Kalmár, Z.; Jancsó, A. *Plaste u. Kautsch.* **1978**, *25*, 340.
2. Bánhegyi, Gy.; Marosi, Gy.; Bertalan, Gy.; Karasz, F. *Coll. Polym. Sci.* **1992**, *270*, 113.
3. DiBenedetto, A.T. *Mat. Sci. Eng. A - Struct.* **2001**, *302(1)*, 74.
4. Marosi, Gy.; Bertalan, Gy.; Rusznák, I.; Anna, P. *Coll. Surfaces* **1986**, *23*, 185.
5. Sahnoune, F.; Lopez-Cuesta, J.M.; Crespy, A. *J. Mater. Sci.* **1999**, *34*, 535.
6. Marosi, Gy., Tohl, A., Bertalan, Gy., Anna, P., Maatoug, M., Ravadits, I., Bertóti, I., Tóth, A. *Composites Part A.* **1998**, *29A*, 1305.
7. Marosi, Gy.; Anna, P.; Csontos, I.; Márton, A.; Bertalan, Gy. *Macromol. Symp.* **2001**, *176*, 189.
8. Marosi, Gy.; Bertalan, Gy.; Balogh, I.; Tohl, A.; Anna, P.; Szentirmay, K. *Flame Retardants '96*, Interscience Commun. LTD Publ. London, 1996; p. 115.
9. Marosi, Gy.; Anna, P.; Balogh, I.; Bertalan, Gy.; Tohl, A.; Maatoug, M. *J. Therm. Anal.* **1997**, *48*, 717.
10. Tidjani, A.; Wald, O.; Pohl, M.-M.; Hentschel, M.P.; Schartel, B. *Polym Degrad. Stab.* **2003**, *82*, 133.
11. Bartholmai, M.; Schartel, B. *Polym. Adv. Technol.* **2004**, *15*, 355.
12. Qutubudin, S.; Fu, X. A.; Tajuddin, Y. *Polymer Bulletin* **2002**, *48*, 145.
13. Marosi, Gy.; Anna, P.; Márton, A.; Bertalan, Gy.; Bóta, A.; Tóth, A.; Mohai, M.; Rácz, I. *Polym. Adv. Technol.* **2002**, *13*, 1103.
14. Kashiwagi, T.; Grulke, E.; Hilding, J.; Harris, R.; Awad, W.; Douglas, J. *Macromol. Rapid Commun.* **2002**, *23*, 761.
15. Marosi, Gy.; Márton, A.; Csontos, I.; Matkó, Sz.; Szép, A.; Anna, P.; Bertalan, Gy.; Kiss, É. *Progr. Colloid Polym. Sci.* **2004**, *125*, 189.
16. Marosi, Gy.; Anna, P.; Bertalan, Gy.; Szabó, Sz.; Ravadits, I.; Papp, J. *Fire and Polymers* (Nelson, G.; Wilkie, C., Eds.) ACS Ser., 797 Washington 2001; p 161.
17. Anna, P.; Zimonyi, E.; Márton, A.; Szép, A.; Matkó, Sz.; Keszei, S.; Bertalan, Gy.; Marosi, Gy. *Macromol. Symp.* **2003**, *202*, 245.
18. Bertalan, Gy.; Rusznák, I.; Trézl, L.; Horváth, V.; Marosi, Gy.; Anna, P. *Verstärkte Plaste 80, Proceeding p.T5/1.* Kammer der Technik, Drezda, 1980.
19. Hermansson, A.; Hjertberg, T.; Sultan, B.A. *Fire and Materials* **2003**, *27*, 51.
20. Marosi, Gy., Bertalan, Gy., Anna, P., Rusznák, I. *J. Polym. Eng.* **1993**, *12 (1-2)*, 34.
21. Preston, C.; Amarasinghe, G.; Hopewell, J.; Shanks, R.; Mathys, Z. *Polym. Degrad. Stab.* **2004**, *84*, 533.

22. Bourbigot, S.; Gilman, J.; Wilkie, C. *Polym. Degrad. Stab.* **2004**, *84*, 483.
23. Zhu, J.; Uhl, F.M.; Morgan, A.; Wilkie, C. *Chem. Mater.* **2001**, *12*, 4649.
24. Marosi, Gy.; Toldy, A.; Anna, P.; Zimonyi, E.; Keszei, S.; Krause, W.; Hörold, S. *Recent Advances in Flame Retardancy of Polymeric Materials XVI*. (Lewin, M., Ed.); BCC Inc., Stamford, USA, 2004; p 79.
25. Mohai, M.; Tóth, A.; Hornsby, P.R.; Cusack, P.A.; Cross, M.; Marosi, Gy. *Surf. Interface Anal.* **2002**, *34*, 735.
26. Marosi, Gy.; Márton, A.; Anna, P.; Bertalan, Gy.; Marosfői, B.; Szép, A. *Polym. Degrad. Stab.* **2002**, *77*, 259.
27. Marosi, Gy.; Márton, A.; Szép, A.; Csontos, I.; Keszei, S.; Zimonyi, E.; Tóth, A.; Almeras, X.; Le Bras, M. *Polym. Degrad. Stab.* **2003**, *82*, 379.
28. German Patent Application Registration No. R 4700 (13.03.2002.)
29. Marosi, Gy.; Bertalan, Gy.; Anna, P.; Ravadits, I.; Bourbigot, S.; Le Bras, M.; Delobel, R. *Recent Advances in Flame Retardancy of Polymeric Materials XI*. (Lewin, M., Ed.); BCC Inc., Stamford, USA, 2000; p 154.
30. Bourbigot, S.; Le Bras, M.; Duquesne, S.; Rochery, M. *Macromol. Mater. Eng.* **2004**, *289*, 499.
31. Anna, P.; Marosi, Gy.; Bourbigot, S.; Le Bras, M.; Delobel, R. *Polym. Degrad. Stab.* **2002**, *77*, 243.
32. Anna, P.; Marosi, Gy.; Bertalan, Gy.; Márton, A.; Szép, A. *J. Macromol. Sci. Phys.* **2002**, *B41*, 1321.
33. Szép, A.; Szabó, A.; Tóth, N.; Anna, P.; Marosi, Gy. *Polym. Degrad. Stab.* (submitted)
34. Chen, Y.; Liu, Y.; Wang, Q.; Yin, H.; Aelmans, N.; Kierkels, R. *Polym. Degrad. Stab.* **2003**, *81*, 215.
35. Wu, Q.; Qu, B. *Polym. Degrad. Stab.* **2001**, *74*, 225.
36. Lewin, M. *Fire Mater.* **2003**, *27*, 1.
37. Marosi, Gy.; Anna, P.; Márton, A.; Matkó, Sz.; Szép, A.; Keszei, S.; Csontos, I.; Marosfői, B. *Proceedings of the 12th International Conference on Additives San Francisco*, 2003, Vol. 12, (Wilkie, C.; Al-Malaika, S., Eds.); ECM Ltd., p 203.
38. Toldy, A.; Tóth, N.; Anna, P.; Marosi, Gy. *Polym. Degrad. Stab.* (accepted)
39. Kashiwagi, T.; Harris, R.H.; Zhang, X.; Briber, R.M.; Cipriano, B.H.; Raghavan, S.R.; Awad, W.H.; Shields, J.R. *Polymer* **2004**, *45*, 881.
40. Anna, P.; Marosi, Gy.; Csontos, I.; Bourbigot, S.; Le Bras, M.; Delobel, R. *Polym. Degrad. Stab.* **2001**, *74*, 423.
41. Ravadits, A.; Tóth, G.; Marosi, A.; Márton, A.; Szép, A. *Polym. Degrad. Stab.* **2001**, *74*, 414.

Chapter 11

Development of New Fire Retardant Additives Based on Hybrid Inorganic–Organic Nanodimensional Layered Compounds: Thermal Degradation of PMMA Composites

Everson Kandare¹, Daniel Hall¹, David D. Jiang²,
and Jeanne M. Hossenlopp^{1,*}

¹Department of Chemistry, Marquette University, P.O. Box 1881,
Milwaukee, WI 53201–1881

²Department of Materials Science and Engineering, Cornell University,
Ithaca, NY 14853

The addition of zinc/copper methacrylate hydroxy double salt or copper hydroxy methacrylate to bulk polymerized PMMA is shown to substantially influence polymer thermal degradation. Addition of 2–4% by weight of either additive is shown to increase the temperature of 50% mass loss by 40–60° C in thermal gravimetric analysis. In cone calorimetry experiments, the additives lead to 20–30% reduction in total heat release but no significant change in peak heat release rate. The polymer/additive structures are best described as microcomposites based on X-ray diffraction and transmission electron microscopy analysis. X-ray diffraction analysis of residues following cone calorimetry indicates formation of reduced copper from copper hydroxy methacrylate.

Introduction

Polymer/clay nanocomposites have been shown to provide improvements in some aspects of polymer thermal degradation behavior, typically lowering peak heat release rates (PHRR) in cone calorimetry measurements and also increasing the temperature required for mass loss in thermal gravimetric analysis (TGA) (1-4). These nanocomposites also often lead to enhanced physical properties by increasing tensile strength, tensile modulus, and flexural strength, elevating the heat distortion temperature and providing corrosion protection (1,2,5). However, not all properties of interest in fire retardancy applications are improved in polymer/clay nanocomposites. Generally the time to ignition decreases and the total heat release (THR) remains unchanged. Optimizing polymer fire retardancy for a particular application may require testing new classes of additives as well as exploring potentially synergistic combinations of different additives (6).

Layered double hydroxides (LDHs) are a class of compounds that are structurally similar to natural smectite clays, except that there are anions rather than cations intercalated into the interlayer domain. LDHs have the general formula $[M^{2+}_x M^{3+}_{1-x} (OH)_2]^{x+} (A^{n-})_{x/n} \cdot mH_2O$, where A^{n-} represents the intercalated anion, and have been investigated as fire retardant nanocomposite additives, exhibiting similar behavior to natural clays (7-11). A potential advantage of synthetic compounds such as LDHs is the possibility of varying the identity of the metals and the anions in order to provide an additional design parameters for additive property optimization.

A more recently emerging class of nanodimensional layered materials, hydroxy double salts (HDSs), are formed from two divalent metals and have the general formula $[(M^{2+}_{1-x} M^{2+}_{1+x}) (OH)_{3(1-y)/n}] A^{n-}_{(1+3y)/n} \cdot mH_2O$ where M^{2+} and M^{2+} represent the different divalent metals (12-15). HDSs are typically synthesized from combinations of Zn, Ni, Cu, and Co and have easily-exchanged anions, thus offering compositional design parameters for optimizing properties. Work in our laboratory has focused primarily to date on HDSs synthesized with Zn and one of the other three cations. Preliminary results obtained in our laboratory on polystyrene/HDS composites suggested that this new class of potential additives lowers PHRR and that metal ion and anion identity play a role in the additive effectiveness (16). Copper-containing HDSs generally exhibited the most significant improvement in thermal degradation properties.

While our preliminary results with HDSs demonstrated that these materials may hold promise for design of new fire retardant additives, the dispersion in

polystyrene was visibly quite poor even when long alkyl chain anions were used to improve the organophilicity of the interlayer domain. These materials may thus be better suited for use with more polar polymers. In the work reported here we explore the use of Zn/Cu HDS and a structurally-related layered copper hydroxide compound as additives for poly(methylmethacrylate) (PMMA).

Experimental

Monomeric methyl methacrylate, $[\text{CH}_2=\text{C}(\text{CH}_3)\text{CO}_2\text{CH}_3]$, and copper (II) methacrylate (97%) $[(\text{H}_2\text{C}=\text{C}(\text{CH}_3)\text{CO}_2)_2\text{Cu}]$, were obtained from Alfar Aesar. The initiator, benzoyl peroxide (BPO), copper acetate monohydrate (98.0%) $[\text{Cu}(\text{CH}_3\text{CO}_2)_2\cdot\text{H}_2\text{O}]$, sodium methacrylate (99.0%) $[\text{H}_2\text{C}=\text{C}(\text{CH}_3)\text{CO}_2\text{Na}]$, and zinc oxide (99.9%) $[\text{ZnO}]$ were obtained from Aldrich Chemical Co. Copper (II) nitrate (98.9%) $[\text{Cu}(\text{NO}_3)_2\cdot 2\frac{1}{2}\text{H}_2\text{O}]$ was obtained from Fisher Scientific Co. and ammonium hydroxide $[\text{NH}_4\text{OH}]$, was obtained from EM Science, Merck. All chemicals were used without further purification with the exception of methyl methacrylate monomer solution freed from the inhibitor by passing through an inhibitor remover column acquired from Aldrich Chemical Co.

Zn/Cu-acetate (ZCA) HDS was prepared by mixing 0.41 g of ZnO (5 mmol) with 1.00 g of copper acetate (5 mmol) in 10 mL of distilled water with vigorous stirring at room temperature (15). The resultant suspension was allowed to stand for 24 hrs after which the precipitate was filtered off and washed several times with water before drying in air at room temperature. A layered hydroxy salt, copper hydroxy nitrate (CHN), was made following a standard literature precipitation method (17). Copper (II) nitrate $[\text{Cu}(\text{NO}_3)_2\cdot 2\frac{1}{2}\text{H}_2\text{O}]$, (10.0 g; 43 mmol) was added to 100 mL of distilled water and the pH of the resultant solution subsequently raised to 8 by dropwise addition of NH_4OH . The solution was let to stand at room temperature for 24 hrs after which the precipitate was filtered off, washed and dried.

Elemental analysis of ZCA, $\text{Cu}_{3.6}\text{Zn}_{1.4}(\text{OH})_{7.6}(\text{CH}_3\text{CO}_2)_{2.4}\cdot 5\text{H}_2\text{O}$, $[\text{Cu}$ (37.2% calc, 35.6% exp), Zn (14.9% calc, 14.8% exp), C (9.4% calc, 9.4% exp), H (4.1% calc, 3.2% exp)], was carried out by Huffman Labs, Colorado, using the Atomic Emission Spectroscopy interfaced with Inductively Coupled Plasma (AES-ICP) for metals determination. The exchange capacity of ZCA was calculated to be ~3.0 meq/gram while an exchange capacity of 4.2 meq/gram would be calculated for CHN, from its nominal formula, $\text{Cu}_2(\text{OH})_3\text{NO}_3$.

Methacrylate anions were partially exchanged for the acetate in ZCA and for

the nitrate in CHN, respectively, by mixing the dried precursor powders with 0.2 M solution of sodium methacrylate. In a typical exchange reaction at room temperature, 10.0 g of ZCA would be mixed with 500 mL of the exchange solution and frequently shaken for 48 hrs. The solution was decanted and replaced with a fresh one for another 48 hrs.

PMMA was synthesized via bulk polymerization. Methyl methacrylate monomer was combined with the initiator, BPO, (1%) and a methacrylate-containing additive. The mixture was initially heated to 90 °C with vigorous stirring until viscous, after which the temperature was then lowered to 60 °C and held constant for 24 hrs. The temperature was then raised to 80 °C and held at that temperature for another 24 hrs followed by vacuum drying the sample at 100° C for 12 hrs to drive off excess monomer. Percent loadings were determined from the final mass of the composite, assuming no loss of HDS during the preparation process. Reference samples of pure PMMA were synthesized in an identical fashion without additives.

X-ray diffraction patterns were obtained using a 2-circle Rigaku diffractometer operating in parafocusing Bragg-Bretano configuration, with a ½° divergence slit, ½° scatter slit, 0.15 mm receiving slit, 0.15 mm monochromator receiving slit. The Cu ($\lambda = 0.154 \text{ \AA}$) radiation source was operated at 50 kV and 20 mA, and data acquisition done in 2 θ steps of 0.036° per 20 s. Powdered samples were mounted on quartz slides using 10% (v/v) GE 7031 varnish in ethanol after it was found that the glue did not affect the patterns. Polymer composite samples were pressed into 1 mm thick platelets, which were then mounted onto vertically oriented sample holders for XRD analysis. Basal spacing of the HDS and layered copper hydroxide salts were obtained from averaging 00 l ($l = 1$ to 3) reflections after fitting the raw spectra to a pseudo-Voigt function using XFIT (18), stripping off the Cu $K\alpha_2$ contribution.

Thermogravimetric analysis (TGA) was performed on a Mattson-Cahn TG-131 device in the temperature range of 40-600 °C in both air and N₂ using a ramp rate of 20 °C/min with samples sizes in the range of 50-60 mg. Differential thermal analysis (DTA) was performed on a SDT 2960 Simultaneous DTA-TGA instrument from 40-600 °C using a heating rate of 20 °C/min in both air and N₂ with sample sizes of 10-15 mg.

PMMA composite samples, 30 g in total mass, were compression molded into square plates of uniform thickness before cone calorimetry was performed on an Atlas Cone 2 instrument at an incident flux of 50 kW/m² with a cone shaped heater. Bright field transmission electron microscopy (TEM) images were collected at 60 kV with a Zeiss 10c electron microscope at Cornell University.

Results and Discussion

Powder X-ray diffraction characterization of the additives is shown in Figure 1. Figure 1A shows data for the copper hydroxy nitrate precursor, which agrees well with literature results for this compound (19), and the copper hydroxy methacrylate (CHM_x) additive synthesized via exchange of methacrylate for nitrate. The exchange is not complete; small features due to the precursor are still evident. The basal spacing increases from 6.9 Å to 13.4 Å when the nitrate anions are exchanged by the larger methacrylate anions. Figure 1B shows data characterizing precursor (Zn/Cu-acetate HDS) and its corresponding methacrylate exchange product (ZCM_x). In this case, two new sets of basal spacings (12.0 Å and 13.7 Å) are observed following methacrylate exchange. A similar effect has been observed in our laboratory when replacing acetate with propionate and butyrate (20) and has also been reported for exchange of butyrate into copper hydroxy acetate (21). The observation of two distinct basal spacings is most likely due to different relative orientations of the anions in the interlayer domain.

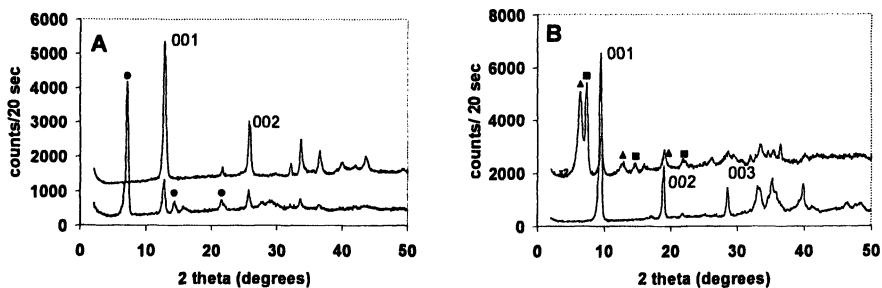


Figure 1. Powder X-ray diffraction analysis of additives, data are offset for clarity in each panel. A. Precursor copper hydroxy nitrate (upper trace) and partially exchanged copper hydroxy methacrylate (CHM_x) (lower trace). 001 progression for CHM_x marked with circles. B. Precursor Zn/Cu-acetate HDS (lower trace) and partially exchanged Zn/Cu-methacrylate (ZCM_x) (upper trace, expanded by factor of two). Two 001 progressions, marked with triangles and squares, respectively, are observed for ZCM_x .

The lower trace in Figure 2 shows the XRD pattern for PMMA- CHM_x -2%, a composite made by loading the polymer matrix with 2% CHM_x modified clay. The peak at $2\theta = 7.5^\circ$, corresponding to a d-spacing of 11.8 Å, suggests that at least some of the additive remains intact in the composite and there is a small reduction in the gallery spacing as compared to the pure additive as synthesized. Similar results were observed with PMMA- ZCM_x -2%, a composite made by loading the polymer matrix with 2% of ZCM_x , shown in the upper trace of

Figure 2. A reduced basal spacing of 11.7 Å was calculated from a rather weak 001 reflection peak at 7.6°. The contraction in the interlayer spacing may be due, at least in part, to the loss of the interlayer water present in the original additives since the polymer composites are vacuum dried at 100°C. However, perturbations on the additive structure due to the surrounding polymer matrix cannot be eliminated based on these data.

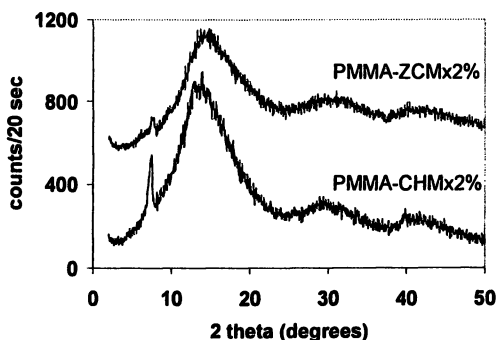


Figure 2. XRD patterns of the PMMA composites, PMMA-ZCM_x-2% (upper trace) and PMMA-CHM_x-2% (lower trace). Traces have been offset for clarity but not otherwise scaled.

X-ray diffraction analysis alone is not sufficient to characterize the dispersion of additives in PMMA. Low and high-resolution TEM images provide additional insight into the quality of the dispersion of additives. Low magnification images allow one to determine whether a microcomposite and/or nanocomposites has been formed, while high magnification images would help one to determine whether intercalation or exfoliation has occurred. TEM images of PMMA-CHM_x-2% and PMMA-ZCM_x-2% are shown in Figure 3.

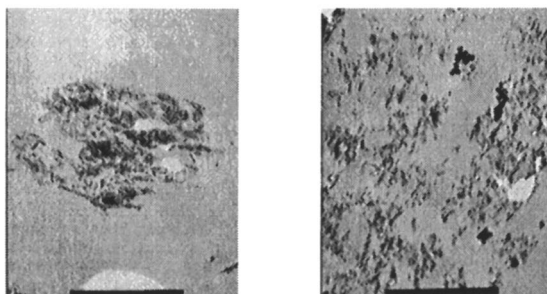


Figure 3. Low magnification (bar = 100 nm) TEM image of: PMMA-CHM_x-2% (left) and PMMA-ZCM_x-2% (right).

The low magnification TEM image of PMMA-CHM_x-2%, shown on the left side of Figure 3, is consistent with the formation of a microcomposite with the additive clumped together, suggesting a poor dispersion in the polymer matrix. The high-resolution image of PMMA-CHM_x-2% (not shown here) does not show any clear evidence of delamination or intercalation, consistent with the clearly evident 001 peak observed in the X-ray diffraction data shown in Figure 2.

The low magnification image of PMMA-ZCM_x-2% shown on the right side of Figure 3 suggests better dispersion of the additive in the polymer matrix, although still with the presence of tactoids. No intercalation or delamination features were observed in the high-resolution image of PMMA-ZCM_x-2% (not shown). We note that the XRD 001 feature for this composite is relatively weak in Figure 2, also consistent with better dispersion of this additive.

Thermogravimetric analysis (TGA) curves of ZCM_x (A), PMMA (B), PMMA-ZCM_x-2% (C), and PMMA-ZCM_x-4% (D) samples in air are shown in Figure 4A. The pure PMMA sample decomposes in three steps in the temperature range of 200–450° C leaving no residue after heating to 600° C. PMMA-ZCM_x-2% and PMMA-ZCM_x-4% begin to lose mass at about the same temperature as pure PMMA. No significant weight losses were observed at 100° C, indicating very little or no physically adsorbed water molecules were contained in these polymer composites. The degradation onset of the composites, as depicted by T_{10%}, the temperature at which 10% of the original mass is lost, is shifted to higher values for the PMMA-layered hydroxy salt composites. TGA curves of CHM_x (A), PMMA (B), PMMA-CHM_x-2% (C), and PMMA-CHM_x-4% (D) are presented in Figure 4B and similar behavior compared with the ZCM_x system is observed. The TGA results are summarized in Table I.

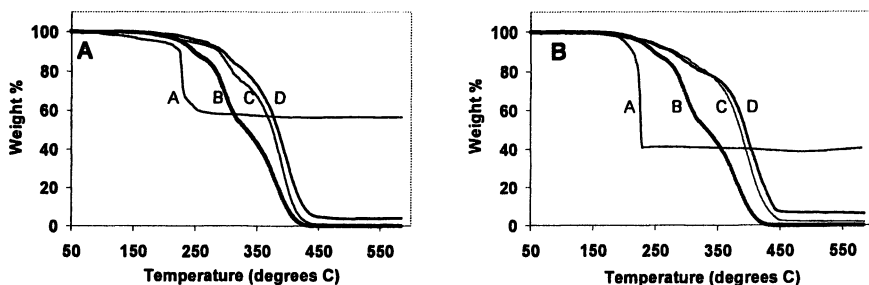


Figure 4. A. TGA curves for (A) ZCM_x, (B) pure PMMA, (C) PMMA-ZCM_x-2%, and (D) PMMA-ZCM_x-4% composites. B. TGA curves for (A) CHM_x, (B) pure PMMA, (C) PMMA-CHM_x-2%, and (D) PMMA-CHM_x-4% composites.

The degradation of the PMMA composite materials occurs in two steps, with the first one probably a result of the weak link scission of PMMA monomeric units involved in head to head linkage, loss of the additive organic content, and or weak links due to disproportionation termination producing vinylidene chain ends. Unreacted initiators of polymerization, in-chain weak links, and free radicals generated from an oxidation of the monomer methyl methacrylate could be initiators for the thermal degradation course of PMMA and its composites (22). This first step accounts for about 30% of the overall weight loss, which suggests that it cannot be solely attributed to the unreacted monomer units. Also, since the composites were made in an air atmosphere, weak peroxides and or hydroperoxides links are expected and these lead to a high degree of chain scission initiation at low temperatures (23).

Table I TGA Results

Sample	$T_{10\%}$ (°C)		$T_{50\%}$ (°C)		$\Delta T_{50\%}$ (°C) ^a		Char (%)	
	Air	N ₂	Air	N ₂	Air	N ₂	Air	N ₂
PMMA	249	248	333	338	0	0	0.1	0.0
CHM _x 2%	282	285	386	388	53	50	1.8	3.2
CHM _x 4%	277	273	394	393	61	55	6.0	7.1
ZCM _x 2%	289	288	375	373	42	35	0.6	0.0
ZCM _x 4%	296	287	384	384	51	46	3.9	3.3

$$^a \Delta T_{50\%} = T_{50\%} (\text{PMMA composite}) - T_{50\%} (\text{PMMA})$$

Chen and coworkers reported that a PMMA nanocomposites sample with 30 wt% MgAl LDH (containing dodecyl sulfate) showed a 45° C improvement in the $T_{50\%}$ value (24). Note that our additives lead to similar improvements at much lower loadings. Zinc polymethacrylate gave a similar increment in the thermal stability at 50% decomposition in work reported by McNeill and coworkers, another indication that the presence of metal atoms in these composites plays a profound role in preventing depolymerization (25). Finally, we also note Chandrasiri and Wilkie have reported (26) a stabilizing effect of SnCl₄ and tetraphenyltin on the thermal degradation of PMMA. They suggested that monomer or polymer radicals combine with Sn-based radicals forming cross-linked char, which then acts as an energy or mass transfer barrier. The $\Delta T_{50\%}$ values reported in Table I for the CHM_x polymer composites are higher than for the corresponding ZCM_x composites and char formation is also greater with the CHM_x additive. Note that the additives used here have a relatively high exchange capacity. Using the TGA data for the additives shown in Figure 4, the estimated residue for the PMMA-ZCM_x-4% would be 2.4% assuming complete combustion of PMMA, whereas 3.9% char was observed for combustion of the

composite in air. Similarly, PMMA-CHM_x-4% would be expected to have 1.6% residue due to the additive alone, while the observed value for the composite heated in air was significantly higher, 6%. Given that CHM_x has a higher copper content, this suggests that this metal may play a particularly important role in the thermal stabilization of the polymer matrix via barrier formation.

Figure 5 shows the TGA and DTA curves for PMMA-ZCM_x-2% and PMMA-CHM_x-2% composites respectively. Pure PMMA TGA and DTA curves are also shown to draw a comparison between its thermal degradation behaviors and those of the polymer composites.

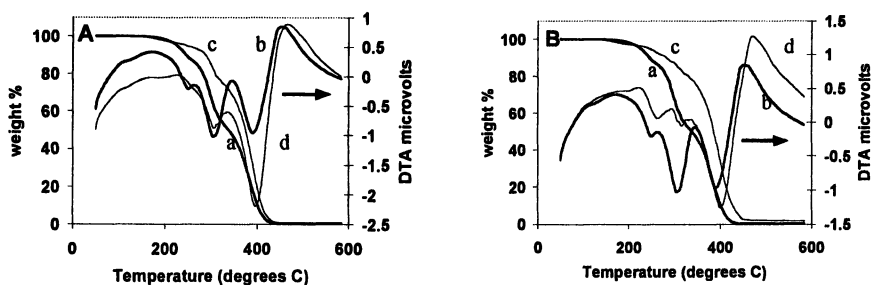


Figure 5. A. TGA and DTA curves for pure PMMA (a and b, respectively) and PMMA-ZCM_x-2% (c and d, respectively). B. TGA and DTA curves for pure PMMA (a and b, respectively) and PMMA-CHM_x-2% (c and d, respectively).

Small changes in the shape of the DTA curves of the PMMA-metal hydroxide composites as compared to pure PMMA are observed. An endotherm in the DTA curve for pure PMMA at ca. 250 °C is not seen in the DTA curve for PMMA-ZCM_x-2% in Figure 5A. The DTA curves for pure PMMA and PMMA-CHM_x-2% shown in Figure 5B are similar, except that the endotherms appear to be shifted to slightly higher temperatures with the additive and a weak exotherm appears at 220 °C for the PMMA-CHM_x-2% composite. While it appears from these data that the additives may influence the PMMA decomposition mechanism, further work is necessary to fully characterize these effects.

Cone calorimetry was used to determine the effects of these additives on PMMA thermal degradation. In particular, we will focus here on time to self-sustained combustion (TSC), peak heat release rate (PHRR), time to peak heat release rate (T_{PHRR}), and total heat released (THR). In most cases where smectite clays or modified clays are used as polymer additives (without synergistic coadditives), the key trends observed are a decrease in TSC, a decrease in PHRR, and little or no change observed in THR (6). Figure 6 shows heat release rate curves for PMMA and PMMA with our additives at two different loadings. Cone data are summarized in Table II.

In contrast to the commonly observed trends for polymer/clay nanocomposites (6), neither CHM_x nor ZCM_x loaded at 2% or 4% lead to any significant decrease in PHRR. The time to peak heat release is slightly decreased for all of the samples containing additives. The time to sustained combustion decreases for samples containing 2% additive but remains approximately the same or is slightly improved with the 4% loading.

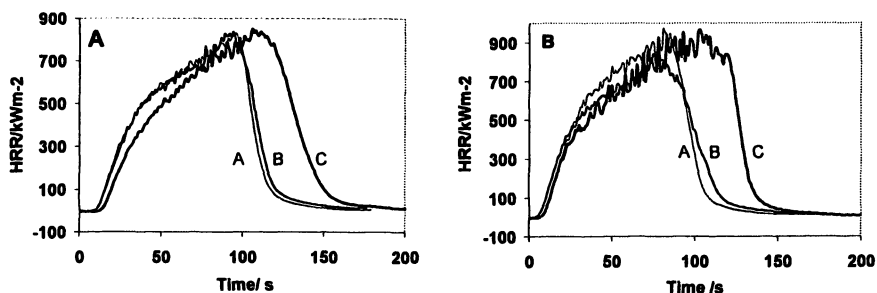


Figure 6. Heat release rate curves. A. 2% loadings (A) PMMA-ZCM_x, (B) PMMA-CHM_x, and for comparison (C) pure PMMA. B. 4% loadings (A) PMMA-ZCM_x, (B) PMMA-CHM_x, and for comparison (C) pure PMMA.

Table II Cone Calorimetry Data

Sample	TSC (s)	PHRR (kW/m ²) (% change ^a)	T _{PHRR} (s)	THR (MJ/m ²) (% change ^a)
PMMA	7.9	874	109	69
PMMA-CHM _x -2%	4.6	846 (-3%)	92	53 (-23%)
PMMA-ZCM _x -2%	4.0	848 (-3%)	96	53 (-22%)
PMMA	4.7	966	104	79
PMMA-CHM _x -4%	5.2	902 (-7%)	87	57 (-27%)
PMMA-ZCM _x -4%	6.2	981 (+2%)	83	56 (-29%)

^a Percentage change relative to pure PMMA sample, comparison data acquired on the same day to control for run-to-run fluctuations.

The most striking result observed here is the significant lowering in total heat release with incorporation of our additives into PMMA. As is clearly evident in Figure 6, combustion ends earlier with the additives. The decrease in THR suggests that the presence of additives results in incomplete combustion of the polymer, also consistent with the extent of char formation observed in TGA

experiments. Both the ZCM_x and the CHM_x additives lead to similar decreases in total heat release, with the 4% loading leading to a slightly larger effect than observed with the 2% loading. We note that the average effective heat of combustion obtained from cone data is unchanged for the 2% additive loadings compared with PMMA (~20 MJ/kg) but is slightly increased for the 4% loading (23-24 MJ/kg).

While both additives lead to similar effects in cone calorimetry analysis, there is, however, a striking difference in the metal-containing species found in the residue remaining after combustion in the cone calorimeter. Figure 7 shows X-ray diffraction analysis of the residues. PXRD patterns of the cone residue revealed the presence of CuO , Cu_2O , and $Cu^{(0)}$ for the PMMA- CHM_x composites and ZnO and CuO for PMMA- ZCM_x composites as shown in Figure 7A and 7B, respectively. The observation of reduced copper in the PMMA sample loaded with CHM_x is consistent with the hypothesis that the copper may play a chemical role in forming polymer-containing char. This is also consistent with TGA experiments where a higher char content was found in PMMA- CHM_x , compared with corresponding loadings of the PMMA- ZCM_x composites (Table I). Some differences in DTA data were also observed for the two additives, again suggesting a possible difference in mechanism due to metal content.

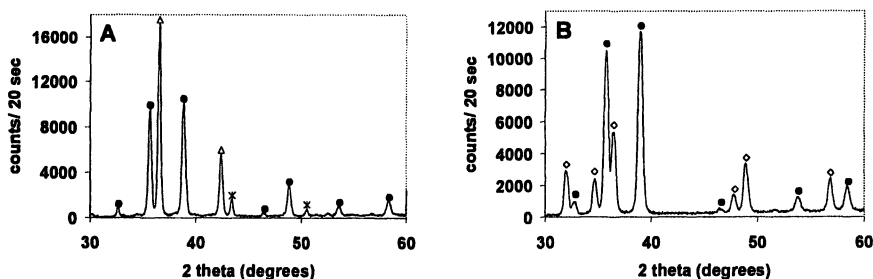


Figure 7. A. XRD patterns of PMMA- CHM_x -4% residue from cone calorimetry reflections assigned to CuO (\bullet), Cu_2O (Δ), and $Cu^{(0)}$ ($*$) reflections are marked. B. XRD patterns of PMMA- ZCM_x -4% residue from cone calorimetry with ZnO (\diamond) and CuO (\bullet) reflections marked; no reduced copper species were observed.

Future experiments including TGA coupled with Fourier transform infrared spectroscopy analysis of vapor phase products (TGA-FTIR) and spectroscopic analysis of the organic content of the chars will be performed in order to provide further insight into the role that the copper content of the additive plays on the combustion process. More detailed analysis of polymer samples synthesized with and without additives is necessary to examine whether the additive influences polymer properties such as molecular weight distribution. In addition,

modification of the organic portion of the additive to improve dispersion should be also be attempted in order to better characterize whether the extent of dispersion is a factor influencing the copper oxidation states in cone residues. For example, using longer chain organic groups with polymerizable end groups, in contrast to the simple methacrylate groups used here, would serve to make the interlayer domain more organophilic, which should enhance dispersion. Use of fully-exchanged additives would also enable us to eliminate any possible contribution of the small amount residual nitrate or acetate to the observed thermal degradation pathways.

Conclusions

Two copper-containing hybrid inorganic/organic layered compounds with nanodimensional interlayer spacing have been tested as fire retardant additives for PMMA. Copper hydroxy methacrylate (CHM_x) and zinc/copper methacrylate (ZCM_x) hydroxy double salt additives each form microcomposites when added to PMMA during bulk polymerization. Both additives serve to increase the temperature required for mass loss in TGA analysis with $T_{50\%}$ found to increase by 40-60° C with 2-4% by mass additive loadings. The CHM_x additive led to slightly larger temperature increases and a greater extent of char formation compared with the same mass percent loading of ZCM_x . Residue remaining from combustion in a cone calorimeter contains reduced copper species for CHM_x but only CuO and ZnO when ZCM_x is used. While TGA, DTA, and X-ray diffraction analysis of combustion residues suggest the possibility of different effects for the two additives on the PMMA thermal degradation pathways, similar results were obtained in cone calorimetry measurements. The presence of either additive at 2-4% loading led to a significant reduction in total heat release but did not reduce the peak heat release rate. While further work is necessary to complete characterization of these new additives, the results presented here demonstrate the potential of these compounds for use as fire retardant additives.

Acknowledgments

Helpful discussions with C.A. Wilkie and coworkers are gratefully acknowledged. Work on this project was initiated with support from the Marquette University Committee on Research.

References

1. Alexandre, M.; Dubois, P. *Mater. Sci. Eng.* **2000**, *R28*, 1.
2. Zhu, J.; Morgan, A.B.; Lamelas, F.J.; Wilkie, C.A., *Chem. Mater.* **2001**, *13*, 3774.
3. Tyan, H.; Leu, C.; Wei, K., *Chem. Mater.* **2001**, *13*, 222.
4. Xie, W.; Gao, Z.; Pan, W.-P.; Hunter, D.; Singh, A.; Vaia, R., *Chem. Mater.* **2001**, *13*, 2979.
5. Yeh, J.-M.; Liou, S.-J.; Lai, C.-Y.; Wu, P.-C., *Chem. Mater.* **2001**, *13*, 1131.
6. Chigwada, G.; Wilkie, C.A., *Polym. Degrad. Stab.* **2003**, *80*, 551.
7. Leroux, F.; Besse, J., *Chem. Mater.* **2001**, *13*, 3507.
8. Bubniak, G. A.; Schreiner, W. H.; Mattoso, N.; Wypych, F. *Langmuir*, **2002**, *18*, 5967.
9. Chen, B.; Qu, B. *Chem. Mater.* **2003**, *15*, 3208.
10. Leroux, F.; Adachi-Pagano, M.; Intissar, M.; Chauvière, S.; Forano, C.; Bess, J.P. *J. Mater Chem.* **2001**, *11*, 105.
11. Messersmith, B.P.; Stupp, S.I. *Chem. Mater.* **1995**, *7*, 454.
12. Morioka, H.; Tagaya, H.; Kadokawa, J.; Chiba, K. *Recent. Res. Devel. Mat. Sci.* **1998**, *1*, 137.
13. Meyn, M.; Beneke, K.; Lagaly, G. *Inorg. Chem.* **1993**, *32*, 1209.
14. Choy, J.; Kwon, Y.; Song, S.; Chang, S. *Bull. Korean Chem. Soc.* **1997**, *18*, 450.
15. Morioka, H.; Tagaya, H.; Karasu, M.; Kadokawa, J.; Chiba, K. *Inorg. Chem.* **1999**, *38*, 4211.
16. Hossenlopp, J.M., *Proc. Conf. Rec. Adv. in Flame Retard. Polym. Mater.* **2004**, *15*, 199.
17. Tanaka, H.; Terada, S. *J. Thermal. Anal.* **1993**, *39*, 1011.
18. Cheary R.W.; Coelho A. A. Programs XFIT and FOURYA, deposited in CCP14 Powder Diffraction Library, Engineering and Physical Sciences Research Council, Daresbury Laboratory, Warrington, England. (<http://www.ccp14.ac.uk/tutorial/xfit-95/xfit.htm>), 1996.
19. Bovio, B.; Locchi, S. J. *Crystallographic and spectroscopic Research.* **1982**, *12*, 507.
20. Kandare, E.; Hossenlopp, J.M, unpublished results.
21. Fujita, W.; Awaga, K. *Inorg. Chem.* **1996**, *35*, 1915.
22. Martin, J. W.; Dickens, B.; Waksman, D.; Bentz, D. P.; Byrd, E. W.; Embree, E.; Roberts, W. E. *J. Appl. Polym. Sci.* **1987**, *34*, 377.
23. Holland, B. J.; Hay, J. N. *Polym. Degrad. Stab.* **2002**, *77*, 435.
24. Chen, W.; Feng, L.; Qu, B. *Solid State Comm.* **2004**, *130*, 259.
25. McNeill, I. C.; Zulfiqar, M.; Urie, C. *Polym. Degrad. Stab.* **1984**, *9*, 239.
26. Chandrasiri, J. A.; Wilkie, C. A. *Polym. Degrad. Stab.* **1994**, *45*, 91.

Chapter 12

Thermal Stability and Flammability of Polymer–Silica Nanocomposites Prepared via Extrusion

Feng Yang, Ria Yngard, Alica Hernberg, and Gordon L. Nelson

College of Science, Florida Institute of Technology, 150 West University
Boulevard, Melbourne, FL 32901

A novel approach, a single-screw extrusion technique, was applied to the preparation of polymer/silica nanocomposites. The thermal properties of the resulting nanocomposites are discussed in terms of silica content and particle size. For PMMA / silica nanocomposites, significant improvement in thermal stabilities of the materials has been shown compared with PMMA itself. On the other hand, although nanocomposites are not flame retardant, less flame retardant additives were needed to achieve the same level of flame retardancy when nanocomposites were used, as seen in PS / silica nanocomposites. Thermal stabilities of PETG/PMMA/silica and PC/silica nanocomposites were also improved, while no significant changes were found when those materials were subjected to UL 94 evaluation.

Over the past decade, polymer nanocomposites have received considerable interest as an effective way for developing new composite materials, and they have been studied widely. Because of the larger surface area and surface energy of the additives when individual particles become smaller, it is not an easy task to obtain homogeneously dispersed organic / inorganic composites when the additives are down sized to nano-scale (1-5). Up to now, five major approaches have been reported for the preparation of organic / inorganic nanocomposites, and they are the sol-gel process (6-10), in-situ polymerization (11,12), solution blending, intercalative polymerization (13-15), and melt intercalation (16,17). Among these approaches, most of them involve polymerization of monomer in the presence of additives, except solution blending and melt intercalation. Melt intercalation has been successful in preparing polymer clay nanocomposites (18), but materials with good physical performance can only be achieved by employing a twin-screw extruder, which is expensive for bulk production of nanocomposites. A new approach utilizing a single screw extruder to prepare nanocomposites was previously reported by us (19-22), and different kinds of polymer/inorganic nanocomposites have been successfully obtained.

In this paper, an approach utilizing a single extruder to achieve polymer/silica nanocomposites was used, and four types of nanocomposites were prepared. They are PMMA/silica, PS/silica, PETG/PMMA/silica and PC/silica nanocomposites. The thermal stabilities and flammability of those nanocomposites are reported.

Experimental

Preparation of polymer/silica nanocomposites

Polymer/silica nanocomposites were obtained by a single screw extrusion technique developed in our laboratory using a 3/4" CW Brabender Table Top Independent Extruder (19-22). Polymer pellets were pre-dried under vacuum at 60 °C for one day to eliminate moisture and solvent. A 2" ribbon die was used at the orifice of the extruder.

Thermal stability of polymer/silica nanocomposites

All the materials were tested with a Hi-Res TGA 2950 thermogravimetric analyzer from Thermal Analysis Co. to evaluate thermal stability. Materials were

preheated to 100°C and held for 5 minutes to eliminate solvent and moisture in the sample before testing. The temperature ramp rate was 10°C/min and temperature scan range was 100~600°C respectively. All tests were performed under a helium atmosphere.

Flammability Evaluation

Oxygen Index testing (OI) was performed on all samples according to ASTM D2863. OI is the minimum oxygen concentration in an oxygen/nitrogen flow that just supports flaming combustion of a sample that burns downward in a candle-like configuration. The burning flame spread rate of all the samples was investigated by the Horizontal Burning Test according to ASTM D635. Vertical burning behavior was accessed using the UL 94 method.

Results and Discussion

PMMA / Silica Nanocomposites

Degradation of polymeric materials involves the scission of long polymer chains into shorter ones. When good interfacial interaction exists in an organic / inorganic composite, the inorganic phase can act as restriction sites for the movement of polymer chains, which typically increases the degradation temperature. In Table I, all silica nanocomposites showed higher degradation temperatures than PMMA itself, as expected, while an increase in degradation temperature with increasing silica content and decreasing particle size was also found.

Considering the fact that there are more particles per weight for smaller size silica than larger size silica, more particles will offer more restriction sites for the polymer chain, the scission of the polymer chain will become more difficult, and thus require more thermal energy for degradation (example, at 5% additive). Moreover, the better interfacial interaction between additives and polymer chain introduced by the deeper penetration of smaller particles in the polymer matrix will also restrict the movement of the polymer chain.

Table I. Thermal stability and flammability of PMMA/silica composites.

<i>Sample*</i>	<i>Temp. at 10% Weight Loss (°C)</i>	<i>Temp. at 50% Weight Loss (°C)</i>	<i>Oxygen Index</i>	<i>Average Burning Rate (cm/min)^a</i>
PMMA	343	379	17.5	4.7
PMMA-40-5	347	391	19.8	7.3
PMMA-40-10	358	398	21.2	7.7
PMMA-40-15	366	401	21.2	8.1
PMMA-30-5	350	385	18.9	7.0
PMMA-30-10	359	394	21.2	6.7
PMMA-30-15	367	411	22.1	7.7
PMMA-20-1	360	389	17.5	6.9
PMMA-20-3	361	388	19.8	7.4
PMMA-20-5	364	392	21.2	7.2
PMMA-20-10	373	403	22.1	8.4
PMMA-20-13	378	408	22.1	8.9
PMMA-16-5	369	397	22.1	7.8
PMMA-16-10	363	397	22.9	8.4
PMMA-7-5	370	399	22.1	6.9
PMMA-7-6	373	403	22.1	6.6

*: The code system can be explained by the following example: PMMA-30-10. The first element is the polymer matrix, which is PMMA in this case. The second element is the nominal size of silica in nm used, and the third element is the concentration of silica in the material in wt%.

a: Burning rate = $450/(t - t_1)$, where t_1 is the burning time from the beginning to 25 mm, and t is the burning time from the beginning to 100 mm (ASTM D635).

Oxygen index is a common test used to evaluate the ease of extinction of plastics. The minimum percentage of oxygen in an oxygen/nitrogen mixture to just sustain the combustion of a top ignited specimen is measured. Table I lists the oxygen indices of PMMA/silica nanocomposites. Oxygen indices of nanocomposites show modest improvement, although fillers in general lead to lower oxygen indices for thermoplastic samples due to less dripping. Real flame retardancy is not achieved, which requires the oxygen index to reach 24~28. Below this number, materials are easily ignited and difficult to extinguish once ignited. The horizontal burning test (ASTM D635) is a test to evaluate the fire spread rate of a small sample. PMMA/silica nanocomposites listed on Table I are not flame retardant materials. They all exhibit substantially higher burning rates and shorter average times of burning compared to PMMA. In another words, they burn faster. However, all the nanocomposites burn without dripping, which

is very different from PMMA, which drips significantly during the test. The phenomenon can be explained by the "wick effect". For some organic/inorganic composites, fire will burn out the organic phase and leave the inorganic phase intact, which will lead to a faster burning rate of the composite.

Polystyrene / Silica Nanocomposites

Table II. Decomposition and flammability of PS/BrPS/ Silica composites.

<i>Composite</i>	<i>Temp. at 10% Weight Loss (°C)</i>	<i>Temp. at 50% Weight Loss (°C)</i>	<i>OI</i>	<i>Average Burning Rate (cm/min)</i>
Polystyrene	389	420	17.3	5.4
PS-1%silica-M1*	403	425	17.0	5.7
PS-3%silica-M1	404	426	17.3	5.8
PS-5%silica-M1	405	427	17.5	6.1
PS-10%silica-M1	406	428	18.1	7.3
35%BrPS-55%PS-10%silica-M1	396	421	25.4	AEB**=1.5cm
PS--5%silica-M2	395	424	18.4	7.1
PS-10%silica-M2	400	428	17.5	6.6
PS-15%silica-M2	402	430	17.8	8.2
35%BrPS-55%PS-10%silica-M2	399	430	24.1	AEB=1.5cm
35%BrPS-65%PS	387	420	23.0	AEB=1.0cm
40%BrPS-60%PS	391	419	24.0	AEB=0.5cm

*all nanocomposites were developed based on silica with nominal diameter of 20 nm.

**AEB = Average Extent of Burning

The decomposition of polystyrene at temperatures between 300 and 500°C in air yields predominantly monomer (55%-67%) (23). In Table II, the temperature at which 10% weight loss and 50% weight loss of the composites occurred are listed.

As shown in Table II, all nanocomposites exhibited a higher degradation temperature than polystyrene itself. The presence of silica modified with either a long (PDMS, polydimethylsiloxane, M2) or short (PTCS, phenethyltrichlorosilane, M1) chain resulted in an increase of the decomposition temperature at 10% and 50% weight loss. An increase in the silica concentration resulted in an increase in the temperature at which the material started to break down. The degradation temperatures for silica treated with PDMS were not significantly different from silica treated with PTCS.

Table III. Vertical burning (UL 94) of PS/BrPS/Silica nanocomposites.

<i>Materials</i>	<i>1st imp¹.(s)</i>	<i>2nd imp.(s)</i>	<i>Notes</i>
PS	104	-	*
PS-1%silica-M1	92	-	*
PS-3%silica-M1	83	-	*
PS-5%silica-M1	68	-	*
PS-10%silica-M1	57	-	*
PS-15%silica-M1	72	-	*
30%BrPS-60%PS-10%silica-M1	3	7	V2
35%BrPS-55%PS-10%silica-M1	1	1	V0
35%BrPS-60%PS-5%silica-M1	2	3	V2
PS-5%silica-M2	49	-	*
PS-10%silica-M2	53	-	*
PS-15%silica-M2	62	-	*
35%BrPS-55%PS-10%silica-M2	1	1	V0
35%BrPS-60%PS-5%silica-M2	5	10	V2
38%BrPS-62%PS	1	1	V2
40%BrPS-60%PS	1	1	V0

imp¹: extinguishing time in seconds after 10 second flame impingement.

*: ignites cotton and burns up to the clamp.

According to the Underwriter's Laboratories vertical fire test protocol (UL94), V0, V1, V2 ratings are obtained depending upon whether self-sustained ignition occurs after applications of a small Bunsen burner flame. The data obtained from this test are listed in Table III. The samples were burned after

conditioning at room temperature for at least 48 hours and at 70°C for 168 hours. The data in Table III indicate that silica composites burned faster than the virgin material (shorter time to burn to the clamp). In the literature, organic/inorganic nanocomposites have shown reduced “flammability” (24-26); however, nanocomposites with only nanoclay and with a V0 rating have not yet been reported. In the present case, materials with 40% of brominated polystyrene added are V0 and with 38% of brominated polystyrene added are V2. When 10% silica is added to polystyrene, only 35% of flame retardant additive is needed to make the material V0. These results were obtained with silica that was treated with either PTCS or PDMS.

Compared with the virgin polymer, polystyrene/silica nanocomposites showed a slight increase in the oxygen index, but not enough to achieve flame retardancy (Table II). Addition of the flame retardant additive to polystyrene causes an increase in OI up to a point where the presence of 40% of brominated polystyrene resulted in a flame retardant material (OI of 24). This result is consistent with what was found in the vertical burning test; polystyrene became flame retardant (V0) when 40% brominated polystyrene was added. The above results also indicate that the addition of nanoscale silica itself to the pure polymer cannot achieve flame retardancy (V0). However, less flame retardant additive is needed to achieve the same level of flame retardancy when silica is present. For example, only 35% instead of 40% of brominated polystyrene is needed when 10% silica was present, in order to achieve V0. The sample has the highest OI, at 25.4 (for 10% silica-M1).

According to data in Table II and Table III, all the polystyrene/silica nanocomposites burn faster than the pure polymer. The average burning rate increased with an increase in silica content, no matter which surface modifier was used, in both vertical and horizontal samples. On the other hand, the addition of flame retardant brominated polystyrene to polystyrene had the expected fire resistance effect.

PETG/PMMA/Silica Nanocomposites

As discussed to this point for two phase organic/ inorganic composites, if the interface is strong enough, the inorganic phase will restrict the movement of the chains of the polymer. Scission of the chains will become more difficult and will result in an increased decomposition temperature. However, for materials with more than two components, the thermal degradation process may be more complicated.

Table IV. Thermal stability and flammability of PETG/PMMA/silica nanocomposites.

<i>Sample</i>	<i>Temp. at 10% Weight Loss</i>	<i>Temp. at 50% Weight Loss</i>	<i>OI</i>	<i>Average Burning Rate (cm/min)</i>
PMMA	341	371	17.5	4.7
PETG	407	429	18.6	Drip to extinguish
PMMA-PETG	378	417	18.4	6.1
PMMA-PETG-1%*	367	406	18.4	5.7
PMMA-PETG-3%	372	408	18.4	5.7
PMMA-PETG-5%	366	406	18.4	5.6

*all nanocomposites were developed based on Aerosil® R972 from Degussa (nominal diameter is 16 nm), and the content of silica was indicated as the third column in sample code.

According to Table IV, the degradation temperature of PETG/PMMA blend is not as high as PETG itself, while higher than PMMA. However, all nanocomposites showed a little lower degradation temperature than the polymer blend. While studies on isothermal degradation will be performed to clarify the cause of early degradation in nanocomposites in a three component system like this, most likely the presence of silica may increase the free volume of the material, and cause the less thermally unstable PMMA, which degrades by simple unzipping, to degrade more easily compared with the blend.

Compared to the virgin polymer, polymer blends and nanocomposites showed little difference from PETG in their fire performance. Both PETG and PMMA are very flammable materials. Without other flame retardant additives, the blend itself will not become more flame retardant. As we reported previously, nanocomposites alone are not flame retardant materials. The results in Table IV can be used as further evidence for our previous conclusion.

According to the data in Table IV, all nanocomposites burn slightly slower than the polymer blend, while the burning rate of PETG can not be obtained because of the severity of the dripping.

PC/Silica Nanocomposites

As a high performance engineering plastic, polycarbonate always gains attention from materials scientists. The disadvantages of polycarbonate materials

are mostly associated with the degradation and weathering performance of these materials. Therefore, improvement in the stability of these materials may be important for the application of polycarbonate.

Table V. Thermal stability and flammability of PC/silica nanocomposites.

<i>Material</i>	<i>Temp. at</i>	<i>Temp. at</i>	<i>Vertical Burn Testing (UL94)*</i>		
	<i>10% Weight Loss</i>	<i>50% Weight Loss</i>	<i>Tf(s)</i>	<i>T1avg(s)</i>	<i>T2avg(s)</i>
Polycarbonate	452	482	124	7.2	17.7
PC-1% silica	456	492	57	5.2	6.2
PC-3% silica	466	497	100	15.7	9.3
PC-5% silica	456	491	118	7.2	22.2

*: all samples dripped and ignited cotton. Tf is the sum of T1 and T2 for 5 samples.

In Table V, all polycarbonate / silica nanocomposites exhibited higher thermal stabilities than polycarbonate itself. The improvement in thermal stability of these materials is consistent with the results of other polymer silica nanocomposites discussed above, and showed further evidence that nanocomposites are more thermally stable. PC/silica nanocomposites also showed impact on the flammability according to vertical burning tests. While all materials subjected to vertical burning testing are V2 rated, after flame times at 1% silica were significantly reduced, Tf of 57s versus 124s.

Conclusion

Polymer / silica nanocomposites were successfully prepared by a single-screw extrusion technique, and four different kinds of polymer / silica nanocomposites were obtained. They are PMMA / silica, PS / silica, PETG/PMMA/silica and PC / silica nanocomposites. All nanocomposites showed significant improvement in thermal stabilities. The thermal degradation of polymers is largely associated with the molecular chain length and segmental chain length. The restriction caused by the presence of additive particles will improve the thermal stabilities of the materials. The flammability of nanocomposites suggests that small amounts of restriction make no significant contribution to the flame retardancy of the materials since fire is largely a surface phenomenon.

Polymer/silica nanocomposites alone are not flame retardant as shown by vertical burning tests and oxygen index. In fact, the materials burned faster, with the exception of polycarbonate. On the other hand, results of PS / silica nanocomposites showed that nanocomposites have a positive impact on the

flame retardancy of materials when combined with FR additives. The addition of 40% of brominated polystyrene to the pure polymer resulted in a flame retardant material with a rating of V0, while less flame retardant additive (35%) was needed in the presence of 10% of silica to achieve the same level of flame retardancy.

References

- 1, Fan, J.; Liu, S.; Qi, Z. *J. Appl. Polym. Sci.*; **2002**; *83*; 66-69.
- 2, Vacatello, M. *Macromolecules*, **2001**, *34*, 1946-1952.
- 3, Ou, Y. ; Yang, F., Yu, Z. *J. Polym. Sci. Part B: Polym. Phys.*, **1998**, *36*, 789-795.
- 4 Yang, F.; Ou, Y.; Yu, Z. *J. Appl. Polym. Sci.*, **1998**, *69*, 355-361.
- 5 Yang, F.; Nelson G. L. "Mechanical and Thermal Properties of PMMA/Silica Nanocomposites Prepared by Extrusion", The 11th International conference, ADDITIVES **2002**.
- 6 Hou, Y.; Zhang M.; Rong M.; Yu G.; Zeng H. *J. Appl. Polym. Sci.*; **2002**, *2768-2775*.
- 7 Egerton, R. *Chem. Mater.*; **1998**; *10*, 3936-3940.
- 8 Tilley, T. D. *Chem. Mater.*; **1996**; *8*, 274-280.
- 9 Harmer, M. A.; Farneth, W. E.; Sun, Q. *J. Chem. Soc.*; **1996**, *118*, 7708-7715.
- 10 Ma J.; Qi Z.; Hu Y. *J. Appl. Polym. Sci.*; **2001**, *82*, 3611-3617.
- 11 Mishra, S.; Sonawane, S. H.; Singh, R. P.; Bendale, A.; Patil, K. *J. App. Polym. Sci.* **2004**, *94*, 116.
- 12 Lan, T.; Pinnavaia, T. J. *Chem. Mater.* **1994**, *6*, 2216.
- 13 Usuki, A.; Kojima, Y.; Kawasumi, M.; Okada, A.; Fukushima, Y.; Kurauchi, T.; Kamigaito, O. *J. Mater. Res.* **1993**, *8*, 1179.
- 14 Usuki, A.; Kato, M.; Okada, A.; Kurauchi, T. *J. App. Polym. Sci.* **1997**, *63*, 137.
- 15 Ni, P.; Li, J.; Suo, J.; Li, S. *J. App. Polym. Sci.* **2004**, *94*, 534.
- 16 Fisher, H.; Gielgens. L.; Koster, T. "Nanocomposites from Polymers and Layered Minerals"; TNO-TPD Report, **1998**.
- 17 Kojima, Y.; Usuki, A.; Kawasumi, M.; Okada, A.; Fukushima, Y.; Kurauchi, T.; Kamigaito, O. *J. Mater. Res.* **1993**, *8*, 1185.
- 18 Giannelis, E. *Adv. Mater.* **1996**, *8*, 29.
- 19 Yang, F.; Nelson, G. L. "PMMA/Silica and Polystyrene / Silica Nanocomposites Prepared via Extrusion", 2nd World Congress Nanocomposites, **2002**, Proceedings.
- 20 Yang, F.; Nelson, G. L. "Mechanical and Thermal Properties of PMMA/Silica Nanocomposites Prepared by Extrusion", The 11th International Conference, ADDITIVES **2002**, Proceedings.

21. Yang, F.; Nelson, G. L. "Thermal Properties and Flammability Study of PMMA / Silica Nanocomposites", The Thirteenth Annual BCC Conference on Flame Retardancy, **2002**, Proceedings.
22. Yang, F.; Nelson, G. L. "Flame Retardant or Not: Fire Performance of Polystyrene / Silica Nanocomposites Prepared via Extrusion", The Fourteenth Annual BCC Conference on Flame Retardancy, **2003**, Proceedings.
23. Giannelis, E. P. *Appl. Organometal. Chem.* **1998**, 12, 675-680.
24. Lewin, M. The Thirteenth Annual BCC Conference on Flame Retardancy; Stamford, Connecticut, **2002**, 1-15.
25. Wilkie, C. A. The Tenth International Conference: ADDITIVES 2001; Hilton Head Island, South Carolina, **2001**, 1-6.
26. Davis, R. D.; Gilman, J. W.; VanderHart, D. L. "Processing Degradation of Polyamide 6 Montmorillonite Nanocomposites", The 11th International conference, ADDITIVES **2002**.

Chapter 13

Effect of Layered Silicate Nanocomposites on Burning Behavior of Conventionally Flame-Retarded Unsaturated Polyesters

B. K. Kandola, S. Nazaré, A. R. Horrocks, and P. Myler

**Centre for Materials Research and Innovation, Bolton Institute,
Deane Road, Bolton BL3 5AB, United Kingdom**

Montmorillonite clay has been modified with a series of organic modifiers. Modified clays have been characterised by X-ray diffraction and thermal analytical techniques. Unsaturated polyester nanocomposites have been prepared by *in-situ* polymerisation. Some clays were fully exfoliated, some indicated combined nano-structures with ordered intercalation and partial exfoliation, and some indicated only microcomposite structures, depending upon type of organic modifier used. Thermal stability and flammability of these samples have been studied by thermal analysis and cone calorimetry. All clays reduce the onset of decomposition temperature of the resin, slightly increase ignition time and total burning time but decrease peak heat release rate (PHRR) values (9-36%) and total heat release rate (THR) (2-16%) compared to resin only sample. In the presence of conventional flame retardant, ammonium polyphosphate (APP), there is a synergistic effect with the nanoclay in terms of increased char formation, reduction in PHRR (60-67%), THR (35-39%) and smoke production (1-13%) compared to resin. Mechanical testing in terms of flexural mode has indicated that inclusion of functionalised nanoclays enhances mechanical performance of the resin.

Introduction

There is a constant demand for efficient and environmentally friendly flame retardants. Organic-inorganic nanocomposites are of significant interest since they frequently exhibit unexpected hybrid properties synergistically derived from two components [1-3]. Montmorillonite, one of the layered silicate clay minerals, is composed of silicate layers with a thickness of about 1 nm. Organic ammonium ions and neutral organic molecules may be intercalated in the interlayer space between the silicate layers [4], which when present in a polymer matrix may lead to increased mechanical and reduced flammability properties at very low loading levels (2 – 5%) [2,3]. The efficiency of clay in modifying the properties of the polymer is primarily determined by its degree of dispersion in the polymer, which in turn depends on the clay particle size and chemistry of the clay [5]. Exfoliation depends upon processing shear conditions, melt rheology and the structure of aliphatic or organic compound to modify the clay [6]. The structure of a layered silicate and its charge density may also influence nanocomposite morphology and degree of exfoliation [6,7].

During the last five years we have been studying the flammability behaviour of unsaturated polyester resin, as cast laminates and glass - reinforced composite structures [8-10]. In our previous publications [10,11], we have used commercially available organically modified clays in preparing unsaturated polyester nanocomposites with and without conventional flame retardants. In this work, the effects of different organic modifiers on nanocomposite formation and thermal, flammability and mechanical properties of the resultant polymer are presented. Due to the limited sample size and numbers available, mechanical performances are only studied in the flexural mode, however, full mechanical characterisation of glass fibre reinforced composite laminates prepared from selected nanoclays and flame retardant unsaturated polyester resins will be discussed in a subsequent publication.

Experimental

Materials

Polyester resin : Orthophthalic, Crystic 471 PALV (Scott Bader) ; Catalyst M (methyl ethyl ketone peroxide, Scott-Bader)

Clays : Cloisite Na⁺ montmorillonite, Na-MMT (Southern Clay Products, USA) modified with different organic modifiers are given in Table 1.

Table I. Treatment / properties of organically modified clays

Clay	Organic modifier	Chemical structure of organic modifier	XRD results d spacing (nm)*
Na-MMT		-	1.17
Cl (i)	Vinyl triphenyl phosphonium bromide		1.77, 0.89, 0.58
Cl (ii)	Vinyl benzyl trimethyl ammonium chloride		1.46, -, 0.48
Cl (iii)	Hexa decyl trimethyl ammonium chloride		1.82, 0.94, 0.56
Cl (iv)	Dodecyl ethyl dimethyl ammonium bromide		1.72, 0.98, 0.61
Cl (v)	N,N-dimethyl-N,N-dioctadecyl quaternary ammonium bromide		2.63, 1.29

Me = $-\text{CH}_3$ Et = $-\text{C}_2\text{H}_5$ Oct = $-\text{CH}_3(-\text{CH}_2-)_{17}$

* Values in bold are characteristic silicate d-spacings, in italics are very small peaks
Flame-retardant (FR) : Ammonium polyphosphate, APP (Antiblaze MCM, Rhodia Specialities)

Modification of sodium montmorillonite

Sodium montmorillonite (Na-MMT) clay has been functionalised with a range of quaternary ammonium and phosphonium salts, as given in Table I. An appropriate salt was dissolved in distilled water and gently agitated to obtain a homogeneous solution of 0.1 M, to which 50g of Na-MMT was added and stirred for 6 hours at room temperature. The resulting mixture was filtered and washed repeatedly with hot water (60 °C) until free of excess organic modifier (tested with AgNO₃ solution). The exchange process was repeated for another 48 hrs and the resulting clay was collected by filtration, washed, finally dried in a vacuum oven (40 °C, 24 hrs) and then ground into a fine powder.

Crude organo-modified clays contain impurities in form of (a) unexchanged / excess organic modifier and (b) an ion exchanged product (sodium bromide/chloride). The residual anions decrease thermal stability of organo clays, whereas the nature of counter cation dictates the onset of degradation of organic modifier on the organically modified clays [12]. Hence, the clays were extracted with ethanol first and then with tetrahydrofuran using routine soxhlet extraction procedures for 4 hours. The clays were dried under high vacuum for 18 hours at 120 °C. The extracted and dried organo-clays were analysed using XRD and TGA.

Preparation of polyester-clay nanocomposites

The polyester-clay nanocomposites incorporating flame retardants have been prepared by in-situ intercalative polymerisation. 5%(w/w) clay was gradually added to the polyester resin, while stirring with a mechanical mixer under high shear (900 rpm). The mixing was carried out for 60 min at room temperature. For samples incorporating flame retardant, 20% (w/w with respect to resin-clay mixture) of the flame retardant was added to the mixture of resin and clay after 20 min of mixing. The percentages of various components in the formulations are given in Table II. Small amounts of samples were taken from the mixture for simultaneous DTA-TGA analysis. For cone calorimetric studies, 1 % (w/w with respect to resin) catalyst was added, laminates were cast and cured at room temperature for 24 hours and post cured at 80°C for 8 hours. Their nanocomposite structures were characterised by X-ray diffraction, XRD.

Table II. Mass percentages of various components in the formulations

Sample	Sample description	Resin (%)	FR (%)	Clay (%)
Res	Resin	100	-	-
Res/Cl	Resin + Clay	95	-	5
Res/FR	Resin + FR	83	17	-
Res/Cl/FR	Resin + Clay + FR	79	17	4

Equipment

X-ray diffraction (XRD) studies were carried out using a Siemens D500 powder diffractometer with a step size of 0.02° , a step time of 1 s and a range of $0-25^\circ$ on the 2-theta scale. Simultaneous DTA-TGA analysis was performed using SDT 2960 TA instruments under flowing air (100 ml/min) and at a heating rate of 10K min^{-1} on 25 mg sample masses. A cone calorimeter (Fire Testing Technology Ltd., UK) was used at an incident heat flux of 50kW/m^2 according to ISO 5660. The flexural moduli of the laminates (coupon sizes $120 \times 12 \times 3$ mm) were measured in three point bending mode according to BS 2782-10: Method 1005:1997, EN 63:1977, with load applied via a computer controlled Instron 4303 tensometer.

Results and Discussion

X-ray diffraction studies

The periodic structures of inorganic clays can be distinguished through X-ray diffraction. Representative XRD patterns for the Cl (i) and (v), their hybrids with resin and with/without APP are given in Fig.1 (a) and (b), respectively. Characteristic d-spacing values for clays and their hybrids with resin and Res/APP for 2-theta in the range $2 - 10^\circ$ only, are given in Tables I and III, respectively. Na-MMT shows a peak at $2\theta = 7.3^\circ$ (d-spacing 1.17 nm, see Fig 1(a)), which has shifted to lower 2θ angles : in Cl (i) to 4.9° (d-spacing 1.77nm, Fig.1(a)), in Cl (ii) to 6.0° (1.46 nm (Table I)), in Cl (iii) to 4.8° (1.82nm (Table I)), in Cl (iv) to 5.1° (1.72nm (Table I)), and Cl (v) to 3.3° (2.63nm, Fig.1(b)).

This shows intercalation of the silicate layers by respective organic molecules. Some clays show up to three Bragg reflections, primary (d_{001}), secondary (d_{002}) and sometimes tertiary (d_{003}). These secondary or tertiary reflections are more prominent in certain clays compared to others, which may be explained by the height of the gallery spacing of the organoclay in relation to thickness of a silicate platelet [6]. This hypothesis is supported by the fact that these reflections are more prominent for organoclays with primary d-spacing 1.77 nm and higher (see Table I). Cl (i) shows prominent secondary peaks at $2\theta = 9.8$ and 15° , Cl (iii) at 9.3 and Cl (v) at 6.7° .

From Fig 1(a), Tables I and III, it can be seen that the Res/Cl (i) and Res/Cl (ii) samples have characteristic clay peaks similar to those of the respective clays, indicating that there is no intercalation of the polymer between the clay layers. These samples correspond to conventionally filled polymers where, at least, each primary particle is dispersed in the polymer matrix. Additional presence of APP does not affect this pattern as seen for respective Res/Cl/APP curves. For Res/Cl (iii) sample, the main peak of Cl (iii) at $2\theta = 4.8^\circ$ has moved to lower 2θ values ($2\theta = 2.5^\circ$) and the d-spacing has increased from 1.76 nm to 3.40 nm, suggesting ordered intercalation of the polymer chains into the organoclay layers. Also, an extremely broad peak (at $2\theta = 5.0^\circ$) indicates exfoliation. According to Bragg equation, $n\lambda = 2d \sin\theta$ and area under each reflection is proportional to $\sin^2(n\pi\phi/2)$, where ϕ is the volume fraction of the structure [6], so broadening of peak can be interpreted as partial exfoliation [13]. The XRD pattern of Res/Cl (iii) system hence, illustrates combined structure with partly exfoliated clay layers and the remaining having ordered intercalation. Presence of APP in Res/Cl (iii)/APP sample has in fact assisted exfoliation of layers because as seen in Table III, the d-spacing is no longer observed for Res/Cl (iii)/APP sample. Res/Cl hybrids containing Cl (iv) and Cl (v) have no characteristic peaks in their respective XRD patterns suggesting that clay layers are completely exfoliated and dispersed at the molecular level into resin. For Res/Cl(iv),(v)/APP samples (see Table III and Fig.1(b)) also the characteristic peaks are missing indicating exfoliation of clay layers. Characteristic XRD peaks of APP and broad resin peaks are unaffected by presence of clays in microcomposite or nanocomposite form as seen from Fig. 1(a) and (b).

In conclusion, XRD studies on the modified clays suggest that the clays modified with longer chain molecules show better exfoliation in polymer-clay nanocomposites than the others.

Mechanical performance studies

The mechanical performances in terms of flexural moduli of the samples containing nanoclays with and without flame retardants have been studied in

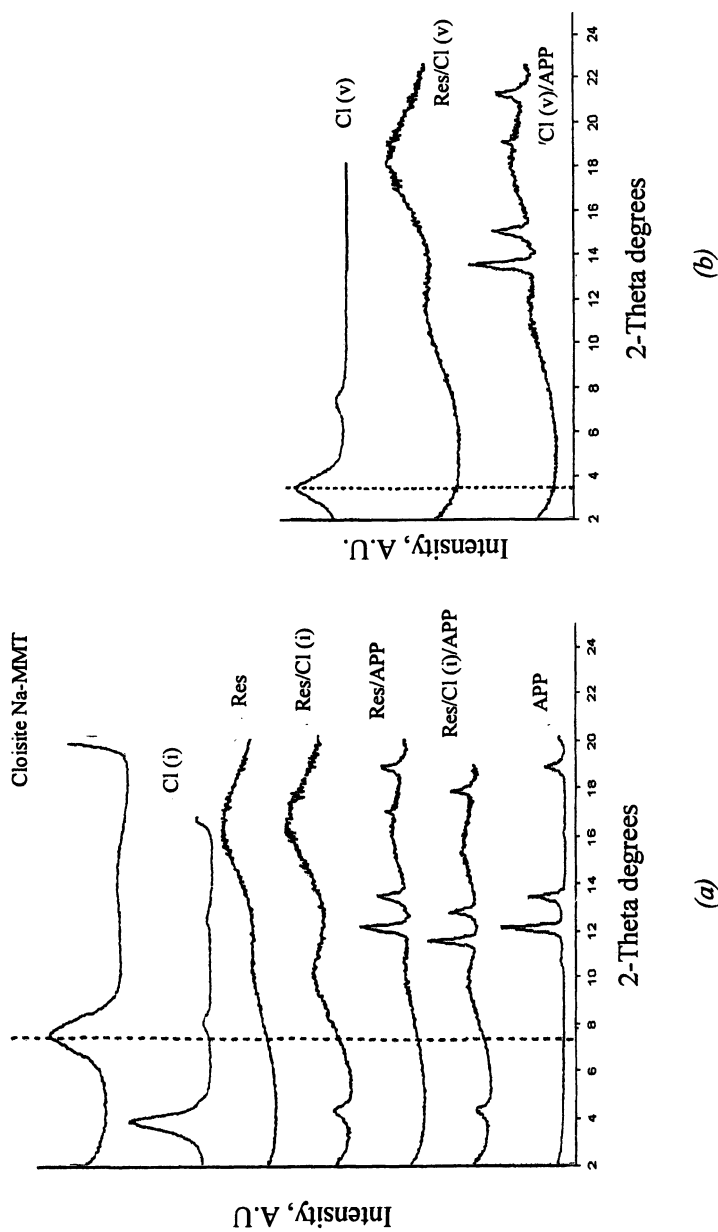


Fig. 1 XRD curves for unsaturated polyester with (a) Cl (i) and (b) Cl (v), with and without APP.

Table III. XRD and mechanical performance results for polyester-clay nanocomposites with and without FRs

Sample	XRD results [#] d-spacing, (nm)	Mechanical properties	
		Flexural modulus, <i>E</i> (GPa)	Stress at failure (MPa)
Res	-	3.3 ± 0.38	50.3 ± 2.3
Res / Cl (i)	1.76	4.5 ± 0.41	63.7 ± 3.1
Res / Cl (ii)	1.44	3.3 ± 0.07	45.5 ± 4.7
Res / Cl (iii)	3.04, 1.76	3.5 ± 0.01	42.1 ± 1.9
Res / Cl (iv)	-	3.3 ± 0.12	38.2 ± 1.3
Res / Cl (v)	-	*	*
Res/APP	-	2.7 ± 0.01	24.7 ± 1.0
Res /Cl (i) / APP	1.74	4.8 ± 0.34	68.2 ± 6.9
Res /Cl (ii) / APP	1.47	3.8 ± 0.18	56.9 ± 4.1
Res /Cl (iii) / APP	-	3.8 ± 0.04	49.3 ± 2.4
Res /Cl (iv) / APP	-	3.9 ± 0.07	45.1 ± 3.1
Res /Cl (v) / APP	-	*	*

[#] Diffraction peaks for 2-theta in the range 2 – 10° only are presented ; * Not tested

three point bending mode and the results are given in Table III. Inclusion of functionalised nanoclays maintains and in some cases enhances flexural modulus and hence, stiffness of the resin from 3.3 to 3.3 - 4.5 GPa, depending upon type of organic modifier of the clay. Stress at failure varies between 38.2 – 63.7 MPa for different Res/Cl samples. Inclusion of APP in resin (Res/APP sample) decreases both modulus (2.7 GPa) and stress at failure (24.7 MPa) of the resin. However additional presence of clay (Res/Cl/APP samples) enhances both modulus (3.8 – 4.8 GPa) and stress at failure (45.1 – 68.2 MPa). Res/Cl/APP samples show improved flexural moduli compared to resin only, Res/Cl and Res/APP samples, and stress at failure compared to Res/Cl and Res/APP samples (see Table III). In terms of reinforcing element, Cl (i) shows better results compared to other clays (see Table III) in enhancing mechanical performance (flexural modulus and stress to failure) of resin, with and without APP.

Thermal analysis

DTA and TGA analysis for all modified clays are given in Table IV. As seen from Table IV and also discussed in our earlier communication [10], the DTA response of Na-MMT is featureless, showing inertness of the inorganic clay. All organically modified clays show exothermic peaks (Table IV) and two or three stages of weight loss represented by respective DTG peaks (given in Table IV). For Cl (i), the main DTA decomposition peak is at 568°C, whereas for all other clays the decomposition peak is in the temperature range 300 - 352°C. This is also corroborated from DTG peaks, where the peak representing major weight loss for Cl (i) is at 574°C and for others in the range 250 - 352°C. This suggests a higher thermal stability of Cl (i). As discussed in detail earlier, on heating all of these clays, the organic component of the clay decomposes first, followed by dehydroxylation of clay layers [10,14]. Mass residues at 600 and 800°C are given in Table IV, which represent the residual silica content after decomposition of the organic component.

Polyester resin starts to decompose above 200°C and the main decomposition occurs between 300 and 400°C [10]. Above 400°C, solid phase oxidation of the char occurs, leaving very little char residue at higher temperatures (1% at 800°C, see Fig 2(a)).

Table IV. Thermal analytical properties of organically modified clays

Clays	DTA results Peak maxima* (°C)	TGA results	
		DTG peak * maxima (°C)	% Mass residue at 600 (°C) 800(°C)
Na-MMT	-	76 ; 665	91 88
Cl (i)	278 Ex(s,b) ; 568 Ex	144 ; 351 ; 574	80 75
Cl (ii)	335 Ex ; 612 Ex(s,b)	252 ; 592	73 66
Cl (iii)	305, 342 Ex(d) ; 618 Ex(s,b)	256 , 593	74 67
Cl (iv)	308 Ex ; 433 Ex(s) ; 621 Ex(s,b)	260, 310 (d) ; 445 ; 607	82 75
Cl (v)	301, 352 Ex(d) ; 455 Ex ; 609 Ex	300 ; 462 ; 634	76 67

Key : Ex = Exotherm ; s = small ; b = broad ; *Values in bold are main decomposition peaks

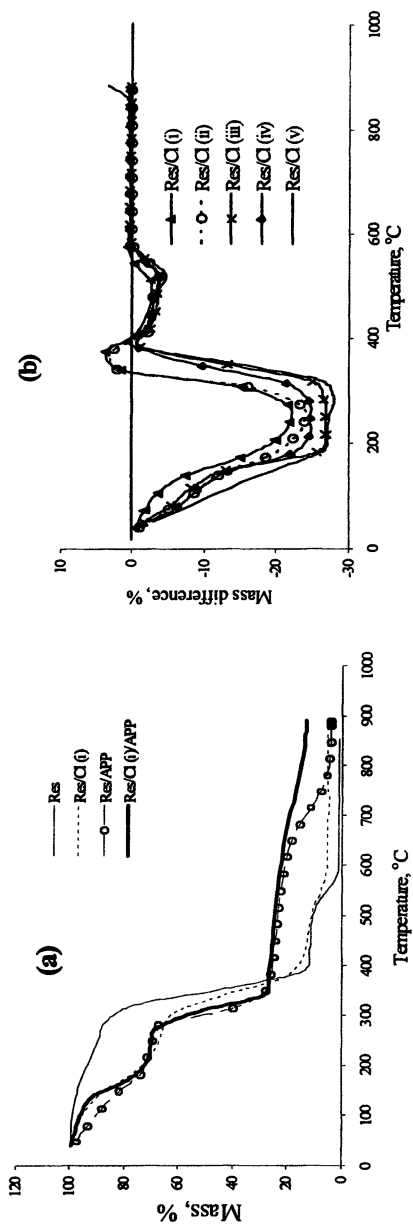
All clays reduce thermal stability of the resin below 400°C and above 600°C increase slightly as can be seen from Fig 2(a) for Cl (i). This is more clear in Fig.2(b), where the difference between TGA experimental and calculated (from weighted average component responses) masses versus temperature (for details see our previous publications [8,15]) for all Res/Cl samples are plotted. Above 600°C, char formations are similar to those expected from respectively calculated values and the type of clay has no effect on residue formation at high temperatures. This gives indication that nanoclays on their own are not effective in increasing residue formation by additional char and hence, reducing flammability of the resins. Ammonium polyphosphate increases residue formation to 3% (see Fig 2(a)) and nanoclays increase this value further to 12-14% as seen for Cl (i) samples in Fig 2(a), presumably as a consequence of carbonaceous char. In Fig 2(c) the difference between experimental and calculated TGA responses for Res/APP and all Res/Cl/APP samples are plotted, where it can be seen that that the thermal stabilities of these formulations are less than expected below 500°C, but after that they are more stable, suggesting synergistic effect of clay and FR combination. Nanoclays are known [2,3,10] to increase thermal stability of the polymer due to formation of a protective surface insulative barrier layer consisting of accumulated silica platelets with a small amount of carbonaceous char. These insulative silicate platelets are claimed to protect the fast volatilization and degradation of the resin and giving more time to react with acid released from APP, leading to more char formation than expected. All clays promote additional char formation above 700°C. This same effect noted for commercially modified clays has been discussed in detail in our previous communication [10].

Effect of clays on residual char formation of resin with and without APP is shown in Fig.2(d), where residual chars for all Res/Cl and Res/Cl/APP samples at 600 and 800°C are reported, after subtracting the residual silica content taken from Table IV. Clays enhance char formation of resin by 2%, whereas with additional presence of APP, more than 10% residual char is observed at 800°C.

Thermal analytical results indicate that all clays have a similar effect on the thermal stability of resin with and without APP. None of the clays shows any distinct behaviour, although there is slight shift in decomposition temperature range, depending upon the type of organic modifier used.

Cone calorimetry

The various parameters recorded by the cone calorimetric test at 50kW/m² heat flux are given in Table V and selected results are shown in Fig. 3. These are derived from respectively averaged curves obtained from three replicate runs for each sample. Thus heat release rate values have an error of $\pm 1 - 9\%$ (See Table V) Presence of clays in general does not affect time to ignition (TTI) of the resin (TTI=34s), although Cl (i) and (ii) slightly increase it to 45 and 40s, respectively. All clays increase flame out (FO) or total burn time of the resin from 136 to 139 – 170s (see Table V). Peak heat release rate (PHRR) of pure resin is reduced with all types of clays from 1153 kW/m² to 743 – 1045 kW/m², depending upon the organic modifier used. These clays also help in reducing total heat release, whereas, smoke production is not affected and even increased in some samples. Effective heat of combustion, H_c is the quantity of heat produced by combustion of a unit quantity of material and hence, may be used to measure the possible flame retarding effects of components present. Except for Res/Cl (i) sample, effective heat of combustion for all other samples is unaffected by presence of clay. In Table V, the fire growth index (FIGRA) [16] values are also given, which is PHRR/TTP (kW/s) and is helpful in ranking the materials in terms of potential fire safety because it combines peak fire size (PHRR) and time to achieve this (time to peak, TTP). FIGRA index of resin (11.5 kW/s) is reduced to (6.5 kW/s) with Cl (i) and 9.8 with Cl (ii). Cl (ii) - (iv) have little effect on this value, however. Mass loss versus time curve in Fig. 3(b) show that clay helps in increasing thermal stability and char formation. In Fig.2(d) char residue after 4 minute period is plotted, where the silica content is accounted for by subtracting the silica values taken from TGA results at 800°C in Table IV and indicate that clays enhance 3.5 – 5% char formation of resin.



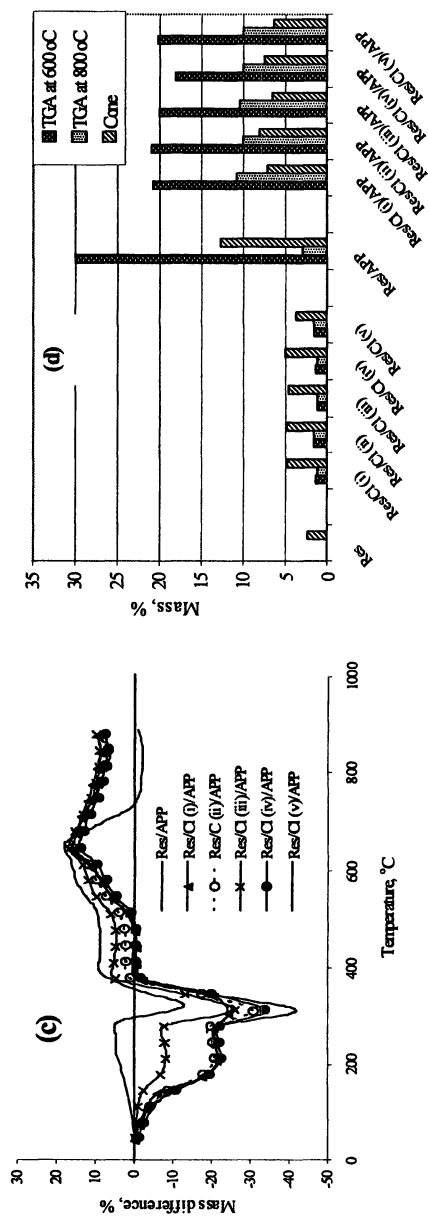


Fig.2. (a) TGA responses of Res and Res/Cl(i) with/without APP in air; (b) percentage residual mass differences (actual - calculated) as a function of temperature for (b) Res/Cl, (c) Res/Cl/APP; (d) residual masses of Res/Cl/APP samples from TGA curves at 600, 800°C and cone results after 4 min exposure at 50kW/m² heat flux

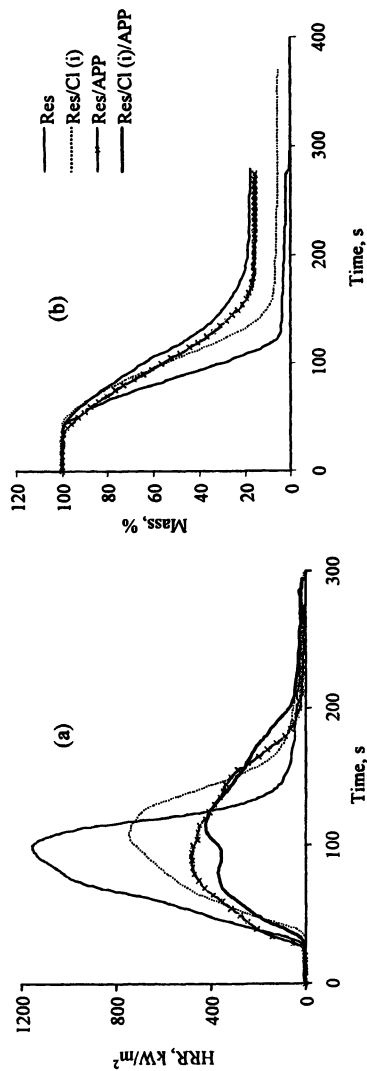


Fig. 3. (a) HRR and (b) mass loss vs time curves for Res and Res/Cl(i) with / without APP at 50kW/m²

The effect of different flame retardants, including ammonium polyphosphate, on the flammability of this particular resin is discussed in depth in a separate publication [11]. As seen from Table V, APP does not help in increasing time to ignition of the resin, but increases flame out time, which is further increased with additional presence of clays. APP in Res/APP sample is effective in reducing PHRR (478 kW/m^2) and THR (52.2 MJ/m^2) compared to pure resin. Clay presence further reduces PHRR ($384 - 457 \text{ kW/m}^2$) and THR ($48.5 - 51.6 \text{ MJ/m}^2$). There are no significant changes in smoke values except for Clay (v) containing sample. APP presence significantly reduces H_c of resin from 33.1 to 19.2 MJ/m^2 , but that of clays increases it again to $23.7 - 24.7 \text{ MJ/m}^2$. FIGRA index is lowered by APP to 5.3 kW/s , which is further lowered by clays to within the range $3.1 - 4.6 \text{ kW/s}$. APP helps in increasing char formation as seen from Figs. 2(d) and 3(b), whereas additional presence of clay has little effect, once the amount of silica residue is accounted for.

Table V. Cone calorimetric results at 50 kW/m^2 heat flux for polyester-clay nanocomposites with and without FRs

Sample	TTI (s)	FO (s)	PHRR (kW/m^2)	FIGRA (kW/s)	THR* (MJ/m^2)	H_c * (MJ/kg)	Smoke* (l)
Res	34	136	1153	11.5	79.0	33.1	761
Res/Cl (i)	45	170	743	6.5	66.5	30.1	814
Res/Cl (ii)	34	139	1045	11.6	68.8	32.1	683
Res/Cl (iii)	32	140	1002	11.1	70.0	37.8	712
Res/Cl (iv)	40	143	1034	10.8	71.7	35.3	732
Res/Cl (v)	33	159	958	9.1	77.9	33.5	835
Res/APP	31	190	478	5.3	52.2	19.2	754
Res/Cl (i)/APP	38	204	419	3.6	48.5	23.7	715
Res/Cl (ii)/APP	36	199	426	4.0	49.9	24.7	706
Res/Cl (iii)/APP	38	202	434	3.9	49.1	24.0	724
Res/Cl (iv)/APP	36	193	484	4.8	51.6	24.4	760
Res/Cl (v)/APP	34	211	384	3.1	50.6	24.5	660

* Values for 4 minute period ; Coefficient of variation ranges are : TTI = 2 - 17 % , FO = 1 - 10 % , PHRR = 1 - 9 % , THR = 2 - 8 % , H_c = 6 - 19 % and Smoke = 1 - 4 %.

In terms of effect of individual clays, Cl (i) increases TTI, reduces PHRR and THR and shows minimum values of H_c and FIGRA (see Table V). Although

this clay does not show intercalation or exfoliation in XRD studies, it surprisingly shows best results for cone studies of all clay/resin combinations tested. This may be due to flame retardant effect of phosphorus group present in the functionalised clay and its higher decomposition temperature (see Table IV). Cl (ii) and (iii) do not show any significant improvement in any of the cone parameters except as reduced FO and smoke values in the Res/Cl (ii)/APP sample, but they do not indicate nanocomposite formation as well. Cl (iv) shows complete exfoliation but does not show any significant improvement in cone parameters. Cl (v) on its own is not very effective in reducing flammability of resin as seen for Res/Cl (v) sample in Table V, but shows best results in presence of APP indicating synergistic effect of organic modifier and APP. In Res/Cl (v)/APP sample, PHRR is reduced by 67%, THR by 36% and smoke by 13% compared to pure resin.

This discussion shows that although nanoclays are effective in reducing flammability of unsaturated polyester resin but they do not do so to the same extent as seen for other polymer-nanocomposites systems. Bharadwaj et al [17] have proposed that exfoliation of clay reduces the cross-linking density of the resin, hence enhancement in certain thermal and mechanical properties due to exfoliated clay is counterbalanced by reduced crosslinking of the resin. This also explain why nanoclays are not very effective in reducing flammability of polymers showing low inherent tendencies to crosslink during thermal degradation, such as the polyester resin used in this work.

Conclusions

In the unsaturated polyester resin used, organically modified nanoclays affect its thermal stability very slightly. Nanoclays reduce onset of decomposition temperature, peak heat release rate and total heat release values. In the presence of conventional flame retardants, typified by APP, flammability of resin-clay-nano/micro composites is considerably reduced compared to unmodified resin. Choice of organic modifier is an important factor affecting degree of intercalation/exfoliation, thermal stability, flammability and mechanical performance of the resultant polymer.

Acknowledgements

The authors wish to acknowledge the financial support from the Engineering and Physical Science Research Council and National Institute of Standards and Technology (NIST), USA, in particular Dr Jeffrey W Gilman for technical and

financial support. They also want to thank Scott-Bader for providing samples and technical support.

References

1. Giannelis, E.P. *Adv. Mater.* **1993**, *8*, 29-35.
2. Gilman, J.W., Kashiwagi, T., Giannelis, E.P., Manias, E., Lomakin, S., Lichtenhan, J.D. In: Le Bras, M., Camino, G., Bourbigot, S., Delobel, R. eds. *Fire Retardancy of Polymers*, The Royal Society of Chemistry: Cambridge, UK, **1998**, 203-221.
3. Kandola, B.K. 'Nanocomposites' In: Horrocks, A.R., Price, D. eds. *Fire Retardant Materials*, Woodhead Publishing Ltd: Cambridge, **2001**, 204-219.
4. Usuki A., Kojima Y., Kawasumi M., Okada A., Fukushima Y. *J.Mater.Res.* **1993**, *8*, 1179-1184.
5. Alexander M., Dubois P. *Mater. Sci. Eng. Rep.* **2000**, *28*, 1-63.
6. Fornes T.D., Hunter D.L., Paul D.R. *Polymer*, **2004**, *45*, 2321-2331.
7. Cho J.W., Paul D.R. *Polymer*, **2001**, *42*, 1083-1094.
8. Kandola B.K., Horrocks A.R., Myler P. Blair D. In : *Fire and Polymers*, Nelson G.L., Wilkie C.A., eds. *ACS Symp. Ser.*, **2001**, *797*, 344-360.
9. Kandola B.K., Horrocks A.R., Myler P. Blair D. *Composites Part A*, **2002**, *33*, 805-817.
10. Kandola B.K., Nazaré S. Horrocks A.R. In : 'Fire Retardancy of Polymers: New applications of mineral fillers', Le Bras M. *et al*, eds. The Royal Society of Chemistry : Oxford, **2005**, 147-160.
11. Nazare S., Kandola B., Horrocks A.R. in preparation
12. Morgan A.B., Haris J.D. *Polymer*, **2003**, *44*, 2313-2320.
13. Liu T.X., Liu Z.H., Ma K.X., Shen L., Zeng K.Y., He C.B, *Composites Sci. Tech*, **2003**, *63*, 331-337.
14. Pramoda K.P., Liu T., Liu Z., He C. Sue H-J. *Polym Deg Stab*, **2003**, *81*, 47-56.
15. Kandola B.K., Horrocks S., Horrocks A.R. *Thermochim Acta*, **1997**, *294*, 113-125.
16. Sundstrom, B. 'Fire hazards, testing, materials and products', <http://www.sp.se/fire/Eng/default.htm>.
17. Bharadwaj R.K., Mehrabi A.R., Hamilton C., Trujillo C., Murga M., Fan R., Chavira A. Thompson A.K. *Polymer*, **2002**, *43*, 3699-3705.

Chapter 14

Mechanistic Aspects of Nanoeffect on Poly(acrylic ester)–GO Composites

TGA–FTIR Study on Thermal Degradation and Flammability of Polymer Layered Graphite Oxide Composites

Jianqi Wang and Zhidong Han

National Laboratory of Flame Retardant Materials, School of Materials Science and Engineering, Beijing Institute of Technology, 100081 Beijing, China

The TGA-FTIR technique has been utilized to study the thermal degradation of poly (acrylic ester) (PAE) and its graphite oxide micro- and nano-composites. Nanocomposite formation is shown by the use of X-ray diffraction and transmission electron microscopy. The influence of graphite oxide on the degradation is followed and cone calorimetry has also been used to ascertain the role of graphite oxide in flame retardancy.

Introduction

Since the initial preparation of graphite oxide (GO) samples by the Hummers method in 1958, the characterization of GO (1, 2) and polymer/GO nanocomposites has been documented in the literature (3-8). Very few publications on the flammability properties of these composites have appeared in the past, but recently, some flame retardant systems of polymer/graphite oxide (GO) were reviewed (9, 10), including poly(acrylic ester) (PAE), a commercial copolymer of butyl acrylate, polyvinyl alcohol (PVA), polyurethane (PU), and polyvinylidene chloride (PVDC).

In order to study the role played by nanocomposite formation in the flammability of polymer layered graphite oxide nanocomposites, the poly(acrylic ester) system has been studied using TGA/FTIR and cone calorimetry.

Experimental

Poly(acrylic ester) (PAE), a commercial copolymer of butyl acrylate, ca 40 wt% or 33 mol%, ethyl acrylate (ca 46 wt% or 48 mol%) and acrylic acid (ca 14 wt% or 19 mol%) was supplied by Beijing Eastern Yakeli Chemical Industrial Corporation. Graphite oxide was synthesized in this laboratory following the Hummers method (2-4) with some modifications (9, 10). The accurate composition of GO is dependent on the oxidation treatment. The micro- and nano-composites were prepared and characterized according to the literature procedure (2).

X-ray diffraction (XRD) was carried out on D/max-RB Japan equipped with Cu-K α generator ($\lambda=0.1540$ nm), operated at 100 mA and 40 kV. Transmission electron microscopy (TEM) experiments were conducted on Hitachi H-800 at an acceleration voltage of 200 kV. Cone calorimetry was carried out on a Stanton-Redcroft cone calorimeter following the ASTM 1356 protocol. The TGA-FTIR measurements were obtained on an Netzsch TG 209 instrument on finely ground samples of about $8 \cdot 10^{-6}$ kg in an Al $_2$ O $_3$ pan in the temperature range 23°-700°C at a heating rate of 10°C/min and a nitrogen flow rate of 20 ml/min. Four samples were studied by TGA-FTIR: GO; PAE; micro-PAE/GO5 and nano-PAE/GO5.

Results and Discussion

XRD and TEM

The XRD traces, shown in figure 1, and the TEM images, shown in figure 2, confirm that nanocomposites have been obtained. GO shows a large peak at a 2θ value a little above 10° which is absent in the XRD trace of the PAE/GO system. From TEM, in the lower magnification image on the left, one can see that there is good nano-dispersion of the graphite oxide throughout the polymer while on the right, in the higher magnification image, only agglomerated graphite oxide layers are seen.

TGA-DTG data

Graphite oxide. The TGA curve of graphite oxide is shown in figure 3, the onset temperatures T_5 and T_{10} , at which 5% and 10% mass loss occurs, show values of 69°C and 242°C , respectively. Two stages can be seen from TGA curve within the temperature range of $25\text{--}200^\circ\text{C}$ and $242\text{--}600^\circ\text{C}$. The infrared spectra show peaks that can be ascribed to the presence of H_2O (3853 , 3744 , 3668 , 1700 , 1512 cm^{-1}) (11) (in general $1850\text{--}1350$ and $4000\text{--}3600\text{ cm}^{-1}$) (12) and CO_2 (2327 cm^{-1}) (11) (in general $720\text{--}635$, $2400\text{--}2250$ and $3700\text{--}3600\text{ cm}^{-1}$) (12). The evolution of H_2O and CO_2 continues to a temperature of 612°C and the behavior is similar to that of expanded graphite (13). There is a large amount of carbon dioxide at high temperatures, due to the oxidation reaction between the carbon in the GO and the oxidants used to form the GO.

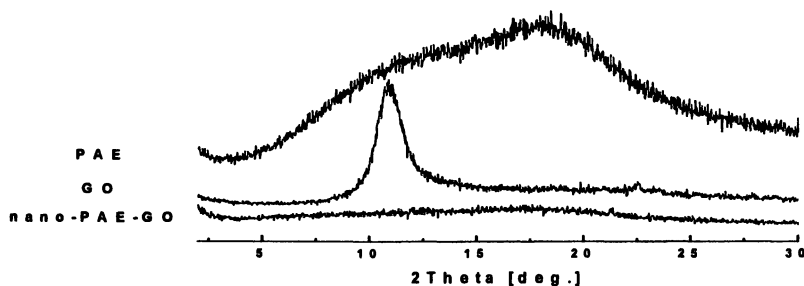


Figure 1. XRD patterns of PAE, GO and PAE/GO nanocomposites.

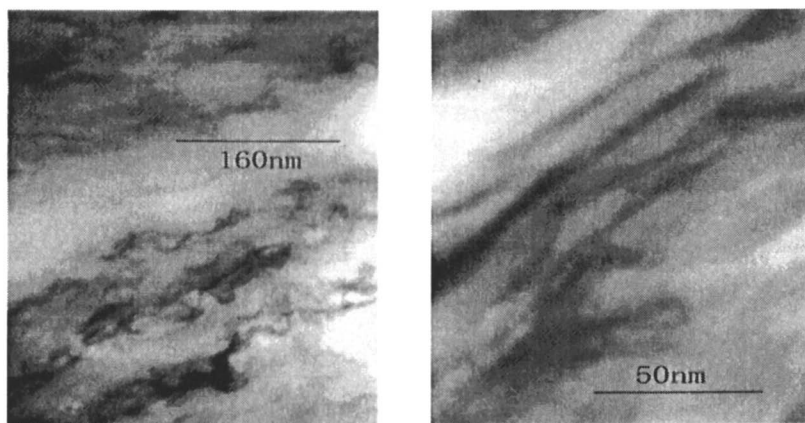


Figure.2 TEM images of nano-PAE/GO (5 %)

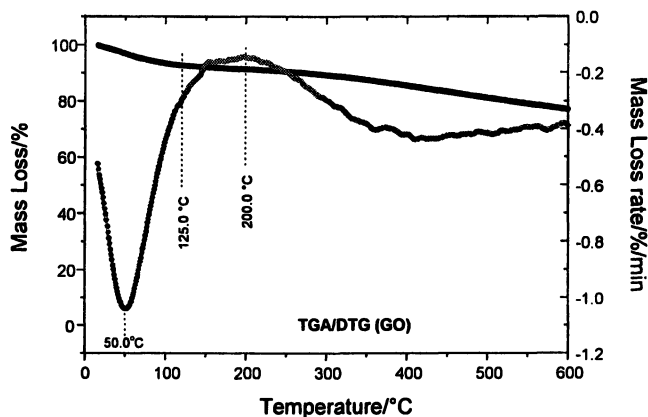


Figure 3. TGA/DTG of GO

Polymer and its microcomposite and nanocomposite. The TGA curves for virgin polymer, its microcomposite and nanocomposites are shown in figure 4 – respectively, and the data is tabulated in table I. The incorporation of GO into PAE gives rise to a reduction in the onset temperatures of the degradation relative to the ne PAE due to the earlier decomposition of GO. A substantial influence of the nano-effect on properties of micro-blending is visible, for example, the nano-structured material displays a higher T_5 , a lower mass loss rate (R_{max}) and an increased amount of residue than micro-PAE/GO5.

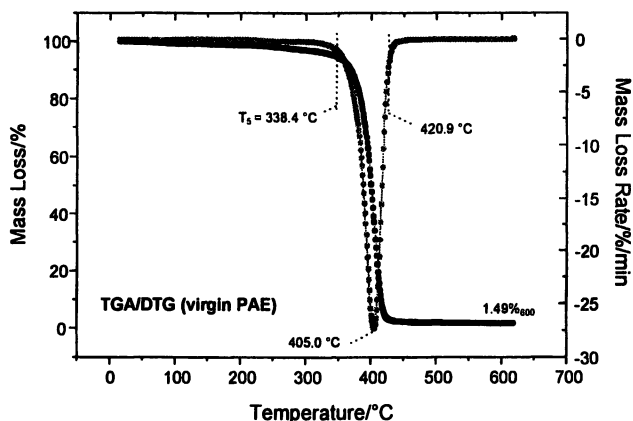


Figure 4. TGA/DTG of virgin PAE

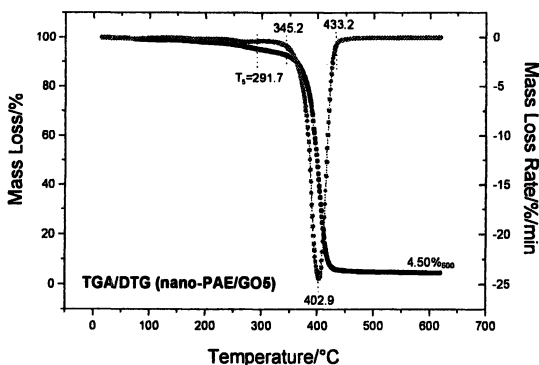


Figure 5. TGA/DTG of micro-PAE/GO5

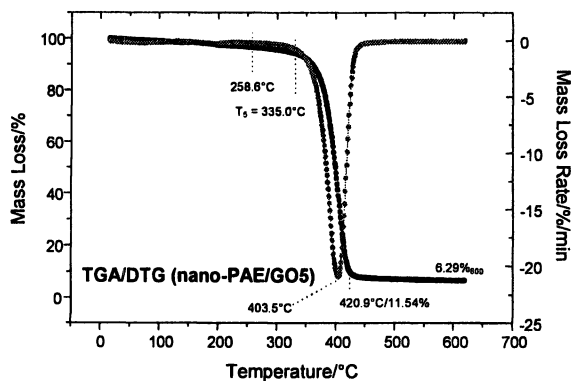


Figure 6. TGA/DTG of nano-PAE/GO5

Table I TGA/DTG Data

System	T ₅ / °C T ₁₀ * / °C	Peak 1 Range / °C	Peak 2 Range / °C T _m / °C	R _{max} / %·min ⁻¹	Residue / % at 600 °C
GO	69 / 242	25-200	242-600 425	0.43	71
PAE	338 / 362	---	300-450 405	27.5	1.5
Micro- PAE/GO5	292 / 358	---	250-450 403	24.8	4.5
Nano- PAE/GO5	335 / 354	---	300-450 404	22.0	6.3

* T₅ and T₁₀ represent the temperature at which 5% and 10% mass loss take place

FTIR spectra

As noted above, pure graphite oxide shows only peaks due to water and carbon dioxide so these spectra are not shown here. On the other hand, the samples which contain polymer do show other peaks and these spectra are shown herein. Based on the TGA curves of PAE, micro- and nano-PAE/GO5 (shown in figures 4 - 6) spectra are shown at two temperatures, *i.e.*, 300° and 500°C.

FTIR spectra of PAE, micro- and nano-PAE/GO5 at 300°C. PAE begins to degrade at 302°C and peaks are observed in the infrared spectra, shown in figure 7, corresponding to tert-butyl group (1394, 1369 cm⁻¹ doublet) (7) and an anhydride group (1852, 1795cm⁻¹ and 1803, 1739 cm⁻¹) (14, 15). A very small amount of poly acrylic ester (2941, 1743, 1166 cm⁻¹) (11) was formed, accompanied by some H₂O (3853, 3744, 3668, 1700, 1512 cm⁻¹).

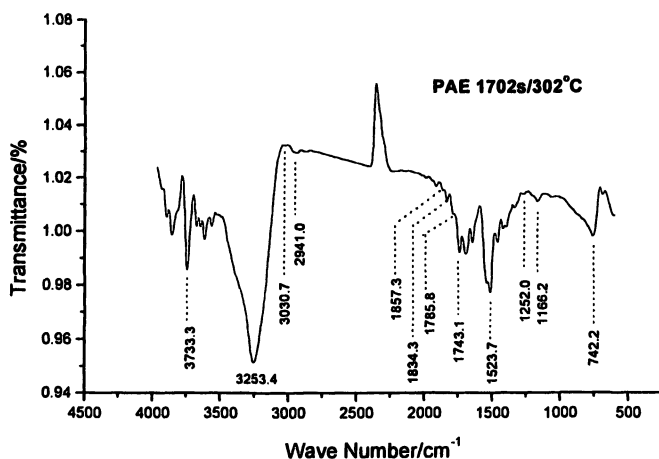
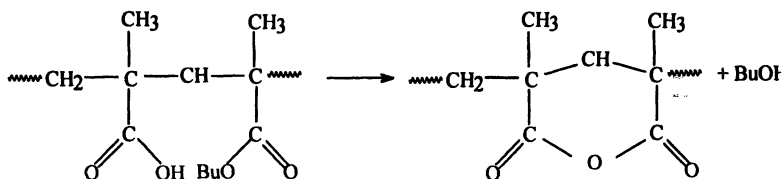
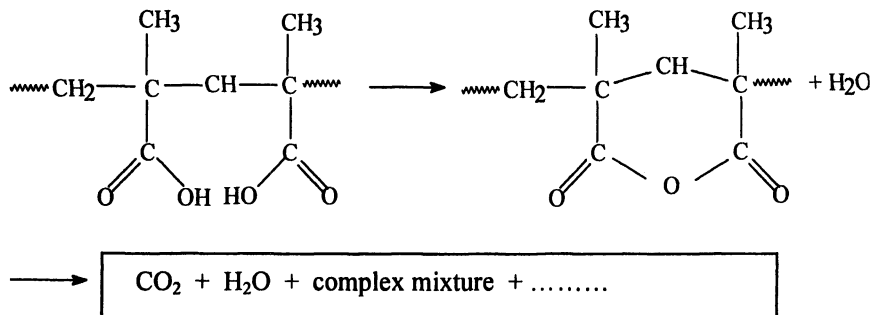


Figure 7 FTIR of PAE 302 °C (1702s)

Unlike the homopolymer, the reactions shown in scheme 1 and 2 may occur during the thermal degradation of the copolymer PAE.



Scheme 1



Scheme 2

Grassie et al. (17, 18) has studied the thermal degradation of some lower alkyl polyacrylates, which indicated close qualitative similarity in the thermal degradation behavior of the polyacrylates (ethyl, *n*-propyl, and *n*-butyl acrylate). The main products are saturated and unsaturated dimers and the amount of olefin is very small (19). Partial oxidation of carbon to CO can be ruled out, because of the absence of absorption in the region where CO should be seen, 2179 and 2115 cm^{-1} (11). This is also supported by a thermal volatilization analysis experiment (TVA) (16).

Micro- and nano-PAE/GO Composites. The FTIR spectra of the microcomposite and nanocomposites are shown in figure 8 and 9, respectively. There is a difference in chemical species between micro-PAE/GO5 and virgin PAE, although no change was observed in the morphology of micro-PAE/GO5 composite compared to a blended mixture of the two (9, 10). In addition to those peaks that appear in virgin PAE, some new peaks at 2963, 1741, 1166 cm^{-1} begin to appear at this temperature in the presence of graphite oxide; these can be assigned to butyl acrylate and ethyl acrylate monomer, dimer and oligomer (11).

For nano-PAE/GO5, the intensity of the anhydride peaks (1852 and 1795 cm^{-1} and 1803, 1739 cm^{-1}) are weaker in the nanocomposites than in the microcomposite, implying that the depolymerization of PAE into monomer, dimer, etc., takes place at the expense of intermediates, like anhydride, etc.

Virgin PAE, Micro- and nano-PAE/GO Composites at 500 °C. Minor yields of monomer, dimer and/or oligomer (2952, 1745, 1156 cm^{-1}) were observed in virgin PAE, shown in figure 10, in the gas phase at 500 °C. Water (3853, 3744, 3668, 1700, and 1512 cm^{-1}) and very little amount of residual carbon dioxide are also observed. This may imply that the polycondensation reaction dominates at 500 °C with the evolution of water.

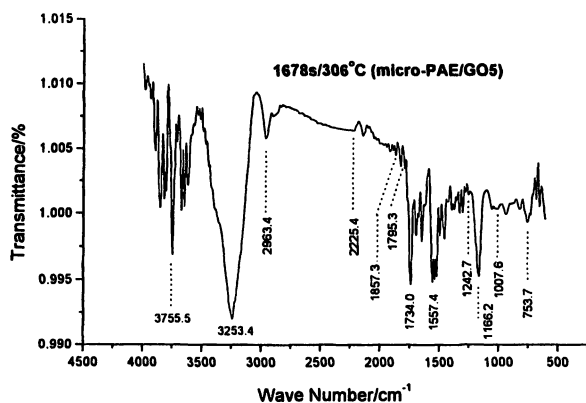


Figure 8. FTIR of micro-PAE/GO5 at 306 °C (1678s)

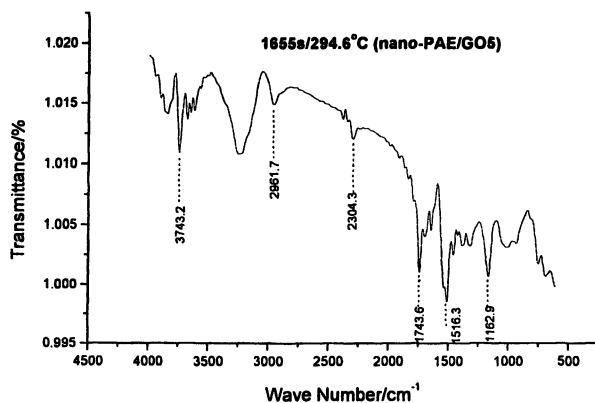


Figure 9. FTIR of nano-PAE/GO5 at 295 °C (1655s)

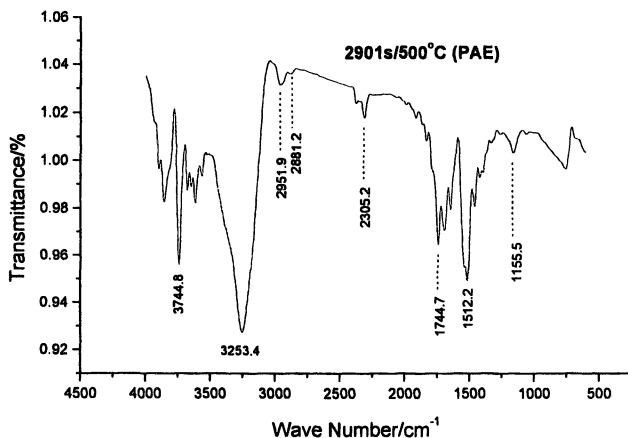


Figure 10. FTIR spectra of PAE at 500 °C (2901s)

The comparison between micro-PAE/GO5 (figure 11) and nano-PAE/GO5 (figure 12) at similar temperatures shows differences in the decreased release of H₂O (3853, 3744, 3668, 1700, 1512 cm⁻¹) and growing amount of carbon dioxide (2350 cm⁻¹). The interaction between PAE and GO at 500°C is likely to be accelerated by the nano-effect, resulting in a large release of CO₂, in addition to the polycondensation reaction.

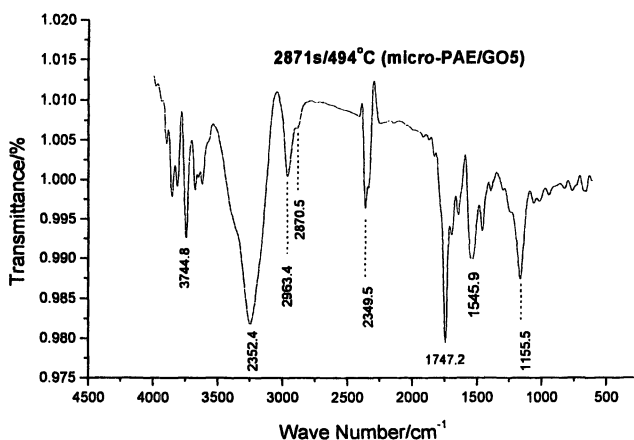


Figure 11. FTIR spectra of micro-PAE/GO5 at 494 °C (2871s)

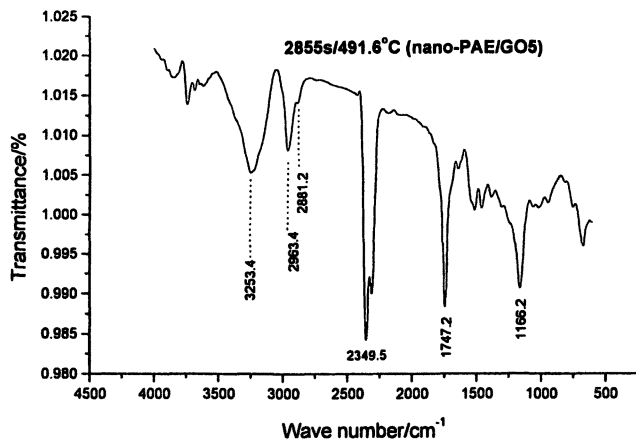


Figure 12. FTIR spectra of nano-PAE/GO5 at 492 °C (2855s)

The function of GO in the flammability of the nanocomposite

The expandable graphite (EG) flake is being used in a growing number of fire retardant applications (13). The effectiveness of the EG additive very much depends on the amount of expansion generated on heating. In contrast, graphite oxide plays its role in flame retardancy in a very different way, since it is almost independent of the amount of expansion. Our previous work (9, 10) indicated that the nano-effect is quite important, as shown by the LOI values, *i.e.* 18.8 % (PAE), 19.3 % (micro-PAE/GO5) and 23.3 % (nano-PAE/GO5); such a change is not seen in the case of the PLS (polymer layered silicates) nanocomposites.

Table II shows the TTI (time to ignition), one of the flammability parameters obtained by cone calorimetry. The nano-effect, defined as $LOI_{\text{nano}} - LOI_{\text{micro}}$, does have an influence on TTI. The barrier mechanism is the commonly accepted process by which clay systems prevent heat and mass transfer to the polymer, as shown by X-ray Photoelectron Spectroscopy (XPS) (9, 10). In order to gain insight into this issue, other factors concerning heat transfer, such as the absorption characteristics of PAE and PAE/GO5 composites, heat loss through thermal conduction to the bulk and radiation to the gas phase, may be considered. Graphite oxide, with its black color, is an infrared absorber. Both heat absorption from external radiant flux (here, from 15 to 35 kW/m²) and low thermal conductivity of GO lead to a higher temperature in the top surface of PAE/GO5 composites. Meanwhile, for pure PAE the temperature results in a lower value over some depth due to the low heat absorption.

Table II. Time to Ignition (TTI) of PAE and its GO composites as a function of the irradiance

<i>Irradiation flux</i> <i>System</i>	15 kW/m ² *	25 kW/m ²	35 kW/m ²
PAE	109	108	62
Micro-PAE/GO5	181	100	54
Nano-PAE/GO5	293	93	39

* See literature (9, 10)

The heat absorption due to the external radiant flux is very low at 15 kW/m² so the difference between PAE and PAE/GO tends to be negligible. At this stage the flame retardancy would mainly be controlled by the barrier mechanism. The reason that nano-PAE/GO5 may possess a longer TTI than micro-PAE/GO5 may result from the thicker and denser barrier. When the external radiant flux increases to 35 kW/m², the heat absorption is growing so fast that a huge heat absorption by GO would give rise to higher thermal conductivity, particularly in the case of the nanocomposite. Consequently, the temperature of surface becomes high enough to initiate the degradation of the underlying polymer, finally, the TTI reverses order, due to the evolution of combustibles (monomer, dimer of PAE and so on), as seen in the TGA/FTIR data. There is also a nano effect seen in the peak heat release rates, as shown in table III.

Table III. Peak heat release rate (PHRR)/kW·m⁻² of PAE/GO5 at various levels of irradiance

<i>Irradiation flux</i> <i>System</i>	15 kW/m ² *	25 kW/m ²	35 kW/m ²
PAE	377	502	624
Micro-PAE/GO5	252 (-33.0%)	449 (-10.6%)	564 (-9.6 %)
Nano-PAE/GO5	178 (-52.8%)	408(-18.7%)	404 (-35.0%)

* See literature (9, 10)

References

1. Hummers, Jr, W.S.; Offeman, R.E. *J. Am. Chem. Soc.*, **1958**, *80*, 1339.
2. Han, Z.; Wang, J. *Chinese J. Inorg. Chem.*, **2003**, *19* 459–461.

3. Han, Z.; Wang, J. *Chinese J. Inorg. Chem.*, **2003**, 19 1366–1370.
4. Matsuo, Y.; Tahara, K.; Sugie, Y. *Carbon*, **1996**, 34, 672.
5. Matsuo, Y.; Tahara, K.; Sugie, Y. *Carbon*, **1997**, 35, 113.
6. Matsuo, Y.; Hatase, K.; Sugie, Y. *Chem. Mater.*, **1998**, 10, 2266
7. Strawhecker, K.E.; Manias, E. *Chem. Mater.* **2000**, 12, 2943.
8. Xu, J.; Hu, Y.; Song, L.; Wang, Q.; Fan, W.; Chen, Z. *Carbon*, **2002**, 40, 445–467.
9. Wang, J.; Han, Z. Proceedings of the 9th European Conference on Fire Retardant Polymers, FRPM'03, Lille, France, 2003.
10. Wang, J.; Han, Z, in *Fire Retardancy of Polymers : New application of mineral fillers* Bras, M. Wilkie, C. and Bourbigot, S. eds., RCS pub. Cambridge UK, 2005, pp 161–178.
11. Stein, S.E. *The NIST/EPA Gas Phase Infrared Database, Version 1.0*, 1992,
12. Camino, G.; DuquesneS.; Delobel, R.; Eling, B.; Lindsay, C.; Roels, T. in *Fire and Polymers, Materials and Solutions for Hazard Prevention*, Ed. G.L.Nelson and C.A.Wilkie, American Chemical Society, Washington, D.C., 2001, pp. 90-109.
13. Krassowski, D.W.; Ford, B.M.. Fire and Materials conference, San Antonio, Texas, 1998
14. Martínez, G.; Sánchez-Chaves, M.; Rocha, C. M.; Ellis, G. *Polym. Degrad. Stab.*, **2002**, 76, 205–210.
15. Wang, J.; Zhou, H.; Jiang L.; Leng G. *Polym. Mat. Sci.Eng. (in Chinese)*, **2003**, 19, 60–63.
16. McNeil, I.C. Developments in Polymer Degradation-1, N. Grassie Ed., Applied Science Publication, 1977, pp 43–66.
17. Grassie, N.; Speakman, J.G. *J. Polym. Sci.*, Part A-1 **1971**, 9, 919.
18. Grassie, N.; Speakman, J.G.; Davis, T.L. *J. Polym. Sci.*, Part A-1, **1971**, 9, 931..
19. Li, J.; Xu, H.; Shi, J.; Li, C.; Bao, C. *Anal. Chim. Acta*, **1999**, 402, 311–318.

Chapter 15

Navy R&D Programs for Improving the Fire Safety of Composite Materials

Usman Sorathia¹ and Ignacio Perez²

¹Naval Surface Warfare Center, Carderock Division, 9500 MacArthur Boulevard, West Bethesda, MD 20817

²Office of Naval Research, 800 North Quincy Street, Arlington, VA 22217

Due to their inherent characteristics, fiber reinforced plastics (FRP), also referred to as polymer matrix based composite materials (PMC), have been making steady inroads into naval military systems for the past 10-15 years. Chief among their characteristics is the stiffness to weight ratio (much better than steel or aluminum), and the resistance to chemical attack (e.g. corrosion resistance). US Navy is currently using sandwich composites in most surface ship topside applications. The sandwich composite consists of brominated vinyl ester resin with glass or carbon reinforcement and balsa wood core. The unprotected vinyl ester based sandwich composite does not meet all of the Navy's fire performance goals for interior applications. In order to use such composites inside the ship for manned spaces, it must be protected with either passive (fire insulation) and/or active (water mist) fire protection systems. Such fire protection adds weight and cost. Navy has invested over \$10M over the last 5 yrs in SBIR (Small Business Innovative Research) and STTR (Small Business Technology Transfer) programs to develop flame resistant polymers suitable for room or low temperature processing by Vacuum Assisted Resin Transfer Molding (VARTM). Such flame resistant resins could then be used to produce sandwich composites that would meet the Navy's fire growth requirements without the need for passive fire protection. In this paper, we have presented summary of some of the R & D

programs that the Navy is pursuing to address this issue. Selected low cost screening test procedures to facilitate such development are also discussed.

Introduction

The 1975 collision involving the USS KENNEDY (CV-67) and the USS BELKNAP (CG 26), and resultant fire, influenced the Navy to improve the survivability of aluminum structures through mineral wool fire insulation. Principal use of steel instead of aluminum in the deckhouse design started with the DDG 51 class ship.

During the past 10-15 years, Navy has experienced a resurgence of interest in the development and application of composites for both primary and secondary load-bearing structures. This growing interest in composite materials is driven by the fleet needs to reduce maintenance, save weight, increase covertness and provide affordable alternatives to metallic components with lower life cycle costs.

Polymer composites are engineered materials in which the major component is fiber reinforcement (typically a fiber made out of carbon, glass or Kevlar) and the minor component is an organic resin binder (such as vinyl ester, epoxy or phenolic resin). Currently, structural composites for U.S. Navy surface ship applications are typically glass reinforced with brominated vinyl ester and balsa wood core. Some recent notable large composite applications are the Advanced Enclosed Mast/Sensor (AEM/S) System for amphibious transport dock ship LPD-17 shown in Figure 1, and topside deckhouse for multi mission surface combatant DD(X).

A significant concern in shipboard application of organic matrix based composites is the possibility that an accidental (or deliberate) fire may ignite the composite material. This may result in the spread of flame on the composite surface, and also release heat and generate potentially toxic smoke. Thus, the localized incidental fire may cause a larger structural fire involving the composite, which now becomes the fuel for the growing fire. In enclosed and confined spaces, such as in ships, the growing fire can lead to a "flashover" condition. "Flashover" is a term that is used to indicate the point during a fire when the internal temperatures in the upper regions of the compartment have increased to the point where the radiant energy from the hot upper layer spontaneously ignites all combustible materials within the compartment. Typically this is on the order of 600°C. If the affected composite component is part of a primary critical structure, the structure may collapse when exposed to

fire. Recent fire incident on the Norwegian Orkla minesweeper, where the fire started in the lift fan room, reinforces the need to select resin and core materials for composite structures with improved flammability characteristics.

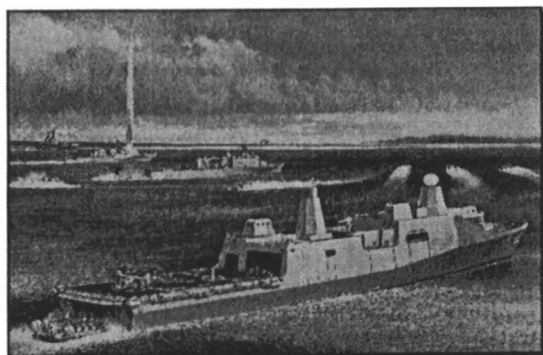


Figure 1: Composite Mast-LPD-17

Fire Performance Requirements

Fire Performance Requirements for Submarines. Fire aboard a submarine threatens the platform itself and must be fought independently with limited onboard resources. The use of structural applications in U.S. Navy submarines is covered by MIL-STD-2031 [1]. Fire performance goals for use of composites in submarines are based on assumptions that a fire should be extinguished or brought under control within 5 minutes. This military standard contains requirements for limiting oxygen index (ASTM D 2863), flame spread index (ASTM E 162), heat release rates (ASTM E 1354), smoke generation (ASTM E 662), fire gas toxicity, quarter and large scale fire tests. For the purpose of this paper, a summarized version of cone calorimeter part of the MIL-STD-2031 acceptance criteria is at 25 kW/m², Time to ignition, 300 s; PkHRR, 50 kW/m²; AHRR, 50 kW/m². At 50 kW/m², 150 s, 65 and 50 kW/m². At 75 kW/m², 90 s, 100 and 100 kW/m². At 100 kW/m², 60 s, 150 and 120 kW/m².

Fire Performance Requirements for Surface Ships. Egress and fire fighting situations onboard surface ships are different than those onboard submarines. In general, fire performance goals for the use of composites in surface ships are based on assumptions that typical time available for fire fighting operations is about 30 minutes.

Design Data Sheet DDS-078-1 [2] covers the fire performance requirements for the use of composites in the topside of surface ship. In most cases, fire performance goals are based on full-scale fire tests as shown in Table I.

Material fire performance goals should be incorporated in conjunction with existing or additional detection, suppression, and fire-fighting systems.

Fire Performance of Current Composite Material System. The US Navy is currently using sandwich composites in most surface ship topside applications. The sandwich composite consists of brominated vinyl ester resin with glass or carbon reinforcement and balsa wood core as shown in Figure 2. Vinyl ester resins are mixtures of styrene and methacrylated epoxy. Styrene has one reactive vinyl group while the vinyl ester monomer has several reactive vinyl end groups. These end groups provide cross-linking capacity and branching while styrene provides linear chain extension. The polymerization reaction proceeds by free radical chain growth. The brominated vinyl ester resin, shown in Figure 3, was selected based on its fire retardant properties, chemical resistance, cost, room temperature curing properties, and ease in large scale processing methods such as Vacuum Assisted Resin Transfer Molding (VARTM).

The cone calorimeter data for sandwich composite and its components is shown in Table II. The unprotected vinyl ester based sandwich composite does not meet all of the Navy fire performance goals for interior applications. For example, in mock up room corner fire tests, the unprotected sandwich composite (critical heat flux for ignition $\approx 15 \text{ kW/m}^2$, ignition temperature $\approx 657\text{K}$) ignites in less than 120 seconds, delaminates from balsa core at approximately 660 seconds, and exhibits total heat release rates of close to 1.0 MW shortly after the burner heat release rate was increased to 300 kW [3]. The combustible nature of vinyl ester based sandwich composite with balsa core, and its propensity to be driven to flashover by small to intermediate fires, is the major difference between the metallic (steel) and polymer matrix based composite structures. On the other hand, balsa core sandwich construction provides superior fire resistance. Fire resistance is the ability of building structures to limit the fire spread from room of fire origin to adjoining spaces, such as bulkheads and overheads, by preventing ignition of items on the non-fire side of the bulkhead (backside).

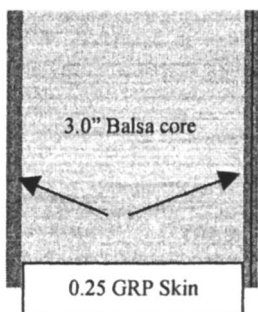


Figure 2: Sketch of a sandwich composite

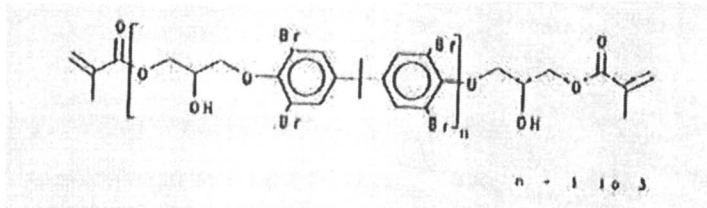


Figure 3: Brominated bisphenol A epoxy vinyl ester resin

New Resin And Core Materials. The US Navy has long recognized the need for the development of new low cost resins and core materials which can be processed by VARTM and which have the mechanical characteristics comparable to vinyl esters and balsa core, but have the superior flammability characteristics comparable to phenolics. To this end, US Navy has invested over \$10M towards the development of new fire restricting resins and foams over the last 5 years. Most of this investment is made through ONR SBIR/STTR as well as internal research programs. The SBIR/STTR program is designed to provide funding to stimulate technological innovation in small business to meet DoD research and development needs. This investment includes the modification of vinyl ester with fire retardants (Marquette University), development of products such as phthalonitrile by Naval Research Laboratory (NRL), modified phenolics by Texas Research Institute (TRI), epoxy and cyanate ester resins based on bisphenol-C (Shade Inc.), polyhedral oligomeric silsesquioxane (POSS) based resins (Hybrid Plastics), nanoclay reinforced vinyl esters (Hydrosize Inc.), improved phenolic foams (University of Southern California, University of North Carolina), and carbon foam (Touchstone Research Laboratory) materials. A more detailed description of some of these research efforts is given in the following sections.

Small Scale Screening Methodology. Most of the tests required to qualify the fire performance of composite systems for naval applications are large-scale tests. When developing new resins and core materials, it is expensive to repeatedly conduct these tests to determine the performance of the most recent design. Instead, more cost-effective small-scale testing is preferable to intermittently evaluate performance.

The U.S. Navy sandwich composite uses balsa core (3.0 inch). The low density core (9.5 pcf) provides superior resistance to heat transmission which yields low temperature rise on the unexposed side during fire resistance tests using UL-1709 fire exposure curve [4]. As such, meeting the requirements for fire resistance (heat transmission) is not an issue with such sandwich composites. It is, however, the combustibility or the high heat release rates of sandwich composite and its components which result in the failure of unprotected composite system in the room corner fire test (ISO 9705). This fire test (100 kW for 10 minutes, 300 kW for 10 minutes) requires that three

Table I. Summary of Fire Performance Goals for Composite Topside Structure

<i>Category</i>	<i>Test Method</i>	<i>Criteria</i>
Surface Flammability	ASTM E-84, ASTM E-84, "Standard Test Method for Surface Burning Characteristics of Building Materials.	Interior applications: Flame spread index : 25 max Smoke developed index: 15 max Exterior applications: Flame spread index: 25 max Smoke data for review by NAVSEA 05P4
Fire Growth	ISO 9705 "Full-scale room test for surface products" Annex A, standard ignition source fire	Net Peak heat release rate less than 500 kW Net Average heat release rate less than 100 kW
Smoke Production	ISO 9705 "Full-scale room test for surface products" Annex A, standard ignition source fire	Peak smoke production rate less than 8.3 m ² /s Test average smoke production rate less than 1.4 m ² /s
Smoke Toxicity	ASTM E662, ASTM E662, Specific Optical Density of Smoke Generated by Solid Materials.	CO: 350 ppm (max); HCl: 30 ppm (max); HCN: 30 ppm (max) Fire Gas IDLH Index, I _{IDLH} < 1;
Fire Resistance and Structural Integrity Under Fire Bulkheads/Overheads/Decks/Doors/	Navy modified: UL 1709 fire curve for 30 minutes using IMO A.754 (18) test procedures IMO App. A. III & A.IV apply Maximum fire test load	Average temperature rise on the unexposed surface not more than 250°F (139°C) Peak temperature rise on the unexposed surface not more than 325°F (180°C) There should be no passage of flames, smoke, or hot gas on the unexposed face Structural Integrity Under Fire (under load): No collapse or rupture of the structure for 30 minutes.

Table II: Cone Calorimeter Data for Sandwich Composite and its Components.

	Vinyl ester, 1483		Glass/vinyl ester 1459		Balsa core, 1447		Sandwich composite, 1257	
Flux, kW/m ²	25	75	25	75	25	75	25	75
Tig (s)	184	21	284	39	22	4	306	28
PkHRR, kW/m ²	161	421	108	159	93	169	121	150
AHRR, kW/m ²	118	235	78	92	30	74	58	99
AHOC, MJ/kg	9.9	9.7	9.7	9.8	6.7	12.3	12.7	10.6
SEA, m ² /kg	169	1937	1300	1536	23	24	933	986
THR, MJ/m ²	74	80	24	27	10	42	80	102
AMLR, g/s m ²	15.0	37.2	8.6	13.7	4.8	8.3	5.8	7.7
Mass loss, %	81	95	17	23	36	87	15	23

AHOC: Average effective Heat of Combustion; SEA: Specific Extinction Area; AMLR: Average Mass Loss Rate.

1483: Brominated vinyl ester resin, no fiber, 0.25 in thick, post cured at 160°F for 4 hrs; 1459: glass reinforced brominated vinyl ester, 0.25 in thick, post cured at 160°F for 4 hrs; 1447: Balsa wood core: 9.5 lb/ft³; 1257: Un-protected sandwich composite, 0.25 in thick composite skins, 3.0 in thick balsa core.

walls and the ceiling of the 8 ft wide, 12 ft deep, and 8 ft high test room to be lined with composite material. The large amount of material required makes this test expensive to evaluate new resins and core materials in the developmental phase.

Tests conducted at Naval Surface Warfare Center, Carderock Division (NSWCCD) show that solid (no core) composite materials which have met the MIL-STD-2031 (SH) cone calorimeter requirements of heat release rates and time to ignition at all four heat fluxes of 25, 50, 75, and 100 kW/m² also meet the requirements of room corner (ISO 9705) fire test with considerable margin of safety [5] as shown in Figure 4.

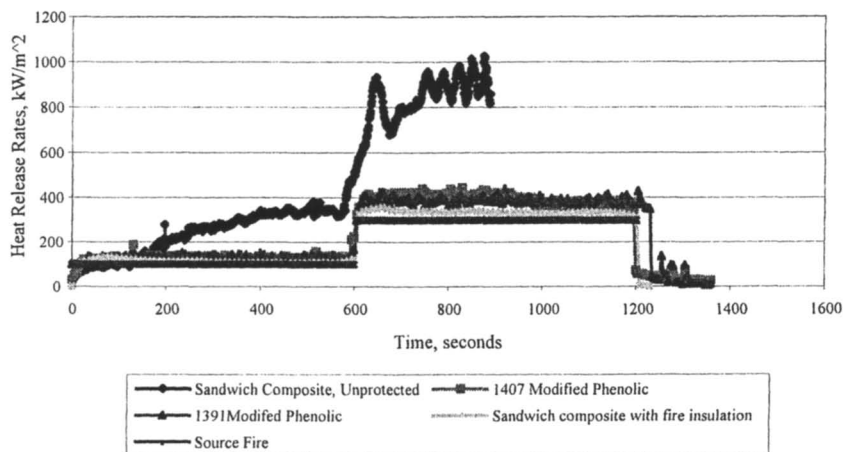


Figure 4: HRR for Selected Composites from ISO 9705 Room Corner Fire Tests.

To facilitate the development and introduction of new resins and core materials, Navy is using the small-scale screening test methodology based on cone calorimeter (ASTM E-1354) which uses the small size coupons (4 x 4").

Fire Retardancy of Vinyl Ester Nanocomposites by Synergy With Phosphorus-Based Fire Retardants. Fire retardancy of vinyl ester nanocomposites was investigated by Prof. Charles Wilkie at Marquette University [6]. In this study, summarized in Table III, synergy between conventional phosphorous-containing fire retardants and vinyl ester nanocomposites was shown through cone calorimetry by reductions in the peak heat release rate (PkHRR), total heat release (THR) and mass loss rate. There was no improvement in the time to ignition (Tig). These reductions were directly proportional to the amount of phosphate added. With both brominated and non brominated resins, the type of clay used showed different effects on the flammability of the nanocomposites formed. The cone calorimetric parameters are comparable to the brominated resin when the systems are not glass

reinforced, but the brominated resin exhibited better performance when glass reinforcement was used.

Table III. Cone Calorimetric Data for PVE +6%15A + phosphate

Sample	tig (s)	PkHRR kW/m ² (% reduction)	THR MJ/m ²	ASEA M ² /kg
Brominated PVE	76	460 (62)	38	19
Pure PVE	82	1197	80	1015
PVE+6%15A+5%RDP	68	856 (32)	69	931
PVE+6%15A+10%RDP	74	643 (46)	58	1003
PVE+6%15A+15%RDP	56	512 (57)	51	1044
PVE+6%15A+30%RDP	81	535 (55)	47	1238
PVE+6%15A+15%TCP	44	670 (44)	47	976
PVE+6%15A+30%TCP	29	299 (75)	38	1350
PVE+6%15A+40%TCP	38	397 (67)	35	1721
brominated PVE	76	460 (62)	38	19

PVE: vinyl ester; 15A: nano clay; RDP = resorcinol di-phosphate;
TCP = tricresylphosphate

Phthalonitrile Resin. Researchers from the Naval Research Laboratory (NRL) developed in the 1980's a new class of high-temperature polymers based on the phthalonitrile system that has attractive properties for composites [7]. The fully cured resin exhibits good thermal and oxidative stability, and possesses useful long-term mechanical properties up to 371°C (700°F). More significantly, there is no indication of a glass transition or softening up to 500°C (932°F). The uncured resin has a low melt viscosity that allows it to be used in a resin transfer molding manufacturing process. This material is one of a short list of materials that has met all small-scale FST requirements as defined in MIL-STD-2031. Figure 5 shows the chemical structure of the Phthalonitrile system. When this monomer cures it forms a triazine network that is known to be very flame resistant. Also, the benzene rings forming the backbone structure are very stable against fire.

One of the shortcomings of this resin system is its relatively high processing temperature ($T_{\text{cure}} = 270^{\circ}\text{C}$) and small processing window ($\Delta T = 40^{\circ}\text{C}$). In a recent development, the same group of researchers have been able to modify the backbone chemistry of the monomer in such a way as to lower the processing temperature to $T_{\text{cure}} = 190^{\circ}\text{C}$ and expand the processing window to ($\Delta T = 140^{\circ}\text{C}$) without affecting the high temperature performance of the resin system. Figure 6 shows the formulation of new resin system where $n=2$ or $n=4$ in the structure.

Preliminary data suggests that the original phthalonitrile and the two new formulations ($n=2$ and $n=4$) show the same onset temperature for thermal degradation (around 500°C). The char yield is over 70% in all cases, and over 80% for $n=4$.

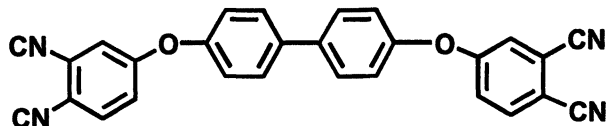


Figure 5: Phthalonitrile (PN) Monomer

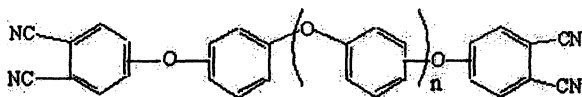


Figure 6: Structure of the New Phthalonitrile Monomers with $n=2$ and $n=4$.

Polyhedral Oligomeric Silsesquioxanes (POSS) Based Resin Systems. Under a STTR program, Hybrid Plastics is developing reduced flammability vinyl esters using a new class of chemical called Polyhedral Oligomeric Silsesquioxanes or (POSS[®]) which is shown in Figure 7. POSS[®]-materials are termed hybrid due to their combined inorganic (silicon based) and organic (carbon based) nature and can be viewed as discrete, chemically-modified particles of silica having dimensions at the nanometer scale. As a result, this technology bridges the property space between hydrocarbon-based plastics and ceramics. The organic portion of the POSS molecule provides compatibility with existing resins thereby enabling their easy incorporation into conventional resins. The inorganic component of the POSS molecule, the $\text{SiO}_{1.5}$ cage, provides the thermal and oxidative stability. Incorporation of POSS[®] combines the beneficial properties of plastics with those of ceramics.

Hybrid Plastics has developed several promising formulations and produced glass-reinforced composites. The most promising formulation has a time to ignition of 268 s, a peak heat release rate of 74 kW/m^2 , and average heat release

rate of 46 at 300 s and the specific extinction area is 39 m²/ kg at a heat flux of 50 kW/m² (8).

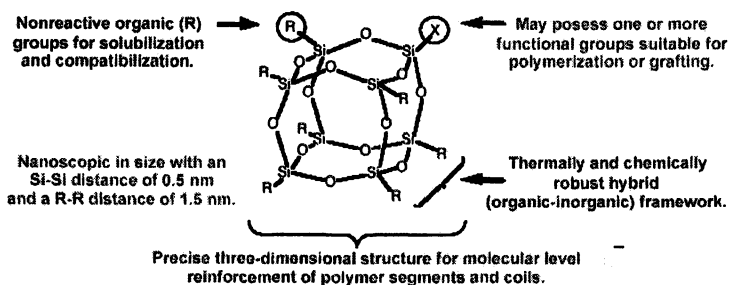


Figure 7: *Polyhedral Oligomeric Silsesquioxanes* or (POSS[®]).

Bisphenol-C Based Resins. Recently, FAA has evaluated bisphenol-C based cyanate ester resin which is shown in Figure 8 [9]. Glass reinforced composites produced from this resin meet the ignitability and heat release rate requirements of MIL-STD-2031 at all four heat fluxes of 25, 50, 75, and 100 kW/m². There is no ignition at either 25 or 50m kW/m² heat flux while at 75 kW/m² the time to ignition is 266 s with a PHRR of 36 kW/m² and an SEA of 74 m²/kg; at 100 kW/m², the time to ignition is 145 s, with a PHRR of 46 kW/m² and an SEA of 115 m²/kg. Low fuel content, high char yields, and halogen inclusion in the polymer structure all contribute to the low heat release rate from bisphenol-C based resins [10]. Based on recent fire tests conducted by NSWCCD, solid composite systems which meet the ignitability and heat release requirements of MIL-STD-2031 are also likely to meet the acceptance criteria from full scale ISO 9705 room corner fire tests without the need for any passive fire protection [5]. In FY05, Shade Inc (SBIR, Phase II) is developing low temperature cure modified bisphenol-C based vinyl ester or epoxy systems which can be processed by VARTM to produce large naval composite structures.

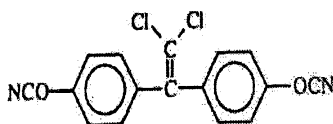


Figure 8. *Bisphenol-C Based Cyanate Ester Resin*.

New Core Materials. The Navy is investigating two different approaches to the development of fire resistant core materials for use in naval sandwich composites. These include carbon foam (Touchstone Research Laboratory), and phenolic foam (University of Southern California and University of North Carolina). These core materials have shown superior reaction to fire characteristics.

Heat release data at incident heat flux of 50 kW/m^2 on several core materials is shown in Figure 9. These included: (1) 1444: Carbon foam, 1.0" thick; (2) 1445: Polymethacrylimide, 1.0" thick, 51 IG; (3) 1446: Polymethacrylimide, 1.0" thick, 110 IG; (4) 1447: Balsa wood core, 9.5 lbs/ft³, 1.0" thick; (5) 1448: PVC foam, HT 90, 1.0" thick; (6) 1449: PVC foam, H 100, 1.0" thick. Data show that carbon foam did not ignite at any of the heat fluxes used in these tests. As such, it is the most flame resistant core material evaluated to-date. Data further show that polymethacrylimide foam core produced high heat release rates. Data further show that balsa wood core chars and appears to have lower average heat release rates than PVC foam cores at 50 kW/m^2 heat flux.

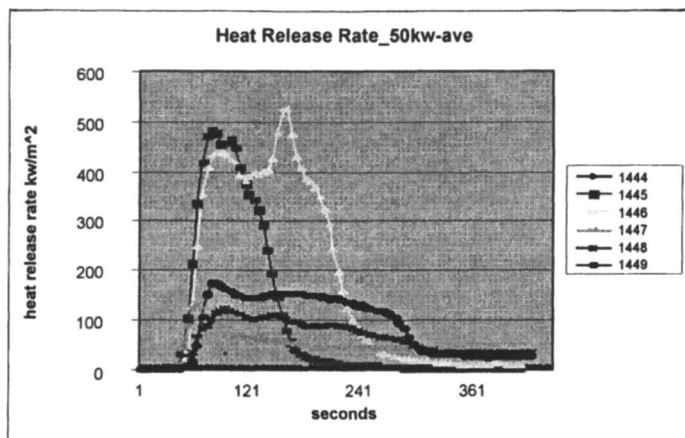


Figure 9: HRR from various cores at 50 kW/m^2

Summary

The U.S. Navy currently uses glass reinforced brominated vinyl ester resin with balsa wood as core for topside sandwich structures. Unprotected vinyl ester sandwich composites do not meet the fire growth requirements of ISO 9705. As such, unprotected vinyl ester based sandwich composites require fire

insulation or sprinkler protection to reduce the fire risk. To meet Naval Sea System Command (NAVSEA) fire performance goals, a sprinkler protected combustible structure offers less protection than a structure protected with fire insulation. As such, the use of fire insulation to protect and prevent ignition of a combustible structure is preferred.

Fire insulation attachment on sandwich composite structures can cost as much as \$35-50 per sq. ft. in labor and material costs. Significant savings can be realized by the development of low temperature cure resins and improved core materials to manufacture composite structures which can meet Naval Sea System Command (NAVSEA) fire performance goals for fire growth without the use of passive fire protection. To this end, the US Navy has invested over \$10M towards the development of new fire restricting resins and foams over the last 5 years. Most of this investment is made through SBIR/STTR programs as well as internal research programs. This investment has resulted in some promising candidates such as low temperature cure phthalonitriles by Naval Research Laboratory (NRL), modified phenolics by Texas Research Institute (TRI), cyanate ester based on bisphenol-C by Federal Aviation Administration (FAA) and their contractors, polyhedral oligomeric silesquioxane (POSS) based resins by Hybrid Plastics, and carbon foam materials by Touchstone Research Laboratory. The efforts to scale up selected promising candidates and perform large scale fire and mechanical tests are expected to continue in the FY05. Furthermore, Navy is investing over \$2M towards the development of alternative passive fire protection materials in FY05 through SBIR programs.

References

1. MIL-STD-2031 (SH), "Fire and Toxicity Test Methods and Qualification Procedure for Composite Material Systems Used in Hull, Machinery, and Structural Applications Inside Naval Submarines," February, (1991).
2. DDS-078-1, Design Data Sheet, Composite Materials, Surface Ships, Topside Structural And Other Topside Applications – Fire Performance Requirements, August 2004.
3. Lattimer, B.Y.; Sorathia, U. *Fire Safety J.* **2003**, *38*, 747-770.
4. Lattimer, B.Y.; Ouellette, J.; Sorathia, U. *Proc. 49th Int SAMPE Symp.*, Vol. 49, May 2004.
5. Lattimer, B.Y.; Sorathia, U. *Proc. 49th Int. SAMPE Symp.*, Vol. 49, May 2004.
6. Chigwada, G.; Jash, P.; Jiang, D.D.; Wilkie, C.A. *Polym. Degrad. Stab.*, in press.
7. Keller, T.M.; Price, T.R. *J. Macromol. Sci.-Chem.* **1982**, *A18*, 931.

8. Lichtenhan, J.D. Progress Report, Reduced Flammability Vinyl Ester Resin Containing No Halogen for use in Large Composite Ship Surface Structures via Nanocomposite Technology, Progress Report July 2004, Hybrid Plastics Inc.
9. Lyon, R.E.; Walters, R.; Gandhi, S. "Combustibility of Cyanate Esters", Federal Aviation Administration, Final Report, DOT/FAA/AR-02/44, June 2002.
10. Walters, R.N. "Fire Resistant Cyanate Ester-Epoxy Blends", Federal Aviation Administration, Final Report, DOT/FAA/AR-02/53, May 2002.

Chapter 16

Synergistic Aspects of the Combination of Magnesium Hydroxide and Ammonium Polyphosphate in Flame Retardancy of Ethylene-Vinyl Acetate Copolymer

Serge Bourbigot¹, Sophie Duquesne¹, Zakia Sébih²,
Sébastien Ségura², and René Delobel²

¹Laboratoire Procédés d'Elaboration de Revêtements Fonctionnels (PERF),
École Nationale Supérieure de Chimie de Lille (ENSCL), B.P 108, 59652
Villeneuve d'Ascq Cedex, France

²Centre de Recherche et d'Étude sur les Procédés d'Ignifugation des
Matériaux (CREPIM), Parc de la Porte Nord, Rue Christophe Colomb,
62700 Bruay-la-Buissière, France

In this work, flame retardancy of ethylene-vinyl acetate copolymer (EVA) is investigated incorporating Mg(OH)₂ (MDH) as flame retardant combined with ammonium polyphosphate (APP) as potential synergist. It is shown that APP is a synergistic agent in EVA-MDH formulations in terms of LOI and cone calorimetry. The interactions between APP and MDH are studied using ²⁵Mg and ³¹P solid state NMR. The formation of magnesium phosphate stabilizing phosphorus in the system and it is proposed that the combination APP/MDH provides a physical/thermal barrier protecting the substrate; this barrier is constituted of magnesium phosphate glass and MgO-like ceramic. The degradation of the polymeric matrix is slowed and the flow of flammable molecules which issue from the degradation of the polymer is reduced.

Introduction

A flame retardant should inhibit or even suppress the combustion process. Depending on their nature, flame retardants can act chemically and/or physically in the solid, liquid or gas phase *1*. They interfere with combustion during a particular stage of this process, e.g. during heating, decomposition, ignition or flame spread. Metal hydroxides such as $\text{Al}(\text{OH})_3$ or $\text{Mg}(\text{OH})_2$ achieve their effect by decomposing endothermically with the release of water, which cools the substrate to a temperature below that required for sustaining the combustion process *2*. The main effect here is to delay the ignition time *34*. A ceramic-like protective layer is then formed (e.g., aluminum or magnesium oxide) which slows the degradation of the polymer and reduces the flow of flammable molecules *4*.

Ethylene-vinyl acetate copolymers (EVA) are widely used in low-voltage electrical wires *5*; their major shortcoming remains their great flammability. One goal of this work is to reduce the flammability of EVA by the incorporation of flame retardants. This can be achieved using $\text{Mg}(\text{OH})_2$ (hereafter called MDH) but high loading must be used to get high limiting oxygen indexes (LOI) and V-0 rating in the UL-94 test *6*.

Previous studies demonstrated the benefit of using a combination of zinc borate with MDH in EVA *47*. Zinc borate acts as a synergist in EVA-MDH formulations, e.g., LOI is increased by 40% and the total heat release in the cone calorimeter (external heat flux of 50 kW/m^2) is decreased by 50% at the same loading of flame retardant (i.e. MDH/Zinc borate). It was postulated *8* that zinc borate degrades into boron oxide which plays the role of a binder in the protective MgO-based ceramic, reinforcing the protective effect of the ceramic layer. This mechanism suggests the formation of a glassy coating, and the idea in this work is to substitute zinc borate with another type of glass former: phosphates. Phosphates, such as ammonium polyphosphate (APP), are known to be both efficient flame retardants and glass formers (formation of phosphorus oxides at high temperature) *1*. The network structure of phosphate glasses is based upon a tetrahedral PO_4 structural unit. The structural behavior of phosphate glasses is well suited for accommodation of various modifier cations (such as, for example, Mg^{2+}) which themselves may stabilize the network. So, it is expected that phosphate will combine these two effects to reinforce the action of MDH in EVA.

In this paper, the action of phosphate in EVA-MDH system is examined using the usual fire testing protocols (cone calorimetry by oxygen consumption

and limiting oxygen index (LOI)). The potential interactions between phosphate and MDH are investigated using thermal analyses and ^{25}Mg and ^{31}P solid state NMR. The role of phosphate in EVA-MDH formulation is then discussed.

Experimental

EVA (Elastane E0119) containing 19 mol.-% vinyl acetate was supplied by ExxonMobil. MDH was a commercial grade (Magnifin H5 from Matinswerk), and APP was supplied by Clariant (Exolit AP422). Table I gives the composition of the formulations.

Table I. Composition of the FR formulations

<i>Formulation</i>	<i>EVA</i> (wt.-%)	<i>MDH</i> (wt.-%)	<i>APP</i> (wt.-%)
EVA-MDH	50	50	0
EVA-MDH/APP (50-x/x)	50	50-x*	x*

*x: percentage by weight of APP in the formulation, $0\% < x < 50\%$

Mixing was carried out in a Brabender roller mixer measuring head (mixer E350 with roller blades, volume 370 cm^3 at 170°C and with 30 rpm rotor speed). LOI (Standard Test Method for Measuring the Minimum Oxygen Concentration to support Candle-like Combustion of Plastics) was measured using a Stanton Redcroft instrument on sheets ($100 \times 10 \times 3\text{ mm}^3$) according to the standard oxygen index test (ASTM D2863/77). FTT (Fire Testing Technology) cone calorimeter was used to carry out measurements on samples following the procedure defined in ASTM E 1354-90. Our protocol involves exposing specimens measuring $100\text{ mm} \times 100\text{ mm} \times 3\text{ mm}^3$ in a horizontal orientation. An external heat flux of 50 kW/m^2 has been used for the experiments. Measured parameters include heat release rate (HRR), time to ignition (t_{ig}) and total heat evolved (THE). When measured at 50 kW/m^2 , parameters are reproducible to within $\pm 10\%$. Cone data reported in this paper are the average of three replicated experiments. Thermogravimetric analyses were carried out at heating rate of 10°C/min in synthetic air flow (Air Liquid grade; flow rate = 60 mL/min) using a Setaram TG 92 thermobalance. In each case, samples (10 mg) were positioned in open vitreous silica pans. The precision on the temperature measurements is $\pm 1.5^\circ\text{C}$ in the range 50°C - 850°C . Solid state ^{25}Mg NMR measurements were performed at 24.5 MHz (9.4 T) on a Bruker Avance 400 with MAS (Magic Angle Spinning) at 7 kHz. Bruker probe heads equipped with a 7 mm rotor

assembly were used. In order to observe the complete FID and so, to get an undistorted spectrum, Hahn spin echo (90° - τ - 180° - τ -aq) was used as suggested by McKenzie 9. A repetition time of 10 s was used for all samples and 5000 scans were used to obtain a good signal to noise ratio. The external reference used was a saturated solution of MgSO_4 . The simulation of the spectra was made using homemade software (Quasar) 10. ^{31}P solid state NMR was performed at 162 MHz on the same spectrometer as above with MAS at 15 kHz and with dipolar decoupling (DD) of protons. Bruker probe heads equipped with a 4 mm rotor assembly were used. A repetition time of 120s was used for all samples. H_3PO_4 in aqueous solution (85%) was used as external reference.

Results and Discussion

The influence of APP in EVA-MDH formulations was first studied using LOI. The percentage of flame retardants (MDH/APP) remains constant, so the benefit of APP in such systems can be evaluated. LOI values of EVA containing pure APP and pure MDH are 25 vol% and 26 vol% respectively. A synergistic effect is observed when the percentage of APP lies between 0.5 wt% and 10 wt% (Figure 1); LOI jumps from 25-26 vol% for the formulations containing the pure components to 30 vol% for the formulation EVA-MDH/APP. This test demonstrated the effect of APP. Previous studies 4,7 carried out using borate as the glass former (as zinc borate) led to the same conclusion. A synergistic effect is observed in terms of LOI at low zinc borate content. When APP concentration is higher than 10 wt%, MDH and APP concentrations are too low to provide protection.

To investigate further the reaction to fire of the systems EVA-MDH/APP, cone calorimeter was used as the fire model. The peak of HRR (PkHRR) of EVA is dramatically decreased using the flame retardant and t_{ig} is significantly increased (40s for the pure EVA compared to 75s for EVA-MDH and EVA-MDH/APP(50/45/5) and to 50s for EVA-MDH/APP(50/25/25)) (Figure 2). PkHRR of EVA-MDH is decreased by 54% while those of the EVA-MDH/APP formulations are decreased by 70%. It is noteworthy that only a small amount of APP permits a strong reduction of the PkHRR and that its action is on the second peak of the HRR curve, spreading out the curve and decreasing the HRR values.

The total heat evolved (THE) of the flame retarded EVA is strongly reduced compared to the pure EVA (65 MJ/m² vs. 110 MJ/m²) (Figure 3). This is sensible, because 50 wt% of fillers (MDH and APP) are incorporated in EVA. They dilute the fuel (EVA) and so, THE is decreased. It is noteworthy that adding 25 wt% APP in the EVA-MDH systems slows the evolution of heat, and this is advantageous for increasing the escape time. This phenomenon was previously observed in the case of EVA-MDH/ZB formulations 7.

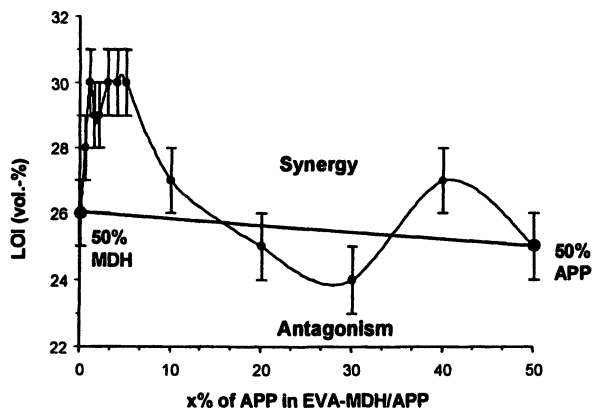


Figure 1. LOI values as a function of the percentage of APP in EVA-MDH/APP (total loading is constant equaling 50 wt.-%)

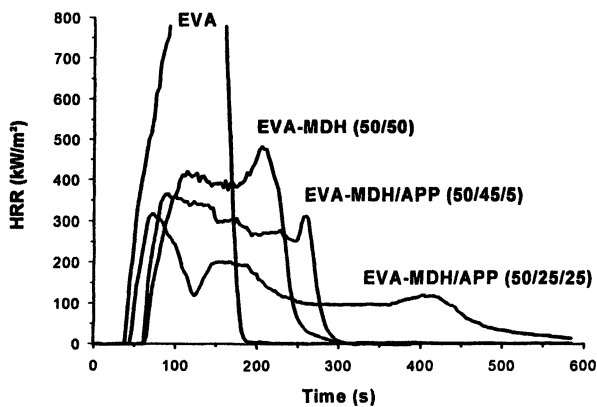


Figure 2. HRR curves versus time of EVA-MDH/APP formulations (external heat flux = 50 kW/m²; the percentage by weight of MDH and APP is given in brackets on the plot)

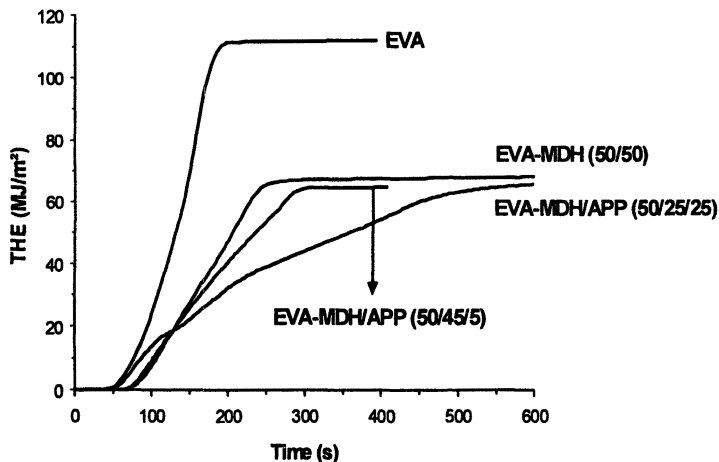


Figure 3. THE curves versus time of EVA-MDH/APP formulations (external heat flux = 50 kW/m^2 ; the percentage by weight of MDH and APP is given in brackets on the plot)

Observation of the residues obtained from the cone calorimeter experiments (Figure 4) demonstrates that the use of APP leads to the formation of a coherent protective shield. As a consequence, it may be assumed that reaction between APP and MDH or between their degradation products takes place and leads to the formation of a protective shield that can spread out the heat release.

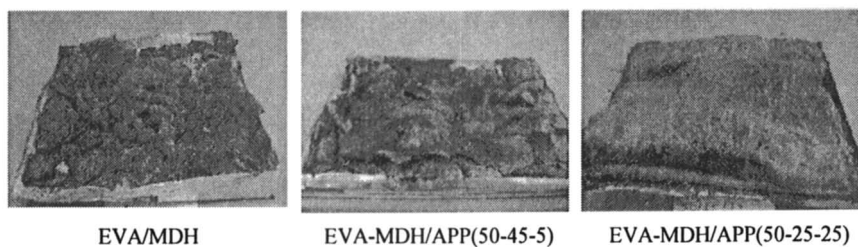


Figure 4. Residues from cone calorimeter experiments

In order to understand the interactions between MDH and APP, thermal degradation of the combination MDH/APP is investigated (Figure 5). APP degrades in two main steps starting, at 300°C and 550°C , corresponding to the evolution of ammonia and water and to the volatilization of phosphorus oxides 11. It gives at 800°C a residue of 20 wt% composed of stable -P-N- compound 11. MDH loses water at 350°C and gives MgO residue of 70 wt%. The TGA curve of MDH/APP (95/5 (wt/wt)) is similar to that of pure MDH and the TGA

curve of MDH/APP (50/50 (wt/wt)) starts to loose mass at 270°C and exhibits a behavior close to that of APP until 400°C. The final residues of the two systems MDH/APP are the same, equaling 70 wt%. This result suggests therefore that the presence of MDH prevents the volatilization of phosphorus oxides at high temperature ($T > 550^\circ\text{C}$).

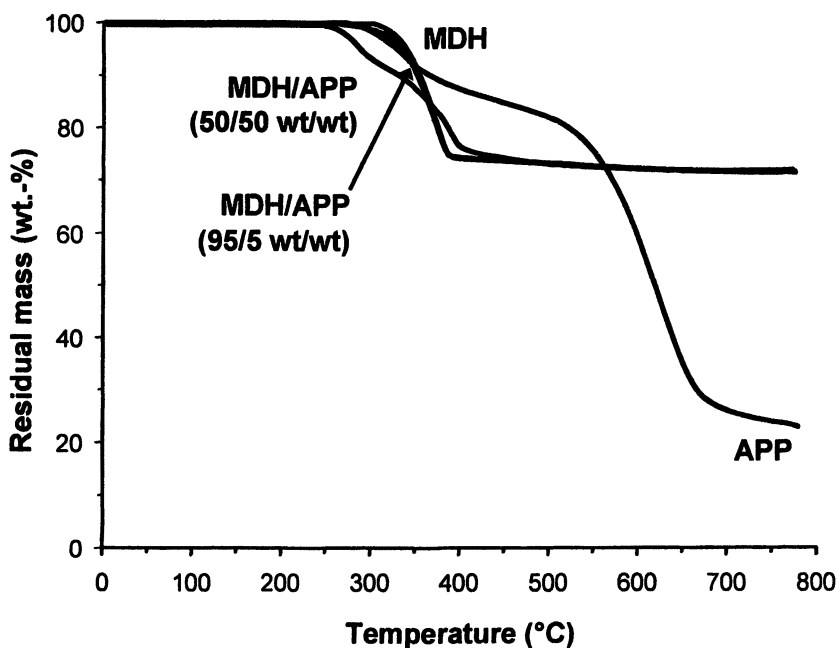


Figure 5. TG curves of pure components (MDH and APP) and of two different ratios of MDH/APP (air flow, heating rate = $10^\circ\text{C}/\text{min}$)

TGA curves (Figure 5) shows several characteristic temperatures corresponding to the steps of degradation of the system MDH/APP (360°C , 395°C , 460°C and 500°C). The systems MDH and MDH/APP (50/50 (wt/wt)) are heat treated at these temperatures for 1 hour in flowing air (this MDH/APP composition has been chosen to detect the interactions between APP and MDH). The ^{25}Mg NMR spectrum of MDH exhibits a typical quadrupolar lineshape ρ which can be simulated (see our previous work in 4). MgO (band at 25 ppm

4) appears at 360°C and a mixture of MgO and MDH is detected at this temperature. At higher temperatures, mainly MgO is observed (the tail on the MgO band suggests the presence of a small amount of MDH). This is reasonable, since MDH dehydrates at about 360°C into MgO. What is noteworthy is that this behavior is modified when MDH is heated combined with APP. At 360°C, the mixture MgO/MDH resulting from the heating of pure MDH contains 30% MgO (amount calculated from the simulated spectrum) but the system MDH/APP prepared in the same conditions, does not yield MgO (Figure 7). MgO is only formed at temperatures higher than 360°C (first detected at 395°C in the NMR spectra up to 500°C (not shown)). This result suggests that APP (or its degradation products) might stabilize MDH and/or MDH or MgO might react with APP (or its degradation products). These assumptions will be discussed in the following.

MAS-DD ^{31}P NMR spectra versus temperature (Figure 8) show the evolution of APP in the MDH/APP (50/50 (wt/wt)) system. At 20°C, the

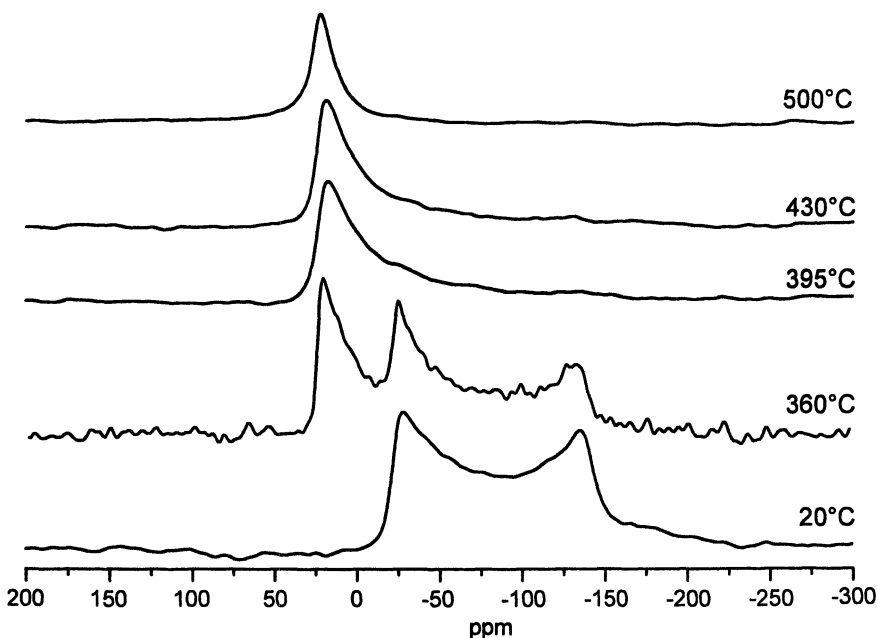


Figure 6. MAS ^{25}Mg NMR spectra of MDH versus the temperature of treatment

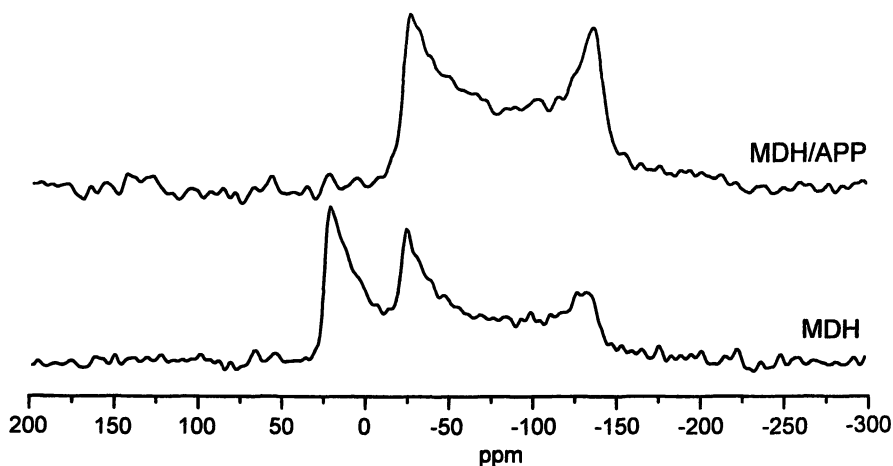


Figure 7. MAS ^{25}Mg NMR spectra of MDH and MDH/APP (50wt/50wt) heat treated at 360°C

spectrum exhibits a split signal at -22 and -24 ppm corresponding to PO_4 units in polyphosphate chains. At 360°C , a broad band centered at -27 ppm appears in the spectrum. The linewidth is due to a continuous distribution of ^{31}P isotropic chemical shifts reflecting the structural disorder such as bond angle and bond length variations and higher coordination sphere disorder. This behavior may be due to the formation of magnesium phosphate glasses *12* because of the chemical shifts typically observed in such glasses and because they can be easily formed heating up a mixture of MgO and phosphate. The assumption of magnesium phosphate does not contradict the ^{25}Mg NMR results because additional experiments (not shown) on different identified magnesium phosphates reveals that the NMR signal is weak and broad, probably because of the large distribution of chemical shifts. At higher temperatures ($T \geq 395^\circ\text{C}$), only one band, centered at -26 ppm, is observed suggesting the formation of magnesium phosphate material. In phosphate material, the network is made of PO_4 tetrahedra that can be classified according to the number of bridging oxygen atoms per PO_4 unit (Q_n). The chemical shift at -26 ppm is evidence of the formation of Q_2 middle groups containing two bridging and two non-bridging oxygen atoms. At 500°C , an additional broad band, centered at -33 ppm and at 0 ppm, appears suggesting the presence of Q_3 branching groups (-33 ppm) and orthophosphate (0 ppm) due to thermooxidative degradation of the phosphate species.

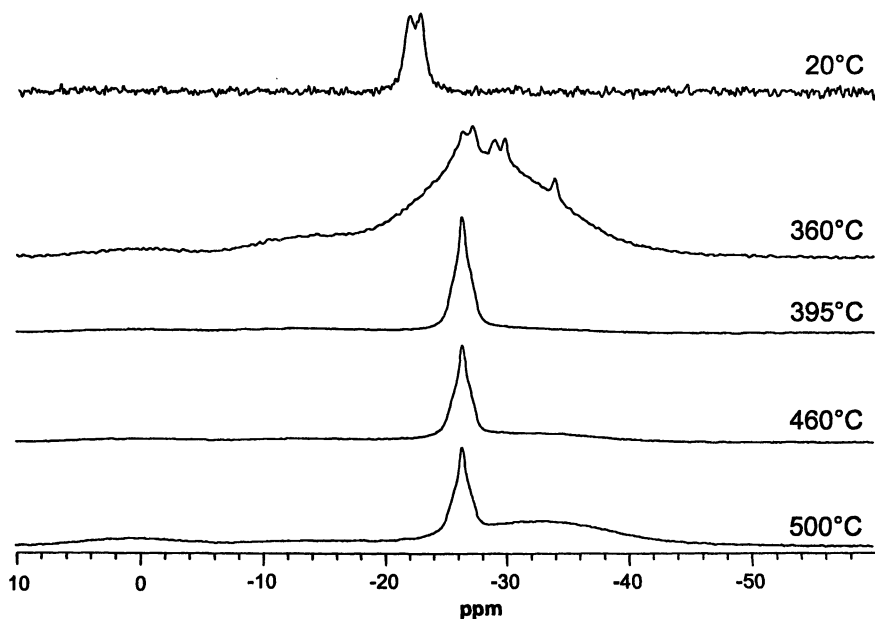


Figure 8. MAS-DD ^{31}P NMR of MDH/APP (50/50 (wt/wt)) versus the temperature of treatment

Figure 9 shows the interactions between APP and MDH upon thermal degradation. The destabilization of the system occurs first between 250°C and 550°C. According to the discussion above, this can be assigned to ammonia and water evolution because of an acid/base reaction between MDH and APP (250°C-350°C) and because of the condensation of phosphate and the formation of magnesium phosphate. At higher temperatures, the stabilization of the system is due to the formation of a stable magnesium phosphate material. Note that formation of magnesium phosphate was confirmed by X-ray diffraction and further characterization will be published in a separate paper.

At $T \leq 360^\circ\text{C}$, the interactions between APP and MDH create the destabilization of APP. There is formation of polyphosphoric acid (PPA), which is able to solubilize MDH. It permits reactions between PPA and MDH (and/or MgO resulting from the degradation of MDH) to make magnesium phosphate. At this stage, short -O-P-O-Mg-O-P- chains are formed *13*. As was mentioned above, no MgO was detected. An explanation of this might be that (i) MgO formed reacts immediately with APP to form magnesium phosphate (not detectable by ^{25}Mg NMR) or (ii) MgO surfaces adsorb water to form MDH. At $T > 360^\circ\text{C}$, there is formation of magnesium phosphate and of MgO. Magnesium phosphate grows around MgO grains and a protective cementitious matrix develops.

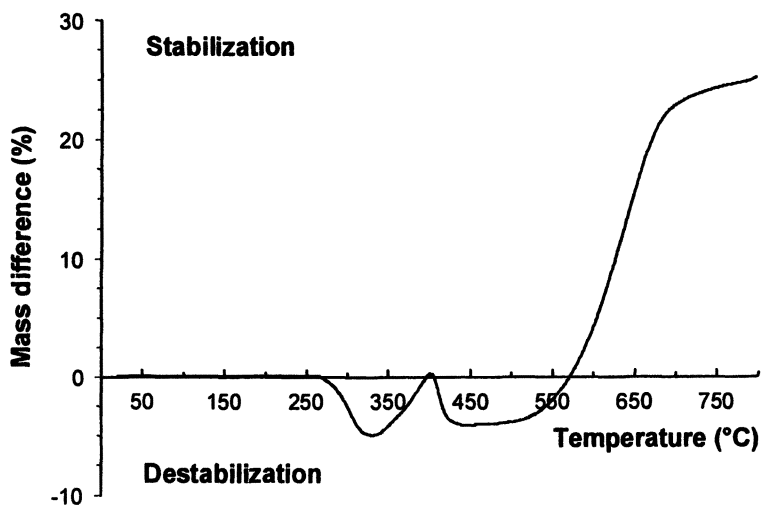


Figure 9. Curve of mass difference of MDH/APP (50/50 (wt/ wt)) between the experimental TG curve and the calculated one (calculation made by linear combination of the experimental TG curves of the pure components) (air flow, heating rate = 10°C/min)

To summarize, heating a mixture of MDH and APP yields the formation of magnesium phosphate material where the Mg cation acts as a network modifier. The formation of this material prevents the volatilization of phosphorus oxides which remain as a protective layer in EVA-MDH/APP.

Conclusion

In this work, we have shown that APP is a synergistic agent in EVA-MDH formulations in terms of LOI and cone calorimetry. The study of the interactions between MDH and APP shows that the presence of MDH prevents the volatilization of phosphorus oxides. The formation of magnesium phosphate material is suggested and might explain the high thermal stability of the protective layer. In the system EVA-MDH containing 5 wt% APP (best formulation), it is proposed that the layer consists of a magnesium phosphate glass stabilizing phosphorus and in an MgO-like ceramic. This combination provides a physical/thermal barrier protecting the substrate. The degradation of the polymeric matrix is slowed and the flow of flammable molecules which issue from the degradation of the polymer is reduced.

Acknowledgment

The authors are indebted to Mister Pankewitch from CREPIM for skilful experimental assistance in cone calorimeter experiments. NMR experiments were made in the common research center of the University of Lille, Mister Bertrand Revel is acknowledged for helpful discussion and experimental assistance.

References

1. Bourbigot, S.; Le Bras, M. *Flammability Handbook*; Troitzsch, J., Ed.; Hanser Verlag Pub.: Munich, 2003, pp 133-157.
2. Hornsby, P.R.; Watson, C.L. *Plastic and Rubber Processing and Applications*, 1986, 6, 169.
3. Bourbigot, S.; Le Bras, M.; Leeuwendal, R., Shen, K.K.; Schubert, D. *Polym. Deg. & Stab.*, 1999, 64, 419.
4. Bourbigot, S.; Carpentier, F.; Le Bras, M.; Fernandez, C. *Polymer Additives*; Al-Malaika, S.; Golovoy, A., Wilkie, C.A., Eds.; Blackwell Science Pub.: London, 2001, pp 271-292.
5. Ray I., and Khastgir D. *J. Appl. Polym. Sci.*, 1994, 53, 297
6. Rotheron R.N. *Particulate-Filled Polymer Composites, : Particulate Fillers used as Flame Retardant*; Rotheron, R.N., Ed.; Longman: Harlow, 1995, Chapter 6.

7. Carpentier, F.; Bourbigot, S.; Le Bras, M.; Delobel, R.; Foulon, M. *Polym. Deg. & Stab.*, **2000**, *69*, 83.
8. Bourbigot, S.; Carpentier, F.; Le Bras, M. *Fire and Polymer*, *ACS Symp. Ser. N° 797*; Gordon, N., Wilkie, C.A., Eds.; American Chemical Society: Washington, DC, **2001**; pp. 173-185.
9. MacKenzie, K. J. D. ; Meinhold, R. H. *American Mineralogist*, **1994**, *79*, 43.
10. Amoureux, J.P. ; Fernandez, C. ; Carpentier, L. ; and Cochon, E. *Phys. Stat. Sol.*, **1992**, *132*, 461.
11. Camino, G., and Luda, M.P. *Fire retardancy of polymers: the use of intumescence*; Le Bras, M.; Camino, G.; Bourbigot, S.; Delobel, R., Eds; Royal Society of Chemistry: Cambridge, **1998**; pp 48-63.
12. Fayon, F.; Massiot, D.; Suzuya, K.; Price, D.L. *J. Non-Cryst. Solids*, **2001**, *283*, 88.
13. Soudée, E.; Péra, J. *Cement Concrete Res.*, **2000**, *30*, 315-321.

Chapter 17

Mechanism for the Reductive Dehalogenation of "Dechlorane Plus" by Mixtures of Antimony(III) Oxide and Polymers

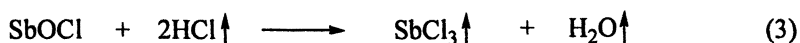
Jing Zhang and William H. Starnes, Jr.*

Departments of Chemistry and Applied Science, College of William and Mary, P.O. Box 8795, Williamsburg, VA 23187-8795

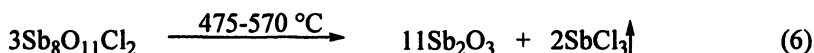
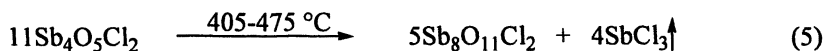
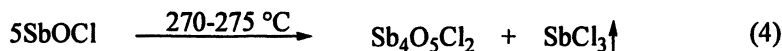
"Dechlorane Plus", a well-known commercial fire retardant made by the Diels-Alder cycloaddition of 1,5-cyclooctadiene to hexachlorocyclopentadiene (two equivalents), undergoes partial reductive dechlorination in polyethylene at 320–330 °C. This reaction is promoted strongly by Sb_2O_3 , but when that additive is present, the reaction is slower and gives lower conversions in polyethylene than in nylon 6,6. These results are demonstrated to argue against dechlorination by a process in which carbanions are intermediates. Instead, the data are shown to support a mechanism involving the abstraction of hydrogen atoms by carbon-centered free radicals formed by C-Cl homolysis.

For many years, antimony-halogen synergism has contributed greatly to the fire retardance of polymers. It is observed in systems that contain both a compound of antimony, such as Sb_2O_3 (commonly called "antimony oxide") and an organic chloride or bromide. The fire retardance occurs in the vapor phase and is believed to involve the scavenging of highly reactive radicals by volatile antimony halides, such as SbCl_3 , that are formed *in situ* (1–3). Surprisingly, however, the mechanisms for the formation of these effective flame inhibitors are incompletely understood.

In systems where Sb_2O_3 and an organic chloride are present, two major routes to SbCl_3 can be envisaged. One of these applies only to chloroorganics that produce hydrogen chloride under fire conditions. In such cases, the HCl can react directly with antimony oxide to form the SbCl_3 , either without the incursion of any detectable intermediates (eq 1) (4) or via an oxychloride such as SbOCl (eqs 2 and 3) (4).

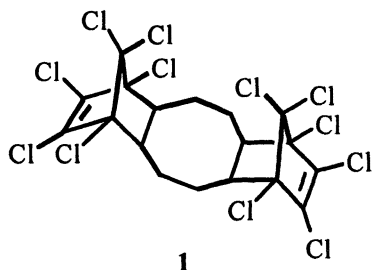


When the starting chloride does not dehydrochlorinate readily, the process that leads to the antimony halide is much less clear. Several of the schemes proposed have been summarized elsewhere (5,6). One possibility for which some evidence is available involves the formation of SbCl_3 from SbOCl in a series of disproportionation reactions (eqs 4–6) (7). Unfortunately, this



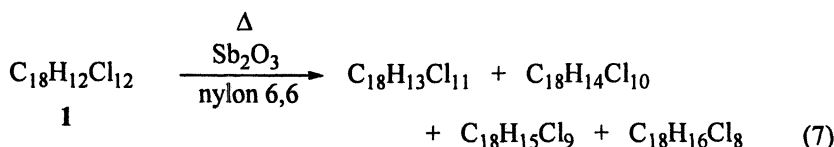
mechanism fails to answer the very important question of how the organically bonded chlorine is transferred to antimony. The organic chemical literature is not very helpful in this regard, as it tends to give the initial impression that antimony oxide may not react cleanly or readily with any organic substrates at all.

"Dechlorane Plus" is the trade name of a very well-known fire retardant, **1** (**8**), that results from the reaction of 1,5-cyclooctadiene with two molar



equivalents of hexachlorocyclopentadiene. Mixtures of this additive with Sb_2O_3 are highly synergistic for flame suppression in certain polymer systems. Dehydrochlorination of **1** would produce an alkene linkage at a bridgehead carbon atom and thus is proscribed by Bredt's rule (**9**). Hence the dechlorination of **1** that eventually leads to SbCl_3 must occur in some other way.

When heated together at ca. 400–700 °C, **1** and antimony oxide were found to evolve SbCl_3 and other chlorine-containing species that presumably were organic (**7**). However, the researchers performing the work (**7**) reported no results for ternary blends of **1**, Sb_2O_3 , and a combustible polymer. Subsequently, the thermolysis of such mixtures was studied in our laboratory (**5**). The polymer used was nylon 6,6, and the experiments were conducted at 320–330 °C in order to avoid the extensive decomposition that was expected to ensue from reactions allowed to run at higher temperatures. The results obtained were very striking. They revealed the occurrence of an unprecedented reductive dechlorination reaction that converted **1** into products that had lost as many as four chlorine atoms (eq **7**). Possible mechanisms for the dechlorination were discussed (**5**),



and it was suggested to play a major role in the creation of SbCl_3 , perhaps via HCl formation followed by some combination of reactions 1–4, or via a mechanism in which chlorine was transferred directly from carbon to antimony (**5**). Support for the latter option came from the discovery that copious amounts of SbCl_3 were evolved from heated mixtures of antimony oxide and hexachlorocyclopentadiene, a retro-Diels-Alder product that would have been formed from **1** *in situ* (**5**).

One of the mechanisms considered (5) for reductive dechlorination began with the reaction of Sb_2O_3 with organically bonded halogen to give the $\text{ClSb}_2\text{O}_3^+$ cation and a carbanion intermediate. Abstraction of a proton by the carbanion would form a C-H bond. Alternatively, the initial stage might yield $\text{ClSb}_2\text{O}_3^\bullet$ and a carbon-centered radical whose acquisition of a hydrogen atom from an existing C-H linkage would complete the elementary reduction process (5).

The polymer used in our earlier study, nylon 6,6, contains NHC=O and $\text{CH}_2\text{C=O}$ groups that are potentially capable of protonating certain types of carbanions. Nylon 6,6 also is a potential donor of hydrogen atoms. Thus its use as a polymeric substrate did not allow us to determine whether the mechanism for dechlorination involves carbanions or free radicals. In order to address this question, we now discuss the results of new pyrolysis experiments in which the matrix polymer was polyethylene (PE). Even though this substrate is a very weak acid indeed, it is an effective donor of hydrogen atoms to many types of free radicals.

Experimental

Materials

Compound 1 and antimony oxide were supplied by the Occidental Chemical Corporation. Polyethylene (density = 0.94 g/mL, Catalog No. 33211-9) was obtained from Aldrich. Tetrahydrofuran (THF) containing 0.031% of BHT (an oxidation inhibitor) was purchased from Fisher. All materials were used as received.

Thermogravimetric Analysis (TGA)

The analyses were carried out with a Shimadzu TG-50 instrument under a nitrogen flow of 50 mL/min. Finely powdered samples for analysis were obtained by grinding with a mortar and pestle at liquid nitrogen temperature. The samples (12–20 mg) were heated to 320 °C at the rate of 10 °C/min, kept at 320 °C for 6.0 h, and then cooled to room temperature at the rate of 50 °C/min. Reproducibilities of the total mass losses were within ± 5 –15% of the final values.

(Gas Chromatography)/(Mass Spectrometry) (GC/MS) Analysis

A Hewlett-Packard GC apparatus (Model 5890 Series II) equipped with a cross-linked methylsiloxane capillary column [12 m \times 0.2 mm (i.d.)] was used

with a Hewlett-Packard Mass Selective Detector (Model 5971A). Data were analyzed with Hewlett-Packard G1034B software for the MS ChemStation (DOS series). The carrier gas was helium, and the temperature of the injection port was 200 °C. After an initial hold period of 2 min at 50 °C, column temperature was increased to 300 °C at the rate of 20 °C/min and then held at 300 °C for 10 min. Products were identified by comparing their retention times and mass spectra with those of materials obtained in a previous study (5). The chlorine contents of various ions were easily deduced from the characteristic relative intensities of peaks whose masses differed significantly only because of variations in their chlorine isotope compositions (10).

Preparative Pyrolysis

Pyrolyses were performed on weighed samples (ca. 2.5 g) of finely powdered blends that were prepared by grinding with a mortar and pestle at liquid nitrogen temperature. Each sample was added to a 25-mL two-necked round-bottom flask that had been preheated in a Wood's metal bath to 325 °C, and the pyrolysis then was carried out for 6.0 h at 325±5 °C under a stream of argon that swept the volatile products into a U-tube cooled to ca. -80 °C. After weighing, the condensate was dissolved in THF and subjected to GC/MS analysis. The nonvolatile residues in the reaction vessel did not contain significant amounts of products that could be removed by attempted extractions with THF or several other common solvents.

Results and Discussion

TGA and Preparative Pyrolysis Data

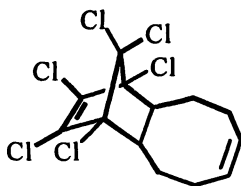
Because of its lack of polar functionality, PE undoubtedly is much less effective than nylon 6,6 as a solvent for **1** and antimony oxide. Hence, the promotion of reductive dechlorination by the antimony additive can reasonably be expected to be less dramatic in PE than in the nylon system. In preliminary trials, this expectation was verified, and for that reason, the isothermal pyrolysis time was extended to 6.0 h in PE [vs 0.5 h in nylon 6,6 (5)] in order to increase the extent of reaction.

In our TGA experiments, pure PE lost 3% of its weight during 100 min, while an 80:20 (w/w) PE:1 mixture lost 12% of its weight during the same time interval. Much of the increased weight loss must have resulted from sublimation of the additive, as had been found in the nylon system (5). However, in parallel experiments with PE:1:Sb₂O₃ at a weight ratio of 72:18:10, the weight loss during 100 min was consistently 17%. Antimony oxide is entirely nonvolatile at

320 °C (5). Thus its ability to enhance the weight loss can be ascribed to its promotion of reductive dechlorination, as had been observed in TGA runs on the nylon system, though there to a greater extent (5).

After ca. 100–120 min, both the PE/1 and the PE/1/Sb₂O₃ mixtures lost no more than an additional 1–2% of their weight up to the total TGA pyrolysis time of ca. 6.5 h. Hence it is apparent that, in both cases, appreciable amounts of the additives were not being converted into products that were volatile at 320 °C. This result is not inconsistent with observations made earlier on the pyrolysis of 1 alone, which indicated the diversion of much of the hexachlorocyclopentadiene formed *in situ* into insoluble (and unidentifiable) material (5).

In preparative pyrolyses, volatile organic product fractions were evolved from both the PE/1 blend and the ternary PE/1/Sb₂O₃ mixture. From GC retention times and mass spectral cracking patterns, these volatile fractions were shown to consist almost entirely of the retro-Diels-Alder product 2 (C₁₃H₁₂Cl₆)



2

and a monoreduction product, C₁₃H₁₃Cl₅. Unlike similar pyrolyses in nylon 6,6 (5), pyrolysis of the PE/1/Sb₂O₃ mixture gave no appreciable yields of products that could be removed from the nonvolatile residue by extraction with THF.

Gas chromatograms of the volatile fractions appear in Figures 1 and 2. They show that antimony oxide caused a major increase in the ratio of monoreduced to unreduced product. Monoreduction product yields were calculated from eq 8

$$\begin{aligned} \% \text{ monoreduction} &= \frac{100 \text{ (moles of } C_{13}H_{13}Cl_5)}{\text{(initial moles of 1)}} \\ &= \frac{100AB/(\text{molecular wt of } C_{13}H_{13}Cl_5)}{C \text{ (initial wt fraction of 1)} / (\text{molecular wt of 1})} \end{aligned} \quad (8)$$

by using the data in Table I and equating the GC area percentages to mole fractions. The tabulated monoreduction percentages show very good reproducibility and confirm the ability of antimony oxide to promote reductive dechlorination in this system.

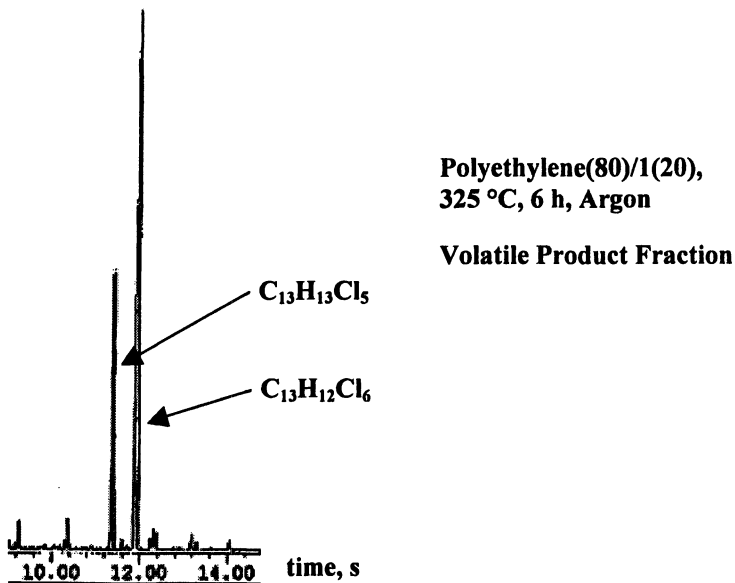


Figure 1. Partial gas chromatogram of the THF-soluble volatile products of a pyrolysis described in the heading. Parenthesized numbers in the heading are percentages by weight.

Mechanistic Implications

Compounds **1** and **2** contain vinyl, dichloromethylene, and tertiary C-Cl bonds. Which of these bonds is reduced to C-H has not been established experimentally. However, the vinyl halo substituents are likely to be bonded much too strongly to be abstracted by a nucleophile, and the nucleophilic abstraction of Cl^+ from a tertiary position, in addition to being entirely unprecedented, would give a carbanion having little, if any, allylic resonance stabilization, owing to poor overlap of its filled p orbital with the π orbital of the adjacent double bond. The most probable locus of Cl^+ abstraction is, therefore, the bridging CCl_2 group. The resultant bridging carbanion would be stabilized considerably by its α -chloro substituent, and its secondary nature also would tend to favor its formation over that of a tertiary ion at a bridgehead position (secondary carbanions are well-known to be more stable, in general, than tertiary carbanions). Now a bridging carbanion formed from **1** or **2**, whether actual or incipient, undoubtedly would undergo a retro-Diels-Alder reaction, such as reaction **9**, at an exceedingly rapid rate, owing to the formation of the aromatic C_5Cl_5^- ion as a product (11–14). Yet from the approximate $\text{p}K_a$ values of several weak Brønsted acids (15), it is clear that neither PE, **1**, nor **2** would be able to protonate C_5Cl_5^- . Consequently, the formation of C_5HCl_5 in this way,

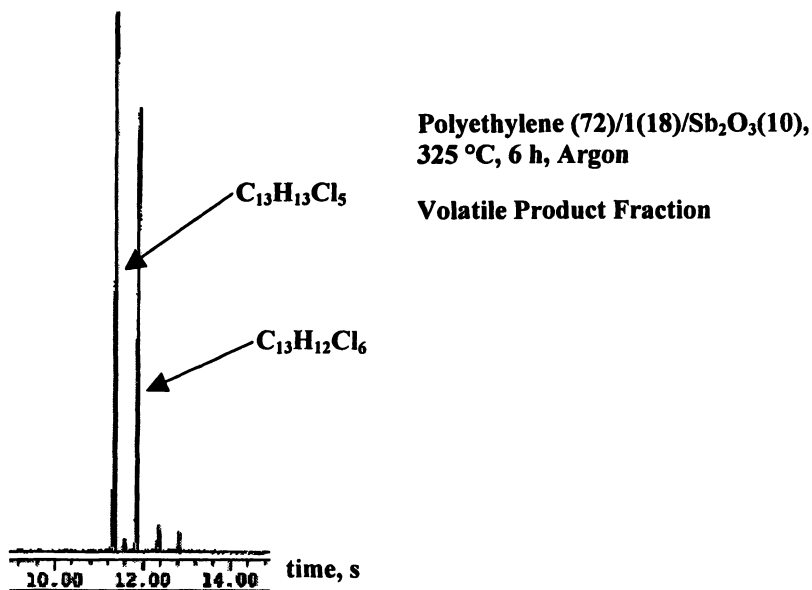


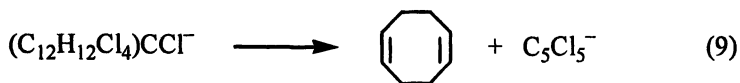
Figure 2. Partial gas chromatogram of the THF-soluble volatile products of a pyrolysis described in the heading. Parenthesized numbers in the heading are percentages by weight.

Table I. Pyrolysis Yield Data and Extents of Monoreduction^a

	<u>PE (80)/1(20)</u>		<u>PE(72)/1(18)/Sb₂O₃(10)</u>	
	<i>Run 1</i>	<i>Run 2</i>	<i>Run 1</i>	<i>Run 2</i>
A: wt of volatile product fraction, g	0.17	0.14	0.31	0.28
B: wt fraction of C ₁₃ H ₁₃ Cl ₅ in A	0.19	0.28	0.52	0.54
C: wt of initial mixture, g	2.55	2.50	2.61	2.49
Monoreduction, ^b %	12	15	64	63

^aNumbers in parentheses are percentages by weight.

^bValues obtained from eq 8.



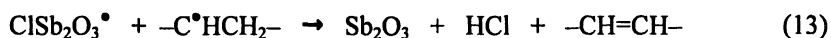
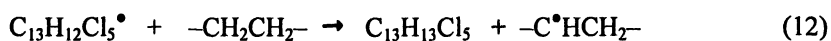
followed by its reaction with 1,5-cyclooctadiene in a Diels-Alder process, is a very unlikely route to $\text{C}_{13}\text{H}_{13}\text{Cl}_5$ in the PE system.

A similar argument can be made against the intermediacy of carbanions in the nylon 6,6 system. Although protons in $\text{CH}_2\text{C}=\text{O}$ and, especially, $\text{NHC}=\text{O}$ structures are much more acidic than those in PE, **1**, or **2**, a comparison of approximate $\text{p}K_a$ values (15) shows that the protonation of C_5Cl_5^- by nylon 6,6 is improbable nonetheless.

In both PE and nylon 6,6, a free-radical mechanism for reductive dechlorination best explains the available facts. The dechlorination occurred to a small extent in both polymers, even when Sb_2O_3 was not present. In view of the lack of evidence for intermediate carbanions, the only reasonable mechanism for this uncatalyzed dechlorination involves C-Cl homolysis and subsequent hydrogen-atom abstraction from the matrix by the resultant C-centered radicals.

The strongest C-Cl bonds in **1** and **2** obviously are the vinyl ones. Thus their homolysis is highly unlikely. Homolysis of the bridgehead C-Cl bonds seems rather improbable, as well. Owing to poor orbital overlap (see above), the resultant C-centered radicals would not enjoy allylic resonance stabilization. In fact, considerable evidence exists to suggest that they actually would be less stable than typical tertiary alkyl radicals (or even secondary ones), owing to their adverse geometry (16). In contrast, C-Cl homolysis in a dichloromethylene bridge would create a secondary C-centered radical that is stabilized appreciably by α -chloro substitution. This homolysis finds some precedent in the ClC-Cl homolysis that has been implicated in the thermolysis of vinylidene chloride polymers (17). On the other hand, the bridging secondary radical would be destabilized to some extent by angle strain. For that reason, a firm conclusion regarding the site of C-Cl homolysis in **1** and **2** cannot be reached at this time. However, this ambiguity obviously does not rule out the involvement of free radicals in reductive dechlorination.

The promotion of dechlorination by Sb_2O_3 can be explained by the mechanism shown in eqs 10–13 (5). An analogous scheme would apply to **1**, of



course, and reactions 10 and 11 conceivably could merge into a single step in which the Sb_2O_3 performs a direct abstraction of a chlorine atom from the

substrate. Reaction 13, though not required, would allow the antimony oxide to function as a true catalyst, and continual repetition of the sequence would lead to products whose dechlorination is more extensive, as was observed in nylon 6,6 (5).

Concluding Remarks

We now believe that in both polyethylene and nylon 6,6, the reductive dechlorination of Dechlorane Plus and its promotion by antimony oxide occur by a mechanism that involves the abstraction of hydrogen atoms by carbon-centered free radicals. Explicit identification of the C-Cl groups that are reduced is envisaged as the objective of further studies in this area.

Acknowledgment

This work was supported by the National Science Foundation under Grant No. CHE-9983374.

References

1. Hastie, J. W. *J. Res. Natl. Bur. Stand., Sect. A* **1973**, *77*, 733–754.
2. Cullis, C. F.; Hirschler, M. M. *The Combustion of Organic Polymers*; Oxford University Press: New York, 1981; pp 276–295.
3. Camino, G.; Costa, L.; Luda di Cortemiglia, M. P. *Polym. Degrad. Stab.* **1991**, *33*, 131–154.
4. Lum, R. M. *J. Polym. Sci., Polym. Chem. Ed.* **1977**, *15*, 489–497.
5. Starnes, W. H., Jr.; Kang, Y. M.; Payne, L. B. *ACS Symp. Ser.* **2001**, *No. 797*, 253–266.
6. A correction of printer's errors in reference 5 has been provided by the publisher and can be obtained from the corresponding author upon request.
7. Costa, L.; Goberti, P.; Paganetto, G.; Camino, G.; Sgarzi, P. *Polym. Degrad. Stab.* **1990**, *30*, 13–28.
8. Markezich, R. L.; Mundhenke, R. F. In *Chemistry and Technology of Polymer Additives*; Al-Malaika, S., Golovoy, A., Wilkie, C. A., Eds.; Blackwell Science: Malden, MA, 1999; pp 151–181.
9. March, J. *Advanced Organic Chemistry*, 4th ed.; Wiley-Interscience: New York, 1992; p 160.
10. Beynon, J. H. *Mass Spectrometry and Its Applications to Organic Chemistry*; Elsevier: New York, 1960; pp 298–299.

11. Finnegan, R. A.; McNees, R. S. *J. Org. Chem.* **1964**, *29*, 3234–3241.
12. Bowman, E. S.; Hughes, G. B.; Grutzner, J. B. *J. Am. Chem. Soc.* **1976**, *98*, 8273–8274.
13. Neukam, W.; Grimme, W. *Tetrahedron Lett.* **1978**, 2201–2204.
14. Blümel, J.; Köhler, F. H. *J. Organomet. Chem.* **1988**, *340*, 303–315.
15. March, J. *Advanced Organic Chemistry*, 4th ed.; Wiley-Interscience: New York, 1992; p 251–253.
16. March, J. *Advanced Organic Chemistry*, 4th ed.; Wiley-Interscience: New York, 1992; pp 192 and 686.
17. Wessling, R. A.; Gibbs, D. S.; DeLassus, P. T.; Obi, B. E.; Howell, B. A. *Encycl. Chem. Technol.* 4th Ed. **1997**, *24*, 882–923 .

Chapter 18

Borates as Fire Retardants in Halogen-Free Polymers

Kelvin K. Shen^{1,*} and Eric Olson²

¹Luzenac/Borax, Huntington Beach, CA 92646 (Kelvin.Shen@Borax.com)

²Luzenac America, Denver, CO 80112 (Eric.Olson@America.Luzenac.com)

Recent development in the use of borates as fire retardants in halogen-free polymers will be reviewed. Particular emphasis will be on the use of *Firebrake* zinc borates ($2\text{ZnO}\cdot 3\text{B}_2\text{O}_3\cdot 3.5\text{H}_2\text{O}$, $4\text{ZnO}\cdot \text{B}_2\text{O}_3\cdot \text{H}_2\text{O}$, and $2\text{ZnO}\cdot 3\text{B}_2\text{O}_3$) in polyolefins. The interaction/beneficial effects of using zinc borate in the presence of magnesium hydroxide and/or alumina trihydroxide will be presented. The results of using co-additives such as silicone/silica, phosphates, and nanoclay in enhancing the zinc borate/metal hydrate fire test performance in Cone Calorimeter and other fire tests will also be presented.

Introduction

One of the many applications of borates is fire retardancy. Boron compounds such as boric acid and borax are well known fire retardants for cellulosic products. Ammonium pentaborate, melamine borate, and barium metaborate are known for their use in fire retardant coatings. However, the low dehydration temperature and/or high water solubility of these borates severely limits their usage in plastics and rubber industries. Colemanite, a natural calcium

borate mineral with a low purity, is mostly used in the rubber modified asphalt roofing membrane. Among all of the boron-containing fire retardants, zinc borate is of the most commercial importance. This paper will be focused on the use of zinc borate as a multifunctional fire retardant in halogen-free polyolefins.

Metal hydroxides, such aluminum trihydroxide (ATH - $\text{Al}(\text{OH})_3$) and magnesium dihydroxide (MDH - $\text{Mg}(\text{OH})_2$), have been used extensively in halogen-free, fire retardant polyolefins. They produce drastically lower levels of smoke and corrosive combustion products than halogen-containing polyolefins. However, high loading levels of ATH and MDH are required. In wire & cable applications, for example, addition levels of these metal hydroxides of more than 60% by weight in polyolefins are generally required to meet the fire standards such as VW-1, IEC332-1 and -3 vertical burn tests. In TPO roofing membrane application, about 40% by weight MDH is required to pass the UL 790 test.

High additive loading has deleterious effect on extrudability/melt viscosity and mechanical properties. These negative impacts can be alleviated or offset by proper selection of base polyolefin polymer, by surface treatment of the additives, and by the addition of a compatibilizer. Recent development efforts are focused on maximizing fire test performance with the use of co-additives and improving the formation of a strong char. A strong char formation is critical in applications such as in jacketing of riser or security cables. Some examples of chemical and physical modifications are:

- Transition metal oxides (ZnO, NiO) treated MDH or ATH
- Nitrate treated ATH
- Zinc stannate treated MDH
- Nano-sized ATH and MDH

Some examples of co-additives are:

- Silicon derivatives- organosiloxane, silica, talc, ceramic frits, zeolite, kaolin, wallastonite
- Nanoclays, nanotubes
- Borates- zinc borate, calcium borate, boron phosphate, borosiloxane, boric oxide
- Phosphorous derivatives- red phosphorus, phosphate esters, melamine polyphosphate, ammonium polyphosphate
- Nitrogen derivatives- melamine, melamine cyanurate,
- Organic compounds- novolak, polyaromatic phenols, polyphenylene oxide, polyacrylonitrile fiber, acrylic-siloxane
- Metal Oxides- zinc oxide, antimony oxide

This paper will review our recent efforts in trying to achieve a more efficient fire retardant, halogen-free polyolefins with the use of *Firebrake* zinc borates as co-additives.

Experimental

Materials

Firebrake[®]ZB ($2\text{ZnO}\cdot 3\text{B}_2\text{O}_3\cdot 3.5\text{H}_2\text{O}$)- This form of zinc borate, combining the optimum effects of zinc and boron oxides, starts to release water at about 290 °C. It has a typical median particle size of 9 microns. A finer grade, *Firebrake* ZB-Fine, has a typical median particle size of 2 microns.

Firebrake[®]500 ($2\text{ZnO}\cdot 3\text{B}_2\text{O}_3$)- An anhydrous form of zinc borate that is offered to meet the demand of high performance engineering plastics processed at temperatures significantly above 290 °C and no significant water release is permitted.

Firebrake[®]415 ($4\text{ZnO}\cdot \text{B}_2\text{O}_3\cdot \text{H}_2\text{O}$)- This patented zinc borate with higher ZnO/B₂O₃ ratio than that of *Firebrake* ZB is stable to 415 °C.

Nano-clay was Cloisite 30B from Southern Clay; Nanofil 5 and Nanofil 15 are from Sud-Chemie. Magnesium hydroxide was Magnefin H5 from Albemarle. Silicon fluid was from GE (SFR100) and Dow-Corning (DC4-7081). Melamine polyphosphate (Melapur 200) from Ciba Specialties. EVA copolymers used were Escorene UL00119 (EVA 19% VA, Melt index 0.65) from Exxon Chemical. Samples for testing were prepared in a Haake mixer with electrical heating. For preliminary tests, small 75 gram batches were made in a Haake 600 mixing head; for cone tests, batch size was 425 grams in a Haake 3000 mixing head. Cam blades were used in both cases. Formulation components were pre-blended and added to the mixer, preheated to 160°C. Mixing was continued at 160°C for 10 minutes.

Results and Discussion

Background

One of the major challenges in developing fire retarding formulations is trying to correlate a small-scale laboratory test with that of intermediate or a large-scale fire test. In wire and cable applications, one normally uses UL 94 (or its modified version) and Oxygen Index tests for pre-screening. In recent years,

the use of Cone Calorimeter has been an increasingly popular tool for screening and research purposes.

In earlier work, Shen et al. reported that *Firebrake* ZB-Fine and ATH can form a porous and hard residue during the combustion of a cross-linked EVA (1-5). Our recent study showed that the sintering/fusion between zinc borate and MDH starts at temperatures between 550 and 700 °C. In wire & cables, for example, this sintered residue is an important thermal insulator for the substrate or unburned polymer. It can prevent short-circuiting and sparking, as well as protecting the underlying insulation material. It was also observed that partial replacement of ATH with *Firebrake* ZB can result in significantly higher Oxygen Index and better fire test performance in a modified UL 94 test but only at high total loadings. Based on DTA and DSC, it was also demonstrated that *Firebrake* ZB can delay and reduce the thermal oxidative peak.

Interestingly enough, Bourbigot reported that replacement of ATH (total 65% in EVA) with *Firebrake* ZB (5%) resulted in a maximum increase in Oxygen Index (from 42.0 to 51.5%.) in a non-cross-linked EVA (6). A similar ratio giving maximum Oxygen Index was also observed with the use of MDH and *Firebrake* 415. Recently, Hull et al. reported that partial replacement of ATH with zinc borate in EVA reduces carbon monoxide yield under fuel rich conditions in their Purser furnace (7).

Duquesne et al. reported that increasing the level of substitution of MDH by *Firebrake* 415 in an EVA (6% VA content, with 60% total loading) displayed significant reduction of rate of heat release (RHR) and an increasingly stronger char (8). They used a dynamic plate-plate rheometer to confirm that increasing *Firebrake* 415 loading can result in 100 fold increase of melt/pyrolysis viscosity in the range of 300-400 °C. They also demonstrated that a strong char that is able to stand pressure of 50 kN/m² was formed with the use of *Firebrake* 415. The strong char with the elimination of surface cracks can prevent volatile gases from reaching the combustion zone. Interestingly enough, Durin-France et al. claimed synergy between *Firebrake* ZB and talc at constant MDH loading in ternary compositions (9). Park et al. reported that the incorporation of zinc borate and talc can increase the flame retardancy of MDH in ethylene-ethylacrylate as evidenced by the Cone Calorimeter test (10). Our recent evaluation results with the use of Cone Calorimeter are presented as follows (11).

MDH or ATH with *Firebrake* Zinc Borates

In the UL 94 test (1/16 in.), the finer zinc borate can generally perform better than the coarser material (i.e. Sub-micron zinc borate > *Firebrake* ZB XF (1.8 microns) > *Firebrake* ZB-Fine (2.5 microns) > *Firebrake* ZB (9 microns). But in

the Cone Calorimeter test, one may not see a similar correlation. To balance the cost/performance, *Firebrake ZB-Fine* was used throughout the study. Figure 1 illustrates that, at 65% loading, ATH in EVA can generate a lower peak rate of heat release (peak HRR) than that of MDH (257 vs. 188 kW/m²). A partial substitution of MDH with *Firebrake ZB-Fine* resulted in not only the significant reduction of first peak HRR but also a drastic reduction and delay of the 2nd major peak of HRR. The latter indicates that there is a significant char/hard residue formation due to the presence of *Firebrake ZB-Fine*. In the case of ATH, although the HRR reduction is not as dramatic, the 2nd peak is flattened out with use of *Firebrake ZB-Fine* that is also an indication of a stronger char formation. The use of a combination of MDH/ATH/*Firebrake ZB-Fine* resulted in better UL-94 performance but no apparent improvement in the HRR. It should be pointed out that both magnesium oxide (a dehydration product of MDH) and aluminum oxide (a dehydration product of ATH) are known to cause glowing combustion in polyolefin and that *Firebrake zinc borate* is known to suppress the glowing combustion.

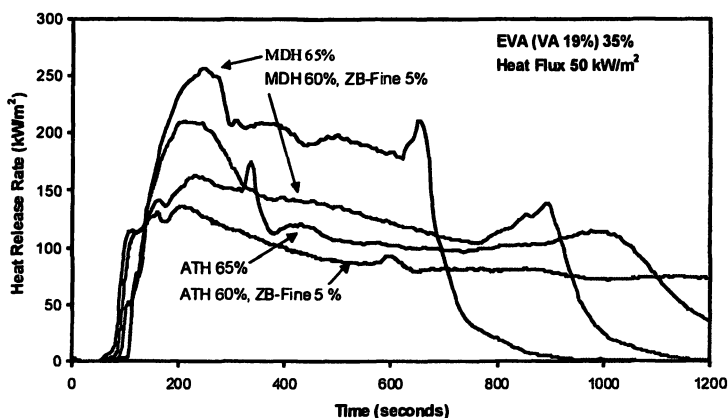


Figure 1. HRR Curves of EVA (35%) Containing MDH or ATH with *Firebrake ZB-Fine* (total loading 65%)

Figure 2 illustrates that, at 60% total loading, an incremental increase in the substitution of MDH with *Firebrake ZB-Fine* resulted in an incremental delay of the HRR peak starting at around 625 second. This is also an indication of a stronger char/ceramic formation at the surface. With 40% MDH and 20% *Firebrake ZB-Fine*, a very strong char is formed (See inserted picture). But it should be noted that, with this high level of substitution, one will lose the vertical flammability test performance.

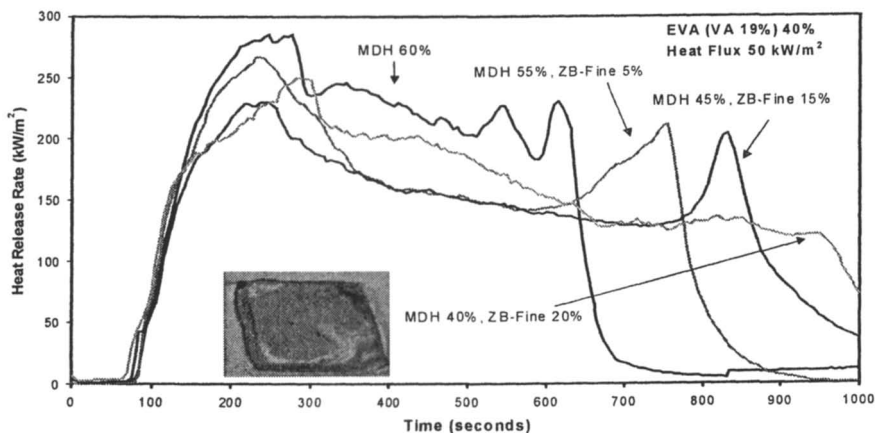


Figure 2. HRR Curves of MDH with Firebrake ZB-Fine (60% total loading)

It is interesting to note that *Firebrake 500* was found to outperform *Firebrake ZB-Fine* in the UL 94 test but not in terms of HRR.

Firebrake ZB / Silicone as Co-additives

Firebrake zinc borate was previously reported to be an effective flame retardant and smoke suppressant in silicone polymers (12). It is believed that the fire retardant action is due to the formation of vitreous borosilicate glass. Marosi also reported that the use of borosiloxane as a fire retardant in polyolefin (13). Matsumoto reported the use of phenylborosiloxane to achieve V-O (1.6 mm) in a transparent polycarbonate with good impact strength (14). Thus, it is reasonable to expect that a combination of *Firebrake ZB*, a silica source, and MDH (or ATH) will have a good fire retardancy effect in polyolefin. Mortimer reported the use of a combination of ATH/*Firebrake ZB*/silicone in polyolefins (15). Guimond reported that, in a blend of MDH/ mLDPE/ethylene-methylacrylate, *Firebrake ZB* and silicone powder showed synergy in Oxygen Index measurement but not in the modified UL 94 test (16). Nakagoma et al. reported the use of a similar combination in ultra-low-density polyethylene for IEEE-383 tray cable applications (17). More recently, Yuu of Hitachi reported the use of a combination of a silicone-acrylic rubber and an unspecified zinc borate as a co-additive in EVA/MDH cable sheathing (Table I) (18).

Table I. Halogen-Free Cable Sheathing Containing Acrylic-Silicone

<u>Components</u>	<u>Examples (parts by wt.)</u>			
	<u>1</u>	<u>2</u>	<u>3</u>	<u>4</u>
EVA	100	100	95	95
MA Grafted LLDPE	-	-	5	5
Mg(OH) ₂	100	100	-	-
Silane-Treated Mg(OH) ₂	-	-	80	120
Silicone-Acrylic Rubber	20	20	5	-
Silicone Rubber	-	-	-	5
Zinc Borate	-	3	15	15
Antioxidant	0.5	0.5	0.5	0.5
<u>Properties</u>				
Tensile Strength (MPa)	12.4	12.2	11.6	8.6
Oxygen Index (%)	31	36	35	33
IEEE383 (cm)	<180	<120	<120	<180

Figure 3 illustrates that, in the presence of MDH, the benefits of using a combination of *Firebrake ZB-Fine/silicone* (SFR100) as a co-additive. The peak HRR can be reduced drastically from 257 to 131 kW/m²; but the TTI was slightly decreased.

The use of DC4-7081 (silicone) and *Firebrake ZB-Fine* give similar results in the Cone Calorimeter test. In both cases, a dramatic smoke reduction was also observed with the addition of either *Firebrake ZB-Fine* or *Firebrake 415* (Figure 4).

Firebrake ZB/Melamine Polyphosphate (MPP) as Co-additives

Recently Daicel reported the use of a combination of MPP/ dipentaerythritol/*Firebrake ZB* in polypropylene (19) (Table II).

Toyo Ink recently reported the use of MDH and various melamine salts, including MPP, in EVA and LDPE (20). Figure 5 illustrates that MPP at 5% substitution of MDH (65% total loading) can result in a drastic reduction in HRR and the formation of an intumescent char. At the same total loading, the use of a combination of *Firebrake ZB-Fine/MPP* can result in even further reduction of HRR and the formation of a stronger intumescent char.

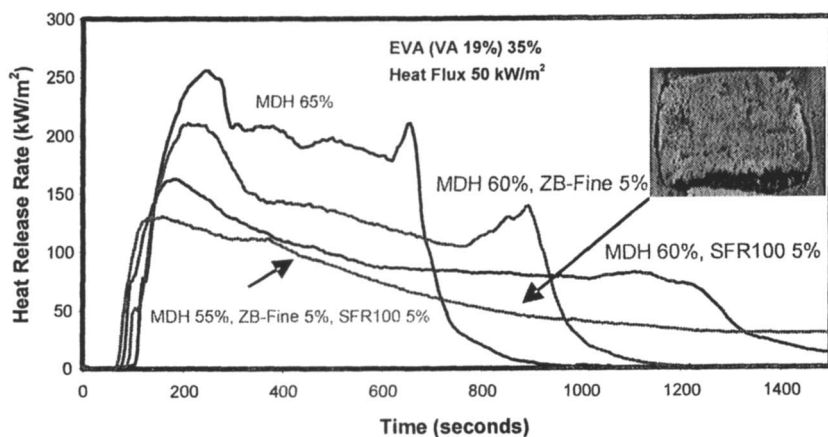


Figure 3. HRR Curves of MDH/Firebrake ZB-Fine/Silicone (total loading 65%) in EVA.

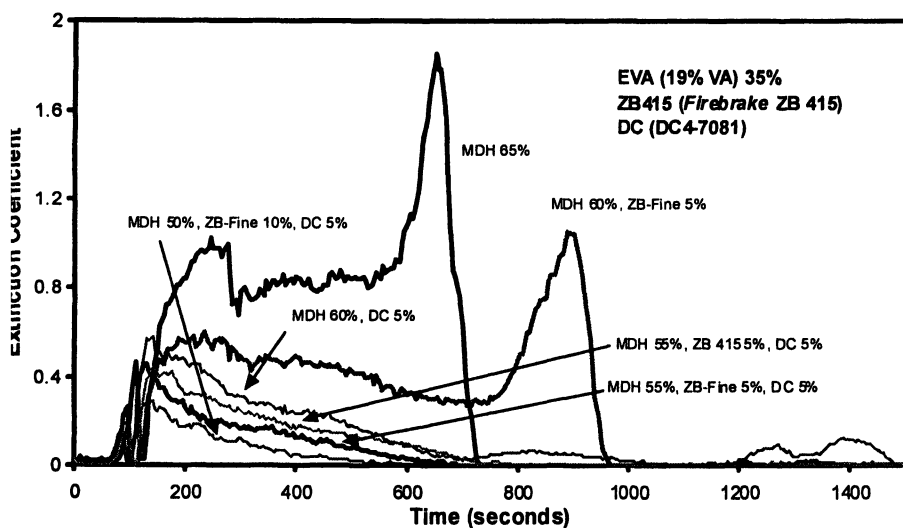


Figure 4. Smoke Reduction of Firebrake ZB-Fine and Silicone in MDH-Containing EVA (total loading 65%, heat flux 50 kW/m²).

Table II. Halogen-Free Polypropylene

<u>Components</u>	<i>Examples (parts by wt.)</i>		
	<u>1</u>	<u>2</u>	<u>3</u>
Polypropylene	100	100	33
Melamine polyphosphate	33	33	33
Dipentaerythritol	16	16	16
<i>Firebrake ZB</i>	-	3	-
Aluminum Silicate	-	-	3
<u>Properties</u>			
UL-94 (3.0 mm)	V-O	V-O	V-O
Peak HRR (kW/m ²)	610	450	530
Soapness	O	O	O

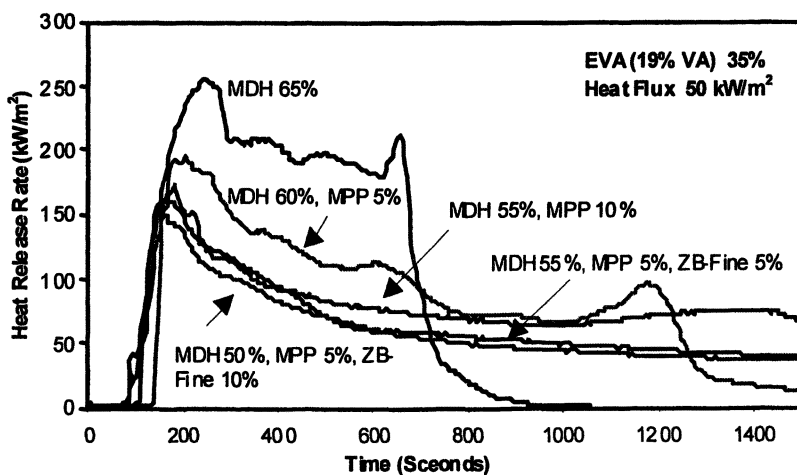


Figure 5. HRR Curves of EVA containing MDH, Melamine Polyphosphate (MPP), and Firebrake ZB-Fine (total loading 65%)

In an attempt to lower the total loading, Figure 6 illustrates the use of *Firebrake* ZB-Fine/MPP in conjunction with MDH at 50% total loading. The combination of MDH (35%)/*Firebrake* ZB-Fine (5%)/MPP (10%) yielded the lowest HRR (reduction of peak HRR from 340 down to about 200 kW/m²). However, these formulations with high substitution all failed the UL-94 test (i.e. not ratable).

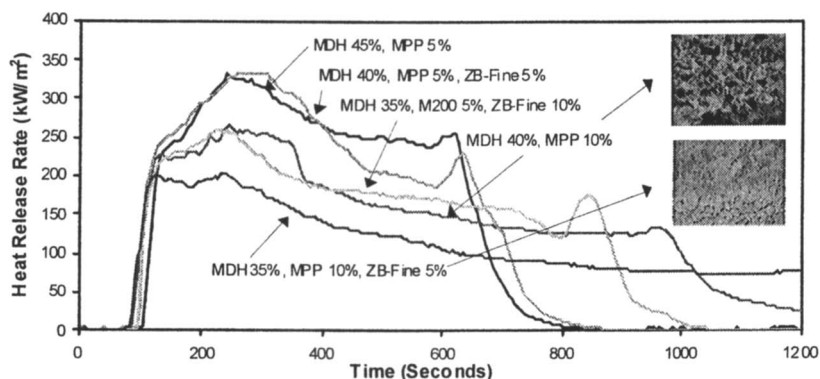


Figure 6. HRR Curves of MDH/Melamine Polyphosphate (MPP)/*Firebrake* ZB-Fine in EVA (total loading 50%, heat flux 50 kW/m²).

Firebrake ZB/Nanoclay as Co-Additive

Beyer reported that nanoclay in EVA containing ATH showed a dramatic decrease of heat release and further improvement of other important fire parameters (21). Lan et al. also reported the use of nanoclay in both halogen-free and halogen-containing polyolefins (22). Figure 7 illustrates the use of a combination of *Firebrake* ZB-Fine and nanoclay (Cloisite 30B) in EVA containing ATH. In this case, *Firebrake* ZB-Fine can improve both the Oxygen Index, UL 94, char formation of the formulation but not the HRR.

Figure 8 illustrates the same combination in EVA containing MDH. The addition of *Firebrake* ZB-Fine in these systems can not only decrease HRR (although slightly) but can also improve the UL-94 test performance. In addition, a stronger char is formed due to the presence of *Firebrake* ZB-Fine.

Conclusions

- *Firebrake* zinc borates reduce the Heat Release Rate and smoke evolution in most metal hydroxide-containing polyolefin formulations.

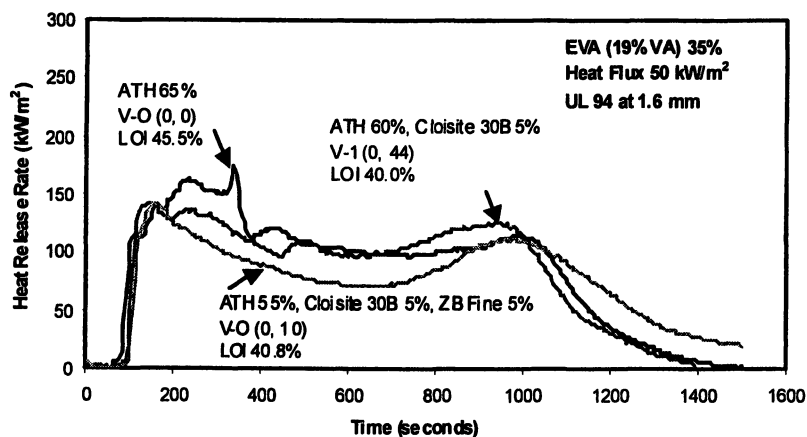


Figure 7. HRR Curves of ATH, Nanoclay, and Firebrake ZB-Fine in EVA (total loading 65%).

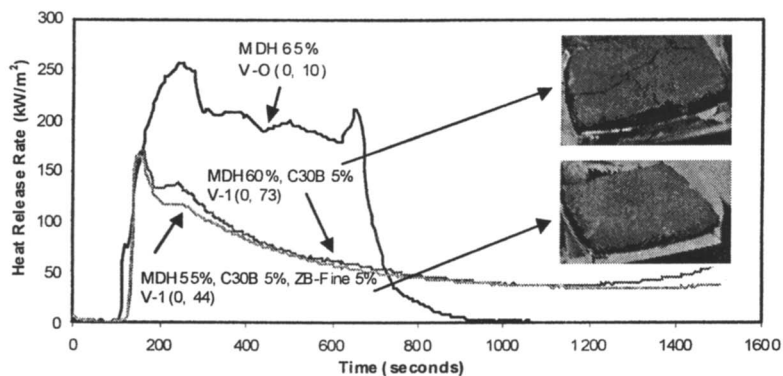


Figure 8. HRR Curves of MDH, Nanoclays, and Firebrake ZB-Fine in EVA (total loading 65%, heat flux 50 kW/m²).

In terms of HRR, *Firebrake* zinc borates appear to be more effective with MDH than with ATH.

- At about 5% substitution of metal hydroxide with *Firebrake* zinc borates, the Oxygen Index test performance can generally be improved.
- *Firebrake* zinc borates can promote the formation of a strong char/ceramic residue that prevents burning drips and delay oxidative pyrolysis.
- With certain co-additives, *Firebrake* can improve smoke, carbon monoxide, and afterglow reduction.
- The use of co-additives such as silicone, melamine phosphate, and nanoclay augment the performance of *Firebrake* zinc borate/metal hydroxide combination.
- *Firebrake* zinc borate is recommended for use in conjunction with ATH or MDH at ratios of about 1:10 to about 2:10 in halogen-free polyolefins.

References

1. Shen, K.K. *Plastics Compounding*, Sept./Oct. 1985.
2. Shen, K.K.; O'Connor R. in "*Plastics Additives*"; Pritchard, G. (Ed.), P. 268, 1998, Chapman & Hall, London.
3. Shen, K.K.; Griffin, T.S. in "*Fire and Polymers*"-ACS Symposium Series 425; Nelson, G.L. (Ed.), p.157 (1990).
4. Shen, K.K. in "*Fire and Polymer*" Symposium, *Proceedings of ACS Fall Meeting- Polymeric Materials*, August 21, Washington, D.C., 91, p. 64 (2000); Shen, K.K.; and Ferm, D.J. in "*Tenth Annual BCC Conference on Flame Retardancy*", Stamford. Conn., May 1999.
5. Shen, K.K.; Schultz, D.S. in "*Rubber Technology-Compounding and Testing for Performance*," Dick, J.S. (Ed.), P. 489, 2001, Hanser, Munich.
6. Bourbigot, S.; Le Bras, M.; Delobel, R. in "*Ninth Annual BCC Conference on Fire Retardant*", Stamford, CT, May 1998.
7. Hull, T.R.; Quinn R. E.; Areri, I. G.; Purser D.A. *Polym. Deg. & Stab.*, **2002**, *77*, 235-242.
8. Duquesne, S.; Le Bras, M.; Delobel, R. *Thirteenth Annual BCC Conference on Fire Retardant*, Stamford, CT, June 2002.
9. Durin-France, A.; Ferry, L.; Lopez Cuesta, J-M.; Crespy, A. *Fire Internat.* **2000**, *49*, 1101.
10. Park, D.H.; Ahn. M. J.; Kim, S.; Lee, G. J. *Proceedings of 50th International Wire & Cable Symposium*, 422 (2000).
11. Shen, K.K.; Olson, E. *Additives 2004*, Clearwater Beach, Florida.
12. Sharp, D.W. *GB 2,140,325A* (1984).
13. Marosi, G.,; Anna,P.; Balogh,L.; Bertalan, G.; Tohl, A. *J.Therm. Anal.*, **1997**, *48*, 717

14. Matsumoto, K.; Ono, Y.; Tsuneishi, H. *US Patent 6,716,952 B1* (2004).
15. Smith, J.P.; Mortimer, J. *European Patent Application 333 514 A1* (1989).
16. Guimond, C. *Proceedings ANTEC 98, Society of Plastics Engineers*, p.3406
17. Nakagoma, K.; Morii, A.; Fujimura, S.; *Jpn. Kokai Tokkyo Koho*, JP 02,150,436.
18. Yuu, S. *Japan Kokai Tokkyo JP 2002-338775A*.
19. Imannishi, S. *European Patent 1 270 613 A2* (2002).
20. Nakane, M. *Japan Kokai Tokkyo Koho JP 2001-151950A*.
21. Beyer, G. *Twelfth Annual BCC conference on Flame Retardants*, Stamford, Conn., June 2001.
22. Lan, T.; Qian, G.; Liang, Y.; Cho, J.W. *Fire Retardant Chemical Association Spring Conference*, San Antonio, Texas, 2002, p.115.

Chapter 19

In Search of Synergy Using Conventional Fire Tests

L. J. Russell, D. C. O. Marney*, and V. P. Dowling

**CSIRO Division of Manufacturing and Infrastructure Technology,
P.O. Box 56, Highett, Victoria 3190, Australia**

Conventional fire testing techniques including UL 94 test, cone calorimetry and oxygen index determination, were used to investigate the interaction between a brominated fire retardant and a proprietary fire performance enhancing additive within a polypropylene matrix. We have focused upon the techniques and methodologies used and the conclusions that may be drawn to gain a better understanding of the system. Analysis of the fire testing results indicates an interaction between the two additives which clearly enhances the fire performance. This work has also shown that the use of multiple fire tests representing different fire models can provide valuable information on the burning process for a particular material.

In this paper we consider the utility of conventional fire testing methodologies to study the interaction between a proposed fire performance enhancing additive (FPEA) and a brominated fire retardant (BFR) within a polypropylene (PP) matrix and whether this interaction has an effect on the fire performance of the PP material. The details of the fire retardant additives will not be discussed due to a confidentiality agreement with an industry partner. The interaction between the two additives may impact upon the fire performance in an additional, antagonistic, or a synergistic manner (1). Troitzsch (1) and Lewin (2) have provided extensive discussions on the modes of action of flame retardants and synergists when combined with plastics. Halogenated organic compounds are well known fire retardant additives for PP. They are generally used in conjunction with antimony trioxide compounds to enhance their fire retardant efficacy (halogen-metal synergistic effect) (3).

Two types of fire retardant systems will be studied. The first system consists of a BFR combined with PP, and the second system combines the FPEA and a BFR with PP. The focus of this work is on the techniques and methodologies used and the conclusions that may be drawn to gain a better understanding of the system during combustion. We present the analysis of the data from the experiments carried out using the cone calorimeter, UL 94 and the oxygen index apparatus.

Combustion of Solid Polymers – Background

The steps involved in the flaming combustion of solid polymers are described schematically in Figure 1. Flaming combustion requires three coupled processes: (i) heating of the polymer, (ii) thermal decomposition / pyrolysis, and (iii) ignition of the gaseous decomposition products. The cycle is completed when an ignition source or thermal feedback of radiant energy from the flame supplies heat to the polymer surface, causing decomposition by thermolytic cleavage of primary chemical bonds in the polymer molecules.

Flammable and non-flammable gaseous pyrolysis products mix and react exothermically with air in the combustion zone above the surface. Carbon dioxide, water and products of incomplete combustion such as carbon monoxide and soot are produced.

For continuous burning to occur, the application of heat (step 4 to step 1) must be sufficient to decompose the material (step 1 to step 3); the temperature must be high enough to ignite decomposition products (step 2 to step 3); and the amount of heat transferred back to the polymer (step 4 to step 1) must be great enough to maintain the cycle when the initially applied source of heat is withdrawn (4). Thus, solving the problem of fire retardancy involves:

- A. Modification of the thermal degradation process,
- B. Quenching of the flame, or
- C. Reduction of the supply of heat from the flame back to the decomposing polymer as shown in Figure 1.

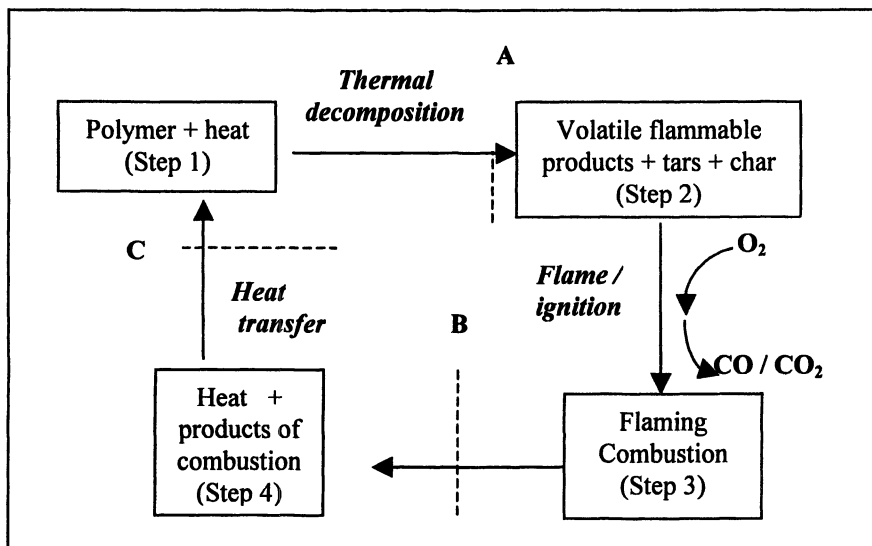


Figure 1. The Polymer Burning Cycle

Experimental

Materials

The materials used were polypropylene, a brominated fire retardant (BFR) and the proprietary fire performance enhancing additive.

Specimen Preparation

The fire retardant additives were premixed with PP in a TK Fielder powder mixer (Type: TR8, 1430 rpm) prior to feeding to a JSW twin-screw extruder set at 190 °C. The extruded material was then pelletised. Specimens for UL 94, Cone Calorimeter and Oxygen Index tests were injection moulded on a Battenfeld BA 800 CDC injection moulder at approximately 200 °C to produce specimens with dimensions specific to each test. Specimens were conditioned at 23 °C and 50 % relative humidity for a minimum of 48 hours prior to fire testing.

The various compositions made from PP, the BFR and the FPEA are given in Table I.

Table I. The compositions of PP/FR material

<i>Material</i>	<i>PP</i>	<i>PP+BFR</i>	<i>PP+FPEA</i>	<i>PP+BFR+FPEA</i>
PP (phr)	100	100	100	100
BFR (phr)		15		15
FPEA (phr)			1	1

Combustion Tests

UL 94 Test

The UL 94 test (5) is commonly used by industry as a quality control or screening procedure. (6, 7, 8, 9) It provides an indication of a material's ability to self-extinguish with ratings of V-0, V-1, V-2 and not rated (NR) (10, 11, 12). For this work we used the UL 94 Vertical Burning Test in accordance with UL 94 Section 8. Tests were conducted on specimens measuring approximately 125 mm x 12 mm x 3 mm.

Cone Calorimetry

The cone calorimeter can be used to examine the performance of fire-retarded plastics (13). It is used to determine heat release rate and mass loss, as well as a number of other fire parameters. It uses the oxygen consumption principle (14) with the assumption that there is a constant relationship between the mass of oxygen consumed from the air and the amount of heat released. It has been demonstrated that a value of 13.1 MJ kg⁻¹ oxygen consumed is appropriate for most polymers (15).

By observing changes in the fire parameters measured in PP during this test, the fire retardancy effectiveness of the BFR and the FPEA can be determined. The parameters considered in this study included the following:

- Effective heat of combustion in MJ kg⁻¹
- Ratio of CO to CO₂ (based on a mole fraction)
- Heat release rate in kW m⁻²
- Mass loss rate in % s⁻¹
- Rate of smoke formation in cm² s⁻¹

A Stanton Redcroft cone calorimeter was used in accordance with ISO 5660-1 (16). The specimens measured 100 mm x 100 mm x 6 mm and were contained within an aluminium tray during testing. The aluminium tray was taller on the sides than the tray specified in ISO 5660-1 (16) to ensure that mass loss was only via volatilisation and combustion. Specimens were positioned horizontally on a load cell within the cone calorimeter and tested at a heat flux of 50 kW m⁻². Three specimens each of PP, PP+BFR and PP+BFR+FPEA material and two of PP+ FPEA were tested, and the results reported in the plots presented in figures 2-6 are the average of these replicates.

Oxygen Index Test

The Oxygen Index (OI) test provides a convenient and reproducible means of assigning a numerical measure to the flammability of materials (17). It measures the minimum level of oxygen necessary to sustain combustion of a material. It is frequently used to compare the effectiveness of fire retardants (18) (19). The higher the OI value, the less likelihood there is for combustion (20).

The OI was determined according to ISO 4589-2 (21). Injection moulded materials were cut into specimens measuring 80 mm x 6 mm x 3 mm (to satisfy the dimension range specified for test specimens of form IV). The ignition procedure used was type A – top surface ignition and a step size of 0.2 % for successive changes in the oxygen concentration was used.

Results and Discussion

The flammability of the fire-retarded formulations was evaluated by UL 94, Oxygen Index and cone calorimeter tests. It was not the purpose of this paper to draw a comparison between these tests as has been done in previous studies (10, 22, 23). Instead, we combined the unique data obtained from each test to gain an understanding of the fire properties of the systems studied and to analyse the interaction between the FPEA and the BFR in a matrix of PP.

UL 94 Test

Analysis of the UL 94 results in Table II show that the addition of BFR to PP improved the UL 94 rating from NR to V-2. The addition of the FPEA to the fire-retarded PP accelerated dripping, as shown by the shorter Time to Drip results. Despite this, the overall result was improved to the more desirable V-0 rating.

The t_1 and t_2 results suggest that the fire retardant action of the BFR was sufficient to extinguish the flame at its source. However, with the addition of the FPEA, a more efficient flame poisoning process was possible (indicated by the failure of the cotton to ignite). This suggests that some gas phase flame poisoning may be taking place. The FPEA also appears to act on the BFR/PP system via a condensed phase action by accelerating the breakdown of the PP (i.e., chain scission (24)), as shown by the Time to Drip results. The lack of flaming drips and the non-ignition of the cotton suggest that the drips retain relatively little heat and thus there is insufficient flammable gases released to maintain the burning. This is shown graphically as stage C in the polymer burning cycle in the previously presented Figure 1.

During UL 94 testing, the BFR/PP material burned with a sooty flame and a black sooty material was deposited on the specimen during combustion. This is attributed to the BFR and is an indication of an inefficient burning process and some condensed phase fire retardant action (25). This, however, was not the case when the FPEA was added to the BFR/PP material.

Table II. UL 94 Test Results

<i>Material</i>	<i>Rating</i>	<i>Ave t_1</i> (s)	<i>Ave t_2</i> (s)	<i>Burning of Cotton</i>	<i>Time to Drip</i> (s)
PP	NR	188	N/A	Yes	13.8
PP+ FPEA	NR	113	N/A	Yes	6.3
PP+BFR	V-2	0.4	0	Yes	8.8
PP+BFR+ FPEA	V-0	0	0	No	8.1

NOTE: t_1 = time that flaming persisted after burner had been removed for the first time; t_2 = time that flaming persisted after burner had been removed for the second time; N/A = flame did not extinguish after first ignition; V-0 = specimen extinguished quickly enough to pass and cotton indicator below the specimen was not ignited (best rating); V-2 = specimen extinguished quickly enough to pass but cotton indicator below the specimen was ignited; NR = no rating (fail); Time to Drip = the time at which the material started to drip measured from the start of the test.

Cone Calorimetry

Effective Heat of Combustion (EHC) is a measure of the efficiency to which the emitted gaseous products are combusted. A low EHC indicates less efficient combustion in the gas phase suggesting better flame retardancy (26). From the

EHC data in Figure 2 it is clear that the effective heat of combustion plateau for PP is reduced by the addition of the BFR and FPEA. This reduction is mainly a function of the BFR, as shown by the EHC curve for PP/BFR system. The addition of the FPEA has relatively little impact upon the EHC plateau.

Closer examination of these curves can also give a clue as to whether the fire inhibition mechanism is occurring in the gas or condensed phase. The addition of the FPEA to the BFR/PP system slows the initial rate at which gaseous products are combusted in comparison with the other systems, (i.e., lower EHC over the first 75 seconds). This suggests that gas-phase flame poisoning mechanisms may occur during this period. The slightly greater emission of CO with respect to CO₂ from the FPEA /BFR/PP system compared to the BFR/PP system, as shown in Figure 3, supports this notion, as CO is the product of incomplete combustion.

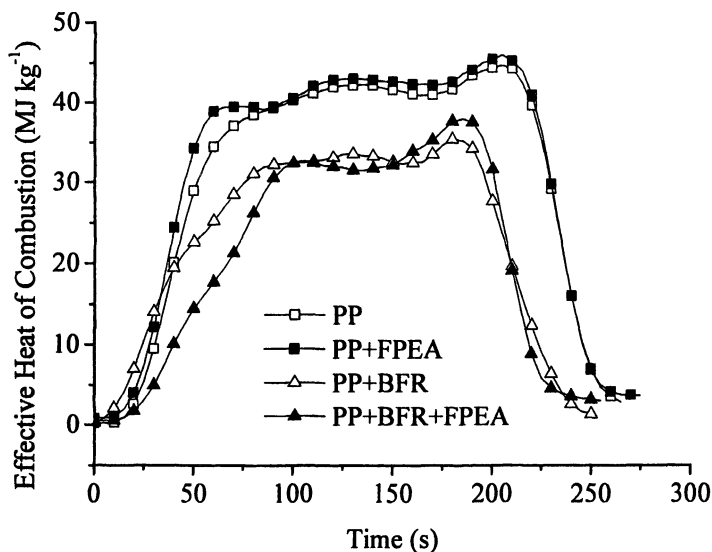


Figure 2. Effective heat of combustion as a function of time for polypropylene and fire-retarded polypropylene at a heat flux of 50 kW m^{-2} . (Average of replicate measurements)

Heat release rate (HRR) is one of the most important parameters for characterising material fire behaviour. It is an indicator of the rate of fire growth and intensity of the fire (27). A more effective fire retardant has a lower HRR

(28). For thermoplastics, HRR in the cone calorimeter increases steadily until there is no significant quantity of material left and the peak is typically followed by an abrupt linear decline to zero, with 100% mass loss. A comparison of the peak HRR for thermoplastics is valid only if specimens are similar in thickness and mass. Peak HRR cannot therefore be used to compare thermoplastic specimens of different thickness.

Figure 4 shows the HRR as a function of time. It can be seen that the fire-retarded systems act to reduce the peak HRR of PP by approximately 15%. The impact of the FPEA upon the BFR system can also be seen in Figure 4. While initially the HRR curves track along similar paths, over the period *ca* 60 to 100 seconds, the heat release rate per unit time of the FPEA /BFR/PP system is about 50% greater. This trend continues until volatile moieties have been consumed and by 125 seconds the curve returns to a similar trend as that for the system containing BFR and PP.

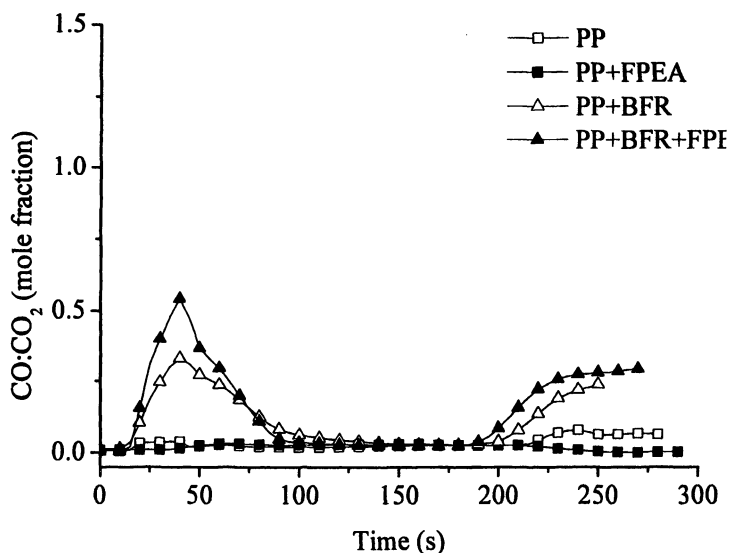


Figure 3. CO/CO_2 ratio (by mole fractions) as a function of time for polypropylene and fire-retarded polypropylene at a heat flux of 50 kW m^{-2} . (Average of replicate measurements)

The HRR behaviour of the FPEA /BFR/PP material is different from the other systems in that it displays a peak plateau at 100-125 seconds. The reasons for this are not clear but appear to relate to degradation processes. This is

illustrated by the mass loss rate curves in Figure 5. During the early stages of combustion the presence of the BFR enhances the rate of mass loss of the PP suggesting an increase in the thermal degradation of the polymer. With the addition of the FPEA to the BFR/PP system, the rate of mass loss and hence the thermal degradation of the PP, is further enhanced.

The effect of the fire retarded systems on the rate of smoke formation as a function of time is shown in Figure 6. There is an increase in the amount of smoke produced from the BFR/PP system relative to the PP system. This increase may be attributed to inefficient combustion caused by flame poisoning as a consequence of chemical interactions between the BFR and flame propagating species. Interestingly, the FPEA /BFR/PP system has a low smoke production rate which suggests a greater degree of oxidation of polymer degradation products.

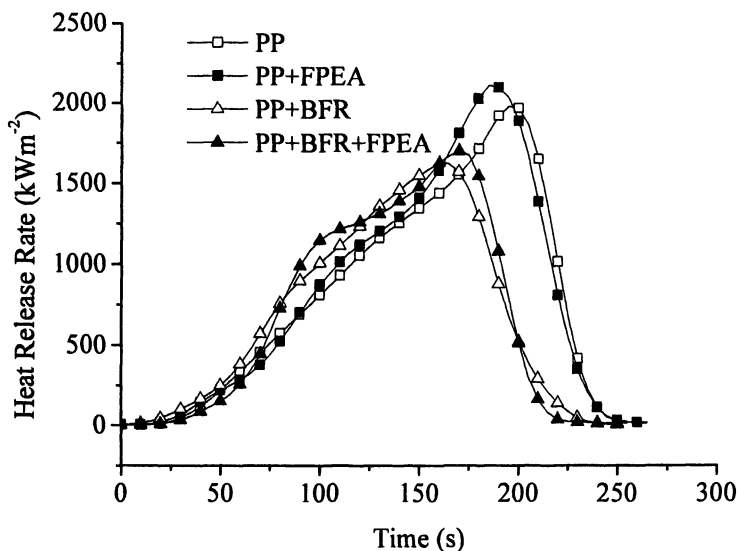


Figure 4. Heat release rate as a function of time for polypropylene and fire-retarded polypropylene at a heat flux of 50 kW m^{-2} . (Average of replicate measurements)

This presents a conundrum in that generally less smoke indicates better combustion. However it is clear from the UL 94 results previously shown in Table II, that the presence of the FPEA with the BFR improves the fire retardancy i.e. contributes to inefficient combustion. This is also shown by the

CO/CO₂ mole ratios previously presented in Figure 3. A possible explanation for this is that the presence of the FPEA acts to increase the thermal degradation of the PP during the early stages of combustion (as shown by the mass loss rate data). By inference, lower molecular weight pyrolysis fragments are generated and these smaller fragments are more flammable and have an increased probability of interaction with the BFR and targeted free radical species. This provides the opportunity for more complete oxidation of volatile products during the thermal degradation of the material, thereby allowing the BFR to be more effective in its role of flame poisoning.

In summary, the cone calorimeter results presented previously in Figures 2, 3 and 4 as well as in Table III indicate that during the first 75 seconds the addition of the FPEA to the BFR/PP system slows the rate at which the gaseous products are combusted suggesting gas phase flame poisoning. During this early stage of the combustion process, the greater formation of CO with respect to CO₂ for systems containing BFR indicates burning inefficiency and confirms gas phase action. The slightly higher CO:CO₂ ratio for the FPEA/BFR/PP material indicates that the FPEA acts on the BFR/PP to further increase the inefficiency of combustion.

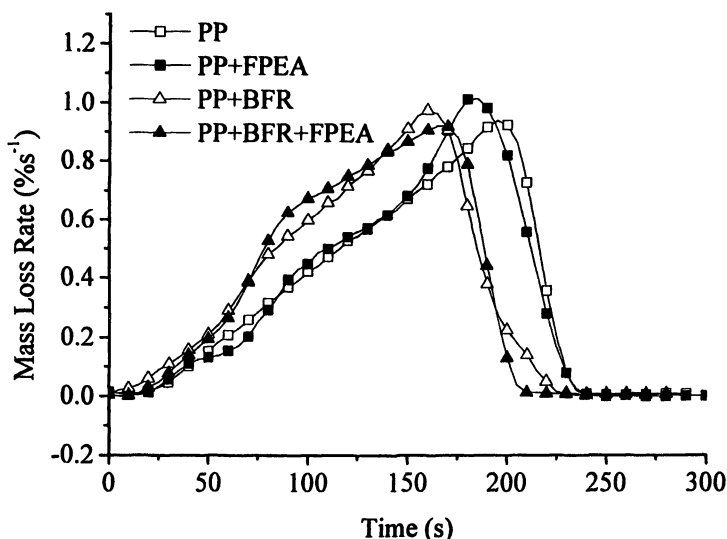


Figure 5. Mass loss rate as a function of time for polypropylene and fire retarded polypropylene at a heat flux of 50 kW m^{-2} . (Average of replicate measurements)

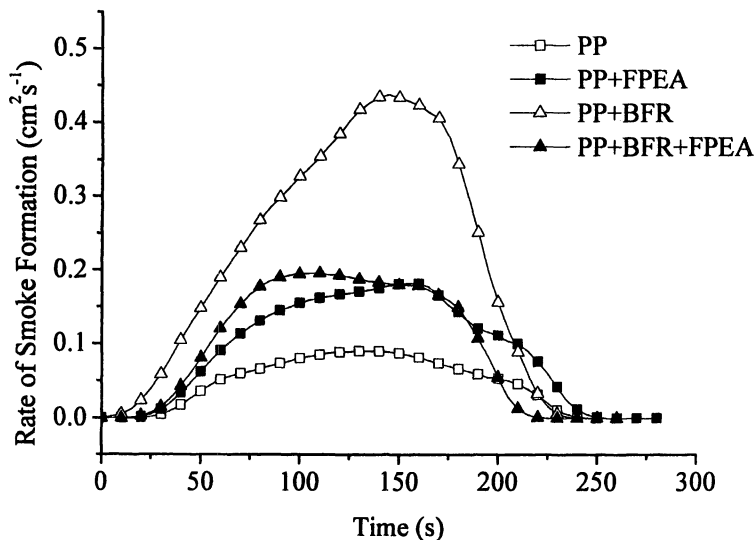


Figure 6. Rate of smoke formation as a function of time for polypropylene and fire-retarded polypropylene at a heat flux of 50 kW m^{-2} . (Average of replicate measurements)

After the first 75 seconds the $\text{CO}:\text{CO}_2$ ratio tends towards zero and there is no further increase in the EHC as it tends to plateau. This indicates the completion of the gas phase fire retardant action and a transition to some other mechanism (most probably condensed phase). It is at this stage in the combustion process that the HRR curves for the FPEA/BFR/PP system increases rapidly compared to the other systems, indicating the commencement of a different fire inhibition mechanism (presumed to be condensed phase).

Table III. Effect of FPEA on Fire Retarded PP

Parameter	PP+BFR	PP+BFR+FPEA	% change
Peak CO/CO_2 (mf)	0.34	0.54	Up by ~60%
EHC (at 50 secs) (MJ kg^{-1})	20	14	Down by 30%
HRR (at 100secs) (kW m^{-2})	860	1145	Up by 33%

Oxygen Index Test

The OI value obtained for PP (17.9) shown in Table IV correlates well with a typical literature value of 17.4 (18, 19). This low OI value indicates that PP is relatively flammable. With the addition of the BFR to PP, the OI value is increased by approximately 50 % to 27.2, indicating improved fire retardancy of the PP. The addition of the FPEA to the BFR/PP system further increases the OI value to 30.7, thus enhancing the fire retardancy of the PP even more. However, unlike the UL 94 test, there was no visual evidence that the presence of the FPEA increased the flow of the polymer away from the flame.

Table IV. OI Test Results

<i>Material</i>	<i>OI (%)</i>
PP	17.87
PP+ FPEA	21.86
PP+BFR	27.22
PP+BFR+ FPEA	30.67

Conclusions

The analyses carried out during the investigation of the fire retardant systems using conventional fire testing techniques, have shown that there was an interaction between the two additives which improved the fire performance of the PP. However it was unclear as to whether this interaction was synergistic or purely additive especially when considering the OI results. Further testing will be carried out in the future using techniques such as nitrous oxide index (NOI) combined with the current OI data, pyrolysis GC-MS, pyrolysis FTIR, TGA-FTIR and pyrolysis NMR to determine whether there was synergy or simply an additive effect of two fire retardants. Such work will need to consider the organic chemistry mechanisms which occur between the two additives in the PP matrix in the time leading up to decomposition and during the fire.

The investigation has shown that the use of multiple fire tests representing different fire models can provide valuable information on the burning process of a fire retarded polymeric system. Further, analysis of the data in a non-standard way provided useful insights into how the range of fire retardant systems functioned.

The cone calorimeter data (EHC, HRR and CO:CO₂ ratios) suggested that the presence of the FPEA in the BFR/PP system altered the behaviour of the polymer via the gas phase during the early stages of combustion, and

subsequently via the condensed phase. The mass loss rate data demonstrated that the proposed synergist acted to accelerate the degradation of the polymer, i.e., condensed phase. The CO and CO₂ gas analyses confirmed that the burning process was more inefficient in the presence of this material.

Further, we have shown that cone calorimeter data can be utilised as an analytical tool to contribute to the understanding of complex interactions between fire retardant additives. As a result of considering the EHC, CO:CO₂ gas ratios and the HRR, we were able to comment upon, and suggest where gas and condensed phase fire retardancy occurred.

The UL 94 and Oxygen Index data were strong indicators of interaction between the two fire retardant additives. Close examination of the UL 94 data indicated that this method of analysing fire properties was not just limited to a pass or fail. Instead it could be used to provide more information about the fire inhibition process by indicating the action or mechanism of the fire retardant; i.e., gas phase, condensed phase or a combination of the two and when they occur in the process.

References

1. Troitzsch, J. H. *Prog. Org. Coat.* **1983**, *11*, 41-69.
2. Lewin, M. J. *Fire Sci.* **1999**, *17*, 3-19.
3. Chiu, S.-H.; Wang, W.-K. *Polymer.* **1998**, *39*, 1951-1955.
4. Grassie, N.; Scott, G. *Polymer Degradation and Stabilisation*; Cambridge University Press: New York, 1985.
5. *Underwriters Laboratories Inc.* UL 94 Standard; Northbrook, IL, 2000.
6. Use of the Cone Calorimeter for Evaluation of Plastics Used in Containers for Flammable Materials. <http://www.mcclureindustries.com/pdf/Cone.pdf> (accessed Jul 2004).
7. Marplex Home Page. http://www.marplex.com.au/application_content/telecommunications.htm (accessed Aug 2004).
8. Erntec Home Page. <http://erntec.net/content/products/?0,3,a001,37> (accessed Oct 2004).
9. M+H Power Systems Home Page. <http://www.mhpower.com.au/Batteries/TechBrochure/techinfo1.htm> (accessed Sep 2004).
10. Hong, S.; Yang, J.; Ahn, S.; Mun, Y.; Lee, G. *Fire Mater.* **2004**, *28*, 25-31.
11. Fernandes Jr., V. J.; Araujo, A. S.; Fonseca, V. M.; Fernandes, N. S.; Silva, D. R. *Thermochim. Acta.* **2002**, *392-393*, 71-77.
12. Ebdon, J. R.; Hunt, B. J.; Joseph, P.; Konkell, C. S.; Price, D.; Pyrah, K.; Hull, T. R.; Milnes, G. J.; Hill, S. B.; Lindsay, C. I.; McCluskey, J.; Robinson, I. *Polym. Degrad. Stab.* **2000**, *70*, 425-436.

13. *Heat Release in Fires*; Babrauskas, V.; Grayson, S. J. Eds.; Elsevier Applied Science: London, 1992; pp 423-446.
14. Babrauskas, V. *Fire Mater.* **1984**, *8*, 81.
15. Huggett, C. *Fire Mater.* **1980**, *4*, 61-65.
16. *International Organisation for Standardisation*; International Standard ISO 5660-1; Geneva, 2002.
17. Nelson, M. *Combustion of Polymers: Oxygen Index Methods*; [Website] <http://www.uow.edu.au/~mnelson/review.dir/oxygen.html>, 2002.
18. Camino, G.; Costa, L. *Polym. Degrad. Stab.* **1988**, *20*, 271-294.
19. *Fire and Polymers II: Materials and Tests for Hazard Prevention*; Nelson, G. L. Eds.; ACS Symposium Series 599; American Chemical Society: Washington, D.C., 1995; pp 1-28.
20. GE Plastics Home Page. <http://www.geplastics.com/resins/devprod/flammabilityt.html> (accessed Sep 2004).
21. *International Organisation for Standardisation*; International Standard ISO 4589-2; Geneva, 1996.
22. Weil, E. D.; Hirschler, M. M.; Patel, N. G.; Said, M. M.; Shakir, S. *Fire Mater.* **1992**, *16*, 159-167.
23. Lyon, R.; *Fire and Flammability. First Annual Conference for the Consortium for Fire Safety, Health and the Environment*; SP Swedish National Testing and Research Institute: Boras, Sweden, 2003.
24. Kaspersma, J.; Doumen, C.; Munro, S.; Prins, A. *Polym. Degrad. Stab.* **2002**, *77*, 323-331.
25. Kuryla, W. C.; Papa, A. J. *Flame Retardance of Polymeric Materials*; Marcel Decker Inc.: New York, 1978.
26. Li, B.; Wang, J. J. *Fire Sci.* **1997**, *15*, 341-357.
27. Tewarson, A. *Fire Mater.* **1980**, *4*, 185-191.
28. *Plastics Flammability Handbook: Principles, Regulations, Testing and Approval*; Troitzsch, J. Eds.; Carl Hanser Verlag: Munich, Germany, 2004; pp 133-157.

Chapter 20

Mechanisms of the Flame Retardant Behavior of Covalently Bonded Phosphorus in Poly(methyl methacrylates)

Dennis Price^{1,*}, L. K. Cunliffe², K. J. Bullett (formally Pyrah)²,
T. R. Hull¹, G. J. Milnes¹, J. R. Ebdon³, B. J. Hunt³,
and P. Joseph³

¹Centre for Materials Research and Innovation, Bolton Institute,
Deane Road, Bolton BL3 5AB, England

²Institute for Materials Research, Cockcroft Building, University
of Salford, Salford M5 4WT, England

³Chemistry Department, University of Sheffield, Dainton Building,
Brook Hill, Sheffield S3 7HF, England

Flammability studies concerned with the fire retardance of an additive fire retardant system of poly(methyl methacrylate), PMMA, containing triethyl phosphate (TEP) and two reactive systems of methyl methacrylate and diethyl 2-(methacryloyloxy)ethylphosphate (DEMEP) and diethyl 2-(acryloyloxy)ethylphosphate (DEAEP) copolymers have already been reported. These studies showed improvements in the fire retardancy when the phosphate group was incorporated into the polymer. The purpose of this work is to establish the different modes of action of the additive and reactive fire retardants and to identify the causes of the different behaviours. A combination of TG with EGA, DSC, laser and microfurnace pyrolysis mass spectrometry and isothermal pyrolysis GC-MS were used for these studies. The greater extent of the condensed phase interactions shown by the MMA/DEAEP case explains why that system has superior flame retarding ability than does the MMA/DEMEP system.

Introduction

We have previously reported our extensive flammability studies of a range of poly(methyl methacrylate) based copolymers in which phosphorus is covalently bonded to the polymer chain (1,2). The advantages of this 'reactive' system over the more common 'additive' approach have been discussed elsewhere (3). This can be seen from the decrease in peak rate of heat release for the PMMA polymer, 633 kWm^{-2} , to 500 kW m^{-2} for the additive system PMMA+TEP, to 360 kWm^{-2} for the copolymer MMA-DEMEP and to 360 kWm^{-2} for the copolymer MMA-DEAEP. The limiting oxygen indices increase in the same order, i.e. 17.2% for PMMA, 22.7% for PMMA+TEP, to 25.0 % for MMA-DEMEP and to 28.1% for MMA-DEAEP. Current studies are concerned with gaining an insight into the significance of the chemical nature of the phosphorus-containing comonomer on the flame retardant mechanism of the resultant copolymer. This paper reports a comparison of the behaviours of acrylate (DEAEP) and methacrylate phosphate (DEMEP) comonomers. In particular, why does the MMA-DEAEP show superior flame retardant behaviour compared to that of MMA-DEMEP? A variety of techniques have been used for these studies. The laser pyrolysis technique (4) provides information as to the initial breakdown of a polymer over the first few milliseconds after its surface is exposed to a very rapid temperature rise as would be the effect of radiation from a fire. The micro-furnace experiment (5) identifies the species evolved as the polymer temperature is raised in a controlled manner. Pyrolysis/GC-MS (6) data can provide insight into the thermal breakdown in these systems and hence the mechanisms of the flame retarding processes. Table 1 provides a comparison of the different reaction conditions generated by these three techniques. Non-isothermal thermogravimetric (TG) studies identify the temperature ranges of the various polymer decomposition steps and the extent of char formation whilst addition of a suitable evolved gas analysis (EGA) technique enables the gas phase products to be monitored. Differential scanning calorimetry (DSC) alongside TG data, can be used to identify any changes occurring within the condensed phase. Information from our current studies will illustrate the value of this combination of techniques.

Experimental

The laser pyrolysis- and microfurnace- mass spectrometry techniques have been described previously (4,5). Pyrolysis in air experiments were conducted at 400°C for 60s in a Wilks pyrolyser (6) with the evolved products subsequently being analysed using a VG Trio-1 GC/MS. A recent innovation is the addition of an infrared analyser, utilising characteristic wavelength specific filters, to monitor the exhaust gas line from a Polymer Laboratories TG 750. This provides continuous profiles of the CO, CO₂ and hydrocarbons (measured as propane + hexane) evolved during a TG experiment.

Table 1: Reaction time-scale of techniques

<i>Technique</i>	<i>Heating Rate</i>	<i>Reaction Period</i>	<i>Comments</i>
LP/TOFMS	1k°C in 0.5 ms	Initial 2 ms	Dynamic Vacuum Primary reactions monitored
Microfurnace- TOFMS	10°C min ⁻¹	40 min	Dynamic Vacuum Temperature dependence of primary products
Py/GC-MS	25→400 °C in about 1s	60s @ 400 °C	Air End product analysis

Materials. The methyl methacrylate/diethyl 2-(acryloyloxy)ethyl phosphate (MMA/DEAEP) and methyl methacrylate/diethyl 2-(methacryloyloxy)ethyl phosphate (MMA/DEMEP) copolymers were synthesised as previously described (1, 2). Their structures and that of the additive triethyl phosphate are shown in figure 1. All of the systems contained 3.5wt% of phosphorus.

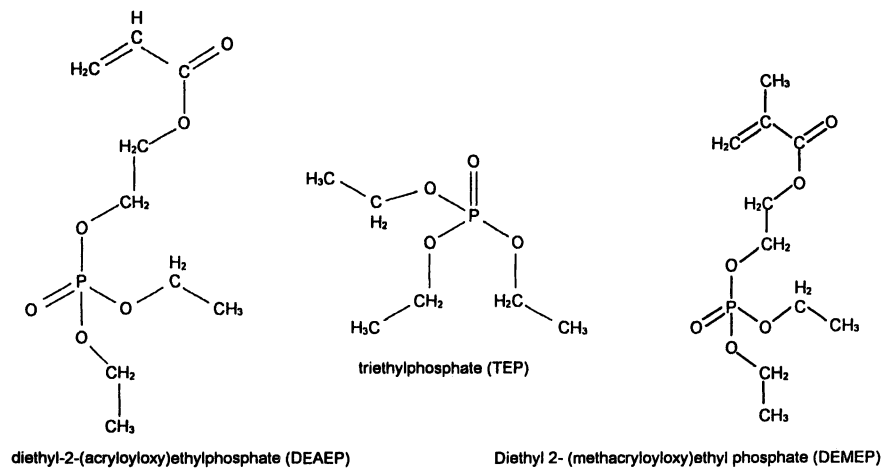


Figure 1. Structures of comonomers and additive used in this work

Results and Discussion

MMA/DEAEP. Two typical time-of-flight mass spectrometric scans from a laser pyrolysis experiment are shown in figure 2. The peaks due to the MMA and DEAEP portions of the copolymer are indicated on the figure. It can be seen that peaks due to fragments from the reactive flame retardant, DEAEP, and for the MMA monomer appear shortly after the laser has been fired. The probable breakdown patterns of the DEAEP component, shown in figure 3, indicate that in a real fire situation, phosphorus-containing fragments are evolved concurrently with the MMA, i.e. the 'fuel', from the copolymer. This would optimise the efficiency of delivery of the flame retardant species into the flame region.

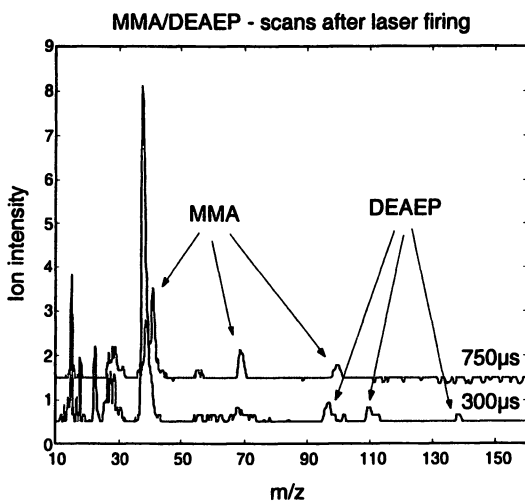


Figure 2. MMA/DEAEP: mass spectra taken 300 and 750 μ s after firing of the laser.

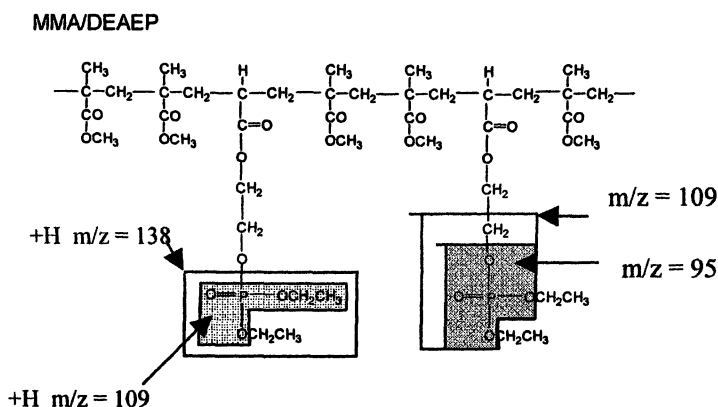


Figure 3. Indication of the source of the ions due to breakdown of the DEAEP component of the MMA/DEAEP copolymer structure.

Supporting evidence was also obtained via the microfurnace experiment. As shown in figure 4, the MMA/DEAEP sample yields fragments larger than the monomer molecular ion (m/z 100) at lower temperatures in the heating process.

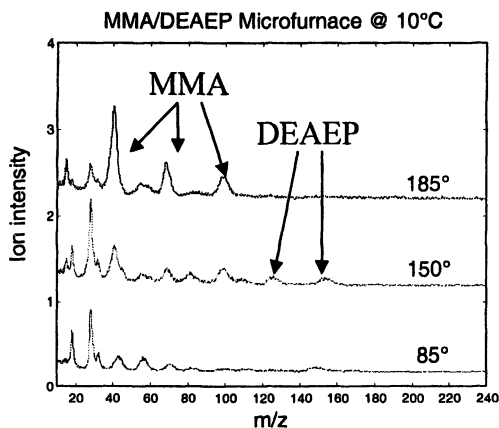


Figure 4. Mass Spectra taken at various temperatures as the sample temperature was raised at $10^{\circ}\text{C min}^{-1}$ in the microfurnace.

Pyrolysis-GC/MS experiments for MMA/DEAEP found that MMA monomer was the major species evolved, see chromatogram in figure 5. This was accompanied by several minor species including a significant contribution from triethyl phosphate (TEP). This would indicate that in a real fire, TEP would initially be released into the flame region thus initiating gas phase flame retardant processes. No trace of the DEAEP comonomer was observed. Thus, the DEAEP unit in the copolymer chain must be involved in condensed phase interactions with the rest of the copolymer chain. One of such interactions must produce the observed TEP.

MMA/DEMPEP. Two typical time-of-flight mass spectrometric scans from a laser pyrolysis experiment are shown in figure 6. The peaks due to the MMA and DEMPEP portions of the copolymer are indicated on the figure. It can be seen that peaks due to fragments from the reactive flame retardant, DEMPEP, and for the MMA monomer appear shortly after the laser has been fired. This indicates that in a real fire situation, phosphorus-containing species would be available to provide flame retardant action as soon as the main polymer decomposition begins.

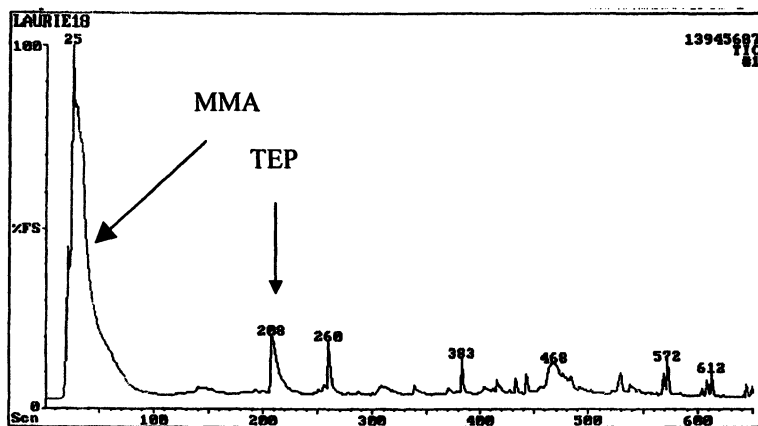


Figure 5. Chromatogram of the gases evolved from MMA/DEAEP at 400°C for 60s. The MMA and triethyl phosphate peaks identified via their mass spectra and retention times.

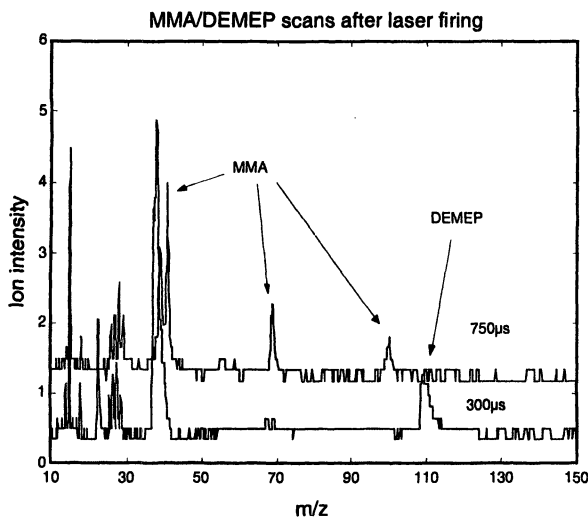


Figure 6. MMA/DEMPEP: mass spectra taken 300 and 750 μ s after firing of the laser.

As in the MMA/DEAEP case, the microfurnace experiments provide supportive evidence to the above proposal. As shown in figure 7, fragments from the DEMEP portion of the copolymer are observed at lower temperatures than were the MMA fragments. Again these peaks are identified in the diagram. The probable breakdown pattern of the copolymer structure, which results in the observed peaks, is indicated in figure 8.

The chromatogram obtained from py/GC-MS studies is shown in figure 9, the peaks being identified by their mass spectra. TEP and DEMEP, the major products of pyrolysis are more abundant than the major comonomer component, MMA. Thus end chain unzipping of the MMA/DEMPEP backbone proceeds essentially in the same manner as PMMA, i.e. yields monomer regardless of whether the methacrylate monomer in the chain is MMA or DEMEP. This is in contrast to the previous MMA/DEAEP case where the DEAEP unit underwent condensed phase interactions and was not detected as a product.

Thus in the case of the MMA/DEMPEP copolymer the net flame retardant action is diminished because more of the phosphorus escapes into the gas phase reducing the extent of the condensed phase action. Previous results for cone calorimetry experiments with these copolymers (7) gave the DEMEP char residue as 8.2% of the original mass with a phosphorus content of 9.8%. The same data for the DEAEP experiments were 10.8% char with 11.3% phosphorus content. This is in line with our current observations and provides an explanation as to why the LOI of MMA/DEMPEP is some 3 units lower than that of MMA/DEAEP.

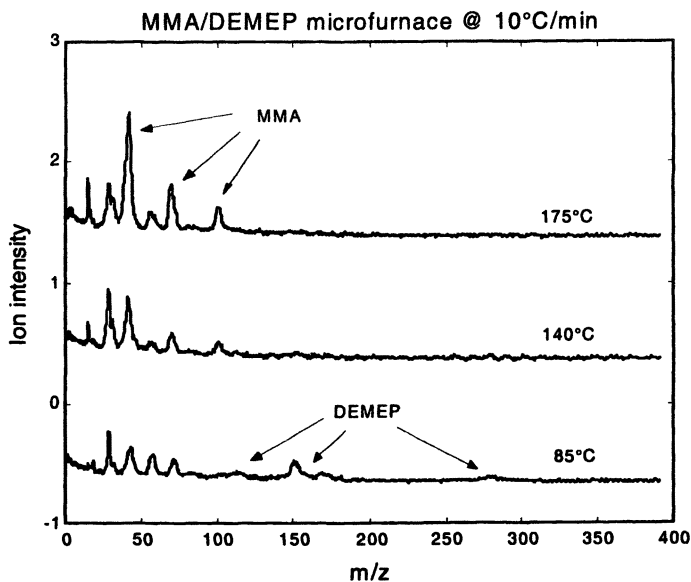


Figure 7. Mass Spectra taken at various temperatures as the MMA/DEMPEP sample temperature was raised at 10°C min⁻¹ in the microfurnace.

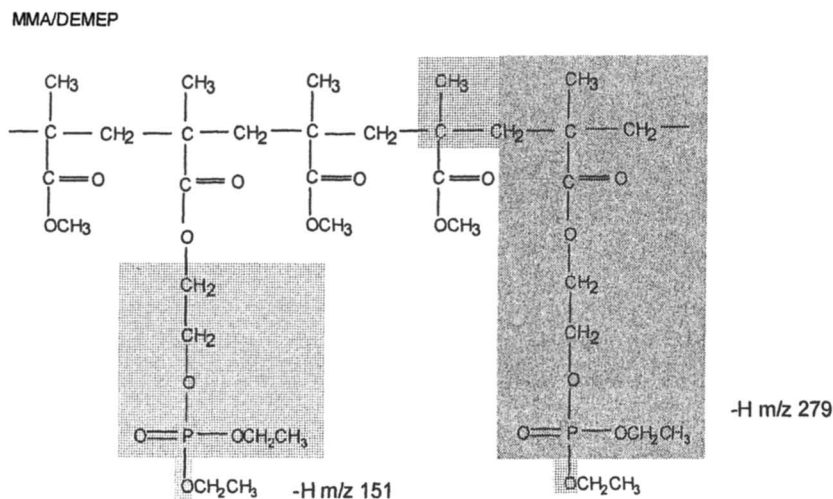


Figure 8. Indication of the source of the ions due to breakdown of the DEMPEP component of the MMA/DEMPEP copolymer structure.

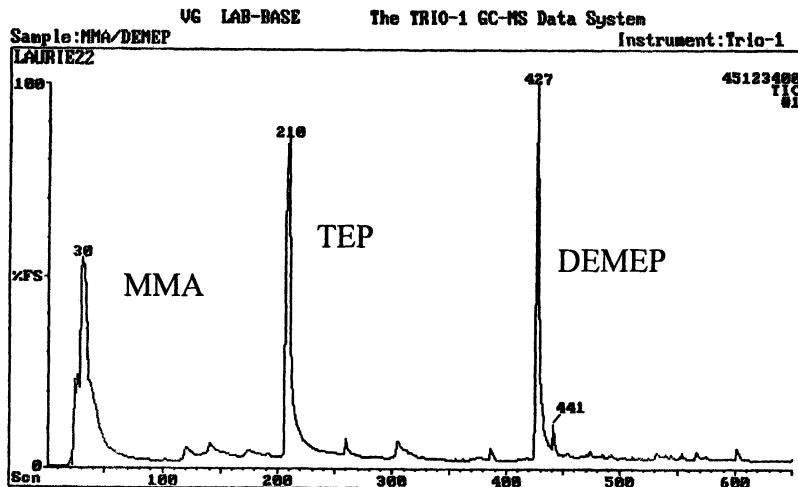


Figure 9 Chromatogram of the gases evolved from MMA/DEMPEP at 400°C for 60s. The MMA, TEP and DEMEP peaks identified via their mass spectra and retention times.

Thermogravimetry/Infrared Evolved Gas Analysis Experiments

The temperature dependent profiles for TG, CO and CO₂ determined for the four systems studied are presented in figures 10 to 12. The TG profiles for the PMMA and PMMA+TEP systems are very similar except that the additive system starts to lose weight at around 100°C, due to loss of the additive, compared to around 200°C for PMMA. The rate of weight loss is also slightly lower for the additive system. In both cases, there is considerably more CO₂ evolved compared to CO. This indicates that oxidation reactions are very efficient. Under these TG conditions and in previous cone calorimetry experiments carried out at 35 kWm⁻² (2), no char residue remained. Thus there was no evidence for a condensed phase flame retardant mechanism occurring in the PMMA+TEP system.

The TG profiles for the reactive systems MMA/DEMPEP and MMA/DEAEP are distinctly different. Decomposition starts at around 150°C. This is

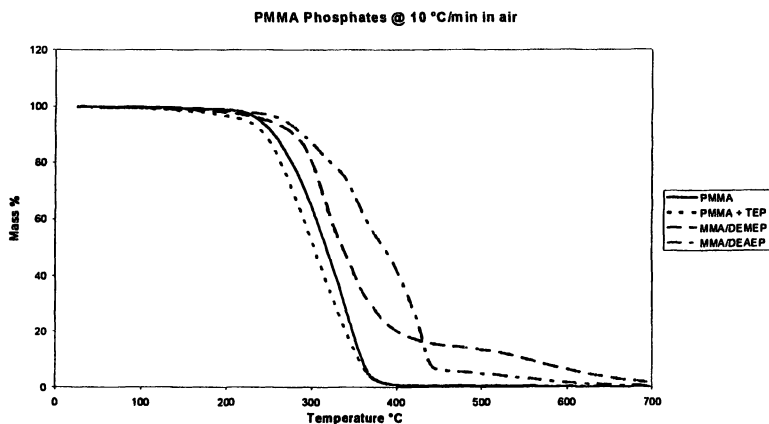


Figure 10 Temperature dependent TG profiles determined in air for the PMMA, PMMA+TEP, MMA/DEMEP and MMA/DEAEP samples. Heating rate $10^{\circ}\text{C min}^{-1}$.

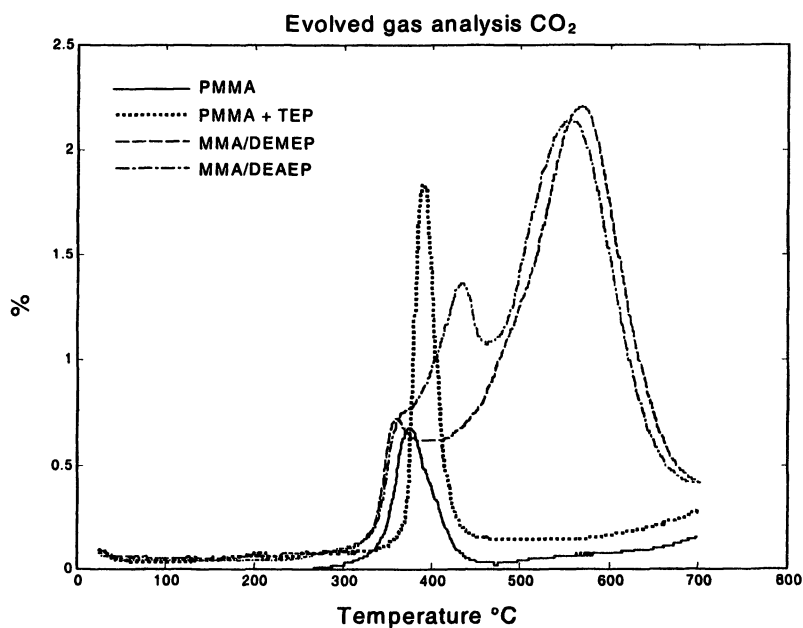


Figure 11 Temperature dependent CO_2 profiles determined in air for the PMMA, PMMA+TEP, MMA/DEMEP and MMA/DEAEP samples. Heating rate $10^{\circ}\text{C min}^{-1}$.

followed by increasing amounts of CO and CO₂ in a two-step process. However in this case, the CO concentration is much closer to that of CO₂ with a CO₂/CO ratio of less than 2 compared to that of the additive system that had a CO₂/CO ratio of about 20. This suggests that a gas phase flame retardant mechanism, inhibiting the conversion of CO to CO₂, occurred in the copolymer systems. Significant condensed phase residues were also observed during the copolymer TG experiments. This also confirms that the covalently bonded phosphorus in the copolymer promoted the formation of char via a condensed phase mechanism. Additionally, the slower evolution of fuel from the copolymers, due to this condensed phase process, may have contributed to the inefficiency of the combustion and the lower CO₂/CO ratio.

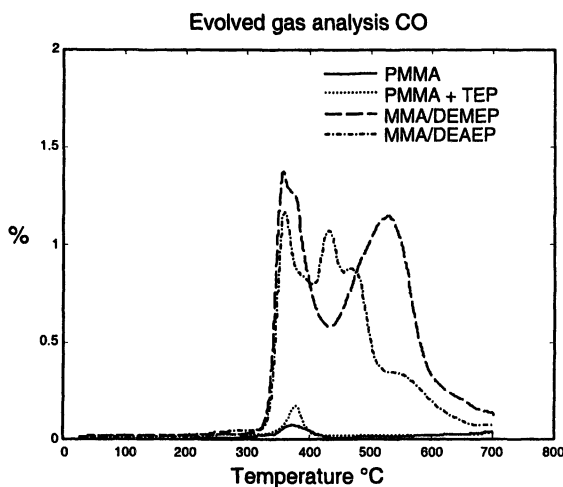


Figure 12 Temperature dependent CO profiles determined in air for the PMMA, PMMA+TEP, MMA/DEMPEP and MMA/DEAEP samples. Heating rate 10°C min⁻¹.

Differential Scanning Calorimetry (DSC)

The DSC curves for PMMA, PMMA + TEP, MMA/DEMPEP and MMA/DEAEP are presented in figure 13. The PMMA and PMMA+TEP curves show predominantly endothermic processes occurring in the condensed phase

with some exothermic gas phase formation of CO and CO₂ above 400°C, as shown in figures 9 and 10. This corresponds to unzipping of the PMMA polymer chain with the release of volatile material, which would act as fuel in any conflagration. In contrast, the MMA/DEMEP and MMA/DEAEP systems show much reduced endotherms. Since the TG data shows less material was lost below 400°C., then an exothermic condensed phase reaction, which in part compensates for the endothermic evolution process, must occur. This is particularly so in the MMA/DEAEP case. This points to the formation of char and hence a condensed phase fire retardant mechanism operating. Again, in each of these two reactive systems there is a significant exothermic process occurring in the condensed phase between 420 and 600°C.

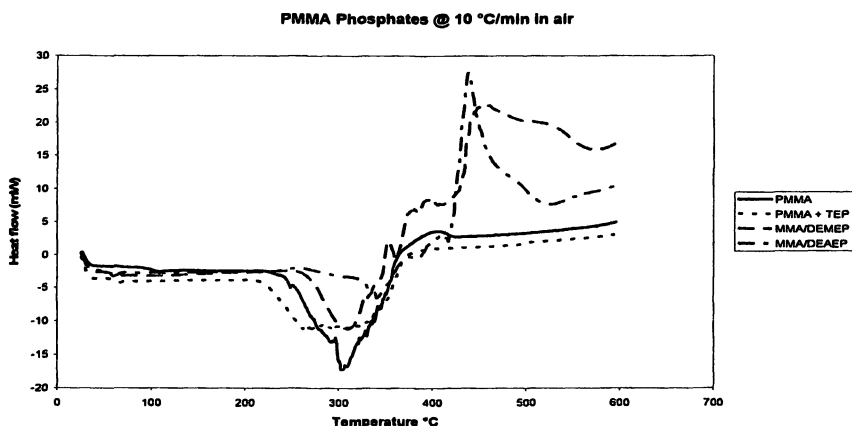


Figure 13. DSC profiles obtained for PMMA, PMMA+ TEP, MMA/DEAEP and MMA/DEMEP.

Summary

The role of phosphorus as an additive in the PMMA + TEP sample seems to be to delay the unzipping of the PMMA, and to some extent inhibit the gas phase conversion of CO to CO₂. The evidence presented here shows that very little residue remains and that the TEP acts in the gas phase to give modest levels of flame retardancy. In the two reactive systems, mass is lost at higher temperatures than in the additive case. This is more pronounced in the MMA/DEAEP case, because the DEAEP component of the copolymer interacts with rest of the polymer chain and is not liberated into the vapour phase. This is in marked contrast to the MMA/DEMEP case where more of the DEMEP comonomer than the major MMA component was observed in the vapour phase following pyrolysis at 400°C in air. In both systems, some of the phosphorus-containing

fragments released in the condensed phase will degrade to some form of phosphoric acid which will promote char formation. The remainder are evolved together with TEP and subsequently inhibit gas phase combustion reactions. The greater extent of the condensed phase interactions shown by the MMA/DEAEP case explains why that system has superior flame retarding ability than does the MMA/DEMEP system.

Acknowledgements

The authors wish to thank EPSRC for financial support. One of us (LKC) wishes to thank the University of Salford for permitting her PhD studies.

References

1. Ebdon, J.R.; Price, D.; Hunt, B.J.; Joseph, P.; Gao, F.; Milnes, G.J.; Cunliffe, L.K. *Polym. Degrad. Stab.* **2000**, *69*, 267-277.
2. Price, D.; Bullett (formally Pyrah), K.; Cunliffe, L.K.; Hull, T.R.; Milnes, G.J.; Ebdon, J.R.; Hunt, B.J.; Joseph, P. *Polym. Degrad. Stab.* **2002**, *77*, 227-233.
3. Price, D.; Pyrah, K.; Hull, T.R.; Milnes, G.J.; Ebdon, J.R.; Hunt, B.J.; Joseph, P.; Konkel, C.S. *Polym. Degrad. Stab.* **2001**, *74* 441-447.
4. Price, D.; Gao, F.; Milnes, G.J.; Eling, B.; Lindsay, C.I.; McGrail, T.P. *Polym. Degrad. Stab.*, **1999**, *64*, 403-410.
5. Price, D.; Milnes, G.J.; Lukas, C.; Hull, T.R. *Int. J. Mass Spec. and Ion Proc.*, **1984**, *60*, 225-235.
6. Faroq, A.; Price, D.; Milnes, G.J.; Horrocks, A.R. *Polym Degrad Stab*, **1991**, *33*, 155-170.
7. K.J. Bullett, PhD Thesis, University of Salford, 2002.

Chapter 21

Synthesis, Characterization, and Cure Properties of a Halogen-Free Phosphate-Based Inherently Flame Retardant Epoxy Resin

Xiaodong Wang

School of Materials Science and Engineering, P.O. Box 61, Beijing
University of Chemical Technology, Beijing 100029, Peoples Republic
of China

A phosphorus-containing oligomer, bis(3-hydroxyphenyl) phenyl phosphate (BHPP), was synthesized through the reaction of phenyl dichlorophosphate and 1,3-dihydroxybenzene, and characterized by elemental analysis, Fourier transform infrared (FTIR), $^1\text{H-NMR}$, and $^{31}\text{P-NMR}$ spectroscopy. Subsequently, phosphate-based epoxy resins, with phosphorus contents of 1 and 2 wt %, were prepared via the reaction of diglycidyl ether of bisphenol-A, BHPP and bisphenol-A, and were characterized by FTIR and gel permeation chromatography. Phenolic melamine, novolac, and dicyanodiamide were used as curing agents to prepare the thermoset resins with the control and the phosphate-based epoxy resins. Thermal analysis investigations revealed that the thermoset resins cured with phenolic melamine exhibited higher glass-transition temperatures than the others, owing to the high rigidity of their molecular chain. Thermogravimetric analysis demonstrated that the decomposition temperatures of the thermoset resins cured with novolac were higher than those of the others. A synergistic flame retardant effect from the combination of the phosphate-based epoxy resin and the nitrogen-containing curing agent has been observed.

Introduction

Epoxy resins have been commercially developed for more than half a century and have many major industrial applications owing to their attractive characteristics and excellent properties (1,2). In the last two decades, there has been a rapid development in the use of epoxy resins in electronic applications, which, in most cases, requires good flame retardancy for the epoxy resins (3,4). Therefore, imparting flame retardancy to epoxy resins has received a great deal of attention and several techniques have been employed. The most common approach is to incorporate halogen atoms into the epoxy resins, so that the brominated epoxy resins can achieve the expected flame retardancy (5-7). However, flame-retardant epoxy resins containing bromine release hydrogen bromide during combustion, which may cause corrosion and toxicity. Environmental effects and health restrictions have been considered in recent years with regard to controlling the inherent flammability of epoxy resins by incorporation of flame-retardant additives. These considerations have led to a reexamination in terms of overall fire hazards of halogen-based epoxy resins and a search for halogen-free and environmentally friendly flame-retardant epoxy resins (8,9).

Phosphorylation is considered to be one of the most efficient methods of conferring flame retardancy on epoxy resins (10,11). Organophosphorus compounds exhibit high flame-retardant efficiency for epoxy resins and have also been found to generate less toxic gas and smoke than halogen-containing compounds (12,13). The decreased destruction of the earth's environment is a noteworthy benefit of replacing halogens with phosphorus in flame-retardant epoxy resins, and the flame retardancy of epoxy resins via phosphorylation has been widely studied (14,15). Some studies indicated that a significant improvement of flame-retardant efficiency was observed when phosphorus and nitrogen were both present in the curing system of the epoxy resins, so the effect of the combination of phosphorus and nitrogen on flame retardancy is of interest (16-19).

It is essential that new environmentally friendly flame retardant systems are developed to meet the constantly changing demand of new regulations, standards and test methods. In this work, we synthesized phosphate-based epoxy resins by incorporating the phosphorus-containing moieties into the molecular backbone of epoxy resins. Several curing agents for these phosphate-based epoxy resins were prepared and the thermal and the flame-retardant properties were investigated. The purpose of this study was to develop new environmentally friendly flame-retardant epoxy resins and to examine a novel curing system, containing phosphorus and nitrogen, which may be synergistic.

These "green" flame-retardant epoxy resins are expected to impart the requirement for environmental protection in electric/electronic applications.

Experimental

Materials. Phenyl dichlorophosphate was purchased from TCI Company, Japan. 1,3-Dihydroxy-benzene, 2-methyl imidazole (2MI), bisphenol A (BPA), triphenyl phosphine (Ph₃P), and all solvents were reagent grade from Aldrich Chemical Co., USA. DGEBA (commercial name: YD-128) with an epoxide equivalent weight (EEW) of 187 g was supplied by Kuk Do Chemical Co., Ltd., Korea. The curing agents, dicyanodiamide (DICY) and novolac with a hydroxyl equivalent weight of 105 g, were supplied by Suzhou Special Chemical Co., China. Phenolic melamine, PS-6313 and PS-6333, with hydroxyl equivalent weights of 148 g and 169 g and nitrogen contents of 20 wt % and 25 wt %, respectively, was kindly supplied by Gun Ei Chemical Industry Co., Ltd., Japan.

Synthesis of bis(3-hydroxyphenyl) phenyl phosphate 1,3-Dihydroxy-benzene, dissolved in dried xylene, was introduced into a four-neck, round-bottom 1000 ml glass flask equipped with a thermometer, a nitrogen inlet, a reflux condenser, and a mechanical stirrer. The mixture was stirred and heated slowly to 70 °C for about 30 min until the 1,3-dihydroxy-benzene had dissolved completely and then the mixture was heated to 90 °C. Phenyl dichlorophosphate was added continuously to the flask at a constant rate over a period of 2 h under a nitrogen atmosphere. The temperature was maintained at 90 °C during the addition of phenyl dichlorophosphate. The reaction mixture was then heated to 125 °C, and then stirred for 2.5 h under a nitrogen atmosphere. The reaction was assumed to end when no more HCl evolution was detected with wet pH test paper. After cooling to room temperature, the precipitant was filtered and recrystallized from tetrahydrofuran (THF). A light yellow crystalline solid, bis(3-hydroxyphenyl) phenyl phosphate (BHPP), (mp 216 °C) was collected by filtration and dried under reduced pressure. Elemental analysis: C, 60.71; H, 4.14; O, 26.87; and P, 8.28%. Calculated for (C₁₈H₁₅O₆P) are C, 60.34; H, 4.18; O, 26.82; and P, 8.66. Infrared spectroscopy: The strong absorption peaks at 1182 cm⁻¹ and 1239 cm⁻¹ indicate the formation of P-O-Ph, while the distinctive absorption peak at 684 cm⁻¹ of the P-Cl stretch in phenyldichlorophosphate disappears. The chemical structure of BHPP can be further confirmed by the other absorption peaks at 973 cm⁻¹, 1015 cm⁻¹ and 1032cm⁻¹ (P-O-Ph); 3550–3200 cm⁻¹ (Ph-OH); and 1264 cm⁻¹ (P=O). NMR spectroscopy: peaks attributable to two hydroxy protons were observed at δ=9.38–9.50 ppm (d, 2H); the protons of the phenol ring protons were found at δ=6.55-7.04 ppm (m, 8H), and those due to the phenyl ring protons were found at δ=7.52-7.95 ppm (m,

5H). The ^{31}P -NMR spectrum of BHPP exhibited an intense single peak at $\delta=15.43$ ppm.

Synthesis of the phosphate-based epoxy resins. DGEBA was introduced into a four-neck, round-bottom 1000 ml glass flask and heated to $120\text{ }^{\circ}\text{C}$ under vacuum for 1h to remove trace water. Then the flask was filled with nitrogen gas and the temperature was raised to $130\text{ }^{\circ}\text{C}$ and BHPP and BPA were added to DGEBA in amounts needed to produce the designed formulation, in which phosphate-based epoxy resins with a phosphorus content (1 wt % and 2 wt %) and an EEW (455 g/eq.) were expected to be obtained. A small amount of Ph_3P or 2MI as a catalyst was added. On basis of the expected phosphorus content and the EEW, the amount of BPA and BHPP could be calculated through the following equations:

$$\frac{100}{E_1} - \left(\frac{W_1}{1/2 \times 358} + \frac{W_2}{1/2 \times 288} \right) = (100 + W_1 + W_2) \times \left(\frac{1}{E_2} \right) \quad (1)$$

$$P (\%) = \frac{W_1 \times 0.0956}{100 + W_1 + W_2} \times 100 \quad (2)$$

where W_1 and W_2 are the weights of BHPP and BPA, respectively, while the amount of DGEBA is 100 g; E_1 and E_2 are the EEWs (455 and 187 g/eq.) of the phosphate-based epoxy resin and DGEBA, respectively; $P (\%)$ is the expected phosphorus content. The reaction mixture was heated to $160\text{ }^{\circ}\text{C}$ and stirred for 4h under a nitrogen atmosphere. The brown phosphate-based epoxy resins with an EEW of about 457 g/eq. (value obtained by an HCl potentiometric titration) were obtained after cooling to room temperature.

The phosphate-based epoxy resin was characterized by FTIR spectroscopy. The characteristic absorption peaks are: 914 cm^{-1} (oxirane ring); 1261 cm^{-1} (P=O); 985 cm^{-1} , 1028 cm^{-1} , 1176 cm^{-1} , and 1245 cm^{-1} (Ph-O-P); 3550 cm^{-1} , 3200 cm^{-1} (Ph-OH), and 1362 cm^{-1} ($-\text{CH}_3$).

A phosphorus-free epoxy resin, used as the control resin for comparison of curing properties with the phosphate-based epoxy resins, was also synthesized via the reaction of DGEBA with BPA. The EEW (around 456 g/eq.) of the control resin was obtained through modulating the weight ratio of DGEBA and BPA to 4.3/1.

Curing procedure of epoxy resins. The control resin and the phosphate-based epoxy resins were cured with DICY, novolac, and phenolic melamine. The curing agents and curing accelerator 2MI were dissolved in methyl cellosolve, then the epoxy resins and the solution of curing agents were mixed homogeneously in an epoxide to hydroxyl equivalent ratio of 1/1. The reaction mixtures were kept at $60\text{ }^{\circ}\text{C}$ for 1 h under vacuum to remove the solvent, then the reaction mixtures were cured at $150\text{ }^{\circ}\text{C}$ for 1.5 h and post cured at $180\text{ }^{\circ}\text{C}$ for

3.5 h. After curing, all samples were cooled to room temperature to prevent stress cracking.

Characterization. The melting point and glass transition temperature (T_g) were determined under a nitrogen atmosphere at a heating rate of 10 °C/min using a Perkin-Elmer Pyris-1 differential scanning calorimetry (DSC) apparatus. Elemental analysis was carried out with a Heraeus CHN-O rapid elemental analyzer with acetanilide as a standard. $^1\text{H-NMR}$ and $^{31}\text{P-NMR}$ spectra were obtained with a Bruker MC-80 NMR spectrometer with dimethyl sulfoxide- d_6 as a solvent. For the $^{31}\text{P-NMR}$ spectrum, phosphoric acid was used as an external standard. Fourier transform infrared spectra (FTIR) were obtained using a Nicolet 205 FTIR spectrometer and KBr pellets. Gel permeation chromatography (GPC) measurements were performed using a Waters 515 GPC with THF as the solvent at a flow rate of 1.0 ml/min. Thermogravimetric analysis (TGA) was performed with a Perkin-Elmer Pyris-1 TGA analyzer at a heating rate of 10 °C/min under an air or a nitrogen atmosphere from 23 °C to 800 °C; the average deviations for degradation temperatures and char residues are 1.4 °C and 1.8 wt %, respectively.

Measurement of flame-retardant properties. Limiting oxygen index (LOI) measurement was performed on sample bars of 65×3.0×0.5mm dimensions using an HD-2 oxygen index apparatus with a magneto-dynamic oxygen analyzer, according to the ASTM D-2863 specification. The UL-94 vertical test was carried out according to the testing method proposed by Underwriter Laboratory.

Results and Discussion

Synthesis of BHPP. BHPP, synthesized through the reaction of phenyldichlorophosphate and hydroquinone, is shown in Figure 1. In the synthesis, the nucleophilically active chlorine in phenyl dichlorophosphate could serve as a reactive site for the electrophilically active hydrogen in hydroquinone. The elemental analysis and spectral characterizations confirmed the chemical structure of BHPP.

Synthesis of phosphate-based epoxy resins. The phosphate-based epoxy resins, whose structure is shown in Figure 2, were synthesized via the reaction of

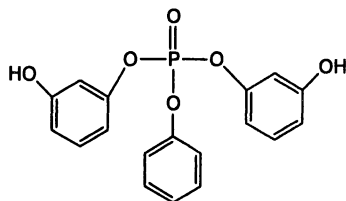


Figure 1. Structure of BHPP

DGEBA with BHPP and BPA, in which BPA was added to adjust the phosphorus content of the epoxy resins. The catalyst was necessary to facilitate the reaction.

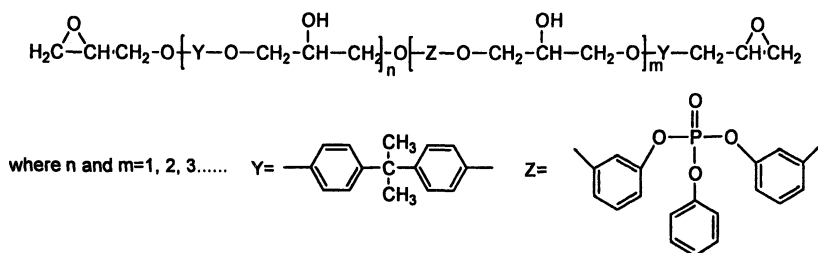


Figure 2 Structure of the phosphate-based epoxy resin.

The progress of the reaction was determined by GPC, as shown in Figure 3. For DGEBA, the main peaks appear at molecular weights of 284, 781, and 1227 with percentages of 81.7 wt %, 16.4 wt %, and 1.7 %, respectively. For the phosphate-based epoxy resin with a phosphorus content of 1 wt % (EP-P1), the peaks at molecular weights of 284 and 781 decrease sharply and the percentages are both lower than at 2 wt %. However, the peak at the molecular weight of 1227 increases rapidly and the percentage reaches 79 wt % and new peaks at molecular weights of 2053 and 4208 appear, which is attributed to the condensation polymerization of DGEBA with BPA and BHPP. Almost the same results were observed for the epoxy resin with the phosphorus content of 2 wt % (EP-P2). The number average molecular weight (M_n) and weight average one (M_w) were also calculated statistically from the data supplied by GPC measurements. One can find a significant increase in the average molecular weights from 431 (M_n) and 595 (M_w) of DGEBA to 1355 (M_n) and 3581 (M_w) of

EP-P1, and 1526 (M_n) and 3962 (M_w) of EP-P2, respectively. These results verified the completion of the reaction of DGEBA with BHPP and BPA.

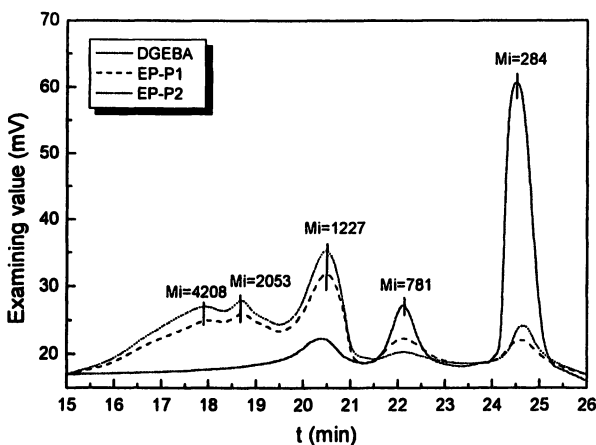


Figure 3 GPC diagrams of DGEBA and the phosphate-based epoxy resins.

Thermal analysis of the cured epoxy resins. T_g is a very important parameter for the thermoset epoxy resins because it establishes the service environment for the epoxy-based materials. In most cases, the epoxy resins are only used at a temperature below T_g . Therefore, identification of the mechanisms responsible for T_g changes and prediction of T_g depression are critical for the design and the application of the epoxy resins and their curing systems. T_g s of the control and the phosphate-based epoxy resins cured with various curing agents, obtained by DSC measurements, are listed in Table I. The T_g s of the phosphate-based epoxy resins cured with the four curing agents were found to be slightly lower than those of the control resin cured with the same four curing agents. It has been reported that incorporating a linear phosphorus-containing group into the epoxy main chain will decrease the rotational barrier of the epoxy and, therefore, reduce the T_g s of the polymers (20). The EP-P1/novolac thermoset resin shows a lower T_g than does EP-P1/DICY, which could be explained from the higher cross-linking density of the EP-P1/DICY thermoset resin compared to the EP-P1/novolac. However, the T_g of the EP-P1/DICY thermoset resin was lower than that of EP-P1/PS-3313 or PS-3333. This may be attributed to the higher rigidity of phenolic melamine compared to DICY, which compensates somewhat for the loss in cross-linking density, though DICY has a higher hydroxyl equivalent weight than the phenolic-melamine resins. The same arguments can be derived from the difference of the

T_g s of the thermoset control resins cured with the four curing agents. It was also found that the T_g of the EP-P2 thermoset resin was always lower than that of the EP-P1 when cured with the same curing agent. BHPP has a much more flexible molecular chain than BPA. Therefore, the reduction in the T_g of the EP-P2 thermoset resins should arise from the decrease in the rigidity of the molecular chain. However, it is still noteworthy that both EP-P1 and EP-P2 exhibited high T_g s, over 130 °C, when cured with the four curing agents. These high T_g values suggest that the phosphate-based epoxy resins prepared in this work could potentially be applied to FR-4 type copper clad laminates (21).

Table I TGA data of the control resin and the phosphate-based epoxy resins (EP-P1 and EP-P2) cured with various curing agents

Sample	T_g (°C)	Temperature at the characteristic weight loss (°C)				T_{max}^* (°C)		Char residue at 700 °C (wt %)
		1 wt %		10 wt %		Air	N_2	
		Air	N_2	Air	N_2			
Control/DICY	135.6	201	212	335	379	417	431	8
EP-P1/DICY	134.5	186	194	321	363	411	425	16
EP-P2/DICY	133.2	152	149	292	278	427	432	19
Control/Novolac	133.7	235	244	396	405	442	449	6
EP-P1/Novolac	131.9	226	239	389	394	439	450	7
EP-P2/Novolac	130.5	197	185	368	374	433	443	13
Control/PS-3313	139.4	187	172	332	354	431	439	6
EP-P1/PS-3313	137.1	180	162	324	341	432	435	16
EP-P2/PS-3313	135.6	161	158	321	347	426	432	18
Control/PS-3333	137.9	213	198	358	366	431	434	8
EP-P1/PS-3333	135.4	194	186	355	352	434	435	16
EP-P2/PS-3333	133.5	178	229	346	365	428	435	18

- The temperature of the rapid degradation.

The TGA data for the thermal degradation of all of the thermoset resins are summarized in Table I. The thermoset control resins cured with the four curing agents are more thermally stable than the cured phosphate-based epoxy resins. The relatively poor thermal stability of the thermoset phosphate-based epoxy resins comes from the phosphorus group degrading at relatively low temperature (22,23). However, the temperature of the rapid degradation for the cured thermoset phosphate-based epoxy resins was found to be much higher than that for the cured thermoset control resins. This phenomenon has been observed in

other phosphorylated polymer systems and is thought to play an important role in improvement of the flame retardancy of the phosphate-based epoxy resins (10). It was also observed that the amount of char residue of the thermoset phosphate-based epoxy resins was much higher than that of the thermoset control resins. On heating, the phosphorus groups of the thermoset resins first decompose to form a phosphorus-rich residue, which prevents further decomposition of the resins by raising the decomposition temperatures and consequently results in a high char yield (24). This char yield has been correlated to the flame retardancy and has been widely referenced in the studies of the flammable properties of polymers (12-14).

The results in Table I also indicate that the EP-P1 or EP-P2/novolac thermoset resin showed a much higher decomposition temperature at a weight loss of 1 wt % and 10 wt % (commonly considered as two important decomposition stages for the polymer degradation) than the other three curing systems both in an air and in a nitrogen atmosphere; but the decomposition temperatures of the DICY/EP-P1 and EP-P2 thermoset resins were the lowest. For phenolic melamine, the degradation temperature of their thermoset resins were moderate. Compared with PS-3133, the decomposition temperature of the EP-P1 or the EP-P2/PS-3333 thermoset resin was much higher. Sato and Yokoyama reported that polymers with a high aromatic content could possess good thermal stability (25,26). Apparently, the molecular chain of novolac is mainly constituted of regular phenol units. The incorporation of these regular phenol units into the backbone enhanced the thermal stability of the EP-P1 or the EP-P2/novolac thermoset resin. It could be also noticed that the EP-P1 or the EP-P2/novolac thermoset resin showed the highest temperature at the rapid weight loss, which may be explained in the same way. Phenolic melamine also contains a phenol group, however, its aromatic content is lower than that of novolac and, therefore, the thermal stability of this thermoset resin was slightly lower than that of novolac. DICY does not contain an aromatic group, thus the thermal stability of its cured resins was the poorest. The TGA data also showed that the thermal stability decreased with increasing phosphorus content of the cured phosphate-based epoxy resins. These results imply that some chain structure or group in BHPP may have poor thermal stability.

From Table I, it is also seen that the EP-P2/DICY thermoset resin has a char residue of 19 wt % at 700 °C, which is greater than that of the other thermoset resins. The char residue (around 18 wt %) of EP-P2/PS-3313 or PS-3333 thermoset resin was slightly lower than that of the EP-P2/DICY thermoset resin, and ranked as the second highest value. The EP-P1/novolac thermoset resin exhibited the lowest char residue of 7 wt % of all the samples. These results implied that the char residue is strongly dependent on the phosphorus and nitrogen contents, and the char residue increases with increasing phosphorus and nitrogen contents. The higher the phosphorus and nitrogen contents, the higher the char residue of the thermoset resin cured with the same curing agent. The

phosphorus-nitrogen ratio is also an important parameter as discussed in a later section. For the curing agents used in these experiments, the nitrogen content of DICY (67 wt %) is much higher than that of phenolic melamine (20 – 25 wt %), while novolac does not contain nitrogen. So the char residue of the thermoset resins cured with the four curing agents increase in the order: DICY > PS-3333 > PS-3313 > novolac. Usually, the degree of oxidation of the thermoset resins can be reduced with an increase in the phosphorus and nitrogen contents at high temperatures; furthermore, the char residue has been correlated to the flame retardancy. The relationship between the char residue and the flame retardancy will be discussed in following section.

Flame-retardant properties. The flame-retardant properties of all the samples were examined by LOI and UL-94 vertical measurements, and the data are listed in Table II. The LOI values of these thermoset resins are noteworthy. From these values, it can be seen that the cured thermoset control resins exhibited poor flame retardant properties. The control resin/novolac thermoset resin does not contain any flame-retardant element and it has a low LOI value of 24 and was not rated in the UL-94 vertical test. However, the thermoset control resins cured with DICY, PS-3133, and PS-3333 could not achieve any significant improvement in flame retardancy through the incorporation of only nitrogen; they also exhibited low LOI values and were not rated according to the UL-94 protocol. As shown in Table II, the EP-P2/DICY thermoset resin exhibited the highest LOI value, 35, of all the samples, and a UL-94 grade of V-0 was achieved. The EP-P1/DICY, EP-P2/PS-3313, and EP-P2/PS-3333 thermoset resins also showed good flame retardancy with the LOI values ranging from 32 to 34, and the UL-94 V-0 grade was achieved for these three thermoset resins. The LOI values of the EP-1 and EP-2/novolac thermoset resins were lower than those of the other thermoset resins and the UL-94 vertical tests for these two thermoset resins only reached the V-2 grade. On the basis of the data, it could be concluded that the LOI values, as an indicator of flame retardancy, could be improved by increasing both the phosphorus and the nitrogen contents.

Generally, a polymer with a phosphorus moiety exhibits good flame retardancy through the formation of a phosphorus-containing char acting as insulation to prevent heat transfer, which will reduce the production of combustible gases during combustion. During combustion, a phosphorus-rich incombustible char layer would form on the surface of the polymer to block the advancing flame. This process can be attributed to a condensed-phase mechanism (27). The higher the phosphorus content, the better is the effect of decreasing the exothermicity of the pyrolysis reaction and decreasing the conductivity of the burning materials. As a result, the flammability can be greatly limited. However, the EP-P2/novolac thermoset resin still exhibited poor flame retardancy, though its phosphorus content was as high as 1.62 wt %. On the other hands, it is found in Table II that all the EP-P/nitrogen-containing curing agent thermoset resins reveal a high degree of non-flammability. These

Table II LOI values and UL94 vertical test results of the control resin and the phosphate-based epoxy resins (EP-P1 and EP-P2) cured with various curing agents

<i>Sample</i>	<i>Phosphorus content (wt %)</i>	<i>Nitrogen content (wt %)</i>	<i>LOI</i>	<i>UL94 grade</i>
Control/DICY	0	2.786	25	NR
EP-P1/DICY	0.947	2.786	34	V-0
EP-P2/DICY	1.888	2.786	35	V-0
Control/Novolac	0	0	24	NR
EP-P1/Novolac	0.812	0	28	V-2
EP-P2/Novolac	1.622	0	28	V-2
Control/PS-3313	0	4.697	25	NR
EP-P1/PS-3313	0.755	4.697	32	V-1
EP-P2/PS-3313	1.511	4.697	34	V-0
Control/PS-3333	0	6.486	25	NR
EP-P1/PS-3333	0.730	6.486	31	V-1
EP-P2/PS-3333	1.462	6.486	33	V-0

results indicate that the synergistic effect of phosphorus and nitrogen plays an important role in the improvement of the flame retardancy. There are two char forming mechanisms: (a) redirection of the chemical reactions involved in decomposition in favor of reactions yielding carbon rather than CO or CO₂ and (b) formation of a surface layer of protective char (28). Although the chemical transformations of phosphate-based compounds and their participation in all stages of the epoxy resin combustion process are not yet fully understood, it is still possible that the phosphate-based thermoset resins undergo chain scission during combustion and the phenyl phosphate group are first stripped from main chains, then the other chain segments tend to decompose with the consequent production of highly volatile and flammable monomers and oligomers. These materials are not inherently flame retardancy. However, when phosphorus and nitrogen are simultaneously incorporated into the thermoset resins, it can be assumed that the good flame retardancy may be based on the concept that nitrogen-containing fragments can eliminate the combustion by producing nitrogen gas, which can exclude oxygen from the burning materials and the nitrogen moiety enhances the formation of the phosphorus-rich char. Therefore, the highly synergistic flame-retardant efficiency comes from the combination of phosphorus and nitrogen elements in the backbone of the thermoset resins.

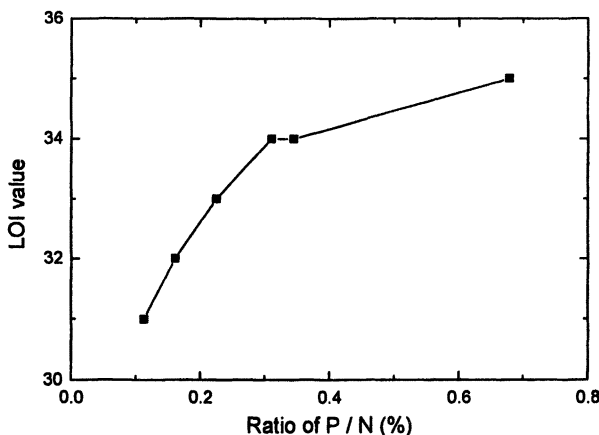


Figure 4 Plot of the LOI value versus the ratio of P/N in the thermoset resin.

In order to obtain more details about the synergistic effect of the combination of phosphorus and nitrogen on flame retardancy, the relationship between the ratio of the phosphorus to nitrogen (P/N) and the LOI is plotted in Figure 4. It is very important to notice that the LOI value increases with an increase in the P/N ratio. This result indicates the effective synergism of phosphorus and nitrogen mainly depends on the ratio of P/N. On the other hand,

as discussed in the previous paragraph, the char residue is correlated to flame retardancy. From the char residue listed in Table I, it was observed that the LOI strongly relied on the char residue and increased with an increase in the amount of char residue. Obviously, an increase in char residue can limit the production of combustible carbon-containing gas and reduce the exothermicity of the pyrolysis reaction and the thermal conductivity of the burning materials, consequently limiting the flammability. The EP-P/novolac system is an exception to this statement, since the char residue for EP-P2/novolac thermoset resin is twice than that for EP-P1/novolac thermoset resin while the LOI values are similar. In general, the higher the char residue, the higher is the LOI value. These results were in good agreement with a solid-phase mechanism of flame retardancy (29,30).

Conclusion

The combination of the phosphate-based epoxy resins prepared in this study and a nitrogen-containing curing agent can provide excellent flame retardancy (UL-94 V-0) as well as good thermal stability. These curing systems of halogen-free epoxy resins will have potential applications in electronic fields with consideration of environmental and health effects.

Acknowledgements

The author greatly appreciated financial support from the *New-Star* Plan by the Beijing Municipal Science and Technology Commission (Grant No.: 954811500).

References

1. Lubin, G. Editor, *Handbook of Composites*; Van Nostrand Reinhold: New York, 1982.
2. Liaw, D. J. *J. Polym. Sci., Part A: Polym. Chem.* **1997**, *63*, 895-901.
3. Wang, C. S.; Liao, J. K. *Polym. Bull.* **1991**, *25*, 559-570.
4. Wang, C. S.; Shieh, J. Y. *Eur. Polym. J.* **2000**, *36*, 433-452.
5. Yang, C. P.; Lee, T. M. *J. Appl. Polym. Sci.* **1987**, *34*, 2733-2745.
6. Mantecon, A.; Cadiz, V.; Serra, A. *Eur. Polym. J.* **1987**, *23*, 481-489.
7. Ichina, T.; Hasuda, Y. *J. Appl. Polym. Sci.* **1987**, *34*, 1667-1675.
8. Chang, S. J.; Chang, F. C. *Polym. Eng. Sci.* **1998**, *38*, 1471-1482.
9. Wang, C. S.; Liu, Y. L.; Hsu, K. Y. *Polymer* **2002**, *44*, 565-573.
10. Wang, C. S.; Lin, C. H. *J. Appl. Polym. Sci.* **2000**, *75*: 429-436.

11. Wang, C. S.; Shieh, J. Y. *Polymer*, **1998**, *39*, 5819-5826.
12. Annakutty, K. S.; Kishore, K. *Polymer* **1988**, *29*, 756-764.
13. Morgan, A. B.; Tour, J. M. *J. Appl. Polym. Sci.* **1999**, *73*, 707-718.
14. Banerjee, S.; Palit, S. K.; Maiti, S. *J. Polym. Sci., Part A: Polym. Chem.* **1994**, *32*, 219-229.
15. Wang, C.S.; Shieh, J. Y. *J. Appl. Polym. Sci.* **1999**, *73*, 353-361.
16. Liu, Y. L.; Hsiue, G. H.; Lee, R. H.; Chiu, Y. S. *J. Appl. Polym. Sci.* **1997**, *63*, 895-901.
17. Chen-Yang, Y. W.; Lee, H. F.; Yuan, C. Y. *J. Polym. Sci., Part A: Polym. Chem.* **2000**, *38*, 972-981.
18. Shau, M. D.; Wang, T. S. *J. Polym. Sci., Part A: Polym. Chem.* **1996**, *34*, 387-396.
19. Wang, T. S.; Parng, J. K.; Shau, M. D. *J. Appl. Polym. Sci.* **1999**, *74*, 413-421.
20. Shieh, J. Y.; Wang, C. S.; *J. Polym. Sci., Part A: Polym. Chem.* **2002**, *40*, 369-378.
21. Nakamura, Y.; Yamaguchi, M.; Okubo, M. *J. Appl. Polym. Sci.* **1992**, *45*, 1281-1290.
22. Liu, Y. L.; Hsiu, C. H.; Chiu, Y. S. Jeng, R. J.; Ma C. *J. Appl. Polym. Sci.* **1996**, *59*, 1619-1625.
23. Liu, Y. L.; Hsiu, C. H.; Chiu, Y. S. *J. Polym. Sci., Part A: Polym. Chem.* **1997**, *35*, 565-574
24. Liu, Y. L.; Hsiue, G. H.; Lan, C. H. *Polym. Degrad. Stab.* **1994**, *32*, 219-227.
25. Sato, M.; Yokoyama, M. *Eur. Polym. J.* **1980**, *16*, 79-87.
26. Sato, M.; Yokoyama, M. *J. Polym. Sci., Part A: Polym. Chem.* **1980**, *18*, 2751-2762.
27. Banks, M.; Ebdon, J. R.; Johnson, M. *Polymer*, **1994**, *35*: 3470-3474.
28. Lu, S. Y.; Hamerton, I. *Prog Polym Sci*, **2002**, *27*: 1661-1712.
29. Wang, X.; Zhang, Q. *Eur Polym J*, **2004**, *40*: 385-396.
30. Cellis, C. F.; Hirschler, M. M. *The Combustion of Organic Polymers*; Clarendon Press: Oxford, 1981.

Chapter 22

Recent Progress in Flame Retardancy of Polyurethane and Polyisocyanurate Foams

Sergei V. Levchik¹ and Edward D. Weil²

¹Supresta U. S. LLC, 1 Livingstone Avenue, Dobbs Ferry, NY 10522

²Polytechnic University, Six Metrotech Center, Brooklyn, NY 11201

The review covers developments since the previous Fire and Polymers symposium which are of commercial significance. The polyurethane foam industry is currently undergoing serious changes because of the banning of some chlorofluorocarbon blowing agents. Moreover, the banning of pentabromodiphenyl ether as a flame retardant requires finding alternative means for avoiding scorch (thermal damage during production exotherms). We discuss recent insights into the scorch mechanism in relation to the choice of flame retardant.

We recently published a review of flame retardants for polyurethanes which are in commercial use (1) and a more comprehensive review covering the literature and patents (2). In the present paper, we will discuss developments of the last four years, since the previous ACS Fire and Polymers symposium in 2000.

Additives in Rigid Foams

The leading method for flame retarding rigid foam at present is to use additives, although reactive diols are occasionally employed where there is some

special requirement. The well-established additives are still tris(2-chloroethyl) phosphate and tris(1-chloro-2-propyl) phosphate. The principal recent change here is the need for higher percentages of these additives due to the use of hydrocarbon blowing agents in place of the ozone-depleting chloro-fluorocarbons.

The roofing test and some other rigid foam flame retardancy tests can be passed with relatively high loadings of chlorinated phosphates alone. Recently, Weil and Levchik (3) reported that the B-2 rating in the German DIN 4102 test can be achieved by the combination of a chlorinated phosphate and pigment grade iron(III) oxide. A significant decrease of smoke was another advantage of that particular combination.

Although the chloroalkyl phosphates continue to dominate, there is an interest especially in Europe in non-halogenated flame retardants. A non-halogenated phosphorus additive, which has found usage in rigid polyurethane foam for several decades is dimethyl methylphosphonate (DMMP). This compound contains 25% phosphorus, the basis of its high flame retardant activity, and only about 8 phr is required in a sucrose-amine based rigid foam. DMMP now has a "R46" (mutagen) labeling in Europe so it is not used much there. Diethyl ethylphosphonate or triethyl phosphate are also effective for the same purpose, and have better label status in Europe.

Bayer has recently introduced dimethyl propylphosphonate (LEVAGARD™ DMPP or LEVAGARD™ VP SP 51009) which they advocate as a replacement for the halogen-containing flame retardants in rigid foams (4). It is a low viscosity liquid, having over 20% P content.

Also, for non-halogen applications of importance in Europe, high molecular weight finely-divided ammonium polyphosphate (APP) has been found effective in pentane-blown polyurethane or polyisocyanurate foams (5). Ammonium polyphosphate combined with a char former and blowing agent to make a complete intumescent system is also useful in both rigid and some flexible foams.

Stabilized red phosphorus, which we recently reviewed (6), also has found usage in Europe in rigid polyurethane foams. It is highly efficient on a weight basis, and can be used at rather low loadings to meet stringent flammability standards. Dispersions in polyol, castor oil or tris(chloroisopropyl) phosphate are variously available from Clariant or Italmatch. Effective combinations of red phosphorus with melamine compounds have recently been patented as flame retardants for polyurethanes in rail vehicles (7).

Expandable graphite can be used as an efficient flame retardant in rigid PU foams in combination with triethyl phosphate, which helps to decrease the heat conductivity and the deleterious physical effect of the graphite (8,9). Compared to pentane-blown polyisocyanurate-polyurethane foams which have an oxygen

index (OI) of about 20-25, an OI of 35 was found for a similar foam with 15 wt. % expandable graphite and 3 wt. % triethyl phosphate.

Reactive Non-halogen Flame Retardants in Rigid Polyurethane Foams

Reactive diols such as VIRCOL™ 82, now Albemarle's ANTIBLAZE™ 82, and Akzo Nobel's FYROL™ 6 or Bayer's LEVAGARD™ 4090N are old products which continue to be used, and perhaps the fact that they are non-halogen reactives will get them more attention. We notice some new studies of FYROL™ 6 in China (10) which confirm that this reactive diol has a char-enhancing mode of action.

Impact of Blowing Agent on Flame Retardancy of Rigid Foams

As mentioned, the chlorofluorocarbon blowing agents are being (or have been) phased out to avoid their upper-atmosphere ozone-depleting action. The use of pentanes (cyclopentane, isopentane, n-pentane or mixture) for blowing of foams in place of chlorofluorocarbon blowing, imposes a need for more flame retardants to counteract the flammability of the blowing agent. The usual flame retardants such as FYROL™ CEF and PCF can still be used but the level will usually have to be raised. It is well known that by raising the isocyanate index to get more isocyanurate structure, a lower level of flame retardant can be used to meet a standard.

A review of blowing agents is available (11). New non-ozone-depleting blowing agents containing fluorine can allow for less flame retardant, or with a high enough isocyanurate content, no flame retardant at all. An example of a non-ozone-depleting blowing agent in commercial development is 1,1,1,3,3-pentafluoropropane or Honeywells' ENOVATE™ 3000 (HFC-245fa) or Solvay's HFC-365mfc. This compound does have a flash point, but can be made less flammable by blending with tetrafluoroethane (HFC-134a) (12,13,14,15). There is also a possible trade-off in the use of a pentane with HFC-245fa. The pentane lowers the cost of the blowing agent but may require an increase in the flame retardant. A typical flame retardant such as tris(chloroisopropyl) phosphate can be then elevated to compensate for the pentane.

Brominated Diols as Reactive Flame Retardants

Brominated diols have been used in rigid urethane foams for many years, specifically Great Lakes PHT-4™ diol or Albemarle SAYTEX™ RB-79 to meet ASTM E-84 Class I or II ratings. The original product has one primary hydroxyl group (faster reacting) and one secondary hydroxyl group (slower reacting). In order to pass the E-84 tunnel test with a class I rating, DeLeon *et al.*(16) recommended the use of a combination of this brominated diol and phosphorus from three different fire retardants, the lowest possible amount of polyether polyol, and the highest possible isocyanate index.

Based on a small scale test simulating performance of the FM 4450 calorimeter (used for roofing insulation testing), blends of the brominated phthalate diol with chlorinated phosphate flame retardants have been recommended (17) as an effective FR combination for this application. Recently, a related tetrabromophthalate diol with both hydroxyl groups primary, thus faster-reacting, has been introduced by Great Lakes.

Dead Sea Bromine Group has introduced a series of proprietary blends of a brominated neopentyl alcohol, a tetrabromobisphenol-based polyether polyol (probably) and a chlorinated phosphate, as SaFRon 6601 and 6700, aimed at rigid foams for the building industry (18).

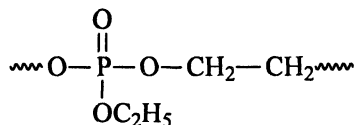
Additives in Flexible Foams

A major fraction of the flexible polyurethane foams used in furniture is flame retarded.

Additives, such as tris(2-chloroisopropyl) phosphate and tris(1,3-dichloro-2-propyl) phosphate are still dominant, although much research has been expended on reactives. Furniture manufacturers in the U.S. usually try to have their foam cushions comply with the CAL 117 tests, which is currently under revision. When and if the California requirements are stiffened, the expected result is more likely to affect the choice of upholstery or force the use of a flame-resistant interliner (19,20). Typical interliners are polyimides, aramides, polybenzimidazoles, woven glass fabric and a melamine-based fiber (BASOFIL™).

Halogen-free Additives for Flexible Foams

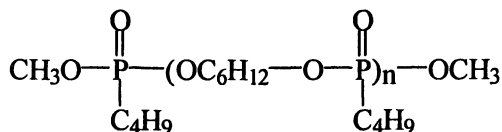
An oligomeric ethyl phosphate additive containing 19% phosphorus has been introduced by Akzo Nobel as FYROL™ PNX. It is an oligomeric additive (21,22) with a repeating unit of the structure:



Because PNx is halogen-free it is especially of interest in Europe, particularly with respect to the automotive industry and their low fogging/VOC emission requirements. In the MVSS 302 test, this oligomer is on average 40-50% more efficient than the chloroalkyl phosphates. In terms of volatile organic content (VOC), PNx compares well with other flame retardants used in the automotive industry, but it becomes especially advantageous because the low use level also helps to maintain low VOC. PNx was suggested for use in automotive applications in combination with alkylated phenyl phosphates, which not only improve the fire retardant performance of PNx, but also decrease its viscosity (23).

PNx also outperforms traditional products in Cal 117A and D test which is a small-scale ignition tests for upholstered furniture. PNx is 50 – 60 % more effective than traditional chlorinated alkyl phosphates. This oligomer was found to be synergistic with tris(dichloroisopropyl phosphate) (24). One advantage of the use of an additive instead of a reactive is that little change needs to be made in the foam formulation.

Oligomeric alkyl phosphonates of the following structure:



were synthesized in the Albright & Wilson laboratories, later acquired by Rhodia, and evaluated in flexible PU foams (25). It was found that 10 php of the oligomeric phosphonate makes foam self-extinguishing.

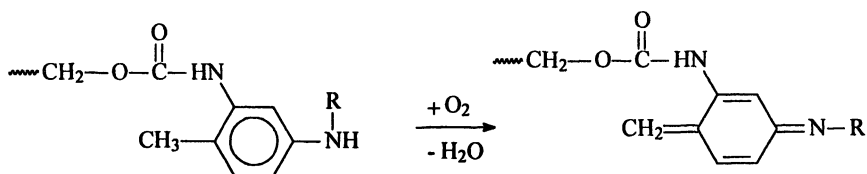
Triaryl phosphates, such as isopropylphenyl diphenyl phosphate, are now finding use in flexible foam formulations sometimes in combination with a bromine-containing additive (see Scorch discussion). A recent introduction by Great Lakes, REOFOS™ NHP, a low viscosity aryl phosphate, is designed to meet MVSS 302 for hot-molded automotive seating, and to be non-fogging (26).

Understanding and Overcoming the "Scorch" Problem in Flexible Foams

In the manufacture of flexible polyurethane foams, allowing the foam to reach an excessively high temperature during the latter stages of foaming, after the addition of the water, can lead to "scorch." This is, minimally, a discoloration of the interior of the foam slab or bun, more seriously a loss of mechanical properties indicative of structural degradation.

It has always been thought that scorch involved some kind of free radical and acid generation chemistry (27), and improved products such as tris(dichloroisopropyl) phosphate with various antioxidants and acid acceptors have been successfully marketed (28,29). Experiments with indicators however show little or no acid in the scorched region of a foam bun. Infrared spectroscopic studies, done either by diffuse reflectance FTIR (E. D. Weil, unpublished) or transmission FTIR, show that the scorched part of a foam bun has a lower unreacted isocyanate group content than the unscorched part. More insight into the chemistry of scorch comes from a study done at University of Turin (30) sponsored by Akzo Nobel. These isocyanate groups are present in the foam because of entrapment in the crosslinked network where they cannot come into proximity with reactive groups. When they are hydrolyzed by water, added to make CO₂ for blowing and urea linkages, these isolated isocyanate groups cannot find an OH or NH to react with, so they generate free amino groups. Aminophenylamido structures, are known to be readily oxidized to quinoneimine structures, which are extremely chromophoric with very strong visible light absorption bands. Spectroscopic evidence for such structures was found in the Turin study.

The question as to why the flame retardants such as the chloroalkyl phosphates aggravate scorch was then addressed. It is known that these structures can alkylate an aminoaryl group, by nucleophilic displacement of the chloride or phosphate anion or both (31). It is also likely that the more electron-rich alkylaminophenyl groups are more readily oxidized than the unalkylated aminophenyl groups. The formation of the chromophoric groups is aggravated, amongst other factors, by the presence of flame retardants with alkylating capabilities such as the chloroalkyl or alkyl phosphates, and this alkylation reaction also adds to the exotherm. Those flame retardants which are most reactive towards the hypothesized arylamino groups tend to be those which aggravate scorch. Many such conjugated structures are likely.



Conversely, phosphorus compounds that cannot alkylate amino groups are those which do not aggravate scorch; examples are aryl phosphates.

Low-Scorch Flame Retardants

The polybromoaromatic compounds are relatively unreactive and act as inert additives under the conditions of scorch, thus foams containing them tend to be scorch-resistant. Consequently, a widely used low scorch flame retardant additive has been a liquid blend of pentabromodiphenyl ether and isopropylphenyl diphenyl phosphate/triphenyl phosphate, both quite stable liquids which perform well together as Akzo Nobel's FYROL™ PBR or Great Lakes' DE-61™ (32). In the early 2000 era, environmental concerns regarding pentabromodiphenyl ether have led to a sharp decline in its usage, regulatory actions in California and in Europe have the effect of a ban, and manufacturing in the U.S. is being discontinued in 2004 (33).

Bromine-containing alternatives introduced into the market include a tetrabromobenzoate ester, Great Lakes FIREMASTER™ BZ-54 (CN 2065) (34) which can be used alone or blended with an alkylphenyl diphenyl phosphate. The stated 54% Br fits an octyl tetrabromophthalate. When used alone, this additive has a favorable effect on flame lamination, and also unlike the pentabromodiphenyl oxide formulations, it does not cause center softening in high resilience foam formulations. Its blend with an alkylphenyl phosphate is Great Lakes new FIREMASTER™ 550, used in both high-resilience and conventional foams (35).

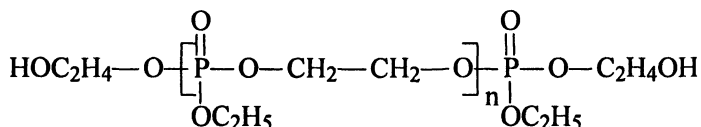
A blend of tribromoneopentyl alcohol and triaryl phosphate has been offered by Dead Sea Bromine for use in non-scorching flexible foam (18). It has high efficiency and provides good thermal and UV stability.

Akzo Nobel Chemicals has developed new highly stable phosphate esters and their blends known as AC003 and AC007 (36,37). AC003 is a non-halogen material of low viscosity with a phosphorus content of 10.9%. AC007 contains 9% phosphorus and 24.5% chlorine. In the MVSS 302 test, the flame retardant efficiency of AC003 is comparable to chlorinated alkyl phosphates and/or pentabromodiphenyl ether at 1.5 pcf but at a density of 1.8 pcf AC003 is less efficient than these conventional additives. The blended product AC007 is more

efficient than chlorinated alkyl phosphates or pentabromodiphenyl ether at 1.5 pcf and comparable at 1.8 pcf. In terms of volatile organic content (VOC), both AC003 and AC007 are superior to pentabromodiphenyl ether and comparable or better than chlorinated alkyl phosphates. AC003 is actually very close to the fogging performance of non-flame-retarded foam. In the CAL 117 A and D tests, AC003 compares favorably with chlorinated alkyl phosphates. AC007 is significantly more efficient than any tested additive at 1.5 pcf. In order to further improve efficiency of AC003 and AC007 these products can be combined with synergists.

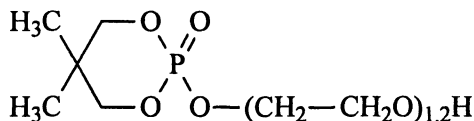
Reactive Flame Retardants for Flexible Foams

A newer halogen-free phosphorus-containing diol was developed by Hoechst for rigid or flexible foams and has been marketed for several years as EXOLIT™ OP 550 by Clariant (38). The product is an ethyl phosphate oligomer diol of the following probable structure:



The primary hydroxyl groups are reactive with TDI and this diol can be used as a partial replacement of the polyol. This diol containing about 17% P can be used for rigid or flexible foams, especially for molded and high density slabstock flexible foams. At relatively low loadings of 4 - 7.5 phr it allows the foam to pass the MVSS 302 automotive test, with superior performance in the fogging test.

Monofunctional phosphates were made in the Daihachi laboratories by reacting cyclic acid phosphates with propylene oxide or ethylene oxide (39) to obtain monohydric alcohols of the structure:



This additive is said to be efficient at 8.5 parts per hundred of polyol in the MVSS 302 automotive test.

Melamine in Flexible Foams

Especially in Europe, melamine has been used for some years as a part of the flame retardant system in flexible foams. It is often used in combination with a haloalkyl phosphate, such as tris(1,3-dichloro-2-propyl) phosphate. A synergistic interaction noted with melamine and TDCPP (but not with the more volatile tris(1-chloro-2-propyl) phosphate TCPP) in combustion-modified high-resilience foam has been recently explained by Bastin *et al.* (40,41) on the basis of a chemical interaction producing char or a difficultly ignitable low-melting semi-solid. The more volatile TCPP escapes before this interaction can take place.

Conclusion

At this time, the older chloroalkyl phosphate additives continue to be predominantly used in both rigid and flexible foams. A number of new candidates have made their appearance, competing for market niches opened up by changes in blowing agent, by the demise of pentabromodiphenyl ether and by the interest in halogen-free, low VOC and reacted-in flame retardants.

References

1. Weil, E.D.; Levchik, S. V., *J. Fire Sci.* **2004**, *22*, 183.
2. Levchik, S.V.; Weil, E.D. *Polym. Int.* **2004**, *53*, 1585.
3. Weil, E.D.; Levchik, S.V. In *Proc. Conf. Recent Adv. Flame Retardancy Polym. Mater.* Stamford, CT, 2003.
4. Mauerrer, O. *PU Magazin*, May, 2003, p 239.
5. Sicken, M.; Schutz, C.; Jung, S. In *Polyurethanes Expo '96*, Las Vegas, NE, 1996, pp 460-466.
6. Weil, E. D., In *Proc. Conf. Recent Adv. Flame Retardancy Polym. Mater.* Stamford, CT, 2000.
7. Avar, G.; Munzmay, T.; Ruckes, A., to Bayer, US Patent Application 20020115812, 2002.
8. Modesti, M.; Lorenzetti, A.; Simoni, F.; Gilbert, M., In *Polyurethanes Expo '01*, Columbus, OH, 2001, pp 623-626.
9. Modesti, M.; Lorenzetti, A., *Polym. Degrad. Stab.* **2002**, *78*, 167.
10. Wang, X.L.; Yang, K.K.; Wang, Y.Z., *J. Appl. Polym. Sci.* **2001**, *82*, 276.
11. Singh, S.N., *Blowing Agents for Polyurethane Foams*; RAPRA Review Reports 142, RAPRA Technology Ltd.: Shawbury, UK, 2002.

12. Williams, D. In *Polyurethanes Expo '02*, Salt Lake City, UT, 2002, pp 135-143.
13. Bogdan, M.; Williams, D.; Verbiest P. *J. Cel. Plast.* **2001**, *37*, 58.
14. Wu, J.; Dillon, D.; Crooker, R. In *Polyurethanes Expo '02*, Salt Lake City, UT, 2002, pp 144-149.
15. Zipfel, L.; Dournel, P. *J. Cell. Plast.* **2002**, *38*, 51.
16. DeLeon, A.; Shieh, D.; Feske F.F. In *Polyurethanes Expo '01*, Columbus, OH, 2001, pp 125-128.
17. Feske, E. F.; Brown, W. R. In *Polyurethanes Expo '02*; Salt Lake City, UT, 2002, pp 32-40.
18. Borms, R.; Wilmer, R.; Bron, S.; Zilberman, Y.; Georgette, P. In *Flame Retardants 2004*; Interscience Communications, London, 2004, pp 73-84.
19. Hirschler, M.M. In *Proc. Fall FRCA Conference*; Cleveland, OH, 2002, pp 1-26.
20. Damant, G. In *Flame Retardants 2004*; Interscience Communications: London, 2004, pp 221-232.
21. Bradford, L.L.; Pinzoni E.; Wuestenenk J. In *Polyurethanes Expo '96*; Las Vegas, NE, 1996, pp 358-361.
22. Blundell, C.; Bright, D.A.; Halchak, T. In *Proc. UTECH 2003*, The Hague, NL, 2003.
23. Bradford, L.L.; Pinzoni E.; Williams, B.; Halchak T. to Akzo Nobel, European Patent 1,218,433, 2003.
24. Bradford, L.L.; Pinzoni E.; Williams, B.; Halchak T. to Akzo Nobel, US Patent 6,262,135, 2001.
25. Harris, C. J.; Woodward, G.; Taylor, A.J.; Manku, J.S. to Albright & Wilson, British Patent 2,319,251, 1998.
26. Rose, R.S.; Buszard D.L.; Philips M.D. and Liu F.J. to Pabu Services, US Patent 6,667,355, 2003.
27. Gray, R.L.; Lee, R.L. In *Plastics Additives*, Pritchard, G. Ed.; Chapman Hall: London, 1998, pp 567-575.
28. Andrews, S. In *60 Years of Polyurethanes*, Kresta, J.E.; Elfred E.W. Eds.; Technomic: Lancaster, 1998, pp 101-119.
29. Williams, B.A.; De Kleine, L.A. to Akzo Nobel, PCT Patent Application 200279315, 2002.
30. Luda, M.P.; Bracco, P.; Costa, L.; Levchik, S.V. *Polym. Degrad. Stab.* **2004**, *83*, 215.
31. Bissell, E.R. *J. Heterocyclic Chem.* **1977**, *14*, 535.
32. Darnerud, P.A. *Environ. Int.* **2003**, *29*, 841.
33. Hardy, M.L.; Bieseemeier, J.; Manor, O.; Gentit, W. *Environ. Int.* **2003**, *29*, 793.
34. Rose, R.S.; Likens, L.J.; Elliott, J.L. In *Proc. Polyurethane Foam Association*, 1966, <http://www.pfa.org/abstracts/ab96.html>

-
35. Jacobs, P.; Rose, R.; Likens, J.; Elliott, J. In *Proc. Polyurethanes World Congress '97*, Amsterdam, NL, 1997, pp 215-219.
 36. Bradford, L.; Williams, B.; Pinzoni, E. In *Proc. Spring FRCA Conference*, Washington, DC, 2000.
 37. Bradford, L.; Pinzoni, M.; Halchak, T. In *Polyurethanes Expo '02*, Salt Lake City, UT, 2002, p 647.
 38. Sicken, M.; Staendeke, H. to Clariant, US Patent 5,985,965, 1999.
 39. Tokuyasu, N.; Matsumura, T. to Daihachi, US Patent 6,127,464, 2000.
 40. Bastin, B.; Paleja, R.; LeFebvre, J. In *Polyurethanes Expo '02*, Salt Lake City, UT, 2002, pp 244-254.
 41. LeFebvre, J.; Bastin, B.; Le Bras, M.; Paleja, R.; Delobel, R. *J. Fire Sci.* **2003**, *21*, 343.

Chapter 23

Fire-Resistant Flexible Foams for High-Risk Cushioning Applications

Chandrasiri Jayakody, Dan Myers, and Carl Ogburn

Chestnut Ridge Foam, Inc., 443 Warehouse Drive, Latrobe, PA 15650

In this paper, the fire-performance characteristics and physical properties of highly flame retarded polyurethane-neoprene compound cushioning products will be discussed. The cushioning product for aviation industry, Airflex, is manufactured in distinct seat and back selections, in a variety of colors for a comprehensive variety of firmness choices. Airflex foam cushioning will easily meet fire-testing standards required by the Federal Aviation Administration (FAA) when tested in composite with properly treated dress covering fabrics. In addition to fire-retardant characteristics, these low-density foam grades show excellent comfort and physical properties. Safeguard™ cushioning products are utilized to make military, institutional, healthcare, psychiatric, university and crib/youth mattresses that need to meet fire performance standards such as CAL. TB No. 129, City of Boston BFD IX-11, NFPA 101® Life Safety Code®, ASTM E-1590, CAL. TB 603 and the US Navy (NAVSEA PD 1-00, NFPA 267-98 modified). The contract furniture applications with these foam grades easily comply with CAL. TB No. 133 and ASTM E-1537 when tested in composite with FR upholstery fabrics. Safeguard™ XL cushioning is designed to provide maximum cushion durability for rail and bus transportation vehicles and comply with component fire performance characteristics in accordance with the Federal Transit Administration (FTA) and Federal Railroad Administration (FRA) regulations.

Introduction

The flexible polyurethane foam industry enjoys an annual market share of billions of dollars. In 2000, the United States alone produced 2,084 million pounds of flexible polyurethane foam. This value represents an average annual growth rate of 1.6% when compared with the production volume of 1995, 1,925 million pounds (1). According to Business Communication Co. Inc., estimations, the applications of flexible polyurethane foams in the year 2000 include furniture (862 million pounds), transportation cushioning (540 million pounds), bedding industry (273 million pounds), carpet underlay (212 million pounds), electrical/electronic (115 million pounds), medical cushioning (44 million pounds) and other uses (38 million pounds) (1).

However, polyurethane foam materials are very flammable, and produce extensive smoke upon burning. Therefore, there is a substantial need for cushioning products with improved fire-retardant characteristics. Fire is a major social issue in the United States and around the world. According to national fire statistics, fire causes billions of dollars in property damages annually and a significant number of casualties. In 2003, the residential structure fires alone resulted in 3145 fatalities (an increase of 17.8%), 14,075 injuries and \$6 billion in property damages (2). In an effort to upgrade fire safety and improve occupant survivability in a case of fire in high-risk institutions such as hospitals, detention facilities, prisons, hotels, and in industries such as aviation, transportation, marine etc., federal, state and local agencies and/or consensus organizations are often imposing fire codes with very strict requirements.

In order to be used in the applications mentioned above, each cushioning product has to meet stringent component or composite fire performance requirements. For example, cushioning products used in the aviation industry shall meet the Federal Aviation Administration (FAA) fire retardant regulations, surface transportation foam grades such as flexible cellular foams used in rail transportation passenger cars, locomotive cabs and public buses shall meet Federal Railroad Administration (FRA) and Federal Transit Administration (FTA) fire performance criteria for flexible cellular foams, cushioning products used in military, healthcare, psychiatric, and university mattress applications shall meet fire performance standards such as US Navy (NAVSEA PD 1-00, NFPA 267-98 modified), California Technical Bulletin 121, 129, City of Boston BFD IX-11, NFPA 101® Life Safety Code®, and ASTM E-1590, and effective January 1, 2005, the mattresses, box springs and futons to be sold in California shall also meet the new open-flame standard, Cal TB 603, foam products used in

contract furniture applications shall meet the California Technical Bulletin 133 fire performance criteria etc.

In this paper, we describe the use of polyurethane-neoprene composite cushioning products to help meet these stringent fire-retardant guidelines in various industrial settings. Such applications include use of these foam materials in aviation, surface transportation, contract furniture, and mattress industries.

Aviation Seat Cushion Applications

Many commercial and regional aircraft seat cushion assemblies are constructed in such a way that in the case of an emergency, when an aircraft is forced to land on water, the seat bottom cushion could be used as a floatation device. In order to be used as a floatation device, the seat bottom cushion must be sufficiently buoyant to support the weight of the passenger in water. This is measured in accordance with FAA Technical Standard Order No. TSO-C72c, buoyancy and extreme temperature tests. According to this test, the seat cushion must be capable of providing at least 15 pounds of buoyancy in fresh water at 85 °F for a period of 8 hours and also be capable of providing at least 15 pounds of buoyancy after conditioning at the temperature extremes (-40°F and 140°F) for at least 8 hours. Since aircraft seat cushions are made of open-cell flexible foam materials which absorb water easily, this requirement is met by fabricating a piece of closed cell floatation foam within the lower depth of the seat cushion. Even though FR foam materials alone meet the oil burner requirement, once this closed cell foam is incorporated into the seat cushion, the cushion assembly may now fail the oil burner requirement as flammable closed cell foam material may contribute to weight loss of more than 10 percent when subjected to the oil burner test. The normal procedure to protect this floatation foam is to cover it with expensive fire barrier fabric materials such as Kevlar® and Nomex® blended fabrics.

The cushioning technologies currently available to meet the above mentioned oil burner test include use of polyurethane-neoprene composite cushioning, use of heat expandable graphite, and use of polyurethane foams encapsulated with expensive Kevlar® type fire barrier fabrics.

The standards used to measure the fire retardancy of aviation seat cushioning are FAR 25.853 (c), Appendix F, Part II, oil burner test and FAR 25.853 (a), Appendix F, Part I, (a), (1), (ii), 12-second vertical Bunsen burner test (3). In addition to foam materials, each individual component of the seat cushion assembly such as fabric coverings, muslin, fire barrier materials, and Velcro must meet the vertical Bunsen burner test requirements.

The fire retardant behavior of six foam grades was evaluated using the vertical Bunsen burner test for cabin and cargo component materials (FAR

25.853 (a), Appendix F, Part I, (a)(1)(i) and (a)(1)(ii)), the oil burner test for seat cushions (FAR 25.853 (c), Appendix F, Part II, Cone Calorimeter (ASTM-E 1354), Buoyancy and extreme temperature tests (FAA Technical Standard Order No. TSO-C72c) and other ASTM test standards such as D 3574. These low-density foam grades, trade named Airflex, have been specifically developed for aircraft seat cushion applications. The average densities and the indentation force deflection ranges (IFD) (at 25% deflection) measured at 2" thickness as well as 4" thickness of all six Airflex foam grades together with recommended applications are presented in the Table I. The miscellaneous applications of Airflex 90-110 grade include carpet underlay, back of the headrest, and skirting around the seat bottom cushions. All density and IFD values are average values and have $\pm 10\%$ ranges.

Table I. Density and IFD ranges for Airflex foam grades and their applications

<i>Foam Grade</i>	<i>Density/IFD Range @ 2" English system (lbs/ft³, lbs)</i>	<i>Density/IFD Range @ 2" Metric system (kg/m³, N)</i>	<i>IFD at 4" lbs (N)</i>	<i>Aircraft Applications</i>
<i>Airflex 15-25</i>	2.7 / 15-25	43.2 / 67-111	30.8 (137)	Seat back
<i>Airflex 30-40</i>	2.7 / 30-40	43.2 / 133-178	40.0 (178)	Seat back
<i>Airflex 20-30</i>	3.6 / 20-30	57.7/89-133	38.3 (170)	Seat bottom
<i>Airflex 40-50</i>	3.6 / 40-50	57.7/178-222	53.8 (239)	Seat bottom
<i>Airflex 55-65</i>	3.6 / 55-65	57.7/245-289	74.9 (333)	Seat bottom
<i>Airflex 90-110</i>	4.5 / 90-110	72.1/400-489	110 (489)	Miscellaneous

FAR 25.853 (a), Appendix F, Part I – Vertical Bunsen Burner Test Results

All six-foam grades easily met both the 12-second and 60-second vertical Bunsen burner test requirements. All samples had 0-sec flame time, 0-sec drip flame time and average burn lengths in the range of 4.0 inch (102 mm) to 5.5 inch (140 mm). The results represent an average of more than 50 test trials.

These foam materials did not burn with a flame and showed no drippings after the removal of the Bunsen burner. The burn length test results are also below the required burn length standards in both the 12-sec and 60-sec tests.

FAR 25.853 (c), Appendix F, Part II – Oil Burner Test Results.

FAR 25.853 (c) is a composite test performed using all seat components. Individual foam grades were also tested with and without upholstery covering materials. Both individual foam grades as well as composite seat cushions easily passed the FAA oil burner requirement for aircraft seat cushions. The modified gun type oil burner, which provides an average thermocouple temperature equal or greater than 1800°F (982°C), is shown in Figure 1.

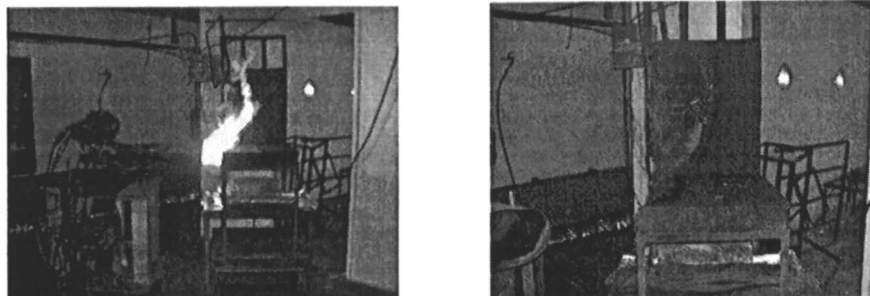


Figure 1. FAA Oil Burner Test for Aviation Seat Cushioning, $t = 0$ minutes (left), at the end of the test (right)

The average weight losses were in the range of 4.0% to 8.5% and the flames self extinguished within 0-1 minutes after the removal of the oil burner flame. The burn length values were significantly lower than the stated requirement (17 inches). One of the great advantages of Airflex foam grades is that they helped to obtain consistent compliance; even with upholstery materials considered most difficult to pass this test such as treated leather materials. With Airflex foam, these leather upholstery materials have shown a greater tendency to pass the oil burner test with less than 10% weight loss as a result of lower weight loss contribution from the foam. Aviation seat cushions made of Airflex foams also showed the lowest weight loss percentages when subjected to FAA oil burner test after repeated wet and dry cleaning of the seat fabrics (5). All these foam grades also passed the Airbus Industrie ATS 1000.001 and Boeing BSS 7239 toxicity test standards.

Cone Calorimeter Test Results

The fire performance characteristics of some Airflex foam grades were also studied using the Cone Calorimeter (ASTM E-1354), the instrument that has emerged as an important tool for the analytical testing of materials for their fire properties. The cone data of 4"x 4"x 2" foam specimens were conducted at 35 and 50 kW/m² exposure in a horizontal orientation using an edge frame. Airflex

20-30 gave a peak heat release rate of 83.0 kW/m² and smoke factor (average) of 7.1 MW/m² at 35 kW/m² exposure. This peak heat release rate value represents a reduction of 85% compared to the molded polyurethane foam, which showed an average peak heat release rate of 564 kW/m² at 35 kW/m² exposure (6). The peak heat release rate and average smoke factor of Airflex 20-30 at 50 kW/m² exposure were 102.3 kW/m² and 9.0 MW/m² respectively. Other Airflex foam grades also showed very low peak heat release rates when tested at 35 and 50 kW/m² exposures. Cone data also showed very low values of average heat release rate, average heat release rate at 3 minutes, total heat release, average effective heat of combustion and average mass loss rate for these foam grades.

Physical Properties

In addition to stringent fire testing standards, improvements in passenger comfort continue to be one of the essential needs of the global airline industry. Comfort experience is a combination of many different factors, including aesthetics. During a journey, aircraft passengers are subjected to both mental and physical stresses. Comfortable seat cushions are instrumental in reducing those stresses. To meet these goals, Airflex seat cushions are designed to achieve longer service life with better firmness retention, less thickness loss over time, higher resiliency, good support factors, and improved aging characteristics. The physical properties of these Airflex foam grades are summarized in Table II.

Flexible Cellular Foam Applications for Passenger Cars and Locomotive Cabs

Variations of this technology can also be utilized to make relatively high density foams (Safeguard™ and Safeguard™ XL) that meet FTA and FRA regulations, such as Radiant Panel flame spread index ($I_s \leq 25$) (ASTM D 3675-01), and ASTM E 662-03 smoke density requirement [D_s (1.5 min) ≤ 100 , D_s (4.0 min) ≤ 175] for flexible cellular foam materials used in passenger cars and locomotive cabs thus finding seat cushion applications in the public surface transportation industry (7). Safeguard™ XL foam grades will meet all FTA and FRA regulations at the density as low as 5.0 lbs/ft³ (80 kg/m³) and the IFD (25% deflection) range of 20-34 lbs (89-133 N) at 2-inch thickness. Radiant panel index values are below 10 and smoke density measured in accordance with ASTM E 662-03 under both flaming and non-flaming modes showed values significantly lower than the stated requirements. Some physical properties of the

Safeguard™ XL foam materials together with radiant panel and smoke density values are shown in Table III.

Table II. Physical Properties of Airflex Foam Grades

<i>Property</i>	<i>Test Method</i>	<i>Airflex Grade</i>	<i>Result</i>
<i>Compression set (50% deflection)</i>	ASTM D3574, Test D, Percent of original thickness	All grades	10% max.
<i>Tensile Strength</i>	ASTM D3574, Test E	All grades (except 90-110) 90-110	10 psi min. (69.0 kPa) 20 psi min (138 kPa)
<i>Elongation</i>	ASTM D3574, Test E	All grades (except 90-110) 90-110	125 % min 80 % min
<i>Tear Strength</i>	ASTM D3574, Test E	All grades	2.0 lbs/in (3.5 N/cm)
<i>Dynamic Fatigue Test by Constant Force Pounding</i>	ASTM D3574, Test I ₃ -IFD loss at 40% deflection (80,000 cycles, 24 hrs after test)	AF 20-30 AF 40-50 AF 55-65	18% max. 18% max. 18% max.
<i>Flex Fatigue</i>	ASTM D1055, Suffix H-250,000 cycles (thickness loss)	All grades (except 90-110)	5% max.
<i>Resilience</i>	ASTM D3574, Test H	All grades	30% min

SOURCE: Reproduced with permission from reference 4. Copyright 2001 BCC.

Contract Furniture Applications

The cushioning products used in contract furniture applications often need to meet the California Technical Bulletin 133 and ASTM E 1537 requirements. These test standards are designed to test seating furniture for use in occupancies that are identified as or considered to be public occupancies. Such facilities include, but are not limited to, nursing homes, healthcare facilities, public auditoriums, hotels and motels, jails and prisons. The ignition source for the Cal 133 shall be a square gas burner with propane gas as a fuel at a volume flow rate of approximately 13 liters per minute for a period of 80 seconds. An ignition source of five double sheets of loosely wadded newsprint contained in an ignition box, may be used as a screening test. The seating furniture fails to meet the requirements of this test procedure if any of the criteria A or any of the Criteria B are exceeded. The criteria A are; 1) a temperature increase of 200°F at the ceiling thermocouple 2) A temperature increase of 50°F at the 4-foot

thermocouple 3) Greater than 75% opacity at the 4-foot smoke opacity monitor 4) carbon monoxide concentration in the room, as measured of 1000 ppm for 5 minutes and e) weight loss due to combustion of 3 pounds in the first 10 minutes of the test. The criteria B include 1) a maximum rate of heat release of 80 kW 2) a total heat release of 25 MJ in the first 10 minutes of the test 3) greater than 75% opacity at the 4-foot smoke opacity monitor and 4) carbon monoxide concentration in the room, as measured in accordance with the procedure of 1000 ppm for 5 minutes (8).

CR foam grades such as Safeguard™ and Safeguard™ XL foams in composite with FR upholstery fabrics are currently being used to make fire resistant contract furniture that often needs to meet the Technical Bulletin 133 requirements.

Table III. Physical and Fire Resistant Characteristics of the Surface Transportation Cushioning.

Property	Test method	Result
Density Range	ASTM D3574, Test A	5.0 – 8.8 lb/ft ³ (80 - 141 kg/m ³)
Indentation force deflection (25% deflection) Range	ASTM D3574, Test B1 Measured at 2" thickness	20- 64 lbs (89-285 N)
Tensile strength	ASTM D3574, Test E	10.0-12.0 psi (69-83 kPa)
Elongation	ASTM D3574, Test E	120-150 %
Tear strength	ASTM D3574, Test E	2.0 - 2.5 lb/in (3.5 - 4.4 N/cm)
Compression set (50% deflection)	ASTM D3574, Test D, Percent of original thickness	10 % max
Resilience	Ball rebound test	30% min
Radiant panel index	ASTM D 3675-01	10.0 max
Smoke density (flaming and non-flaming modes at 1" thickness)	ASTM E662-03 Ds (1.5 min) Ds (4.0 min)	100 max 175 max

Mattress Applications

The importance of preventing mattress fires has been recognized for many years, and a number of standards for flame retardancy of the mattresses have been introduced. In 1972, a federal performance standard applicable to mattresses on a nationwide basis was codified in 16 CFR Part 1632, "Standard for the Flammability of Mattresses and Mattress Pads" by Consumer Products Safety Commission (CPSC) (9). This was issued to protect the public from the unreasonable risks of death, personal injury, and property damage associated with fires that resulted from the ignition of mattresses by cigarettes. However, even when mattresses meet the requirements of the Cigarette Ignition Standard, these mattresses pose deadly results when exposed to open-flame ignition sources such as matches, candles and lighters. The open-flame ignition of mattresses/bedding continues to cause a significant number of deaths and injuries. Between 1996 and 1998, an estimated 20,800 residential structure fires are attributed to mattress and bedding fires. These fires caused 2,200 injuries, 380 fatalities, and \$104 million in property damages (10). The leading causes of mattress and bedding fires are children playing and smoking, each cause 25%, arsons accounts for 16%, and electrical and open flames, each causes 9% (10). According to another report issued by CPSC in 1997, about 70% of the open flame fires involved child play and that 68% of the open flame deaths were to children playing with matches, lighters, candles and other open flame sources. The mattress was ignited directly by open flame in about 24% of the cases. However, bedding was the first item to ignite in about 60% of the cases (11).

In order to address the hazards associated with open flames, the Bureau of Home Furnishing and Thermal Insulation (BHFTI) recently introduced the California Technical Bulletin No. 603, Requirements and Test Procedure for Resistance of a Mattress/Box Spring Set to a large Open-Flame which is in effective 1st January, 2005 (12). This minimum requirement protocol provides a means of determining the burning behavior of mattress/foundation sets intended for any use by measuring specific fire test responses when the test specimen, a mattress plus foundation, is subjected to a specific flaming ignition source under well-ventilated conditions. When tested accordance with Cal TB 603, a mattress, a futon or a mattress/box spring set fails to meet the requirements of this test procedure if the peak rate of heat release exceeds 200 kW and total heat release exceeds 25 MJ in the first 10 minutes of the test. The BHFTI CAL TB 604 (draft) will address the flame resistance of filled bedclothing (13). The CPSC also published Advanced Notice of Proposed Rulemaking 16 CFR Part 1633 to develop a federal standard to address open flame ignition of mattresses/bedding in 2001 (11). Based on public comment, the CPSC should approve the final standard, which may go into effect as early as January, 2006. (14).

The California Bureau of Home Furnishing and Thermal Insulation also addressed the hazards associated with the ignition of mattresses in public institutions with Technical Bulletin No. 129, published as a draft standard in 1992 (15). It has since been adopted as a voluntary consensus standard by the American Society of Testing and Materials (ASTM) as ASTM E-1590. ASTM E-1590 and NFPA 267 use essentially the same test protocol as CAL TB 129 but contain no pass/fail criteria. The standard has also been embodied in NFPA's 101® Life Safety Code®, 2000, Section 10.3.4. (16). However, the failure criteria of Cal TB No. 129, maximum rate of heat release of less than 100 kW and a total energy release of less than 25 MJ in the first 10 minutes of the test have been modified to a maximum rate of heat release of less than 250 kW and a total energy release of less than 40 MJ in the first five minutes of the test in the Life Safety Code®.

Safeguard™ and Airflex foams can be utilized to make traditional flat surfaces or convoluted with “waffle design” or similar convoluted surfaces to meet the mattress flammability standards mentioned above. Airflex, Safeguard™ foams used to encapsulate fire-retardant polyurethane, has demonstrated excellent performance when fire-tested in composite to California Technical Bulletin No. 603 and No. 129. The use of Safeguard™ or Airflex as an exterior cushioning barrier provides facility occupants and consumers additional escape time in the event of a mattress being exposed to cigarettes or open flame ignition sources. In addition, the application as a resilient cushioning “barrier” eliminates potential “wear and tear” changes in long term testing performance which are possible with many fabric type barriers. This concept provides a beneficial and economical choice of fire-resistant mattresses for hospitals, nursing homes, universities and residential bedding.

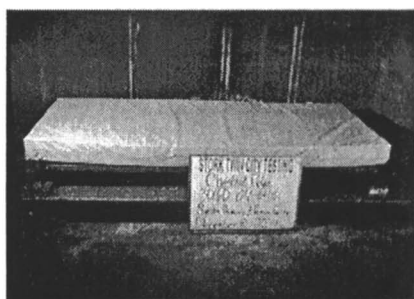
A comparison of the TB 603 open flame test results of a Siesta university or a long-term healthcare mattress in comparison to test criteria is shown in the Table IV. This mattress is constructed with Cal TB 117 foam core encapsulated with half-inch (12.7 mm) thickness CR Safeguard™ neoprene compound cushioning. The test results indicate extremely low values compared to the TB 603 criteria. The peak heat release rate value, 24.5 kW, showed a reduction of 88% and a total heat release rate value at 10 minutes of 1.4 MJ, showed a reduction of 94% compared to the TB 603 test criteria. During the test, all signs of combustion ceased after 6 min and 11 seconds of the test. Figure 2 shows before and after images of the mattress.

For increased fire-performance, Safeguard™ or Airflex cushioning can be used to make mattresses in a 4-6 inch (10.2-15.2 cm) full thickness for

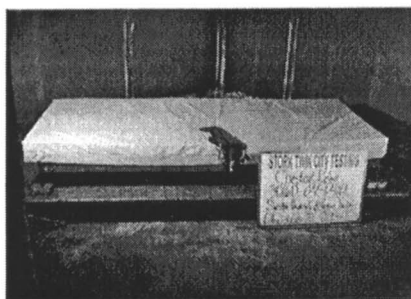
psychiatric and military applications to achieve high levels of comfortability as well as durability.

Table IV. Cal. TB No. 603 open flame test results of Siesta university or long-term healthcare mattress

<i>Test parameter</i>	<i>TB 603 Criteria</i>	<i>Results</i>	<i>Pass/Fail</i>
<i>Peak rate of heat release</i>	200 kW	24.5	Pass
<i>Total heat release @ 10 min</i>	25.0 MJ	1.4 MJ	Pass



Before Test



After Test

Figure 2. Cal TB 603 Test: Before and after images of the Siesta university or long-term healthcare mattress

US Navy Shipboard Mattress Applications

US Navy shipboard mattress/bedding assemblies must meet the NAVSEA PD-1-00, NFPA 267-98 (modified) standard test requirements for fire characteristics of mattresses and bedding assemblies exposed to flaming ignition source. In this modified test, the "T" burner was replaced with a 12" x 12" Ottawa silica sand burner and tested at 50 kW for the first 5-minutes and then increased to 100 kW for the remaining 10-minutes (Figure 3) as described in section 4.4.2.3.2 of the NAVSEA PD-1-00.

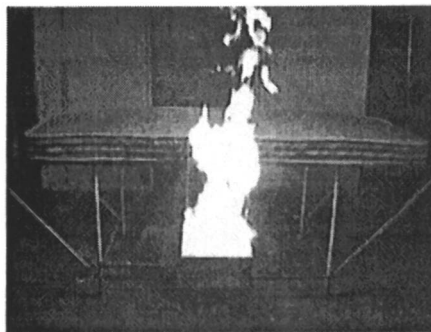


Figure 3. NAVSEA PD-1-00, NFPA 267-98 (modified) test with sand burner

These requirements are a) net peak heat release rate shall not exceed 150 kW b) no flaming droplets and c) average specific extinction area (Ave. SEA) shall not exceed 300 m²/kg. The Airflex foam mattresses prepared with 4 to 6 inch full thickness construction as well as inner spring constructions with Safeguard™ foam topper pads with LS-200(C) neoprene quilt backing will easily meet these requirements. The results are shown in Table V.

Table V. NAVSEA PD 1-00, NFPA 267-98 (Modified) Standard Test Results for Mattresses and Bedding Assemblies Exposed to Flaming Ignition Source (A) Shipboard Full Depth Mattress ; (B) Shipboard Innerspring Mattress Constructed with Safeguard™ Topper Pads & LS 200c Neoprene Quilt Backing (Mattress Dimensions: 76"x26"x4" Fabric: 100% FR Cotton).

	<i>Requirement</i>	<i>Results Mattress (A)</i>	<i>Results Mattress (B)</i>
Net Peak HRR	Shall not exceed 150 kW	23 kW	25 kW
Flaming Droplets	Shall not be formed & dropped	No flaming droplets	No flaming droplets
Ave. SEA	Shall not exceed 300 m ² /kg	66 m ² /kg	16 m ² /kg

The net peak heat release rate obtained for a 4" (10.2 cm) full depth mattress was 23 kW, an 85% reduction compared to the requirement. In addition, this foam mattress did not produce any flaming droplets. The average specific extinction area was 66 m²/kg, a reduction of 78 % compared to the requirement.

For the innerspring version of the mattress, these values were 25 kW of net peak heat release rate (83 % reduction with respect to the requirement), average specific extinction area of 16 m²/kg (a reduction of 95% compared to the requirement). This mattress also showed no flaming droplets.

Conclusions

Airflex is an open-cell, breathable, fire-resistant cushioning manufactured in distinct seat and back cushioning selections, in a variety of colors for comprehensive variety of firmness choices. In addition to lightweight, comfort, and excellent physical properties, the Airflex foam grades consistently and easily meet all fire-testing standards required by the Federal Aviation Administration including full-scale FAR 25.853 (c), Appendix F, Part II, oil burner test with weight loss ranging from 4.0% to 8.5% depending on the seat construction. Since these foam grades are highly flame resistant, it is not necessary to cover them with expensive fire blocking fabric materials (except the base of the seat bottom cushion with floatation foam fabrication) to meet the oil burner requirements. These foam grades and Safeguard™ cushioning grades can also be used to make healthcare, psychiatric, institutional, military, university, residential, and crib/youth mattresses that need to pass fire performance standards such as CAL. TB Nos. 121, 129, and 603, City of Boston BFD IX-11, ASTM E-1590, NFPA 101® Life Safety Code®, 2000, Section 10.3.4, and the US Navy (NAVSEA PD 1-00, NFPA 267-98 modified). The contract furniture applications with these foam grades easily comply with CAL. TB 133 and ASTM E-1537. Safeguard™ XL cushioning is designed to provide maximum cushion durability for rail and bus transportation vehicles and comply with component fire performance characteristics in accordance with the FTA and FRA regulations.

Cone calorimeter test results of Airflex, Safeguard™, and Safeguard™ XL cushioning products, even at 50 kW/m² heat exposure showed very low values for heat release rates, mass loss rates.

Disclaimer: Flammability results are based on small-scale laboratory tests for purpose of relative comparison and are not intended to reflect the hazards presented by these or any other materials under actual fire conditions.

References

1. *Opportunity Report*; Business Communication Company, (ISBN:1-56965-266-X), 1996.
2. Karter Jr., M.J. "Fire Loss in the United States During 2003", National Fire Protection Association, October, 2004.
3. *Aircraft Materials Fire Test Handbook*, DOT/FAA/AR-00/12, Office of Aviation Research, Washington, D.C., Final Report, April 2000.
4. Jayakody, C.; Myers, D.; Romanish, G.; Crocker, M.; Bridge, J.; Ogburn, C. The 12th Annual BCC Conference in Flame Retardancy, Stamford, CT, 2001.
5. Hasselbrack, S. "Alternate Cleaning Technologies" Phase III of IV; The Boeing Commercial Airplane Group; December, 2001.
6. Jayakody, C.; Myers, D.; Sorathia, U.; Nelson, G.L. *J. Fire Sci.*, **2000**, 18, 430-455.
7. *Federal Register*; Rail Passenger Equipment: Guidelines for selecting materials to improve their fire safety characteristics, Department of Transportation, 1984; Vol. 64.
8. *Technical Bulletin 133*; Flammability Test Procedure for Seating Furniture for Use in Public Occupancies, Bureau of Home Furnishing and Thermal Insulation, Department of Consumer Affairs, State of California; January, 1991.
9. The Standard for the Flammability of Mattresses and Mattress Pads, 16 CFR Part 1632, Consumer Product Safety Commission, May, 1991.
10. *Topical Fire Research Series*; US Fire Administration, March, 2002; Vol. 2, Issue 17.
11. *Federal Register*; October 2001; Vol. 66, No. 197.
12. *California Technical Bulletin 603*; Requirements and Test Procedure for Resistance of a Mattress/Box Spring Set to a Large Open-Flame, Bureau of Home Furnishing and Thermal Insulation, Department of Consumer Affairs, State of California, January 2004.
13. *Technical Bulletin 604 (Draft)*; Test Procedure and Apparatus for the Flame Resistance of Filled Bedclothing, October 1, 2004.
14. *Bed Times*; October 2004, p 56.
15. *Technical Bulletin 129*; Flammability Test Procedure for Mattresses for Use in Public Buildings, October, 1992.
16. NFPA 101® Life Safety Code® 10.3.4; 2003 Edition.

Chapter 24

Molecular Modeling of the Thermal Decomposition of Polymers

**Stanislav I. Stoliarov^{1,*}, Phillip R. Westmoreland², Huiqing Zhang²,
Richard E. Lyon³, and Marc R. Nyden⁴**

¹Galaxy Scientific Corporation, 3120 Fire Road, Egg Harbor
Turnpike, NJ 08234

²Chemical Engineering Department, University of Massachusetts at
Amherst, Amherst, MA 01003

³W. J. Hughes (FAA) Technical Center, Fire Safety Branch AAR-440,
Atlantic City International Airport, NJ 08405

⁴Building and Fire Research Laboratory, National Institute of Standards
and Technology (NIST), Gaithersburg, MD 20899

Applications presented in this chapter demonstrate the potential for using quantum chemical methods and molecular simulations to determine the mechanisms and rates of the thermal decomposition of polymers. Our expectation is that these capabilities can be used to predict materials flammability and develop strategies to improve fire resistance. The thermal decompositions of poly(dihydroxybiphenylisophthalamide) and bisphenol C polycarbonate are investigated by performing density-functional calculations of potential energy surfaces of model compounds representing the polymers. Reactive molecular dynamics, a relatively new technique that extends conventional molecular dynamics to modeling chemical reactions, is used to simulate the thermal decomposition of polyisobutylene. The advantages and limitations of both computational approaches are discussed.

Introduction

Computational chemistry, which embraces the application of methods of quantum, classical, and statistical mechanics to molecules and molecular assemblies, offers new possibilities for the investigation of materials flammability. In principle, these methods can be used to determine the mechanisms and calculate the rates of thermal decomposition reactions, thereby providing guidance for the development of new and more fire-resistant materials. Indeed, the ability of these methods to predict thermodynamics and kinetics of chemical reactions involving small gas-phase molecules is well established (1, 2). Unfortunately, the extension of the methods to large molecules, such as polymers, in the condensed phase introduces many conceptual and computational challenges. Nevertheless, the results from our recent studies (3-6) demonstrate that it is possible to obtain valuable information about the mechanism and kinetics of polymer decomposition by means of computational chemistry.

Here we present an overview of our studies of the thermal decompositions of poly(dihydroxybiphenylisophthalamide) (3), bisphenol C polycarbonate (4), and polyisobutylene (6). Poly(dihydroxybiphenylisophthalamide) (PHA) and bisphenol C polycarbonate (BPC) are among the most fire-resistant polymers ever tested. Their thermal degradation results in the formation of a large amount of char (about 50 % by weight) and the release of nearly noncombustible gasses (7, 8). In an effort to determine the source of this exceptional fire performance, the decomposition chemistries of both PHA and BPC were investigated by performing quantum chemical calculations to determine the most probable reaction paths. Based on the results of these calculations, the chemical mechanisms responsible for the unusual high-temperature behavior of these materials were proposed. A relatively new method, called reactive molecular dynamics (RMD), was employed to study the thermal decomposition of polyisobutylene (PIB). The results of the RMD calculations provided a detailed, dynamic picture of the decomposition process and led to important observations about the kinetics of key elementary reactions.

Quantum Chemical Calculations of Reaction Paths

The B3LYP density-functional method (9) was used in combination with the 6-31G(d) and 6-31G(d,p) basis sets (10) to calculate potential energies of model

compounds representing the molecular structures of PHA and BPC. The model compounds contained up to 19 multi-electron (non-hydrogen) atoms. This method was chosen to achieve the maximum accuracy within a reasonable computational time. A basis set with additional functions on the hydrogen atoms (the 6-31G(d,p) basis set) was used for the PHA calculations because of the expectation that these atoms play an important role in the decomposition process.

Potential energy surfaces of the model compounds (i.e. dependencies of potential energies of the compounds on internal atomic coordinates) were carefully examined in order to identify transition states leading to chemical transformations. Intrinsic reaction coordinate (IRC) reaction-path-following calculations (11) were performed for the transition states in order to establish the connected reactants and products. The structures of the reactants, products, and transition states were optimized. The energies of the optimized structures were corrected for zero-point energy contributions. No corrections for basis set superposition errors were made. These energies were subsequently used in the analyses of chemical mechanisms. During the analyses of competing reactions, it was usually assumed that the most probable reaction channel is the one with the lowest energy barrier. However, only differences in energy larger than 40 kJ/mol, which is about twice the average error of the method (4), were considered as a conclusive evidence of the domination of one reaction channel over the other. All quantum chemical calculations were carried out using the Gaussian 98 package of programs (12).

PHA

It is well established (7) that, when heated, PHA converts to polybenzoxazole (PBO), which is an extremely thermally stable material. To a large degree, this explains the high fire resistance of PHA. However, the detailed mechanism of the decomposition reaction, which is shown in Figure 1, is not known.

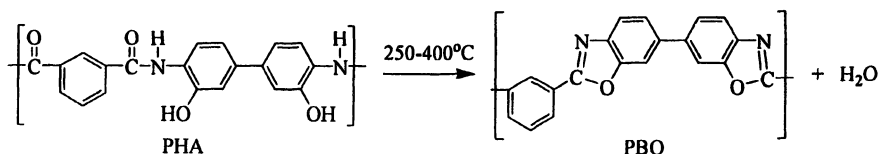


Figure 1. Thermal decomposition of PHA.

In order to determine the mechanism, we analyzed the potential energy surface of a model compound, HA, shown in Figure 2. This compound represents a PHA fragment that undergoes the cyclodehydration reaction. Our analysis led to the conclusion that this reaction is not a single-step process. Before HA cyclizes, it has to undergo a keto-enol rearrangement. Two possible mechanisms for this rearrangement are shown in Figure 2. The direct transfer of a hydrogen atom (top diagram) has a substantial energy barrier. However, this barrier is reduced by almost a factor of 3 when an external hydroxyl group participates in the rearrangement (bottom diagram). Presumably, the hydroxyl group comes from an adjacent PHA chain (which was represented by vinyl alcohol in the calculations) or a water molecule, which is an expected contaminant.

Two conformations of the EN compound, which is formed as a result of the keto-enol rearrangements, were found to be capable of cyclization. These conformations are depicted in Figure 3. Transformations between EN conformers require between 30 and 70 kJ/mol and are omitted here. A detailed description of these transformations can be found in (3). According to the mechanisms presented in Figure 3, the cyclization of EN may proceed through a single transition state (top diagram) or through a sequence of two transition states separated by an intermediate (bottom diagram). The latter reaction path is much more energetically accessible and, thus, more probable. Regardless of whether or not an external hydroxyl group is involved in the keto-enol rearrangement, the total energy required for the cyclodehydration of HA is about 170 kJ/mol. This is significantly less than 320 kJ/mol that is required to break the backbone of PHA (3). On this basis, it was concluded that the polymer should convert to PBO before any fragmentation of the chains takes place, which is consistent with experimental observations.

BPC

As shown in Figure 4, hydrogen chloride, carbon dioxide, and char are among the major products of the thermal decomposition of BPC (8). The unusually high char yield suggests that cyclization and crosslinking dominate the decomposition process. In order to determine the mechanism of the process, we examined a number of reactions that could potentially lead to cyclization and/or

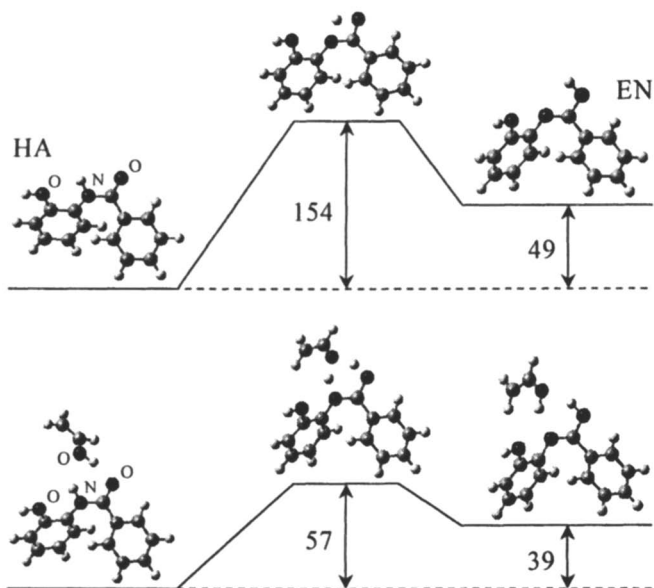


Figure 2. Keto-enol rearrangements. Energy values are in kJ/mol

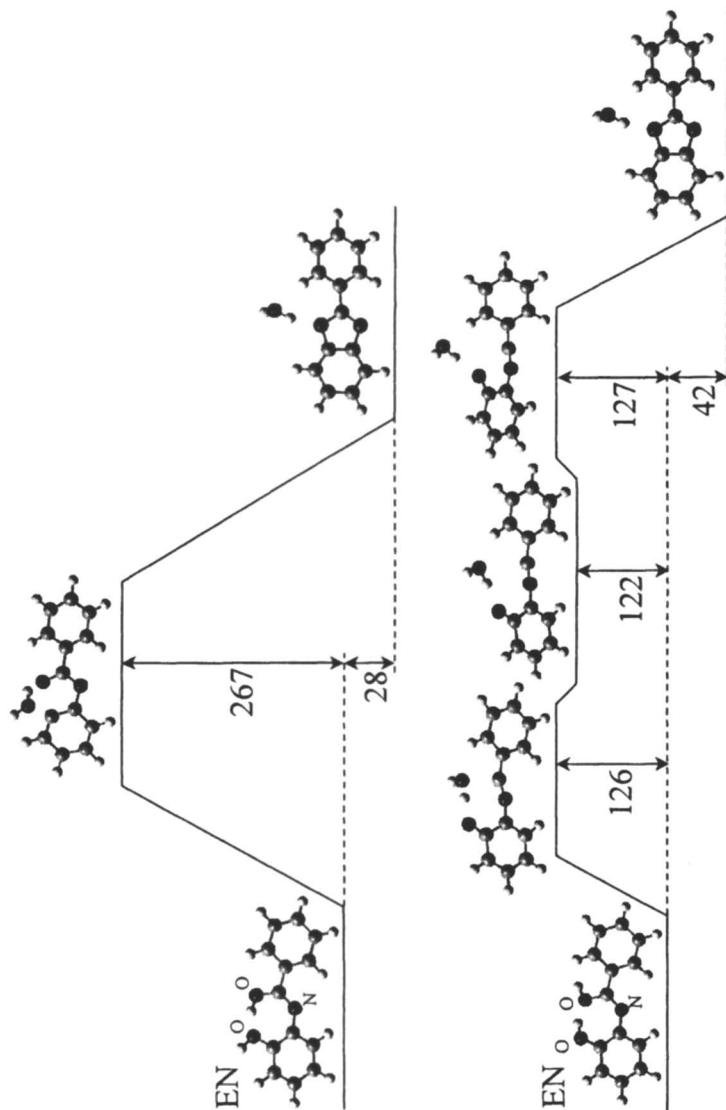


Figure 3. Cyclizations. Energy values are in kJ/mol.

crosslinking of the polymer. The reaction paths for Cl_2 elimination, one-step HCl elimination, C-Cl bond dissociation, and Cl-atom shift were calculated. According to the calculations, the energy barriers of these reactions are 400, 380, 330, and 300 kJ/mol , respectively. The first two reactions were ruled out based on energetics. A detailed description of these reactions is given in (4). The last two reactions were found to be both energetically and mechanistically similar. The Cl-atom shift was identified as the key reaction that takes place at the initial stages of the thermal decomposition. However, the possibility that the C-Cl bond dissociation also plays a major role in the decomposition process could not be ruled out.

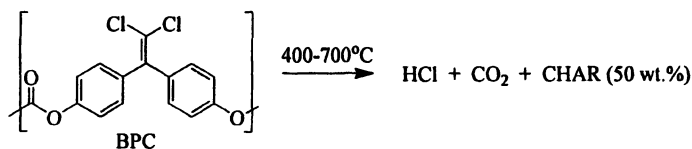


Figure 4. Thermal decomposition of BPC.

The Cl-atom shift is a reaction where a chlorine atom moves from its original position in BPC onto the adjacent phenyl ring. The reaction path, which was calculated using the β,β -dichlorostyrene model compound, is shown in Figure 5. Once the shift occurs, the Cl atom can move freely around the ring structure. The fact that a Cl atom can bond with one as well as two phenyl rings (4) indicates that, in an environment with a high density of the rings, migration of the atom from one ring to another will also require little or no energy. Thus, the Cl-atom shift in BPC should be similar to the C-Cl bond dissociation, with the exception that the energy required for the former reaction is lower due to the stabilization provided by Cl-phenyl interactions.

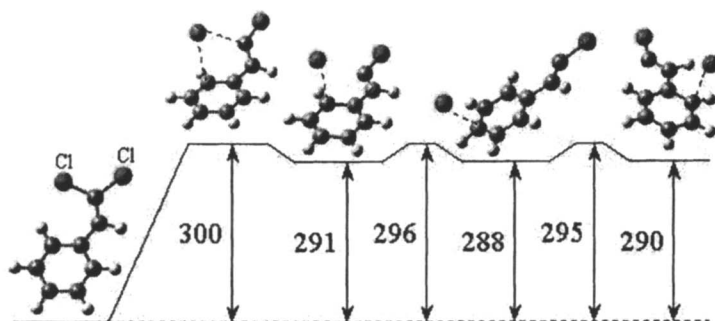


Figure 5. Cl-atom shift. Energy values are in kJ/mol .

Cl atoms migrating around and between the phenyl rings are likely to abstract hydrogens attached to the rings. According to the mechanisms shown in Figure 6, these abstraction reactions have relatively low energy barriers. The reactions lead to cyclization and to the formation of phenyl radical sites. In the context of decomposing BPC structure, this results in internal cyclization of the polymer and the formation of highly reactive centers capable of establishing strong covalent crosslinks between the chains. Chlorovinyl radical sites, which are formed as a result of the Cl-atom shifts, may also be involved in crosslinking. In addition, these radical sites may participate in phenyl-ring shifts followed by eliminations of the Cl atoms (4), which, in turn, lead to the formation of diphenylacetylene structural elements in the decomposing polymer. The cyclization and crosslinking reactions, which result in the formation of char, are expected to compete with the scissions of the O-C(O) backbone bonds (the weakest covalent bonds in BPC (4)), which result in fragmentation of the polymer chains and the subsequent elimination of CO₂.

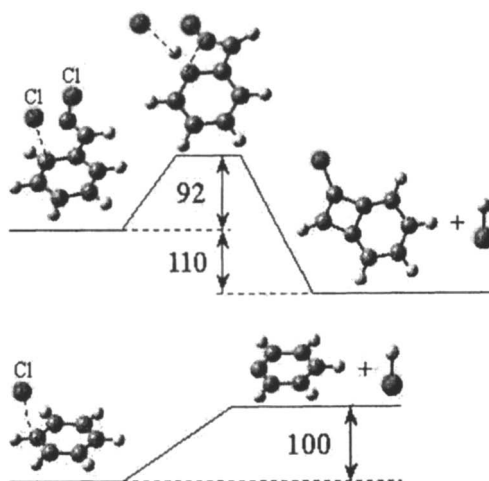


Figure 6. Abstractions of H atoms by Cl atoms. Energy values are in kJ/mol.

Reactive Molecular Dynamics

The RMD method is based on conventional molecular dynamics, which makes use of analytical expressions (force field) that define the interactions between atoms. The atomic trajectories, obtained by numerical integration of the classical equations of motion, provide a time-resolved description of the system

under study. The feature that distinguishes RMD from other force-field-based implementations of molecular dynamics is that it is capable of modeling chemical reactions.

The current implementation of RMD, a detailed description of which is given in (6), uses a version of the Consistent Valence Force Field (13), which was modified and calibrated to accommodate some general features of reactive potential energy surfaces. In this force field, the energy of a molecular system is represented as a sum of contributions from covalent bonds (defined by Morse potentials), bond angles (including torsions), and non-bonded interactions. In order to model chemical transformations, the RMD employs the following algorithm. After every time step of molecular dynamics, fractional bond orders, which are defined as $1 - V/D$, where V/D is the ratio of the bond energy to the bond dissociation energy, are computed for every covalent bond. The bond orders are then compared to a pre-defined bond-dissociation criterion (BDC). If a fractional bond order is less than or equal to BDC , the bond is eliminated and the atoms that had been connected are labeled as chemically active (if the bond order is higher than BDC , no action is taken with respect to that bond). Next, a set of new bonds is generated, consisting of all possible covalent interactions between the chemically active atoms. The most energetically favorable subset of the new bonds that complies with the rules of atomic valence is selected. If the total number of bonds to an atom is equal to its valence and the fractional bond order of each of its bonds is higher than BDC , then the chemically active label is removed from the atom. Otherwise, if an atom retains its chemically active status, it is allowed to form one additional bond; provided that the sum of the bond orders associated with the valence + 1 bonds to that atom does not exceed its valence. This feature is used to describe chemical reactions that occur via so-called hypervalent transition states, such as abstraction or radical disproportionation reactions. Once the bond analysis is complete and the structural information is updated, the next time step of molecular dynamics is executed.

It should be noted that, as the result of the procedure described above, the bonds between atoms are not formally removed unless they are replaced by new more energetically favorable bonds. For the purpose of quantifying chemical events, a covalent bond between atoms is considered to be broken when its energy is within $0.25RT$ (R is the ideal gas constant and T is the simulation temperature) of the dissociation energy. The bond-dissociation criterion determines whether covalently bonded atoms are eligible to participate in chemical reactions. In the simulations described below, BDC was set to 0.8, which means that an atom was labeled as chemically active when at least one of its stretched covalent bonds reached the energy that was equal to or higher than 20 % of the bond dissociation energy. The RMD is implemented as a Fortran/C computer code, MD_REACT program, interfaced with Discover 95, which is

commercially available molecular dynamics software offered by Accelrys Inc^a. The function of the MD_REACT is to compute the reactive force field, while Discover 95 updates the molecular geometry based on the solution of the equations of motion.

PIB

The thermal decomposition of PIB has been studied experimentally by a number of investigators (14-16). According to these studies, the mechanism of the decomposition can be summarized by the set of reactions shown in Figure 7.

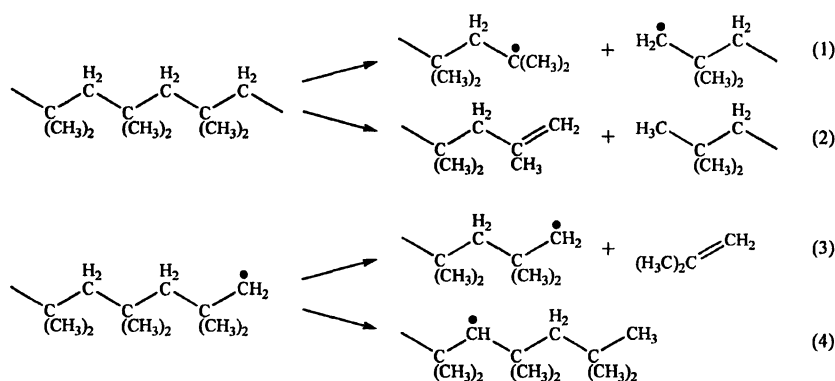


Figure 7. Mechanism of the thermal decomposition of PIB.

In all studies, homolytic scissions of the backbone and depolymerization reactions (reactions 1 and 3 in Figure 7) are considered to be important. There are, however, notable disagreements between investigators regarding the roles and mechanisms of reactions involving transfer of a hydrogen atom (reactions 2 and 4 in Figure 7).

Four single-chain models of PIB consisting of 4, 14, 50, and 150 isobutylene units were used in the RMD simulations of the decomposition process. Periodic boundary conditions were employed in the simulations involving the 14, 50, and 150-unit models to account for the condensed-phase

^a Certain commercial equipment, instruments, materials, or companies are identified in this paper in order to adequately specify the procedure. This in no way implies endorsement or recommendation by NIST.

environment. The 4-unit model, however, was treated as a single gas-phase molecule. Simulations were performed at a series of temperatures between 1300 and 1750 K. The lowest temperature was dictated by the necessity to observe reactive events within computationally feasible simulation times. The thermal motion was initiated by assigning each atom a velocity, with Cartesian components chosen at random from a Maxwell-Boltzmann velocity distribution. The reactive dynamics were run for 5-100 ps (longer times were used at lower temperatures and with smaller models). In order to accumulate statistics on chemical reactions, between 11 and 70 RMD simulations were done for each model at every temperature.

A still frame from an RMD trajectory of the 150-unit model of PIB is shown in Figure 8. According to the results of the simulations, homolytic backbone scission and subsequent depolymerization of the resulting radicals (reactions 1 and 3 in Figure 7) are the dominant decomposition reactions for all models within the examined range of temperatures. The only hydrogen transfer reactions observed in the simulations were hydrogen abstractions involving small molecules (smaller than the dimer). Aside from occasional terminations of the depolymerization process, these reactions had little effect on the decomposition of the polymer chains.

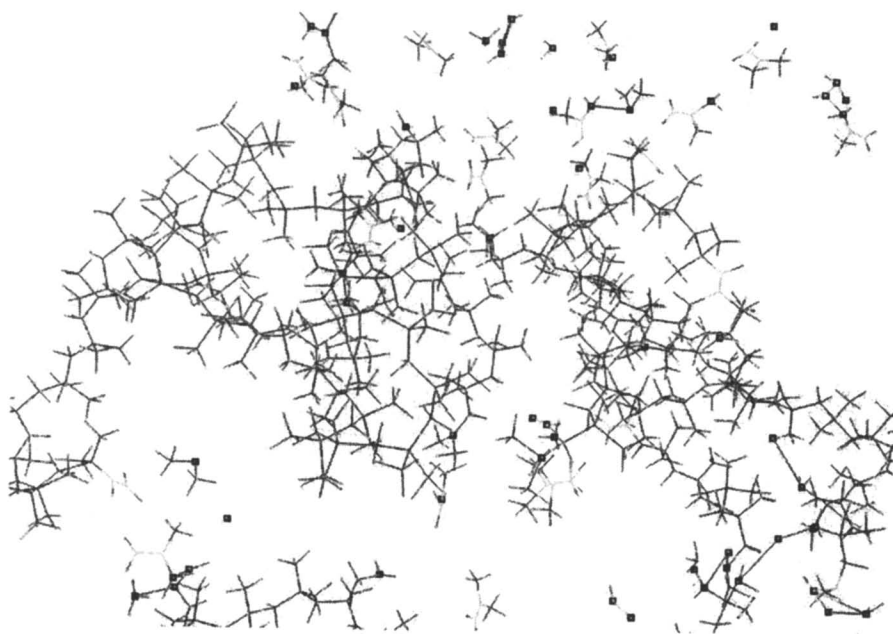


Figure 8. The 150-unit model of PIB after 10 ps of reactive dynamics at 1525 K. The black dots are chemically active atoms.

The times to the first backbone scission determined from the simulations were used to calculate the rate constants of the initiation reaction. The rate constants were normalized by the initial number of backbone bonds in the PIB models to provide a common basis for comparing results from models having different chain lengths. Arrhenius fits of the temperature dependence of the rate constants revealed that the pre-exponential factors and activation energies decrease systematically with increasing size of the model. The Arrhenius parameters change from a pre-exponential factor of $2 \times 10^{17} \text{ s}^{-1}$ and an activation energy of 240 kJ/mol, obtained for the 4-unit model (gas-phase tetramer), to a pre-exponential factor of $1 \times 10^{15} \text{ s}^{-1}$ and an activation energy of 170 kJ/mol, obtained for the 150-unit model. Based on the observation of these trends, it was concluded that the kinetics of the backbone scission reaction is affected by the density and by the degree of polymerization of the decomposing polymer. This means that the conventional approach to the kinetic modeling of polymer decomposition, in which the chain scission rate constants are assigned values obtained from the measurements performed on small gas-phase molecules, is not generally valid. This approach should be modified to account for the potential effects of the macromolecular environment on the rate of the scission reactions. For a complete description of the RMD simulations and comparison of the simulation results with experimental observations, see (6).

Concluding Remarks

Each of the computational approaches discussed in this chapter has its own advantages and limitations. The quantum chemical approach is an effective tool for mapping complex chemical transformations that are localized on a small segment of a polymer structure. The information obtained from the quantum chemical calculations can be used in combination with statistical reaction rate theories (17) to determine rate constants of the model reactions. However, it is not clear whether the calculated rate constants would represent the kinetics of the corresponding reactions in the polymer melt because the presence of the surrounding molecular structure (the condensed-phase) is ignored in the calculations.

The application of RMD makes it possible to capture the effects of the condensed-phase environment. Unlike in the case of the quantum chemical approach, RMD simulations do not require a priori assumptions about reaction mechanisms. However, despite these advantages, RMD does have several drawbacks. Currently, the computationally accessible time scales of these calculations are several orders of magnitude shorter than what is needed to make direct comparisons with experimental measurements on burning polymers. Even more important is the issue of force field accuracy. In order for RMD to produce

reliable quantitative results, the force field should be able to reproduce reactive potential energy surfaces with chemical accuracy (be accurate within about 5 kJ/mol). The development and validation of a force field that is capable of this level of accuracy, even for a small number of chemical elements, is a grand challenge. Further complications arise from the fact that RMD uses classical mechanics to simulate quantum mechanical systems. That is, there is no accounting for the discrete nature of molecular vibrations or tunneling. It is apparent that, to a large degree, RMD and the quantum chemical approach (combined with statistical reaction rate theories) are complementary. We are actively pursuing the development of methodologies that combine best features of both approaches.

References

1. *Computational Thermochemistry: Prediction and Estimation of Molecular Thermodynamics*; Irikura, K. K.; Frurip, D. J., Eds.; ACS Symposium Series; ACS: Washington, DC, 1998.
2. *Modern Methods for Multidimensional Dynamics Computations in Chemistry*; Thompson, D. L., Ed.; World Scientific: Singapore, 1998.
3. Zhang, H. Ph.D. thesis, University of Massachusetts Amherst, Amherst, MA, 2004.
4. Stoliarov, S. I.; Westmoreland, P. R. *Polymer* **2003**, *44*, 5469.
5. Stoliarov, S. I.; Westmoreland, P. R.; Nyden, M. R.; Forney, G. P. *Polymer* **2003**, *44*, 883.
6. Stoliarov, S. I.; Lyon, R. E.; Nyden, M. R. *Polymer* **2004**, *45*, 8613.
7. Zhang, H.; Farris, R. J.; Westmoreland, P. R. *Macromolecules* **2003**, *36*, 3944.
8. Stewart, J. R. Technical Report DOT/FAA/AR-00/39; U. S. Department of Transportation: Washington, DC, 2000.
9. Becke, A. D. *J. Chem. Phys.* **1993**, *98*, 5648.
10. Hehre, W. J.; Radom, L.; Schleyer, P. v. R.; Pople, J. A. *Ab Initio Molecular Orbital Theory*; Wiley-Interscience: New York, 1986.
11. Gonzalez, C.; Schlegel, H. B. *J. Phys. Chem.* **1990**, *94*, 5523.
12. Frisch, M. J.; Trucks, G. W.; Schlegel, H. B.; Scuseria, G. E.; Robb, M. A.; Cheeseman, J. R.; Zakrzewski, V. G.; Montgomery, J. A. Jr.; Stratmann, R. E.; Burant, J. C.; Dapprich, S.; Millam, J. M.; Daniels, A. D.; Kudin, K. N.; Strain, M. C.; Farkas, O.; Tomasi, J.; Barone, V.; Cossi, M.; Cammi, R.; Mennucci, B.; Pomelli, C.; Adamo, C.; Clifford, S.; Ochterski, J.; Petersson, G. A.; Ayala, P. Y.; Cui, Q.; Morokuma, K.; Malick, D. K.; Rabuck, A. D.; Raghavachari, K.; Foresman, J. B.; Cioslowski, J.; Ortiz, J. V.; Stefanov, B. B.; Liu, G.; Liashenko, A.; Piskorz, P.; Komaromi, I.; Gomperts, R.; Martin,

- R. L.; Fox, D. J.; Keith, T.; Al-Laham, M. A.; Peng, C. Y.; Nanayakkara, A.; Gonzalez, C.; Challacombe, M.; Gill, P. M. W.; Johnson, B.; Chen, W.; Wong, M. W.; Andres, J. L.; Head-Gordon, M.; Replogle, E. S.; Pople, J. A. *Gaussian 98*, Revision A.9; Gaussian, Inc.: Pittsburgh, PA, 1998.
13. Dauber-Osguthorpe, P.; Roberts, V. A.; Osguthorpe, D. J.; Wolff, J.; Genest, M.; Hagler, A. T. *Proteins: Structure, Function and Genetics* **1988**, *4*, 31.
 14. Madorski, S. L. *Thermal degradation of organic polymers*; Interscience Publishers: New York, 1964.
 15. Sawaguchi, T.; Seno, M. *Polymer* **1996**, *37*, 5607.
 16. Lehrle, R. S.; Pattenden, C. S. *Polym. Degrad. Stab.* **1999**, *63*, 321.
 17. Gilbert, R. G.; Smith, S. C. *Theory of Unimolecular and Recombination Reactions*; Blackwell Scientific: Oxford, 1990.

Chapter 25

Smoke Toxicity Measurements of Automotive Materials

**Keith R. Willson, Marc L. Janssens, A. Leigh Griffith,
Karen C. Carpenter, and Jason P. Huczek**

**Department of Fire Technology, Southwest Research Institute,
6220 Culebra Road, San Antonio, TX 78238-5166**

A recent research program conducted for the Motor Vehicle Fire Research Institute examined the yields of gases generated during the combustion of automotive materials. Eighteen materials taken from the exterior of a passenger van and a sports coupe were exposed to radiant heat fluxes of 20, 35, and 50 kW/m² using a Cone Calorimeter. Gas samples taken from the exhaust duct were analyzed using an FTIR spectrometer to quantify the yields of CO, CO₂, HCl, HCN, and NO_x. Three materials, representing low, intermediate, and high peak CO concentrations in the Cone Calorimeter testing, were further evaluated using two commonly used smoke chamber test methods: ASTM E 662 and ISO 5659-2. Yield data are presented for each of the materials tested, along with a discussion of the test methods and the relationships between the results generated by the various methods.

A recent research program conducted for the Motor Vehicle Fire Research Institute (MVFRI) examined the yields of toxic gases generated during the combustion of exterior automotive materials. These gases contribute to physical incapacitation, loss of motor coordination, faulty judgment, disorientation, restricted vision, and panic, all of which inhibit or prevent egress from a burning vehicle. Irritants such as halogen gases (HCl, HF, and HBr) and nitric oxide are generally not fatal during inhalation, but can cause post exposure fatality due to pulmonary damage. Asphyxiants such as CO and HCN can cause loss of consciousness and possibly death during exposure.

Several fire scenarios contribute to the number of deaths and injuries in post-crash motor vehicle fires. The program reported in this paper focuses on fires following a front-end collision that originate in the engine compartment and propagate to the passenger compartment. The smoke toxicity measurements reported below were obtained in conjunction with a flammability study on automotive materials that was conducted for the National Highway Traffic Safety Administration (NHTSA).

Material Suite

Materials for this study were selected based on previous full-scale studies conducted at the Factory Mutual Research Center (currently FM Global Research) (1,2) and flammability studies performed at the Building and Fire Research Laboratory (BFRL) of the National Institute of Standards and Technology (NIST) on parts taken from a passenger van and a sports coupe (3,4). Ten parts were selected from a 1996 Dodge Caravan, and eight parts were selected from a 1997 Chevrolet Camaro. Tables I and II show the list of parts, along with the base polymer composition of each component. Components of each part that could be separated were tested individually.

Toxic Gas Measurements

The concentrations of toxic gases generated by the materials used in this study were quantified using a ThermoNicolet Magna 560 Fourier Transform Infrared (FTIR) spectrometer with a 2-meter gas cell, calibrated at a resolution of $\frac{1}{2} \text{ cm}^{-1}$ against known concentrations of the toxic gases to be quantified. Yield data were then calculated from the measured concentrations and mass loss data. Combustion byproducts were generated using three different methods: Cone Calorimetry (ASTM E 1354 (5)) and two variations of smoke chamber tests (ASTM E 662 (6) and ISO 5659-2 (7)).

Table I. 1996 Dodge Caravan Test Samples

<i>Part Number</i>	<i>Description</i>	<i>Base Composition</i>
5235267AB	Battery Cover	Polyethylene
4861057	Resonator Structure	Polypropylene
53030508	Resonator Intake Tube	Polypropylene/EPDM
4678345	Air Ducts	Polyethylene or Polypropylene
4683264	Brake Fluid Reservoir	Polypropylene
4860446	Kick Panel Insulation Backing – Rubber Side	Polyvinylchloride
4857041A	Headlight – Clear Lens	Polycarbonate
4857041A	Headlight – Black Casing	Polycarbonate
4716345B	Fender Sound Reduction Foam	Polystyrene
4716832B	Hoodliner Face	Polyethylene terephthalate
4716051	Windshield Wiper Structure	Glass reinforced thermoset polyester resin cross-linked with styrene

Table II. 1997 Chevrolet Camaro Test Samples

<i>Part Number</i>	<i>Description</i>	<i>Base Composition</i>
10296526	Front Wheel Well Liner	Polypropylene/ Polyethylene copolymer
10297291	Air Inlet	Polyethylene/ Polypropylene
10278015	Hood Insulator – Foil Side	Polyamide 6 and phenolic binder (Novalac)
10278015	Hood Insulator – Fiber Side	Phenolic binder (Novalac)
52465337	Radiator Inlet/Outlet Tank	Polyamide 6,6
22098787	Engine Cooling Fan	Polyamide 6
26019594	Power Steering Fluid Reservoir	Polyamide 6,6
10310333	Laminated Windshield	Unknown
52458965	Heater Module Blower Motor Housing	Polypropylene

Cone Calorimeter Measurements

All eighteen parts were tested in duplicate in the Cone Calorimeter at three different radiant heat fluxes: 20, 35, and 50 kW/m². Specimens of small parts were prepared by piecing together smaller sections cut from each part.

The method used to collect gas samples and determine the concentrations of the various gases followed the recommendations of ASTM E 800 (8) and the SAFIR report (9). A horizontal, multi-holed, stainless steel sampling probe with holes oriented downstream was used to collect samples from the Cone Calorimeter exhaust duct. The PTFE-lined transfer line was heated to a temperature of 150°C to prevent losses due to condensation in the line.

Samples were collected semi-continuously throughout each test. Eight IR scans were collected and added into a single IR spectrum to improve the signal-to-noise ratio. The data calculated from each spectrum represented the average gas concentration over the collection period (approximately 30 seconds). Multiple spectra were collected during each test, resulting in a concentration profile as a function of time.

Yields of CO were calculated for each specimen at each exposure level. Data for average CO yields from the 50-kW/m² exposures are presented in Tables III and IV. Yields at lower heat fluxes were generally comparable or lower. They were also less repeatable, due to the lower measured concentrations.

Four of the materials were made of nitrogen-containing polymers. The gases generated by these materials were analyzed to quantify the levels of NO_x and HCN. The data for average yields from the 50-kW/m² exposures are presented in Table V.

Table III. Average CO Yields for 1996 Dodge Caravan Test Samples at 50 kW/m² Cone Calorimeter Exposure

<i>Part Number</i>	<i>Description</i>	<i>CO Yield (mg/g)</i>
5235267AB	Battery Cover	13
4861057	Resonator Structure	28
53030508	Resonator Intake Tube	21
4678345	Air Ducts	24
4683264	Brake Fluid Reservoir	25
4860446	Kick Panel Insulation Backing – Rubber Side	9.0
4857041A	Headlight – Clear Lens	50
4857041A	Headlight – Black Casing	54
4716345B	Fender Sound Reduction Foam	52
4716832B	Hoodliner Face	140
4716051	Windshield Wiper Structure	36

Table IV. Average CO Yields for 1997 Chevrolet Camaro Test Samples at 50 kW/m² Cone Calorimeter Exposure

<i>Part Number</i>	<i>Description</i>	<i>CO Yield (mg/g)</i>
10296526	Front Wheel Well Liner	31
10297291	Air Inlet	21
10278015	Hood Insulator – Foil Side	DNI ^a
10278015	Hood Insulator – Fiber Side	50
52465337	Radiator Inlet/Outlet Tank	13
22098787	Engine Cooling Fan	15
26019594	Power Steering Fluid Reservoir	26
10310333	Laminated Windshield	2.7
52458965	Heater Module Blower Motor Housing	25

^a Did Not Ignite. The very low mass loss made the yield calculation extremely unreliable.

Table V. Average NO_x and HCN Yields for Nitrogen-Containing Test Samples at 50 kW/m² Cone Calorimeter Exposure

<i>Part Number</i>	<i>Description</i>	<i>NO_x Yield (mg/g)</i>	<i>HCN Yield (mg/g)</i>
10278015	Hood Insulator – Foil Side	DNI ^a	DNI ^a
52465337	Radiator Inlet/Outlet Tank	15	5.0
22098787	Engine Cooling Fan	12	4.5
26019594	Power Steering Fluid Reservoir	1.4	6.3

^a Did Not Ignite. The very low mass loss made the yield calculation extremely unreliable.

The Kick Panel Insulation Backing – Rubber Side (Part Number 4860446) was the only part made from chlorine-containing material used in this study. The gas generated by this part was analyzed to quantify the level of HCl. The average yield during the 50-kW/m² exposure was 2.7 mg/g.

Smoke Chamber Measurements

Three parts were chosen for further testing based on the maximum CO concentrations ($[\text{CO}]_{\text{max}}$) measured using the Cone Calorimeter. The three parts represented high, low, and intermediate $[\text{CO}]_{\text{max}}$. None of the materials chosen contained significant amounts of nitrogen, and only one (Kick Panel Insulation Backing – Rubber Side, Part Number 4860446) contained significant amounts of chlorine. Information about these parts is listed in Table VI. These parts were tested in general accordance with ISO 5659, Part 2, and in general accordance with ASTM E 662.

Table VI. Parts Used for Smoke Chamber Measurements

<i>Part Number</i>	<i>Description</i>	<i>Base Composition</i>	<i>[CO]_{max}</i> <i>(ppm)</i>
4857041A	Headlight – Clear Lens	Polycarbonate	400
4716832B	Hoodliner Face	Polyethylene terephthalate	210
4860446	Kick Panel Insulation Backing – Rubber Side	Polyvinylchloride	46

In ISO 5659, Part 2, a horizontally oriented specimen is exposed to a radiant heat flux while enclosed in a 914 x 914 x 610-mm, airtight chamber. A load cell is used to record mass loss of the specimen. For the purposes of this study, three specimens of each of the three parts were tested in each of three exposure modes: a heat flux of 25 kW/m² with a pilot flame, a heat flux of 25 kW/m² without a pilot flame, and a heat flux of 50 kW/m² without a pilot flame. During the testing of the second and third specimen for each mode, the evolved gases were sampled from the geometrical center of the test chamber within three minutes of the time when the maximum specific optical density of smoke was reached. The gas samples were then analyzed as described above to determine the peak concentrations of toxic gases. Average yields were then determined on the basis of the mass of each toxic gas in the chamber and the total mass loss at the time of sampling. Peak CO concentrations and average CO yields are listed in Tables VII and VIII. Peak HCl concentrations and average HCl yields for the Kick Panel Insulation Backing–Rubber Side specimens are listed in Table IX.

In ASTM E 662, a vertically oriented specimen is exposed to a radiant heat flux while enclosed in a 24 x 36 x 24-inch, airtight chamber. For the purposes of this study, two specimens of each of the three parts were tested in each of two exposure modes: a heat flux of 25 kW/m² with a pilot flame, and a heat flux of 25 kW/m² without a pilot flame. Smoke gases were sampled for three minutes, starting four minutes after the start of the exposure. The gas samples were then analyzed as described above to quantify the levels of toxic gases. CO concentrations and average CO yields are listed in Table X. Peak HCl

Table VII. Peak CO Concentrations and Average CO Yields (ISO 5659-2, 25 kW/m²)

<i>Description</i>	<i>Non-Piloted</i>		<i>Piloted</i>	
	<i>Peak</i> <i>[CO]</i> <i>(ppm)</i>	<i>Average</i> <i>Yield</i> <i>(mg/g)</i>	<i>Peak</i> <i>[CO]</i> <i>(ppm)</i>	<i>Average</i> <i>Yield</i> <i>(mg/g)</i>
Headlight – Clear Lens	2	1	17	3
Hoodliner Face	5100	180	3700	110
Kick Panel Insulation Backing – Rubber Side	89	25	190	4

Table VIII. Peak CO Concentrations and Average CO Yields (ISO 5659-2, 50 kW/m²)

<i>Description</i>	<i>Non-Piloted</i>	
	<i>Peak [CO] (ppm)</i>	<i>Average Yield (mg/g)</i>
Headlight – Clear Lens	1300	74
Hoodliner Face	3500	150
Kick Panel Insulation Backing – Rubber Side	990	25

Table IX. Peak HCl Concentrations and Average HCl Yields for Kick Panel Insulation Backing – Rubber Side (ISO 5659-2, Various Exposures)

<i>Exposure</i>	<i>Peak [HCl] (ppm)</i>	<i>Average Yield (mg/g)</i>
25 kW/m ² , Non-Piloted	36	12
25 kW/m ² , Piloted	19	3
50 kW/m ² , Non-Piloted	1200	49

**Table X. CO Concentrations and Average CO Yields
(ASTM E 662, 25 kW/m²)**

<i>Description</i>	<i>Non-Piloted</i>		<i>Piloted</i>	
	<i>Peak</i>	<i>Average</i>	<i>Peak</i>	<i>Average</i>
	<i>[CO]</i> <i>(ppm)</i>	<i>Yield</i> <i>(mg/g)</i>	<i>[CO]</i> <i>(ppm)</i>	<i>Yield</i> <i>(mg/g)</i>
Headlight – Clear Lens	3	2	500	26
Hoodliner Face	2300	71	1900	82
Kick Panel Insulation Backing – Rubber Side	630	11	990	30

**Table XI. HCl Concentrations and Average HCl Yields for Kick Panel
Insulation Backing – Rubber Side (ASTM E 662, Various Exposures)**

<i>Exposure</i>	<i>Peak</i> <i>[HCl]</i> <i>(ppm)</i>	<i>Average</i> <i>Yield</i> <i>(mg/g)</i>
25 kW/m ² , Non-Piloted	570	27
25 kW/m ² , Piloted	610	27

concentrations and average HCl yields for the Kick Panel Insulation Backing – Rubber Side specimens are listed in Table XI. The average yields were calculated on the basis of the measured concentrations and total specimen mass loss.

Discussion

The CO yields measured in this study were compared with literature values, and a qualitative comparison was made between the measurements made under highly-ventilated conditions and those made in under-ventilated conditions. Finally, industry standards were used to evaluate the performance of each material tested using the smoke chamber techniques.

Comparison with Literature Values

Tewarson has published CO yield data for a variety of polymeric materials generated using the ASTM E 2058 Fire Propagation Apparatus designed by FM Global (10,11). Table XII shows a comparison between the CO yields measured for the materials used in this study and Tewarson's data. The reported values for the polyethylene, polypropylene, and polyamide materials are averages of the results obtained from the samples designated as such in Tables I and II.

Table XII. Comparison of Measured CO Yields with Data Published by Tewarson

<i>Material</i>	<i>Number of Parts</i>	<i>CO Yields (mg/g)</i>	
		<i>Tewarson</i>	<i>Measured Values</i>
Polyethylene, Polypropylene	7	24	24 ± 6
Polycarbonate	1	54	50
Polyamide	3	38	18 ± 7
Polystyrene	1	60	52
Polyvinylchloride	1	63	9

There is reasonable agreement between the results from this study and Tewarson's data for the polyethylene/polypropylene, polycarbonate, and polystyrene materials. The lower values generally seen in this study may be reflective of the difference in ventilation between the Cone Calorimeter and the Fire Propagation Apparatus. The poor agreement between the values for the polyamide and polyvinylchloride materials may be an indication of significant differences in the formulations of the materials used in this study and those used in Tewarson's work.

Comparison of Dynamic vs. Static Results

Smoke toxicity data were collected using two different types of fire scenarios. The Cone Calorimeter is a well-ventilated scenario; fresh air is pulled past the specimen throughout the test. The smoke chamber tests are under-ventilated; the combustion takes place in an airtight chamber. A comparison of the results generated by the two methods clearly shows that the levels of toxic gases generated during a combustion event are strongly influenced by the details of the combustion scenario.

The three parts used in the smoke chamber measurements were chosen based on their performance in the Cone Calorimeter tests. Specifically, the Kick Panel Insulation Backing – Rubber Side (Part Number 4860446) was chosen for its low $[\text{CO}]_{\text{max}}$ value, the Hoodliner Face (Part Number 4716832B) was chosen for its intermediate $[\text{CO}]_{\text{max}}$ value, and the Headlight – Clear Lens (Part Number 4857041A) was chosen for its high $[\text{CO}]_{\text{max}}$ value.

The $[\text{CO}]_{\text{max}}$ data from the smoke chamber tests show a different relationship among the three parts. At the 25-kW/m² exposures, the Headlight material produced the lowest $[\text{CO}]_{\text{max}}$ values, rather than the highest. The $[\text{CO}]_{\text{max}}$ values for the other two parts were ordered as with the Cone Calorimeter data. The Headlight material showed an increase in $[\text{CO}]_{\text{max}}$ value relative to the other two parts in the 50-kW/m² ISO 5659-2 test.

Another important observation to be made concerning the comparison between the Cone Calorimeter measurements and the smoke chamber measurements is the relative difficulty in obtaining repeatable data. Due to the dilution of the exhaust stream in the Cone Calorimeter test, the levels of toxic gases in the exhaust stream are quite low. As stated above, while data were collected at three different heat fluxes (20, 35, and 50 kW/m²), only the tests conducted at 50 kW/m² generated sufficient concentrations of toxic gases in the exhaust stream to allow the concentrations to be reliably determined using the FTIR technique. The smoke chamber techniques allow the toxic gases to build up in the airtight test chamber, allowing the concentrations to rise to readily quantifiable levels.

These two observations, that the results of a toxicity analysis are strongly influenced by the specific fire scenario employed, and that quantitative gas analysis is made more difficult in highly ventilated conditions, need to be taken into account when crafting acceptance criteria based on smoke toxicity determinations. The fire scenario used in the evaluation of candidate materials must be carefully chosen so as to mimic as closely as possible the conditions that are likely to be present in an actual fire. When highly ventilated conditions are required, consideration must be given to designing more sensitive quantitative gas analysis techniques.

Acceptance Thresholds

Part 2 of Annex 1 to the IMO FTP Code (12), Airbus Industrie ABD 0031 (13), and Bombardier SMP 800-C (14) are industry standards that place limits on the amount of toxic gases that may be generated by burning materials used in ships, aircraft, and ground transportation vehicles, respectively. The limits specified in each method are listed in Table XIII. The results presented above were evaluated in general accordance with the requirements of these methods.

Table XIII. Toxic Gas Concentration Limits (ppm)

<i>Gas Species</i>	<i>IMO</i>	<i>Airbus</i>	<i>Bombardier</i>
CO ₂	NS ^a	NS ^a	90,000
CO	1450	1000	3500
HF	600	100	100
HCl	600	150	500
HBr	600	NS ^a	100
NO _x	350	100	100
HCN	140	150	100
SO ₂	200	100	100

^a None Specified. No limit is specified in the standard.

Part 2 of Annex 1 to the IMO FTP Code requires materials to be tested according to ISO 5659, Part 2, with the modifications and gas analysis described above.

Both Airbus Industrie ABD 0031 and Bombardier SMP 800-C require materials to be tested in general accordance with ASTM E 662. While ABD 0031 makes use of the gas analysis described above, SMP 800-C specifies an absorptive sampling procedure or a demonstrated equivalent.

As shown in Table XIV, all three materials meet the requirements of Bombardier SMP 800-C, assuming that the FTIR analysis used for this study yields results equivalent to the absorptive procedure referenced in the method. The Kick Panel Insulation Backing – Rubber Side (Part Number 4860446) fails to meet the requirements of both Airbus Industrie ABD 0031 and Part 2 of Annex 1 to the IMO FTP Code, due to excessive HCl production in both the piloted and non-piloted modes. The Hoodliner Face (Part Number 4716832B) fails to meet the requirements of Part 2 of Annex 1 to the IMO FTP Code due to excessive CO production in all three of the ISO 5659, Part 2 exposure modes.

Table XIV. Acceptability of Materials According to Various Criteria

<i>Description</i>	<i>IMO</i>	<i>Airbus</i>	<i>Bombardier</i>
Headlight – Clear Lens	Pass	Pass	Pass
Hoodliner Face	Fail	Pass	Pass
Kick Panel Insulation Backing – Rubber Side	Fail	Fail	Pass

It is interesting to note that the only material that meets the criteria for all three specifications is the Headlight – Clear Lens (Part Number 4857041A). This is the material that was chosen for this part of the study based on its *high* peak CO concentration, as measured in the Cone Calorimeter.

Conclusions

This study has provided useful information to the transportation industry and policymakers regarding the quantification of toxic gases generated during automobile fires. Measured values of the concentrations of toxic gases are consistent with previously published data. Differences observed between CO yields measured in this study and those published by Tewarson are most likely due to minor differences in the combustion scenarios, and differences in the material formulations. The strong relationship between the details of the fire scenario and the toxic gas yields has been demonstrated, and has been shown to

be an important issue to consider when developing material acceptance criteria. Finally, three industry standards that define acceptance criteria for materials used in their respective industries have been used to evaluate the performance of the materials used in this study.

Comparison with full scale testing is necessary to determine what, if any, relationship exists between the results of the small scale tests described in this report and the actual toxic gas yield from components in a burning vehicle. A proposal was submitted to NHTSA for a series of full-scale vehicle burn tests to explore this relationship. At this time it is not clear if and when this proposal will be funded.

Acknowledgements

The authors of this paper would like to acknowledge the support of both the Motor Vehicle Fire Research Institute (MVFRI) and the National Highway Traffic Safety Administration (NHTSA) for this project. In particular, we are thankful for the assistance and contributions of Dr. Kennerly H. Digges and Dr. R. Rhoads Stephenson of MVFRI and Mr. Carl Ragland of NHTSA.

References

1. Santrock, J. *Evaluation of Motor Vehicle Fires Initiation and Propagation, Part 3: Propagation in an Engine Compartment Fire in a 1996 Passenger Van*; General Motors Corporation: Warren, MI, 2001.
2. Santrock, J. *Evaluation of Motor Vehicle Fires Initiation and Propagation, Part 7: Propagation of an Engine Compartment Fire in a 1997 Rear Wheel Drive Passenger Car*; General Motors Corporation: Warren, MI, 2002.
3. Ohlemiller, T.; Shields, J. *Burning Behavior of Selected Automotive Parts from a Minivan*; NISTIR 6143; National Institute of Standards and Technology: Gaithersburg, MD, August 1998.
4. Ohlemiller, T.; Shields, J. *Burning Behavior of Selected Automotive Parts from a Sports Coupe*; NISTIR 6316; National Institute of Standards and Technology: Gaithersburg, MD, April 2001.
5. ASTM E 1354. *Annual Book ASTM Standards 2003*, 04.07.
6. ASTM E 662. *Annual Book ASTM Standards 2003*, 04.07.
7. ISO 5659-2:1999. *Plastics - Smoke generation - Part 2: Determination of optical density by a single-chamber test*; International Organization for Standardization: Genève, Switzerland.
8. ASTM E 800. *Annual Book ASTM Standards 2003*, 04.07.

9. Hakkarainen, T. *Smoke gas analysis by Fourier transform infrared spectroscopy - The SAFIR project*; VTT Research Notes; Technical Research Centre of Finland: Espoo, Finland, 1999.
10. ASTM E 2058. *Annual Book ASTM Standards 2003*, 04.07.
11. Tewarson, A. Generation of Heat and Chemical Compounds in Fires. In *SFPE Handbook of Fire Protection Engineering*, 3rd Edition; DiNenno, P., Walton, W. D., Eds.; National Fire Protection Association: Quincy, MA, 2002.
12. IMO FTP Code Annex 1 Part 2. *FTP Code International Code for Application of Fire Test Procedures*, International Maritime Organization: London, 1998.
13. Airbus ABD0031, *Fireworthiness Requirements Pressurized Section of Fuselage*; Airbus: Toulouse, France, 2003.
14. Courcy, Y. *Bombardier Material and Process Specification SMP 800-C, Toxic Gas Generation*; Bombardier: Montréal, Canada, November 16, 1994.

Chapter 26

Products of Rigid PVC Burning under Various Fire Conditions

Krzysztof Lebek, T. Richard Hull, and Dennis Price

**Centre for Materials Research and Innovation, University of Bolton,
Deane Road, Bolton BL3 5AB, United Kingdom**

The low flammability of PVC as a bulk polymer is counterbalanced by its higher toxicity in a fire. Rigid PVC has been subjected to decomposition, early well-ventilated and developed, low-ventilation flaming combustion in a tube furnace (the Purser furnace) following the methodology described in IEC 60695-7-50. Analysis of the temperature profiles within the tube furnace showed stratification at low air flow rates and uneven mixing within the tube. Conversely, within the effluent dilution chamber, it was shown that complete mixing had taken place. In comparison with hydrocarbon polymers, yields of carbon monoxide are shown to increase in the presence of HCl, giving high levels of fire toxicity for both well ventilated and low ventilation conditions. Under smouldering conditions, large quantities of HCl are evolved but most of the carbon remains as residue.

Introduction and Background

PVC is widely used for wire and cable jacketing and insulation (replacing natural rubber), for pipes and conduits (replacing metallic tubing) and for window frames (replacing wood). As a consequence of the widespread use of PVC-based materials, they are often present at the scene of a fire and it is, therefore, of interest to investigate their behaviour. Toxic gases are the cause of most fire fatalities, and carbon monoxide poisoning is responsible for the majority of these deaths (1). Its contribution to the toxicity and irritancy of fire gases has been the subject of much recent debate. It is acknowledged that small-scale tests do not generally accurately represent the burning conditions occurring in a fully developed fire. Since most fire deaths result from breathing fire gases, and real-scale fires are very expensive to set up, there is a need for a robust means of replicating real-scale fires on a small scale.

UK fires cost 600 lives and £4.9 billion per year. The main killer in fire is carbon monoxide. CO is colourless and odourless, so it is inhaled unnoticed. CO combines with haemoglobin in blood, forming carboxyhaemoglobin which is 200 times more stable than oxyhaemoglobin, dramatically reducing the oxygen supply to the cells and the brain.

The toxicity of CO may be expressed as an LC_{50} . This is the concentration of CO at which 50% of the population would be expected to die in a fixed time, normally within 30 minutes. This has been quoted (2) as 5700 ppm.

Different strategies have been employed in order to replicate these fire types on a small scale. Closed box tests, such as NBS smoke chamber, attempt to estimate combustion toxicity in an atmosphere that starts off well-ventilated but which becomes increasingly oxygen depleted during the test. These suffer from a lack of definition of fire conditions, which change during the test, and so are not suitable for use in fire safety engineering.

More sophisticated are the flowing air tests of which four established methods exist for small-scale measurement of fire gas toxicity: the DIN 53436 (3), the FM Fire Propagation Apparatus [ASTM E2058] (4), the French test [NFX70-100] (5) and the Purser furnace [BS 7990 (6) and IEC 60695-7-50 (7)]. Only the Purser furnace is capable of forcing a steady state under the most toxic oxygen depleted conditions. It does so by feeding the sample and air into a tube furnace at fixed rates, so that the flame front is held stationary relative to the furnace. This makes it the only small-scale apparatus capable of giving reliable data on the product yields over the full range of fire conditions.

Figure 1 presents a simplified view of the first step of the decomposition of PVC, showing the theoretical maximum yield of HCl. Above 190°C, HCl evolution is rapid and autocatalytic. The resultant conjugated polyene then undergoes scission, resulting in the formation of benzene, toluene, polyaromatic species and carbonaceous char, depending on the conditions. Decomposing

organochlorine compounds can also form a mixture of toxic compounds such as phosgene, chlorobenzene, chlorotoluene, dichlorobenzene and chlorinated dibenzodioxins and dibenzofurans (8,9) at lower concentrations, which can be detected by FTIR or GC-MS.

PVC generates very dense smoke in the initial phase of the fire. The fire effluent gases are corrosive and contain approximately five times the amount of carbon monoxide, compared to polyolefins such as PE, PP. Tests performed according to ASTM 1354-90 using the cone calorimeter (10) showed the main corrosive and irritant gas is hydrogen chloride which can be evolved from unplasticised PVC with a yield of up to the maximum theoretical yield of 0.58 g/g of polymer, based on the atomic weights on the elements.

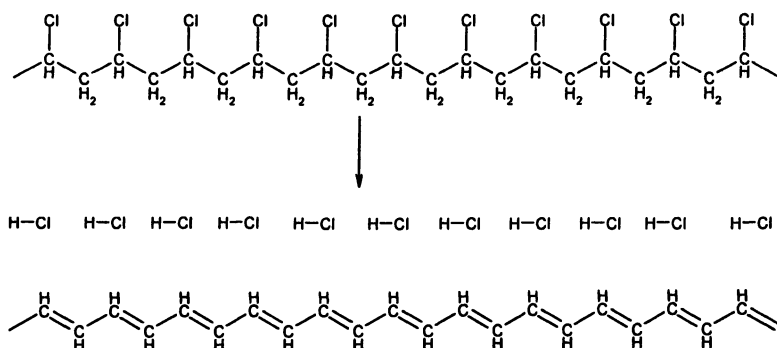


Figure 1. Simplified first step of decomposition of PVC

Experimental

Materials. Rigid PVC pellets obtained from Northern Industrial Plastics, Manchester, U.K. were used for this study.

The Purser furnace. The Purser furnace (11,12) (figure 2) consists of a tube furnace (13) through which a polymer sample is driven at a fixed rate, while being supplied with a fixed feed rate of primary air. This tube furnace has two major advantages over other small-scale physical fire models for studying fire toxicity. By fixing the fuel and primary air feed rates, the equivalence ratio (fuel to air ratio over stoichiometric fuel to air ratio) can be carefully controlled. By driving the sample into a rising temperature gradient within the furnace, increasing the applied heat flux, combustion is forced even under reduced ventilation. In this way, steady state burning is set up before the hottest part of the furnace is reached, and provided steady flaming is obtained, the results are largely independent of the furnace temperature. Furnace temperature profiles have been recorded and reported elsewhere (14). The effluent from the tube is

made up to 50 litres per minute with secondary air by dilution within the chamber.

The secondary oxidiser is supplied with gaseous sample taken from the effluent dilution chamber. The temperature is set at 900 °C so that partially burnt molecules, benzene, CO, and soot particles are oxidised to CO₂. Carbon dioxide concentrations in effluent dilution chamber and secondary oxidiser are detected using non-dispersive infrared analysers (Edinburgh Sensors Ltd.). The oxygen concentration in the effluent dilution chamber is measured using a paramagnetic analyzer (Servomex Ltd.). The carbon monoxide concentration is measured using an electrochemical cell (City Technology Ltd.). HCl was trapped by a series of three bubblers into deionised water and titrated against 0.1M sodium hydroxide, using congo red as an indicator.

Toxic product yields were determined using the IEC 60695-7-50 tube furnace method which controls the rate of burning through the sample feed rate. The ratio of primary to secondary air is altered, and once steady state conditions have been established, the fire toxicity at different fire conditions can be determined. The PVC was studied using the experimental conditions relating to the 3 fire scenarios described in IEC 60695-7-50 (Table I). The feed rate was set to 1 g/min by loading the sample boat which travelled at a speed of 35.6 mm/s. Flaming combustion occurred within the first half of the tube furnace before the temperature maxima was reached.

Table I Fire types according IEC 60695-7-50.

<i>fire type</i>	<i>furnace temperature /°C</i>	<i>primary air flow /l/min</i>	<i>secondary air flow /l/min</i>
smouldering	350	1.1	48.9
well-ventilated flaming	650	22.6	27.4
developed fire-low ventilation	825	2.7	47.3

Results

Oxygen Concentration

Figure 3 shows data for three different fire types. For a developed fire, the steady state occurred from 9 to 26 minutes. For other conditions a shorter steady state was observed. Under smouldering conditions ignition does not take place, but smoke appears. During well-ventilated flaming, ignition occurs, and there is a significant drop in the oxygen concentration. Flaming reaches a peak, and then subsides in the latter part of experiment.

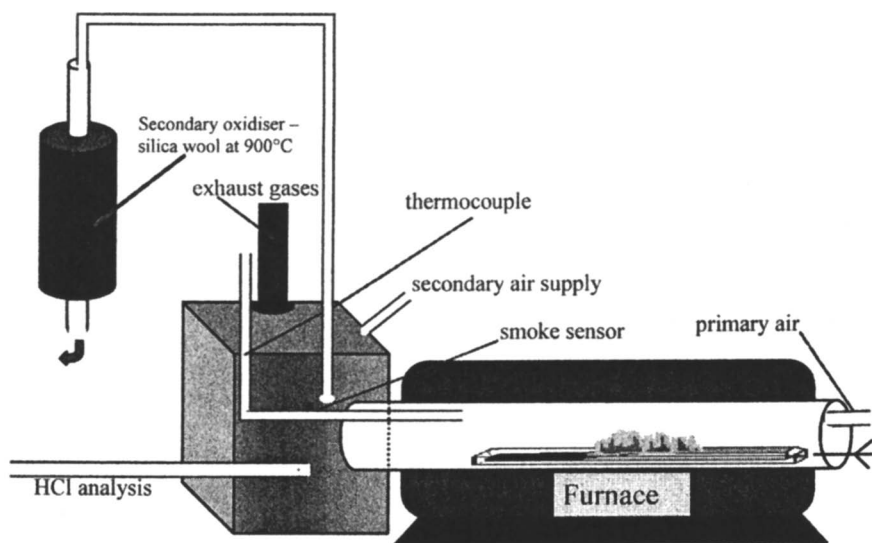


Figure 2. The Purser Furnace

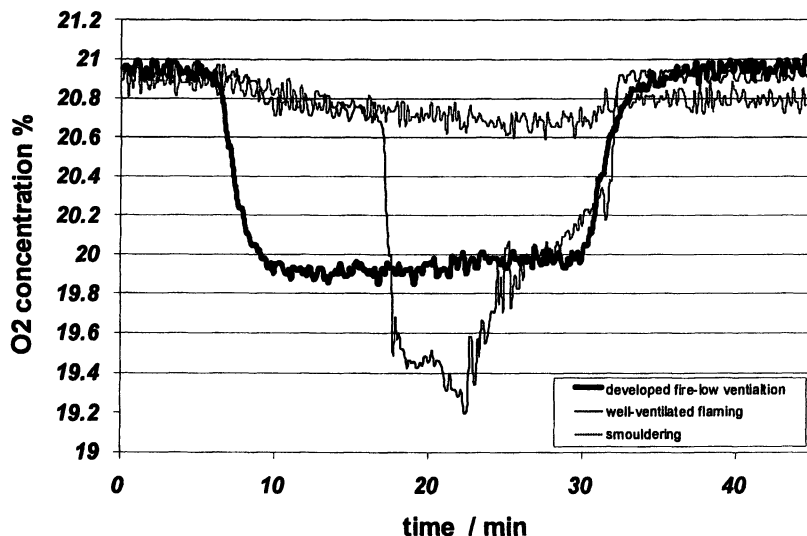


Figure 3. Variation of oxygen concentration during experimental runs

Carbon Dioxide

Figures 4 and 5 show the variations of CO_2 for the effluent dilution chamber and secondary oxidiser during runs. In figure 4, the steady state for the developed fire is observed between 10 and 25 minutes, showing a deviation only at the start and at the end. The deviation at the start shows a slow ignition process, and the peak at the end may be due to an increase in flaming once all the HCl has been pyrolysed. As dehydrochlorination occurs at 190°C , the supply of HCl would finish before the residual char further along the sample boat had been oxidised. The drop in CO_2 concentration between 20 and 25 minutes suggests temporary extinction of flaming for the well ventilated flaming scenario. During smouldering, only very low concentrations of CO_2 were observed.

Greater concentrations of CO_2 are observed for the secondary oxidiser because inside the secondary oxidiser the temperature is always 900°C and all carbonaceous material is converted into CO_2 . The concentration of CO_2 during smouldering at 350°C showed a slow increase, corresponding to the longer distance the boat needed to travel into the furnace in order to achieve a steady state.

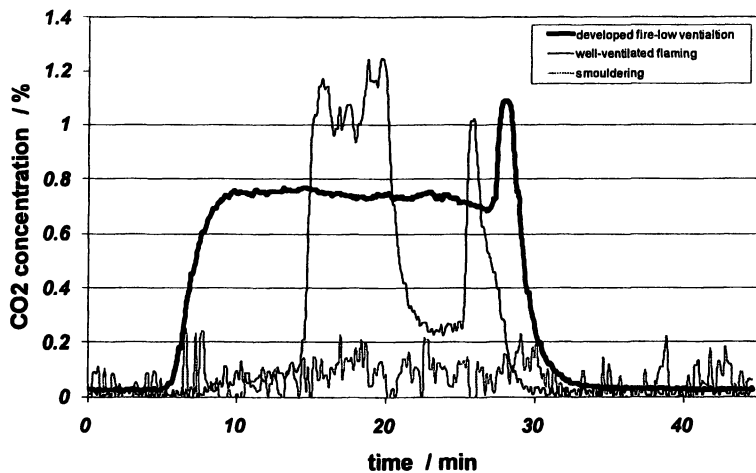


Figure 4. Variation of CO₂ concentration in effluent dilution concentration during experimental runs

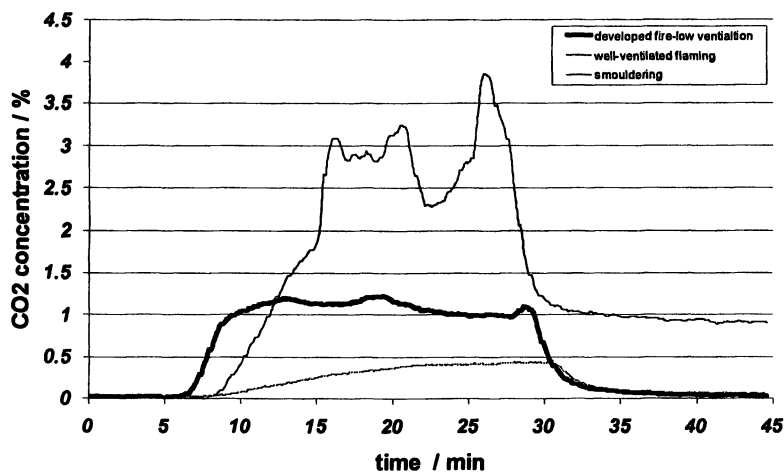


Figure 5. Variation of CO₂ concentration in secondary oxidiser during experimental runs

Carbon Monoxide

Figure 6 shows the variation of carbon monoxide with time. Again the longest steady state was obtained under fully developed conditions, since the higher furnace temperature means that the sample is exposed to temperatures above ignition for a greater period of travel of the sample boat. The sharp rise in the CO concentration, between 17 and 20 minutes during well ventilated flaming, suggests some inhibition mechanism (possibly by HCl) which resulted in temporary extinction of flaming by reducing heat feedback to the sample.

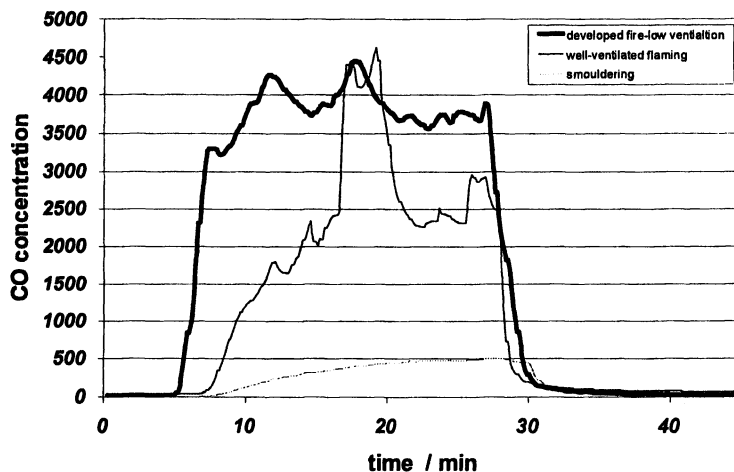


Figure 6. Variation of CO concentration during experimental runs

It is very important to assess CO concentration because this is the most significant toxicant found in a real fire. The highest CO concentration occurred for a developed fire at low ventilation and the lowest CO concentration occurred for smouldering. There is a very strong correlation between fire conditions and CO yield. For a developed fire at low ventilation, the CO yield is nearly 6 times greater than for smouldering and 3.5 times greater than for well-ventilated. As CO is the main toxic element from fires, this shows the importance of fire scenario on the fire gas toxicity.

Optical Density

Figure 7 shows hazard from smoke (presented as optical density). For well-ventilated flaming much more smoke is produced than for other conditions. The lowest level of smoke is produced during smouldering fire types.

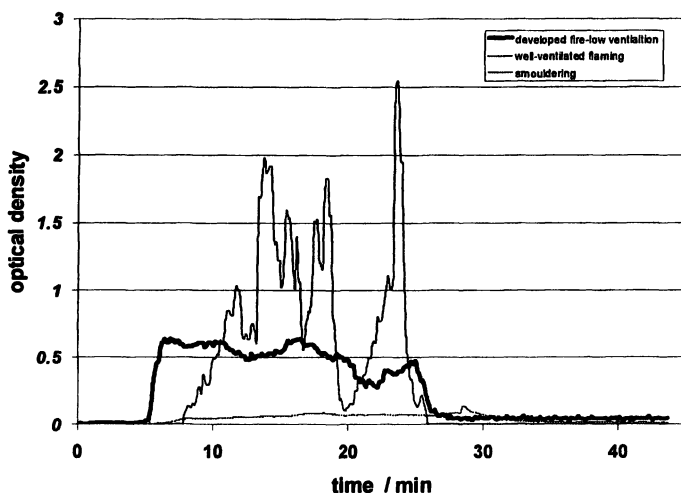


Figure 7. Variation of optical density during experimental runs

HCl Detection

The assessment of fire gas toxicity of halogen-containing materials, such as PVC, requires measurement of HCl evolution, which makes a major contribution to the fire gas irritancy, (as an irritant gas which suppresses breathing and so hinders escape), most notably under smouldering conditions (where the smouldering may be driven by heat or fuel from other sources). A methodology for determination of HCl, which is extremely soluble in condensable vapours, and easily adsorbed onto many other surfaces, was developed. Starting with pellets of rigid PVC, the determination was optimised in order to get consistent and quantitative yields of HCl from PVC. Initially it was believed that the best approach would be to sample the gas directly from the furnace tube, where it would not have had a chance to condense.

In some preliminary work using slightly different ventilation conditions to IEC 60695-7-50, comparison was made of the HCl concentrations at the top and

bottom of tube (Figure 8), and at the top and bottom of the effluent dilution chamber (Figure 9). For low ventilation conditions inside the tube, six times more HCl was detected at the top of the tube than at the bottom (Table II). Based on this information, subsequent samples were only taken from effluent dilution chamber.

The variations in the data led to temperature measurements within the tube, and the unexpected discovery of stratification within the furnace tube, with the hottest layers at the top at low air flow rates, and in the middle at higher air flow rates. Further, the HCl concentration was found to vary significantly according to the position of the probe in the furnace tube. Conversely, grab samples taken from the effluent dilution chamber were found to give nearly quantitative yields of HCl from PVC under certain conditions, and consistent yields under all conditions. Subsequent analysis from different positions within the effluent dilution chamber verified that adequate mixing had taken place within the chamber.

Table II Comparison HCl yield for top and bottom the tube furnace

<i>material</i>	<i>temp. °C</i>	<i>HCl yield in tube %</i>	<i>HCl yield in chamber %</i>
Pure PVC sample taken from top of tube	350	19.9	36.5
Pure PVC sample taken from bottom of tube	350	4.5	35.0
Pure PVC sample taken from top of tube	825	48.1	
Pure PVC sample taken from bottom of tube	825	4.7	47

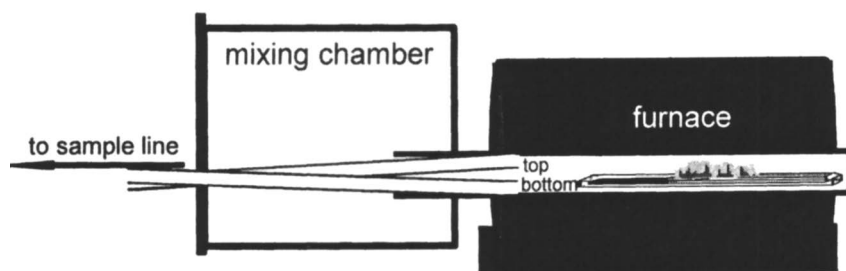


Figure 8. Measurements from top and bottom of tube furnace

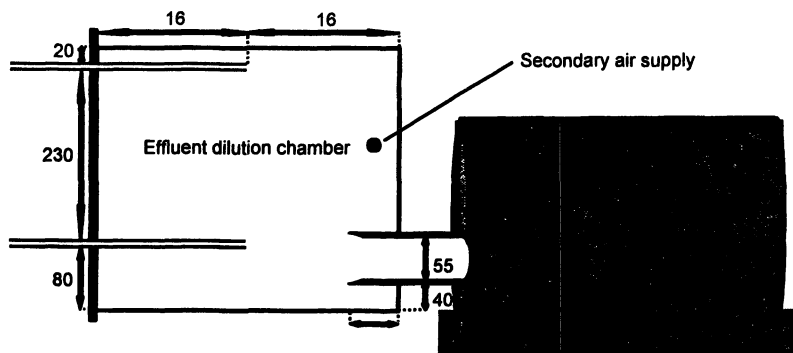
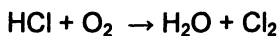


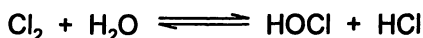
Figure 9. Comparison concentrations of HCl on top and bottom of effluent dilution chamber

This demonstrates that the concentrations in different parts of the effluent dilution chamber are the same because the results obtained (for both sampling lines) were the same. HCl chain strips from PVC at low temperature ($\sim 200^\circ\text{C}$), so at 350°C fairly high HCl concentrations are observed. However, because only the total HCl is measured during the run, it is not possible to quantify the amount of chlorine remaining in the undecomposed material, particularly during smouldering. This is because the maximum furnace temperature is 350°C , and many parts will be below 200°C . At 825°C nearly all the furnace will be above 200°C , so HCl loss from the polymer will be complete. HCl was measured from the secondary oxidiser in order to determine the organochlorine content of the fire effluent, by difference with the effluent dilution chamber HCl yield.

The deionised water in the bubbler from the secondary oxidiser showed evidence of chlorine formation, a yellow colour and bleaching of the congo red indicator. This arises from oxidation of HCl, which is favourable at 900°C .



The Cl_2 then undergoes partial hydrolysis to hydrochloric and hypochlorous acid.



There also seems to be evidence for some loss of HCl in the tubing running to the secondary oxidiser, most obviously at 825°C when the organochlorine compound concentration is lowest.

Summary of Results for Different Fire Types

Table III shows the data for the decomposition of PVC under the three fire conditions. The mass loss for smouldering could correspond to loss of all HCl (58.5%) plus loss of a smaller portion of the aromatic residue. More complete decomposition occurs for the two flaming fire conditions with around 90 and 99% mass loss. The oxygen concentration (average concentration for a steady state), taken from the effluent dilution chamber shows only a small level of oxygen uptake by the sample, which concurs with the low levels of CO₂ produced. Under smouldering conditions there is only a small yield of CO₂ in the effluent dilution chamber, but a larger concentration of products of incomplete combustion. Surprisingly, under well-ventilated flaming, there is a similar low yield of CO₂ in the fire effluent, but a much higher concentration of products of incomplete combustion. This suggests that if flaming occurred it was only partial or sporadic. This brings into question the lack of guidance in the IEC standard over the continuity of the flaming condition. By contrast, BS 7990 stipulates that if flaming is not continuous the furnace temperature should be increased in 25°C steps and the experiment repeated until steady flaming occurs. At the fully developed fire stage, despite the lower concentration, there is a higher yield of CO₂ but still a larger yield of products of incomplete combustion.

The carbon monoxide yield is consistently high in proportion to the amount of mass lost. Under smouldering conditions, there is little release of carbonaceous material, but a significant CO yield. Under well-ventilated and developed fire/low-ventilation conditions, potentially toxic levels of CO are clearly evident. The CO₂/CO ratio, which is normally around 100 for well-ventilated flaming for hydrocarbon polymers, is very low, due to the inhibiting effect of HCl on the conversion of CO to CO₂. The HCl yield for the PVC under different fire conditions shows that significant chain stripping yielding HCl, aromatics and char precursors is occurring, even under smouldering conditions. The theoretical maximum yield of HCl from the PVC is 0.585 g/g, suggesting that considerable HCl is lost (or converted to Cl₂ and not then hydrolysed), particularly at 825°C for the fully developed fire condition. The slightly lower yields of HCl from the secondary oxidiser for the developed fire condition, giving an apparent negative organochlorine yield, may arise from deposition of HCl between the effluent dilution chamber and the secondary oxidiser, or may be within the limits of experimental error.

Table III Summary of results for different fire types

	<i>smouldering</i>	<i>Well-ventilated</i>	<i>Developed fire-low ventilation</i>
Mass loss %	63.81	89.65	98.93
O ₂ concentration %	20.75	19.95	19.5
CO ₂ yield as g/g polymer	0.0947	0.1038	0.6612
Secondary CO ₂ yield as g/g polymer	0.3659	1.5298	0.9516
Products of incomplete combustion as g CO ₂ /g polymer	0.2712	1.426	0.2904
CO yield as g/g polymer	0.0268	0.0437	0.1550
HCl yield as g/g polymer	0.37	0.48	0.55
Secondary HCl as g /g polymer	0.39	0.51	0.51
Organochlorine as g HCl/g polymer	0.02	0.03	-0.04
Smoke as optical density	0.0688	0.0769	0.3662

Conclusions

The Purser Furnace is capable of forcing a steady state under the most toxic oxygen depleted conditions, even for intrinsically low flammability materials, such as rigid PVC. HCl yields must be undertaken carefully to minimise loss of analyte. The measurements of fire gas concentrations taken from the effluent dilution chamber are more reliable than those taken directly from the tube, where stratification appears to occur, particularly at low primary air flow rates. At higher furnace temperatures, greater yields of HCl, CO, CO₂ are observed, but in contrast to CO or smoke, the HCl yield is less dependent on fire conditions. It should be noted that toxic yield assessment may also be dependent on concentration and identity of the organochlorine species detected through secondary oxidation.

References

1. Fire statistics United Kingdom 1997, Home Office Statistical Bulletin, p13 Issue 25/98 (1998)
2. ISO/TR9122-5:1993 Toxicity testing of fire effluents – Part 5: Prediction of toxic effects of fire effluents
3. Purser D. A.; Fardell P. J.; Rowley J.; Vollam J.; Bridgeman B. An improved Tube Furnace method for the generation and measurement of toxic combustion products under a wide range of fire conditions. Flame Retardant '94 Conference, London (1994)
4. Standard Test Methods for Measurement of Synthetic Polymer Material Flammability Using a Fire Propagation Apparatus (FPA) ASTM E2058: **2002**
5. NFX 70-100 (06/86) Essais de comportement au feu, analyse de gaz de pyrolyse et de combustion, methode au four tubulaire, **1986**
6. BS 7990 : 2003. Tube furnace method for the determination of toxic product yields in fire effluents, **2003**
7. Toxicity of fire effluent - Estimation of toxic potency: Apparatus and test method; IEC 60695-7-50:2002, **2002**
8. Paul K. T. *Fire Mater*, **1989**, 14, 43-58
9. Hirschler M. M. *Eur. Polym. J.* **1986**, 22, 153-160
10. Sultan B. Å.; Ericsson K.; Hirvensalo M.; Hjertberg T.; Hanninen M.; Novel halogen free flame retardant polyolefins intended for internal wiring- Properties and flame retardant mechanism. 47th International Wire & cable symposium, 1998, Philadelphia, USA
11. Price D.; Ebdon J. R.; Hull T. R.; Milnes G. J.; Hunt B. J. in *Fire and Polymers, Materials and Solutions for Hazard Prevention*, Ed. G. L. Nelson and C.A. Wilkie, ACS Symposium series 797, 2001, pp.307-320.
12. Hull T. R.; Carman J. M.; Purser D. A. *Polym. Int.* **2000**, 49, 1259-1265
13. BS 7990:2003 Tube furnace method for the determination of toxic product yield in fire effluents
14. Carman J. M.; Purser D. A.; Hull T. R.; Price D.; Milnes G. J. *Polym. Int.* **2000**, 49, 1256-1258

Chapter 27

Methodology for Small-Scale Toxic Hazard Assessment of Burning Cables

T. Richard Hull, Claire L. Wills, Krzysztof Lebek, Keith Paul, and Dennis Price

**Centre for Materials Research and Innovation, University of Bolton,
Deane Road, Bolton BL3 5AB, United Kingdom**

The IEC 60695-7-50 tube furnace method using the Purser furnace was used to create three fire conditions and study the fire toxicity of four typical whole cables replicating the protective behaviour of the sheathing found in a real fire. The results for the plasticized PVC cables show some HCl and traces of CO and CO₂ and significant smoke under smouldering conditions, CO, CO₂ and HCl and copious quantities of smoke under well-ventilated flaming conditions, and large quantities of CO and organic materials under fully developed flaming conditions. The results for the polyolefin (Casico) sheathed cables show very little pyrolysis, with only slight smoke and CO and little CO₂ or oxygen depletion during smouldering, and quite high levels of CO and CO₂ under well-ventilated and fully developed flaming conditions. The fire toxicity of these cables has been quantified through the calculation of the fractional effective dose calculated using the Purser and N-Gas models, and the rank order of toxicity is shown to be the same for each case.

Introduction

The tube furnace method has become established for assessment of the fire toxicity of materials. The work sets out to establish and assess the suitability of the (Purser) tube furnace for assessing the toxic hazard of composite products, using electrical cables as proof of concept. The present work compares the bench-scale yields of toxic products of four whole cables under three established fire types, in order to assess their fire toxicity.

The majority of deaths in fires result from inhalation of toxic gases (1). Many of these arise from burning synthetic polymer based materials. Carbon monoxide is acknowledged to be the most toxicologically significant element in fire gases, preventing oxygen transport by the formation of carboxyhaemoglobin. The presence of CO₂ in blood, which stimulates hyperventilation, increases the respiration rate and hence the hazard from the toxic components of the fire gas. Oxygen depletion deprives the body of oxygen (hypoxia) with fatal consequences at concentrations below 14%. A large number of other toxic and irritant gas species also contribute to the hazard from fire gases to a lesser extent. In this work, during the decomposition of PVC cables, the high yields of HCl are singled out because of their significant contribution. Until recently, fire (or smoke) toxicity was only specified for certain high risk applications. Currently, estimation of lethal toxic potency of fire effluents is of increased importance as prescriptive standards of fire behaviour for product acceptance (e.g. meeting a certain UL 94 rating) are replaced by holistic performance based fire codes requiring overall levels of fire safety to be maintained. New buildings now require assessment by fire safety engineers in terms of flammability and fire gas toxicity within the time required to escape (2).

Fire gas toxicity can be quantified in terms of a fractional effective dose (FED) (3), calculated from fire gas concentrations and published animal toxicity data for each gas. This approach avoids the use of animals for routine product testing, which is not permitted in Europe. The ratio of the concentrations of each species to its lethal concentration (LC₅₀) is summed for all toxicologically significant species. An FED of 1 indicates a lethal gas mixture. This simple approach has been modified to provide two standard methods of assessment of fire gas toxicity. Both give similar results, one, the N-Gas model developed at NIST (USA) and the other, the Purser model developed at the FRS division of BRE (UK). The methods differ in that the N-Gas model assumes that only the effect of the main toxicant CO is enhanced by the increase in respiration rate caused by high CO₂ concentrations (which increases as a step function), while in the Purser model the effect of all the toxic and irritant species is increased by higher CO₂ concentrations (rising continuously with increase of CO₂ concentration).

The yield of toxic gases from burning polymers is highly dependent on both the fire conditions and the material formulation (4). The factors controlling a material's fire gas toxicity are generally poorly understood, but have been shown to be somewhat independent of material for many non-fire retarded C, H, and O polymers (5), and highly dependent on fire conditions. The difficulties in predicting large scale behaviour on a small-scale have left this area neglected in the development of fire retarded materials. Large scale ventilation-controlled fires generate far higher concentrations of toxic products than small-scale well-ventilated fires.

The yields of toxic products are highly dependent on the fire conditions. As an enclosure fire develops, the temperature increases and oxygen concentration decreases. This has been set out as series of characteristic fire types (6), from smouldering, 1b in Table I, to post-flashover, 3b. After flashover the gases above the fire plume can form a reactive hot layer. In addition to oxygen concentration, the CO₂/CO ratio is often a useful indicator of fire type.

Table I. Characteristic fire types (BS 7899-2:1999) (6).

<i>Revised classification of fire types</i>	<i>Temperature (°C)</i>		<i>Oxygen to Fire (%)</i>	<i>Fire effluents</i>	
	<i>Fire</i>	<i>Hot Layer</i>		<i>Oxygen from fire %</i>	<i>CO₂/CO</i>
<i>Fire stage or fire type</i>					
1. Non-flaming					
a) Self-sustaining	450-600	RT	21	>20	1 to 5
b) Oxidative pyrolysis (smouldering)	300-600	<50	21	>20	1 to 5
c) Non-oxidative pyrolysis	300-600	<50	0	0	<5
2. Well-ventilated flaming	>700	<500	>15	5 to 21	>20
3. Less well-ventilated flaming					
a) Small underventilated fires in closed compartments.	>700	<500	<15	0 to 12	2 to 20
b) Post-flashover fires in large compartments (fully developed).	>700	500 to 1000	<15	0 to 12	2 to 20

Large scale fire tests, where transition through the different fire types occurs, show the highest levels of the most toxic species CO (and coincidentally also HCN) under oxygen-depleted conditions (3a and 3b in Table 1). These are the conditions where the heat flux is sufficient to drive the decomposition and pyrolysis processes forward, but there is insufficient oxygen to allow the combustion reactions to go to completion.

In bench-scale tests, fully-developed conditions are much more difficult to replicate, and most bench-scale fire models are more suited to the much less toxic early, well-ventilated fire types. Some other fire models enclose the sample, which starts off well-ventilated, but becomes increasingly oxygen depleted during burning. Neither provides the data the fire safety engineers require to predict the toxicity of real-scale fires. The defining feature of fully developed flaming is that the rate of burning is controlled by the air feed rate, not by the fuel supply or radiant flux. To replicate this on a small-scale requires control of the air feed rate for a particular burning rate. Small scale physical fire models for the prediction of toxic product yields are only valid for fully developed low-ventilation fire types when the air feed rate is fixed for a particular rate of burning.

One of the only bench-scale physical fire models capable of replicating a ventilation controlled steady state is the tube furnace apparatus (7) (Purser furnace). The apparatus differs from those described above (the well-ventilated and closed box apparatuses) in that the sample is fed into the furnace tube at a fixed rate (typically 1 g min^{-1}) alongside a fixed air flow, which may be above, at, or below the stoichiometric (chemical) air requirement. As the sample moves into the furnace, so it experiences increasing radiant flux intensity, until it ignites, then the flame spreads to a slightly cooler part of the furnace. At low oxygen concentrations, where ignition is more difficult, the sample reaches a hotter part of the furnace before igniting, and again, the flame will stabilise itself, as it spreads a little way back up the tube. Two standard methods exist which both use the same apparatus. As this is the only bench scale fire toxicity assessment apparatus capable of replicating steady state underventilated flaming, there is considerable interest in the differences between the two. BS 7990:2003 and IEC 60695-7-50 differ in the methodology used to define the fire types. In real-scale underventilated fires, the fire will grow until it is limited by the oxygen supply. In bench-scale tests, the oxygen requirement must be known in order to simulate this. Since typical polymer-based materials may be of unknown composition, and contain up to 70% inorganic fillers the fuel content, and hence the oxygen requirement of the material will not be known. IEC 60695-7-50 defines extremes of under and over-ventilation, which ensure that the conditions have been met. BS 7990:2003 uses the more sophisticated equivalence ratio approach, where the oxygen requirement is determined beforehand, and then the underventilated conditions are replicated by using twice the stoichiometric fuel/air ratio. These differences are illustrated in table II.

Thus the IEC 60695-7-50 method used in this work uses an established tube furnace apparatus, with an experimental protocol which is independent of the material's formulation. Three different fire types are established, for smouldering (non-flaming) using 1.1 litres per gram of fuel at 350°C , and by the use of extremes of overventilation for a well-ventilated fire (flaming) using 22.6

litres of air per gram of material, at 650°C, and for a fully developed underventilated fire (flaming) using 2.7 litres of air per gram of material at 825°C. These scenarios correspond to the standard fire types.

Table II. Furnace conditions corresponding to characteristic stages of burning behaviour

<i>Fire Type</i>	<i>Temperature (°C)</i>	<i>IEC 60695-7-50 Primary air flow (l/min)</i>	<i>BS 7990 Primary air flow (l/min)</i>
1b Smouldering (non flaming fires)	350	1.1	2
2 Well ventilated flaming	650	22.6	10
3a Small underventilated flaming fires	650		Twice stoichiometric fuel/air ratio
3b Fully developed under ventilated fires	825	2.7	Twice stoichiometric fuel/air ratio

These two methods are generally applicable to materials which are used in pellet or granulated form. However, the design of cable materials, which typically have a fire retarded sheath surrounded by a more flammable core of insulation material, such as LDPE surrounding copper conductors, have an inhomogeneity which is unlikely to be accurately represented by burning the individual components separately. Fortunately, their linear construction makes them ideal for tube furnace work, where they can be burned whole.

Experimental

All the cables were of comparable flammability, having passed the single wire burning test IEC 332-1, the industry standard criteria for general applications. A length of cable is mounted vertically, supported in two places, the flame from a gas burner is applied to the bottom at an angle of 45° to the cable for a fixed time (corresponding to the diameter of the cable), and the cable is classified as self-extinguishing if the distance from the lower edge of the top support to the onset of charring is between 50 and 540 mm. Two compositions were studied, one based on PVC and the other on polyolefin polymers, each used as both data cables (Cat. 5) and power cables (NHMH and NYM), selected in order to compare the toxic product yields of two widely used polymer systems, in the two most common cable formats. The formulations followed standard industry practice. Only the outer sheath was made of a different material, with the inner using polyolefin insulation, except for the PVC power cable which had

PVC for sheath, bedding and insulation. The formulations are shown in Table III. The PVC materials contained a PVC plasticizer (found to be di-isooctyl-phthalate) and chalk. Thermogravimetric analysis showed that PVC A and PVC C contains around 22% plasticizer, 22% chalk and 56% PVC, PVC B contains around 80% chalk.

Table III Cable designation and formulation

Type	Insulation	Bedding	Sheath
NHMH	polypropylene	EPR/chalk	Casico
NYM	PVC A	PVC B	PVC C
Cat. 5	MDPE	None	Casico
Cat. 5	MDPE	None	PVC C

The polyolefin material, Casico(TM) contains ethylene-acrylate copolymer, chalk (30%) and silicone elastomer. The flame retardant mechanism of Casico is complex, related to a number of reactions, e.g. ester pyrolysis of acrylate groups, formation of carbon dioxide by reaction between carboxylic acid and chalk, ionomer formation and formation of an intumescent structure stabilized by a protecting char (8). All four cables were supplied by Borealis AB (Sweden).

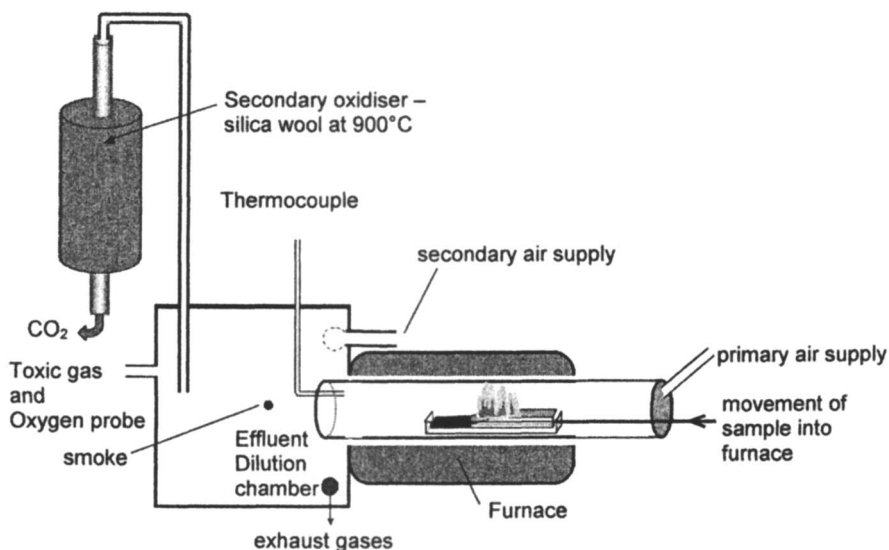


Figure 1. The tube furnace apparatus (Purser furnace)

The apparatus is described elsewhere (4), and shown in figure 1 with the addition of a secondary oxidiser, following the IEC 60695-7-50 standard method. The cable burning was conducted at a feed rate of 1 g min^{-1} of combustible material under the three different fire conditions 1b, 2 and 3b

described above (Table II). Whole cables were used, with the non-metallic parts of the cable (i.e. polymer, plasticizer and filler) were together taken as the "combustible material". The method differs slightly from the standard method in that power cables with a high linear density, and bundles of two to three data cables were fed in at a lower sample boat speed in order to keep the fuel feed rate close to a constant 1 g min^{-1} .

Oxygen depletion and yields of carbon dioxide, carbon monoxide and smoke were determined for each fire condition, as described elsewhere in this volume (9). For the PVC cables, hydrogen chloride was collected by drawing a metered volume of fire gas effluent through three bubblers containing deionised water and determined using a titrimetric method, described elsewhere (9). In addition, the incompletely oxidised products were determined by further oxidation, at 900°C in excess air over silica wool, and the secondary CO_2 and HCl concentrations determined.

Results and Discussion

Steady state burning was achieved for all cables and fire conditions except, under well-ventilated conditions, PVC power cables appeared to extinguish flaming in the last 30% of the run time, and the NHMH power cable burnt with intermittent flaming, corresponding to the physical observation of the inner LDPE fuel bursting through the protective sheath. Table IV shows the percentage mass loss of non-metallic material lost under each of the different fire conditions, during the steady state part of the burn. This characterizes the experiment in terms of the amount of pyrolysis products available for combustion. At 350°C for smouldering combustion, the mass loss of the PVC samples arises from a combination of plasticiser loss and dehydrochlorination, where that for the polyolefin cable is very low. For the well-ventilated condition, mass losses are much higher, in each case amounting to between 56 and 68%. This corresponds to a loss of most of the carbonaceous material, leaving a predominantly inorganic residue. The mass loss for the developed fire condition at 825°C is slightly higher, corresponding to decomposition of chalk (CaCO_3 to CaO and CO_2) of and greater efficiency of char oxidation.

Figure 2 shows the CO_2 yield for each of the cable samples (lower section), the total CO_2 yield measured from the secondary oxidiser (both sections), and the products of incomplete combustion (upper section) expressed as grams of CO_2 per gram of non-metallic material. In each case the ratio is based on the mass charge of material, not the mass loss of material. Although the CO_2 may arise from CaCO_3 , by reaction with HCl or above 750°C by thermal decomposition, from the composition of the cables and stoichiometry, this can only account for a maximum yield of 0.15 g/g of CO_2 . The remainder corresponds to the extent and efficiency of burning of each of the cable materials.

Table IV. Percentage of non-metallic mass loss of cable compounds

	<i>PVC data cable</i>	<i>PVC Power cable</i>	<i>FR Polyolefin Power cable</i>	<i>FR Polyolefin data cable</i>
<i>Smouldering (350°C)</i>	39.2	44.7	3.8	1.8
<i>Well-ventilated flaming (650°C)</i>	62.3	56.6	67.5	58.6
<i>Developed fire – low ventilation (825°C)</i>	75.8	59.1	72.7	71.2

During smouldering, the yield of CO₂ is very low for all materials except the PVC power cable, where it is surprisingly high at 0.35 g/g, which can only be partially accounted for as chalk decomposition by HCl, and may arise from decomposition of the phthalate ester plasticizer. Under the well-ventilated fire condition at 650°C, conversion of CO to CO₂ is much more efficient, for all samples except the PVC power cable. Under fully developed fire conditions at 825°C similarly high levels of CO₂ are observed for all the samples except the PVC power cable. The products of incomplete combustion data represents the organic component of the fire gas. Compounds such as CH₄, partially oxidised species CH₃CHO and CO, and soot would all be included. During smouldering, the surprisingly complete oxidation of the volatile part of the all-PVC power cable, compared with the PVC-sheathed data cable is again evident, together with small but significant degrees of pyrolysis of the polyolefin materials. Under the developed flaming condition all samples except the polyolefin data cable show higher levels of incomplete combustion than under the fully developed condition at 825°C. However, the additional 0.15 g/g of CO₂ from the decomposing chalk accounts for much of the difference. This suggests that for the cables studied here, neither the well-developed or the fully developed fire condition are conducive to complete oxidation.

Figure 3 shows the yield of carbon monoxide, the principal toxic gas in fires. CO results from incomplete combustion, which can arise from:

- Insufficient heat (e.g. during smouldering).
- Quenching of the flame reactions (e.g. when halogens are present in the flame, or ventilation overcools the flame).
- Insufficient oxygen (e.g. in post-flashover fires, large radiant heat fluxes pyrolyse the fuel even though there is not enough oxygen to complete the reaction).

The CO yield shows a similar trend to that of CO₂ under smouldering conditions, with little carbonaceous material released from either of the polyolefin cables. Under well-ventilated conditions all samples show low yields

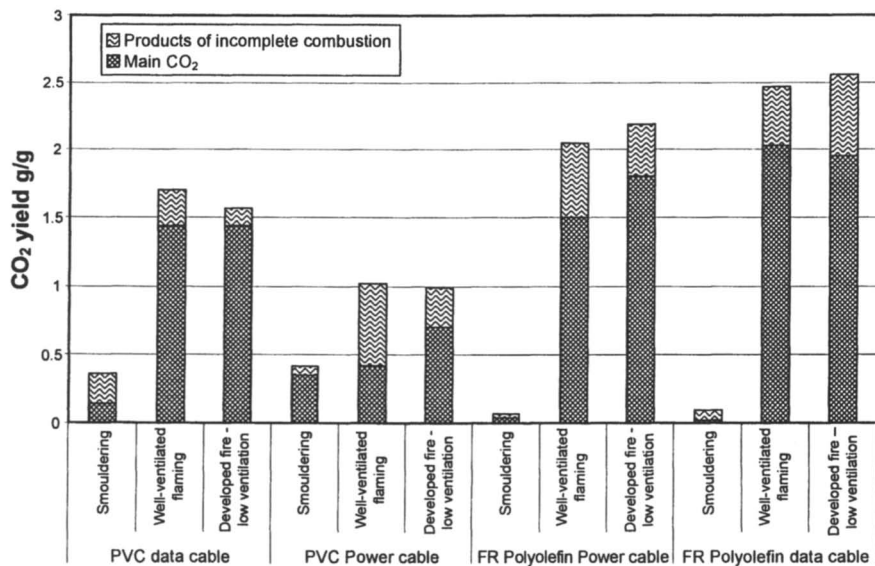


Figure 2. CO₂ yield in g/g of non-metallic material into furnace (lower section is yield from main chamber, total height is yield from secondary oxidiser, and upper section is yield of CO₂ from products passing unburnt from main chamber).

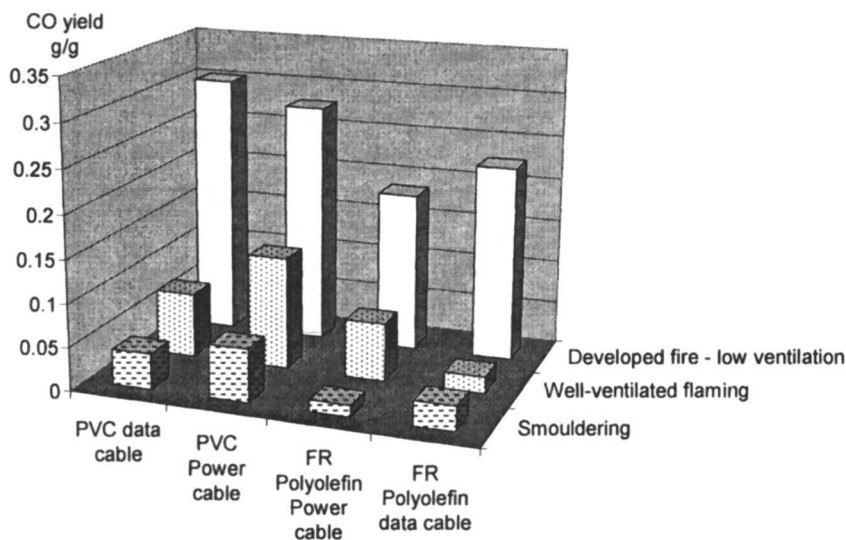


Figure 3. Variation Carbon monoxide yield for the three fire conditions in g/g of non-metallic material into furnace.

of CO, with a progressive increase from polyolefin data cable < polyolefin power cable < PVC data cable < PVC power cable. However, under fully developed fire conditions, all samples show a dramatic increase in CO yield, increasing in the order from polyolefin power cable < polyolefin data cable < PVC power cable < PVC data cable. This reversal from data cable to power cable may be due to the influence of higher levels of oxygen in promoting char oxidation of the thicker sheaths formed by the decomposing power cables.

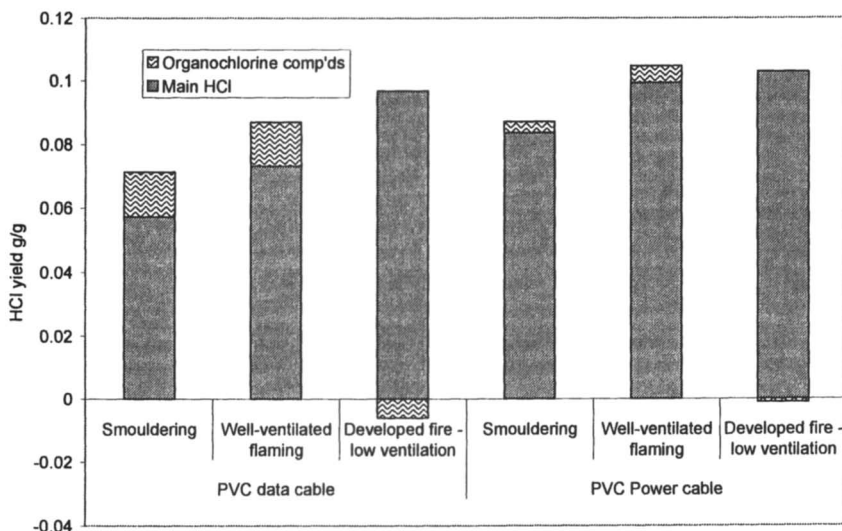


Figure 4. HCl yield for the three fire conditions in g/g of non-metallic material for PVC cables (lower section is yield from main chamber, total height is yield from secondary oxidiser, and upper section is yield of organochlorine compounds).

Figure 4 shows the HCl yield for the PVC containing materials under different fire conditions. This shows that significant chain stripping yielding HCl, aromatics and char precursors is occurring, even under smouldering conditions. The HCl produced could either be released directly into the gas phase, or could be trapped by reaction with the chalk.



The quantity of chalk present in the sample is theoretically sufficient to trap all the HCl, though the transport properties of the decomposing cable, and the relatively large size of the chalk particles clearly allows significant quantities of HCl to escape. Further support for HCl trapping by chalk comes from the surprisingly high yield of CO₂ under smouldering conditions as discussed earlier.

Under fully developed flaming conditions, chalk that has been converted to CaO is not capable of trapping HCl, giving correspondingly higher yields both of HCl and of CO₂. The theoretical maximum yield of HCl from the PVC power cable is around 0.3 g/g, suggesting that considerable HCl is trapped or lost, even at 825°C for the fully developed fire condition. The slightly lower yields of HCl from the secondary oxidiser for the developed fire condition, giving a notional negative organochlorine yield may arise from deposition of HCl between the effluent dilution chamber and the secondary oxidiser, or may be within the limits of experimental error.

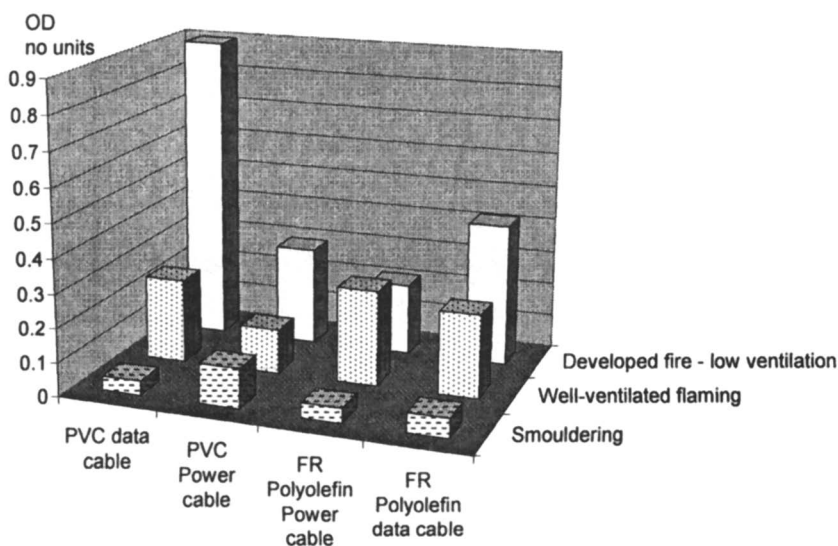


Figure 5. Smoke production expressed as optical density (OD)

Figure 5 shows the smoke production, which shows similar levels of obscuration for all cables under smouldering, well-ventilated and even developed fire conditions, which is surprising since PVC is normally associated with the highest smoke yields. The PVC power cable shows three times the average smoke yield under smouldering conditions, but half the average smoke yield under well-ventilated flaming. Under developed fire conditions, the data cables perform significantly worse than the power cables, with the polyolefin cable producing twice the smoke of the corresponding power cable, and the PVC data cable producing 3½ times more than its corresponding power cable. This probably arises from the more rapid pyrolysis of the thinner sheath material. The mechanisms of smoke production are not well understood, but the presence of particulates is likely to influence the radiant flux from the flame, which in turn may impact on the large scale fire behaviour.

Figure 6 shows the total fractional effective dose, calculated using the N-Gas model with steady state data, taken over the central 5 minutes of the run. This shows the total FED using the N-Gas model and the individual contributions to it, CO (increased by the higher respiration rate caused by carbon dioxide), hypoxia, and hydrogen chloride. Under smouldering conditions, for PVC cables, the major contribution to the FED comes from HCl. Under well-ventilated flaming, and developed fire low-ventilation conditions, the major contribution to the fire gas toxicity comes from the carbon monoxide for all cables, but is significantly higher for PVC based cables. This is probably caused by interference of the flame reactions by the more stable $\text{Cl}\cdot$ radical, which reduce the concentration of the more reactive $\text{H}\cdot$ and $\text{OH}\cdot$ radicals, preventing oxidation of CO to CO_2 .

Figure 7 shows a comparison of four methodologies for the calculation of fractional effective dose. Two of the graphs show the results of the FED calculation taken over the "central 5 minute period of the test" as specified in IEC 60695-7-50, and two taken over the full duration of the run, neglecting the fluctuations at the start and finish. The two pairs of graphs also show the differences between the N-Gas model and the more sophisticated Purser model for the calculation of FED. The rank order correlation between the two calculation methods is extremely good, and the actual FED values obtained show good correlation, given the fluctuations inherent within the fire data. In fire safety engineering, FEDs generally use a safety factor of three, making differences between the two methodologies insignificant.

Conclusions

A bench scale method of predicting the fire toxicity of linear products, based on a materials test method has been described. This correlates with other test data, and uniquely allows material balances to be calculated, allowing quantification of possible losses. This has allowed inhomogeneous products, such as cables to be investigated in a scenario related to end use, which is likely to be a much better model of fire behaviour than testing the individual components (fire retarded sheath, bedding and insulation) separately.

The tube furnace model provides toxic gas yields for specified fire conditions, independent of the material's flammability. The standard test method used in this work provides interesting fire toxicity data for the conditions defined by the standard. However, the PVC power cable did not appear to undergo flaming combustion for the whole duration of the run, and the polyolefin power cable underwent intermittent combustion. In both cases, the very high ventilation rate of 22.6 l/min is likely to have had a quenching impact on the flame, as has been reported in other work on the same apparatus.

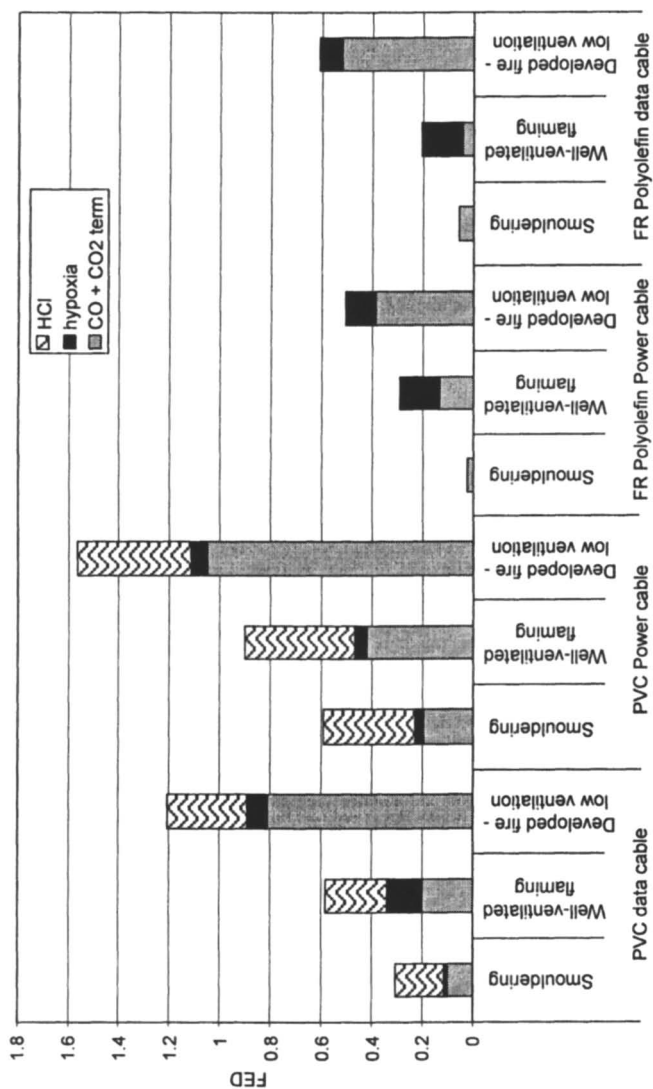


Figure 6. Fractional effective dose (FED) data showing the effects of the three contributions

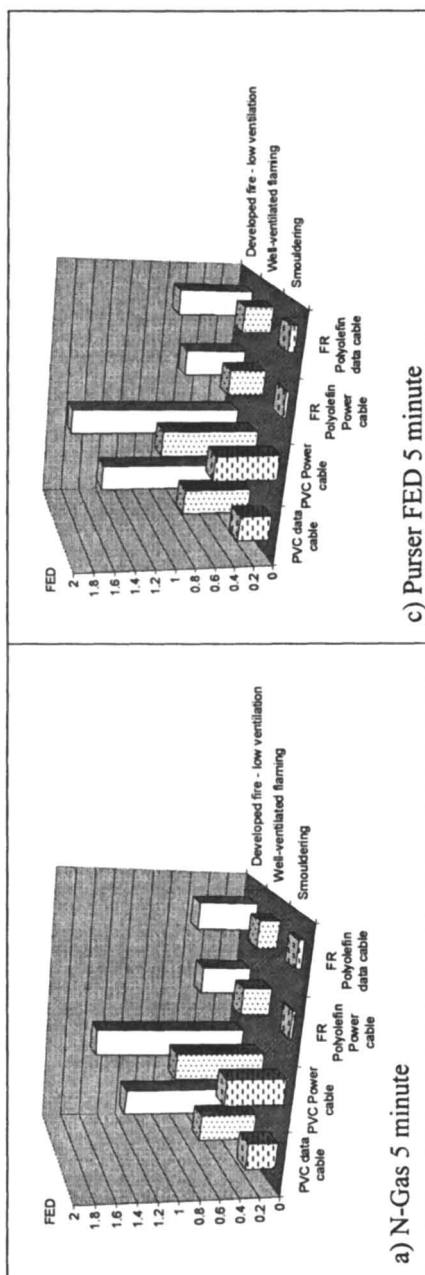


Figure 7. Fractional Effective Doses (FEDs) calculated by a) N-Gas 5 minute, b) N-Gas Full burn, c) Purser FED 5 minute, and d) Purser FED full burn time. Continued on next page.

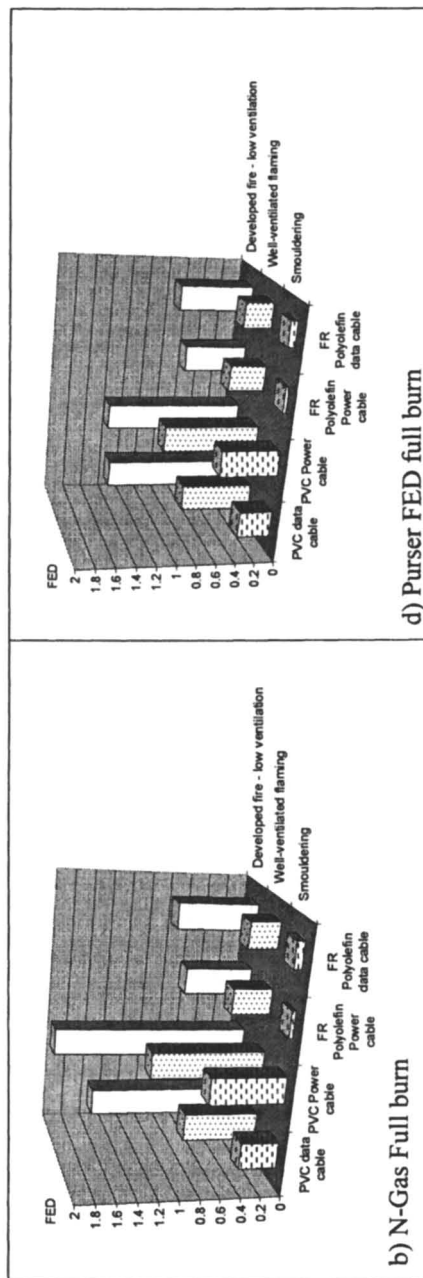


Figure 7. Continued.

With respect to the individual cables it is observed that most yields and especially CO (but not HCl), are highly dependent on conditions. The FED reflect both the yield of toxic products, and the degree of combustion. Under smouldering conditions, HCl is the major contributor to the toxic hazard, but its significance diminishes with the severity of the fire.

Little difference is observed (especially in the relative ranking of hazard) between the Purser (FRS) and N-Gas (NIST) models. The selection of a 5 minute steady state versus the total burn time is subjective, but has a minimal effect on the overall rankings in the cases reported here.

Acknowledgements

We would like to thank EPSRC and the European Association of Producers of Flame Retarded Olefinic Cable Compounds (FROCC) for the provision of one project studentship each to support this work.

References

1. *Fire Statistics United Kingdom 2002*; Office of the Deputy Prime Minister: London, April 2004.
2. *Life threat from fires – Guidance on the estimation of time available for escape using fire data*; ISO TS 13571:2001
3. *Estimation of lethal toxic potency of fire effluents*; ISO 13344:1996.
4. Hull, T. R.; Quinn, R. E.; Areri, I. G.; Purser, D. A. *Polym. Degrad. Stab.* **2002**, *77*, 235-242.
5. Hull, T. R.; Carman, J. M.; Purser, D. A. *Polym. Int.*; **2000**, *49*, 1259-1265.
6. *Assessment of hazard to life and health from fire - Part 2: Guidance on methods for the quantification of hazards to life and health and estimation of time to incapacitation and death in fires* [Fire Types Table p18]. BS 7899-2:1999
7. Purser, D. A.; Fardell, P. J.; Rowley, J.; Vollam, S.; Bridgeman, B.; Ness, E. M. *Proceedings of the Flame Retardants '94 Conference*, Interscience Communications, London 1994
8. Hermansson, A.; Hjertberg, T.; Sultan, B.-Å. *Fire Mater.*; **2003**, *27*, 51-70.
9. Lebek, K.; Hull, T. R.; Price, D; in this volume.

Chapter 28

Alternatives to Thermal Curing in Diacetylene-Containing Carboranylenesiloxanes

Manoj K. Kolel-Veetil and Teddy M. Keller

**Advanced Materials Section, Code 6127, Chemistry Division,
Naval Research Laboratory, Washington, DC 20375**

The dilutions in crosslinking density in the thermally and thermo-oxidatively stable, diacetylene-containing inorganic-organic hybrid oligomers of poly(carboranylenesiloxanes) have resulted in rendering the network polymers derived from them elastomeric in nature. While the crosslinking reactions of the diacetylenes require high temperatures and protracted curing times, avenues of diacetylene-curing with less demanding conditions should add to the possibilities of their potential applications. Several alternative avenues for the curing of the diacetylenes have been explored and the preliminary results are reported.

The recent rapid advance of modern technology has resulted in an increasing demand for new high performance materials in a wide variety of engineering applications. Such materials are increasingly expected to function under unusual service conditions. In the aerospace industry, the need especially for high temperature elastomers, plastics, and ceramics that have thermal,

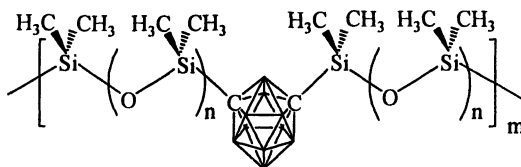


Figure 1: Poly(carboranylenesiloxane)s.

thermo-oxidative, and hydrolytic stability and that can also maintain flexibility to well below ambient temperatures is severe. In this regard, the linear polymers of carboranylenesiloxanes (Figure 1) stand out as excellent candidates due to their exceptional thermal, thermo-oxidative, and elastic properties (1). The properties of these linear polymers may be enhanced further by their conversion into extended network polymers. During the early development of the carboranylenesiloxane chemistry, the available method for the production of a network polymer from a precursor carboranylenesiloxane was by the polymerization in air (at 315°C for 300h) of the vinyl groups of a pendant vinyl-containing carboranylenesiloxane by organic peroxides (2). However, in recent times, research in this area has resulted in the development of extended network systems of carboranylenesiloxanes that were produced either by the thermal polymerization of the diacetylene groups (PCSA networks) (Figure 2) (3) or by the hydrosilation of vinyl or ethynyl groups (Figure 3) (4). While the hydrosilation reaction proceeded at ambient conditions, the thermal curing required the exposure of the materials to temperatures in excess of 250°C for several hours. The networks produced from the thermal reactions, however, were observed to be tougher than the networks obtained from the hydrosilation reactions. The parent precursor, 1 (Figure 2), of the diacetylene-cured network contained the disiloxyl unit as the constituent siloxane moiety and produced networks that were plastic in nature on thermal curing (5). The crosslinked materials were observed to have high weight retention on thermal treatment to 1000°C in both N₂ and air (weight retention in N₂ = 87% and in air = 92%) and consequently were found to possess exceptional ceramic characteristics, thereby allowing their applications as both high temperature plastics and ceramics. Subsequent research to produce high temperature elastomeric versions of these materials resulted in the recent development of crosslinked network carboranylenesiloxane systems by the manipulation of the crosslinking density in 1 (6). A reduction in the crosslinking density in 1 by the lowering of the concentration of constituent diacetylene units yielded products with decreased

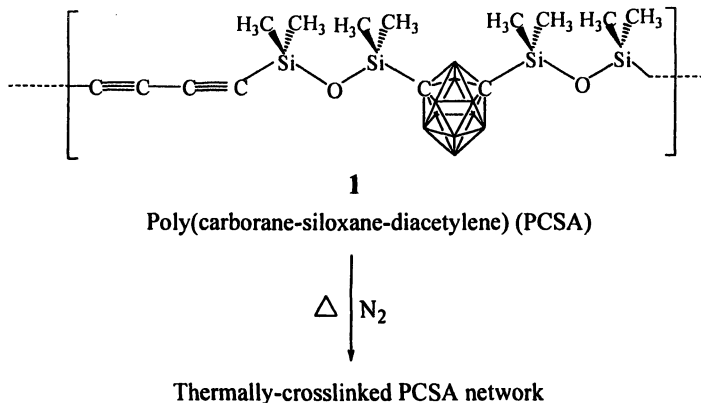


Figure 2: Thermal curing of a PCSA oligomer into a network system.

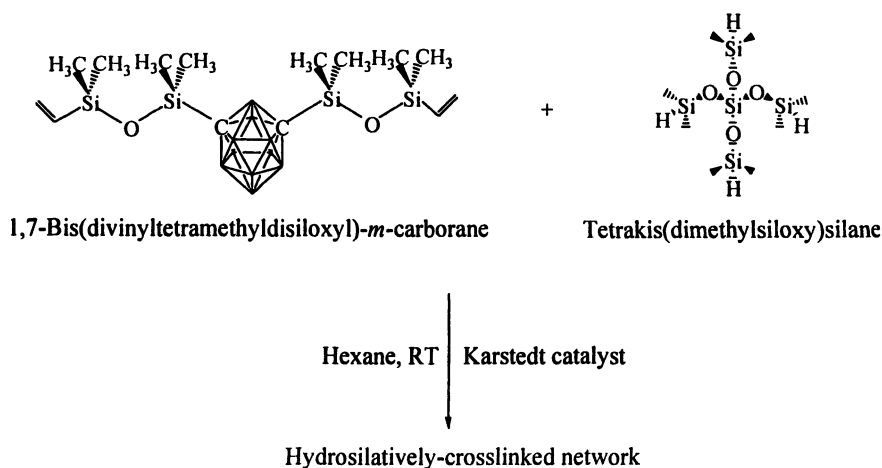


Figure 3: Network formation by the hydrosilylation reaction of a vinylcarboranylenesiloxane with a branched crosslinking siloxane.

glass transition temperatures. However, the products were still observed to predominantly possess a plastic nature at ambient conditions. In order to further improve the elasticity of these diacetylene-diluted products, the constituent siloxyl unit was changed from disiloxyl to the more flexible trisiloxyl unit. As expected, the substitution rendered the network products derived from these altered precursors elastomeric at ambient conditions (Figure

4) (7). Thus, the network systems of carboranylenesiloxanes that are currently available encompass the gamut of elastomers, plastics, and ceramics. However, the conditions for the thermal curing of the diacetylene-diluted versions of both **1** and its trisiloxyl derivatives still require thermal treatment at high temperature (250°C and above) as required for **1**. Hence, in an attempt to make these systems more amenable to applications at ambient conditions, four avenues were explored that required much milder conditions for the curing of diacetylenes. The explored avenues included the curing of the diacetylenes in **1** by UV irradiation, TaCl₅-catalyzed polymerization, W(CO)₆-catalyzed photo polymerization and Rh₂(μ-Cl)₂(COD)₂-catalyzed hydrosilation reaction. The preliminary results of the studies are reported.

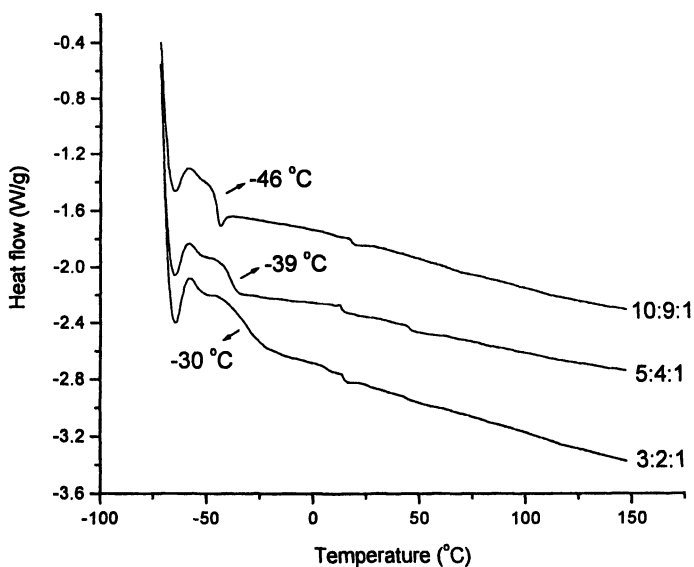


Figure 4: DSC thermograms of three diacetylene-diluted systems of poly(carborane-trisiloxane-diacetylene) systems with varying ratios of siloxane:carborane:diacetylene.

Experimental

The synthesis of **1** was performed by following a published procedure (5). All of the reactions were carried out under inert conditions using standard Schlenk line techniques. Toluene (anhydrous, 99.8%) and diethyl ether (Et₂O, anhydrous, 99.9%) were used as received from Aldrich. 1,1,3,3,5,5,7,7-Octamethyltetrasiloxane was used as received from Gelest. The metal catalysts, tantalum(V) chloride (TaCl₅, 99.99%), tungsten hexacarbonyl (W(CO)₆, 99.9+%), and chloro(1,5-cyclooctadiene)rhodium(I) dimer (Rh₂(μ-Cl)₂(COD)₂, 98%) were used as received from Aldrich. (Cp)₂Ta=CH(CMe)₃Cl was synthesized following a published procedure (8).

Thermogravimetric analyses (TGA) were performed on a SDT 2960 Simultaneous DTA-TGA analyzer. Differential scanning calorimetry (DSC) studies were performed on a DSC 2920 modulated DSC instrument. All thermal experiments were carried out at a heating rate of 10°C/min and a nitrogen flow rate of 100cc/min. The UV-curing studies were performed using a Model 22-UV lamp (115 V, 60 Hz, 4w) obtained from Chemical Engineering Inc., Santa Rosa, CA. Infrared (IR) spectra were obtained on a Nicolet Magna 750 Fourier transform infrared spectrometer.

Polymerization reactions:

(a) UV-curing reactions: A 1M solution of compound **1** in Et₂O was placed on a NaCl infrared disk. On evaporation of the solvent, a fine film was deposited on the surface of the disk. An IR spectrum of this sample was obtained as a reference and the film was exposed to the radiation of a UV lamp. The FTIR spectrum of the film was monitored periodically for several days.

(b) TaCl₅-catalyzed curing of the diacetylenes in 1: To a flame-dried Schlenk flask was added 0.450 g (1.000 mmol) of **1** and 5 mL of toluene under argon. The resulting brown solution was placed in an oil bath at 85°C. In a separate flame-dried Schlenk flask, 0.023 g (0.066 mmol) (polymer to catalyst ratio = 15:1) of TaCl₅ was dissolved in 2.5 mL of toluene under argon at 80°C yielding a bright yellow solution. The Ta solution was then transferred to the polymer solution via cannula. In about an hour, a darkening of the reaction solution was observed. The reaction was allowed to proceed for 3 days. After this period, the solvent was removed under vacuum to yield a rubbery dark blackish-brown product.

The reactions involving polymer:TaCl₅ and polymer:Cl₂Ta=CH(CMe)₃Cl at ratios of 1:1 and 15:1, respectively, were carried out following the procedure described above.

(c) $W(CO)_6$ -catalyzed photo polymerization of 1: A mixture of 0.450 g (1.000 mmol) of **1** and 0.023 g (0.066 mmol) of $W(CO)_6$ was placed in a quartz photo reactor under argon. The solids were dissolved in 5 mL of hexane at room temperature and the solution was exposed to wavelengths $>300\text{nm}$ for a day. After this period, the solvent was removed under vacuum to yield a rubbery blackish-brown product.

(d) $(Rh_2(\mu-Cl)_2(COD)_2)$ -catalyzed hydrosilation of 1: To a flame-dried Schlenk flask was added 0.225 g (0.500 mmol) of **1** and 0.330 mL (1.000 mmol) of 1,1,3,3,5,5,7,7-octamethyltetrasiloxane in 1 mL of toluene under argon. The golden brown solution was placed in an oil bath at 70°C . A solution of 0.010 g (0.020 mmol) of $Rh_2(\mu-Cl)_2(COD)_2$ in 0.50 mL of toluene was prepared in another flame-dried Schlenk flask and the contents were cannulated into the former flask under argon. The solution turned blackish-brown immediately. The progress of the reaction was monitored periodically by infrared spectroscopy. After an hour of reaction, the solvent was removed under vacuum to leave behind a rubbery black product.

Results and Discussion

UV-curing reactions: Solid state photo polymerization of diacetylenes was first discovered by G. Wegner in 1969 (9). Innumerable examples have appeared in the literature on this area (10). The efficacy of photo polymerization by UV exposure in **1** was found to be poor compared to the solid-state polymerization of diacetylenes. The progress of the curing was monitored by IR spectroscopy. On complete curing, the diacetylene absorption at around 2079 cm^{-1} in the FTIR spectrum of the uncured sample was found to completely disappear from the corresponding spectrum of the cured sample which was dark brown in color (Figure 5). To achieve any appreciable extent of curing, the films (cast on a NaCl IR disk) had to be irradiated with UV radiation for an extended period (several days). The same level of cure could be achieved more rapidly (in about 2 hours) under harsher thermal cure conditions ($250\text{--}400^\circ\text{C}$) (7). The slowness of the UV-curing could be attributed to a lack of proximal ordering/stacking of the diacetylene centers, which results in the enhancement of the rate of solid state polymerization by irradiation in the solid phase (11).

$TaCl_5$ -catalyzed curing of the diacetylene units in 1: In the literature, a plethora of examples of transition-metal catalyzed metathetical polymerization of olefins and alkynes involving metallacyclobutadiene intermediates are known (12). Among the catalysts, $TaCl_5$ is known to be especially effective for the

polymerization of acetylenes (13). Hence, TaCl_5 was chosen for the polymerization reaction studies of **1**. A reaction at an oligomer to catalyst ratio of 15:1 was allowed to proceed for 3 days since periodic FTIR analysis of the reaction mixture exhibited the remnant of the diacetylene stretch at 2079 cm^{-1} during the first two days of the reaction. The reaction was repeated at an oligomer to catalyst ratio of 1:1 and resulted in the disappearance of the diacetylene absorption in 2h. Hence, in the former reaction it is believed that, at the low catalyst concentration, the availability and ability of the diacetylene units to polymerize at the Ta centers are greatly reduced due to the initial

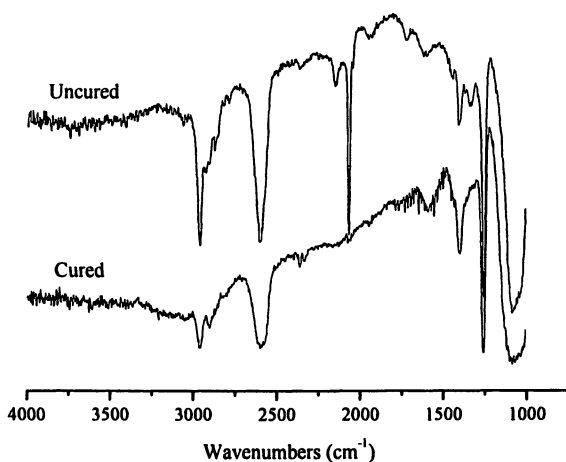


Figure 5: IR spectra of the cured and uncured samples of **1**.

formation of a viscous gel during the reaction. Thus, a rapid curing of the diacetylene units is thwarted under such a condition. This was also apparent in the DSC thermogram of the intermediate reaction product after 2 days (Figure 6). There were two endothermic transitions centered at -44°C and -30°C within the developing networked system attributed to glass transition temperatures of distinct regions in the product. The production of a $\text{Ta}=\text{C}$ species during the polymerization could be argued based on the observation that a similar polymerization reaction catalyzed by $(\text{Cp})_2\text{Ta}=\text{CH}(\text{CMe})_3\text{Cl}$ which contained an alkylidene species was found to accelerate the reaction. The polymerization reaction using this catalyst was complete in 4h at 80°C . In the TaCl_5 -catalyzed

reaction, the initial formation of a catalytically active Ta=C species, derived from the diacetylene units in **1**, perhaps has a long induction period thereby causing the polymerization to be slow. Thus a probable mechanism for the reaction could involve the initial formation of a Ta=C (Ta-vinylidene) species from a diacetylene unit followed by the metallacyclobutadiene formation and the propagation steps (Figure 7). Such a mechanism has been proposed previously in transition metal-catalyzed polymerization of alkynes (14). The polymerization products were determined to have high thermal stabilities on treatment to 1000°C (weight retention in N₂ = 85% and in air = 91%).

W(CO)₆-catalyzed photo polymerization of 1: In 1985, Landon et al. reported the room temperature photo polymerization of alkynes in the presence of W(CO)₆ (15). A tungsten-vinylidene/alkylidene intermediate was postulated as the reactive intermediate in the polymerization. As **1** was susceptible to a metathetical polymerization involving a Ta-alkylidene intermediate, a photo polymerization of **1** using W(CO)₆ seemed reasonable. In a reaction conducted at room temperature at a polymer:catalyst ratio of 15:1 in the presence of wavelengths >300nm, a complete polymerization was observed in 24h as determined by the absence of a diacetylene stretch at 2079cm⁻¹ in the FTIR spectrum of the product. The product from the polymerization was determined to have similar thermal stabilities on treatment to 1000°C as observed for the TaCl₅-catalyzed product (weight retention in N₂ = 86% and in air = 92%). It seems reasonable that the rate of the polymerization could be enhanced if the

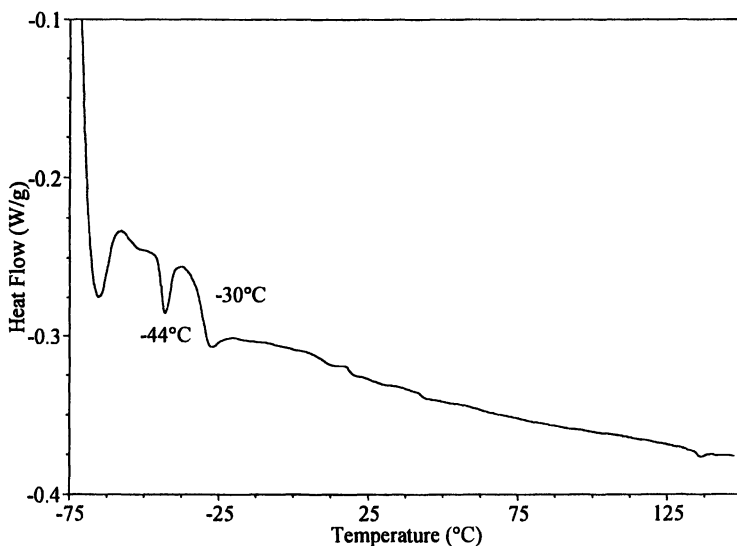


Figure 6: DSC thermogram of the network produced from the TaCl₅-catalyzed polymerization of **1**.

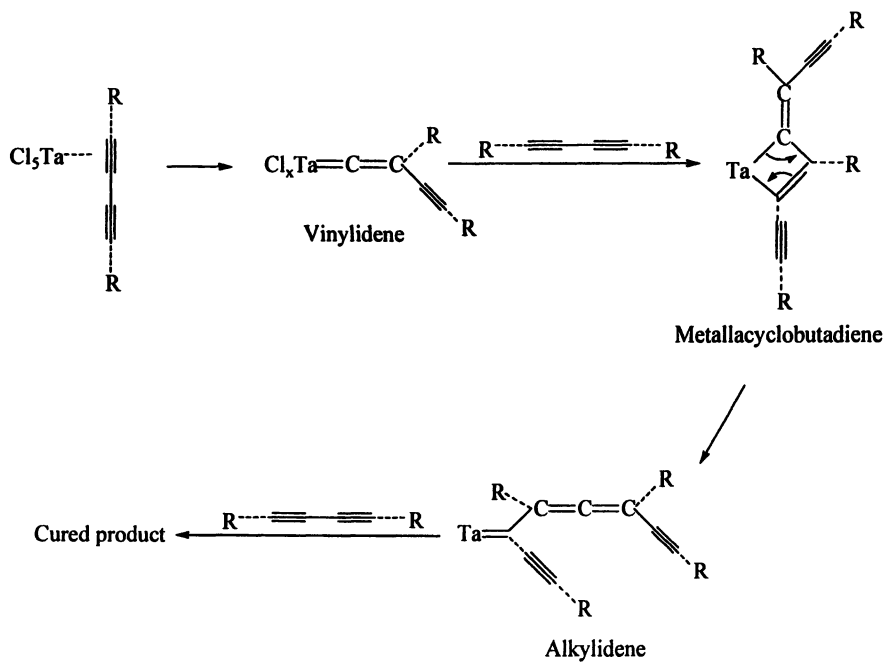


Figure 7: A proposed mechanism for the TaCl₅-catalyzed polymerization of 1.

reaction was carried out at a higher temperature. Since a W-vinylidene/alkylidene species is believed to be the catalytically active species, the use of a preformed tungsten-alkylidene catalyst is also expected to further expedite the rate of the polymerization.

Rh₂(μ-Cl)₂(COD)₂-catalyzed hydrosilation of 1: Examples of the polymerization of terminal alkynes by hydrosilation are vast in the literature (16). A few examples of hydrosilation reactions of butadiynes are also known (17). Among the catalysts, Rh₂(μ-Cl)₂(COD)₂ stands out as an especially active catalyst for the hydrosilation of alkynes. The Rh₂(μ-Cl)₂(COD)₂-catalyzed hydrosilation reaction of 1 with 1,1,3,3,5,5,7,7-octamethyltetrasiloxane proceeded rapidly in toluene at 70 °C. The darkening of the reaction mixture was instantaneous. The reaction was very effective even at an oligomer to catalyst ratio of 25:1. It is probable that an even lower ratio might suffice for a reasonably fast reaction rate. The completion of the polymerization was monitored by the disappearance of the diacetylene absorption at 2079 cm⁻¹ in the FTIR spectrum of the reaction mixture, which occurred within an hour from the start of the reaction. The product, expected to possess a complex network structure (Figure 8), was blackish-brown in appearance. The thermal and thermo-oxidative stabilities of the product as determined by TGA analyses were reasonably high (weight retentions; In N₂ = 60%; In air = 72%). The product exhibited a T_g value that was below -65°C.

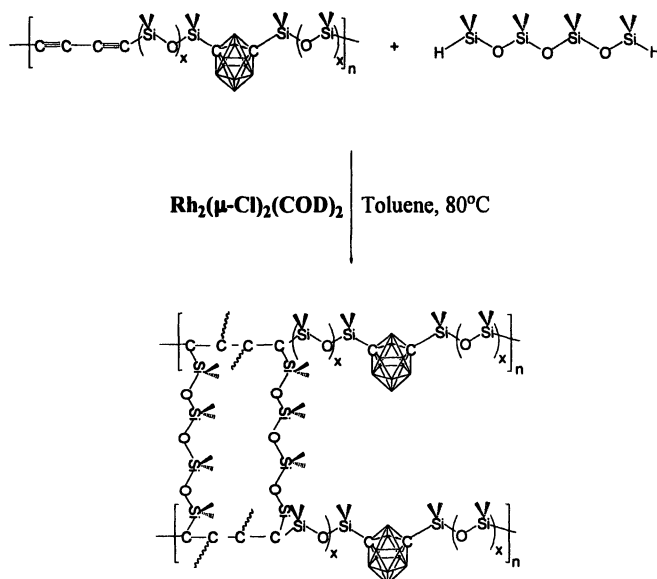


Figure 8: A simplified depiction of the network formed from the Rh₂(μ-Cl)₂(COD)₂-catalyzed hydrosilation of 1 by octamethyltetrasiloxane.

Conclusions

This study involved the exploration of four alternative strategies to the thermal curing of diacetylene-containing carboranylenesiloxanes. The radiation (UV)-cured polymerization seems rather inefficient. However, the Ta-cured metathetical polymerization, the $W(CO)_6$ -catalyzed photo polymerization, and the $Rh_2(\mu-Cl)_2(COD)_2$ -catalyzed hydrosilation of **1** appear promising. The $Rh_2(\mu-Cl)_2(COD)_2$ -catalyzed hydrosilation, which did not involve polymerization of the diacetylenes, produces a product that was not thermally and thermo-oxidatively stable as the ones produced using the other three avenues. However, the reaction is found to have the fastest rate among the four compared alternatives. While $TaCl_5$, $(Cp)_2Ta=CH(CMe)_3Cl$ and $W(CO)_6$ catalysts operate utilizing a $M=C$ reactive entity and yield products of similar thermal and thermo-oxidative stabilities, $(Cp)_2Ta=CH(CMe)_3Cl$ seems to offer the fastest rate for the polymerization by this route owing to a preformed $Ta=C$ entity. It is probable that a photo catalyst more active than $W(CO)_6$ could also affect the polymerization at a rate comparable to or faster than that of $(Cp)_2Ta=CH(CMe)_3Cl$. Additionally, in solid state UV cured reactions, the established means of activation of the diacetylene unit is by the generation of radical species which propagate by reacting with similar species in the ordered solid (*18*). In the current study, the lack of a long range order perhaps thwarts such propagation in **1**. In contrast, in the transition metal catalyzed polymerizations, the presence of the catalytic transition metal sites facilitate the orientation of reactive radical species into a metallacyclobutadiene moiety for propagation. Hence, the mechanistic limitations make the UV cured reactions less viable than the metathetical reactions for the curing of **1**. In addition, it is possible that the energy of the UV radiation used in the current study was not sufficient to produce enough reactive radicals for propagation. If this is the case, the solid-state polymerization of **1** could be made viable if a more intense high energy radiation source such as an electron beam source is utilized in place of a UV radiation source.

References

1. Dvornic, P.R.; Lenz, R.W. *High Temperature Siloxane Elastomers*; Huthig & Wepf: New York, 1990.
2. Hedaya, E.; Kawakami, J.H.; Kopf, P.W.; Kwiatkowski, G.T.; McNeil, D.W.; Owen, D.A.; Peters, E.N.; Tulis, R.W. *J. Polym. Sci., Polym. Chem. Ed.*, **1977**, *15*, 2229-2238.
3. Henderson, L.J.; Keller, T.M. *Polym. Preprints*, **1993**, *34(1)*, 345-346.
4. Kolel-Veetil, M.K.; Keller, T.M. *Polymer Preprints*, **2004**, *45(1)*, 579-580.

5. Henderson, L.J.; Keller, T.M. *Macromolecules*, **1994**, *27*, 1660-1661.
6. Kolel-Veetil, M.K.; Keller, T.M. *J. Mater. Chem.* **2003**, *13*, 1652-1656.
7. Kolel-Veetil, M. K.; Keller, T. M. *Chem. Mater.* **2004**, *16*, 3162-3167.
8. Schrock, R. R. *J. Am. Chem. Soc.* **1974**, *96*, 6796-6797.
9. Wegner, G. Z. *Naturforsch., B: Anorg. Chem., Org. Chem., Biochem., Biophys., Biol.* **1969**, *24B*, 824-829.
10. (a) Ogawa, T. In *Polymeric Materials Encyclopedia*; Salamone, J. C. Eds.; CRC press: Boca Raton, FL, **1996**, Vol. 8, p 5725-5748. (b) Kricheldorf, H. R.; Schwarz, G. In *Handbook of Polymer Synthesis*; Kricheldorf, H. R., Eds.; Marcel Dekker: New York, **1991**, Chapter 27, p 1629-1652.
11. Hammond, P. T.; Rubner, M. F. *Macromolecules* **1997**, *30*, 5773-5782.
12. (a) Wallace, K. C.; Liu, A. H.; Davis, W. M.; Schrock, R. R. *Organometallics* **1989**, *8*, 644-654. (b) Schrock, R. R.; Luo, S.; Zanetti, N. C.; Fox, H. H. *Organometallics* **1994**, *13*, 3396-3398. (c) Masuda, T.; Hyano, S.; Iwawaki, E.; Nomura, R. *J. Mol. Cat. A: Chem.* **1998**, *133*, 213-220. (d) Hayano, S.; Masuda, T. *Macromolecules* **1999**, *32*, 7344-7348.
13. Masuda, T.; Isobe, E.; Higashimura, T. *Macromolecules* **1985**, *18*, 841-845.
14. Ohff, A.; Burlakov, V. V.; Rosenthal, U. *J. Mol. Cat. A: Chem.* **1996**, *108*, 119-124.
15. Landon, S.J.; Schulman, P.M.; Geoffroy, G.L. *J. Am. Chem. Soc.* **1985**, *107*, 6739-6740.
16. For reviews on hydrosilation of alkynes (a) Ojima, I. In *The Chemistry of Organic Silicon Compounds*; Patai, S.; Rappoport, Z., Eds.; John Wiley & Sons, Ltd.: New York, **1989**; p 1479-1492. (b) Armitage, D. A. In *Comprehensive Organometallic Chemistry*; Vol. 2; Wilkinson, G.; Stone, F. G. A.; Abel, E. W., Eds.; Pergamon: Oxford, England, **1982**; Vol. 2, p 117-133. Some other reports: (c) Lewis, L. N.; Sy, K. G.; Bryant, G. L.; Donahue, P. E. *Organometallics* **1991**, *10*, 3750-3759. (d) Wang, F.; Neckers, D. C. *J. Organomet. Chem.* **2003**, *665*, 1-6. (e) Field, L. D.; Ward, A. J. *J. Organomet. Chem.* **2003**, *681*, 91-97.
17. For hydrosilation reactions of butadiynes: (a) Kusumoto, T.; Hiyama, T. *Chem. Lett.* **1985**, 1405-1410. (b) Kusumoto, T.; Ando, K.; Hiyama, T. *Bull. Chem. Soc. Jpn.* **1992**, *65*, 1280-1287. (c) Tillak, A.; Pulst, S.; Baumann, W.; Baudisch, H.; Kortus, K.; Rosenthal, U. *J. Organomet. Chem.* **1997**, *532*, 117-124.
18. Bubeck, C.; Tieke, B.; Wegner, G. *Mol. Cryst. Liq. Cryst.* **1983**, *96*, 109-115.

Chapter 29

Processable Phthalonitrile Resins with High-Thermal and Oxidative Stability

Matthew Laskoski, Dawn D. Dominguez, and Teddy M. Keller

**Materials Chemistry Branch, Code 6127, Naval Research Laboratory,
Washington, DC 20375-5320**

A processable multiple aromatic ether-linked phthalonitrile with high thermal and oxidative stability has been synthesized and characterized. The oligomeric phthalonitrile monomer was prepared in a two-step, one-pot procedure using an excess amount of resorcinol and 4,4'-difluorobenzophenone in a N,N-dimethylformamide/toluene mixture and K_2CO_3 as the base followed by end-capping with 4-nitrophthalonitrile. The monomer was thermally crosslinked in the presence of bis(4-[4-aminophenoxy]phenyl)sulfone forming a void-free thermoset. Thermal, oxidative, and mechanical measurements were performed on the resulting polymer. The polymer exhibits excellent thermal and oxidative stability, superior mechanical properties, and low water absorption

Thermosetting polymers containing terminal phthalonitrile units are a unique class of high temperature materials having a variety of potential uses in the adhesive (1) and electronic (2,3) industries and as a matrix resin in structural applications (4). Phthalonitrile composites have superior flame resistant properties when compared to other polymeric composites. Phthalonitriles are the only thermosetting materials that meet the Navy's stringent requirement of MIL-STD-2031 (6) for use as the matrix resin in polymeric composites aboard Naval submarines (4a,b). In the past twenty years, a variety of high temperature materials have been developed by incorporating aromatic units within polymeric systems containing phthalonitrile (5) end units. To date, the majority of phthalonitrile resins have high melting points and short processing windows and result in somewhat brittle thermosets once thermally cured. This limits the use of these resins in a broad variety of applications.

Recent research in this area has focused on the incorporation of aryl ether-containing linkages between the terminal phthalonitrile units (7). It has been determined that the necessity of using low cost organic reactants, a short reaction synthetic scheme, and low temperature processing of the resin are essential to the viable use of organic resins in various composite applications. New phthalonitrile monomers have been prepared utilizing a two-step, one-pot reaction (5b). This synthetic approach results in a phthalonitrile system with a lower melting point and a broader processing window for easy conversion to crosslinked polymers, which will allow phthalonitrile resins to compete with other high performance polymeric systems. The synthesis, polymerization, and material properties of a newly developed phthalonitrile resin based on resorcinol will be described. The thermal and physical properties of this material will be compared to those of a phthalonitrile system based on bisphenol A.

Experimental

All starting materials were of reagent grade and used without further purification. The synthesis of the oligomeric multiple aromatic ether-containing phthalonitrile **6b** prepared from bisphenol A and 4,4'-difluorobenzophenone has been described previously (7b,8). Differential scanning calorimetric (DSC) analysis was performed using a TA Instruments DSC 2920 modulated thermal analyzer at a heating rate of 10 °C min⁻¹ and a nitrogen purge of 50 cm³ min⁻¹. Thermogravimetric analysis (TGA) was performed using a TA Instruments SDT 2960 Simultaneous DTA-TGA at a heating rate of 10 °C min⁻¹ under a nitrogen or air purge of 50 cm³ min⁻¹. Infrared (IR) spectra were recorded as films deposited on NaCl plates using a Nicolet Magna FTIR 750 spectrometer. ¹H-NMR was performed using a Brüker ADVANCE 300 spectrometer.

A TA Instruments AR-2000 Rheometer, in conjunction with an environmental testing chamber for temperature control and torsion fixtures, was used to monitor the response of samples (50 mm x 13 mm x 2 mm) to oscillatory testing. The measurements were made in nitrogen over the temperature range of

~ 40 to 450 °C. A temperature ramp of 3 °C min⁻¹ was used to determine the storage modulus and damping factor ($\tan \delta$) of the material at a frequency of 1 Hz and a strain of 2.5×10^{-2} %. Normal force control was utilized throughout the tests to keep the samples taut.

Preparation of the Oligomeric Multiple Aromatic Ether-Containing Phthalonitrile (6a).

To a 100 mL, three-necked flask fitted with a thermometer, a Dean-Stark trap with condenser, and a nitrogen inlet were added resorcinol (1a) (10.0 g, 90.8 mmol), 4,4'-difluorobenzophenone (2) (9.90 g, 45.4 mmol), powdered anhydrous K₂CO₃ (9.40 g, 68.1 mmol), toluene (10 mL), and N,N-dimethylformamide (DMF) (60 mL). The resulting mixture was degassed with argon, the Dean-Stark trap was filled with toluene, and the mixture was heated to reflux at 135 - 145 °C for 12 - 18 h or until no more water was collected in the Dean-Stark trap. The toluene was then removed by distillation and the reaction mixture was cooled to 50 °C. At this time, 4-nitrophthalonitrile (5) (15.7 g, 90.7 mmol) was added in one portion and the reaction mixture was heated at 80 °C for 6 - 8 h. The mixture was cooled to ambient temperature and poured into a 5 % aqueous KOH solution resulting in the formation of a solid. The material was broken up and collected by filtration at reduced pressure. The white solid was dissolved in chloroform (200 mL) and washed with 200 mL of a 5 % aqueous NaOH solution, 200 mL of distilled water, 200 mL of a 5 % aqueous HCl solution, and finally 200 mL of water until neutral. The solvent was removed *in vacuo* and the solid vacuum dried to yield 6a (27.3 g, 92 %). ¹H-NMR (300 MHz, CDCl₃): δ 7.85-7.70 (m, aromatic-H), 7.57-7.25 (m, aromatic-H), 7.12-6.97 (m, aromatic-H), 6.92-6.78 (m, aromatic-H). IR [cm⁻¹]: ν 3074 (C=CH), 2232 (CN), 1650 (C=O), 1587 (C=C), 1477 (aromatic), 1307 (aromatic), 1307 (C-O), 1244 (CH₃), 1162 (C-O), 928 (C-O), 842 (aromatic).

Formulation of 6 and Aromatic Amine Composition

To the melt of 6 at 200 °C was added 3 weight % of bis(4-[4-aminophenoxy]phenyl)sulfone (*p*-BAPS). Once the curing additive had been evenly dispersed by stirring, the sample was cooled and used in the DSC and TGA cure studies.

Polymerization and TGA Studies on Thermoset 7

Solid samples of 6 containing 3 weight % of *p*-BAPS were added to TGA pans. The mixtures were cured under nitrogen by heating at 270 °C for 12 h,

300 °C for 3 h, 350 °C for 6 h, 375 °C for 8 h and 425 °C for 8 h. Polymer 7 formed as a film on the bottom of the pan. The thermal and thermo-oxidative properties of the polymer film were then determined from 50-1000 °C.

Rheometric Measurement Sample Preparation

Samples for rheometric measurements were prepared by degassing **6** under vacuum at 275 °C for 4 h in a mold with cavity dimensions of 65 mm x 13 mm. The temperature of the mold was reduced to 220 °C, *p*-BAPS (3 weight %) was added with stirring and the resulting mixtures were degassed for an additional 30 min. The samples were cooled, placed in an oven, and heated at 270 °C for 12 h, 300 °C for 3 h, 350 °C for 6 h, 375 °C for 8 h and 425 °C for 8 h. The cured samples were removed from the mold and sanded to a thickness of approximately 2 mm.

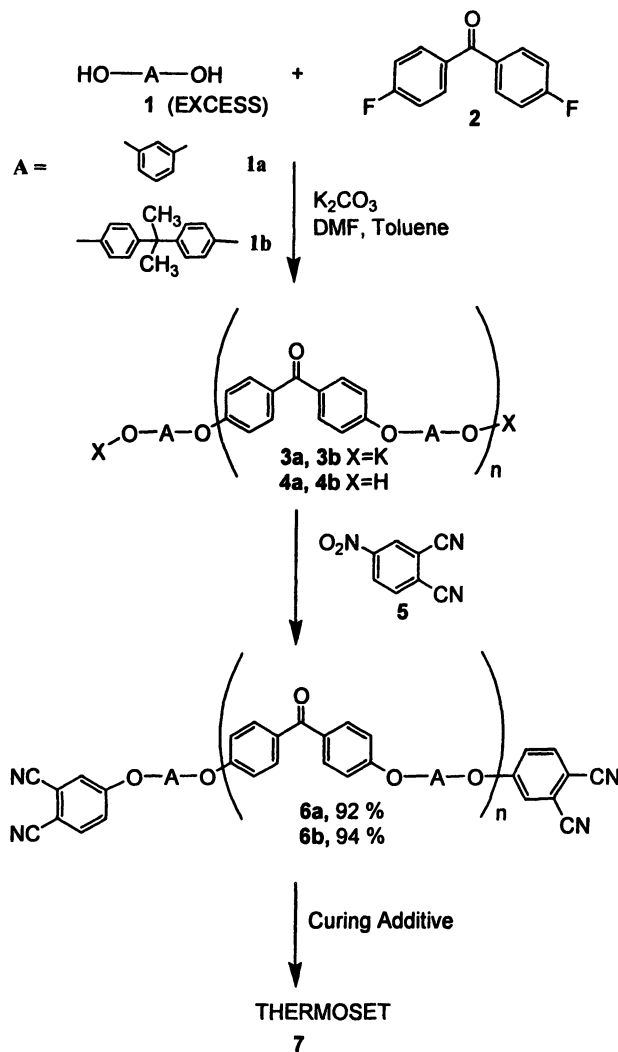
Results and Discussion

Synthesis

The reaction of 4,4'-difluorobenzophenone **2** with a bisphenol **1** has been utilized to incorporate aryl ether linkages into the interconnecting unit of a multiple aromatic ether phthalonitrile **6**. (Scheme 1) The oligomeric phthalonitriles **6** were prepared by a two-step, one-pot procedure from the reaction of **1** and **2** in the presence of potassium carbonate as the base, followed by the reaction of the potassium diphenolate-terminated intermediate **3** via a nitro displacement reaction involving 4-nitrophthalonitrile **5**. The oligomeric phthalonitriles were isolated in 92 - 94 % yield. Phthalonitriles **6** were readily soluble in common organic solvents such as toluene, DMF, acetone, dichloromethane, and chloroform. The reaction was performed in DMF and a minimal amount of toluene to allow azeotropic distillation of the water that formed as a by-product in the reaction. The reaction mixture was stirred at solvent reflux (135 - 145 °C) until no more water was collected in the Dean-Stark trap. The length of the spacer between the terminal phthalonitrile groups can be varied by simply changing the ratio between **1** (excess) and **2**.

IR analysis was used to monitor and determine the progress of the synthetic reactions producing monomers **6**. The spectra of thin films of the hydroxyl-terminated intermediates **4**, which were isolated by acidic workup of **3**, were examined. During the reaction involving **3** and **5** resulting in the formation of **6**, the most notable features were the disappearance of the hydroxyl functionality at approximately 3420 cm⁻¹ and the appearance of the nitrile functionality at

about 2232 cm^{-1} . Once the hydroxyl peak was fully diminished, the reaction was essentially complete.



Scheme 1. Preparation of oligomers 6 and thermosets 7.

The neat curing of phthalonitrile resins has been shown to proceed very slowly even during extended periods at elevated temperatures. Consequently, the resulting monomers 6 (Figure 1) were cured by the incorporation of a minute amount of the highly thermally stable curing additive,¹⁴ *p*-BAPS, to allow the

thermoset formation reaction to proceed quickly and at a low temperature. The incorporation of aromatic ether spacers between the reactive terminal phthalonitrile units generated oligomeric monomers **6a** and **6b** which exhibited softening temperatures around 60 and 75 °C, respectively. Both monomers were completely free flowing around 130 - 150 °C, and therefore had a long processing window before reaction with the curing additive occurred at around 250 °C. Cost effective composite fabrication techniques such as filament winding, resin infusion molding, and resin transfer molding (RTM) may be feasible with these systems at low initial resin processing temperatures.

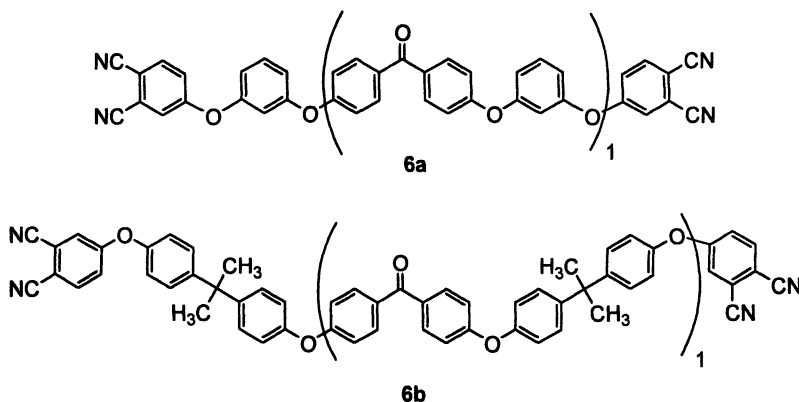


Figure 1. Structure of oligomeric phthalonitriles **6a** and **6b**.

Characterization

Polymerization of **6** where $n \approx 1$ was achieved and studied using DSC analysis in the presence of small quantities of *p*-BAPS (**9**) to afford **7**. For the study, **6** was cured with 3 weight % of *p*-BAPS. The DSC thermograms obtained by heating at 10 °C min⁻¹ to 400 °C revealed endothermic transitions at approximately 60 and 75 °C for **6a** and **6b**, respectively. These transitions corresponded to a softening of **6** from the amorphous phase. Both resins also displayed an exothermic transition commencing around 250 °C and ending at approximately 350 °C, which was attributed to the reaction of **6** with *p*-BAPS.

Rheometric measurements were performed on samples of **7** cured to 425 °C with 3 weight % *p*-BAPS under identical conditions. Figure 2 shows a plot of the storage modulus for samples of **7** up to 500 °C. The storage modulus for **7a** varied from 1625 to 830 MPa when heated from 30 to 500 °C, respectively. The storage modulus for **7b** changed from 1290 to 725 MPa over the same

temperature range. In addition, **7a** exhibited a higher storage modulus than **7b** at any given temperature. The lower modulus for **7b** could be a result of the longer aromatic ether spacer and the reduced crosslinking density in **7b** relative to **7a**. Since the phthalonitrile end units are closer together for **7a**, it is easier for the curing additive to find the ends. Figure 3 shows the damping factor ($\tan \delta$) for polymer **7** cured to 425 °C. When heated to 500 °C, **7a** and **7b** both exhibited peaks commencing at 400 °C. The observed peak maxima appeared near the sharpest decline of the storage modulus. At 500 °C, polymers **7a** and **7b** maintained 51 and 56 % of their initial storage modulus, respectively. It is important for these materials to maintain structure integrity if they are to be used at elevated temperatures (*4c*).

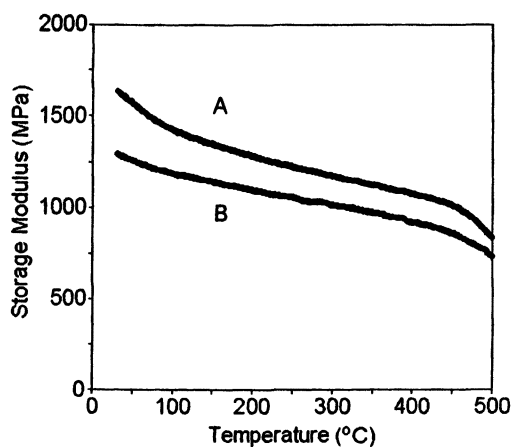


Figure 2. Storage modulus for polymer 7 cured with 3 weight % p-BAPS: (A) polymer 7a, (B) polymer 7b.

The thermal and thermo-oxidative properties were investigated between 50 and 1000 °C in a TGA chamber. Figure 4 shows the TGA thermograms for **7** cured to 425 °C with 3 weight % *p*-BAPS. Polymer **7a** and **7b** displayed similar thermal properties despite the fact that **7b** contains approximately 7 % by weight of aliphatic moieties. When heated under inert conditions, polymers **7a** and **7b** retained about 95 % weight at 545 °C and exhibited char yields of 77 % and 79 %, respectively, at 1000 °C. Polymer **7b** exhibited a slightly higher char yield relative to **7a**. Further studies are being performed to determine the effect of heating to such high temperatures on the mechanical and other physical properties of **7a** and **7b**. When polymers **7a** and **7b** were heated in air, a weight retention of 95 % was observed at 550 and 535 °C, respectively, with decomposition occurring between 600 and 900 °C for both polymers.

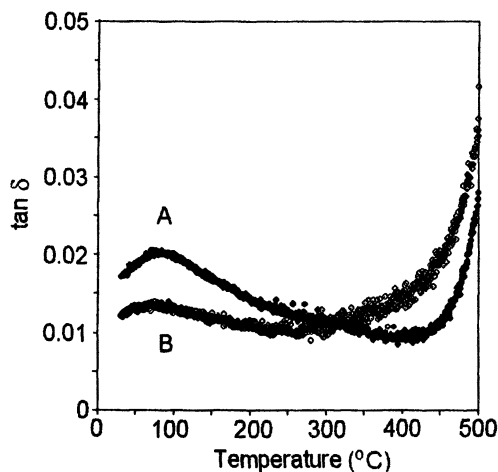


Figure 3. Damping factor ($\tan \delta$) for polymer 7 cured with 3 weight % *p*-BAPS: (A) polymer 7a, (B) polymer 7b.

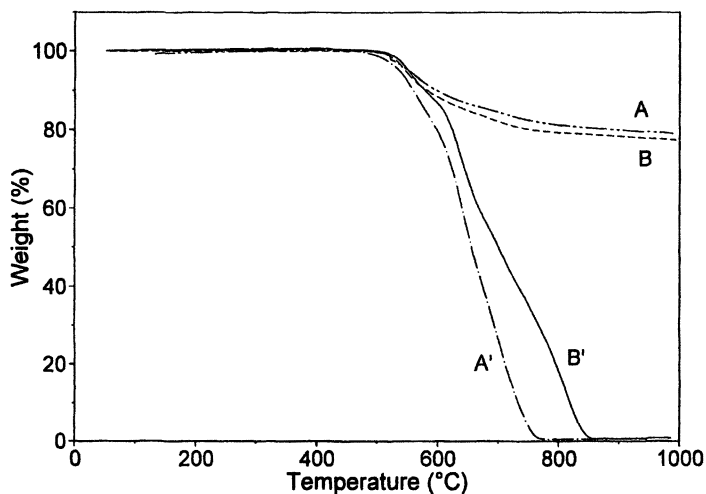


Figure 4. Thermogravimetric analysis of polymer 7 heated to 1000 °C under inert and oxidizing environments: 7b under N_2 (A) and air (A') and 7a under N_2 (B) and air (B').

The oxidative stability for polymer 7 was examined over extended periods. Figure 5 shows an oxidative aging plot for samples of 7a and 7b heated stepwise to 375 °C under air in 8 h temperature intervals. Table 1 indicates the percent of total weight loss over the various temperature intervals. Upon heating to the maximum temperature of 375 °C, a total weight loss of around 5 and 8 % for 7a and 7b, respectively, was observed. The majority of the weight loss occurred on the final segment at 375 °C for both polymers.

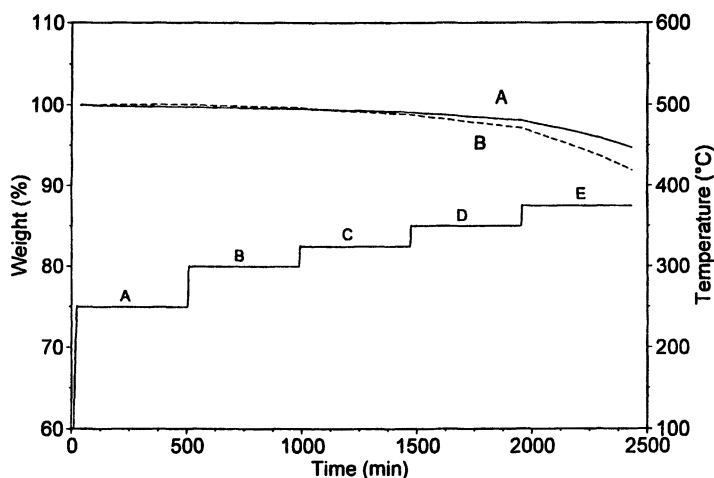


Figure 5. Oxidative aging of polymer 7 at various temperatures: (A) 7a and (B) 7b.

Table I. Data for oxidative aging of polymers 7a and 7b.

Segment	Temperature (°C)	Total Weight Loss for 7a (%)	Total Weight Loss for 7b (%)
A	250	0.1	0.2
B	300	0.3	0.4
C	325	0.7	1.0
D	350	1.7	3.0
E	375	5.0	8.0

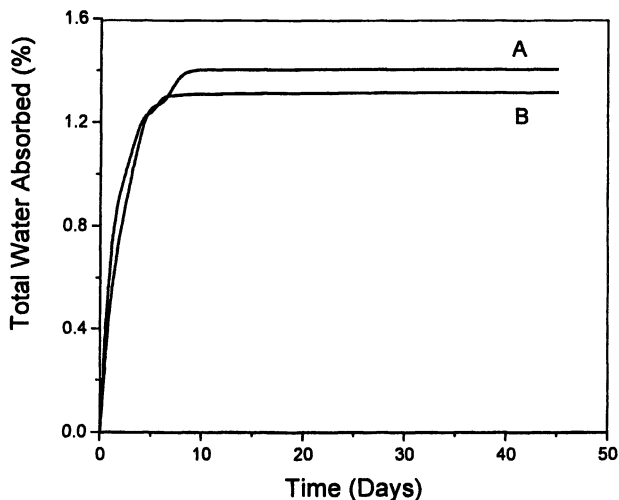


Figure 6. Plot of the weight of water absorbed over time for thermosets (A) 7a and (B) 7b.

Another important feature of phthalonitrile thermosets is their ability to resist significant water absorption over extended periods in aqueous or high humidity environments. Figure 6 shows a water absorption plot for samples of thermosets 7a and 7b soaked at ambient temperature in distilled water. The graph illustrates that the majority of water is absorbed within the first week. The maximum amount of water absorbed over the course of 45 days was approximately 1.4 and 1.3 % by weight for 7a and 7b, respectively. The curve also appears to level off after approximately 10 days. For the use of these materials in high humidity or aqueous environments, this limited water absorption is a significant advantage over other high performance, high temperature polymers.

Conclusion

The described synthetic scheme provides a method for the formation of a series of multiple aromatic ether-linked phthalonitriles **6** with an aryl ether spacer between the reactive phthalonitrile end groups. The monomers were prepared via a two-step, one-pot reaction. The monomers **6** exhibit an amorphous softening temperature below 100 °C and are completely free flowing

around 130 to 150 °C. This low softening temperature lengthens the processing window and therefore enhances the processability. Since polymers 7 do not soften until nearly 500 °C and maintain structural integrity at elevated temperatures once fully cured they are good candidates for structural and microelectronics applications. Thermal studies show that polymers 7 exhibit excellent thermal and oxidative properties and limited water absorption.

Acknowledgments

The authors would like to thank the Office of Naval Research for financial support of this project.

References

1. Keller, T. M.; Roland, C. M. *U. S. Patent Appl.* 7,841,945, 1992.
2. Keller, T. M. "Stable Polymer Conductor," *Proceedings of the 18th International SAMPE Technical Conference*, 1986, 31, 528.
3. (a) Keller, T. M. *CHEMTECH* 1988, 18, 635. (b) Giuliani, J. F.; Keller, T. M. *Sensors Mater.* 1989, 1, 2247.
4. (a) Sastri, S. B.; Armistead, J. P.; Keller, T. M. *Polymer Comp.* 1996, 17, 816. (b) Sastri, S. B.; Armistead, J. P.; Keller, T. M.; Sorathia, U. *Polymer Comp.* 1997, 18, 48. (c) Fowler, G. "Applications of High Temperature Composites on Supersonic Missiles," *Proceedings of the 34th International SAMPE Technical Conference-Baltimore, MD, November, 4-7, 2002*, 1123.
5. (a) Keller, T. M. *Polym. Mater. Sci. Eng.* 1988, 58, 1039. (b) Keller, T. M. *Chem. Mater.* 1994, 6, 302. (c) Dominguez, D. D.; Keller, T. M. *Poly. Prep.* 2002, 43, 991. (d) Keller, T. M. *Polym. Prep.* 1987, 28, 37. (e) Keller, T. M. *Polym. Mater. Sci. Eng.* 1988, 58, 1039.
6. MIL-STD-2031 (SH), Fire and Toxicity Test Methods and Qualification Procedure for Composite Material Systems Used in Hull, Machinery and Structural Applications Inside Naval Submarines; 1991.
7. (a) Dominguez, D. D.; Keller, T. M. "The Development of Low Melting Phthalonitriles," *Proceedings of the 34th International SAMPE Technical Conference-Baltimore, MD, November, 4-7, 2002*, 1111. (b) Laskoski, M.; Dominguez, D.D.; Keller, T. M. *Polym. Mater. Sci. and Eng.* 2004, 91, 164.
8. Laskoski, M.; Dominguez, D. D.; Keller, T. M. *Macromolecules*, 2004, submitted for publication.
9. (b) Keller, T. M.; Price, T. K. *J. Macromol. Sci - Chem.* 1982, A18 (6), 931. (c) Sastri, S. B.; Keller, T. M. *J. Polym. Sci., Part A: Polym. Chem.* 1999, 37, 2105.

Author Index

- Bertalan, Gy., 117
Bourbigot, Serge, 89, 200
Bullett, K. J. (Pyrah), 252
Camino, G., 21
Carpenter, Karen C., 321
Chigwada, Grace, 8, 103
Cochez, M., 36
Cogen, Jeffrey M., 48
Costa, Luigi, 75
Costache, Marius, 8
Cuesta, J. M. Lopez, 36
Cunliffe, L. K., 252
Delobel, René, 89, 200
Dominguez, Dawn D., 378
Dowling, V. P., 237
Duquesne, Sophie, 89, 200
Ebdon, J. R., 252
Falqui, L., 21
Ferriol, M., 36
Finocchiaro, P., 21
Frache, A., 21
Griffith, A. Leigh, 321
Hall, Daniel, 131
Han, Zhidong, 172
Hernberg, Aliea, 144
Horrocks, A. R., 155
Hossenlopp, Jeanne M., 131
Huczek, Jason P., 321
Hull, T. Richard, 252, 334, 348
Hunt, B. J., 252
Jang, Bok Nam, 8
Janssens, Marc L., 321
Jayakody, Chandrasiri, 291
Jiang, David D., 103, 131
Joseph, P., 252
Kandare, Everson, 131
Kandola, B. K., 155
Keller, Teddy M., 366, 378
Keszei, S., 117
Kolel-Veetil, Manoj K., 366
Laachachi, A., 36
Laskoski, Matthew, 378
Lebek, Krzysztof, 334, 348
Lefebvre, J., 89
Leroy, E., 36
Levchik, Sergei V., 280
Lin, Thomas S., 48
Luda, Maria Paola, 75
Lyon, Richard E., 306
Manferti, C., 21
Marney, D. C. O., 237
Marosi, Gy., 117
Matkó, Sz., 117
Milnes, G. J., 252
Morgan, Alexander B., 48
Myers, Dan, 291
Myler, P., 155
Nazaré, S., 155
Nelson, Gordon L., 1, 144
Nyden, Marc R., 306
Ogburn, Carl, 291
Olson, Eric, 224
Paul, Keith, 348
Perez, Ignacio, 185
Price, Dennis, 252, 334, 348
Recourt, P., 89
Russell, L. J., 237
Sébih, Zakia, 200

- Ségura, Sébastien, 200
Shen, Kelvin K., 224
Sorathia, Usman, 185
Starnes, William H., Jr., 213
Stoliarov, Stanislav I., 306
Tartaglione, G., 21
Valesella, Simona, 75
Wang, Jianqi, 172
Wang, Xiaodong, 266
Weil, Edward D., 280
Westmoreland, Phillip R., 306
Whaley, Paul D., 48
Wilkie, Charles A., 1, 8, 61, 103
Wills, Claire L., 348
Willson, Keith R., 321
Yang, Feng, 144
Yngard, Ria, 144
Zanetti, Marco, 75
Zhang, Huiqing, 306
Zhang, Jing, 213
Zhang, Jinguo, 8, 61
Zheng, Xiaoxia, 8

Subject Index

A

Activating interphases, ethylene-vinyl acetate (EVA) copolymer nanocomposites, 121–122

Adaptive interphases

flame retardant additives, 125

See also Interphases (IP)

Additives

flexible foams, 283–284

halogen-free, for flexible foams, 283–284

Airflex

aviation seat cushions, 293–294

open-cell breathable cushioning, 291, 303

See also Cushioning applications

Algorithm, reactive molecular dynamics, 314

Alkyl phosphonates

structure of oligomeric, 284

Aluminum trihydrate (ATH)

with *Firebrake* zinc borates, 227–229

fire retardant for polypropylene, 61–62

nanocomposites with

polypropylene, 67*f*

thermogravimetric analysis, 65

thermogravimetric analysis of

composites with polypropylene (PP), 66*f*

See also Polypropylene–metal hydroxide nanocomposites

Ammonium polyphosphate (APP)

cone calorimetry of polyester–clay nanocomposites with/without, 169*t*

conventional flame retardant, 155, 157*t*, 201

effect on flammability of polyester resin, 169

glass formers, 201

protecting interphases, 124–125

rigid and flexible foams, 281

synergist in ethylene vinyl acetate (EVA) copolymer, 200, 211

See also Ethylene vinyl acetate

(EVA); Magnesium hydroxide (MDH); Polyester–clay nanocomposites

Ammonium salt, counterion of clay in nanocomposite, 11

Antimony(III) chloride

formation, 214

mixtures with Dechlorane Plus, 215

Antimony(III) oxide

promoting dechlorination, 221–222

synergism with halogen, 214

Automotive materials. *See* Smoke

toxicity of automotive materials

Aviation seat cushions

cone calorimetry, 295–296

density and indentation force

deflection (IFD) ranges, 294*t*

Federal Aviation Administration (FAA), 292

fire retardancy standards, 293–294

floatation device, 293

oil burner test, 293, 295

physical properties, 296, 297*t*

vertical Bunsen burner test, 294

See also Cushioning applications

B

Barrier mechanism

fire retardancy by nanocomposites, 10–11

- poly(methyl methacrylate) (PMMA), 14
- Bis(3-diethoxyphosphonyl-4-hydroxyphenyl)propane, fire retardant comonomer, 23, 24
- 5,5'-Bis(diethoxyphosphonyl)-6,6'-dihydroxy-3,3,3',3'-tetramethyl-1,1'-spirobiindane [SpiroP], fire retardant comonomer, 23, 24
- Bis(3-hydroxyphenyl) phenyl phosphate (BHPP)
 structure, 271*f*
 synthesis, 268–269, 270
See also Epoxy resins
- Bisphenol C based resins, cyanate ester resin, 195
- Bisphenol C polycarbonate (BPC)
 Cl-atom shift, 312*f*
 H atom abstractions by Cl atoms, 313*f*
 quantum chemical calculations, 309, 312–313
 thermal decomposition, 312*f*
See also Modeling thermal decomposition
- Blowing agent, impact on flame retardancy of rigid foams, 282
- Bond-dissociation criterion (BDC), reactive molecular dynamics, 314
- Borates
 aluminum trihydroxide (ATH) or magnesium hydroxide (MDH) with *Firebrake* zinc borates, 227–229
 applications in fire retardancy, 224
 background for, in polymer fire retarding formulations, 226–227
 co-additives, 225
 colemanite, 224–225
 experimental, 226
Firebrake ZB/melamine polyphosphate (MPP) as co-additives, 230, 233
Firebrake ZB/nanoclay as co-additive, 233
Firebrake ZB/silicone as co-additives, 229–230
Firebrake zinc borates, 233, 235
 halogen-free cable sheathing containing acrylic-silicone, 230*t*
 halogen-free polypropylene, 232*t*
 heat release rate (HRR) curves of ethylene vinyl acetate (EVA) containing MDH or ATH with *Firebrake* ZB-fine, 228*f*
 HRR curves of ATH, nanoclay, and *Firebrake* ZB-fine in EVA, 234*f*
 HRR curves of EVA containing MDH, MPP, and *Firebrake* ZB-fine, 232*f*
 HRR curves of MDH, nanoclay, and *Firebrake* ZB-fine in EVA, 234*f*
 HRR curves of MDH/*Firebrake* ZB-fine/silicone in EVA, 231*f*
 HRR curves of MDH with *Firebrake* ZB-fine, 229*f*
 smoke reduction of *Firebrake* ZB-fine and silicone in MDH-containing EVA, 231*f*
 zinc borate, 225
- Brominated diols, reactive flame retardants, 283
- Brominated fire retardant. *See* Polypropylene
- Brominated vinyl ester resin sandwich composite, 188
 sketch of sandwich composite, 188*f*
 structure, 189*f*
- Bureau of Home Furnishing and Thermal Insulation (BHFTI), mattress, 299
- Burning cables
 bench-scale tests, 351
 cable designation and formulation, 353*t*
 carbon dioxide yield, 354–355, 356*f*
 carbon monoxide yield, 355, 356*f*, 357

Casico™ containing ethylene-acrylate copolymer, 353
 chalk trapping HCl, 357–358
 characteristic fire types, 350*t*
 comparison of methodologies for fractional effective dose (FED) calculation, 359, 361*f*, 362*f*
 experimental, 352–354
 FED data, 358–359, 360*f*
 furnace conditions by fire type, 352*t*
 HCl yield, 357–358
 methodology defining fire types, 351–352
 percentage non-metallic mass loss of cable compounds, 354, 355*t*
 Purser furnace, 351, 353*f*
 smoke production as optical density, 358
 steady state burning, 354
 tube furnace apparatus, 351, 353*f*
See also Poly(vinyl chloride) (PVC)
 Burning cycle, polymers, 238, 239*f*

C

Cables. *See* Burning cables
 Calcium carbonate, trapping HCl with cable burning, 357–358
 Calcium magadiite
 polyethylene-*co*-vinyl acetate (EVA) nanocomposites, 53, 54*f*
See also Polyethylene-*co*-vinyl acetate (EVA) nanocomposites
 California Bureau of Home Furnishing and Thermal Insulation, mattress, 300
 Caprolactone-containing clay, polymer nanocomposites, 13
 Carbocation, counterion of clay in nanocomposite, 11–12
 Carbon dioxide (CO₂)

decomposition of poly(vinyl chloride), 339, 340*f*
 temperature dependent profiles for poly(methyl methacrylate) (PMMA) copolymers, 261, 262*f*
 yield for burning cable samples, 354–355, 356*f*
 Carbon foam, new core materials, 196
 Carbon monoxide (CO)
 decomposition of poly(vinyl chloride) (PVC), 341
 fire deaths, 349
 temperature dependent profiles for poly(methyl methacrylate) (PMMA) copolymers, 261, 263*f*
 toxicity, 335
 yield from burning polymer cables, 355, 356*f*, 357
See also Smoke toxicity of automotive materials
 Carboranylesiloxanes
 development of, chemistry, 367
 diacetylene-cured network
 precursor, poly(carborane-siloxane-diacetylene) (PCSA) (1), 367, 368*f*
 differential scanning calorimetry (DSC) of network from TaCl₅-catalyzed polymerization of (1), 373*f*
 DSC thermograms of three diacetylene-diluted systems of poly(carborane-trisiloxane-diacetylene), 369*f*
 experimental, 370–371
 infrared spectra of cured and uncured (1), 372*f*
 network formation, 367–368
 polymerization reactions, 370–371
 proposed mechanism for TaCl₅-catalyzed polymerization of (1), 374*f*
 Rh₂(μ-Cl)₂(COD)₂-catalyzed hydrosilation of (1), 371, 375
 structure of polymer, 367*f*

- TaCl₅-catalyzed curing of diacetylene units in (1), 370, 371–373
- thermal curing of PCSA oligomer into network, 367, 368*f*
- thermogravimetric analysis (TGA), 370
- UV-curing reactions, 370, 371
- W(CO)₆-catalyzed photo polymerization of (1), 371, 373, 375
- Cars**
- cushioning products, 296–297, 298*t*
- See also* Cushioning applications; Smoke toxicity of automotive materials
- Ceramizing interphases**
- clay particle accumulation on surface, 128
- See also* Interphases (IP)
- Chalk, trapping HCl with cable burning, 357–358**
- Chemical compatibilization, polymer composites, 118**
- Chlorofluorocarbon blowing agents, impact on flame retardancy of rigid foams, 282**
- Cigarette Ignition Standard, mattress applications, 299**
- Clay**
- caprolactone-containing, 13
- effect on residual char formation with polyester–clay nanocomposites, 165, 166*f*, 167*f*
- efficiency of modifying polymer properties, 156
- oligomerically modified (COPS), 12–13, 62
- organic and inorganic magadiites, 49–50
- peak heat release rate (PHRR) reduction of polymers with, 14*t*
- phosphorus fire retardants as additives to, 15–16
- thermal analytical properties of organically modified, 164*t*
- treatment/properties of organically modified, 157*t*
- tropylium-modified, 12
- See also* Epoxy–clay nanocomposites; Nanocomposites; Polyester–clay nanocomposites; Polystyrene clay nanocomposites
- Co-additives**
- aluminum trihydroxide (ATH) or magnesium hydroxide (MDH) with zinc borates, 227–229
- examples, 225
- zinc borate/melamine polyphosphate (MPP), 230, 233
- zinc borate/nanoclay, 233
- zinc borate/silicone, 229–230
- See also* Borates
- CO₂/CO ratio, poly(methyl methacrylate) (PMMA) copolymers, 261, 263**
- CO/CO₂ ratio, polypropylene and fire-retarded PP, 243, 244*f***
- Colemanite, borate, 224–225**
- Combustion**
- cone calorimetry, 240–241
- oxygen index test, 241
- solid polymers, 238, 239*f*
- tests, 240–241
- UL-94 test, 240
- Compatibilization, chemical and mechanical, 118**
- Composites**
- accidental fires, 186–187
- See also* Navy research and development programs; Poly(acrylic ester)/graphite oxide (PAE/GO) composites; Poly(methyl methacrylate) (PMMA) composites; Sandwich composite
- Composite topside structure, fire performance goals, 190*t***

- Compounding, poly(vinyl chloride) (PVC)/clay and PVC/organoclay nanocomposites, 77**
- Cone calorimetry**
 aviation seat cushions, 295–296
 bisphenol C based cyanate ester resin, 195
 epoxy–clay nanocomposites, 31–33
 ethylene vinyl acetate–magnesium hydroxide/ammonium polyphosphate (EVA–MDH/APP), 203, 204*f*
 evaluating nanodispersion, 13–14
 intumescent formulations, 98*t*
 poly(acrylic ester)/graphite oxide (PAE/GO) nanocomposite, 182–183
 polyester–clay nanocomposites, 165, 169–170
 polyethylene-*co*-vinyl acetate (EVA) magadiite nanocomposites, 55–56, 57*f*, 58*f*
 polyhedral oligomeric silsesquioxanes (POSS) resins, 194–195
 poly(methyl methacrylate) (PMMA) composites, 139–141
 polypropylene and fire-retarded PP, 242–247
 polypropylene expandable nanocomposites, 126, 127*f*
 polypropylene–metal hydroxide nanocomposites, 68–69, 70*f*, 71*f*, 72*f*
 polystyrene clay nanocomposites, 111–114
 residues of EVA–MDH/APP, 205
 sandwich composite, 188
 sandwich composite and components, 191*t*
 smoke toxicity of automotive materials, 324–325
 vinyl ester nanocomposites with phosphorus-based fire retardants, 192–193
- Consumer Products Safety Commission (CPSC), mattress applications, 299**
- Contract furniture**
 cushioning products, 297–298
See also Cushioning applications
- Copolymers. *See* Ethylene vinyl acetate (EVA); Polyethylene-*co*-vinyl acetate (EVA) nanocomposites; Poly(methyl methacrylate) (PMMA) copolymers; Poly(vinyl chloride) (PVC)-based nanocomposites**
- Copper-containing hybrid inorganic/organic compounds. *See* Poly(methyl methacrylate) (PMMA) composites**
- Copper hydroxy methacrylate (CHM). *See* Poly(methyl methacrylate) (PMMA) composites**
- COPS clay. *See* Oligomerically modified clay (COPS)**
- Core materials, fire resistant, for naval sandwich composites, 196**
- Costs, Navy R&D programs, 197**
- Crosslinked networks. *See* Carboranylensiloxanes**
- Cured epoxy resins. *See* Epoxy resins**
- Curing**
 phthalonitrile resins, 382–383
See also Carboranylensiloxanes
- Cushioning applications**
 aviation seat cushions, 293–296
 cone calorimeter test results, 295–296
 contract furniture applications, 297–298
 density and indentation force deflection (IFD) ranges for Airflex foam grades, 294*t*
 fire performance requirements, 292–293
 mattress, 299–303
 oil burner test results, 295

open flame test results for mattress, 300, 301*t*
 passenger cars and locomotive cabs, 296–297
 physical and fire resistant characteristics of surface transportation cushioning, 298*t*
 physical properties for aviation cushions, 296, 297*t*
 US Navy shipboard mattress, 301–303
 vertical Bunsen burner test results, 294

D

Damping factor, phthalonitrile resins, 384, 385*f*

Deactivating interphases, ethylene-vinyl acetate (EVA) copolymer nanocomposites, 121–122

Deaths, fire, 1–2, 349

Decabromodiphenyl oxide (DBDO), nanocomposite fire retardant, 18

Dechlorane Plus

experimental, 216–217

free-radical mechanism for reductive dechlorination in PE and nylon 6,6, 221

gas chromatograms of polyethylene (PE) with, and Sb_2O_3 , 219*f*, 220*f*

gas chromatography/mass spectrometry (GC/MS) analysis, 216–217

mechanistic implications, 219, 221–222

method for thermogravimetric analysis (TGA), 216

mixtures with Sb_2O_3 , 215

monoreduction product yields, 218

possible mechanisms for dechlorination, 215–216

preparative pyrolysis, 217

promotion of dechlorination by Sb_2O_3 , 221–222

pyrolysis yield data and extents of monoreduction of PE with, and Sb_2O_3 , 220*t*

structure, 215

TGA and preparative pyrolysis data for, in polyethylene, 217–218

trade name, 215

Dechlorination. *See* Dechlorane Plus

Decomposition

PVC cables, 349

See also Poly(vinyl chloride)

(PVC)

Degradation

poly(methyl methacrylate)

(PMMA) composites, 138–139

polystyrene nanocomposites, 10–11

Developed fire/low ventilation

carbon dioxide yield for burning cable samples, 354–355, 356*f*

poly(vinyl chloride)

decomposition, 345, 346*t*

Development. *See* Navy research and development programs

Diacetylene-curing. *See*

Carboranylenesiloxanes

Dibromostyrene, incorporation for nanocomposites, 18

Diels–Alder reaction, dispersing, coupling interphases, 119–120

Diethyl 2-(acryloyloxy)ethylphosphate (DEAEP)

copolymer with methyl

methacrylate (MMA), 255, 257

source of ions for DEAEP

breakdown, 256*f*

structure, 255*f*

See also Poly(methyl methacrylate)

(PMMA) copolymers

Diethyl 2-

(methacryloyloxy)ethylphosphate (DEMPEP)

copolymer with methyl

methacrylate (MMA), 257, 259

- source of ions for DEMEP
breakdown, 260*f*
structure, 255*f*
See also Poly(methyl methacrylate)
(PMMA) copolymers
- Differential scanning calorimetry
(DSC)
diacetylene-diluted systems of
poly(carborane-trisiloxane-
diacetylene), 369*f*
network from poly(carborane-
siloxane-diacetylene), 373*f*
poly(methyl methacrylate)
(PMMA) copolymers, 263–
264
- Diglycidyl ether of bisphenol-A
(DGEBA). *See* Epoxy–clay
nanocomposites; Epoxy resins
- Dimethyl methylphosphonate
(DMMP), rigid polyurethane foam,
281
- Diols, brominated, reactive flame
retardants, 283
- Dispersing, coupling interphases
reactive surfactants, 119–120
See also Interphases (IP)
- Dynamic thermal analysis (DTA),
polyester–clay nanocomposites,
163–165
- E**
- Effective heat of combustion (EHC),
polypropylene and fire-retarded PP,
242–243
- Effluent dilution chamber
carbon dioxide concentration, 339,
340*f*
HCl detection, 343, 344*f*
- Elastomer interphases
ethylene-vinyl acetate (EVA)
copolymer nanocomposites,
120–121
See also Interphases (IP)
- Environmentally friendly flame
retardants. *See* Epoxy resins
- Epoxy–clay nanocomposites
2,2-bis(3-diethoxyphosphonyl-4-
hydroxyphenyl) propane [BisP],
23, 24
5,5'-bis(diethoxyphosphonyl)-
6,6'-dihydroxy,3,3,3',3'-
tetramethyl-1,1'-spirobiindane
[SpiroP], 23, 24
characterization methods, 25
cone calorimetry, 31–33
experimental, 23–25
fire retardant comonomer
structures, 24
materials, 23
methods, 24
morphological characterization,
25–27
silicate content, 22–23
thermal characterization, 27, 29–31
thermogravimetry, 27, 29–31
transmission electron microscopy
(TEM), 27, 28*f*
variation of d-spacing of pristine
montmorillonite (MMT) and
after sonication by x-ray
diffraction (XRD), 26*t*
XRD, 25, 27
XRD patterns of NANOFIL 848 in
different physical states, 26*f*
- Epoxy resins
bis(3-hydroxyphenyl) phenyl
phosphate (BHPP) synthesis
method, 268–269
characterization methods, 270
curing procedure, 269–270
diglycidyl ether of bisphenol-A
(DGEBA), 268, 269
environmentally friendly flame
retardant systems, 267–268
experimental, 268–270
flame resistance, 22
flame-retardant properties, 275–
278

- gel permeation chromatography (GPC) diagrams of DGEBA and phosphate-based, 272*f*
- limiting oxygen index (LOI) values of control and phosphate-based, 276*t*
- phosphorylation, 267
- plot of LOI value vs. ratio of P/N in thermoset resin, 277*f*
- structure of BHPP, 271*f*
- structure of phosphate-based, 271*f*
- synthesis of BHPP, 270
- synthesis of phosphate-based, 269, 270–272
- thermal analysis of cured, 272–275
- thermogravimetric analysis (TGA) of control resin and phosphate-based, 273*t*
- UL 94 vertical test results of control and phosphate-based, 276*t*
- See also* Epoxy–clay nanocomposites
- Ethylene vinyl acetate (EVA) copolymers and nanocomposites, 11
- deactivation/activation interphases, 121–122
- elastomer interphases, 120–121
- experimental, 202–203
- flame retardant formulations of magnesium hydroxide (MDH) and ammonium polyphosphate (APP), 202*t*
- heat release rate (HRR) curves of, containing MDH or aluminum trihydroxide (ATH) with zinc borate, 228*f*
- HRR curves vs. time of EVA/MDH/APP formulations, 203, 204*f*
- influence of APP in EVA–MDH formulations, 203, 204*f*
- limiting oxygen index (LOI) values vs. percentage APP in EVA–MDH/APP, 203, 204*f*
- reducing flammability of copolymers, 201
- residues from cone calorimeter experiments, 205*f*
- rheology modifying interphases, 123–124
- thermal degradation of MDH/APP combination, 205–206, 209, 210*f*
- thermogravimetric curves for degradation of MDH/APP, 206–207
- total heat evolved (THE) of flame retarded EVA vs. pure EVA, 203, 205*f*
- viscosity-temperature plots of EVA and FR–EVA containing MMT, 123*f*
- zinc borate/nanoclay as co-additive in EVA, 233, 234*f*
- See also* Ammonium polyphosphate (APP); Borates; Polyethylene-*co*-vinyl acetate (EVA) nanocomposites
- Evolved gas analysis CO₂, poly(methyl methacrylate) (PMMA) copolymers, 261, 263*f*
- Evolved gas analysis CO₂, poly(methyl methacrylate) (PMMA) copolymers, 261, 262*f*
- Expandable graphite (EG) fire retardant applications, 182
- rigid polyurethane foam, 281–282
- Expandable graphite nanocomposites, peak heat release rate (PHRR) reduction of polymers with, 14*t*
- Expandable nanocomposite, separating interphases, 126, 127*f*
- Extrusion preparation of polymer/silica nanocomposites, 145

See also Polymer/silica
nanocomposites

F

Federal Aviation Administration
(FAA). *See* Aviation seat cushions

Fillers, thermal stability, 94, 95*f*

Fillers, inorganic. *See* Intumescent
systems

Fire

collision involving USS
KENNEDY and USS
BELKNAP, 186

rate in United States, 2
statistics, 1–2

Firebrake zinc borates
materials, 226

See also Borates

Fire growth, test, 190*t*

Fire growth index (FIGRA),
polyester–clay nanocomposites,
165, 169*t*

Fire performance

goals for composite topside
structure, 190*t*
intumescent formulations, 97–100

Fire performance requirements
brominated vinyl ester resin in
sandwich composite, 188, 189*f*
submarines, 187
surface ships, 187–188

Fire resistance, test, 190*t*

Fire retardancy

future of nanocomposites, 18
mechanisms of, by
nanocomposites, 9–11
polymer/clay nanocomposites,
8–9
vinyl ester nanocomposites with
phosphorus-based fire
retardants, 192–193

See also Nanocomposites

Fire retardants

additives for polypropylene matrix,
238, 240*t*

background of, formulations, 226–
227

covalently bonded phosphorus,
253, 264–265

Dechlorane Plus, 215

dibromostyrene, 18

halogen-containing additives, 18
phosphorus, 15

resorcinol diphosphate, 16–17

structure of cation in phosphate-
containing clay, 15*f*

styrene nanocomposites using
phosphate-containing clays, 16*f*
tricresylphosphate, 16–17

See also Poly(methyl methacrylate)
(PMMA) copolymers;
Polypropylene

Fire safety. *See* Navy research and
development programs

Fire stability, polymers, 4

Fire testing

poly(methyl methacrylate)–
organically modified
montmorillonite (OMMT) and
PMMA–TiO₂–OMMT
nanocomposites, 43–45
poly(methyl methacrylate)–TiO₂
nanocomposites, 42–43

Fire types

bench-scale models, 351
decomposition of poly(vinyl
chloride), 345, 346*t*
description, 337, 350*t*
furnace conditions, 352*t*
methodology defining, 351–352
small scale, 335
See also Poly(vinyl chloride)
(PVC)

Flame retardancy

control and phosphate-based cured
epoxy resins, 275–277
impact of blowing agent on, of
rigid foams, 282

- mineral fillers in polymers, 37
rigid foam tests, 281
- Flame retardants**
brominated diols as reactive, 283
low-scorch, 286–287
melamine in flexible foams, 288
nature, 201
reactive, for flexible foams, 287
reactive non-halogen, in rigid polyurethane foams, 282
See also Fire retardants
- Flammability**
function of graphite oxide, 182–183
PETG/poly(methyl methacrylate) (PMMA)/silica nanocomposites, 151*t*
PMMA/silica nanocomposites, 147*t*
polycarbonate/silica nanocomposites, 152*t*
polystyrene/silica nanocomposites, 148*t*
- Flammability data, polyethylene-co-vinyl acetate (EVA) magadiite nanocomposites, 55–56**
- Flashover, term, 186–187**
- Flexible foams**
melamine in, 288
passenger cars and locomotive cabs, 296–297, 298*t*
reactive flame retardants for, 287
understanding and overcoming scorch problem, 285–286
See also Cushioning applications; Foams; Polyurethane foams
- Foams**
halogen-free additives for flexible, 283–284
low-scorch flame retardants, 286–287
melamine in flexible, 288
See also Cushioning applications; Polyurethane foams
- Fourier transform infrared (FTIR) spectroscopy, poly(acrylic ester)/graphite oxide (PAE/GO) composites, 178–181, 182*f***
- Fractional effective dose (FED) comparison of four methodologies for calculation, 359, 361*f*, 362*f* effects of three contributions for polymer cables, 358–359, 360*f* fire gas toxicity, 349
See also Burning cables**
- Furniture contract applications, 297–298
See also Cushioning applications**
- G**
- Gel permeation chromatography (GPC), phosphate-based epoxy resins, 271–272**
- Glass transition temperature (T_g), poly(methyl methacrylate) (PMMA)–TiO₂ nanocomposites, 39–40**
- Grafted elastomers, compatibilization, 118**
- Graphite nanocomposites peak heat release rate (PHRR) reduction of polymers with, 14*t*
See also Poly(acrylic ester)/graphite oxide (PAE/GO) composites**
- Graphite oxide (GO) function in flammability of nanocomposite, 182–183 preparation, 173
See also Poly(acrylic ester)/graphite oxide (PAE/GO) composites**
- Green flame retardants epoxy resins, 267–268
See also Epoxy resins**

H

- Halogen-containing additives,
nanocomposite fire retardant, 18
- Halogen-free additives, flexible
foams, 283–284
- Halogen-free polymers. *See* Borates
- Halogen gases. *See* Smoke toxicity of
automotive materials
- HCN gas. *See* Smoke toxicity of
automotive materials
- Heat release rate (HRR)
composites for ISO 9705 room
corner fire tests, 192*f*
cone calorimetry, 31
core materials for sandwich
composite, 196
ethylene vinyl acetate–magnesium
hydroxide/ammonium hydroxide
(EVA–MDH/APP), 203, 204*f*
HRR curves of EVA containing
MDH or ATH with zinc borate,
228*f*
HRR curves of MDH with zinc
borate, 229*f*
intumescent formulations, 99*f*
polyester–clay nanocomposites,
165, 168*f*
polyethylene-*co*-vinyl acetate
(EVA) magadiite
nanocomposites, 55–56, 57*f*,
58*f*
poly(methyl methacrylate)
(PMMA) and PMMA/TiO₂
compositions, 42*f*
poly(methyl methacrylate)
(PMMA) and PMMA with
OMMT and OMMT-*n*TiO₂
compositions), 44*f*
polypropylene and fire-retarded PP,
243–245
polystyrene clay nanocomposites,
112*f*, 113*f*
See also Peak heat release rate
(PHRR)
- High performance materials
increasing demand, 367
See also Carboranylenesiloxanes
- Hybrid Plastics, polyhedral oligomeric
silsesquioxanes (POSS) resins,
194–195
- Hydrogen chloride (HCl)
decomposition of poly(vinyl
chloride), 342–345
detection in effluent dilution
chamber, 343, 344*f*
detection in tube furnace, 343
oxidation, 344
yield from burning polymer cables,
357–358
See also Smoke toxicity of
automotive materials
- Hydroxy double salts (HDSs)
cone calorimetry data of PMMA,
PMMA–CHM, and PMMA–
ZCM, 139, 140*t*
degradation of PMMA composite,
138
dispersion in poly(methyl
methacrylate) (PMMA), 136–
137
elemental analysis, 133
exchange of methacrylate anions
for acetate in ZCA (ZCM), 133–
134
experimental, 133–134
general formula, 132
heat release rate (HRR) curves of
PMMA–ZCM, PMMA–CHM,
and pure PMMA, 140*f*
low and high-resolution
transmission electron
microscopy (TEM) images,
136–137
new fire retardant additives, 132–
133
powder X-ray diffraction (XRD)
analysis of additives, 135
preparation of Zn/Cu-acetate
(ZCA), 133

thermogravimetric analysis (TGA)
 of ZCM, PMMA, and PMMA–
 ZCM samples, 137, 138*t*
 XRD analysis of cone residues, 141
 XRD patterns of PMMA
 composites, 135–136
See also Poly(methyl methacrylate)
 (PMMA) composites

I

Infrared spectroscopy

cured and uncured poly(carborane-
 siloxane-diacetylene) samples,
 372*f*

See also Fourier transform infrared
 (FTIR) spectroscopy

Inorganic fillers. *See* Intumescent
 systems

Inorganic/organic layered compounds.

See Poly(methyl methacrylate)
 (PMMA) composites

Interphases (IP)

activating monolayer, 122

adaptive interphases, 125

ceramizing interphases, 128

deactivating/activating, 121–123

deactivation of flame retardant
 (FR) particles, 122

dispersing, coupling interphases,
 119–120

elastomer interphases, 120–121

ethylene-vinyl acetate copolymer
 (EVA), 118

expandable nanocomposite, 126

expandable polypropylene
 nanocomposite, 126, 127*f*

flame retardancy performance, 118

microgel structure of interacting
 interphases around FR
 nanoparticles, 123*f*

montmorillonite (MMT) and
 organophilic MMT (OMM), 118
 OMM, intercalated (IMM), 118

protecting interphases, 124–125

Raman imaging of EVA-Mg(OH)₂-
 MMT, EVA-Mg(OH)₂-OMM,
 and EVA-Mg(OH)₂-IMM, 121*f*

rheology modifying interphases,
 123–124

separating interphases, 126, 127*f*

transporting interphases, 125

viscosity-temperature plots of EVA
 and FR-EVA containing MMT,
 123*f*

XRD plots of OMM and with
 phosphorylated polyol
 intercalated OMM, 126*f*

Intumescent systems

association of, with mineral fillers,
 90

composition of formulations, 93*t*

cone calorimeter data, 98*t*

copolymer of ethylene/vinyl acetate
 (EVA), 91

experimental, 91–94

fire performance of intumescent
 formulations, 97–100

FTIR spectra of lamellar double
 hydroxide (LDH) and LHD with
 dodecyl sulfate (LDH–DS), 91,
 92*f*

FTIR spectra of sodium dodecyl
 sulfate (SDS), 91, 93*f*

heat release rate (HRR) and weight
 loss curves, 99*f*

LDH–DS, 91

materials, 91, 93

methods, 93–94

montmorillonite (MMT), 90

nature of mineral filler on fire
 retardant properties, 90–91

samples after UL94 tests, 98*f*

thermal stability of intumescent
 formulations, 95–97

thermal stability of nanofillers, 94,
 95*f*

X-ray diffraction (XRD) pattern of
 LDH–DS, 91, 92*f*

Investments, Navy research and development, 189, 197

L

Lamellar double hydroxide (LDH)

exchanging nitrate for dodecyl sulfate (DS), 91

FTIR spectra of LDH and LDH-DS, 91, 92*f*

preparation, 91

thermal stability, 94, 95*f*

X-ray diffraction pattern of LDH-DS, 91, 92*f*

See also Intumescent systems

Layered double hydroxides (LDHs)

fire retardant nanocomposite additives, 132

See also Hydroxy double salts (HDSs)

Limiting oxygen index (LOI)

ammonium polyphosphate (APP) in ethylene vinyl acetate (EVA)-magnesium hydroxide, 203, 204*f*

control and phosphate-based cured epoxy resins, 276*t*

LOI value vs. ratio of P/N in thermoset epoxy resins, 277*f*

poly(methyl methacrylate) (PMMA)-TiO₂ nanocomposites, 39-40

Locomotive cabs

cushioning products, 296-297, 298*t*

See also Cushioning applications

M

Magadiites

organic and inorganic, 49-50

See also Polyethylene-*co*-vinyl acetate (EVA) nanocomposites

Magnesium hydroxide (MDH)

ammonium polyphosphate (APP)

as synergist, 200, 201, 211

composites with polypropylene, 67*t*

curve of mass difference of

MDH/APP, 210*f*

fire retardant for polypropylene, 61-62

flame retardant formulations of ethylene vinyl acetate (EVA), 202

influence of ammonium

polyphosphate (APP) in EVA-MDH formulations, 203, 204*f*

²⁵Mg NMR spectra of, and

MDH/APP vs. temperature of treatment, 208*f*

²⁵Mg NMR spectra of, vs.

temperature of treatment, 207*f*

nanocomposites with

polypropylene, 68*f*

³¹P NMR of MDH/APP vs.

temperature of treatment, 209*f*

thermal degradation of combination of MDH/APP, 205-206, 209, 210*f*

thermogravimetric analysis, 65

thermogravimetric analysis of composites with polypropylene (PP), 66*f*

See also Ethylene vinyl acetate

(EVA); Polypropylene-metal hydroxide nanocomposites

Magnesium magadiite

polyethylene-*co*-vinyl acetate

(EVA) nanocomposites, 53, 54*f*

See also Polyethylene-*co*-vinyl

acetate (EVA) nanocomposites

Markets, resins sales, 3*t*

Mass loss rate curves, polypropylene

and fire-retarded PP, 244-245,

246*f*

Mass spectrometry (MS)

breakdown of diethyl 2-

(acryloyloxy)ethylphosphate

(DEAEP), 256*f*

- breakdown of diethyl 2-(methacryloyloxy)ethylphosphate (DEMPEP), 260*f*
 laser pyrolysis MS, 253, 254*t*, 257
 reaction time-scale techniques, 254*t*
See also Poly(methyl methacrylate) (PMMA) copolymers
- Mattress**
 Bureau of Home Furnishing and Thermal Insulation (BHFTI), 299
 California BHFTI, 300
 Cigarette Ignition Standard, 299
 open flame test results, 300, 301*t*
 prevention of, fires, 299
 US Navy shipboard applications, 301–303
 waffle design, 300
See also Cushioning applications
- Mechanical compatibilization, polymer composites**, 118
- Mechanical performance**
 polyester–clay nanocomposites with/without flame retardants (FR), 162*t*
 studies of polyester–clay nanocomposites, 160, 163
- Mechanisms**
 barrier, 10–11, 14
 char formation by flame retardant, 37
 fire retardancy by nanocomposites, 9–11
 formation of antimony(III) chloride, 214
 free-radical, for reductive dechlorination, 221
 promotion of dechlorination by Sb_2O_3 , 221–222
 reductive dechlorination, 215–216
 TaCl₅-catalyzed polymerization of poly(carborane-siloxane-diacetylene), 374*f*
- Melamine, flexible foams**, 288
Melamine polyphosphate (MPP)
 zinc borate and, in polypropylene, 230, 233
 zinc borate and MPP in ethylene vinyl acetate (EVA) copolymer, 230, 232*f*, 233*f*
- Metal hydroxides**
 achieving effect, 201
 halogen free polyolefins, 225
See also Polypropylene–metal hydroxide nanocomposites
- Metal oxides. *See* Titanium dioxide (TiO₂)**
- Microgel network, rheology**
 modifying interphases, 123–124
- Military. *See* Navy research and development programs**
- Mineral fillers**
 association of intumescent systems with, 90
 intumescent formulations, 93*t*
 polymer flame retardancy, 37
See also Intumescent systems
- Modeling thermal decomposition**
 bisphenol C polycarbonate (BPC), 309, 312–313
 Cl-atom shift in BPC, 312*f*
 cyclizations during rearrangements of HA model compound, 309, 311*f*
 H abstraction by Cl atoms in BPC, 313*f*
 mechanism of thermal decomposition of PIB, 315*f*
 poly(dihydroxybiphenylisophthalamide) (PHA), 308–309
 polyisobutylene (PIB), 315–317
 potential energy surface of model compound HA, 310*f*
 quantum chemical calculations of reaction paths, 307–313
 reactive molecular dynamics (RMD), 313–317
 RMD method, 313–315
 RMD trajectory of 150-unit model of PIB, 316*f*

Models, bench-scale fire, 351

Montmorillonite (MMT)

- adaptive interphases, 125
- composition, 156
- deactivating/activating interphases of systems containing MMT and $\text{Mg}(\text{OH})_2$, 122
- dimethyl ditallow ammonium cation exchange (MMT-DT), 77, 78*t*
- improving fire retardant properties of polymers, 90
- materials, 23
- modification of sodium, 158
- morphology of poly(vinyl chloride)-based nanocomposites containing MMT-DT, 79, 81*f*
- organically modified MMT (OMMT), 37–38
- thermal stability, 94, 95*f*
- transmission electron microscopy (TEM) of OMMT nanocomposites, 38–39
- transporting interphases, 125
- treatment/properties of organically modified, 157*t*
- X-ray diffraction (XRD), 26*f*

See also Epoxy–clay nanocomposites; Polyester–clay nanocomposites; Poly(methyl methacrylate) (PMMA) nanocomposites; Poly(vinyl chloride) (PVC)-based nanocomposites

Morphology

- epoxy–clay nanocomposites, 25–27
- poly(methyl methacrylate) (PMMA) nanocomposites, 38–39
- poly(vinyl chloride)-based nanocomposites, 79–80, 81*f*

Motor Vehicle Fire Research Institute (MVFRI)

- toxic gas examination, 322

See also Smoke toxicity of automotive materials

Multilayer interphase (IP)

- ethylene-vinyl acetate copolymer (EVA), 118
- flame retardancy performance, 118

See also Interphases (IP)

N

Nanoclay, zinc borate and, in ethylene vinyl acetate (EVA) copolymer, 233, 234*f*

Nanocomposites

- ammonium salt as counterion of clay, 11
- amount of clay and peak heat release rate (PHRR), 9–10
- barrier mechanism, 10–11
- caprolactone-containing clay, 13
- carbocation as counterion of clay, 11–12
- cation containing styrene oligomer, 12–13
- cone calorimetry for nanodispersion evaluation, 13–14
- degradation of polystyrene, 10–11
- dibromostyrene, 18
- ethylene vinyl acetate copolymers (EVA), 11
- evaluation of tricresylphosphate and resorcinol diphosphate (RDP), 16–17
- expectations for future of, in fire retardancy, 18
- formation, 9
- halogen-containing additives, 18
- HRR curves for styrene, using phosphate-containing clays, 16*f*
- HRR curves for polystyrene and its, and both with 15% RDP, 17*f*
- mechanisms of fire retardancy by, 9–11

- oligomerically modified clays, 12
 phosphorus fire retardants, 15
 polymer/clay, 8
 reduction in PHRR for polymers
 with clay and graphite, 14*t*
 role of surfactant, 11–13
 structure of cation in phosphate-
 containing clay, 15*f*
 styryltropylium cation for
 modifying clays, 12*f*
 surface by x-ray photoelectron
 spectroscopy, 10
 synergy between, formation and
 conventional fire retardants, 14–
 18
 technology adaptations, 118
 vinyl ester, with phosphorus-based
 fire retardants, 192–193
See also Epoxy–clay
 nanocomposites; Polyethylene-
co-vinyl acetate (EVA)
 nanocomposites; Polymer/silica
 nanocomposites; Poly(methyl
 methacrylate) (PMMA)
 nanocomposites;
 Polypropylene–metal hydroxide
 nanocomposites; Polystyrene
 clay nanocomposites; Poly(vinyl
 chloride) (PVC)-based
 nanocomposites
- Nanodispersion, cone calorimetry for
 evaluation, 13–14
- Nano-effect
 definition, 182
 poly(acrylic ester)/graphite oxide
 (PAE/GO) nanocomposite, 182–
 183
- Nanofillers, thermal stability, 94, 95*f*
- Naphthenate-containing clays
 preparations, 105
 structures of naphthenate-
 containing ammonium salts,
 106*f*
 thermogravimetric analysis, 111*t*
 X-ray diffraction data for, 107*t*
- See also* Polystyrene clay
 nanocomposites
- National Highway Traffic Safety
 Administration (NHTSA)
 smoke toxicity, 322
See also Smoke toxicity of
 automotive materials
- Navy research and development
 programs
 bisphenol-C based resins, 195
 brominated vinyl ester resin in
 sandwich composite, 188, 189*f*
 carbon foam, 196
 collision involving USS
 KENNEDY and USS
 BELKNAP, 186
 composite Mast-LPD-17, 187*f*
 cone calorimeter data for sandwich
 composite and components,
 191*t*
 fire performance goals for
 composite topside structure,
 190*t*
 fire performance of current
 composite material system, 188,
 189*f*
 fire performance requirements for
 submarines, 187
 fire performance requirements for
 surface ships, 187–188
 flashover conditions, 186–187
 heat release rate (HRR) of various
 cores, 196*f*
 interest in composite materials, 186
 investments, 197
 new core materials, 196
 new resin and core materials, 189
 phenolic foam, 196
 phthalonitrile resin, 193–194
 polyhedral oligomeric
 silsesquioxanes (POSS) based
 resin systems, 194–195
 room corner fire test, 192
 sandwich structures, 196–197
 shipboard applications, 186

small scale screening methodology, 189, 192
 vinyl ester nanocomposites with phosphate-based fire retardants, 192–193
 Navy submarines, phthalonitrile resins, 379
 Network formation. *See* Carboranylenesiloxanes
 Nitrogen oxides. *See* Smoke toxicity of automotive materials
 Nuclear magnetic resonance (NMR)
²⁵Mg NMR of magnesium hydroxide (MDH) vs. temperature treatment, 207f
²⁵Mg NMR of MDH and MDH/ammonium polyphosphate (APP) vs. temperature treatment, 208f
³¹P NMR spectra vs. temperature for APP evolution in MDH/APP, 207–208, 209f

O

Oil burner test, aviation seat cushions, 293, 295
 Oligomerically modified clay (COPS) nanocomposites, 12–13
 X-ray diffraction of polypropylene (PP) nanocomposites with, 63, 64f
See also Polypropylene–metal hydroxide nanocomposites
 Open flame test results, mattress, 300, 301t
 Optical density
 decomposition of poly(vinyl chloride), 342
 smoke production, 358
 Organically modified montmorillonite (OMMT)
 morphology of nanocomposites with, 38–39

thermal stability of OMMT nanocomposites, 40–41
See also Poly(methyl methacrylate) (PMMA) nanocomposites
 Organomagadiite
 polyethylene-*co*-vinyl acetate (EVA) nanocomposites, 53, 55f
See also Polyethylene-*co*-vinyl acetate (EVA) nanocomposites
 Oxidative stability, phthalonitrile resins, 386
 Oxygen concentration, decomposition of poly(vinyl chloride) (PVC), 337, 339f
 Oxygen depletion, fires, 349
 Oxygen index
 flammability evaluation, 146
 PETG/PMMA/silica nanocomposites, 151t
 PMMA/silica nanocomposites, 147t
 polypropylene and fire-retarded PP, 241, 248
 polystyrene/silica nanocomposites, 148t, 150
 test method, 241

P

Passenger cars
 cushioning products, 296–297, 298t
See also Cushioning applications
 Peak heat release rate (PHRR)
 cone calorimetry evaluating nanodispersion, 13–14
 poly(acrylic ester)/graphite oxide (PAE/GO), 183t
 polyethylene-*co*-vinyl acetate (EVA) magadiite nanocomposites, 55–56, 57f, 58f
 poly(methyl methacrylate) (PMMA) and PMMA with organically modified montmorillonite (OMMT) and

- OMMT–nTiO₂ compositions),
44f
- vinyl ester nanocomposites with
phosphorus-based fire
retardants, 192–193
- See also* Heat release rate (HRR)
- Pentane, impact on flame retardancy
of rigid foams, 282
- Phenolic foam, new core materials,
196
- Phosphate additives, flexible foams,
283–284
- Phosphate-based epoxy resins
structure, 271f
synthesis, 270–272
- See also* Epoxy resins
- Phosphate fire retardants
aggravating scorch, 285–286
flexible foams, 287
glass formers, 201
melamine in flexible foams, 288
nanocomposites, 15–16
- Phosphorus fire retardants
comonomers for epoxy–clay
nanocomposites, 21, 23, 24
vinyl ester nanocomposites with,
192–193
- See also* Poly(methyl methacrylate)
(PMMA)
- Phosphorylation, epoxy resins, 267
- Phthalonitrile resins
absorbed water vs. time for
thermosets, 387f
characterization, 383–387
damping factor for thermosets, 385f
experimental, 379–381
monomer, 194f
Naval Research Laboratory (NRL),
193–194
neat curing, 382–383
oxidative stability, 386
polymerization and
thermogravimetric studies on
thermoset, 380–381
- preparation of oligomeric multiple
aromatic ether-containing
phthalonitrile, 380
- preparation of oligomers and
thermosets, 382
- resistance to water absorption, 387
- rheometric measurement sample
preparation, 381
- storage modulus of thermoset, 384f
- structure of monomers, 194f
- structure of oligomeric
phthalonitriles, 383f
- synthesis, 381–383
- tan delta for network polymers,
385f
- thermal and thermo-oxidative
properties, 384
- thermogravimetric analysis (TGA)
of thermoset, 385f
- thermosetting polymers, 379
- Plasticizers, poly(vinyl chloride)
(PVC) nanocomposite, 85, 86f, 87
- Plastics, North American, production,
3t
- Poly(acrylic ester)/graphite oxide
(PAE/GO) composites
cone calorimetry, 182–183
experimental, 173
- Fourier transform infrared (FTIR)
spectra, 178–181
- FTIR comparison of micro-
PAE/GO5 and nano-PAE/GO5,
181f, 182f
- FTIR of micro- and nano-PAE/GO
composites, 179, 180f
- FTIR of PAE, micro- and
nanocomposites at 300°C, 178–
179
- FTIR of virgin PAE, micro- and
nano-PAE/GO at 500°C, 179,
181
- function of GO in flammability of
nanocomposite, 182–183
- nano-effect, 182

- peak heat release rate (PHRR) of PAE/GO5, 183*t*
- reactions during thermal degradation of copolymer PAE, 178–179
- TGA/DTG data, 177*t*
- TGA (thermogravimetric analysis) of GO, 174, 176*f*
- TGA of PAE, its microcomposite and nanocomposite, 176, 177*f*
- time to ignition (TTI) of PAE and GO composites, 182, 183*t*
- transmission electron microscopy (TEM), 174, 175*f*
- X-ray diffraction (XRD) method, 173
- XRD traces, 174
- Polyamide blends
nanocomposites, 8
peak heat release rate (PHRR) reduction of, with clay and graphite, 14*t*
- Polybromoaromatic compounds, scorch-resistant, 286
- Polycarbonate (PC), PC/silica nanocomposites, 151–152
- Poly(dihydroxybiphenylisophthalamide) (PHA)
cyclizations, 309, 311*f*
keto-enol rearrangements, 310*f*
quantum chemical calculations, 308–309
thermal decomposition, 308*f*
See also Modeling thermal decomposition
- Polyester–clay nanocomposites
ammonium polyphosphate (APP) as flame retardant (FR), 155, 157*t*, 159*t*, 162*t*
cone calorimetry, 165, 169–170
effect of flame retardants on flammability of resin, 169
equipment, 159
experimental, 156–159
fire growth index (FIGRA), 165, 169*t*
formulations, 159*t*
heat release rate (HRR) and mass loss vs. time curves, 168*f*
mechanical performance studies, 160, 163
modification of sodium montmorillonite, 158
preparation, 158
thermal analysis, 163–165, 166*f*, 167*f*
treatment/properties of organically modified clays, 157*t*
X-ray diffraction (XRD) studies, 159–160, 161*f*
XRD and mechanical performance results for, with and without FRs, 162*t*
- Polyethylene
gas chromatograms of PE with Dechlorane Plus and antimony oxide, 219*f*, 220*f*
pyrolysis yield and monoreduction of, with Dechlorane Plus and Sb₂O₃, 220*t*
reductive dechlorination, 221
thermogravimetric analysis (TGA) of PE with Dechlorane Plus and antimony oxide, 217–218
See also Dechlorane Plus
- Polyethylene-*co*-vinyl acetate (EVA) nanocomposites
analytical data for EVA formulations, 52*t*
clay cation in interface of polymer and clay, 49–50
cone calorimeter and flammability data, 55–56
degree of clay dispersion in magadiite-containing formulations, 52–53
EVA + Mg(OH)₂ + magadiite (MGD) formulations, 51*t*
experimental, 50–51

- heat release rate (HRR) curves of formulations with organic and inorganic magadiites, 57*f*, 58*f*
- inorganic magadiites, 53, 54*f*
- magadiite, 49–50
- organomagadiite, 53, 55*f*
- transmission electron microscopy (TEM) and X-ray diffraction (XRD) data, 52–53
- Polyhedral oligomeric silsesquioxanes (POSS) resin systems, reduced flammability vinyl esters, 194–195
- Polyisobutylene (PIB)
 - 150-unit model after 10 ps of reactive dynamics, 316*f*
 - mechanism of thermal decomposition, 315*f*
 - reactive molecular dynamics (RMD), 315–317
 - See also* Modeling thermal decomposition
- Polyisocyanurate foams, ammonium polyphosphate (APP), 281
- Polymer layered silicate nanocomposites (PLSN)
 - flame retardant improvements, 76
 - See also* Poly(vinyl chloride) (PVC)-based nanocomposites
- Polymers
 - combustion of solid, 238, 239*f*
 - fire safety, 2
 - fire stability of, 4
 - North American plastics
 - production, 3*t*
 - resins sales by major markets, 3*t*
 - See also* Modeling thermal decomposition; Smoke toxicity of automotive materials
- Polymer/silica nanocomposites
 - experimental, 145–146
 - flammability evaluation, 146
 - PETG/PMMA/silica nanocomposites, 150–151
 - PMMA/silica nanocomposites, 146–146, 146–148
 - polycarbonate/silica nanocomposites, 151–152
 - polystyrene/silica nanocomposites, 148–150
 - preparation, 145
 - thermal stability, 145–146
- Poly(methyl methacrylate) (PMMA)
 - barrier mechanism, 14
 - peak heat release rate (PHRR) reduction of, with clay and graphite, 14*t*
 - PETG/PMMA/silica nanocomposites, 150–151
 - PMMA/silica nanocomposites, 146–148
- Poly(methyl methacrylate) (PMMA) composites
 - anion exchange of zinc/copper-acetate (ZCA) forming zinc/copper methacrylate (ZCM), 133–134
 - combustion with additives and char formation, 140–141
 - cone calorimetry, 139, 140*t*
 - copper hydroxy nitrate and copper hydroxy methacrylate (CHM) additive, 133–134
 - degradation, 138
 - dispersion of additives in, 136–137
 - effect of SnCl₄ and tetraphenyltin on thermal degradation, 138–139
 - experimental, 133–134
 - future experiments for role of copper content of additives, 141–142
 - hydroxy double salts (HDSs), 132–133
 - low and high-resolution transmission electron microscopy (TEM) images, 136–137
 - powder X-ray diffraction (XRD) analysis of additives, 135*f*

- TGA curves (thermogravimetric analysis) curves of CHM, PMMA, and PMMA-CHM samples, 137*f*
- TGA curves of ZCM, PMMA, and PMMA-ZCM samples, 137*f*
- TGA results, 138*t*
- XRD pattern for PMMA-ZCM and PMMA-CHM, 135-136
- XRD patterns of PMMA-CHM and PMMA-ZCM cone residues, 141
- Poly(methyl methacrylate) (PMMA) copolymers
- additive triethyl phosphate (TEP), 252, 253, 255*f*
 - comonomers diethyl 2-(methacryloyloxy)ethylphosphate (DEMPEP) and diethyl 2-(acryloyloxy)ethylphosphate (DEAEP), 253, 255*f*
 - differential scanning calorimetry (DSC), 263-264
 - experimental, 253, 255
 - gases from MMA/DEAEP, 258*f*
 - gases from MMA/DEMPEP, 261*f*
 - mass spectra of MMA/DEAEP, 256*f*, 257*f*
 - mass spectra of MMA/DEMPEP, 259*f*, 260*f*
 - MMA/DEAEP, 255, 257
 - MMA/DEMPEP, 257, 259
 - reaction time-scale techniques, 254*t*
 - source of ions for DEAEP breakdown, 256*f*
 - source of ions for DEMPEP breakdown, 260*f*
 - structures of DEMPEP, DEAEP and additive TEP, 255*f*
 - temperature dependent CO₂ profiles for PMMA, PMMA/TEP, MMA/DEMPEP, and MMA/DEAEP, 262*f*
 - temperature dependent CO profiles for PMMA, PMMA/TEP, MMA/DEMPEP, and MMA/DEAEP, 263*f*
 - thermogravimetry/infrared evolved gas analysis experiments, 261-263
- Poly(methyl methacrylate) (PMMA) nanocomposites
- experimental, 37-38
 - fire testing of, samples by melt blending, 42-45
 - flame retardant mechanism, 37
 - glass transition temperature and limiting oxygen index (LOI) measurements for TiO₂ nanocomposites, 39-40
 - heat release rate (HRR) curves of, 44*f*
 - instrumentation, 38
 - materials and processing, 37-38
 - morphology of nanocomposites, 38-39
 - photos of cone calorimeter residues, 43*f*, 46*f*
 - PMMA-OMMT and PMMA-TiO₂-OMMT nanocomposites, 43-45
 - PMMA-TiO₂ nanocomposites, 42-43
 - thermal stability of TiO₂ and OMMT nanocomposites, 40-41
 - transmission electron microscopy (TEM) of, with organically modified montmorillonite (OMMT) and TiO₂, 38-39
- Polypropylene
- CO/CO₂ ratio vs. time for PP and fire-retarded PP, 244*f*
 - combustion tests, 240-241
 - cone calorimetry, 242-247
 - cone calorimetry method, 240-241
 - effective heat of combustion (EHC) vs. time for PP and fire-retarded PP, 243*f*
 - effect of proprietary additive on fire-retarded PP, 247*t*

- elastomer interphases, 120
 experimental, 239–241
 fire retardant additives, 238, 240*t*
 fire retardants for, 61–62
 future combustion testing, 248
 heat release rate (HRR) vs. time for
 PP and fire-retarded PP, 244–
 245
 mass loss rate vs. time for PP and
 fire-retarded PP, 246*f*
 oxygen index test, 241, 248
 peak heat release rate (PHRR)
 reduction of, with clay and
 graphite, 14*t*
 rate of smoke formation vs. time
 for PP and fire-retarded PP, 247*f*
 separating interphases of
 expandable nanocomposite, 126,
 127*f*
 specimen preparation, 239–240
 UL 94 results, 241–242
 UL 94 test method, 240
 zinc borate/melanine
 polyphosphate (MPP) as co-
 additives, 230, 233
- Polypropylene–metal hydroxide
 nanocomposites**
 aluminum trihydrate (ATH) and
 magnesium hydroxide (MDH)
 fire retardants, 61–62
 characterization of formation by X-
 ray diffraction (XRD), 63, 64*f*
 cone calorimetry, 68–69
 experimental, 62–63
 heat release rate (HRR) curves for
 PP and combinations with MDH
 and oligomerically modified
 clay (COPS), 71*f*, 72*f*
 HRR curves for PP, PP with ATH
 and nanocomposites, 70*f*
 instrumentation, 62–63
 materials, 62
 tensile properties, 72, 73*t*
 TGA curves of PP and ATH
 composites, 66*f*
- TGA curves of PP and MDH
 composites, 66*f*
 TGA curves of PP–ATH
 nanocomposites, 67*f*
 TGA curves of PP–MDH
 nanocomposites, 68*f*
 TGA data of metal hydroxides
 ATH and MDH, 65*t*
 thermogravimetric analysis (TGA),
 63, 65, 67
- Polystyrene**
 barrier mechanism for,
 nanocomposites, 10–11
 peak heat release rate (PHRR)
 reduction of, with clay and
 graphite, 14*t*
 PS/silica nanocomposites, 148–150
See also Polymer/silica
 nanocomposites
- Polystyrene clay nanocomposites**
 cone calorimetry, 111–114
 experimental, 104–106
 heat release rate (HRR) for bulk
 polymerized styrene
 nanocomposites of Np clay,
 112*f*
 HRR for bulk polymerized styrene
 with NpDD clay, 113*f*
 HRR for melt blended polystyrene
 in presence of Np clay, 113*f*
 instrumentation, 104–105
 materials, 104
 modification of clay, 105–106
 preparation of methyl-
 naphthenatedidecylmethylammo-
 nium salt NpDD, 105
 preparation of naphthenate Np salt,
 105
 preparation of NpTL and BTL
 salts, 105
 structures of naphthenate-
 containing ammonium salts,
 106*f*
 thermogravimetric analysis, 110–
 111

- transmission electron microscopy (TEM), 108, 109*f*, 110*f*
- X-ray diffraction (XRD), 106, 107*t*
- XRD traces of PS–Np clay nanocomposites by bulk polymerization, 108*f*
- Polyurethane foams
- additives in flexible foams, 283–284
 - ammonium polyphosphate (APP), 281
 - brominated diols, 283
 - dimethyl methylphosphonate (DMMP), 281
 - expandable graphite, 281–282
 - industry for flexible, 292
 - reactive non-halogen flame retardants in rigid, 282
 - scorch problem in flexible foams, 285–286
- See also* Cushioning applications
- Poly(vinyl chloride) (PVC)
- carbon accumulation, 10
 - carbon dioxide for effluent dilution chamber and secondary oxidizer, 339, 340*f*
 - carbon monoxide by fire type, 341
 - char forming polymer, 76
 - chlorine formation, 344
 - comparing HCl yield from top and bottom of effluent dilution chamber, 343, 344*f*
 - comparing HCl yield from top and bottom of tube furnace, 343
 - decomposition, 335–336
 - decomposition under three fire conditions, 345, 346*t*
 - developed fire with low ventilation, 345, 346*t*
 - experimental, 336–337
 - fires causing toxic gases, 335
 - fire types, 337, 345, 346*t*
 - HCl detection during burning, 342–345
 - methods for small-scale measurement of toxic gases, 335
 - optical density by fire type, 342
 - oxidation of HCl, 344
 - oxygen concentration by fire type, 337, 339*f*
 - Purser furnace, 336–337, 338*f*, 353*f*
 - secondary oxidizer, 337
 - simplified first step of decomposition of PVC, 336*f*
 - smoldering conditions, 345, 346*t*
 - uses, 335
 - well-ventilated burning, 345, 346*t*
- See also* Burning cables
- Poly(vinyl chloride) (PVC)-based nanocomposites
- abbreviations and composition of materials, 78*t*
 - characterization methods, 77–78
 - compounding for PVC/clay composite and PVC/organoclay nanocomposites, 77
 - experimental, 77–78
 - intercalated nanocomposites using montmorillonite (MMT-DT), 79
 - intercalated nanocomposites using nanofiller FH-DT (dimethyl ditallow ammonium cation exchange), 80
 - microcomposite PVC/FH vs. nanocomposites, 82–83
 - nanocomposite morphology, 79–80, 81*f*
 - plasticized PVC and PVC nanocomposite, 85, 86*f*, 87
 - TGA of PVC-VA, PVC-VA/FH, PVC-VA/FH-DT, and PVC-VA/MMT-DT, 84*f*, 85*f*
 - thermal degradation, 82–87
 - thermogravimetric analysis (TGA) of PVC, PVC/FH, PVC/FH-DT, and PVC/MMT-DT, 82*f*, 83*f*
- Production, North American plastics, 2, 3*t*

Protecting interphases, sensitivity of fire retardants, 124–125

Purser furnace

decomposition of poly(vinyl chloride) (PVC), 336–337
schematic, 338*f*, 353*f*

See also Burning cables

Q

Quantum chemical calculations

bisphenol C polycarbonate (BPC), 309, 312–313

modeling reaction paths, 307–308

poly(dihydroxybiphenylisophthalamide) (PHA), 308–309, 310*f*, 311*f*

See also Modeling thermal decomposition

R

Reactive coupling, dispersing, coupling interphases, 119–120

Reactive molecular dynamics (RMD)

150-unit model of polyisobutylene (PIB), 316*f*

algorithm, 314

bond-dissociation criterion (BDC), 314

mechanism of thermal

decomposition of PIB, 315*f*

method, 313–315

polyisobutylene (PIB), 315–317

See also Modeling thermal decomposition

Reactive surfactants

compatibilization, 118

dispersing, coupling interphases, 119–120

See also Interphases (IP)

Research. *See* Navy research and development programs

Research costs, Navy R&D programs, 189, 197

Resins sales, major markets, 3*t*

Resorcinol diphosphate, nanocomposite fire retardant, 16–17

Retardancy. *See* Nanocomposites

Rh₂(μ-Cl)₂(COD)₂-catalyzed hydrosilation, poly(carborane-siloxane-diacetylene), 371, 375

Rheology modifying interphases microgel type network, 123–124

See also Interphases (IP)

Rheometric measurement, phthalonitrile resins, 381, 383–384, 385*f*

Rigid foams

brominated diols, 283

impact of blowing agent on flame retardancy of, 282

Rigid poly(vinyl chloride). *See* Poly(vinyl chloride) (PVC)

Room corner fire test, fire performance goal, 190*t*, 192

S

Sandwich composite

brominated vinyl ester resin, 188, 189*f*

cone calorimeter data, 191*t*

fire insulation attachment, 197

heat release rate, 196*f*

new core materials, 196

sketch, 188*f*

small scale screening methodology, 189, 192

Sb₂O₃. *See* Antimony(III) oxide

Scorch problem

low-scorch flame retardants, 286–287

understanding and overcoming, in flexible foams, 285–286

- Screening methodology, fire
performance of composite systems,
189, 192
- Seating furniture, cushioning products,
297–298
- Secondary oxidizer
carbon dioxide concentration, 339,
340*f*
experimental, 337
See also Poly(vinyl chloride)
(PVC)
- Separating interphases
expandable nanocomposite, 126,
127*f*
See also Interphases (IP)
- Shipboard, mattress applications, 301–
303
- Silica
thermal stability, 94, 95*f*
See also Polymer/silica
nanocomposites
- Silicates. *See* Epoxy–clay
nanocomposites
- Silicone, zinc borate and, in ethylene
vinyl acetate (EVA) copolymer,
229–230
- Siloxanes. *See*
Carboranylenesiloxanes
- Small scale screening methodology,
fire performance of composite
systems, 189, 192
- Smoke chamber measurements,
automotive materials, 325–326,
328
- Smoke formation rate, polypropylene
and fire-retarded PP, 245,
247*f*
- Smoke production
optical density, 358
test, 190*t*
- Smoke toxicity, test, 190*t*
- Smoke toxicity of automotive
materials
1996 Dodge Caravan test samples,
323*t*
1997 Chevrolet Camaro test
samples, 323*t*
acceptability of materials by
various criteria, 331*t*
acceptance thresholds, 330–331
average CO yields for 1996 Dodge
Caravan test samples, 324*t*
average CO yields for 1997
Chevrolet Camaro test samples,
325*t*
average NO_x and HCN yields for
nitrogen-containing test
samples, 325*t*
CO concentrations and average CO
yields, 328*t*
comparison of dynamic vs. static
results, 329–330
comparison with literature values,
328–329
cone calorimeter measurements,
324–325
Fourier transform infrared (FTIR)
spectrometer, 322
HCl concentrations and average
HCl yields for kick panel
insulation backing, 328*t*
materials for study, 322, 323*t*
Motor Vehicle Fire Research
Institute (MVFRI), 322
parts for smoke chamber
measurements, 326*t*
peak CO concentrations and
average CO yields, 326*t*, 327*t*
peak HCl concentrations and
average HCl yields for kick
panel insulation backing, 327*t*
smoke chamber measurements,
325–326, 328
toxic gas concentration limits, 330*t*
- Smoldering
carbon dioxide yield for burning
cable samples, 354–355, 356*f*
decomposition of poly(vinyl
chloride), 345, 346*t*
- Sodium dodecyl sulfate (SDS)

- FTIR spectra of SDS, 91, 93*f*
See also Intumescent systems
- Sodium magadiite
 polyethylene-*co*-vinyl acetate
 (EVA) nanocomposites, 53, 54*f*
See also Polyethylene-*co*-vinyl
 acetate (EVA) nanocomposites
- Sodium montmorillonite
 modification, 158
See also Montmorillonite (MMT)
- Solid polymers, combustion, 238, 239*f*
- Storage modulus, phthalonitrile resins,
 383–384
- Structural integrity, test, 190*t*
- Styrene oligomers, organically
 modified clays in nanocomposites,
 12–13
- Styryltropylium cation, counterion of
 clay in nanocomposites, 12
- Submarines
 fire performance requirements, 187
 phthalonitrile resins, 379
- Surface flammability, test, 190*t*
- Surface ships, fire performance
 requirements, 187–188
- Surface transportation
 cushioning products, 296–297, 298*t*
See also Cushioning applications
- Surfactants
 reactive, 118
 role of, in nanocomposites, 11–13
 synthesis of reactive, and Raman
 spectroscopic monitoring, 120*f*
- Synergism
 antimony-halogen, 214
See also Ammonium
 polyphosphate (APP);
 Dechlorane Plus; Polypropylene
- Synthetic plastics, production, 2, 3*t*
- T**
- TaCl₅-catalyzed curing
- diacetylenes in poly(carborane-
 siloxane-diacetylene), 370, 371–
 373
 proposed mechanism, 374*f*
- Tan delta, phthalonitrile resins, 384,
 385*f*
- Tensile properties, polypropylene–
 metal hydroxide nanocomposites,
 72, 73*t*
- Test methods, fire performance goals,
 190*t*
- Thermal analysis, cured epoxy resins,
 272–275
- Thermal curing. *See*
 Carboranylenesiloxanes
- Thermal degradation
 poly(acrylic ester) (PAE), 178–179
See also Modeling thermal
 decomposition
- Thermal stability
 clays in polyester nanocomposites,
 163–165
 intumescent formulations, 95–97
 nanofillers, 94, 95*f*
 PETG/PMMA/silica
 nanocomposites, 151*t*
 PMMA/silica nanocomposites,
 147*t*
 polycarbonate/silica
 nanocomposites, 152*t*
 polymer/silica nanocomposites,
 145–146
 poly(methyl methacrylate)
 nanocomposites with TiO₂ and
 organically modified
 montmorillonite (OMMT), 40–
 41
 polystyrene/silica nanocomposites,
 148*t*
See also Poly(vinyl chloride)
 (PVC)-based nanocomposites
- Thermogravimetric analysis (TGA)
 control and phosphate-based cured
 epoxy resins, 273–274

- epoxy-clay nanocomposites, 27, 29–31
- graphite oxide (GO), 174, 176*f*
- intumescent formulations, 95, 96*f*
- magnesium hydroxide, ammonium polyphosphate, and combinations, 205–207
- metal hydroxides, 65
- phthalonitrile resins, 384, 385*f*
- plasticized poly(vinyl chloride) nanocomposites, 85, 86*f*, 87
- poly(acrylic ester)/graphite oxide (PAE/GO) composites, 174, 176–177
- polyester-clay nanocomposites, 163–165, 166*f*, 167*f*
- poly(methyl methacrylate)–copper hydroxy methacrylate (PMMA–CHM), CHM, and PMMA, 136–137
- poly(methyl methacrylate) (PMMA) copolymers, 261–263
- poly(methyl methacrylate)–zinc/copper methacrylate (PMMA–ZCM), ZCM, and PMMA, 136–137
- polypropylene (PP) and aluminum trihydrate (ATH) composites, 66*f*
- polystyrene clay nanocomposites, 110–111
- poly(vinyl chloride-*co*-vinyl acetate) (PVC-VA) nanocomposites, 84–85
- poly(vinyl chloride) (PVC) nanocomposites, 82–83
- PP and magnesium hydroxide (MDH) composites, 66*f*
- PP–ATH nanocomposites, 67*f*
- PP–metal hydroxide nanocomposites, 63, 65, 67, 68*f*
- Thermosetting polymers. *See* Phthalonitrile resins
- Time to ignition, poly(acrylic ester)/graphite oxide (PAE/GO), 182, 183*t*
- Titanium dioxide (TiO₂)
 glass transition temperature and limiting oxygen index (LOI) measurements of nanocomposites, 39–40
 thermal stability of, nanocomposites, 40–41
See also Poly(methyl methacrylate) (PMMA) nanocomposites
- Total heat evolved (THE), ethylene vinyl acetate–magnesium hydroxide/ammonium hydroxide (EVA–MDH/APP), 203, 205*f*
- Toxicity
 fire gas, 349
 fire performance of polymers, 2
See also Burning cables; Poly(vinyl chloride) (PVC); Smoke toxicity of automotive materials
- Transmission electron microscopy (TEM)
 epoxy-clay nanocomposites, 27, 28*f*
 poly(acrylic ester)/graphite oxide (PAE/GO) composites, 174, 175*f*
 polyethylene-*co*-vinyl acetate (EVA) magadiite nanocomposites, 52–53, 54*f*, 55*f*
 poly(methyl methacrylate)–copper hydroxy methacrylate (PMMA–CHM), 135–136
 poly(methyl methacrylate) nanocomposites with TiO₂ and organically modified montmorillonite (OMMT), 38–39
 poly(methyl methacrylate)–zinc/copper methacrylate (PMMA–ZCM), 135–136
 polystyrene clay nanocomposites, 108, 109*f*, 110*f*

Transportation. *See* Cushioning applications; Smoke toxicity of automotive materials

Transporting interphases
flame retardant additives, 125
See also Interphases (IP)

Tricresylphosphate, nanocomposite
fire retardant, 16–17

Triethyl phosphate (TEP)
additive, 255
pyrolysis of poly(methyl methacrylate) (PMMA)
copolymers, 257, 258f, 259, 261f
structure, 255f
See also Poly(methyl methacrylate) (PMMA) copolymers

Trityl (triphenylmethyl) ion,
counterion of clay in
nanocomposite, 11–12

Tropylium-modified clay,
nanocomposites and thermal
stability, 12

Tube furnace apparatus. *See* Purser
furnace

U

UL 94 test
control and phosphate-based cured
epoxy resins, 276t
method, 240
polypropylene and fire-retarded PP,
241–242

Ultraviolet (UV) curing, diacetylenes
in poly(carborane-siloxane-
diacetylene), 370, 371

United States Navy
shipboard mattress applications,
301–303
See also Navy research and
development programs

Unsaturated polyesters
flammability behavior, 156

See also Polyester–clay
nanocomposites

V

Vacuum assisted resin transfer
molding (VARTM), brominated
vinyl ester resin, 188

Ventilation
carbon dioxide yield for burning
cable samples, 354–355, 356f
decomposition of poly(vinyl
chloride), 345, 346t

Vertical Bunsen burner test, aviation
seat cushions, 293–294

Vertical burning
polycarbonate/silica
nanocomposites, 152t
polystyrene/silica nanocomposites,
149t

Vinyl acetate. *See* Polyethylene-co-
vinyl acetate (EVA)
nanocomposites; Poly(vinyl
chloride) (PVC)-based
nanocomposites

Vinyl chloride. *See* Poly(vinyl
chloride) (PVC)-based
nanocomposites

Vinyl ester nanocomposites, fire
retardancy of, with phosphorus-
based fire retardants, 192–193

W

Waffle design, mattress, 300
Water absorption, phthalonitrile
resins, 387

W(CO)₆-catalyzed photo
polymerization poly(carborane-
siloxane-diacetylene); 371, 373,
375

Wide angle X-ray scattering (WAXS)
clay interlayer spacing, 77

intercalated poly(vinyl chloride)-based nanocomposites, 79–80, 81*f*

X

X-ray diffraction (XRD)

clay and hybrids in resin and with/without ammonium polyphosphate (APP), 159–160, 161*f*

clay in different physical states, 26*f*

copper hydroxy methacrylate (CHM), zinc/copper methacrylate (ZCM) and precursors by powder XRD, 135

COPS (oligomerically modified clay) and polypropylene nanocomposites, 63, 64*f*

epoxy–clay nanocomposites, 25, 27

lamellar double hydroxide with dodecyl sulfate (LDH-DS), 91, 92*f*

poly(acrylic ester)/graphite oxide (PAE/GO) composites, 174

polyester–clay nanocomposites with/without flame retardants (FR), 162*t*

polyethylene-*co*-vinyl acetate (EVA) magadiite nanocomposites, 52–53

poly(methyl methacrylate)–CHM and PMMA–ZCM composites, 135–136

polystyrene clay nanocomposites, 106, 107*t*, 108*f*

residues of cone calorimetry of PMMA–CHM and PMMA–ZCM, 141

variation of d-spacing of clay and after sonication, 26*t*

X-ray photoelectron spectroscopy, evaluating surface of degrading polymer, 10

Z

Zinc borate

synergist in ethylene vinyl acetate–magnesium hydroxide, 201

See also Borates

Zinc-copper methacrylate (ZCM)

product. *See* Poly(methyl methacrylate) (PMMA) composites